

**Investigating the role of GABA<sub>A</sub>  
Receptor  $\alpha$ 1 and  $\alpha$ 2 Subunits in  
Synapse Formation**

Jessica Edith ARAMA



**SCHOOL OF PHARMACY**

A thesis presented for the Degree of  
Doctor in Philosophy

I, Jessica Arama confirm that the work presented in this thesis is my own. Where information has been derived from other sources, I confirm that this has been indicated in the thesis.

## **Acknowledgment**

Firstly, I would like to thank my supervisor, Dr. Jasmina Jovanovic for her support and her help throughout the course of my PhD. The way she cared, listen and trusted me gave me the strength to believe in myself and to do my best in her team. Through her motivation and passion for science, she has been more than a supervisor, she has been, and still is, a truly inspirational figure to me. I would also like to thank Pr. Alex Thomson without whom this PhD would not have been possible.

I would like to thank all the people who scientifically participated in this work:

I would like to thank Pr. Anne Stephenson for her advice and for letting us using her equipment so many times. I would like to thank Dr. Sarah cousins for her precious help and advice. I would like to thank Emmanuel Samuel and Dr. Sibylle Heidelberger from the Laboratory of Mass spectrometry at the school of Pharmacy, and Dr. Yuqin Wang and Dr. Suska Sumova from Swansea University, for their help with Mass Spectrometry experiments.

My colleagues and Friends, Laura Brown and Martin Nicholson: I would like to thank you both for your presence, your support and your help. Thank you for being here for me on a daily basis in the most amazing way.

I would like to thank Agota Biro for her support and her precious advice and Antoine Bremaud for his very important help with statistical analysis.

I would also like to thank all the people who psychologically supported me in this work:

I would like to thank Magali Burher. Her help was more than precious.

My family: My mum, my dad, my sisters Lea and Ava and my brothers Arry and Alec: I would like to thank you for everything you brought in my life, for your advice and love, for believing in me and pushing me to pursue my dream.

I would also like to thank my uncles, aunties and cousins who have been so supportive and amazing to me throughout my PhD.

I would like to thank my Grandfather Daniel Nataf (z"l) who has been a true inspiration and a model, and even if he left us during my PhD, I know that he took good care of me

from where he is. I would also thank my Grandmother Michele Nataf, who is the most amazing woman I know. Thank you for your presence, your advice and your support.

I would like to thank my grandparents Sylvain and Edith Benillouche who have been so supportive throughout my PhD. You are so important to me, I hope that I made you proud.

I would like to thank all my friends from London and from Paris who have made my journey so nice and fun.

Finally, the last but none the least, I would like to thank my husband who has been the hub of my life for so long and who has been the most supportive, amazing and caring person I have ever met. Thank you Antoine for your patience of living with a “PhD student/wife” and everything that comes with it! This work would not have been possible without you, see? I finally admit it...



## Abstract

GABA<sub>A</sub> receptors, the essential functional components of the inhibitory synapses in the brain, have recently been demonstrated to play a structural role during synapse formation. The subunit composition of these receptors is known to determine their synaptic localization, but how different receptor subunits influence the formation of inhibitory synapses is currently unknown.

The first aim of my thesis was to investigate whether these synaptogenic effects of GABA<sub>A</sub>Rs may be mediated by their large N-terminal extracellular domains. I have cloned, expressed and purified the N-terminal extracellular domains of the  $\alpha$ 1 and  $\alpha$ 2 subunits of GABA<sub>A</sub> receptors using the baculovirus/Sf9 cell system. When added to the GABAergic medium spiny neurones over a period of 14 days *in vitro*, these proteins were able to adhere to the cell surface and promote GABAergic synapse formation. As I was interested to study the molecular mechanisms that could mediate such effects, I used proteomics and mass spectrometry to search for potential trans-synaptic interacting proteins of  $\alpha$ 1 or  $\alpha$ 2 subunits which could bind specifically to the N-terminal extracellular domains of these subunits.

In parallel, I have investigated how the activity of GABA<sub>A</sub> receptors influences the proper positioning and the assembly of inhibitory synapses in primary cultures of medium spiny neurones. In these experiments, GABA<sub>A</sub> receptor activity was blocked over the time period of 7 or 14 days in culture and cell survival, as well as the inhibitory synapse formation, were assessed. I have observed very specific structural changes in the density and distribution of  $\alpha$ 1- or  $\alpha$ 2-containing synapses under these conditions. My results indicate that the activity of GABA<sub>A</sub> receptors plays a central role in the formation and maintenance of different types of inhibitory synapses formed between GABAergic neurones during development.

**Abstract Presented at the BNA Conference,**

**London 2013**

**Formation, maturation and specificity of inhibitory synapses in primary cultures of striatal medium spiny neurones**

Jessica E. Arama, Karine Abitbol, Celine Fuchs, F. Anne Stephenson, Alex M Thomson and Jasmina N. Jovanovic

*UCL School of Pharmacy 29-39 Brunswick square WC1N 1AX London*

Basal ganglia play an essential role in motor coordination and cognitive functions. The GABAergic medium spiny neurones account for ~98 % of all the neurones in the basal ganglia, and are mediators of essentially all functions attributed to this brain region (Tepper and Bolam, 2004). The loss of these neurones in Huntington's disease (Pauly et al., 2012), or the loss of dopamine-dependent regulation of their activity in Parkinson's disease result in motor disorders and loss of voluntary motor control (Obeso et al., 2008). Central to the normal functioning of the medium spiny neurones is integration of excitatory and inhibitory synaptic inputs: the former mediated by glutamatergic corticostriatal and thalamostriatal afferents, and the later mediated by GABAergic interneurones and medium spiny neurones axon collaterals (Picconi et al., 2012). Thus, changes in synaptic innervation of these neurones are key determinants of the inhibitory tone of their projections and the overall functional status of their synaptic targets outside of the basal ganglia.

In this study we have investigated formation, maturation and specificity of GABAergic synapses formed between the medium spiny neurones *in vitro*. Medium spiny neurones, cultured from the embryonic E17 striatal tissue, formed a highly homogenous population and displayed a number of properties that are similar to their *in vivo* counterparts (Goffin et al., 2010). Our experiments demonstrate that development of GABAergic synapses in this system is a highly regulated process which involves clustering of specific subtypes of GABA<sub>A</sub> receptors in the vicinity of presynaptic GABAergic terminals immunoreactive for glutamate decarboxylase (GAD)-

65. During maturation, the two most abundant types of synapses incorporating either  $\alpha 1$  or  $\alpha 2$  subunit of GABA<sub>A</sub> receptors were found to undergo distinct changes in the overall density as well as the size of postsynaptic clusters.

Using immunofluorescence and confocal imaging we have observed that from 7 to 14 days *in vitro* the density of  $\alpha 1$ -containing synapses was increased in parallel with the size but not the overall density of postsynaptic GABA<sub>A</sub> receptor clusters. The density of  $\alpha 2$ -containing synapses was increased in correlation with the overall density of postsynaptic GABA<sub>A</sub> receptor clusters while their size was decreased. In parallel with these morphological changes, we detected an increase in the amplitude and frequency of spontaneous inhibitory postsynaptic currents recorded from voltage-clamped neurones in the whole-cell configuration. In addition, dual whole-cell recordings of synaptically connected pairs of neurones revealed that action potential-activated synaptic events, an indication of synapse maturity, occurred after 12-14 days *in vitro*. Finally, using Ca<sup>2+</sup> indicator fluo-4-AM, we have demonstrated that depolarizing activity of GABA<sub>A</sub>Rs detected initially becomes a hyperpolarizing activity during the period of synaptic maturation.

Thus, formation and maturation of  $\alpha 1$ - and  $\alpha 2$ -GABA<sub>A</sub>R containing synapses appear to be driven by different molecular mechanisms which are currently under investigation.

**Abstract presented at FENS Conference,**

**Milan 2014**

**Investigating the role of GABA<sub>A</sub> Receptor  $\alpha$ 1 and  $\alpha$ 2 Subunits in Synapse  
Formation**

Jessica E Arama, Laura E. Brown, F. Anne Stephenson, Alex M. Thomson and  
Jasmina N. Jovanovic

*UCL School of Pharmacy, 29-39 Brunswick Square, WC1N 1AX London, UK*

GABA<sub>A</sub> receptors (GABA<sub>A</sub>Rs), the essential functional components of the inhibitory synapses in the brain, have recently been demonstrated to play a structural role during synapse formation by promoting the adhesion of inhibitory axon terminals (Fuchs et al., 2013). The subunit composition of these receptors is known to determine their functional and pharmacological properties (Olsen and Sieghart, 2009), as well as their subcellular and synaptic localization (Thomson and Jovanovic, 2010, Gross et al., 2011), but how different receptor subunits influence the formation of inhibitory synapses is currently unknown.

The first aim of my thesis was to investigate whether these synaptogenic effects may be mediated by the large N-terminal extracellular domains of GABA<sub>A</sub>Rs. We have cloned and expressed the N-terminal extracellular domains of the  $\alpha$ 1 and  $\alpha$ 2 subunits of GABA<sub>A</sub>Rs ( $\alpha$ 1 and  $\alpha$ 2 ECDs) using Bac-to-Bac CT-TOPO expression system in Sf9 cells, and established a protocol for their purification. The expressed proteins of ~26 kDa were found to be immunoreactive with the corresponding extracellular domain-specific antibodies and glycosylated. These proteins were added to the GABAergic medium spiny neurone cultures at different concentrations and time points over a period of 14 days *in vitro*. The controls included the extracts of untransfected Sf9 cell which were taken through the same purification protocol. Immunolabelling of the  $\alpha$ 1 and  $\alpha$ 2 purified extracellular domains with specific antibodies revealed that these proteins were able to adhere to the cell surface. To analyse formation of synaptic

contacts, we performed immunolabelling with specific pre- and postsynaptic GABAergic markers. This analysis demonstrated that the addition of purified proteins, but not the controls, resulted in an increase in the size and the density of  $\gamma 2$ -containing GABA<sub>A</sub>R clusters in association with the GAD65-positive presynaptic terminals, suggesting that the extracellular domains of GABA<sub>A</sub>R subunits may have synaptogenic effects in GABAergic synapse formation. As we were interested to know what mechanism could trigger such effect, we searched for a potential specific presynaptic binding partner of the  $\alpha 1$  or  $\alpha 2$  ECDs. Together with affinity chromatography and proteomics, mass spectrometry analysis allowed us to identify two heparin sulphate proteoglycans Pikachurin and Perlecan, which could potentially be involved during specific GABAergic synapse formation.

In parallel, we investigated how the activity of GABA<sub>A</sub> receptors influences the proper positioning and the assembly of inhibitory synapses. We have suppressed the GABA<sub>A</sub> receptor activity in the medium spiny neurone cultures using a competitive antagonist bicuculline over the time period of 7 or 14 days in culture. We have observed prominent cell loss at concentrations of bicuculline higher than 25  $\mu$ M suggesting that GABA<sub>A</sub> receptor activity is necessary for the survival of these neurones during development. Using lower concentrations of bicuculline, we have observed very specific structural changes in the density and distribution of  $\alpha 1$ - or  $\alpha 2$ -containing synapses formed between the medium spiny neurones. This indicates that the activity of GABA<sub>A</sub> receptors plays a central role in the formation and maintenance of different types of inhibitory synapses during development.

## List of Abbreviations

°C	Degree celsius
µg	Microgram
µl	Microliter
5-HT3 receptor	Serotonin receptor
AcMNPV	Autographa Californica multiple nucleopolyhedrovirus
ACN	Acetonitrile
AIS	Axon initial segment
AP	Alkaline Phosphatase
AP2	Adaptator protein 2
APs	Action potentials
APS	Ammonium per sulfate
ATP	Adenosin Triphosphate
BAC	Bacterial artificial chromosomes
BCA	bicinchronic acid
BCIP	5-bromo-4-chloro-3'-indolyphosphate
BIG2	Brefeldin A-inhibited GTP/GDP exchange factor 2
Bip	Binding Immunoglobulin protein
bp	Base pairs
BSA	Bovine Serum Albumin
BZ-I	Benzodiazepine 1
BZ-II	Benzodiazepine 2
CA-1	Cornu Ammonis 1
CaCl <sub>2</sub>	Calcium chloride
CCK	Cholecystokinin
CCVs	Clathrin coated vesicles
ChAT	Choline Acetyltransferase
Cl <sup>-</sup> /HCO <sub>3</sub> <sup>-</sup>	Chloride/bicarbonate
CLSM	Confocal Laser Scanning Microscopy
CO <sub>2</sub>	Carbon dioxide
CR	Calreticulin
Cu <sup>2+</sup>	Copper
Cys-loop	Cystein loop
D1/2R	Dopamine 1/2 Receptor
Da	Dalton
DARPP-32	Dopamine- and cAMP-regulated neuronal phosphoprotein
DGC	Dystrophin/Glycoprotein complex
DIV	Days in vitro
DMSO	Dimethyl sulfoxide
DNA	Desoxyribo Nucleic Acid
DOC	Deoxycholate
E.coli	Escherichia coli
ECDs	Extracellular domains
EDTA	Ethylenediaminetetraacetic acid
EEAT3	Glutamate transporter 3
EGFP	Enhanced Green Fluorescent protein
ER	Endoplasmic reticulum
ERAD	Endoplasmic reticulum associated degradation
ERM	Ezrin-radixin-moesin
EtOH	Ethanol
FRAP	Fluorescent photobleaching after recovery
FSI	Fast spiking interneurons
GABA	γ-aminobutyric acid
GABA <sub>A</sub> Rs	GABA <sub>A</sub> Receptors
GABA <sub>B</sub> Rs	GABA <sub>B</sub> Receptors
GABA <sub>C</sub> Rs	GABA <sub>C</sub> Receptors
GABARAP	GABA <sub>A</sub> Rs associated protein
GAD 65	Glutamate Decarboxylase 65
GAD 67	Glutamate Decarboxylase 67

GEF	Guanylate exchange factor
GFP	Green fluorescent protein
GlyRs	Glycine receptors
GODZ	Golgi specific DHHC zinc finger protein
GPCRs	G-protein-coupled receptors
GPE	Globus Pallidus External
GPI	Globus Pallidus Internal
GPM	Globale Proteome Machine
GRIF	GABA <sub>A</sub> Rs interacting factor
GTP	Guanosin triphosphate
HAP1	Huntingtin associated protein 1
HBSS	Hank's balanced salt solution
HEK 293	Human Embryonic Kidney 293
HEPES	4-(2-hydroxyethyl)-1-piperazineethanesulfonic acid
His-tag	Histidine tag
HRP	Horseradish Peroxidase
IDA	Iminodiacetic acid groups
IPI	International protein index
IPSCs	Inhibitory Post Synaptic Currents
IQR	Interquartile range
Kb	Kilobases
KCC 2	K <sup>+</sup> Cl <sup>-</sup> Co transporter 2
KCl	Potassium chloride
kDa	Kilodaltons
KH <sub>2</sub> PO <sub>4</sub>	Potassium phosphate monobasic
KO	Knock out
LB medium	Luria broth medium
LGE	Lateral Ganglionic eminences
lhx 6/7	LIM Homeobox protein 6/7
LNS	Laminin Neurexin Sex hormone
mA	Milliamper
MAP2	Microtubule associated protein 2
mg	Milligram
MgCl <sub>2</sub>	Magnesium chloride
MGE	Medial ganglionic eminences
MgSO <sub>4</sub>	Magnesium sulfate
min	Minute
mIPSC	Miniature inhibitory postsynaptic current
ml	Milliliters
MOI	Multiplicity of infection
mRNA	Messenger Ribonucleic Acid
MS	Mass spectrometry
MS/MS	Tandem mass spectrometry
MSN	Medium Spiny Neurone
Na <sub>2</sub> HPO <sub>4</sub>	Anhydrous sodium phosphate dibasic
NaCl	Sodium chloride
NaHCO <sub>3</sub>	Sodium bicarbonate
NBT	Nitro-blue tetrazolium
NCAM	Neuronal cell adhesion molecule
Ni <sup>2+</sup>	Nickel
Ni-NTA	Nitrilotriacetic acid
NKCC 1	Na <sup>+</sup> K <sup>+</sup> Cl <sup>-</sup> Co transporter 1
Nkx2.1	NK2 Homeobox 1
NL 1-3	Neuroigin 1-3
nm	Nanometers
NOS	Nitric oxide synthase
NP-40	Tergitol-type NP-40
NPY	Neuropeptide Y
NSF	N-ethylmaleimid sensitive factor
PBS	Phosphate Buffered saline

PCR	Polymerase chain reaction
PFA	Paraformaldehyde
pfu	Plaque forming unit
P <sub>H</sub>	Polyhedron promoter
pH	Potential hydrogene
pKa	Acid dissociation constant
PKA	Protein kinase A
PKC	Protein kinase C
pLGICs	Pentameric ligand-gated ion channels
Plic1/2	Protein links integrin-associated proteins with the cytoskeleton1/2
PLTS	Persistant and Low threshold spike interneurons
ppm	Part per million
PPN	Pedunculo pontine Nucleus
PRIP1/2	Phospholipase C-related catalytically inactive protein 1/2
PSD	Postsynaptic density
PTP $\delta$	Presynaptic tyrosine phosphatase receptor
PV	Parvalbumin
Q-TOF	Quadruple-Time-of-flight
g	Revolution per minute
s.e.m	Standard error of the mean
S.O.C medium	Super optimal broth medium
SCAM	Synaptic cell adhesion molecule
SDS	Sodium dodecyl sulfate
SDS/PAGE	Sodium Dodecyl Sulphate Polyacrylamide Gel Electrophoresis
sec	Seconds
Sf9 cells	Spodoptera Frugiperda cells
SFM	Serum Free Medium
sIPSCs	spontaneous inhibitory postsynaptic current
Slitrack	Slit and NRT-like family member 3
SNpc/SNc	Substantia Nigra pars compacta
SNpr/SNr	Substantia Nigra pars reticulata
SOM	Somatostatin
S-SCAM	Synaptic Scaffolding molecule
STN	Subthalamic nucleus
STR	Striatum
TANs	Tonically active neurones
TBS	Tris-Buffered Saline
TEMED	Tetramethylethylenediamine
TMs	Transmembrane domains
T-test	Student's test
TTX	Tetrodotoxin
UPS	Ubiquitin proteasome system
V	Volts
VDCC	Voltage Dependent Calcium Channel
VGAT	Vesicular GABA Transporter
VGLUT	Vesicular Glutamate Transporter
VIAAT	Vesicular Inhibitory amino acid Transporter
$\mu$ m	Micromol



## Table of Contents

Chapter one .....	19
1. Introduction.....	20
1.1 The GABAergic Synapse .....	20
1.1.1 The presynaptic GABAergic nerve terminal .....	21
1.1.1.1 Synthesis of GABA.....	21
1.1.1.2 Vesicular loading of GABA.....	22
1.1.1.3 GABA uptake by transporters .....	22
1.1.1.4 Degradation of GABA.....	22
1.1.2 The postsynaptic specialisations of GABAergic synapses .....	23
1.1.2.1 The structure of ionotropic GABA <sub>A</sub> Rs.....	24
1.1.2.2 Clustering of GABA <sub>A</sub> Rs .....	27
1.1.2.3 The functional and pharmacological heterogeneity of GABA <sub>A</sub> R subtypes.....	30
1.1.3 Synaptic cleft spanning proteins.....	35
1.1.3.1 Neurexins/ Neuroligin.....	36
1.1.3.2 NCAM .....	37
1.1.3.3 Dystrophin/glycoprotein complex (DGC) .....	38
1.1.3.4 Slitrack3 and PTP $\delta$ .....	38
1.1.3.5 Postsynaptic GABA <sub>A</sub> Rs.....	39
1.2 Intracellular trafficking of GABA <sub>A</sub> Rs.....	39
1.2.1 Synthesis and intracellular trafficking of GABA <sub>A</sub> Rs .....	39
1.2.1.1 Assembly of postsynaptic GABA <sub>A</sub> Rs.....	39
1.2.1.2 Degradation of misfolded subunits: ERAD .....	41
1.2.1.3 Export to the Golgi apparatus and Post-translational modification by glycosylation..	42
1.2.2 Endocytosis and recycling of GABA <sub>A</sub> Rs .....	43
1.2.2.1 Clathrin-dependent endocytosis.....	43
1.2.2.2 Phosphorylation-dependent regulation of endocytosis.....	44
1.2.2.3 Recycling of GABA <sub>A</sub> Rs.....	45
1.3 Development of GABAergic synapses .....	46
1.3.1 Regional expression of GABA <sub>A</sub> Rs across the embryonic brain .....	46
1.3.2 Regional expression of GABA <sub>A</sub> Rs across the adult brain.....	46
1.3.3 Physiological properties of GABAergic synapses throughout development .....	48
1.3.3.1 Developmental switch .....	48
1.3.3.2 GABA <sub>A</sub> Rs-mediated hyperpolarisation in mature neurones .....	48
1.4 The basal ganglia .....	49
1.4.1 Structure and functionality of the basal ganglia .....	49
1.4.1.1 The direct and indirect pathway .....	50
1.4.1.2 Pathophysiology of the basal ganglia.....	52
1.4.1.3 Development of the basal ganglia.....	53

1.4.2	Characteristics of the medium spiny neurones.....	54
1.4.2.1	Physiological properties of MSNs .....	54
1.4.3	Inhibitory mechanisms in the neostriatal microcircuitry .....	57
1.4.3.1	Feed-forward inhibition of MSNs by GABAergic interneurons.....	58
1.4.3.2	Feedback inhibition by axon collaterals of MSNs .....	59
1.4.4	Other neuronal types in the striatum .....	60
1.4.4.1	Cholinergic interneurons .....	60
1.4.4.2	The PLTS interneurons.....	61
1.4.5	Expression of GABA <sub>A</sub> R subunits in the adult striatum .....	62
	Chapter two.....	64
2.	Experimental procedures.....	65
2.1	Primary cultures of embryonic medium spiny neurones.....	65
2.2	Fluorescent immunolabelling and confocal imaging .....	66
2.3	Confocal analysis .....	68
2.4	Analysis of synaptic parameters.....	68
2.5	Statistical analysis.....	69
2.6	Protein assays.....	70
2.6.1	Bradford Assay.....	70
2.6.2	BCA Assay .....	71
2.7	Methanol/Chloroform extraction of proteins.....	72
2.8	SDS PAGE and electrophoresis.....	72
2.9	Immunoblotting.....	74
	Chapter three .....	77
3.	Expression and purification of N-terminal extracellular domains of GABA <sub>A</sub> R $\alpha$ 1 and $\alpha$ 2 subunits using Bac-to-Bac Baculovirus/ Sf9 cells expression system .....	78
3.1	Introduction.....	78
3.1.1	Aims .....	81
3.2	Methods .....	82
3.2.1	The Bac-To-Bac Expression System.....	82
3.2.2	Blunt-End TOPO cloning of $\alpha$ 1 and $\alpha$ 2 ECDs in pFastBac/CT TOPO His vector .....	83
3.2.2.1	Primers design and PCR amplification of the $\alpha$ 1 and $\alpha$ 2 ECDs DNA sequences.....	83
3.2.2.2	Gel extraction of DNA from agarose gel.....	85
3.2.2.3	Blunt-end TOPO Cloning in pFastBac CT-Topo His vector.....	86
3.2.2.4	Transformation in One Shot Mach1 <sup>TM</sup> T1 <sup>R</sup> Chemically Competent E.Coli.....	86
3.2.2.5	Miniprep protocol: purification of DNA using QIAprep Spin Miniprep Kit (QIAGEN) ..	86
3.2.2.6	Transposition of $\alpha$ 1 and $\alpha$ 2 ECDs into DH10Bac E.Coli.....	87
3.2.3	Sf9 cell culture.....	91
3.2.3.1	Suspension culture.....	91
3.2.5	Generating P1 and P2 viral stocks from transfected Sf9 cells.....	92

3.2.5.1	Transfection procedure: cationic liposome-mediated transfection using Cellfectin II® Reagent	92
3.2.5.2	Harvesting P1 viral stock and cell lysis for immunoblot analysis	92
3.2.5.3	SDS/PAGE and Immunoblotting	93
3.2.5.4	Generating P2: Amplification of the viral stock	93
3.2.6	Partial purification of $\alpha 1$ and $\alpha 2$ ECDs under native conditions using Tris-HCl buffer and Probond Resin	94
3.2.7	Partial purification of $\alpha 1$ and $\alpha 2$ ECDs under native conditions using $\text{NaH}_2\text{PO}_4$ based buffers and Ni-NTA Resin	95
3.3	Results	97
3.3.1	Insertion of DNA sequence of $\alpha 1$ or $\alpha 2$ N-terminal ECD into Baculoviruses	97
3.3.2	Baculoviruses-infected Sf9 cells express $\alpha 1$ and $\alpha 2$ ECDs	102
3.3.3	Optimising protein expression	103
3.3.4	Optimisation of the purification of $\alpha 1$ and $\alpha 2$ ECDs from infected Sf9 cells	105
3.3.4.1	Purification of $\alpha 1$ and $\alpha 2$ ECDs using ProBond columns	105
3.3.4.2	Purification of $\alpha 1$ and $\alpha 2$ ECDs using Ni-NTA columns	107
3.4	Discussion	109
Chapter four		112
4.	Investigating the potential synaptic binding partners of the extracellular domains of GABA <sub>A</sub> R subunits $\alpha 1$ and $\alpha 2$	113
4.1	Introduction	113
4.1.1	Aims	114
4.2	Methods	114
4.2.1	Proteomics and Mass spectrometry- First and second round	114
4.2.2	Mass spectrometry and analysis	118
4.2.2.1	Analysis with GPM database	119
4.2.2.2	Analysis with MASCOT database	121
4.2.3	Binding assays of $\alpha 1$ and $\alpha 2$ ECDs	123
4.2.4	Immunohistochemistry	124
4.2.5	Immunocytochemistry	124
4.2.6	Immunoblotting	125
4.2.7	<i>In vitro</i> binding assays	125
4.2.8	Co-immunoprecipitation	126
4.3	Results	130
4.3.1	HSPG Pikachurin was found bound to $\alpha 2$ -ECD-Ni-NTA	132
4.3.1.1	GPM DB analysis	132
4.3.1.2	MASCOT DB analysis	134
4.3.2	Binding assays of $\alpha 1$ or $\alpha 2$ ECDs with Neurexins and Neuroligin 2	136
4.3.2.1	The $\alpha 1$ and $\alpha 2$ ECDs do not bind to Neuroligin 2 but bind specifically to Neurexins	136
4.3.3	Investigating the binding of Pikachurin to the GABA <sub>A</sub> R $\alpha 2$ subunit	138

4.3.3.1	Pikachurin is partially co-localised with the GABA <sub>A</sub> R $\alpha$ 2 subunit in the embryonic cortex.	138
4.3.3.2	Synaptic localisation of pikachurin in cultured neurones .....	140
4.3.3.3	Detection of pikachurin in brain lysates using immunoblotting .....	141
4.3.3.4	In vitro binding of pikachurin to $\alpha$ 1- or $\alpha$ 2-ECD-Ni-NTA columns .....	142
4.3.3.5	Co-immunoprecipitation of pikachurin with the $\alpha$ 2 subunit of GABA <sub>A</sub> Rs .....	144
4.4	Discussion .....	146
	Chapter five.....	151
5.	GABAergic synapse formation: study of embryonic MSNs development.....	152
5.1	Introduction.....	152
5.1.1	Aims .....	154
5.2	Methods .....	155
5.2.1	Primary cultures of MSNs.....	155
5.2.2	Immunocytochemistry .....	155
5.2.3	Confocal analysis .....	155
5.2.4	Analysis of synaptic parameters.....	156
5.2.5	Statistical analysis .....	156
5.3	Results .....	158
5.3.1	A specific decrease in the total density of $\alpha$ 1 single and mixed GABA <sub>A</sub> R clusters is observed from 7 to 14 DIV .....	158
5.3.2	The percentage of synaptic over the total GABA <sub>A</sub> R clusters is modified from 7 to 14 DIV .....	167
5.3.3	The connectivity between MSNs is increased during development of GABAergic synapse.....	171
5.3.4	Developmental changes in the size of GABA <sub>A</sub> R clusters are determined by the type of $\alpha$ subunit incorporated.....	171
5.3.5	The density and size of gephyrin clusters are increased from 7 to 14 DIV .....	176
5.3.6	The density of $\alpha$ 1, $\alpha$ 2 and $\alpha$ 1/ $\alpha$ 2 mixed GABA <sub>A</sub> R clusters co-localising with gephyrin is increased from 7 to 14 DIV.....	181
5.3.7	The proportion of GABA <sub>A</sub> R clusters co-localising with gephyrin as a percentage of the the total GABA <sub>A</sub> R clusters is increased from 7 to 14 DIV.....	184
5.4	Discussion.....	186
	Chapter six.....	191
6.	The regulation of GABAergic synapse formation by GABA signalling .....	192
6.1	Introduction.....	192
6.1.1	Aims .....	195
6.2	Methods .....	195
6.2.1	Primary cultures of medium spiny neurones.....	195
6.2.2	Treatments with bicuculline .....	195
6.2.3	Immunocytochemistry .....	195
6.2.4	Analysis of images using confocal microscopy.....	196
6.2.4.1	Analysis of bicuculline treatment on cell survival .....	196

6.2.4.2	Confocal analysis.....	196
6.2.4.3	Analysis of synaptic parameters .....	197
6.2.5	Statistical analysis.....	197
6.3	Results .....	199
6.3.1	Treatment of MSN cultures with bicuculline from 4-7 DIV .....	199
6.3.1.1	Treatment of medium spiny neurones with 50 $\mu$ M bicuculline from 4 to 7 DIV provoked cell death .....	199
6.3.1.2	The density of GABA <sub>A</sub> Rs per dendrite was not affected after 25 $\mu$ M bicuculline treatment from 4 to 7 DIV.....	203
6.3.1.3	The proportion of synaptic clusters as a percentage of the total clusters was not affected by 25 $\mu$ M bicuculline treatment from 4 to 7 DIV.....	211
6.3.1.4	The connectivity between medium spiny neurones was not changed after treatment with 25 $\mu$ M bicuculline from 4 to 7 DIV .....	214
6.3.1.5	The size of $\alpha$ 2-containing GABA <sub>A</sub> R clusters is decreased after treatment with 25 $\mu$ M bicuculline from 4 to 7 DIV .....	215
6.3.2	Treatment of MSN cultures with bicuculline from 7-14 DIV .....	220
6.3.2.1	Treatment of medium spiny neurones with 50 $\mu$ M bicuculline from 7 to 14 DIV provoked cell death .....	220
6.3.2.2	The density of synaptic $\alpha$ 2 single GABA <sub>A</sub> R clusters per dendrite was increased after 25 $\mu$ M bicuculline treatment from 7 to 14 DIV. ....	224
6.3.2.3	The proportion of synaptic as a percentage of total $\alpha$ 2 single GABA <sub>A</sub> receptor clusters was increased after treatment with 25 $\mu$ M bicuculline from 7 to 14 DIV .....	232
6.3.2.4	The connectivity between medium spiny neurones was not changed after treatment with 25 $\mu$ M bicuculline from 7 to 14 DIV .....	236
6.3.2.5	$\alpha$ subunit-specific effects on cluster size of bicuculline treatment from 7 to 14 DIV	237
6.4	Discussion.....	242
	Chapter seven.....	248
7.	The formation of GABAergic synapses is enhanced in the presence of the exogenous extracellular domains (ECDs) of GABA <sub>A</sub> R $\alpha$ 1 and $\alpha$ 2 subunits .....	249
7.1	Introduction.....	249
7.2	Methods .....	251
7.2.1	Purification of ECDs under sterile conditions.....	251
7.2.2	Deglycosylation of ECDs.....	252
7.2.3	Treatment of MSN cultures with $\alpha$ 1 or $\alpha$ 2 ECDs.....	254
7.2.4	Immunocytochemistry .....	254
7.2.5	Analysis of synaptic parameters.....	255
7.2.6	Statistical analysis.....	256
7.3	Results .....	257
7.3.1	Purification of $\alpha$ 1 and $\alpha$ 2 ECDs under sterile condition .....	258
7.3.2	Deglycosylation of $\alpha$ 1 and $\alpha$ 2 ECDs.....	259
7.3.3	Treatment of 4-7 DIV MSN cultures with purified $\alpha$ 1 or $\alpha$ 2 ECDs.....	261
7.3.3.1	Treatment of MSN cultures with $\alpha$ 1 or $\alpha$ 2 ECDs from 4 to 7 DIV revealed that the exogenous proteins adhere to the neuronal cell surface.....	261

7.3.3.2	The total density of $\gamma 2$ -containing GABA <sub>A</sub> Rs per dendrite of MSNs is increased after the treatment with $\alpha 1$ or $\alpha 2$ ECDs from 4 to 7 DIV .....	266
7.3.3.3	The connectivity between MSNs is increased by the $\alpha 1$ or $\alpha 2$ ECD treatments from 4 to 7 DIV	269
7.3.3.4	The size of $\gamma 2$ -containing GABA <sub>A</sub> Rs is increased after the treatment with $\alpha 1$ or $\alpha 2$ ECDs from 4 to 7 DIV .....	271
7.3.3.5	Analysis of gephyrin clusters in MSN following the treatments with $\alpha 1$ or $\alpha 2$ ECDs from 4 to 7 DIV .....	273
7.3.4	Treatment of 7-14 DIV MSN cultures with purified $\alpha 1$ or $\alpha 2$ ECDs.....	275
7.3.4.1	The treatment of MSN cultures with purified $\alpha 1$ or $\alpha 2$ ECDs from 7 to 14 DIV revealed that the exogenous proteins are adhering to the neuronal cell surface .....	275
7.3.4.2	The total density of $\gamma 2$ -containing GABA <sub>A</sub> Rs per dendrite of MSNs is increased after the treatment with $\alpha 1$ or $\alpha 2$ ECDs from 7 to 14 DIV .....	280
7.3.4.3	The connectivity between MSNs is increased by the $\alpha 2$ ECD treatments from 7 to 14 DIV	283
7.3.4.4	The size of the $\gamma 2$ -containing GABA <sub>A</sub> Rs is increased after the treatment with $\alpha 1$ or $\alpha 2$ ECDs from 7 to 14 DIV .....	285
7.3.4.5	Analysis of gephyrin clusters in MSNs following the treatments with $\alpha 1$ or $\alpha 2$ ECDs from 7 to 14 DIV .....	287
7.4	Discussion.....	289
	Chapter eight.....	293
8.	Discussion .....	294
8.1	The HSPG protein pikachurin binds to the extracellular domain of GABA <sub>A</sub> R $\alpha 2$ subunit	295
8.2	The $\alpha 2$ -containing synapses are favoured compared to $\alpha 1$ -containing synapses during maturation of GABAergic MSNs in vitro .....	297
8.3	Activity-dependent regulation of GABAergic synapse formation .....	298
8.4	The N-terminal extracellular domains of $\alpha 1$ and $\alpha 2$ GABA <sub>A</sub> R subunits have synaptogenic effects .....	300
8.5	Limits of the analysis of GABAergic synapses .....	303
9.	Bibliography.....	307
10.	Appendix .....	322

# Chapter one

## 1. Introduction

The brain functioning relies on a balance between excitation and inhibition (Cline, 2005). This is clear from many studies of diseases such as epilepsy, where a decrease in inhibitory inputs can lead to massive brain oscillatory activity (Ronner et al., 2009), or Parkinson's disease, in which an imbalance between excitation and inhibition within striatal-thalamo-cortical connections leads to motor and cognitive impairments (Linás et al., 1999). An imbalance of excitation and inhibition may also provoke several neurological diseases including autism (Mariner et al., 1986), Tourette's syndrome (Singer and Minzer, 2003) and schizophrenia (Wassef et al., 2003). Inhibitory synapses are neuronal cell junctions specialised to mediate the fast inhibitory transmission in the central nervous system. Despite the crucial role played by inhibitory transmission in the brain, little is known about the early molecular events leading to the development of such synapses.

### 1.1 *The GABAergic Synapse*

In the vast majority of inhibitory synapses, transmission is mediated by the presynaptically-released neurotransmitter  $\gamma$ -aminobutyric acid (GABA), which binds to postsynaptic GABA-gated chloride/bicarbonate channels, also known as GABA<sub>A</sub> receptors (GABA<sub>A</sub>Rs). The main role of GABAergic synaptic transmission is to control neuronal excitability in order to generate oscillations that underlie cognitive processes (Ben-Ari et al., 2007). Via GABA<sub>A</sub>Rs, GABAergic networks affect probably every neuron in the central nervous system and regulate major neuro-developmental processes (Tyagarajan and Fritschy, 2014). The ultrastructure of GABAergic synapses appears symmetric which means that the pre- and postsynaptic elements appear equally dense as opposed to glutamatergic synapses. GABAergic terminals mostly contact the dendritic compartment and the cell soma while the glutamatergic synapses are mostly found on the dendritic spines (Tretter and Moss, 2008).



### 1.1.1 The presynaptic GABAergic nerve terminal

GABA is one of the most abundant inhibitory neurotransmitter in the central nervous system (Mohler et al., 1995), and is the neurotransmitter operating at the GABAergic inhibitory synapses in the brain. These synapses are characterised by presynaptic nerve terminals where GABA is synthesised, and postsynaptic elements expressing receptors for GABA. At the vast majority of synapses, GABA<sub>A</sub> receptors are accumulated or clustered at the postsynaptic membrane, closely apposing the presynaptic nerve terminals (Tretter et al., 2008).

#### 1.1.1.1 *Synthesis of GABA*

GABA is present in concentration of 1-10 mM in the vertebrate brain (Kuriyama et al., 1966). This neutral amino acid is the result of the L-decarboxylation of glutamate (glutamic acid) by the rate-limiting enzyme Glutamate Decarboxylase (GAD) (Collins, 1972, Erlander et al., 1991). In the brain, separate genes encode for two isoforms of GAD, GAD 65 and GAD 67 (Figure 1). These two enzymes differ by their molecular size (65 and 67 kDa), amino-acid sequence, antigenicity, and localisation (Soghomonian and Martin, 1998). GAD65 is located in the nerve ending where it synthesises GABA for vesicular release (which represents about 30 % of total GABA). On the other hand, GAD 67 is in the cytosol and widely expressed along neuronal processes where it synthesises the remaining 70 % of the total GABA (Soghomonian and Martin, 1998). GABA is released from the presynaptic terminal by exocytosis of small synaptic vesicles filled with the neurotransmitter. There is evidence that GAD65 and the vesicular GABA transporter VGAT (=VIAAT, vesicular inhibitory amino acid transporter) interact directly (Figure 1), suggesting that conversion of glutamate into GABA and subsequent vesicular uptake of the transmitter may be tightly coupled processes (Jin et al., 2003).

#### 1.1.1.2 *Vesicular loading of GABA*

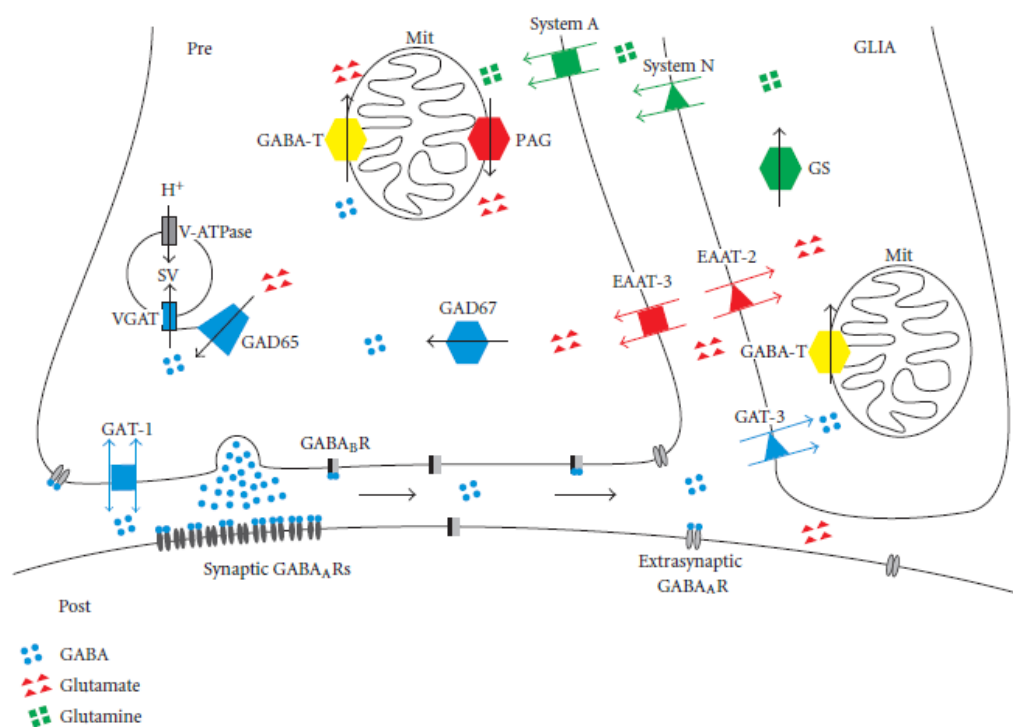
VGAT is a ten-transmembrane helix protein initially identified in *C.Elegans* in 1997 (McIntire et al., 1997). GABA uptake by VGAT into synaptic vesicles depends on a driving force provided by the vacuolar H<sup>+</sup>-ATPase. This pump creates an electrochemical protons gradient that is coupled to transport of neurotransmitter in the opposite direction (Edwards, 2007). Additionally, chloride gradients between vesicle lumen and presynaptic cytosol may contribute to the vesicular loading of GABA (Ahnert-Hilger and Jahn, 2011).

#### 1.1.1.3 *GABA uptake by transporters*

The membrane-bound GABA transporters (GAT) move GABA across the cell membrane from the synaptic cleft back into the presynaptic element (Figure 1). The direction and efficacy of this Na<sup>+</sup>-coupled transport results from the driving electrochemical gradient and is usually directed inwardly (Roth and Draguhn, 2012). GABA transporters are differentially expressed throughout the brain but GAT-1 is the most abundant transporter in the rodent neuronal cells while GAT-3 is mostly present in glial cells (Minelli et al., 1996, Conti et al., 1998b). Another way of GABA enrichment is transmitter synthesis from glutamate. Thanks to EAAT3 which are membrane-bound glutamate transporter molecule found in the presynaptic terminals of inhibitory interneurons, GABA can be synthesised in the presynaptic element after recapture of glutamate (Conti et al., 1998a, Roth and Draguhn, 2012).

#### 1.1.1.4 *Degradation of GABA*

GABA is catalysed by the GABA transaminase (GABA-T) which is present in mitochondria of glial cells and neurones (Jung et al., 1977). After transamination, GABA and  $\alpha$ -ketoglutarate produce succinic semi-aldehyde and glutamate. It is estimated that more than 90 % of all GABA in the mammalian brain is degraded in this way and contributes to energy metabolism in the tricarboxylic acid cycle (Roth and Draguhn, 2012).



**Figure 1: The presynaptic element of GABAergic synapses (Roth and Draguhn, 2012).**

The axonal ending of an inhibitory interneurone (Pre) is drawn on the left, a glial cell (GLIA) on the right. The bottom structure indicates a postsynaptic membrane of a target cell (Post), for example, a pyramidal cell. Transporters are marked by flanking arrows, and synthesising or degrading enzymes are marked by a central arrow. Transporters are colour-matched to substrates: GABA is shown as blue particles, glutamate in red and glutamine in green. Enrichment of glutamate in excitatory neurones involves uptake by glia cells, conversion into glutamine, export via “system N” glutamine transporters followed by uptake into neurones by “system A” glutamine transporters and conversion into glutamate. GS: glutamine synthase, Mit: mitochondrion, PAG: phosphate-activated glutaminase, SV: synaptic vesicle, and V-ATPase: vacuolar type H<sup>+</sup> ATPase, GAD65/7: Glutamate Acid Decarboxylase 65/7, GABA-T: GABA transaminase, GAT-1: GABA transporter 1, V-GAT: Vesicular GABA transporter, EAAT-3: Glutamate transporter 3.

### 1.1.2 The postsynaptic specialisations of GABAergic synapses

The action of GABA is mediated by two different classes of receptors, the metabotropic and ionotropic receptors. The metabotropic GABA<sub>B</sub> receptors are members of the family of G-protein-coupled receptors (GPCRs). They are composed of seven transmembrane domains and are coupled to Ca<sup>2+</sup> and K<sup>+</sup> channels via heterotrimeric G-proteins and second messengers (Bowery et al., 2002). These receptors are found postsynaptically where they modulate specific responses, but also presynaptically where they inhibit neurotransmitter release (Hines et al., 2011).

### 1.1.2.1 *The structure of ionotropic GABA<sub>A</sub>Rs*

GABA<sub>A</sub> and GABA<sub>C</sub> receptors belong to the superfamily of nicotinic heteropentameric 'Cys-loop' ligand gated ion channels which also include the nicotinic acetylcholine, glycine and 5-HT<sub>3</sub> receptors (Lüscher and Keller, 2004). They are both Cl<sup>-</sup>/HCO<sub>3</sub><sup>-</sup> channels but they have different pharmacological properties (Bowery et al., 2002). GABA<sub>C</sub> receptors are only found in neurones of retina and are insensitive to bicuculline and baclofen. In addition, these receptors are composed of hetero- or homo-pentamers of p1-3 subunits (Bowery et al., 2002).

GABA<sub>A</sub> receptors are the major inhibitory receptors in the central nervous system. Deficits in GABA<sub>A</sub>R-mediated neurotransmission are at the origin of multiple disorders of the central nervous system such as epilepsy, anxiety and mood disorders, and neurodevelopmental pathologies such as autism, Fragile X, and schizophrenia (Ortells and Lunt, 1995). They were first identified accordingly to their pharmacological properties (Olsen and Sieghart, 2008). These receptors are activated by GABA and by selective agonists such as muscimol and isoguvacine, and blocked by bicuculline, picrotoxin, and others. They are also modulated by benzodiazepines, barbiturates, ethanol, neurosteroids and others (Macdonald and Olsen, 1994).

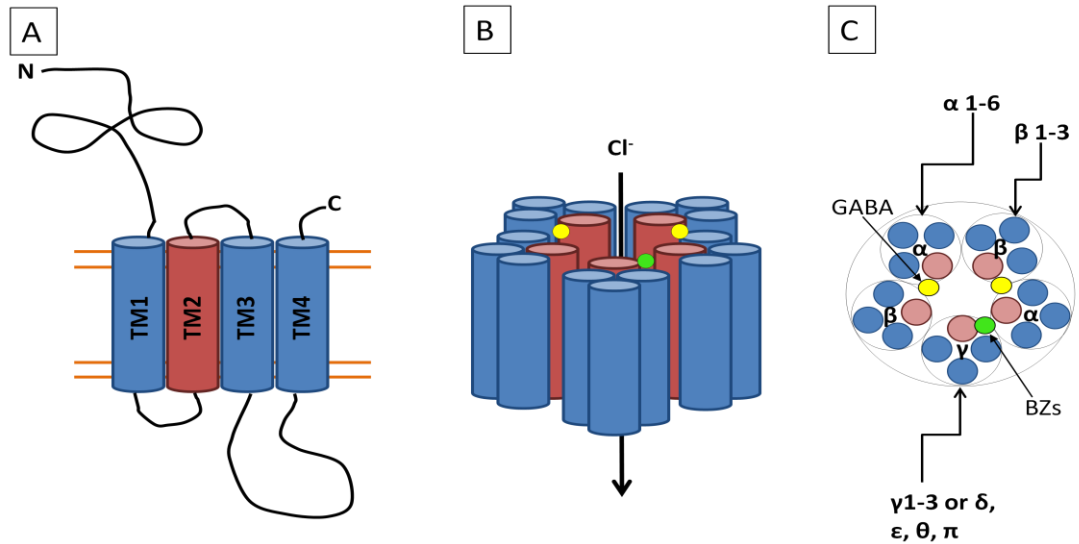
Sixteen subunits of GABA<sub>A</sub>Rs are encoded by different genes grouped in seven different classes ( $\alpha_{1-6}$ ,  $\beta_{1-3}$ ,  $\gamma_{1-3}$ ,  $\delta$ ,  $\pi$ ,  $\epsilon$ , and  $\theta$ ). The structure of the receptor subunits is highly conserved (Unwin, 1993). They all consist of a large (about 200 amino acids) extracellular N-terminal hydrophilic domain, followed by four transmembrane hydrophobic domains (TMs) with a large cytoplasmic-loop between TM3 and TM4, and a small extracellular C-terminal domain (Figure 2) (Sieghart et al., 1999). GABA<sub>A</sub> receptors are organised as pentamers of subunits surrounding a central pore that forms an ion channel (Figure 2). The first crystal structure of a GABA<sub>A</sub>R, the human  $\beta 3$  homopentamer, has revealed architectural elements unique to eukaryotic Cys-loop receptors and explained the mechanistic consequences of multiple disease mutations (Miller and Aricescu, 2014). Interestingly, the receptor has been co-crystallised with a

novel agonist, benzamidine (serine-protease inhibitor) which is capable of inducing desensitisation.

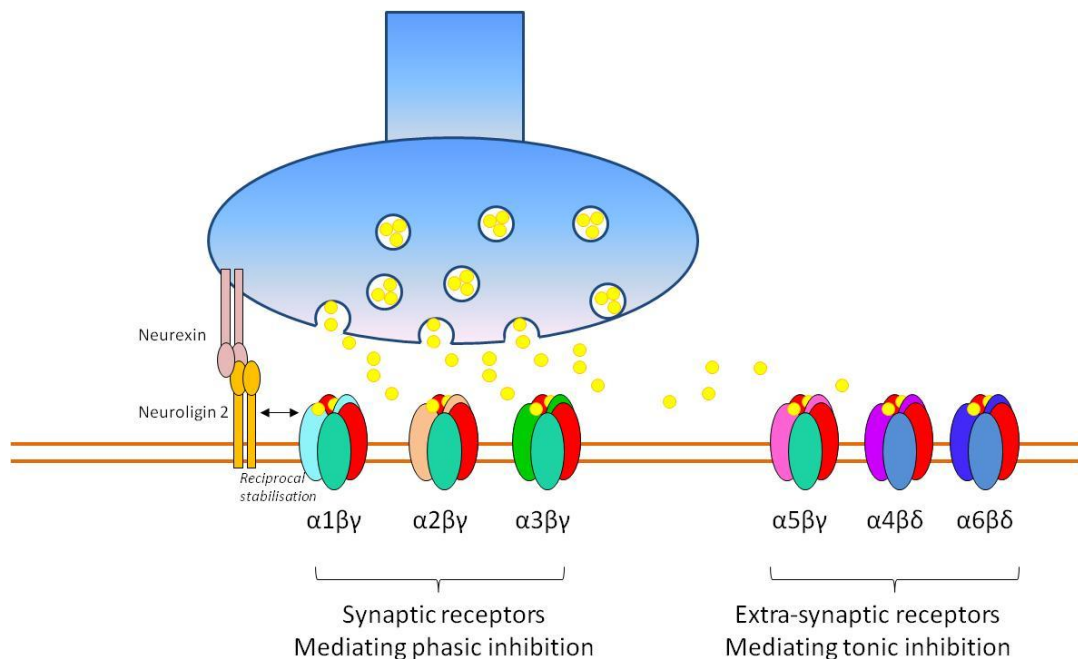
Although the stoichiometry of native receptors has not been fully described, the assembly of heteropentameric GABA<sub>A</sub>Rs in heterologous model systems has been shown to occur with a stoichiometry of 2 $\alpha$ :2 $\beta$ :1 $\gamma$  subunits (Tretter et al., 1997, Farrar et al., 1999) (Figure 2). The major benzodiazepine binding site is at the  $\alpha/\gamma$  subunits interface while the two GABA binding sites lie between  $\alpha/\beta$  subunits (Olsen and Sieghart, 2008) (Figure 3).

Many different combinations of subunits are theoretically possible. Nevertheless, due to restrictions imposed during the assembly of GABA<sub>A</sub>Rs, only a dozen are able to access the neuronal cell surface (Jacob et al., 2008, Olsen and Sieghart, 2008). The  $\alpha$ ,  $\beta$  and  $\gamma$  subunits have to be combined to form a functional synaptic GABA<sub>A</sub>R. The  $\pi$ ,  $\delta$  and  $\epsilon$  subunits seem to replace the  $\gamma$  subunit in some cases (Sieghart et al., 1999). The  $\delta$  subunit is almost exclusively present in  $\alpha 6$  subunit-containing GABA<sub>A</sub>Rs in cerebellar granule cells. This subunit is also combined with  $\alpha 4$  subunit in dentate gyrus, neostriatum and some cortical layers (Olsen and Sieghart, 2008). The  $\epsilon$  subunit is rare but can replace  $\gamma$  or  $\delta$  in certain brain areas such as hypothalamus.

GABA<sub>A</sub>Rs composed of  $\alpha 1$ ,  $\alpha 2$ ,  $\alpha 3$  or  $\alpha 5$  subunit together with  $\beta$  and  $\gamma$  subunits are largely synaptically expressed and mediate phasic inhibition in the brain (Saliba et al., 2007, Jacob et al., 2008). On the other hand,  $\alpha 4$  or  $\alpha 6$  subunit combined with  $\beta$  and  $\delta$  subunit GABA<sub>A</sub>Rs are predominantly extrasynaptic receptors and mediate tonic currents in response to GABA spill-over from synaptic release sites (Jacob et al., 2008) (Figure 3).



**Figure 2: Structure of GABA<sub>A</sub>Rs.** **A.** GABA<sub>A</sub>Rs consist of a large extracellular N-terminal domain, four hydrophobic transmembrane domains (TM1-TM4), a large intracellular loop between TM3-TM4 and a small extracellular C-terminal domain. **B.** GABA<sub>A</sub>Rs assemble into heteropentameric  $\text{Cl}^-$  permeable channels composed of two  $\alpha$ , two  $\beta$  and one  $\gamma$  subunit. The binding of two molecules of GABA (yellow) or Benzodiazepines (green) triggers the entry of chloride in to the postsynaptic cell. **C.** Sixteen genes encode for the different subunits ( $\alpha$ 1-6;  $\beta$ 1-3;  $\gamma$ 1-3;  $\delta$ ,  $\pi$ ,  $\epsilon$ , and  $\theta$ ). Benzodiazepine (green) binding site is at the interface between  $\alpha$  and  $\gamma$  subunits, whereas GABA (yellow) binding site is between  $\alpha$  and  $\beta$  subunits.



**Figure 3: Localisation of GABA<sub>A</sub>Rs.** The  $\alpha$ 1-3 together with  $\beta$  and  $\gamma$  subunit containing GABA<sub>A</sub>Rs are localised to synaptic sites and are responsible for phasic inhibition, whereas  $\alpha$ 4 or  $\alpha$ 6 and  $\delta$  subunit-containing GABA<sub>A</sub>Rs are mainly extrasynaptic and mediate tonic inhibition resulting from ambient GABA. The  $\alpha$ 5 subunit-containing GABA<sub>A</sub>Rs are localised to both synaptic and extrasynaptic sites. Neurexin and Neuroligin 2 are adhesion molecules exhibiting robust synaptogenic effects. Neurexin 2 $\beta$  has been shown to interact with the  $\alpha$ 1 subunit of GABA<sub>A</sub>Rs.

### 1.1.2.2 Clustering of GABA<sub>A</sub>Rs

At inhibitory synapses, the postsynaptic density (PSD) is precisely facing the presynaptic active zone and contains a high concentration of GABA<sub>A</sub>Rs. Sophisticated mechanisms enable the assembly of macromolecular complexes and the selective clustering of the GABA<sub>A</sub>Rs at the appropriate subcellular sites. Although different clustering mechanisms exist, the predominant scaffolding protein which clusters GABA<sub>A</sub>Rs at the postsynaptic membrane is gephyrin (Tyagarajan and Fritschy, 2014).

#### 1.1.2.2.1 Synaptic clustering of GABA<sub>A</sub>Rs

##### 1.1.2.2.1.1 Gephyrin-dependent clustering and collybistin

Gephyrin was originally co-purified with the glycine receptor from the mammalian brain (Prior et al., 1992). This 93 kDa protein regulates the clustering of these receptors by cross-linking their  $\beta$  subunit to tubulin and microtubules (Kneussel and Betz, 2000).

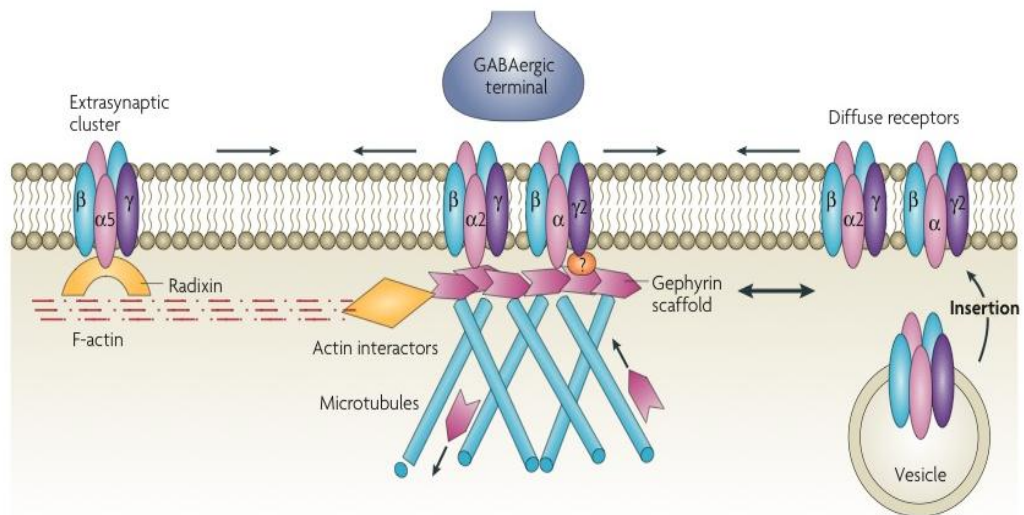
Immunocytochemical studies have revealed that gephyrin is present at GABAergic synapses (Kneussel and Betz, 2000). In the brain, it is enriched at postsynaptic sites which contain GABA<sub>A</sub>Rs subtypes composed of  $\alpha(1-3)$ ,  $\beta(2-3)$  and  $\gamma 2$  subunits (Jacob et al., 2008). It has been shown that gephyrin binds directly to GABA<sub>A</sub>Rs via the intracellular loop of the  $\alpha 1-3$  GABA<sub>A</sub>Rs subunits (Tretter et al., 2008, Mukherjee et al., 2011, Tretter et al., 2011). Therefore, gephyrin is responsible for clustering of GABA<sub>A</sub>Rs at the postsynaptic membrane of GABAergic synapses. Reducing gephyrin expression affects accumulation of  $\alpha 2$ - or  $\gamma 2$ -containing GABA<sub>A</sub>Rs without modifying the overall cell surface levels of these subunits (Kneussel et al., 1999, Jacob et al., 2005). Live imaging has revealed that clusters that formed in the absence of gephyrin were significantly more mobile compared to the control neurones (Jacob et al., 2005).

The interaction of gephyrin with GABA<sub>A</sub>Rs is not only via a direct binding. Gephyrin also interacts with collybistin, a guanylate exchange factor (GEF) (Kins et al., 2000, Harvey et al., 2004). A knock-out of collybistin results in a selective loss of synaptic GABA<sub>A</sub>Rs clusters, increased levels of anxiety and impaired spatial learning memory (Papadopoulos et al., 2007, Thomson and Jovanovic, 2010). All together, these data suggest that gephyrin and its binding partners promote clustering of synaptic GABA<sub>A</sub>Rs (Figure 4).

#### 1.1.2.2.1.2 Gephyrin-independent clustering

In gephyrin knock-out mice, synaptic GABA<sub>A</sub>Rs clusters are formed at the cell surface and mIPSC are detected, suggesting that these receptors are able to form functional clusters in the absence of gephyrin (Kneussel and Betz, 2000, Lévi et al., 2004). Although the mechanisms involved are not fully characterised, it is likely that they involve other GABA<sub>A</sub>R interacting proteins. One such protein is radixin, an ERM (ezrin, radixin, moesin)-family protein which has been identified as a specific interactor of the  $\alpha 5$  subunit of GABA<sub>A</sub>Rs (Loebrich et al., 2006). In neurones, depletion of radixin significantly decreases  $\alpha 5$ -containing GABA<sub>A</sub>Rs clusters while the total levels of  $\alpha 5$  subunit remained unchanged (Loebrich et al., 2006). Activated radixin is able to bind  $\alpha 5$  subunit and F-actin, which suggests that radixin directly links  $\alpha 5$  subunit and actin cytoskeleton (Figure 4). Radixin binding domain is highly conserved between  $\alpha 5$  and  $\alpha 1-3$  subunits suggesting that radixin plays an important role in clustering of other types of GABA<sub>A</sub>Rs.





**Figure 4: Cell surface trafficking and clustering of GABA<sub>A</sub>Rs.** (Jacob et al., 2008) Newly assembled GABA<sub>A</sub>Rs are primarily inserted into the plasma membrane outside of synapses. Synaptic receptors are recruited from extrasynaptic pools by lateral diffusion mediated by unknown mechanisms. Synaptic GABA<sub>A</sub>Rs are maintained and stabilised by gephyrin clusters, which mediate association between the receptors and the microtubules. An alternative mechanism for GABA<sub>A</sub>Rs clustering is mediated by radixin which interact with the  $\alpha 5$  subunit and F-actin.

#### 1.1.2.2.2 Extrasynaptic clustering of GABA<sub>A</sub>Rs

In neuronal cells, GABA<sub>A</sub>Rs are expressed as synaptic and extrasynaptic receptors. Most receptors are distributed first to the extrasynaptic sites. Depending on their subunit composition, some subtypes of GABA<sub>A</sub>Rs will remain extrasynaptic while others will become predominantly synaptic overtime (Bogdanov et al., 2006). For example, the  $\alpha 5\beta 2$  receptors, found in hippocampal pyramidal cells, are mostly extrasynaptic and contribute to tonic GABAergic currents, although some  $\alpha 5\beta 2$  have also been found in synapses (Luscher et al., 2011). In addition,  $\alpha 6\beta \delta$  are diffused and exclusively located at extrasynaptic and perisynaptic sites of cerebellar granule cells. Similarly to some of  $\alpha 5$  subunit-containing receptors,  $\delta$ -containing GABA<sub>A</sub>Rs also mediate tonic inhibition in the brain (Jacob et al., 2008). The same situation was observed in dentate gyrus where  $\alpha 4\beta \delta$  are mainly extrasynaptic and mediate tonic inhibition (Fritschy and Brünig, 2003). In general,  $\alpha$  subunits contained in extrasynaptic receptors have a higher affinity for GABA than those present in synaptic GABA<sub>A</sub>Rs (Saxena and Macdonald, 1994).

In contrast, most of the  $\gamma 2$  subunit-containing GABA<sub>A</sub>Rs are synaptic (Danglot et al., 2003, Thomas et al., 2005). Mice deficient for  $\gamma 2$  subunit show a significant decrease in the level of synaptic GABA<sub>A</sub> receptor clusters, while the extrasynaptic receptors are only slightly affected (Crestani et al., 1999, Schweizer et al., 2003).

Over the recent years, it has become clear that cell surface expressed GABA<sub>A</sub>Rs are relatively dynamic entities because a significant number of receptors can move within the plasma membrane in and out of the synaptic compartments (Figure 3b) (Thomas et al., 2005). Using a fluorescent bungarotoxin and electrophysiological recordings, it has been shown that synaptic GABA<sub>A</sub>Rs are recruited from the extrasynaptic sites (Bogdanov et al., 2006). Single particle tracking of  $\gamma 2$  subunit revealed that at mixed GABAergic/Glycinergic synapses of motor neurones in culture, GABA<sub>A</sub>Rs can be rapidly exchanged between synaptic and extrasynaptic compartments (Lévi et al., 2008).

In addition, fluorescent recovery after photobleaching studies (FRAP) have shown that extrasynaptic GABA<sub>A</sub>Rs have a higher degree of lateral mobility than synaptic receptors (Jacob et al., 2008). The retention of GABA<sub>A</sub>Rs at synaptic sites results from their association with gephyrin clusters. Down regulation of gephyrin results in increased lateral mobility of GABA<sub>A</sub>Rs, facilitating their accumulation at extrasynaptic sites (Jacob et al., 2005). Dynamic regulation of interactions between GABA<sub>A</sub>Rs and scaffold proteins such as gephyrin, is likely to play a central role in regulating the number of postsynaptic receptors (Arancibia-Carcamo and Kittler, 2009).

### 1.1.2.3 *The functional and pharmacological heterogeneity of GABA<sub>A</sub>R subtypes*

#### 1.1.2.3.1 The subunit composition of GABA<sub>A</sub>R influences GABAergic synaptic pharmacology

Structural heterogeneity of GABA<sub>A</sub>Rs is thought to be the basis of their physiological and pharmacological heterogeneity (Olsen and Sieghart, 2009).

GABA<sub>A</sub>Rs contain binding sites for clinically important drugs such as benzodiazepines, barbiturates and anaesthetics (Homanics et al., 1997).

Benzodiazepines are muscle relaxants, anticonvulsants, sedative and anxiolytic drugs (Macdonald and Olsen 1994). They are positive allosteric modulators of GABA<sub>A</sub>Rs which increase the chloride channel opening frequency (Macdonald and Olsen, 1994) and the affinity for GABA. The benzodiazepine binding site is located in a pocket between the  $\alpha$  and  $\gamma$  subunits (Ernst et al., 2003, Henschel O, 2008) (Figure 2). Pharmacological studies have determined that  $\alpha$ 1-,  $\alpha$ 2-,  $\alpha$ 3- and  $\alpha$ 5- subunit containing GABA<sub>A</sub>Rs are 'benzodiazepine-sensitive', while  $\alpha$ 4- and  $\alpha$ 6-GABA<sub>A</sub>Rs are not and are therefore classified as 'benzodiazepine-insensitive' (Benson et al., 1998, Wingrove et al., 2002).

The presence of one histidine residue (H101) in the  $\alpha$ 1 subunit of GABA<sub>A</sub>Rs forms a high affinity binding site for diazepam or nonbenzodiazepines such as zolpidem (Olsen and Sieghart, 2009) which is classified as benzodiazepine site 1 (BZI). Other subclasses of  $\alpha$  subunits-containing GABA<sub>A</sub>Rs ( $\alpha$ 2-5), with lower affinity for diazepam and zolpidem contain a lower affinity binding site which is classified as benzodiazepine site 2 (BZ II).

By introducing a point mutation in histidine 100 (histidine to arginine substitution) in individual  $\alpha$  subunits in transgenic mice, Rudolph et al., 1999 have demonstrated that  $\alpha$ 2- GABA<sub>A</sub>Rs mediate the anxiolytic effects of diazepam, while  $\alpha$ 1-subtypes mediate the sedative effect of the drug (Benson et al., 1998, Löw et al., 2000, McKernan et al., 2000, Olsen and Sieghart, 2009). Thus, in mice expressing the mutated  $\alpha$ 1 subunit, sedative effects of diazepam were abolished but the anxiolytic effects were still present (Benson et al., 1998, Rudolph et al., 2001). Likewise, the anxiolytic effects of  $\alpha$ 2 were abolished in  $\alpha$ 2 mutant mice, although the sedative effects mediated by  $\alpha$ 1 subunit containing GABA<sub>A</sub>Rs were still present (Rudolph et al., 1999, McKernan et al., 2000). Consequently,  $\alpha$ 1-GABA<sub>A</sub> receptors are thought to be operating in neuronal circuits that

are functionally distinct from those involved in other behavioural responses to benzodiazepines (Fritschy and Brünig, 2003). Functional specificity of neuronal circuits expressing different types of  $\alpha$  subunits was further supported by studies of  $\alpha 5$  subunit knock-out mice which have demonstrated that these mice show enhanced cognitive performance in hippocampal-dependent learning tasks (Collinson et al., 2002, Ali and Thomson, 2008, Thomson and Jovanovic, 2010).

#### 1.1.2.3.2 The kinetic properties of $\alpha 1$ - vs. $\alpha 2$ -containing GABA<sub>A</sub>Rs correspond to the physiological properties of the synapses

The structural basis for the functional diversity may be explained by selective targeting of GABA<sub>A</sub> receptors to synapses formed with different types of presynaptic inhibitory interneurons. For example, more than 18 types of presynaptic GABAergic neurones innervate hippocampal CA1 pyramidal cells which express about 14 different subtypes of GABA<sub>A</sub>Rs. Using quantitative electron microscopy and electrophysiology, it has been determined that  $\alpha 1$ -GABA<sub>A</sub>Rs are significantly more abundant in synapses formed with fast-spiking parvalbumin (PV) basket cells, while the  $\alpha 2$ -GABA<sub>A</sub>Rs are more often found contacted by regular spiking cholecystokinin (CCK) basket cells (Thomson et al., 2000, Nyíri et al., 2001, Klausberger et al., 2002, Fritschy and Brünig, 2003). However, these findings are controversial. Using the freeze fracture immunogold labelling (FRIL) method, which is a lot more sensitive than standard immunogold labelling, both  $\alpha 1$ - and  $\alpha 2$ -containing GABA<sub>A</sub>Rs were found present in all the somatic synapses of the CA1 hippocampal neurones (Kasugai et al., 2010). This has suggested that there was no specificity between the  $\alpha$  subtype of GABA<sub>A</sub>R expressed in the postsynaptic membrane and the identity of the presynaptic basket cell (Kasugai et al., 2010).

However, in other types of synapses, a specificity of association between presynaptic inhibitory interneurons with different firing patterns and postsynaptic GABA<sub>A</sub>Rs subtypes is observed. Interestingly, this association is also in agreement

with the kinetic properties of responses mediated by different  $\alpha$  subunits. For example, it has been observed that  $\alpha 2$ -containing GABA<sub>A</sub>Rs are predominantly expressed at the axon initial segment (AIS) compared to  $\alpha 1$ -containing GABA<sub>A</sub>Rs (Panzanelli et al., 2011). Interestingly, the  $\alpha 1$ -GABA<sub>A</sub>Rs are characterised by five-fold faster kinetics of deactivation than the  $\alpha 2$ -GABA<sub>A</sub> receptors (Brussaard et al., 1997, McClellan and Twyman, 1999, Vicini et al., 2001). Thus,  $\alpha 1$ -GABA<sub>A</sub>Rs subtypes are more likely to carry high-frequency signals whereas  $\alpha 2$ -GABA<sub>A</sub>Rs might be more efficient as an on/off switch of neuronal activity, especially at the axon initial segment where they are highly concentrated (Fritschy and Brünig, 2003). The fact that a high concentration of  $\alpha 2$ -containing GABA<sub>A</sub>Rs is present at the AIS is more likely to be related to specific clustering mechanisms present in the AIS only rather than the presence of a specific presynaptic input (Panzanelli et al., 2011). If GABA<sub>A</sub>Rs subtypes were randomly distributed over the neuronal compartments, specific behavioural and cognitive functions mediated by GABAergic synapses would not be possible (Thomson and Jovanovic, 2010). It remains to be determined if the presence of different  $\alpha$  subunits is sufficient to regulate distribution of GABA<sub>A</sub>Rs over different neuronal compartments.

#### 1.1.2.3.3 Analysis of sequence similarity between $\alpha 1$ and $\alpha 2$ subunit of GABA<sub>A</sub>Rs

Pairwise sequence alignment (Needle EMBOSS program) was done with the full sequence of  $\alpha 1$  and  $\alpha 2$  subunits of GABA<sub>A</sub>Rs (Figure 5). The GABA binding site sequence is highly conserved between the two subunits although one serine in the  $\alpha 1$  sequence is replaced by a lysine in the  $\alpha 2$  sequence. This difference could be at the origin of a difference in the affinity for GABA between the two subunits. Although the two subunits share 79.5 % of identity and 86.5 % of similarity, different regions could be at the origin of the specificity observed between  $\alpha 1$  and  $\alpha 2$  subunits-containing synapses. Notably, while the four transmembrane domains are very similar, the extracellular domains (N- and C-terminal) as well as the intracellular loop seem to be



### 1.1.3 Synaptic cleft spanning proteins

Neurons receive multiple inputs from different neurotransmitter systems. An appropriate match between the released neurotransmitter and its corresponding postsynaptic receptors is essential for synapse formation and function (Fritschy and Brünig, 2003). For normal functioning of GABAergic synapses, it is essential to have GABA<sub>A</sub>Rs present at the postsynaptic membrane. The efficacy of transmission is further increased by clustering of GABA<sub>A</sub>Rs at these postsynaptic sites. However, how is this regulated during synapse formation and whether the activation of GABA<sub>A</sub>Rs plays a role in these processes remains unclear.

Some evidence suggests that activation of GABA<sub>A</sub>Rs by released GABA may not be at the origin of clustering of these receptors (Benson et al., 1998, Varoqueaux F, 2002). Hippocampal neurons were cultured in isolation at a density which allowed formation of auto-synapses (Rao et al., 2000). Distribution of the pre and postsynaptic markers of GABAergic and glutamatergic synapses has been correlated with the neurotransmitter phenotype of the neurone. Under such conditions, 60 % of synaptic appositions were mismatched incorporating glutamatergic presynaptic elements and GABA<sub>A</sub> postsynaptic clusters. Moreover, 57 % of clusters were not opposed to any presynaptic element. According to this paper, GABAergic input is not necessary for clustering of GABA<sub>A</sub> receptors, but it may be a synaptogenic signal common to glutamatergic and GABAergic synapses (Rao et al., 2000). However, in neurons receiving extensive GABAergic innervation only, no mismatch was observed, suggesting that GABAergic synapse formation may be dependent on specific pre- and postsynaptic interactions rather than the activity of GABA<sub>A</sub>Rs. Nevertheless, chronic blockade of action potential-mediated synaptic events with tetrodotoxin (TTX) or of GABA<sub>A</sub> receptors with bicuculline did not affect GABA<sub>A</sub>R clustering (Craig et al., 1996).

Taken together, these data suggest that GABA is not required for differentiation and clustering of postsynaptic GABA<sub>A</sub>Rs. If GABA is not crucial for formation of GABAergic synapses, other components of these synapses may play an important

role. Several proteins present pre or postsynaptically that span all or part of the synaptic cleft have been identified and studied for their role in GABAergic synapse formation and maintenance.

#### 1.1.3.1 *Neurexins/ Neuroligin*

Interactions between the presynaptic neurexins and postsynaptic neuroligins are known to regulate synapse formation. Neurexin ( $\alpha$ 1-3,  $\beta$ 1-3) are presynaptic adhesion proteins that exhibit robust synaptogenic activity and are essential for the binding of proteins involved in neurotransmitter release (Fairless et al., 2008). All three  $\alpha$ -neurexins are composed of six LNS (Laminin Neurexin Sex hormone) binding domains which are principal sites for alternative splicing leading to more than 2000 potential variants (Missler and Südhof, 1998, Fairless et al., 2008, Thomson and Jovanovic, 2010). In addition, presynaptic  $\alpha$ -neurexins promote clustering of postsynaptic GABA<sub>A</sub>Rs associated with gephyrin (GABA<sub>A</sub>Rs scaffolding protein) and neuroligin-2 (Kang et al., 2008) (Figure 2). Triple knock-out mice lacking all three  $\alpha$ -neurexins show 50 % reduction in GABAergic synapses in comparison with wild-type mice, and die at birth (Missler et al., 2003). The interaction between neurexins and neuroligins is thought to be sufficient to induce postsynaptic differentiation of both glutamatergic and GABAergic synapses (Graf et al., 2004). In addition, it has been shown that neurexin 2 $\beta$  directly interacts with the extracellular domain of  $\alpha$ 1 subunit of GABA<sub>A</sub>Rs, and that increasing neurexin expression decreased GABAergic but not glutamatergic synaptic transmission (Zhang et al., 2010).

Neuroligins (NL1-4) are postsynaptic interactors of neurexins and they contain only one LNS domain (Kang et al., 2008). Although neuroligins exhibit less extensive alternative splicing of their LNS domain, their distribution across different types of synapses is specific. It has been demonstrated that NL2 is specifically present and involved in GABAergic synapse formation (Varoqueaux et al., 2004), while NL1



promotes glutamatergic synapse formation. On the contrary, NL3 aggregates at both types of synapses forming complexes with other neuroligins (Budreck and Scheiffele, 2007). In a model proposed by Huang and Scheiffele (Huang and Scheiffele, 2008), NL2 and GABA<sub>A</sub>Rs stabilize each other, through extracellular cis-interactions or via scaffolding proteins such as gephyrin (Figure 2). In addition, in neuronal cultures, the over-expression of NL2 increases specifically the amplitude of inhibitory postsynaptic currents (IPSCs), while a pharmacological blockade of neuronal activity prevents this synaptogenic effect (Chubykin et al., 2007, Huang and Scheiffele, 2008). This result suggests that NL2 promotes a postsynaptic synaptogenic effects and that this partially depends on GABA<sub>A</sub>R activity.

Multiple evidence converges to suggest that synaptic signalling mediated by GABA may engage the neuroligin-neurexin cell adhesion system to regulate activity-dependent development of inhibitory synapses and innervation patterns (Huang and Scheiffele, 2008).

Taken together, these data suggest that neurexin/neuroligin complex and GABA signalling play important roles in inhibitory synapse development, stabilising both pre- and postsynaptic elements.

#### 1.1.3.2 *NCAM*

Other cell adhesion molecules present in the synaptic cleft could also play a role in synapse formation, such as NCAM (neuronal cell adhesion molecule) which is enriched at GABAergic synapses (Pillai-Nair et al., 2005). In this study, the role of the extracellular domain of NCAM was explored with the use of a transgenic mouse line which over-expressed a soluble form of the extracellular domain of this protein. These mice exhibited a striking decrease in synaptic innervation arising from a subpopulation of GABAergic interneurons in frontal cortical areas and in amygdala. Thus, the overexpression of the extracellular domain of NCAM seems to perturb the cortical and amygdala circuitry by interfering with presynaptic function of GABAergic interneurons.

### 1.1.3.3 *Dystrophin/glycoprotein complex (DGC)*

Another multiprotein complex co-localised with GABA<sub>A</sub>Rs at GABAergic synapses is the dystrophin/glycoprotein complex (DGC). Immunohistochemical and functional studies have demonstrated that DGC also plays an important role in inhibitory synapse formation (Knuesel et al., 1999, Knuesel et al., 2000, Brünig et al., 2002, Lévi et al., 2002). DGC is a large multiprotein complex containing at least ten proteins such as dystrophin and dystroglycan (Blake et al., 2002, Arancibia-Carcamo and Kittler, 2009). Dystrophin has been found in  $\alpha$ 1 and  $\alpha$ 2 subunit-containing GABA<sub>A</sub>R synapses in the cerebral cortex, hippocampus and cerebellum (Knuesel et al., 2000). The size and number of cell surface GABA<sub>A</sub>Rs clusters were decreased significantly in dystrophin mutant mice (Knuesel et al., 1999). As a consequence, the frequency and amplitude of miniature inhibitory post synaptic currents (mIPSC) in Purkinje cells were significantly lower than in wild-type mice (Kueh et al., 2008). This result suggests that DGC may play an important role in stabilising GABA<sub>A</sub>Rs at synapses (Knuesel et al., 2000). Other components of DGC are selectively present at inhibitory synapses such as  $\alpha$ - and  $\beta$ -dystroglycan and syntrophin (Lévi et al., 2002). The  $\beta$ -dystroglycan indirectly binds neuroligin-2 via S-SCAM (Synaptic scaffolding molecule) and form a tri-partite complex of S-SCAM,  $\beta$ -dystroglycan and neuroligin-2 that may function as a postsynaptic link at inhibitory synapses between the DGC/ neurexin complex and the neuroligin/ neurexin complex (Sumita et al., 2007, Arancibia-Carcamo and Kittler, 2009). However, the role of this complex in cell surface expression and synaptic localisation of GABA<sub>A</sub>Rs remains unclear.

### 1.1.3.4 *Slitrack3 and PTP $\delta$*

It has been recently suggested that Slit and NRT-like family member 3 (Slitrk3) act as postsynaptic adhesion molecules which selectively interact with the presynaptic tyrosine phosphatase receptor PTP $\delta$  (Takahashi et al., 2012). This transsynaptic interaction was shown to promote only inhibitory synaptic formation in co-cultures of

fibroblasts expressing *slitrk3* and rat hippocampal neurones. In addition, *slitrk3*-deficient mice exhibited a decrease in inhibitory synapse number and function in hippocampal CA1 neurones as well as increased seizure susceptibility and spontaneous epileptiform activity. However, GABAergic synapses were still able to form, suggesting that this mechanism is not required to prime the formation of inhibitory synapses.

#### *1.1.3.5 Postsynaptic GABA<sub>A</sub>Rs*

Interestingly, it has been recently proposed that GABA<sub>A</sub>Rs themselves can promote GABAergic synapse formation in a co-culture model of  $\alpha 1/\beta 2/\gamma 2$  stably transfected HEK 293 cells and GABAergic embryonic medium spiny neurones (Fuchs et al., 2013). This study provided the first evidence that GABA<sub>A</sub>Rs can be sufficient to initiate the formation of synaptic contacts. A significant increase in synapse formation and strength was observed when NL2 was co-expressed with GABA<sub>A</sub>Rs in the HEK 293 cells, suggesting a synergetic effect of the two postsynaptic proteins.

### **1.2 Intracellular trafficking of GABA<sub>A</sub>Rs**

#### **1.2.1 Synthesis and intracellular trafficking of GABA<sub>A</sub>Rs**

GABA<sub>A</sub>Rs subunits are assembled within the endoplasmic reticulum (ER). This process has a critical role in determining the heterogeneity of GABA<sub>A</sub>Rs expression at the cell surface (Jacob et al., 2008). Only those receptors which have been assembled in the appropriate conformation are able to exit the ER. Misfolded proteins or unassembled subunits are retained within the organelle and sent to the proteasome for degradation.

##### *1.2.1.1 Assembly of postsynaptic GABA<sub>A</sub>Rs*

Assembly of GABA<sub>A</sub>Rs into pentamers involves the initial formation of  $\alpha\beta$  subunit heterodimers. The N-terminal domains of these subunits associate with two chaperone proteins involved in the folding control quality in the ER: binding

immunoglobulin protein (BiP) and calnexin (Connolly et al., 1996a, Kleizen and Braakman, 2004, Luscher et al., 2011). These two chaperones are the most abundant in the ER and play a critical role in folding of every newly translated protein. They are both located on the luminal side of the ER allowing a direct binding to the N-terminal domains of nascent subunits (Arancibia-Carcamo and Kittler, 2009, Luscher et al., 2011) (Figure 6).

The first insights into the assembly mechanisms of GABA<sub>A</sub>Rs originate from studies using the heterologous HEK 293 cells systems. To determine the stoichiometry and subunit arrangement of GABA<sub>A</sub>Rs, the ratio of subunits in recombinant  $\alpha 1\beta 3\gamma 2$  receptors was determined by immunoblotting from the relative signal intensities of antibodies directed against the N-terminal or the cytoplasmic loop (Tretter et al., 1997). This method allowed determination of the subunit stoichiometry of two  $\alpha$  subunits, two  $\beta$  subunits, and one  $\gamma$  subunit in fully assembled GABA<sub>A</sub> receptors. Similar experiments showed that while  $\alpha 1\beta 3$  and  $\alpha 1\beta 3\gamma 2$  receptors expressed in HEK 293 were able to form pentamers,  $\alpha 1\gamma 2$  or  $\beta 3\gamma 2$  receptors mostly form heterodimers (Tretter et al., 1997). In addition, the residues 58-67 within  $\alpha$  subunit isoforms were shown to be important in the assembly of receptors containing  $\alpha\beta$  and  $\alpha\beta\gamma$  subunits. Deletions of these residues, which are highly conserved in all  $\alpha$  subunit isoforms, resulted in the retention of  $\alpha$  subunits in the endoplasmic reticulum. These residues present on the N-terminal extracellular domain mediate oligomerisation of the  $\alpha 1$  subunit with  $\beta 3$  and thus, play a critical role in the assembly of GABA<sub>A</sub>Rs (Taylor et al., 2000).

The fundamental role of the  $\alpha$  and  $\beta$  subunits in the first assembly steps has been confirmed by the knockout mice studies. Deletion of these subunits resulted in a considerable loss of postsynaptic GABA<sub>A</sub>R (Homanics et al., 1997, Kralic et al., 2002, Luscher et al., 2011). In contrast, the  $\gamma 2$  subunit is not necessary for the assembly and export to the cell surface of GABA<sub>A</sub>Rs but is essential to confer a functional BZ sensitivity (Taylor et al., 2000). Following disruption of the  $\gamma 2$  subunit gene, 94 % of the BZ sites were absent in brains of neonatal mice. However the level of expression and

localisation of GABA<sub>A</sub>R subunit was not altered when  $\gamma 2$  gene expression was disrupted, showing a loss of only 22 % of GABA binding sites, and is therefore dispensable for assembly of  $\alpha$  and  $\beta$  subunits (Günther et al., 1995).

GABA<sub>A</sub>R subunits deficient mice have provided clues for a specific assembly of subunits into heteromeric receptors *in vivo*. For example, deletion of the  $\alpha 6$  subunit induced a loss of  $\delta$  subunit in cerebellar granules cell surface (Nusser et al., 1999). Likewise,  $\alpha 4$  subunit levels are decreased in the forebrain of  $\delta$  knock-out mice, whereas the level of  $\alpha 1$  subunit was unchanged (Korpi et al., 2002, Peng et al., 2002). Moreover,  $\gamma 2$  subunit levels are increased in these  $\delta$  knock-out mice, suggesting a compensatory role of  $\gamma 2$  in absence of  $\delta$  subunit (Tretter et al., 2001, Korpi et al., 2002). This data suggests that subunits compete to find their preferential oligomerisation partners in the ER. However, the underlying mechanisms are still unknown (Jacob et al., 2008).

#### 1.2.1.2 *Degradation of misfolded subunits: ERAD*

Misfolded or unassembled subunits are retained and degraded in the ER. The exit of GABA<sub>A</sub>R subunits from the ER is regulated by constitutive ER-associated degradation (ERAD) of  $\alpha$  and  $\beta$  subunit. ERAD involves protein ubiquitylation and degradation by the ubiquitin-proteasome system (UPS) (Jacob et al., 2008) (Figure 6).

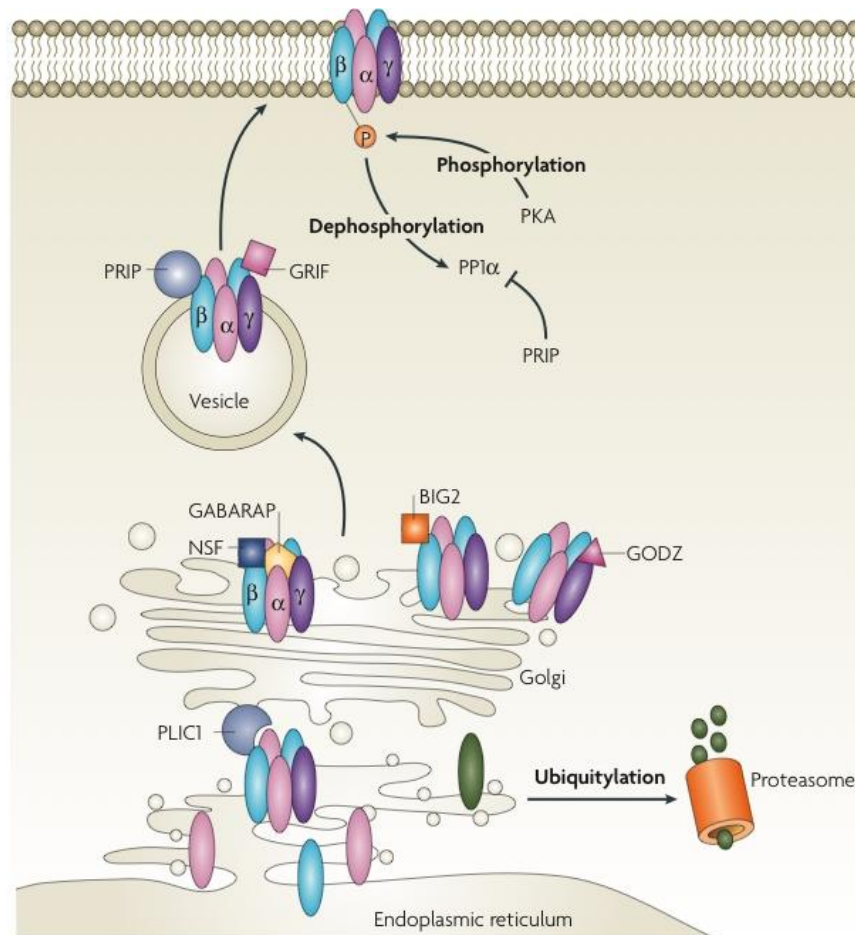
Exit of GABA<sub>A</sub> receptor subunits from the ER is mediated by a ubiquitin related protein Plic-1/2 (Protein Links Integrin-associated proteins with the Cytoskeleton-1/2) which inhibits ubiquitylation and ERAD of  $\alpha$  and  $\beta$  subunits (Luscher et al., 2011). It has been demonstrated that Plic-1 interacts directly with GABA<sub>A</sub>R subunits intracellular domains using the yeast-two hybrid system (Bedford et al., 2001). This interaction protects the subunits from proteasome-dependent degradation in the ER and stabilizes receptor assembly (Bedford et al., 2001). Moreover, Plic-1 is concentrated in the perinuclear ER, the nucleus and in association with intracellular membranes near inhibitory synapses (Bedford et al., 2001, Luscher et al., 2011) (Figure 6). Therefore, by

increasing the stability of receptor pools, Plic-1 binding increases the number of GABA<sub>A</sub>Rs that are available for insertion into the plasma membrane (Bedford et al., 2001).

#### *1.2.1.3 Export to the Golgi apparatus and Post-translational modification by glycosylation*

After their assembly in the ER, GABA<sub>A</sub>Rs are transported to the Golgi apparatus and segregated into vesicles to finally reach plasma membrane. Numerous proteins such as GABARAP, NSF, PRIPs, BIG2 or GRIF (see Figure 6) can interact (directly or indirectly) with the intracellular loop of the  $\beta$  subunits and modify intracellular trafficking of GABA<sub>A</sub> receptors (Connolly et al., 1996b, Wang et al., 1999, Kittler et al., 2001, Kanematsu T, 2002, Chen and Olsen, 2007).

In addition, post-translational modification by palmitoylation mediated by Golgi-specific DHHC Zinc finger protein (GODZ) of the  $\gamma$  subunit, can facilitate GABA<sub>A</sub>Rs trafficking (Keller et al., 2004, Rathenberg et al., 2004) (Figure 6).



**Figure 6: Synthesis and intracellular trafficking of GABA<sub>A</sub> Receptors.** (Jacob et al., 2008) GABA<sub>A</sub>Rs subunits are synthesised and assembled into pentameric channels in the endoplasmic reticulum. Misfolded or unassembled proteins are degraded by ubiquitylation in the proteasome. Plic-1 prevents ubiquitylation of subunits and degradation, facilitating the accumulation of GABA<sub>A</sub>Rs at the cell surface. GABARAP allows translocation of assembled subunits from ER via Golgi apparatus to the cell surface, by direct interaction with the  $\gamma$  subunit. BIG2 and NSF are localised in the Golgi apparatus and promote GABA<sub>A</sub>Rs insertion into the plasma membrane. GODZ is a Golgi-specific enzyme which palmitoylates the intracellular loop of  $\gamma$ 2 subunit which facilitate insertion of GABA<sub>A</sub>Rs at synaptic sites. GRIF is involved in GABA<sub>A</sub>Rs trafficking but the exact role is unclear. PRIPs have essential role in trafficking and phosphorylation state of GABA<sub>A</sub>Rs.

## 1.2.2 Endocytosis and recycling of GABA<sub>A</sub>Rs

### 1.2.2.1 Clathrin-dependent endocytosis

The number of GABA<sub>A</sub>Rs expressed at the cell surface is regulated by internalisation (endocytosis) into the postsynaptic compartment (Kittler et al., 2000). Endocytosis occurs in a clathrin- and dynamin-dependent manner and is mediated by the interaction of GABA<sub>A</sub>R subunit  $\beta$  and  $\gamma$  intracellular domains with the clathrin adaptor protein AP2 (Kittler et al., 2000, Arancibia-Carcamo and Kittler, 2009) (Figure 7). In hippocampal neurones,  $\beta$  and  $\gamma$  subunit intracellular domains can interact directly with the  $\mu$ 2 subunit

of the clathrin adaptor protein AP2 (Arancibia-Carcamo and Kittler, 2009). Consequently, disruption of this system by blocking the interaction of dynamin and amphiphysin results in an increase of GABA<sub>A</sub>R expression at the cell surface and a consequent increase in amplitudes of mIPSC (Kittler et al., 2000). The AP2 binding domain present in the intracellular domains of the  $\beta$  subunits contains the site of phosphorylation by serine and threonine kinases (Kittler et al., 2005).

#### 1.2.2.2 *Phosphorylation-dependent regulation of endocytosis*

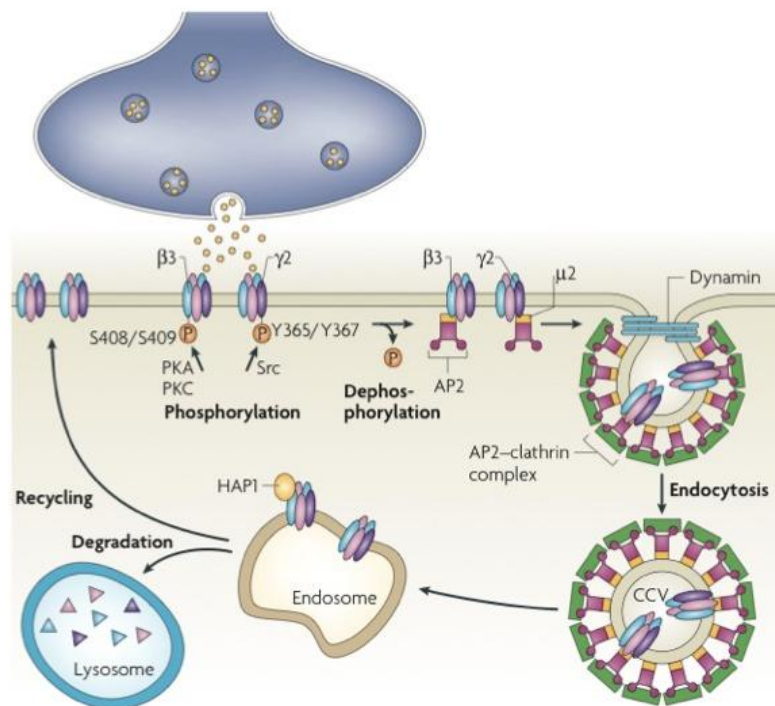
Phosphorylation of the AP2 binding domain prevents the interaction with AP2, indicating that AP2 binds GABA<sub>A</sub>R with high affinity and facilitates their internalisation preferentially when  $\beta$  subunit is dephosphorylated (Kittler et al., 2005, Luscher et al., 2011). Therefore, injecting neurones with a non-phosphorylated form of  $\beta$ 3 that competes with the interaction of the endogenous  $\beta$  subunit with AP2, resulted in an increase of mIPSC (Kittler et al., 2005). This interaction facilitates the recruitment of GABA<sub>A</sub>R into the endocytic pathway and thus is an important mechanism that regulates inhibitory synaptic strength and synaptic plasticity (Kittler et al., 2000). More importantly, the AP2 binding site of  $\beta$ 1 and  $\beta$ 3 subunits can be phosphorylated by PKC and PKA, while  $\beta$ 2 subunit can only be phosphorylated by PKC (Brandon et al., 2003, Luscher et al., 2011). This indicates that modulation of GABA<sub>A</sub>R endocytosis may occur in a subtype-specific manner. GABA<sub>A</sub>R can also bind directly with a high affinity to the  $\mu$ 2 subunit of AP2 via the intracellular loop of the  $\gamma$ 2 subunit (Kittler et al., 2008) (Figure 7). A YGYECL motif in intracellular loop of  $\gamma$ 2 subunit exhibits high affinity for AP2, and this interaction is negatively regulated by the phosphorylation of the two tyrosines by Src Kinases (Kittler et al., 2008) (Figure 7). Similarly to what has been already shown with the  $\beta$ 3 subunit, the dialysis of a blocking peptide of the  $\gamma$ 2/AP2 interaction leads to an increase of mIPSC amplitude as a consequence of an increase in the number of GABA<sub>A</sub>R at the cell surface (Kittler et al., 2008). Therefore, GABA<sub>A</sub>R cell surface expression can be regulated in a phosphorylation-dependent manner by at



least two different mechanisms for AP2/clathrin-dependent internalisation mediated by the  $\beta$  and  $\gamma$  subunits (Figure 7) (Arancibia-Carcamo and Kittler, 2009).

### 1.2.2.3 Recycling of GABA<sub>A</sub>Rs

Over a short time period, GABA<sub>A</sub>R are internalised and rapidly recycled to the cell surface, but over a long-time period, they are degraded. In neuronal cultures, Huntingtin associated protein 1 (HAP1) inhibits degradation of GABA<sub>A</sub>R by interacting with  $\beta$ 1-3 subunits, facilitating the recycling of the receptor and thus, accumulation of GABA<sub>A</sub>R at the cell surface (Kittler et al., 2004) (Figure 7).



**Figure 7: Constitutive endocytosis and recycling of GABA<sub>A</sub>Rs** (Jacob et al., 2008). Clathrin-dependent endocytosis is the major internalisation process for GABA<sub>A</sub>Rs recycling. Phosphorylation of  $\beta_3$  and  $\gamma_2$  subunits by PKA/C and Src respectively, stabilises GABA<sub>A</sub>Rs at the cell surface. However, dephosphorylation of these sites allows binding of the AP2 and receptor endocytosis via clathrin-coated vesicles (CCVs). HAP1 prevents degradation of GABA<sub>A</sub>Rs by interaction with  $\beta$  subunits and promotes recycling of GABA<sub>A</sub>Rs, thus leading to an increase in the number of GABA<sub>A</sub>Rs at synaptic sites

### **1.3 Development of GABAergic synapses**

#### **1.3.1 Regional expression of GABA<sub>A</sub>Rs across the embryonic brain**

The subunits of GABA<sub>A</sub>Rs are differentially expressed both temporally and spatially throughout the mammalian brain (Sur et al., 2001). From embryonic to adult brain, pattern of expression of each subunit has been characterised using *in situ* hybridisation, immunohistochemistry and co-immunoprecipitation.

*In situ* hybridisation and immunohistochemistry studies revealed that in the embryonic brain, different patterns of expression have been observed for thirteen GABA<sub>A</sub>Rs subunit mRNAs tested (Laurie et al., 1992, Fritschy et al., 1994). Initially, the  $\alpha 2$ ,  $\alpha 3$ ,  $\alpha 5$ , the three  $\beta$  subunits and  $\gamma$  subunits were found to be the most abundant subunits in the embryonic brain and during the first two postnatal weeks. After two postnatal weeks, the levels of  $\alpha 2$  subunit starts to decrease (Fritschy et al., 1994) and at the same time,  $\alpha 1$ ,  $\alpha 4$ ,  $\alpha 6$ ,  $\beta 2$  and  $\gamma 2$  mRNA levels increase until they become and remain the most abundant GABA<sub>A</sub>Rs subunits in the adult brain (Laurie et al., 1992). This differential subunit expression pattern happens in parallel with the change in the functional outcome of GABA<sub>A</sub>Rs activation from depolarisation to hyperpolarisation. In the developing brain, GABAergic synapses are immature and most GABA<sub>A</sub>Rs are present outside of the synapses. At this stage,  $\alpha 2$ ,  $\alpha 3$  and  $\alpha 5$ , which have a greater affinity for GABA, are the most abundant subunits. However, once mature synapses are formed, most of GABA<sub>A</sub>Rs contain the  $\alpha 1$  subunit.

#### **1.3.2 Regional expression of GABA<sub>A</sub>Rs across the adult brain**

Among the  $\alpha$  subunits,  $\alpha 1$  is present in all area of the adult brain and is often co-localised with  $\beta 2$  and  $\gamma 2$  subunit (Sieghart and Sperk, 2002). A genetic deletion (knock-out) of  $\alpha 1$  subunit causes a loss of 50 % of total GABA<sub>A</sub>Rs in the adult rat brain (Sur et al., 2001). The  $\alpha 2$  subunit is widely expressed during development but has limited expression in the adult brain. This subunit is present in the hippocampus,

cerebral cortex, hypothalamus, basal ganglia, certain thalamic nuclei and amygdala (Mohler et al., 1995, Pirker et al., 2000). In addition,  $\alpha 3$  subunit is moderately present in the adult brain, and mainly found in cerebral cortex and nucleus reticularis (Pirker et al., 2000). The  $\alpha 4$  subunit is mainly expressed in the thalamus, hippocampus and cortex. The  $\alpha 5$  subunit is rarely expressed in the adult brain except in the hippocampus (Sieghart and Sperk, 2002). The expression of  $\alpha 6$  subunit is restricted to the cerebellar granule cells (Pirker et al., 2000, Olsen and Sieghart, 2008).

All three  $\beta$  subunits are widely expressed in the adult brain. Nevertheless,  $\beta 2$  is the most widely expressed as knock-out mice show a decrease in 50 % of GABA<sub>A</sub>Rs in brain (Sur et al., 2001). Although the  $\beta 3$  subunit is relatively highly expressed in different brain areas,  $\beta 1$  is very rare. Moreover, a deletion of  $\beta 3$  or  $\gamma 2$  produces a lethal phenotype evident within 1 h after birth, suggesting an essential role played by these two subunits in brain development (Homanics et al., 1997, Tretter et al., 2001).

The vast majority of GABA<sub>A</sub>Rs contain the  $\gamma 2$  subunit which is the most abundant  $\gamma$  subunit in the rat brain based on *in situ* hybridisation of mRNA (Laurie et al., 1992, Wisden and Seeburg, 1992) and immunohistochemistry (Mohler et al., 1995). The  $\gamma 1$  and  $\gamma 3$  subunits are more restricted to certain areas as their level of expression decrease during development (Günther et al., 1995). However, the high levels of  $\gamma 1$  subunit expression are found in the substantia nigra, pallidum, amygdala and septum (Pirker et al., 2000).

The  $\delta$  subunit is virtually absent in the developing brain (Mohler et al., 1995). Nonetheless, in the adult brain,  $\delta$  subunit is often combined with  $\alpha 6$  subunit in cerebellar granule cells and associated with  $\alpha 4$  subunit in dentate gyrus, neostriatum and some cortical layers (Olsen and Sieghart, 2008).

### **1.3.3 Physiological properties of GABAergic synapses throughout development**

#### *1.3.3.1 Developmental switch*

Despite the inhibitory role of GABA in the adult brain, it has been demonstrated that GABA<sub>A</sub>Rs activation leads to depolarisation of cell membrane and excitation in developing neurones (Ben-Ari et al., 2007). During development, the intracellular chloride concentration gradually decreases (Ben-Ari et al., 2007). These changes of neuronal chloride homeostasis are dependent on the differential expression of two cation-chloride co-transporters. In immature neurones, Na<sup>+</sup>/K<sup>+</sup>/Cl<sup>-</sup> co-transporter NKCC1, which pumps chloride into the neurones, is expressed at approximately fourteen times higher levels than in mature cells (Bormann, 2000). On the other hand, the levels of K<sup>+</sup>/Cl<sup>-</sup> co-transporter KCC2, which pumps the chloride out of the cell, are lower in developing than in mature neurones. Therefore, in developing neurones, when postsynaptic GABA<sub>A</sub>Rs are activated, an efflux of negatively charged ions causes a depolarisation of the cell. This depolarising effect provides a strong excitatory drive that can generate action potentials and opening of voltage-dependant Ca<sup>2+</sup> channels (VDCCs) during the first two post-natal weeks (Ben-Ari et al., 2007).

#### *1.3.3.2 GABA<sub>A</sub>Rs-mediated hyperpolarisation in mature neurones*

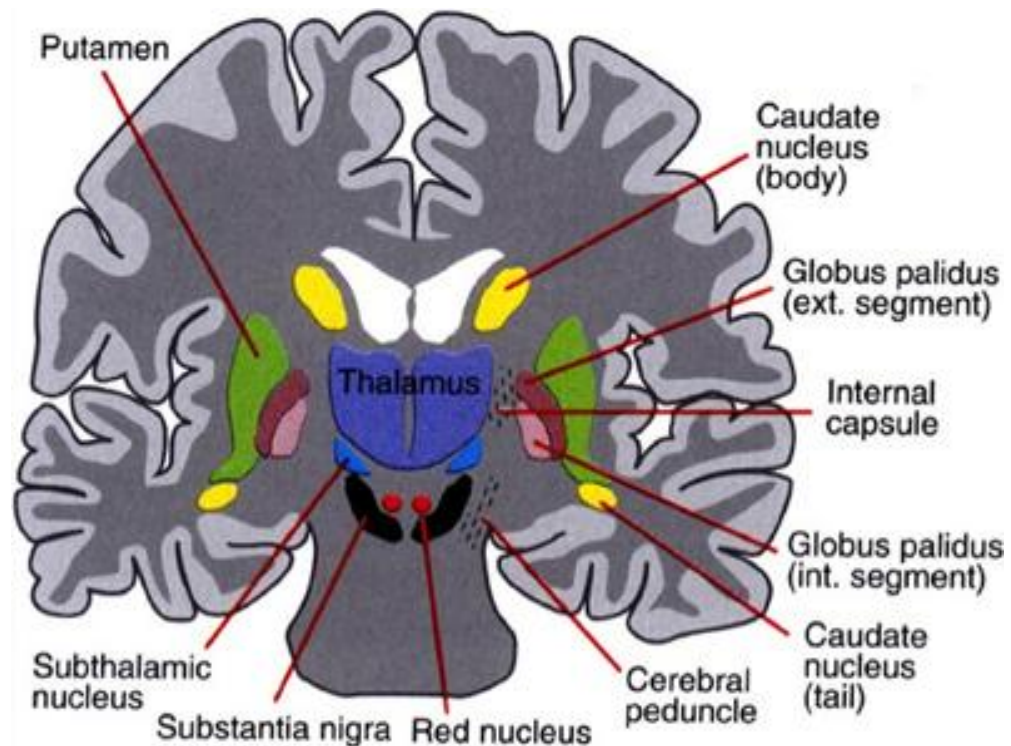
Once GABA is released into the synaptic cleft, it exerts its effect through activation of ionotropic GABA<sub>A</sub> or GABA<sub>C</sub> receptors, or metabotropic GABA<sub>B</sub> receptors. Fast synaptic inhibition is mainly mediated by GABA<sub>A</sub> receptors (Macdonald and Olsen, 1994). The binding of two molecules of GABA to GABA<sub>A</sub>Rs triggers the opening of a channel permeable to chloride and bicarbonate ions. The Cl<sup>-</sup> equilibrium potential is near the resting membrane potential and, in most mature neurones, intracellular chloride is low. Therefore, activation of GABA<sub>A</sub>Rs leads to a rapid chloride influx into the cell. The entry of negatively charged ions causes hyperpolarisation of the membrane potential and inhibition of neuronal activity (Rivera et al., 1999).

## **1.4 The basal ganglia**

### **1.4.1 Structure and functionality of the basal ganglia**

The basal ganglia consist in a group of subcortical nuclei involved in a variety of processes such as motor, associative, cognitive and mnemonic functions (Bolam et al., 2000). The basal ganglia are composed of the striatum (or caudate-putamen), the globus pallidus (external GPe, and internal GPi segments), the subthalamic nucleus (STN) and the *Substantia Nigra* (dorsal part: *pars compacta* SNc, and ventral part: *pars reticulata* SNr) (Figure 8). While the dorsal part of the basal ganglia is involved in motor and associative functions, the ventral part of this area which includes the ventral striatum (or nucleus accumbens), the ventral pallidum and the ventral tegmental area, is associated with limbic functions.

The main structure receiving the cortical information to the basal ganglia is the striatum, although the STN is also a primary recipient of information from outside the basal ganglia. The striatum is composed of the caudate nucleus, putamen (neostriatum) and nucleus accumbens (ventral striatum). Most of the inputs that the striatum receives come from nearly all the cerebral cortex in a topographical manner. For example, the prefrontal cortex projects to the anterior caudate while the somatosensory and motor cortex project onto the posterior putamen (Bolam et al., 2000) (Figure 9).



**Figure 8: The basal ganglia** (Leisman et al., 2014). The basal ganglia, which regulate motor control, are also implicated in the circuits that confer human reasoning and adaptive function. The Basal ganglia are key elements in the control of reward-based learning, sequencing, motor action and cognitive function. This brain region is made up of five subcortical nuclei: the globus pallidus, caudate, putamen, substantia nigra and the subthalamic nucleus.

#### 1.4.1.1 *The direct and indirect pathway*

The corticostriatal information is first transmitted to the striatum which conveys the information to the output structures of the Basal ganglia via two different pathways (Figure 9):

- A direct inhibitory pathway from the striatum to the SNr and GPi.
- An indirect pathway which first involves an inhibitory connection from the striatum to the GPe, which is then relayed by the inhibitory projection from the GPe to the STN and to the output nuclei, and finally via an excitatory connection from the STN to the SNr/ GPi.

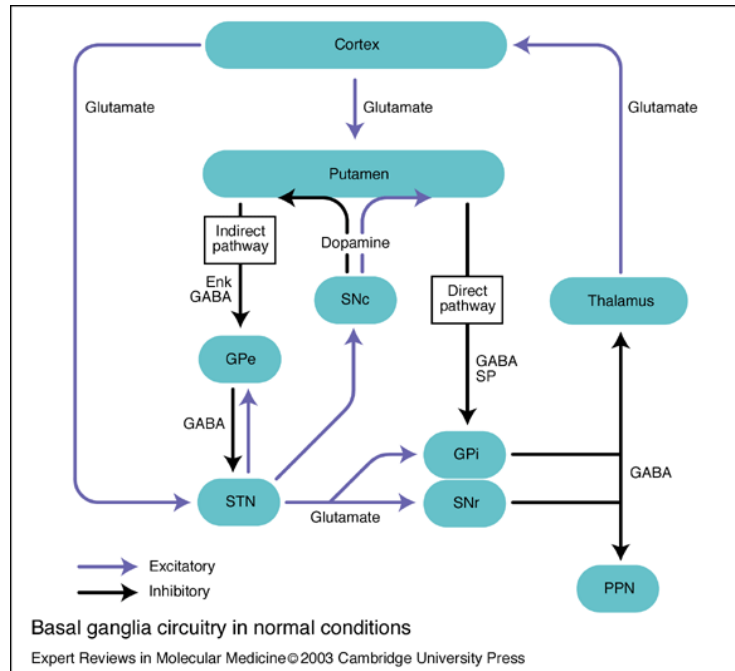
The output signal from the basal ganglia under resting conditions is inhibitory because most of the neurones present within the basal ganglia are GABAergic and tonically active (Chevalier and Deniau, 1990). Activation of the direct pathway by glutamatergic cortical inputs triggers a disinhibition of the medium spiny neurone

(MSN) networks, thus triggering activation of the basal ganglia targets and is associated with 'basal ganglia behaviour'. This is explained by the fact that the MSNs involved in the direct pathway are directly in contact with the neurones of the GPi and of the SNr. As both the MSNs and output neurones of the GPi are GABAergic, the release of GABA following their activation will provoke a disinhibition of the targets of the basal ganglia.

In contrast, if the indirect pathway is activated, the firing of basal ganglia output neurones is increased, provoking the inhibition of the basal ganglia targets. Mechanistically, the MSNs involved in the indirect pathways are forming synapses with the neurones of the GPe. These GPe neurones which are also GABAergic are in direct contact with the neurones from the STN, which in turn are in contact with those from the output nuclei of the basal ganglia. The neurones of the GPe are also in direct contact with the output neurones of the basal ganglia. Thus, activation of MSNs via the indirect pathway will have two effects. First, disinhibition of the GPe neurones will provoke the excitation of the neurones from the STN which in turn will increase the excitation of the output neurones. Second, inhibition of the GPe neurones will have a direct disinhibitory effect on the GABAergic output neurones of the Basal ganglia. Taken together, these two ways taken by the indirect pathway lead to an increase of the firing of the output neurones of the basal ganglia which is ultimately, inhibiting the targets of the basal ganglia, and potentially providing a termination to any basal ganglia associated movement (Mink and Thach, 1993).

Neurones projecting in the direct or indirect pathway are equal in proportion in the striatum. Interestingly, both populations can be distinguished according to the peptide transmitter they release when activated on one hand, and by the type of dopamine receptor they express on the other hand (Durieux et al., 2011). Neurones projecting in the direct pathway release substance P and dynorphine as co-transmitters and express type 1 dopamine receptor ( $D_1R$ ) predominantly. Upon the release of the dopamine from the SNc, the  $D_1R$ -expressing MSN are activated and release GABA to

the SNr, via the direct pathway. On the other hand, MSNs projecting in the indirect pathway co-release enkephalin when activated. In addition, these neurones are inhibited when dopamine is released from the SNc as they express mostly D<sub>2</sub>R (Pauly et al., 2012). Interestingly, this indicates the fact that dopamine plays critical role in the co-activation of the direct and indirect pathways.



**Figure 9. The basal ganglia projections and connections (Lewis et al., 2003).** Parallel neuronal networks of the striatum connect and integrate functions between the basal ganglia nuclei, various region of the cerebral cortex and the thalamus. In the motor circuit, cortical neurones project in a somatotopic pattern to the posterolateral putamen, where they synapse through glutamatergic neurones onto the medium spiny neurones. These striatal neurones are GABAergic and depending on the co-transmitter they release, belong to the direct or indirect pathway. The direct pathway connects the striatum to the internal globus pallidus (GPi) and the substantia nigra par reticulata (SNr). These two nuclei are the output nuclei of the Basal ganglia and project to the brainstem and thalamus, and from the thalamus back to the cortex. The projection of the GPi/SNr on the thalamus is inhibitory, while the thalamic projection to the cortex is excitatory. The indirect pathway pass through synaptic connections in the external segment of the GP (GPe) and then the subthalamic nucleus (STN) before connecting the striatum to the output nuclei of the Basal ganglia. The output from the STN to the GPi/SNr is excitatory. Excitatory projections are shown in blue; inhibitory projections are shown in black. Abbreviation: PPN, pedunclopontine nucleus.

#### 1.4.1.2 Pathophysiology of the basal ganglia

Some movement disorders result from imbalances in the direct and indirect pathways in the basal ganglia. Hypokinetic disorders (of which Parkinson disease is the best-known example) are characterised by impaired initiation of movement and



reduced amplitude of voluntary movements. Hyperkinetic disorders (of which Huntington's disease is the most representative example) are characterised by excessive motor activity provoking involuntary movements and decreased muscle tone. Despite their antagonism, both of these movement disorders are linked with specific disturbances within the basal ganglia thalamo-cortical motor circuit. It has been shown that over or under activity of the indirect pathway results in hypokinetic or hyperkinetic disorders, respectively (Albin et al., 1989). Parkinsonian animal models revealed that due to the loss of dopaminergic input from the SNc to the striatum, the indirect pathway activity was increased while the direct pathway activity was decreased. This shift leads to an increased activity in the GPi which results in increased inhibition of the thalamocortical and midbrain tegmental neurones and thus the hypokinetic features of the disease (Kandel, 2013).

#### *1.4.1.3 Development of the basal ganglia*

The embryonic telencephalon is divided into the pallial and subpallial domains which give rise to dorsal structures such as the cortex and ventral structures such as the striatum and globus pallidus, respectively (Jain et al., 2001). More specifically, the striatum and pallidum derive both from the lateral and the medial ganglionic eminences in the telencephalon (LGE and MGE, respectively) (Marin et al., 2000). The adult striatum is mostly composed of projecting medium spiny neurones and different classes of interneurones such as PV-, SOM- expressing and cholinergic interneurones. But when exactly in the development, these neuronal populations coming from the ganglionic eminences invade the striatum remains unclear.

Striatal projection neurones and SOM<sup>+</sup> interneurones derive both from the LGE while the cholinergic interneurones derive from the MGE (Olsson et al., 1998). Transplantation studies have demonstrated that LGE progenitors from the embryonic rat develop into cells with striatal projection neuron phenotype around E14-15 (Deacon et al., 1994). In contrast, the progenitors in the MGE develop into cholinergic

interneurones around E12-15 in the rat and express Nkx2.1 homeodomain protein together with *lhx 6/7* LIM-homeobox genes. These proteins are crucial for striatal interneurones specification especially for cholinergic and SOM<sup>+</sup> interneurones (Olsson et al., 1998, Marin et al., 2000). The role of NKX2.1 in the differentiation and specification of interneurones has been assessed by staining the striatum of wild type and *nkx2.1* mutant mice with markers such as ChAT, NPY and CR. As a result, the KO mice lacked most of the interneurone populations in the E18 mouse striatum (which corresponds to E19 in the rat) compared to wild type and died few hours after they were born (Marin et al., 2000).

## **1.4.2 Characteristics of the medium spiny neurones**

### *1.4.2.1 Physiological properties of MSNs*

#### 1.4.2.1.1 Neurochemical characterisation of cultured MSNs *in vitro*

The properties of cultured MSNs have been analysed extensively by immunocytochemistry and fluorescent microscopy (Falk et al., 2006). The characterisation of the phenotype of cultured MSNs was first determined using GAD 65 and GAD 67 immunolabelling. Consistent with the staining *in vivo* in the adult striatum, 90 % of MSNs were positive for both isoforms with GAD 65 being largely expressed in neurites.

In addition, the expression of D<sub>1</sub>R and D<sub>2</sub>R was characterised in 4 to 18 DIV cultured MSNs. The results show that 92 % of neurones expressed one or the other receptor at more mature stages. Interestingly, a shift was observed in the expression of dopamine receptors: while D<sub>1</sub>R expression was decreasing, D<sub>2</sub>R levels were increasing during neuronal maturation. Most of the neurones expressed both subtypes of receptors although they were located differently. D<sub>1</sub>R expression was patchy around one side of the soma while D<sub>2</sub>R were uniformly distributed around the soma. Additionally, both were found expressed in neurites. These results indicated that the *in vitro* model is consistent with the *in vivo* in that there is a relatively high expression of

dopamine receptors in the striatum compared to other regions. However, it failed to show distinct populations of neurones as most of the neurones expressed both types of receptors. The shift in the expression of D<sub>1</sub>R vs. D<sub>2</sub>R observed could indicate a progression towards a more mature stage *in vitro* with distinct populations of neurones observed in the adult brain. By activating D1- and/or D2-dopamine receptors, it has been shown that dopamine decreases the number of functional GABAergic synapses formed between the embryonic MSNs with associated changes in the spontaneous synaptic activity (Goffin et al., 2010). In DA-MSN co-cultures, after 5 or 10 DIV, the presence of DA neurones increased the number of MSN spines containing PSD-95 together with an increase in mEPSCs frequency (Fasano et al., 2013). These results suggest that the newly formed spines presented the functional postsynaptic machinery preparing the MSNs to receive additional glutamatergic contacts, thus providing a synaptogenic effect of dopamine on MSN development.

To characterise further the phenotype of these neurones, substance P and enkephalin were labelled and their expression was determined using semi-quantitative analysis (Falk et al., 2006). In this culture, 50 % of neurones expressed substance P in the somatic compartment but no correlation between the expression of D<sub>1</sub>R and Substance P was observed. In addition, less than 50 % of neurones expressed enkephalin which does not correspond to the *in vivo* labelling. In the striatum, there are more than 50 % of enkephalin positive MSNs. This discrepancy could reflect the immature stage of the culture system.

Finally, the potassium channels expressed in cultured MSNs were characterised. Potassium channels are highly diverse group of ion channels important for the regulation of electrical excitability of neurones and maintenance of the resting membrane potential (Hille, 2001). The potassium channels expression pattern in culture of MSNs was similar to that of *in vivo* in the adult striatum (Falk et al., 2006).

#### 1.4.2.1.2 Electrophysiological properties of MSNs *in vitro*

Using single cell patch clamp method, the electrophysiological properties of cultured MSNs with studies performed in slices *in vitro* were compared (Falk et al., 2006). All the recorded neurones showed rapid inactivation characteristics of the A-type  $K^+$  current. This current represented more than 60 % of the  $K^+$  current, corresponding to the *in vivo* studies (Wilson and Kawaguchi, 1996). With voltage clamp recordings, a large number of neurones displayed a continuous firing pattern ranging in frequency from 0.11 to 1.56 Hz. This low level of electrical activity found *in vivo* and *in vitro* reflects clearly the intrinsic properties of MSNs (Falk et al., 2006).

#### 1.4.2.1.3 Characteristics of MSNs *in vivo*

The striatum receives extensive excitatory inputs from the cortex and thalamus that predominantly target the spines of MSNs. In order to know if any selectivity applies to the formation of such synapses, bacterial artificial chromosomes (BAC) transgenic mice were developed with enhanced green fluorescent protein (EGFP) reporting the presence of D1 or D2 receptors. Different types of inputs were identified by the selective expression of the vesicular glutamate transporter type 1 (VGluT1) by corticostriatal afferents and VGluT2 by thalamocortical afferents. It was demonstrated that the proportion of synapses formed by cortical or thalamic terminals was similar for both D1 and D2-expressing MSNs (Doig et al., 2010). In addition, qualitative analysis revealed that individual cortical or thalamic terminals were able to form synaptic contacts with both types of MSNs. These findings demonstrate that there is no correlation between the origin of the input onto the striatum and the subtype of MSN receiving it. Both cortical and thalamic afferents are likely to be critical in the control of MSNs and thus provide an equally fundamental role in the Basal ganglia function.

Although the degree of segregation between the two populations of MSNs have been debated for a long time, recent anatomical studies have shown a specific repartition of the two neuronal populations using BAC transgenic mice expressing

EGFP under the control of D1 receptor- or D2 receptor-specific promoters (Gangarossa et al., 2013). It has been proved that while the striatonigral ( $D_1R^+$ ) and striatopallidal ( $D_2R^+$ ) MSNs are randomly distributed in the rostral part of the dorsal striatum, the caudal part of the dorsal striatum, adjacent to the GPe, is almost uniquely composed of  $D_1R$ -expressing MSNs. However, the function of this particular region within the striatum remains to be established.

Interestingly,  $D_1R$ -expressing MSNs are of particular interest as they are activated upon dopamine release. In the striatum, but also in the prefrontal cortex, the  $D_1R$ s activated by dopaminergic input trigger the cAMP/PKA signalling pathway. In the striatum, the cAMP/PKA response is much stronger, faster and longer lasting than in the pyramidal cortical neurones (Castro et al., 2013). It has been shown that in the striatum, the  $D_1R^+$  MSNs express molecular determinants that enable them to conduct much more efficiently the cAMP/PKA signal. Indeed, the lower level of type 4 phosphodiesterase activity (which does not damp the cAMP/PKA signal in the striatum), adenylyl cyclase activity and DARPP-32 (phosphatase inhibitor prolonging PKA activity) contribute strongly to the efficiency of MSNs in responding to brief dopamine stimuli (Castro et al., 2013).

### **1.4.3 Inhibitory mechanisms in the neostriatal microcircuitry**

The GABAergic striatal microcircuitry is composed of a projecting MSNs and interneurones, which are in minority. The connectivity within this microcircuitry is divided into two main categories: the inhibition mediated by axon collaterals of medium spiny neurones, and the inhibition mediated by neighbouring interneurones, mostly by fast spiking interneurones (FSIs) onto MSNs (Mallet et al., 2005). There are two main classes of interneurones in the striatum: the fast spiking interneurones (FSIs) and the persistent and low-threshold spike interneurones (PLTSs) (Kawaguchi, 1993). Neurochemically, while FSIs express the calcium-binding protein, parvalbumin (PV), the PLTS interneurones express neuropeptides such as somatostatin (SOM),

neuropeptide Y (NPY) or the enzyme nitric oxide synthase (NOS) (Gittis and Kreitzer, 2012). For a long time, the MSN network and their interconnection was considered to provide the majority of striatal GABAergic inhibition and to sharpen and shape the output of MSNs. GABAergic interneurons represent only 2 % of the total rat neostriatum cell population but their input is crucial for a proper functioning of the Basal ganglia. Recent studies, mostly from *in vivo* paired recordings, have shown that the feed-forward inhibition provided by the fast spiking interneurons dominates and is much more efficient in blocking the generation of spikes in MSNs (Planert et al., 2010).

#### 1.4.3.1 *Feed-forward inhibition of MSNs by GABAergic interneurons*

By exerting a powerful and widespread feed-forward inhibition of both striatonigral and striatopallidal MSNs, FSIs regulate the way cortical information is processed within the striatum (Mallet et al., 2005, Planert et al., 2010). In addition, FSIs may not selectively inhibit direct MSNs (*d*MSNs) or indirect MSNs (*i*MSNs), but rather efficiently and similarly inhibit a large subset of neighbouring MSNs of both types. The depressing nature of FSIs mediated inhibition makes it tuned to transmitting the onset of FSI activity, enabling FS cells to mediate efficient synchronised inhibition after cortical excitation (Mallet et al., 2005). The role of such inhibition may be in preventing MSNs to discharge after cortical stimulation but also, to allow synchronisation of output target of MSNs without completely silencing them.

The FSI-MSN and MSN-MSN inhibition observed in the microcircuitry of the striatum is very different in terms of the dynamic and prevalence regardless of the type of postsynaptic MSN. The FSI-MSN connectivity was shown to be several times more prevalent than MSN-MSN connectivity. This big difference could be attributed to the localisation of both types of synapses. As FSI-MSN synapses are perisomatic and MSN-MSN synapses are more distal, the signal of the first type of synapse is less likely to be attenuated than the second one. Interestingly, the FSIs present in the neocortical microcircuit share not only the same physiological properties as those constituting the

striatal microcircuitry but also share the similar networks properties and function in mediating feed-forward inhibition to their respective targets (Planert et al., 2010).

More importantly, the dichotomy between direct and indirect pathway MSNs contributes to the regulation of this network (Gerfen and Surmeier, 2011). One of the major projections to FSIs originates from GPe neurones and is preferentially controlled by the indirect pathway MSNs, complementing the one mediated by the axon collateral projections of MSNs (Bevan et al., 1998). It has been shown that bath application of dopamine elicited a depolarisation with an increase in membrane input resistance of FSIs *in vitro* (Bracci et al., 2002). These effects were mimicked by the D1-like dopamine receptor agonist SKF38393 but not by the D2-like agonist quinpirole. In contrast, GABAergic currents evoked by intrastriatal stimulation were reversibly depressed by dopamine and D2-like, but not D1-like, agonists. These results showed that endogenous dopamine exerts a dual excitatory action on FSIs by directly depolarising them (through D1-like receptors) and by reducing their synaptic inhibition (through presynaptic D2-like receptors).

#### 1.4.3.2 *Feedback inhibition by axon collaterals of MSNs*

Although the feedback inhibition mediated by MSNs on neighbouring MSNs is not as prevalent as the feedforward inhibition mediated by FSIs on MSNs, they both contribute to the processing of cortical input (Plenz, 2003). Unitary connections between MSNs are individually weak but in aggregate, they can be at the origin of a substantial inhibition that might be important for creating distinct assemblies within the striatal microcircuitry (Tepper and Bolam, 2004).

In contrast to FSI-mediated inhibition, striatopallidal and striatonigral MSNs receive sparse and variable, depressing and facilitating synaptic inputs from nearby MSNs (Planert et al., 2010). The dynamics of MSN-MSN synapses are very different and a lot more variable than that observed in FSI-MSN synapses. The synaptic dynamics does not seem to depend on the type of interconnected MSNs, but

interestingly, individual presynaptic neurones induce similar dynamic responses in different types of targets, which is not the case in other types of microcircuitry where the same presynaptic neurone may induce drastically different response to different types of targets (Reyes et al., 1998).

Unlike most of the facilitating connections observed in cortical areas, the facilitation mediated by MSN-MSN synapses was masked by a simultaneously occurring depressing component. This interplay might be at the origin of the variability observed in MSN-MSN connectivity (Planert et al., 2010). In addition, the feedback inhibition provided by neighbouring MSNs acts principally at the dendrites to control local excitability as well as the overall level of activity of the spiny neurones (Wickens et al., 1991).

Mature MSNs possess a highly polarised resting membrane potential at -80 to -90 mV. Following the release of GABA from neighbouring MSNs, the relatively depolarised  $E_{Cl^-}$  induces a membrane potential range of -30 mV which is not sufficient to create an action potential as the spike threshold of MSNs is -45 mV. For MSNs at rest, GABA depolarisation might facilitate further excitatory input. By contrast, for MSNs near the action potential threshold, the GABAergic input might control the timing of postsynaptic action potential (Plenz, 2003).

#### **1.4.4 Other neuronal types in the striatum**

##### *1.4.4.1 Cholinergic interneurones*

The cholinergic interneurones compose approximately 0.3 % of the total striatal population. Although their number is low, they play a major role in the striatal microcircuitry. These neurones receive excitatory cortical and thalamic inputs as well as GABAergic inputs from MSNs and dopaminergic inputs from the SNr (Reynolds and Wickens, 2004, Tepper and Bolam, 2004). Their dense and widespread local axon collateral plexus is restricted to the striatal matrix where they target mostly MSNs and GABAergic interneurones and the effect of released acetylcholine is mediated through



muscarinic and nicotinic receptors (Koos and Tepper, 2002). *In vivo* cellular recordings showed that cholinergic interneurons fire regularly and slowly, with long duration action potentials and slow after-hyperpolarisation spikes, which makes them clearly distinguishable from the rest of striatal neurons. These tonically active neurons (TANs) respond to visual or auditory cues that predict saliency or reward with a stereotypic pause of 200 ms in their activity in response to cues (Reynolds and Wickens, 2004, Tepper and Bolam, 2004). The cholinergic interneurons are the elements in the neostriatal circuit underlying the reward-based learning and motivated behaviour (Tepper and Bolam, 2004). Activation of these interneurons has been shown to indirectly increase synaptic GABA events in MSNs through GABAergic interneurons (English et al., 2012, Luo et al., 2013a).

#### 1.4.4.2 *The PLTS interneurons*

The persistent and low threshold spike (PLTS) interneurons are GABAergic interneurons distinguished by the absence of PV and the presence of NPY, SOM, NOS and NAPDH diaphorase. They compose 0.8 % of the total cell population in the neostriatum of the rat and have the least dense axonal arborisation of all interneurons. They receive both cholinergic and dopaminergic input. Inhibitory inputs from these interneurons onto MSNs are not readily detected with whole-cell recordings and connectivity is sparse (Gittis and Kreitzer, 2012).

The NPY<sup>+</sup> interneurons have been identified as neurogliaform (NGF) cells and shown to be crucial in mediating striatal cholinergic regulation (English et al., 2012). Although all four subclasses of striatal GABAergic interneurons are activated directly by nicotinic agonists, the NPY<sup>+</sup> interneurons are most prominent in regulating the inhibition of MSNs during nicotinic activation (Luo et al., 2013a). In this paper, it has been shown that all the striatal interneurons have nicotinic acetylcholine receptor (nAChR) and that they all make detectable direct synaptic connections with MSNs except NPY<sup>+</sup> PLTS.

Using the striatum slice preparation and chronically dopamine-depleted MSNs, it was demonstrated that the chronic removal of dopamine provoked a shift of activity of GABAergic PLTS interneurons from single-spike to bursting pattern and an increase in the efficacy of GABAergic synaptic transmission (Dehorter et al., 2009). This led in turn to the generation of oscillatory giant bursts of GABA currents by one-half of the MSN population in the striatum (Dehorter et al., 2009).

The last subclass of interneurons is composed of neurons expressing the calcium binding protein, calretinin. They represent 0.8 % of the neostriatal cells in the rat and are relatively sparse in the caudal part of the striatum. Similar to FSIs, these calretinin-expressing interneurons exert a strong monosynaptic inhibition on MSNs that can delay or block spiking (Tepper and Bolam, 2004), however, their contribution to the striatal microcircuitry functioning remains unclear.

#### **1.4.5 Expression of GABA<sub>A</sub>R subunits in the adult striatum**

The expression of different GABA<sub>A</sub>R subunits was characterised throughout the adult rat basal ganglia using immunohistochemistry. A regional segregation between the various  $\alpha$  subunit variants was observed, while the  $\beta$ 2/3 and  $\gamma$ 2 subunits were widely expressed throughout the basal ganglia (Fritschy and Mohler, 1995). The  $\alpha$ 1 and  $\alpha$ 2 subunits were the most predominant  $\alpha$  subunits found in the striatum. The  $\alpha$ 5 subunit was also present. In addition, the sub-cellular localisation of the GABA<sub>A</sub>Rs in the striatum of the rat was investigated. Post-embedding immunolabelling revealed the presence of  $\alpha$ 1,  $\beta$ 2/3 and  $\gamma$ 2 subunits of the GABA<sub>A</sub>Rs at the soma, dendrites and spines at symmetrical synapses of MSNs and/or interneurons (Fujiyama et al., 2000). Interestingly, double labelling for the  $\beta$ 2/3 subunit and GABA revealed only 60 % of co-localisation. More recently, the localisation of GABA<sub>A</sub>Rs throughout the GPe was investigated according to the type of synapses they were part of (Gross et al., 2011). In this paper, electrophysiological recordings and pharmacology followed by immunolabelling were combined in order to determine the cellular distribution of  $\alpha$ 1,  $\alpha$ 2

and  $\alpha 3$  GABA<sub>A</sub>R subunits in relation to striatopallidal (Str-GP) and pallidopallidal (GP-GP) synapses. It has been shown that while  $\alpha 1$  subunit is expressed in both synapses in the soma and dendrites, the  $\alpha 3$  subunit expression was restricted to the perisomatic synapses, a region mostly contacted by local axon collaterals (GP-GP synapses). In contrast, the  $\alpha 2$  subunit was mostly present in dendritic compartments where striatal synapses are located (Str-GP synapses). Thus, due to the kinetic properties conferred by each individual  $\alpha$  subunit, this specific distribution is likely to contribute differentially to both physiological and pathological patterns of activity (Gross et al., 2011).

Additionally, it has been suggested that the  $\beta 3$  subunit plays a central role in the basal tonic current seen in striatopallidal projection neurones from young mice and that the deletion of this subunit in KO mice resulted in a high decrease of MSN excitability (Janssen et al., 2011).

It is becoming increasingly clear that different subtypes of GABA<sub>A</sub>Rs, the main component of the GABAergic synapses, are playing a central role in regulating the formation and maintenance of specific GABAergic synapse. GABA<sub>A</sub>Rs heterogeneity is still poorly understood but the evidence available suggests that GABA<sub>A</sub>R subtypes which are different in subunit composition, represent distinct entities with specific functions and pharmacological profiles, and with unique spatio-temporal mRNA and protein expression patterns during brain development (Fritschy and Panzanelli, 2014). The purpose of this investigation was to determine further the role of GABA<sub>A</sub>R  $\alpha 1$  and  $\alpha 2$  subunits during specific GABAergic synapse formation. In particular, we were interested in the structural role played by the N-terminal extracellular domains of  $\alpha 1$  and  $\alpha 2$  subunit during the formation of GABAergic synapses in the developing basal ganglia.

# Chapter two

## **2. Experimental procedures**

### **2.1 Primary cultures of embryonic medium spiny neurones.**

One day prior to culture preparation, glass coverslips were placed in 24 well plates and incubated in a humidified 37°C/5% CO<sub>2</sub> incubator with 120 µl of poly-L-Lysine (100 µg/ ml) overnight. The coverslips were washed 2 times with water and then coated for 3-5 h with laminin (10 µg/ ml). Dissection tools were sterilized in 70 % EtOH.

Medium spiny neurone cultures were prepared using embryonic striatal tissue as described previously (Goffin et al., 2010). Embryonic striatal tissue was isolated from rat embryos at gestation stage E16 to E19. First, the pregnant female rat (adult Sprague-Dawley, Harlan UK) was euthanized by carbon dioxide inhalation, placed on her back and sprayed with 70 % EtOH. The skin was cut around the abdomen with care taken to avoid contamination by fur and without breaking the abdominal membrane. With smaller scissors and a microsurgery straight-tip forceps, the membrane was cut and embryos were removed from the uterus, placed into a 100 mm Petri dish containing ice cold phosphate buffered saline (PBS). Under the Laminar Flow Hood (Bassair), embryos were removed from their individual placentas and decapitated. The heads were placed in another Petri dish containing ice cold PBS. With a pair of microsurgery straight-tip forceps, the skin and skull were peeled away; the brain was taken out of the skull and placed into a new 100 mm dish containing Hank's balanced salt solution (HBSS; Invitrogen) at 4°C. HBSS consisted of the following components (mM): NaCl (137.93); KCl (5.33); sodium bicarbonate (NaHCO<sub>3</sub>; 4.17), potassium phosphate monobasic (KH<sub>2</sub>PO<sub>4</sub>; 0.44); anhydrous sodium phosphate dibasic (Na<sub>2</sub>HPO<sub>4</sub>; 0.34); D-Glucose (5.5); pH 7.4. Then, with the dorsal aspect of the brain facing up, the rhomb encephalon was removed and the brain was separated into two hemispheres. The meninges were removed carefully from the cortices and hippocampus. In order to access to the striatum the hippocampus was carefully removed. The striatum (containing the caudate nucleus and putamen, including the

striatal neuroepithelium and subventricular zone) was removed and transferred to a sterile 60 mm Petri dish containing HBSS at 4°C.

All the striatal tissue was then minced to small pieces of tissues (<1 mm) with the micro dissecting forceps. All the pieces were then collected with a Pasteur pipette into a 15 ml conical tube. The tissue was allowed to settle and the remaining medium was removed until 0.5-0.8 ml of HBSS was left in the tube. With a fire-polished Pasteur pipette, tissue was triturated with six to eight strokes. With a second Pasteur pipette polished to approximately 30 % of its original tip diameter, the cells were dissociated slowly until the solution was homogeneous. Live cells were counted by Trypan blue exclusion test, in which 10 µl of Trypan blue (0.4 %) was added to 10 µl of cells and 40 µl of HBSS and 10 µl was loaded into haemocytometer (Sigma-Aldrich). Once the total number of viable cells was counted, ~75, 000 cells were plated per coverslip into Neurobasal medium containing B27 Supplement, glutamine (2 mM), penicillin (100 Units), streptomycin (100 µg) and glucose (6 mM; all from Invitrogen). B27 supplement was included since it significantly improves the differentiation and survival of embryonic cultured neurones (Brewer et al., 1993). The cell suspension was swirled several times during the course of the plating to ensure even dispersion of cells. Cells were incubated in the complete Neurobasal medium in a humidified 37°C/5% CO<sub>2</sub> incubator for 4 to 14 days prior to experimentation.

## **2.2 *Fluorescent immunolabelling and confocal imaging***

Imaging fluorescent staining was performed using confocal laser scanning microscopy (CLSM), a widely used high-resolution imaging (optical sectioning) technique that offers enhanced contrast and definition compared to more traditional widefield fluorescence microscopy. In a conventional light microscope, object-to-image transformation takes place simultaneously for all object points. In contrast, in a confocal LSM, the specimen is irradiated in a pointwise fashion (serially). A microscope objective is used to focus a laser beam onto the specimen, where it excites

fluorescence. The fluorescent radiation is collected by the objective and efficiently directed onto the detector via a dichroic beam-splitter. The wavelength range of the fluorescence spectrum is selected by an emission filter, which also acts as a barrier blocking the excitation laser line. The pinhole is arranged in front of the detector, on a plane conjugate to the focal plane of the objective. Light coming from planes above or below the focal plane is out of focus when it hits the pinhole, so most of it cannot pass the pinhole and therefore does not contribute to forming the image (Wilhelm).

After 7 or 14 days in vitro (DIV), cells were washed twice briefly with PBS and fixed using 4 % (w/v) paraformaldehyde (PFA) and 4 % (w/v) sucrose in PBS for 10 min at the room temperature with slow agitation. The paraformaldehyde preserves the tissue by cross-linking proteins and thereby, maintaining the relative positions of cellular structures while the sucrose allows cells to preserve their osmolarity, therefore preventing the leakage of important constituents. Following fixation, cells were washed twice briefly and three times for 5 min with PBS at room temperature with slow agitation. In order to quench the excess of PFA, PBS was removed and cells were incubated with 0.3 M glycine in PBS (Sigma-Aldrich), followed by 2 quick washes and three washes of 5 min in PBS. In order to obtain labelling of cell surface proteins, blocking buffer containing bovine serum albumin (BSA) 2 % (w/v) in PBS was added for 1 h. Subsequently, blocking buffer was removed and cells were incubated with the primary antibodies diluted in 2 % BSA (w/v) / PBS overnight at 4°C. The following day, cells were washed twice quickly and three times for 5 min in PBS. Then, they were incubated in blocking solution containing 2 % BSA (w/v) in PBS for 30 min. For labelling of intracellular proteins, cells were permeabilised with 0.1 % Triton X-100 (v/v) in blocking (2 % BSA (w/v) / PBS), for 15 min. The primary antibodies diluted in 2 % BSA (w/v) / PBS were added and incubated for 2 h. Cells were washed three times for 5 min in PBS and blocking buffer containing 1 % BSA in PBS was added for 30 min. Fluorescently-labelled Alexa Fluor secondary antibodies were diluted at 1/750 dilution (v/v) in 1 % BSA (w/v) / PBS and added to the cells for 1 h protected from light. Cells

were washed three times for 5 min with PBS and mounted on glass slides with the Prolong Gold anti fade reagent (Invitrogen). Images were captured with an LSM 710 laser scanning confocal microscope (Zeiss) with the 63x or 40x 1.4NA Oil DIC Plan-Apochromat M27 lens.

### **2.3 Confocal analysis**

Immunolabelling was analysed using Zeiss LSM 710 confocal microscope with a Plan-Apochromat 63x/1.4 Oil DIC lens. Threshold for each channel was calculated from the background staining intensity and then removed from the image. To count the density and size of  $\alpha$ 1- and  $\alpha$ 2-containing GABA<sub>A</sub> receptor clusters or gephyrin clusters, puncta were defined as immunoreactive profiles greater than  $0.1 \mu\text{m}^2$ , with the mean intensity of each cluster equal or higher than double the standard deviation of intensity which was indicated by the Zen 2009 Programme. The defined clusters were encircled and their properties noted by hand.

The density and size of  $\alpha$ 1 clusters were first calculated, followed by the  $\alpha$ 2 clusters. Then,  $\alpha$ 1 clusters which were mixed with  $\alpha$ 2 (minimum of 50 % overlapping) were separated from  $\alpha$ 1 clusters and analysed as a separate group. The same process was applied to  $\alpha$ 2 mixed clusters. Because the ratio between the density of  $\alpha$ 1 and  $\alpha$ 2 clusters was different among mixed clusters, these populations were kept and analysed separately, although in most of the cases, they represented the same population of mixed clusters. Therefore, we did not separate these two types of mixed clusters when we analysed their co-localisation with gephyrin.

### **2.4 Analysis of synaptic parameters**

As a criterion for synaptically localised clusters, I determined whether these clusters were in close apposition to the GAD-65-positive presynaptic nerve terminal. A minimum of 50 % overlap was used to estimate the close apposition between the postsynaptic clusters and the presynaptic terminals. The same criterion was used to determine the density and proportion of  $\alpha$ 1 and/or  $\alpha$ 2-containing clusters co-localised with gephyrin.



The total density of GAD-65 immunoreactive puncta forming contacts along the first 20  $\mu\text{m}$  length of primary dendrites was counted separately to determine the density of presynaptic inputs.

## **2.5 Statistical analysis**

Once all the parameters were measured, they were copied into an Excel file and sorted into different groups according to their size, co-localisation with GAD-65 and kind, single or mixed clusters:

- All  $\alpha 1$  single clusters
- $\alpha 1$  single clusters which are co-localised with GAD-65
- All  $\alpha 2$  single clusters
- $\alpha 2$  single clusters which are co-localised with GAD-65
- All  $\alpha 1$  mixed clusters
- $\alpha 1$  mixed clusters which are co-localised with GAD-65
- All  $\alpha 2$  mixed clusters
- $\alpha 2$  mixed clusters which are co-localised with GAD-65
- All gephyrin clusters
- $\alpha 1$  single clusters which are co-localised with gephyrin
- $\alpha 2$  single clusters which are co-localised with gephyrin
- mixed clusters which are co-localised with gephyrin

Subsequently, the data was analysed using Origin Pro 9.0 32 Bit software. Normal (Gaussian) distribution of the pooled data was first tested using the Shapiro-Wilk and Kolmogorov-Smirnov tests. Since the data did not follow a normal distribution and the categories were independent, non-parametric statistical analysis was carried out using the Mann Whitney test with an interval of confidence of 95 %. Because they represent a robust measure of central tendency when distributions are not normally distributed, the medians and their interquartile range (Q3-Q1) were used to describe the data and evaluate statistical dispersion. With the groups following normal

distribution, statistical analysis was done using two sample Student's t-test. The total density of clusters was evaluated along the length of 20  $\mu\text{m}$  of primary dendrite for each cell. The density of synaptic clusters was also evaluated along the 20  $\mu\text{m}$  of dendrites for each cell in a whole population of clusters. The proportion of synaptic clusters was determined as a percentage of the total clusters for each dendrite. The percentage of the synaptic/total clusters was tested as above and subsequently compared using parametric (Student's t-test) or non-parametric statistical tests (Mann-Whitney). A Gaussian fit was added to the bar graphs but most of the populations were not following a normal distribution.

## **2.6 Protein assays**

### **2.6.1 Bradford Assay**

The Coomassie dye protein assay was used to detect the protein concentration in non-denatured samples. In this assay, the proteins present in the sample bind to the Coomassie dye because of the acidity of the reagent. This binding results in a shift in the absorbance of the dye from 465 nm to 610 nm, changing the colour of the dye from reddish/brown to blue. The development of colour in Bradford protein assay is associated with the presence of arginine, lysine and histidine amino-acids in the peptide sequence of proteins. Thus, the amount of Coomassie dye bound to each protein is approximately proportional to the density of positively charged amino-acids found in the peptide sequence. Usually, standards were prepared by serial dilutions of 1 mg/ml BSA in  $\text{H}_2\text{O}$  + 5  $\mu\text{l}$  of the buffer in which proteins were present. Then, 2 ml of the Bradford dye mixture (Bradford dye and deionised water 1:5 ratio, Bio-Rad) was added to the sample (5  $\mu\text{l}$ ) and the standards. Solutions were quickly vortexed as the incubation time is very short. The absorbance at 595 nm was determined using spectrophotometer (Beckman-Coulter). The standard curve was constructed by determining the absorbance of BSA standards (1, 2, 3, 4, 5, 10, 15, 20 and 25  $\mu\text{g}$ ),

fitting these points to a linear curve. The concentration of protein lysates was estimated using the standard curve.

### **2.6.2 BCA Assay**

The concentration of samples denatured with 2 % SDS was measured using the BCA Protein Assay (Thermo Scientific Pierce) which is a colorimetric assay detecting the reduction of copper by proteins in presence of an alkaline medium (the Biuret reaction). This detection relies on a highly sensitive and colorimetric detection of the  $\text{Cu}^+$  by the bicinchoninic acid (BCA). The first step is the chelation of copper with protein in an alkaline environment to form a light blue complex. In this reaction, peptides containing three or more amino acid residues form a coloured chelate complex with cupric ions. In the second step of the colorimetric reaction, the bicinchoninic acid (BCA) reacts with the reduced cation that was formed previously ( $\text{Cu}^{1+}$ ). The BCA/copper complex has a linear absorbance at 562 nm with increasing protein concentrations over a working range of 10-2.000  $\mu\text{g}/\text{ml}$ . The reaction leading to BCA colour formation is strongly influenced by the presence of four amino acid residues (cysteine or cystine, tyrosine and tryptophan) in the sequence of the protein. Sample concentrations were determined based on the standards of BSA. After protein sample were denatured in 2% SDS, 5  $\mu\text{l}$  of each was diluted in water (100  $\mu\text{l}$ ) and standards were prepared by serial dilutions of 1 mg/ml Bovine Serum Albumin (BSA) in  $\text{H}_2\text{O}$  + 5  $\mu\text{l}$  of 2% SDS. Then, 2 ml of the BCA mixture (Reagent A and B at a ratio of 50:1) was added to the samples and the standards. Solutions were incubated in a 37°C water bath over 30 min for the reaction to occur. The absorbance at 562 nm was determined using spectrophotometer (Beckman-Coulter). The standard curve was constructed by determining the absorbance of known BSA samples (1, 2, 3, 4, 5, 10, 15, 20 and 25  $\mu\text{g}$ ), and fitting these points to a linear curve. The concentration of protein lysates was estimated using the standard curve.

## **2.7 Methanol/Chloroform extraction of proteins**

Detergents (SDS) or salt (NaCl) can be removed from protein samples by precipitation of proteins with a mixture of chloroform (organic solvent) and methanol (a polar solvent, dissolving polar molecules) resulting in dry protein material. This dry protein material can be resuspended in various buffers and used in experiments. Moreover, it is often useful to resuspend proteins in a smaller volume in order to load small well combs gels.

The samples were split so that a maximum of 150  $\mu$ l was present per tube. First, four volumes of methanol were added to each sample (600  $\mu$ l) and vortexed. Subsequently, one volume of chloroform was added (150  $\mu$ l) and vortexed. Finally, three volumes of ddH<sub>2</sub>O (450  $\mu$ l) were added and vortexed, and the solution precipitated. The proteins were centrifuged for 1 min at 14,000 g. Two phases (the top phase containing methanol and water, the bottom phase containing chloroform) were separated by a white phase in the middle containing the proteins (Folch et al., 1951). The top layer was removed, leaving some of the aqueous/organic interphase, and three volumes of methanol (450  $\mu$ l) were added. After mixing, the proteins were centrifuged for 4 min at 14,000 g. The supernatants were poured off and the protein pellets tap dried for 15 min.

## **2.8 SDS PAGE and electrophoresis**

Proteins were separated according to their molecular mass using sodium dodecyl sulphate polyacrylamide gel electrophoresis (SDS/PAGE) (Raymond and Weintraub, 1959). In their native form, proteins fold into a variety of shapes and with different net charge depending on their amino acid composition. The rate of migration of native proteins through a gel matrix depends on their relative compactness and charge rather than their molecular mass. To overcome this problem, protein samples are denatured with the anionic detergent SDS the reducing agent  $\beta$ -mercaptoethanol and by boiling at 95°C. Because SDS binds to proteins with a ratio of 1.4 g of SDS for

1g of protein, the denatured proteins are uniformly negatively charged. Thus, when a current is applied, all SDS-bound proteins present in a sample migrate through the gel towards the positively charged electrode allowing separation of proteins based on their mass alone. Proteins with the lowest mass travel faster through the gel than those with greater mass because of the sieving effect of the gel matrix. Therefore, the lowest mass proteins are detected at the bottom of the gel, while the highest molecular mass proteins are at the top of the gel.

We have used discontinuous SDS/PAGE because this method “stacks” proteins into a very narrow zone prior to separation (the stacking gel), resulting in enhanced band sharpness and resolution (Ornstein, 1964). This method promotes the use of two different gels: an upper, large pore (5% polyacrylamide) “stacking gel” with a pH of 6.8 and a lower separating gel, varying in pore size (from 8 to 12 %) with a pH of 8.8. When electrophoresis starts, the glycine from the running buffer enters the stacking gel. Because the pH of the gel is lower than the pKa of glycine, it enters the gel with a net charge of zero. It moves slowly through the sieving of the stacking gel, lagging behind the strongly charged Cl<sup>-</sup> ions. As these two species separate, a region of low conductivity, with a high voltage drop is created between them. This is known as the Kohlrausch discontinuity, which provokes the rapid entrance of the proteins through the large pores of the stacking gel. When the Kohlrausch discontinuity enters the separation gel, the increase in pH ionises the glycine molecules so that they move faster until the discontinuity disappear. The stacked proteins separate as they enter the second, higher sieving gel.

Depending on the molecular mass of the protein of interest, a 7, 10 or 12 % polyacrylamide gel was made in a gel sandwich formed using plates of size 16 x 10 cm with a spacer of 1 mm thick. The gel was prepared by mixing 30 % acrylamide, 10 % SDS, 10 % ammonium per sulphate (polymerising agent) (APS, 2.5 µg/ml), TEMED (N, N, N'-tetramethylethylenediamine, catalysing the polymerisation) (1 µg/ml), 1.5 M Tris-HCl (pH 8.8, all from Sigma-Aldrich) and water, for a final volume of 30 ml. The gel was

poured into the space between the assembled glass plates, over-layered with a layer of water-saturated isobutanol and allowed to polymerize. After two to three hours, isobutanol was washed off with distilled water.

After polymerisation, the 5% polyacrylamide stacking gel was prepared with 30 % acrylamide solution, 10 % SDS, 10 % APS (2.5 µg/ml), TEMED (1 µg/ml), 1.0 M Tris- HCl (pH 6.8) and water for a final volume of 10 ml. The mixture was poured on top of the separation gel, and a 10-, 15- or 20-well comb was inserted into gel. During the polymerisation time (one hour), 120-200 µg of protein were mixed with 30 µl of 5X Laemmli sample buffer (312.5 mM Tris, pH 8; 10 % SDS; 50 % glycerol; 25 % β-mercaptoethanol) and SDS 2% was added to a final volume of 150 µl. The molecular weight marker (mixture of standard proteins with known molecular masses, 5 µl, GEHealthcare) was mixed with 30 µl of 5X sample buffer and 115 µl of 2% SDS. The tubes were vortexed, boiled at 95°C for 5 min and centrifuged for 1 min. Once the gel was polymerised, the comb was carefully removed and the wells were washed quickly with H<sub>2</sub>O and running buffer in order to remove un-polymerised polyacrylamide. Samples were loaded and the gel was run in the Hoeffer SE 600 Ruby running tank unit (Amersham B10) overnight with a constant voltage of 55 V.

## **2.9 Immunoblotting**

The term “blotting” refers to the transfer of biological samples from a gel to a membrane and the subsequent detection of protein on the surface of the membrane, first introduced by H Towbin in 1979 (Towbin et al., 1979). Following separation, proteins were transferred onto a nitrocellulose membrane (Whatman 3 mm 46x57 cm) using the Hoefer TE62 Tank transfer unit (Amersham Biosciences UK Ltd.) according to manufacturer’s guidelines. Transfer was performed overnight at a constant current of 150 mA. Following transfer, nitrocellulose membranes were stained with Ponceau S to visualise proteins and thus determine whether the transfer was optimal. To remove Ponceau S staining, membranes were washed with deionised water and subsequently

washed with TBS (Tris Buffer Saline)/ Tween buffer (50 mM Tris, pH 7.5, 200 mM NaCl, and 0.05 % Tween-20). The membranes used in immunoblotting have a high affinity for proteins; therefore, after the transfer of the proteins from the gel, it is important to block the remaining surface of the membrane to prevent non-specific binding of the detection antibodies. Thus, the membranes were incubated in TBS-Tween with 1.5 % dry milk for 30 min at room temperature with agitation. The primary antibodies were diluted to the optimal concentration in the same buffer, added to the membranes and incubated overnight at 4°C with agitation. The membranes were washed twice quickly with agitation and twice for 10 min in TBS-Tween with 1.5 % dry milk in order to remove any exceeding unbound antibodies and to block the membranes before the addition of the secondary antibodies. The secondary antibodies coupled with either alkaline-phosphatase (AP) or horseradish peroxidase (HRP) (prepared in 5 ml of TBS-Tween with 1.5 % skim milk) were incubated with the membranes for 1 h at room temperature with agitation. The membranes were washed twice quickly and twice for 10 min in the same buffer, followed by washings with TBS/ 0.05 % Tween and subsequently washed with TBS for the same time.

If the secondary antibody was coupled to alkaline phosphatase, the proteins of interest were revealed by incubating the membrane with 5 ml of alkaline phosphatase buffer (1M Tris-HCl pH 9.5; 5M NaCl; 1M MgCl<sub>2</sub>; 1% Tween 20) containing 17.5 µl of BCIP (5-bromo-4-chloro-3'-indolyphosphate p toluidine salt) and 35 µl of NBT (Nitro-blue tetrazolium chloride, both from Sigma-Aldrich) which yields an intense, insoluble purple precipitate when reacted with alkaline phosphatase. The advantage of alkaline phosphatase reaction is that its rate remains linear allowing sensitivity to be improved by allowing the reaction to proceed for a longer time period. However, the increased reaction time leads to higher background and darker colour of the membrane.

The HRP reaction has a higher activity rate than AP, a good stability and wide availability of substrates. The immunoblots which were incubated with secondary antibodies coupled with HRP were incubated with the ultra-sensitive enhanced

chemiluminescent substrate (SuperSignal West Femto Chemiluminescent, Thermo Scientific). This type of substrate offers a signal that is a transient product of the enzyme HRP-substrate reaction and which persists only as long as the reaction is occurring. Thus, if the substrate is used up or the enzyme becomes inactive, the signal is lost. Therefore, the conditions were optimised so that the signal could last for a minimum of 8 hours. The images were taken using GeneGnomeXRQ, Syngene; a digital chemiluminescence imaging equipment.



# Chapter three

### **3. Expression and purification of N-terminal extracellular domains of GABA<sub>A</sub>R $\alpha$ 1 and $\alpha$ 2 subunits using Bac-to-Bac Baculovirus/ Sf9 cells expression system**

#### **3.1 Introduction**

Brain function is based on a balance between excitation and inhibition. In healthy brain, this balance is essential for all function activities, including representation of sensory information, cognitive processes such as decision making, sleep and motor control (Cline, 2005). During development, the balance between excitation and inhibition is at the core of the establishment of neuronal projections and synaptic wiring (Cline, 2005). An imbalance between excitation and inhibition underlies a large range of diseases such as autism (Mariner et al., 1986), Tourette's syndrome (Singer and Minzer, 2003), schizophrenia (Wassef et al., 2003) or epilepsy (Galanopoulou, 2010). In the central nervous system, inhibition is mostly mediated by GABAergic synapses. The main role of GABAergic synaptic transmission is to control neuronal excitability and to synchronize neuronal networks in order to generate oscillations that underlie cognitive processes (Ben-Ari et al., 2007). GABAergic synapses regulate probably every neuron in the central nervous system and coordinate major neuro-developmental processes (Tyagarajan and Fritschy, 2014). Via its action on GABA<sub>A</sub>Rs, GABA exerts a multitude of actions on developmental processes well before excitatory synapses are functional, playing an initial regulatory role in migration, cell growth and synapse formation in the immature brain (Ben-Ari et al., 2007). Thus, understanding how GABAergic synapses are formed is crucial for our understanding of brain development in health and disease. GABAergic synapses are characterised by presynaptic nerve terminals where GABA is synthesised, and postsynaptic elements expressing receptors for GABA. At the vast majority of synapses, GABA<sub>A</sub> receptors are accumulated or clustered at the postsynaptic membrane, closely apposing the presynaptic nerve terminals (Tretter et al., 2008). Sixteen subunits of GABA<sub>A</sub>Rs are encoded by different

genes grouped in seven different classes ( $\alpha_{1-6}$ ,  $\beta_{1-3}$ ,  $\gamma_{1-3}$ ,  $\delta$ ,  $\pi$ ,  $\epsilon$ , and  $\theta$ ). The heteropentameric structure of the receptor subunits is highly conserved (Unwin, 1993). At the synaptic contacts, GABA<sub>A</sub>Rs are composed of two  $\alpha$ , two  $\beta$  and one  $\gamma$  subunit. The significance of the GABA<sub>A</sub>Rs heterogeneity is still poorly understood but the evidence available suggests that GABA<sub>A</sub>R subtypes which are different in subunit composition, represent distinct entities with specific functions and pharmacological profiles, and with unique spatio-temporal mRNA and protein expression patterns during brain development (Fritschy and Panzanelli, 2014).

To investigate the role played by GABA<sub>A</sub>R subtypes during GABAergic synapse formation, we decided to focus our study on the most prominent and specifically distributed subunits in the embryonic and adult brain, the  $\alpha 1$  and  $\alpha 2$  subunits (Mohler et al., 2002). These two subunits endow GABA<sub>A</sub>Rs with different kinetic properties and localisation within the brain. Initially, the  $\alpha 2$  subunit is one of the most abundant subunits in the embryonic and perinatal brain. After the second postnatal week, the level of  $\alpha 2$  subunit starts to decrease (Fritschy et al., 1994). However, at the same time, the level of  $\alpha 1$  subunit mRNA increases until it becomes the most abundant GABA<sub>A</sub>R  $\alpha$  subunit in the adult brain (Laurie et al., 1992). This differential subunit expression pattern happens in parallel with the change in the functional outcome of GABA<sub>A</sub>Rs activation from depolarisation to hyperpolarisation. Thus understanding the structural role played specifically by these two subunits during the brain development is of crucial importance.

To study the role of  $\alpha 1$  and  $\alpha 2$  subunits of GABA<sub>A</sub>Rs during the establishment of the first synaptic contacts in the developing brain, we focused our experiments on the structural role played by the extracellular domains (ECDs) of each subunit. Each of the GABA<sub>A</sub>R subunits consists of a large (about 200 amino acids) extracellular N-terminal hydrophilic domain, followed by four transmembrane domains (TMs) with a large cytoplasmic-loop between TM3 and TM4, and a small extracellular C-terminal domain

(Sieghart et al., 1999). While the cytoplasmic loop of  $\alpha$  subunits is involved in intracellular protein-protein interactions, promoting clustering of GABA<sub>A</sub>Rs by gephyrin, and thus participating in the formation of functional synapses (Tretter et al., 2008, Mukherjee et al., 2011, Tretter et al., 2011), the role played by the ECD of the GABA<sub>A</sub>R subunits during the formation of GABAergic synapses is poorly understood. It has been recently demonstrated that GABA<sub>A</sub>Rs themselves can promote GABAergic synapse formation in a co-culture model of  $\alpha 1/\beta 2/\gamma 2$  stably transfected HEK 293 cells and GABAergic embryonic medium spiny neurones (Fuchs et al., 2013). This study provided the first evidence that GABA<sub>A</sub>Rs can be sufficient to initiate the formation of synaptic contacts. It is likely that, if the  $\alpha$  subunits were involved in the proper positioning of the pre and postsynaptic elements, this would be promoted by trans-synaptic interactions involving the ECDs which are the largest domains of these subunits exposed in the synaptic cleft.

To study the role of the  $\alpha 1$  and  $\alpha 2$  ECDs during GABAergic synapse formation, we decided to express and purify these domains from baculovirus/ Sf9 insect cells expression system. Because the  $\alpha 1$  and  $\alpha 2$  ECDs are known to be N-glycosylated proteins (Miller and Aricescu, 2014), the use of Sf9 cells in our experiments was crucial.

The first paper illustrating the use of the baculovirus *Autographa Californica* multiple nucleopolyhedrovirus (AcMNPV) to produce recombinant interferons in insect cells was published in 1983 (Smith et al., 1983). During the thirty years since this first publication, the baculovirus-based expression technology has been largely improved and is now used world-wide to produce a large range of proteins of scientific interest (van Oers et al., 2014). The Sf9 cells enable us to produce recombinant proteins on a very large scale and are well adapted for glycosylated proteins as their post-translational modification system have been engineered to produce N-glycans that are very similar to those in mammalian cells, thus providing an adequate glycosylation of

the proteins of interest (Breitbach and Jarvis, 2001). Previously, Sf9 cells were successfully used for the expression of GABA<sub>A</sub> and glycine receptors (Srinivasan et al., 1999, Elster et al., 2000, Cascio et al., 2001). Different truncated forms of the ECD of GABA<sub>A</sub>R  $\alpha$ 1 subunit were expressed in Sf9 cells in order to establish the structural role of the  $\alpha$ 1 subunit ECDs in the formation of the GABA binding site and the assembly of GABA<sub>A</sub>Rs (Srinivasan et al., 1999). In addition, a better understanding of the assembly of GABA<sub>A</sub>Rs was provided by experiments in which Sf9 cells were infected with  $\alpha$ 1/ $\beta$ 2/ $\gamma$ 2 subunits (Elster et al., 2000). Moreover, the expression and purification of the  $\alpha$ 1 glycine receptor from baculovirus infected cells was optimised and provided a better understanding of the structure of this receptor (Cascio et al., 2001). All together, these findings supported and confirmed the idea that the Sf9 cells expression system was the most suited system to purify the extracellular domains of GABA<sub>A</sub>R subunits  $\alpha$ 1 and  $\alpha$ 2.

### **3.1.1 Aims**

In this chapter the main aims of our research were:

1. To produce baculoviruses incorporating the DNA sequences of  $\alpha$ 1 and  $\alpha$ 2 ECD.
2. To optimise the infection of Sf9 cells with each baculovirus and the expression of the recombinant proteins.
3. To optimise the purification of the His-tagged- $\alpha$ 1 and - $\alpha$ 2 ECDs from infected Sf9 cells by affinity chromatography.

## 3.2 *Methods*

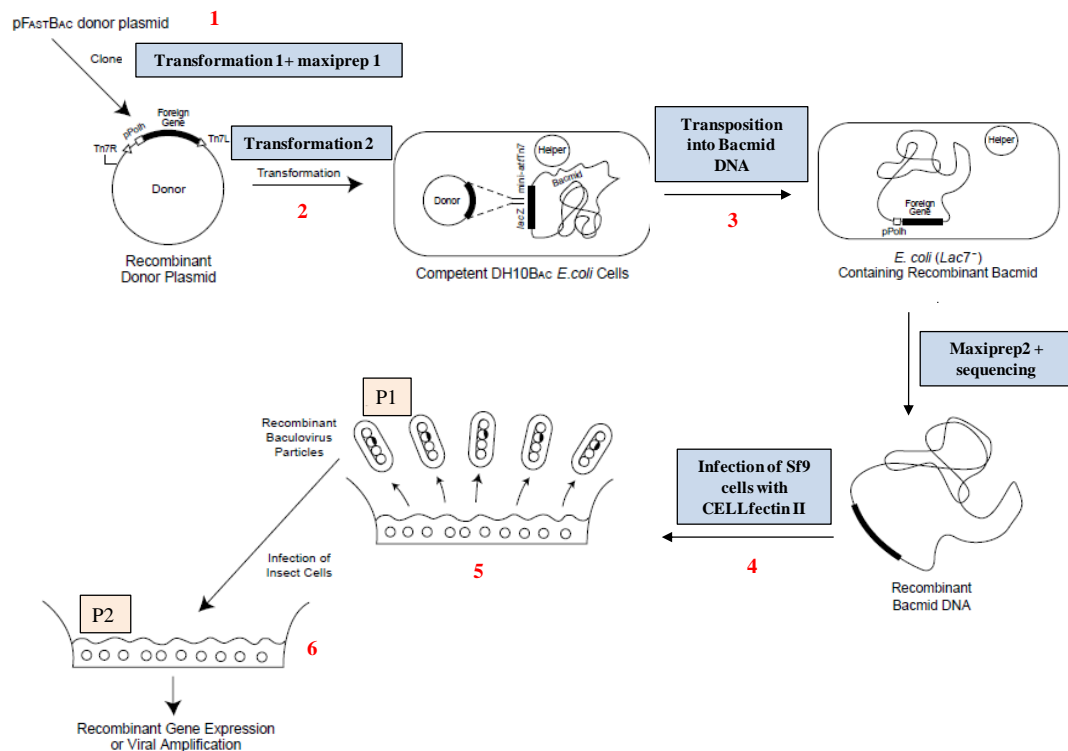
### 3.2.1 The Bac-To-Bac Expression System

The Bac-to-Bac Baculovirus Expression System is a rapid and efficient method to generate recombinant baculoviruses (Ciccarone et al., 1998) from infected Sf9 cells. This method is based on a site-specific transposition of an expression cassette (pFastBac CT-TOPO vector containing Tn7 transposon) into a baculovirus shuttle vector (bacmid) propagated in *E.Coli*. The Bac-to-Bac Baculovirus Expression System provides a pFastBac vector into which the DNA of interest can be cloned. In these experiments, the CT-TOPO pFastBac vector was used because it contains 6x Histidine-tag at the C-terminus end of the insertion site. Similarly to the other available vectors, the expression of the gene of interest is under the control of the *Autographa californica* multiple nuclear polyhedrosis virus, (AcMNPV) polyhedron ( $P_H$ ) promoter, which allows a high-level of expression in infected Sf9 cells. This expression cassette is flanked by two Tn7 sites, a gentamicin resistance gene and SV 40 polyadenylation signal to form a mini Tn7 (Figure 10).

The DH10Bac *E.Coli* strain into which the recombinant vector is transformed contains a baculovirus shuttle vector (Bacmid DNA) with a mini-*att*Tn7 target site and a helper plasmid. Once the pFastBac expression plasmid is transformed into DH10Bac *E.Coli* cells, transposition occurs between the miniTn7 present on the plasmid and the target mini-*att*Tn7 present on the bacmid DNA. The helper plasmid provides specific proteins that are required for the transposition to occur (Figure 10).

Once the recombinant Bacmid is isolated from DH10Bac *E.Coli* cells, it is transfected into Sf9 cells with the help of Cellfectin II Reagent to generate a recombinant baculovirus which will be used for preliminary experiments. First, the P1 viral stock is generated. This low titer viral stock (generally  $> 10^6$  plaque forming unit (pfu)/ ml) is used to infect another culture of Sf9 cells and amplify the viral stock. Post-P1 infection (48 h), the Sf9 cells secrete a large amount of viral particles: the high titer P2 viral stock (generally  $> 10^7$  pfu/ml) is generated,

collected and used to infect Sf9 cells from which recombinant proteins are extracted. Once the baculovirus stock is amplified, it is used to infect Sf9 cells at a larger scale and purify the Histidine-tagged proteins of interest (Figure 10).



**Figure 10. Generation of recombinant baculovirus using Bac-to-Bac Baculovirus Expression System. (1)** The sequence of interest is PCR-amplified and inserted into pFastBac/CT TOPO His vector. After transformation in One Shot Mach1 T1R *E.Coli*, antibiotic-resistant positive clones are selected and the recombinant pFastBac CT-TOPO plasmid is extracted from cells using the Qiagen Plasmid Maxi kit. **(2)** Then, the transposition of the recombinant DNA into Chemically competent DH10Bac *E.Coli* cells (containing the Bacmid DNA) is performed. **(3)** Recombinant DNAs is transposed into bacmid DNA and antibiotic selection is performed. The resistant clones are selected and purified using the Qiagen Plasmid Maxi kit. **(4)** Purified recombinant baculoviruses are transfected into Sf9 cells in combination with CellFectin II reagent (Invitrogen). **(5)** After infection, the cells secrete viral particles containing the recombinant bacmids: the P1 viral stock is generated and collected. **(6)** P1 viral stock is used to infect newly cultured Sf9 cells in order to have a higher titer viral stock (viral amplification/generation of P2). This figure was adapted from Bac-to-Bac Baculovirus Expression System User Guide 10359, Life Technologies.

### 3.2.2 Blunt-End TOPO cloning of $\alpha 1$ and $\alpha 2$ ECDs in pFastBac/CT TOPO His vector

#### 3.2.2.1 Primers design and PCR amplification of the $\alpha 1$ and $\alpha 2$ ECDs DNA sequences.

Primers were designed using the DNA sequence of  $\alpha 1$  and  $\alpha 2$  GABA<sub>A</sub>R subunits from *Mus Musculus*. The forward primers corresponded to the first thirty

nucleotides of the full-length  $\alpha 1$  or  $\alpha 2$  DNAs. The reverse primers were designed to correspond to the last thirty nucleotides before the first predicted transmembrane domain of each subunit. The complementary sequence of the last thirty nucleotides was determined and subsequently reversed in order to have the 5'-3' nucleotide sequence of the reverse primer. The melting temperature and GC-content of each primer were determined in order to check for their compatibility during future PCR experiments.

**Table 1. Sequence and characterisation of primers used to amplify  $\alpha 1$  and  $\alpha 2$  ECDs.** Two- or three- step PCR was carried out with each full-length sequence (originally in pRK5 vector).

	DNA Sequences 5'-3' (30nt)	T <sub>m</sub> (°C)	GC (%)
$\alpha 1$ -Forward primer	atgaagaaaagtcgggggtctctctgactat	46.67	78.58
$\alpha 1$ - Reverse primer	aaagtagccaattttctcttcaagtggaa	43.3	70.15
$\alpha 2$ - Forward primer	atgaagacaaaattgagcacatgcaatgtat	40	75.93
$\alpha 2$ -Reverse primer	cccaattttcttttcaagtggaaatgagc	33.3	68.84

**Table 2. PCR amplification of  $\alpha 1$  ECD: Reaction mix.**

	$\alpha 1$ ( $\mu$ l)	DNA template ( $\mu$ l)	No DNA control ( $\mu$ l)
DNA 100 ng	1	1	0
10x enhancer solution (1X final)	5	5	5
10x amplification buffer (1X final)	5	5	5
50 mM dNTPs (10 mM final)	0.5	0.5	0.5
50 mM MgSO <sub>4</sub> (1 mM final)	1	1	1
Primers (10 $\mu$ M final)	1.5	1	1.5
Platinum <i>pfx</i> DNA polymerase (1 unit)	0.5	0.5	0.5
H <sub>2</sub> O	35	35	36

**Table 3. PCR of  $\alpha 1$  ECD: Thermal cycle parameters**

	Time (min)	Temperature (°C)
Initial denaturation	2	94
denaturation	15 sec	94
Annealing	0	0
Extension	1	68
Final Extension	10	72
35 cycles		



**Table 4. PCR amplification of  $\alpha 2$  ECD: Reaction mix.**

	$\alpha 2$ ( $\mu$ l)	DNA template ( $\mu$ l)	No DNA control ( $\mu$ l)
DNA 100 ng	1	1	0
10x amplification buffer (1X final)	5	5	5
50 mM dNTPs (10 mM final)	0.5	0.5	0.5
50 mM MgSO <sub>4</sub> (1mM final)	1	1	1
Primers (10 $\mu$ M final)	1	1	1
Platinum <i>pfx</i> DNA polymerase (1 unit)	1	1	1
H <sub>2</sub> O	40.5	40.5	41.5

**Table 5. PCR of  $\alpha 2$  ECD: Thermal cycle parameters**

	Time (min)	Temperature ( $^{\circ}$ C)
Initial Denaturation	2	94
Denaturation	1	94
Annealing	1	55
Extension	1	72
Final Extension	10	72
25 cycles		

The amplified products were analysed by agarose gel electrophoresis (1.2 %) in the presence of Ethidium Bromide and visualised under the UV light.

### 3.2.2.2 *Gel extraction of DNA from agarose gel*

The bands were cut out from the gel and weighted. Three volumes of gel solubilisation buffer (L3) for every volume of gel were mixed and heated up to 50 $^{\circ}$ C for 15 min. Once DNA was dissolved, it was transferred into filtered column and spun down at 14,000 g for 1 min. The DNA remaining in the filter was washed one time with washing buffer (W1). After spinning, flow-through was discarded and the tube was spun again for 3 min to remove any residual EtOH from the column. Then, DNA was eluted with elution buffer and stored at 4 $^{\circ}$ C for short term storage or aliquoted and stored at -20 $^{\circ}$ C for longer term storage.

### 3.2.2.3 *Blunt-end TOPO Cloning in pFastBac CT-Topo His vector*

TOPO cloning was set up as described in the table below (in a final volume of 6  $\mu$ l). Insert-to-vector ratio of 1:1 was recommended. The reaction was gently mixed and after 5 min at the room temperature (22-23°C), the mixture was placed on ice.

**Table 6. Blunt-End TOPO Cloning of the amplified DNAs into pFastBac CT-TOPO vector.**

Reagent	Vector only (negative control) ( $\mu$ l)	Vector +PCR Insert ( $\mu$ l)	Vector +DNA template (positive control) ( $\mu$ l)
Control PCR Product	0	1	1
Sterile Water	4	3	3
Salt Solution	1	1	1
pFastBac/ CT-TOPO	1	1	1

### 3.2.2.4 *Transformation in One Shot Mach1<sup>TM</sup> T1<sup>R</sup> Chemically Competent E.Coli*

Each cloning reaction (2  $\mu$ l) was added to the chemically competent *E.Coli* and mixed gently. The pUC19 plasmid DNA (2  $\mu$ l), provided by Invitrogen, was used as a positive control for the transformation. The vials were incubated on ice for 30 min, heat-shocked for 30 sec at 42°C in water bath, and then placed on ice for 2 min. After adding 250  $\mu$ l of warm super optimal broth with catabolite repression (S.O.C medium), the vials were placed at 37°C in a shaking incubator (225 g) for 1 h. For each transformation reaction, 25  $\mu$ l or 100  $\mu$ l was spread onto the pre-warmed agar plates containing ampicillin (100  $\mu$ g/ $\mu$ l). In order to control the transformation efficiency, 10  $\mu$ l of the pUC19 transformation was spread on plates as recommended. All the plates were then incubated upside-down at 37°C over-night. After 24 h, 10 colonies of each transformation were picked and analysed.

### 3.2.2.5 *Miniprep protocol: purification of DNA using QIAprep Spin Miniprep Kit (QIAGEN)*

The 10 ampicillin-resistant clones were selected and amplified in a 4 ml suspension of lysogeny broth medium (LB medium) with 100  $\mu$ g/ $\mu$ l of ampicillin over-

night in a shaking incubator at 37°C. The DNAs were extracted from the suspension bacterial culture and purified using Miniprep kit from QIAGEN following the protocol provided with this kit.

#### 3.2.2.5.1 Analysis of positives clones

The concentration of purified DNA was measured using nanodrop (Thermoscientific) and DNA was loaded on a 1.2 % agarose gel to check purity and quality of DNA. In order to confirm the insertion of DNA fragments and their orientation, two PCR reactions were performed for each sample using the Phusion PCR Master Mix (Finnzymes). The first PCR reaction was carried out using the polyhedrin forward and SV40 reverse primers which bind to small sequences in the vector flanking the sequence of interest (data not shown). The second PCR reaction was carried out using the forward primer overlapping with the first 30 bp of  $\alpha 1$  or  $\alpha 2$  and the SV40 reverse primer (Figure 17). Analysis of this PCR product was carried out by agarose gel electrophoresis. Positive clones were confirmed by sequencing.

#### 3.2.2.5.2 Extraction and purification of pFastBac CT-TOPO His vectors containing the $\alpha 1$ or $\alpha 2$ ECD sequences.

From each transformation, two positive clones were inoculated in 200 ml of LB medium with 100  $\mu\text{g}/\mu\text{l}$  of ampicillin in a shaking incubator at 37°C overnight. The culture was centrifuged at 5000 g for 10 min at 4°C. The supernatant was removed and pellets were frozen for 1-2 h at -20°C. A Maxiprep was performed using GenElute HP Plasmid Maxiprep kit (Sigma-Aldrich) following the protocol provided with the kit. The DNA concentration was measured with a nanodrop (Nanodrop 1000 spectrophotometer, Thermo Scientific).

#### 3.2.2.6 *Transposition of $\alpha 1$ and $\alpha 2$ ECDs into DH10Bac E.Coli*

##### 3.2.2.6.1 Transformation of $\alpha 1$ and $\alpha 2$ recombinant pFastBac CT-TOPO plasmids into MAX Efficiency<sup>R</sup> DH10Bac<sup>TM</sup> Chemically Competent *E.Coli*

LB agar plates containing 50 µg/ml of kanamycin, 7 µg/ml of gentamicin, 10 µg/ml of tetracycline, 100 µg/ml of Bluo-gal and 40 µg/ml of IPTG were prepared in advance. For each transposition, one vial of MAX Efficiency<sup>R</sup> DH10Bac<sup>TM</sup> Chemically Competent *E.Coli* cells was thawed on ice. Once defrosted, 100 µL of the cells were transferred into pre-chilled 15 ml tubes and 1 ng of α1- or α2-containing CT-TOPO pFastBac plasmids, or 50 pg of pUC19 were incorporated onto the cells, respectively. As a positive control for the future Sf9 cells infection, 1 ng of pFastBac Gus plasmid (provided by Invitrogen) was also transformed into *E.Coli* cells. The bacterial cells were incubated on ice for 30 min and heat-shocked for 45 sec at 42°C in a water bath without agitation. The tubes were immediately transferred to ice for 2 min and 900 µl of room temperature S.O.C medium was added to the cells. Each transformation was shaken at 37°C at 225 g for 4 h and the pUC19 transformation at 225 g for 1 h. After incubation, three different dilutions ( $10^{-1}$ ,  $10^{-2}$ , and  $10^{-3}$ ) of each transformation were plated onto previously prepared agar plates. The pUC19 transformation reaction was plated onto agar plates containing 100 µg/ml of ampicillin. The plates were incubated upside-down for 48-72 h at 37°C.

#### 3.2.2.6.2 Isolation of recombinant Bacmid DNAs

The bacmid DNA confers a resistance to kanamycin. The insertion of the mini-Tn7 into mini-attTn7 cassette on the bacmid disrupts the expression of LacZα peptide, so colonies containing the recombinant bacmid are white. After incubation, blue/white screening was done. Only “truly-white” colonies were picked and re-streaked onto new plates (containing 50 µg/ml of kanamycin, 7 µg/ml of gentamicin, 10 µg/ml of tetracycline, 100 µg/ml of bluo-gal and 40 µg/ml of IPTG) and incubated for 24 h at 37°C. All the colonies that had been confirmed to have a white phenotype were inoculated into a 2 ml LB medium culture containing 50 µg/ml of kanamycin, 7 µg/ml of gentamicin, 10 µg/ml of tetracycline in a shaker incubator (250 g) overnight at 37°C.

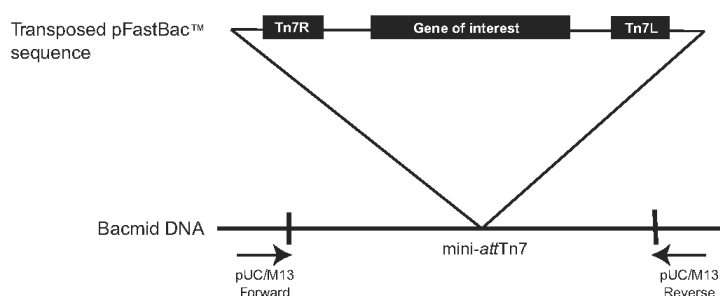
#### 3.2.2.6.3 Miniprep on recombinant Bacmid DNA

In order to isolate the recombinant Bacmid DNA from MAX Efficiency<sup>R</sup> DH10Bac<sup>TM</sup> Chemically Competent *E.Coli* cells, miniprep was performed following the PureLink<sup>TM</sup> HiPure Plasmid DNA Miniprep Kit protocol (Invitrogen). DNA is re-suspended in 40  $\mu$ l of TE buffer, and placed on ice until DNA is completely dissolved. Low concentrated Bacmids were aliquoted and kept at -20°C.

#### 3.2.2.6.4 Analysis of positive clones

Analysis of positive clones containing  $\alpha$ 1 or  $\alpha$ 2 sequence was done using PCR.

Reaction mixture and conditions for amplification are included in Table 7 and 8.



**Figure 11. Analysis of recombinant bacmid by PCR.**

Figure adapted from the Bac-to-Bac Baculovirus Expression System User Guide 10359, Life Technologies. Recombinant bacmid DNA is greater than 135 kb in size which interferes with a reliable detection of the insert. It is therefore recommended to perform PCR instead in order to verify the presence and orientation of the inserts into bacmid DNAs by using different combinations of primers. Puc/M13 forward and reverse primers were used in the first place to confirm the presence of the insert into the bacmid DNA.

**Table 7. PCR amplification of recombinant bacmid DNAs: reaction mix 1.**

	$\alpha$ 1 or $\alpha$ 2 ( $\mu$ l)	Gus control ( $\mu$ l)	No DNA (-) Control ( $\mu$ l)
DNA 100 ng	10	10	0
10x PCR buffer (1X final)	5	5	5
50 mM MgCl <sub>2</sub>	1.5	1.5	1.5
10 mM dNTPs (10 $\mu$ M final)	1	1	1
Primers pUC / M13 forward and reverse (10 $\mu$ M final)	1.25	1.25	1.25
Platinum <i>Taq</i> DNA polymerase	0.5	0.5	0.5
H <sub>2</sub> O	30.75	30.75	30.75

**Table 8. PCR of recombinant bacmid DNAs: Thermal cycle parameters 1.**

	Time (min)	Temperature (°C)
Initial Denaturation	3	94
Denaturation	45sec	94
Annealing	45sec	55
Extension	5	72
Final Extension	7	72
30 cycles		

In order to check if  $\alpha 1$  and  $\alpha 2$  ECDs were inserted in the right orientation in selected clones, another PCR was performed using the corresponding specific forward primers and the pUC / M13 reverse primer (Figure 11) as shown in Tables 9 and 10.

**Table 9. PCR amplification of recombinant bacmid DNAs: reaction mix 2**

	$\alpha 1$ or $\alpha 2$ ( $\mu$ l)	Gus control ( $\mu$ l)	No DNA (-) control( $\mu$ l)
DNA 100 ng	10	1	0
10x PCR buffer (1X final)	5	5	5
50 mM MgCl <sub>2</sub>	1.5	1.5	1.5
10 mM dNTPs (20 $\mu$ M final)	1	1	1
$\alpha 1$ or $\alpha 2$ forward, and pUC/ M13 reverse (10 $\mu$ M final)	1.75	1.75	1.75
Platinum <i>Taq</i> DNA polymerase	0.5	0.5	0.5
Sterile water	28.5	28.5	28.5

**Table 10. PCR of recombinant bacmid DNAs: Thermal cycle parameters 2**

	Time (min)	Temperature (°C)
Initial Denaturation	3	94
Denaturation	45 sec	94
Annealing	45 sec	55
Extension	5	72
Final Extension	7	72
30 cycles		

Once the orientation was confirmed, the DNA was extracted from agarose gel slices and the eluted DNA was analysed by sequencing using a UCL Sequencing Facility (<http://www.ucl.ac.uk/stemcells/infrastructure>). Once the sequence of each clone was confirmed, DNA was isolated using the PureLink™ HiPure Plasmid DNA Maxiprep Kit protocol (Invitrogen), specifically adapted for DNA Bacmid isolation.

Highly concentrated bacmids were aliquoted and kept at -20°C for future Sf9 cells-infection experiments.

### **3.2.3 Sf9 cell culture**

#### *3.2.3.1 Suspension culture*

Sf9 cells were isolated from the parental *Spodoptera Frugiperda* cell line IPLB-Sf21-AE. They were adapted to suspension growth in Sf-900 II SFM (Serum Free Medium, Gibco). The cells were supplied by Invitrogen in a cryogenic vial containing  $1.5 \times 10^7$  viable cells. The pellets were rapidly defrosted in a 37°C water bath added to 125 ml shake flask containing 27 ml of pre warmed Sf-900 II SFM. The loosen cap flask was then placed in a  $28 \pm 0.5^\circ\text{C}$  non-humidified, ambient air-regulated incubator on an orbital shaker platform rotating at 130 rotation per min (g). The cells were split for the first time when they reached the density of  $2 \times 10^6$  cells/ml. The density of cells was determined by Trypan blue exclusion method. Briefly, 10  $\mu\text{l}$  of suspension was taken out and added to a micro centrifuge tube. Trypan blue (10  $\mu\text{l}$ ) and medium (1/4 dilution) were added to the cells. The mixture was loaded onto a haemocytometer chamber. The total density of cells contained in the flask was determined using the formula: Density of cells  $\times 4 \times 1.1 = \times 10^4$  cells/ml. The viability of the culture was calculated using the following formula: Viability =  $(1 - (\text{density of dead cells} / \text{total density of cells})) \times 100$ . After two weeks in culture, the viability of cells was over 90 % and the cells were ready to be split at  $5 \times 10^5$  cells/ml by diluting them in pre-warmed Sf-900 II SFM (27°C). If cells were kept in mid-log growth (logarithmic phase), the density of cells was doubled every 24-30 hours. To reduce the accumulation of cell debris and metabolic waste by-products in shaker culture, the cells were gently spun down (100 g for 10 min) once every three weeks and the pellet re-suspended in fresh medium.

#### *3.2.4 Adherent cultures*

SF9 cells were also grown in adherent cultures. To initiate an adherent culture from frozen vial ( $1 \times 10^7$  cells), cells were thawed in a pre-warmed T-25  $\text{cm}^2$  flask

containing 4 ml of Sf-900 II SFM. After 30 min in the incubator, cells were attached. Medium containing DMSO was removed and replaced by 5 ml of fresh Sf-900 II SFM. After 24 h, the medium was changed and viability of cells estimated. When cells reach confluency (> 80 %), they were sub-cultured by sloughing them with a Pasteur pipette. Cells were counted and added to a new flask with a required density.

### **3.2.5 Generating P1 and P2 viral stocks from transfected Sf9 cells**

#### *3.2.5.1 Transfection procedure: cationic liposome-mediated transfection using Cellfectin II® Reagent*

Before they were infected, cells were healthy, at low passage (P8-12) and the viability was over 95 %. In a 6 well dish containing 2 ml of pre-warmed Sf-900 II SFM,  $9 \times 10^5$  cells/ml were plated and placed at 28°C for 1 h. During this time, the transfection mixture was prepared by adding 2 µg of recombinant bacmid DNA into 100 µL of Sf-900 II SFM medium. In another tube, 8 µl of Cellfectin II Reagent were diluted in 100 µL of Sf-900 II SFM. The Cellfectin II solution was added to the bacmid DNA solution, mixed gently and incubated at room temperature for 15 min. While the lipid/DNA complexes were forming, the Sf9 cells were washed once with 2 ml of Sf-900 II SFM. Then, 0.8 ml of Sf-900 II SFM was added to each tube containing Cellfectin II and bacmid DNA and mixed gently. The Sf-900 II SFM was removed from all the wells and replaced with 500 µl of the mixture containing Cellfectin and bacmid DNA. After 5 h at 28°C, the transfection mixture was removed, 2 ml of fresh Sf-900 II SFM were added and the cells were incubated for 72 h. To avoid the drying of wells, 2 ml of fresh Sf-900 II SFM were added again 48 h post infection.

#### *3.2.5.2 Harvesting P1 viral stock and cell lysis for immunoblot analysis*

Following 72 h of incubation, the medium containing viral particles was carefully removed, centrifuged 6 min at 500 g and filter-sterilized with a 0.22 µm filter. It was kept at 4°C and protected from light. The cells were washed in 2 ml of PBS, harvested and lysed with 200 µl of 2 % SDS. The cell lysate was collected; the samples were



boiled for 10 min at 95°C, sonicated for 15 sec and frozen at -20°C for future analysis of protein expression by SDS/PAGE and Immunoblotting.

#### 3.2.5.3 *SDS/PAGE and Immunoblotting*

Expression of proteins was analysed by SDS/PAGE and immunoblotting as described in the Experimental Procedure Chapter, Section 2.8. Once transferred onto the nitrocellulose membrane, the proteins were incubated with the 6xHis-tag-, the  $\alpha 1$ - or  $\alpha 2$ - specific antibodies (Table 11) in 1.5 % milk-TBS-Tween overnight at 4°C. After washing, the proteins were revealed using an alkaline phosphatase conjugated secondary antibody, and BCIP/NBT colour reaction.

#### 3.2.5.4 *Generating P2: Amplification of the viral stock*

In order to get a viral stock with a higher titre, the P1 viral stock was used to re-infect cells. The Multiplicity of Infection (MOI) was estimated as MOI= 0.1.

The following formula was used to calculate how much P1 viral stock should be added to the cells:

$$\text{Inoculums required (ml)} = \frac{\text{MOI (pfu/ cell)} \times \text{density of cells}}{\text{Titre of viral stock (pfu/ ml)}}$$

The titre of P1 was assumed to be  $1 \times 10^6$  plaque forming unit (pfu)/ml (low titre). Sf9 cells were plated at the density of  $2 \times 10^6$  cells/ml into 6 well dish, and incubated at 28°C for 1 h to allow attachment. The appropriate amount of P1 viral stock was added and cells were incubated for 48 h. Then, the media was collected, spun down and filter-sterilized and the cells were harvested and lysed in 2 % SDS for further analysis of protein expression by SDS/PAGE and Immunoblotting.

**Table 11. Antibodies used for immunoblotting analysis of  $\alpha 1$  and  $\alpha 2$  ECD expression in Sf9 cells.**

primary antibodies				secondary antibodies		
Specificity	Origin	Dilutions	Source and Characterisation	Specificity (AP)	Dilutions	Source
GABA <sub>A</sub> $\alpha 1$	Rabbit	1:500	(Duggan and Stephenson, 1990)	Goat anti-rabbit	1: 5000	ThermoScientific 31340
GABA <sub>A</sub> $\alpha 2$	Rabbit	2 $\mu$ g/ ml	(Mhatre et al., 1993)	Goat anti-rabbit	1: 5000	Same as above
6xHis-tag	Mouse	1: 1000	Abgent AM1010a	Rabbit anti-mouse	1: 2500	Pierce Biotechnology 31329

### 3.2.6 Partial purification of $\alpha 1$ and $\alpha 2$ ECDs under native conditions using Tris-HCl buffer and Probond Resin

Sf9 cells in suspension culture (40 ml) were infected with  $\alpha 1$  and  $\alpha 2$  P2-viral stocks with an MOI of 2, and incubated for 72 h at room temperature. Cells were spun down at 800 g for 10 min, and pellets were resuspended in 1 ml of Tris-HCl buffer (20 mM Tris pH 7.5, 300 mM NaCl, 1 % NP40, Protease inhibitors cocktail (containing antipain, PMSF, chemostatin, leupeptin, pepstatin A, all at 5  $\mu$ g/ $\mu$ l, ThermoScientific)). Then, the cells were lysed by three freeze/thaw cycles and sonicated on ice for 40 sec. Solubilisation was carried out for 45 min on ice with gentle agitation. Cell lysates were spun down at 3000 g for 15 min at 4°C. The collected supernatant was carefully removed from the pellet. Small fractions of lysates were collected at each of these steps and analysed by SDS/PAGE and immunoblotting.

The ProBond resin is a sepharose resin that is coupled with iminodiacetic acid groups (IDA). IDA is loaded with Ni<sup>2+</sup> ions and binds Ni<sup>2+</sup> by three coordination sites. Beads were obtained in 20 % ethanol and 50 % slurry from Invitrogen. Beads were prepared by pipetting 1 ml of the resuspended resin into one eppendorf tube per affinity chromatography. After the beads were centrifuged at 800 g for 1 min, the supernatant was removed and 1 ml of sterilised deionised water was added to wash the beads. The beads were re-suspended in water and centrifuged at 800 g for 1 min at 4°C. The same

procedure was repeated twice with Tris-HCl buffer (1 ml). Once the buffer was removed, 500 µl of Tris-HCl buffer was added to the beads to reach 50/50 slurry.

The capacity of Ni<sup>2+</sup> column was between 1-5 mg of histidine-tagged protein for 1 ml of resin. Considering that approximately 10-20 % of the total yield of protein collected represented the protein of interest, all the collected supernatant from infected Sf9 cells was added to 1 ml of beads. The binding was done at 4°C with rotation for 1.5 h. The columns were spun down at 800 g for 1 min, supernatant was collected and 1 ml of Tris-HCl buffer was added to the beads. After quick vortex, the mixture was spun down and the supernatant was collected. This washing step was repeated 5 times.

The following day, 500 µl of the elution buffer (Tris-HCl buffer containing 250 mM Imidazole, pH 8.0) was added to the beads. After 10 min of incubation, beads were spun down at 800 g and the supernatant was collected. Elution step was repeated 6 times. In order to remove Imidazole, all the collected elution fractions were pulled together and dialysed overnight at 4°C against PBS. After dialysis, the sample concentration was measured by BCA assay, and proteins were snap-frozen in the liquid nitrogen and stored at -20°C. Samples of 100 µl were collected at each step of the protein purifications and analysed by SDS/ PAGE and immunoblotting.

### **3.2.7 Partial purification of α1 and α2 ECDs under native conditions using NaH<sub>2</sub>PO<sub>4</sub> based buffers and Ni-NTA Resin**

Sf9 cells in suspension culture (100 ml) were infected with α1- or α2- P2 viral stocks with an MOI of 2, and incubated for 72 h at room temperature. Cells were split into two 50 ml tubes and spun down at 800 g, for 10 min and pellets were washed in 1x PBS in order to remove any compounds from the growth medium that could interfere with the binding to the nickel beads. Pellets were resuspended in 3 ml of hypotonic lysis buffer (20 mM NaH<sub>2</sub>PO<sub>4</sub> pH 8.0, 0.5 % NP-40, Protease inhibitors cocktail 5 µg/µl) followed by three freeze/thaw cycles and sonication for 30 sec on ice. The lysates were split into two tubes and rotated for 30 min at 4°C to complete cell lysis. Cell lysates

were spun down at 3000 g for 15 min at 4°C. The collected supernatant was carefully removed from the pellet and snap-frozen with liquid nitrogen. The proteins contained in the pellet were resuspended in the solubilisation buffer (50 mM NaH<sub>2</sub>PO<sub>4</sub> pH 8.0, 150 mM NaCl, 2 % NP-40, 1 % DOC, and protease inhibitors cocktail 5 µg/µl) and pulled back together. Once resuspended, proteins were homogenised using a sintered-glass homogeniser with which 4 to 5 strokes were done on ice, in order to avoid degradation. Subsequently, proteins were solubilised on a rotating plate for 1.5 h at 4°C and spun down at 3000 g for 15 min at 4°C. The collected supernatant was dialysed overnight in dialysis buffer (50 mM NaH<sub>2</sub>PO<sub>4</sub> pH 8.0, 300 mM NaCl, 1 % Triton X-100).

The following day, the proteins were collected and the protein concentrations were measured using the Bradford Assay. Glycerol (20 % final) was added to 1 mg of proteins, and they were added to the prepared beads. Ni-NTA agarose uses nitrilotriacetic acid (NTA), a tetradentate chelating ligand, in a highly cross-linked 6 % agarose matrix. NTA binds Ni<sup>2+</sup> ion by four coordination sites. Therefore, NTA resin minimizes leaching of the metal from the solid support (resin) and allows for more stringent purification conditions than ProBond. Beads were prepared by pipetting 800 µl of resuspended beads (50/50 slurry) into one eppendorf tube per affinity chromatography. After they were spun down at 1000 g for 4 min, 400 µl of water were added in order to wash beads. The procedure was repeated one more time. Then, 400 µl of binding buffer (dialysis buffer containing 20 % glycerol) were added to the eppendorf tube which was gently inverted and spun down at 1000 g for 4 min. The procedure was repeated one more time. The supernatant was removed and 1 mg of extracted proteins was added to the beads to bind overnight at 4°C. The following day, the columns were spun down at 800 g for 2 min and the supernatant after binding was removed. The beads were washed two times in the binding buffer for 5 min with rotation. Then, they were washed three more time in the binding buffer which does not contain Triton X-100 for 10 min with rotation. Finally, the proteins were eluted with the elution buffer (binding buffer containing 100 mM EDTA pH 6.0; 250 mM Imidazole, and

with protease inhibitors) by incubating on the rotating plate overnight at room temperature.

The next day, the columns were spun down at 800 g for 2 min and incubated with elution buffer two more times for 10 min with rotation. The elution fractions were then dialysed overnight against PBS containing 300 mM NaCl and the concentration of proteins was measured the day after with the Bradford assay. The proteins were aliquoted and snap-frozen. At each step, samples of 100  $\mu$ l were lysed with SDS, and kept at -20°C for the analysis of the protein purification by SDS/PAGE and immunoblotting as described in the Chapter 2, Sections 2.8-2.9.

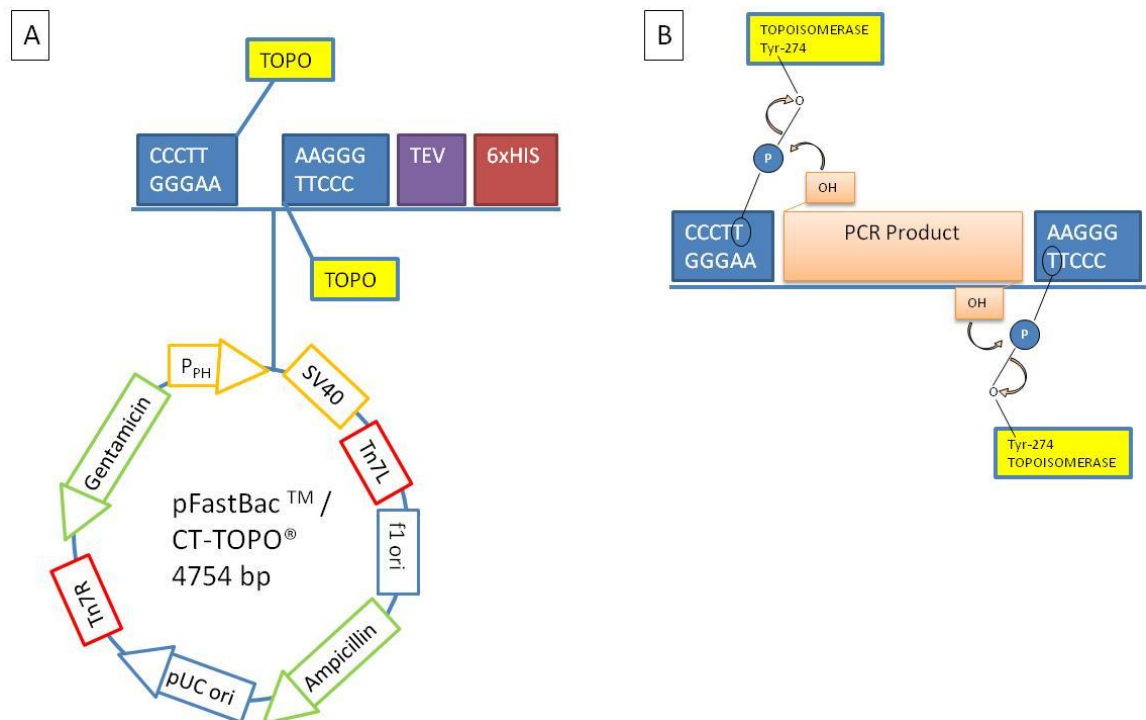
### **3.3 Results**

We used a commercially available Bac-To-Bac Expression System (Life Technologies, Invitrogen) to generate recombinant baculovirus strains expressing the large N-terminal Extracellular domains (ECDs) of GABA<sub>A</sub>R  $\alpha$ 1 or  $\alpha$ 2 subunits. The procedure included the preparation of the recombinant bacmid DNA, followed by the preparation of the recombinant baculovirus stocks. The recombinant baculoviruses with  $\alpha$ 1 or  $\alpha$ 2 ECD were used to infect the Sf9 cells and test the expression of the proteins. Finally  $\alpha$ 1 and  $\alpha$ 2 ECDs were partially purified from infected Sf9 cells.

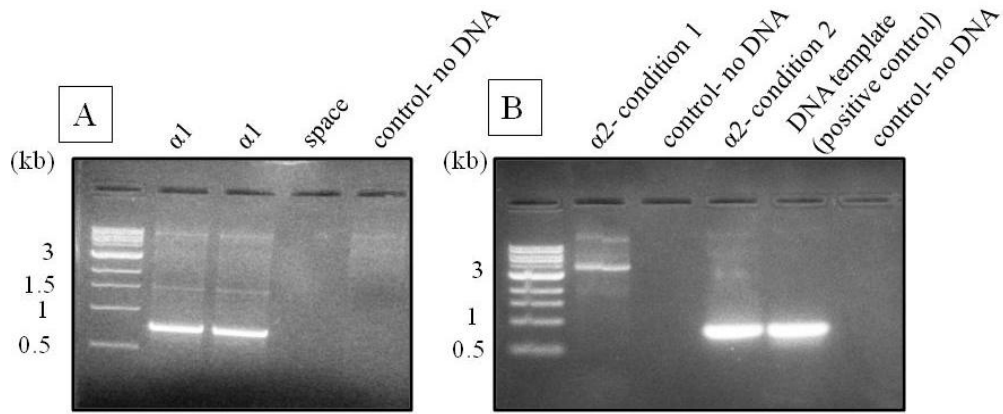
#### **3.3.1 Insertion of DNA sequence of $\alpha$ 1 or $\alpha$ 2 N-terminal ECD into Baculoviruses.**

The initial step included preparation of the recombinant pFastBac constructs containing the sequence encoding the initial 223 N-terminal amino acids of the  $\alpha$ 1 and  $\alpha$ 2 subunits terminating at the start of the predicted first transmembrane domain. Cloning into the pFastBac CT-TOPO vector required blunt end PCR products which were obtained using PCR amplification of these sequences from pRK5 expression constructs in the presence of the appropriate primers and Platinum Pfx DNA polymerase. As shown in the Figure 12, the blunt-end TOPO cloning is based on the

use of the linearised cloning vector with *Vaccinia* topoisomerase I covalently bound to the 3' end of the each DNA strand. The presence of topoisomerase I facilitates the insertion of the blunt-end sequence into the vector. PCR products were obtained using a three-step PCR procedure (condition 1) for  $\alpha 1$  and a two-step (condition 2) for  $\alpha 2$  constructs. As expected,  $\alpha 1$  PCR product contained approximately 756 base pairs and  $\alpha 2$  approximately 753 base pairs (Figure 13). A positive control for the three-step PCR procedure used for generation of the blunt-end  $\alpha 2$  PCR product was provided by the Invitrogen kit.



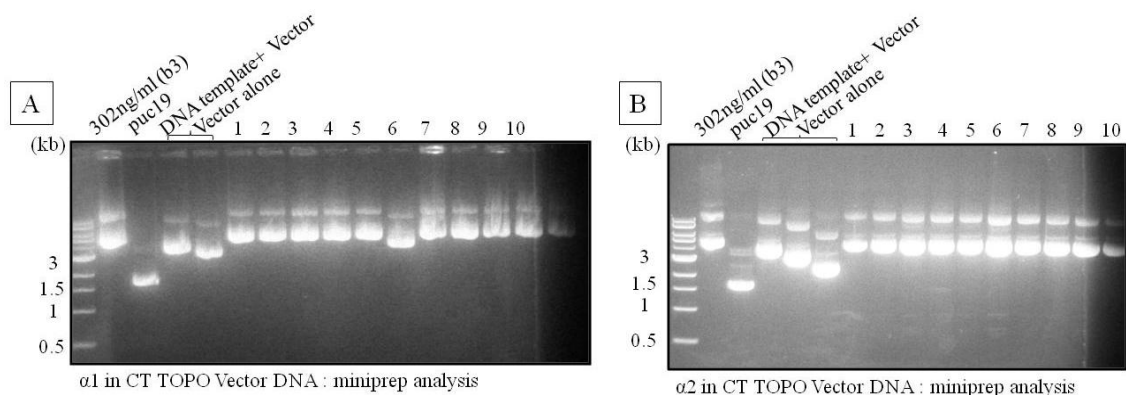
**Figure 12. The pFastBac CT-TOPO His vector and the TOPO-cloning.** Figure adapted from the Bac-to-Bac Baculovirus Expression System User Guide 10359, Life Technologies. **A.** The expression of the gene of interest is controlled by the Polyhedrin promoter ( $P_{PH}$ ) for high-level expression in Sf9 cells. This expression cassette is flanked by the left and right arms of Tn7 (Tn7L and Tn7R). It also contains a gentamicin and ampicilline resistance genes. In addition, it contains an SV40 polyadenylation signal to form a mini Tn7. The pFastBac CT-TOPO His vector contains six histidines on 3' of the insertion site. The Tobacco Etch Virus (TEV) recognition site allows removal of the 6xHistag if needed. DNAs of  $\alpha 1$  and  $\alpha 2$  ECDs were inserted into the vector by TOPO cloning by the topoisomerases bound to the vector DNA sequence. **B.** Topoisomerase I from *Vaccinia* virus is bound to DNA at specific sites in order to cleave the phosphodiester backbone after 5' -CCCTT in one strand of DNA. The released energy allows the DNA of interest to be inserted into the vector.



**Figure 13. Blunt end PCR products of the  $\alpha 1$  and  $\alpha 2$  ECDs.** **A.** The  $\alpha 1$  PCR product was 756 bp. Only one PCR condition (3 steps PCR) was sufficient to amplify the  $\alpha 1$  product. **B.** The  $\alpha 2$  PCR product was 753 bp. Two conditions of PCR were tested for the  $\alpha 2$  insert. The first condition was the same as the one used for  $\alpha 1$  (three steps PCR) and the second condition was a two-step PCR. The first condition did not give any amplification of  $\alpha 2$  sequence. The control PCR product (750 bp, DNA template only tested with  $\alpha 2$ ) was amplified with a two-step PCR.

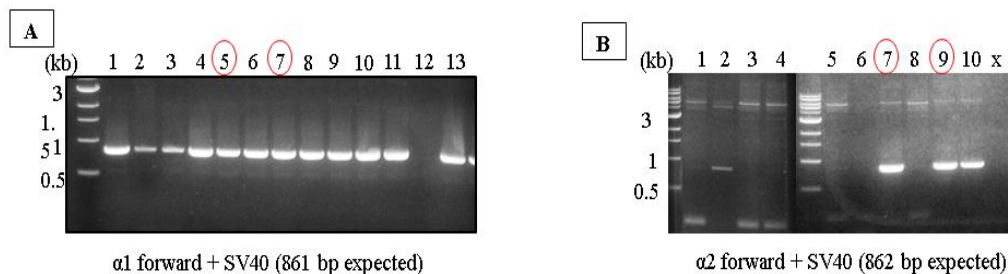
PCR products ( $\alpha 1$ ,  $\alpha 2$  and control) were gel-purified and cloned into a pFastBac CT-TOPO vector which contains a sequence of six histidines at the 3' end of the inserted sequence (Figure 12). This was followed by the transformation of One Shot Mach1 T1 Chemically competent *E.coli*. Then, positive clones (from 10-16 clones) were selected and DNA isolated using PureLink HiPure Mini Plasmid Purification Kit.

Isolated DNA was analysed using agarose gel electrophoresis as shown in the Figure 14. A small difference in size was observed between DNA isolated from different colonies (~ 5 kb) and the DNA template, the empty vector (4754 bp) and pUC19.



**Figure 14. Analysis of the  $\alpha 1$  and  $\alpha 2$  CT-TOPO constructs isolated from positive clones after transformation in Mach1 *E.Coli*.** **A. and B.** The bands above 3 kb correspond to the DNA extracted from positive clones. The first lane corresponds to the  $\beta 3$  subunit DNA used as a control. The second lane (pUC19) is the miniprep of the control of transformation; the third lane is the control of PCR (DNA template). The fourth lane is the DNA extracted from bacteria transformed with an empty vector. Other lanes represent the DNA of 10 clones transformed with  $\alpha 1$  (**A**) or  $\alpha 2$  (**B**) ECDs in pFastBac CT-TOPO Vector.

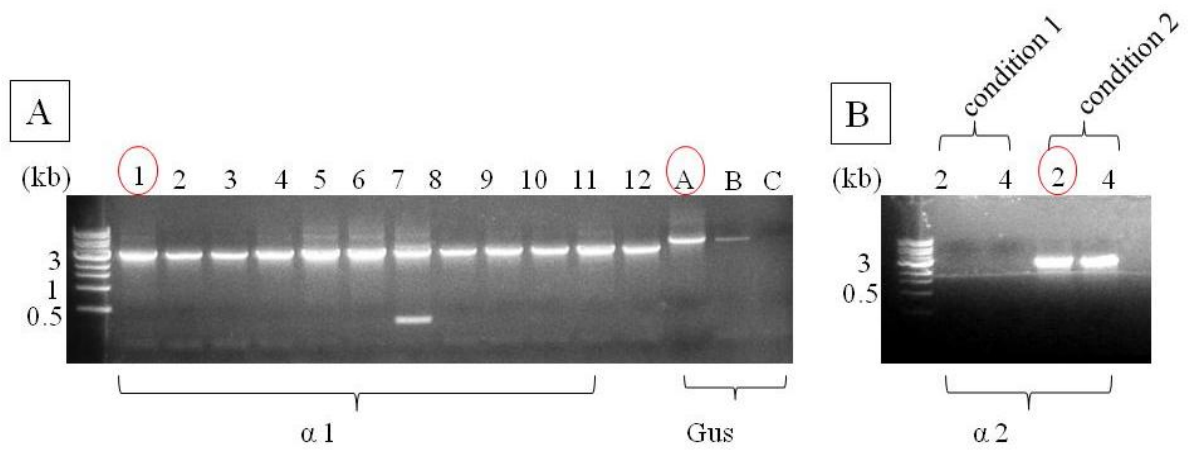
In order to test if the inserts were correctly orientated in the vector, PCR amplification was carried out using the  $\alpha 1$  or  $\alpha 2$  forward primer and SV40 reverse primers which bind to the vector sequence. A band of approximately 860 bp was observed in most clones for  $\alpha 1$  (Figure 15) and in only three clones for  $\alpha 2$  (Figure 15). Clones #5 and #7 for  $\alpha 1$ , and clones #7 and #9 for  $\alpha 2$  were further purified using the PureLink Hi Pure Plasmid Prep Kit and sequenced.



**Figure 15. PCR test for the correct orientation of  $\alpha 1$  and  $\alpha 2$  ECDs sequences inserted into pFastBac CT TOPO His Vector.** **A.** Most of the  $\alpha 1$  clones have inserted the  $\alpha 1$  sequence in the right 5'- 3' orientation (except clone 12). PCR amplification was done with the forward  $\alpha 1$  primer and the SV 40 reverse primer. **B.** Only three clones had inserted the  $\alpha 2$  sequence in the right orientation (clone 7, 9 and 10). PCR amplification was done with the forward  $\alpha 2$  primer and SV40 reverse primer. In both PCR amplifications, the amplified product was approximately 860 bp. The clones circled in red were used for transposition into baculovirus DNA.

Recombinant pFastBac CT-TOPO His vectors were transformed into MAX Efficiency DH10 BAC *E.coli* which contains a baculovirus shuttle vector (bacmid) with a mini-*attTn7* target site and a helper plasmid which promotes transposition of the mini-Tn7 element from the pFastBac donor plasmid into the bacmid. The bacmid propagates in DH10 Bac cells as a large plasmid that contains a kanamycin-resistance gene and can complement a *lacZ* deletion present on the chromosome to form colonies that are blue ( $Lac^+$ ) in the presence of Bluo-gal and IPTG. Following successful transposition into the mini-*attTn7* attachment site, expression of the *LacZ* $\alpha$  peptide was disrupted giving rise to white colonies on a background of blue colonies which contained just the original bacmid. White colonies were selected through a blue/white screening and DNA was purified. Successful transposition of the  $\alpha 1$  and  $\alpha 2$  sequence was verified by PCR using primers which bind to the sequences flanking the insert (pUC/M13 forward and reverse) obtained from Invitrogen (Figure 16).

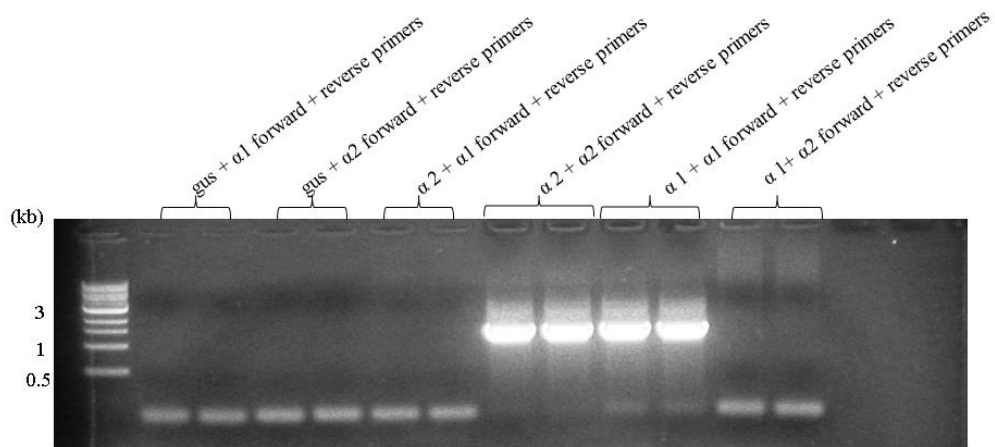




**Figure 16. PCR analysis of the transposition of  $\alpha 1$  and  $\alpha 2$  ECDs into the bacmid DNA.** The PCR amplification of  $\alpha 1$  and  $\alpha 2$  ECDs and control sequence Gus transposed into bacmid DNAs was done using Puc/M13 forward and reverse primers (baculovirus sequence primers flanking the insert). **A.** PCR amplification of  $\alpha 1$  ECDs sequence (1-12) and control Gus sequence (A-C). **B.** PCR amplification of  $\alpha 2$  ECDs sequence using two different PCR conditions. A clone inserted in the bacmid should result in a band at 4420 bp while an empty vector should result in a band at 350 bp. Clones  $\alpha 1.1$ ,  $\alpha 2.2$  and Gus.A are situated at the right molecular weight and have been selected for further experiments.

All  $\alpha 1$  clones contained a band at 3170 bp which reflects the presence of the insert. Transposition of the positive control plasmid pFastBac Gus was detected only in the clone A yielding a PCR product of ~ 4420 bp. Only two  $\alpha 2$  positive clones were obtained containing a band of ~ 4 kbp. The  $\alpha 1$  positive clone #1 and the  $\alpha 2$  positive clone #2 (Figure 16) were purified further using the PureLink HiPure Plasmid Prep kit (Invitrogen) and confirmed by sequencing.

The final confirmation of the successful cloning was obtained by PCR using the  $\alpha 1$  and  $\alpha 2$  forward primers and pUC/ M13 reverse primers, which revealed a band of expected size (~1100 bp) in lanes containing  $\alpha 1$  and  $\alpha 2$  bacmid DNAs. The pFastBac Gus was used as a negative control in this test (Figure 17). The PCR products were sequenced confirming that no mutations in the  $\alpha 1$  and 2 sequences were introduced during the cloning.

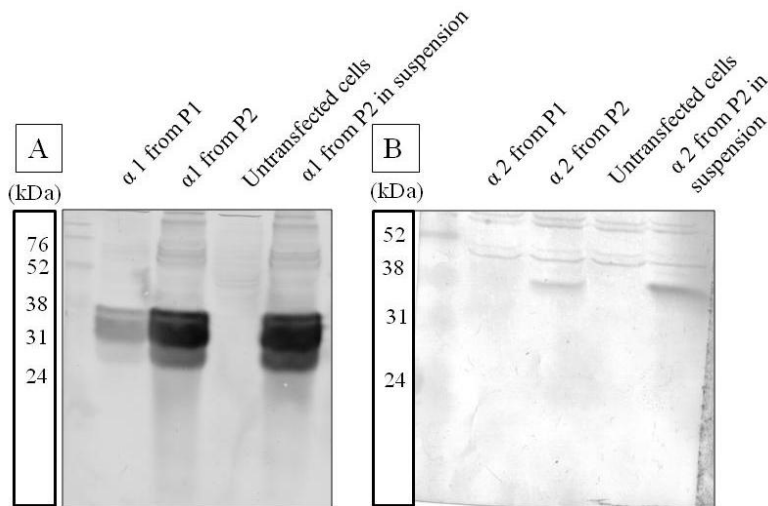


**Figure 17. PCR analysis of the transposition of  $\alpha 1$  and  $\alpha 2$  ECD sequences into the bacmid DNA.** This PCR was done using the maxiprep DNA with different combinations of primers. Gus DNA was tested with  $\alpha 1$  or  $\alpha 2$  forward and reverse primers, as a negative control. The  $\alpha 2$  DNA was tested with  $\alpha 1$  primers and with  $\alpha 2$  primers. As expected, only the second combination worked, giving a band around 1.1 kb. The DNA was tested with  $\alpha 1$  forward and reverse primers but also with  $\alpha 2$  primers. As expected, only the first combination worked.

### 3.3.2 Baculoviruses-infected Sf9 cells express $\alpha 1$ and $\alpha 2$ ECDs

Purified bacmid DNA was transfected into *Spodoptera frugiperda* Sf9 insect cells using the CellFECTIN II reagent which was supplied with the Bac-to-Bac TOPO Expression System. Cells were incubated for up to 72 h until the first signs of cell lysis were observed. The medium was collected and this was labelled as the P1 baculovirus stock. This stock was used to infect a new culture of Sf9 cells in preliminary expression assays and for production of the high titre P2 baculovirus stock. After collecting the medium from infected cultures, cells were lysed with 2 % SDS and the expression of  $\alpha 1$  and  $\alpha 2$  ECDs was detected using SDS/PAGE and immunoblotting with specific antibodies (Figure 18). Due to cell lysis provoked by the viral infection, the total protein yield of infected cells was generally lower in comparison with the control untransfected cells. Expression of the  $\alpha 1$  and  $\alpha 2$  ECDs (both at  $\sim 30$  kDa) was detected specifically in lanes containing the extracts from cells transfected with the bacmid DNA constructs (labelled as P1) and from P1-infected cells (labelled as P2). A major band of  $\sim 30$  kDa and two lower minor bands were detected in these extracts which could represent different glycosylated forms, degradation or truncation of these proteins. The molecular weight of the detected proteins is compatible with the predicted mass of these proteins

of ~ 26 kDa. Detection of  $\alpha 2$  ECDs revealed significantly weaker bands likely reflecting the lower affinity of the  $\alpha 2$  specific antibody compared to  $\alpha 1$  specific antibody. The expression of  $\alpha 1$  and  $\alpha 2$  ECDs was amplified approximately six times between P1-labelled infected cells and P2-labelled infected cells. Moreover, production of  $\alpha 1$  and  $\alpha 2$  ECDs was further increased when Sf9 cells are cultured in suspension in comparison with the adherent monolayer cultures (Figure 18).

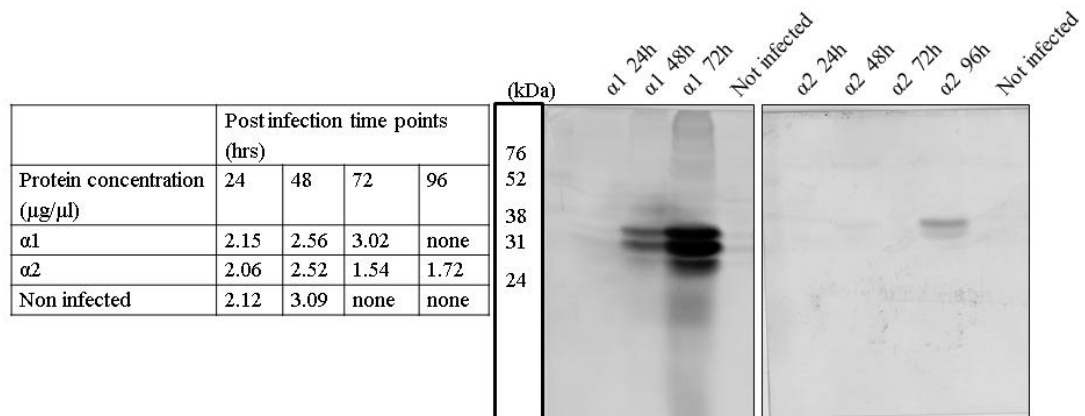


**Figure 18. The  $\alpha 1$  and  $\alpha 2$  ECDs are expressed in Sf9 cells infected with P1 and P2 viral stocks. A. and B.** The  $\alpha 1$  and  $\alpha 2$  protein expression from infected Sf9 cells was analysed by loading 200  $\mu$ g of protein on 12 % SDS/PAGE and immunoblotting with  $\alpha 1$  and  $\alpha 2$  specific antibodies, respectively. The lowest molecular weight bands of  $\alpha 1$  and  $\alpha 2$  ECDs are around 26 kDa (as expected). The higher molecular weight bands could correspond to glycosylated forms of these proteins (to be confirmed). The level of expression of  $\alpha 1$  ECDs in P2-labelled infected cells was six times higher than the level of expression  $\alpha 1$  ECDs in P1-labelled infected cells.

### 3.3.3 Optimising protein expression

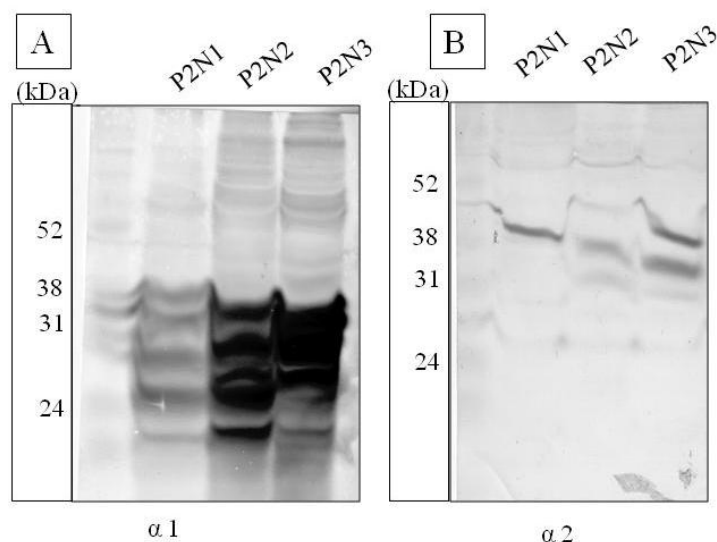
We decided to perform a time course experiment in order to determine the optimal post-infection time to collect infected Sf9 cells. Therefore, we infected cells at the same multiplicity of infection of 0.1 (see Methods, 3.2.5.4) and assayed for recombinant protein expression at different times post-infection (24, 48, 72 and 96 hours post-infection). The Sf9 cells were plated in 6 well plates and infected with each of the P2 viral stocks ( $\alpha 1$ - and  $\alpha 2$ - bacmid DNAs). Non-infected cells were used as a negative control. The cells were harvested and lysed at different time points and analysis of protein expression was performed by SDS/PAGE and immunoblotting.

Immunoblotting with specific antibodies indicated that the level of production of each protein increases in time as the virus propagates in culture. The highest level of expression was detected 72 h after the infection with  $\alpha 1$ -bacmid DNA and 96 h after the infection with  $\alpha 2$ -bacmid DNA (Figure 19). However, after 96 h the vast majority of cells appeared lysed increasing the risk of protein degradation (data not shown).



**Figure 19. Time course experiment of the expression of  $\alpha 1$  and  $\alpha 2$  ECDs in infected Sf9 cells.** Adherent cell cultures were infected with P2 viral stock and incubated for 24 h, 48 h, 72 h or 96 h. Protein extracts from P3-labelled infected cells were prepared in 2 % SDS and analysed by SDS/PAGE and immunoblotting with specific antibodies. Three bands between 24 kDa and 35 kDa were observed for  $\alpha 1$  and two bands for  $\alpha 2$ . The production of  $\alpha 1$  and  $\alpha 2$  increased from 24 to 96 h. The optimal expression was reached at 72 h for cells infected with  $\alpha 1$  or  $\alpha 2$  baculoviruses, and 96 h with  $\alpha 2$  baculovirus.

Three different P2 viral stocks were used to infect Sf9 cells, P3 viral stocks (culture medium) were discarded and cells were lysed with 2 % SDS. For each experiment, the protein expression was analysed by SDS/PAGE and immunoblotting with specific antibodies (Figure 20). The highest level of expression was detected in the third experiment. Therefore, the P2 viral stock collected in the third experiment was isolated and used to infect Sf9 cells for further purification experiments.



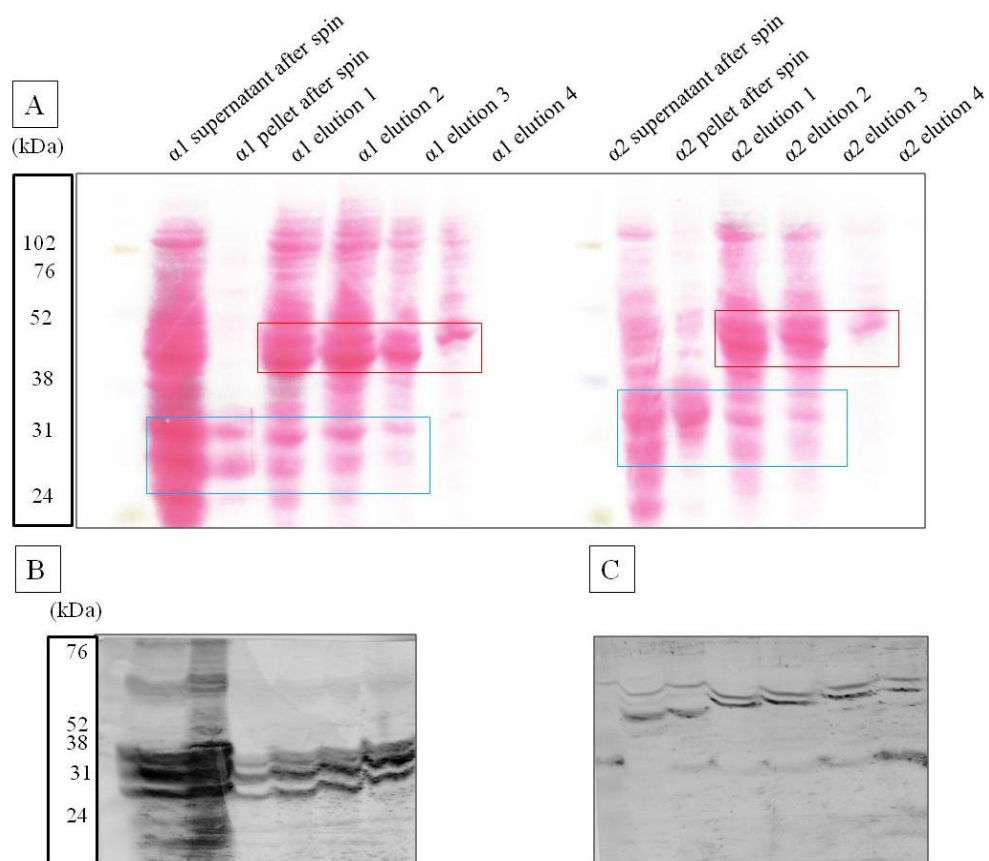
**Figure 20. Expression of  $\alpha 1$  and  $\alpha 2$  ECDs from three independent experiments.** Three independent infections of Sf9 cells were carried out with P2 viral stocks. The medium was removed and infected Sf9 cells were lysed with 2 % SDS. 150  $\mu$ g of extracted proteins were loaded on 12 % polyacrylamide gel. The estimation of protein expression was analysed by SDS/PAGE and immunoblotting with specific  $\alpha 1$  (A) or  $\alpha 2$  (B) antibodies and alkaline-phosphatase conjugated secondary antibodies. Three bands were observed in all the three experiments for  $\alpha 1$  and  $\alpha 2$ . However, in the last experiment, the production of  $\alpha 1$  and  $\alpha 2$  was more efficient. The variability between experiments could be explained by differences in cell viability or passage.

### 3.3.4 Optimisation of the purification of $\alpha 1$ and $\alpha 2$ ECDs from infected Sf9 cells

#### 3.3.4.1 Purification of $\alpha 1$ and $\alpha 2$ ECDs using ProBond columns.

The  $\alpha 1$ - and  $\alpha 2$ - ECDs expressed in Sf9 cells were initially purified using ProBond columns as described in this Chapter, Section 3.2.6. Figure 21 shows the total protein distribution after the transfer onto a nitrocellulose membrane visualised using Ponceau S staining (staining all the proteins present in the sample). The presence of many bands was detected in the supernatants. However, only three bands in the case of  $\alpha 1$ , and two bands in the case of  $\alpha 2$  were detected in pellets. The same bands were also detected in eluted fractions (1-4, indicated by the blue rectangle). These bands could potentially correspond to  $\alpha 1$  and  $\alpha 2$  ECDs. This will be confirmed by incubation with specific  $\alpha 1$  or  $\alpha 2$  antibodies. In addition, prominent contaminating band of ~50 kDa was detected in the supernatants and the eluted fractions (indicated by the red rectangle). Following incubation with the specific antibodies, the presence of

$\alpha 1$  and  $\alpha 2$  proteins was confirmed in all the analysed fractions (Figure 21). The amount of these proteins was particularly high in the pellet fraction. Once eluted, all the fractions were pulled and dialysed against PBS overnight. The concentration of samples was measured using the BCA assay and the total yield of about 2.1 and 1.7 mg of protein was estimated for  $\alpha 1$  and  $\alpha 2$  fractions, respectively. However, the contribution of the contaminating bands to the total protein yield was significant and it precluded the use of these samples in further experiments (Figure 21).



**Figure 21. The distribution of the  $\alpha 1$  and  $\alpha 2$  ECDs isolated using the ProBond affinity chromatography.** **A.** Sf9 cells were infected with P2 viral stocks and lysates were prepared 72 hours post-P2 infection. Samples were collected at each step of purification (25  $\mu$ l) and analysed by SDS/PAGE and Immunoblotting. This figure shows the Ponceau S staining, after transferring the proteins onto the nitrocellulose membrane. The first lane represents the proteins contained in the supernatant collected after the first centrifugation following cell lysis. The second lane is the pellet resulting from the same step. The lanes 3 to 6 represent the four elution fractions. The red rectangles represent a 52 kDa contaminating protein. The blue rectangles outline the proteins that may correspond to  $\alpha 1$  and  $\alpha 2$  ECDs between 24 and 31 kDa. **B and C.** The nitrocellulose membranes shown in **A** were incubated with the  $\alpha 1$  or  $\alpha 2$  specific antibodies, respectively, followed by incubation with the secondary alkaline phosphatase-conjugated antibody. Approximately the same amount of  $\alpha 1$  and  $\alpha 2$  ECDs was present in the supernatant and pellet after lysis and centrifugation, but also increasing amount of each protein was observed in the elution fractions. Three bands between 31 and 38 kDa representing the  $\alpha 1$  ECDs and two bands representing the  $\alpha 2$  ECDs were revealed.

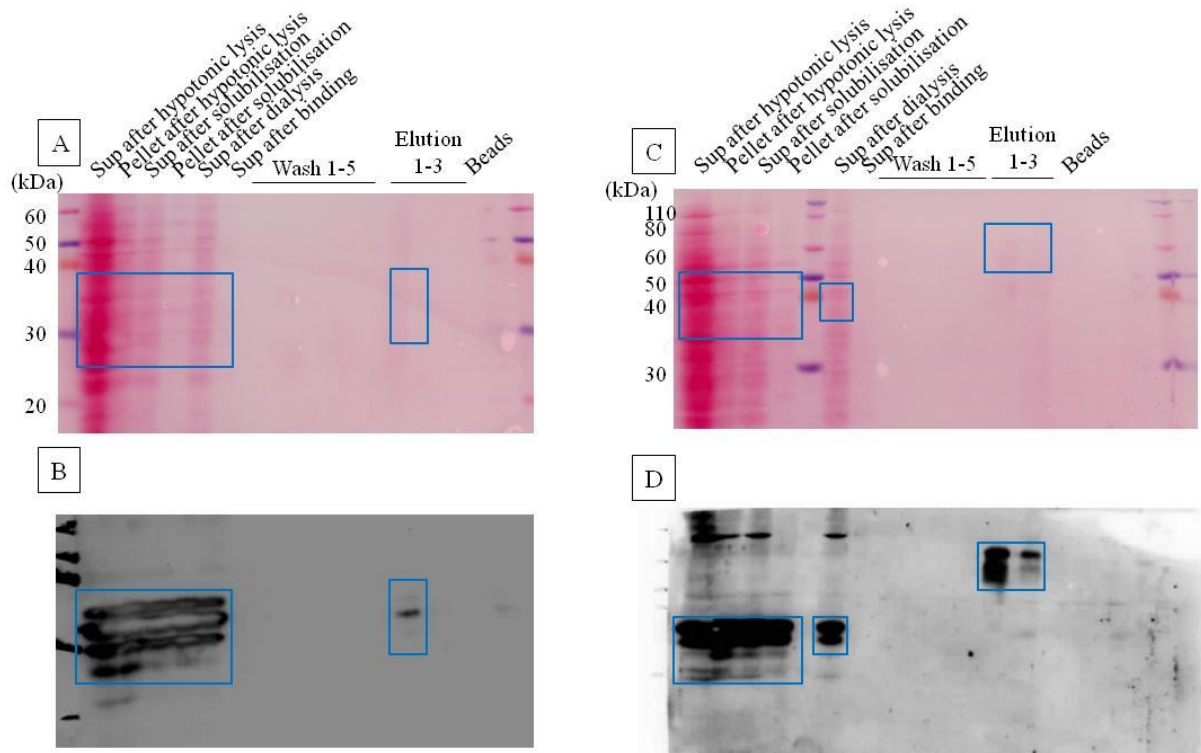
In order to separate  $\alpha 1$  and  $\alpha 2$  proteins from the contaminating bands, we incubated small fractions of supernatants with the Pro-bond  $\text{Ni}^{2+}$  beads. After binding, four different elution buffers were tested:

- 1) 20 mM Tris-HCl buffer pH 7.5;
- 2) 20 mM Tris-HCl buffer, pH 6.5
- 3) Tris-HCl Buffer, pH 7.5 + 10 mM Imidazole
- 4) 20 mM Tris-HCl Buffer, pH 7.5 + 300 mM NaCl

However, none of these conditions proved optimal for the elution of the specific proteins in the absence of the contaminating bands (data not shown).

#### 3.3.4.2 *Purification of $\alpha 1$ and $\alpha 2$ ECDs using Ni-NTA columns*

As we could not avoid this contaminating protein in our pellet using ProBond beads, we decided to purify the  $\alpha 1$ - and  $\alpha 2$ - ECDs by chromatography affinity using Ni-NTA resin columns as described in this Chapter, Section 3.2.7. Figure 22 shows the total protein distribution after the transfer onto a nitrocellulose membrane visualised using Ponceau S (Figure 22A, 22C). The presence of many bands on both membranes was detected in the supernatants and throughout the experiment. In this experiment, no contaminating bands were detected in the supernatants or in the eluted fractions. Following incubation with the specific antibodies and Horseradish-Peroxidase secondary antibodies, the presence of  $\alpha 1$  and  $\alpha 2$  proteins was confirmed in all the fractions up to the first elution (Figure 22B, 22D). In the first immunoblot (Figure 22B), the  $\alpha 1$  ECD was present in high concentration in the first fractions from the supernatant after hypotonic lysis up to the dialysed fraction. Finally, the  $\alpha 1$  ECD is retrieved in the first elution fraction. In the second immunoblot (Figure 22D), the  $\alpha 2$  ECD was present in high concentration in the first fractions from the supernatant hypotonic lysis up to the dialysed fraction. Finally, the  $\alpha 2$  ECD is retrieved in the first two elution fractions but at a higher molecular weight, around 70 kDa, suggesting that proteins may have aggregated.



**Figure 22. Ponceau S staining of  $\alpha 1$  and  $\alpha 2$  ECDs purified from Ni-NTA columns.** Sf9 cells were infected with  $\alpha 1$  baculovirus- or  $\alpha 2$  baculovirus P2 viral stocks and lysates were prepared 72 hours post- P2 infection. Purification of  $\alpha 1$ - (A and B) and  $\alpha 2$ - (C and D) ECDs was performed with Ni-NTA beads based chromatography affinity. Samples were collected at each step of purification and analysed by SDS/PAGE and Immunoblotting. **A.** This image shows the Ponceau S staining. The first lane represents the migration pattern of the molecular weight marker. The next two lanes represent the supernatant and pellet after the hypotonic lysis (2-3). The next two lanes (4-5) represent the supernatant and pellet after the solubilisation. Then, the lane 6 shows the proteins content of the supernatant after dialysis while the lane 7 represent the protein content of the supernatant after the binding. The lanes 8-12 represent the protein content of the five washes followed by the three elutions (13-15). Finally, the beads fraction represents what was left bound to the beads after the last elution. The blue squares represent an estimation of the localisation of  $\alpha 1$  ECDs on the membrane. **B.** Immunoblotting with the  $\alpha 1$  specific antibody. The immunoblot was revealed using HRP-coupled secondary antibody. The  $\alpha 1$  ECD is detected between 28 and 35 kDa. **C.** This image shows the Ponceau S staining, after transferring the proteins onto the nitrocellulose membranes. The first two lanes represent the supernatant and pellet after the hypotonic lysis (1-2). The next two lanes (3-4) represent the supernatant and pellet after the solubilisation. The lane 5 represents the molecular weight marker. Then, the lane 6 shows the proteins content of the supernatant after dialysis while the lane 7 represent the protein content of the supernatant after the binding. The lanes 8-12 represent the protein content of the five washes followed by the three elutions (13-15). Finally, the beads fraction represents what was left bound to the beads after the last elution. The blue squares represent an estimation of the localisation of  $\alpha 2$  ECDs on the membrane. **D.** The membrane was washed and processed through immunoblotting by incubating with  $\alpha 2$  specific antibody. The immunoblot was revealed using HRP-coupled secondary antibody. The  $\alpha 2$  ECD is detected between 30 and 38 kDa.



### **3.4 Discussion**

In this chapter, we employed the baculovirus/Sf9 cells expression system to express and purify the N-terminal extracellular domains of GABA<sub>A</sub>R  $\alpha$ 1 and  $\alpha$ 2 subunits. Once the mouse sequences were inserted by CT-TOPO cloning into the bacmid DNA, Sf9 cells were infected with  $\alpha$ 1 or  $\alpha$ 2 baculoviruses. After performing a time course experiment in order to determine the best infection conditions, the infected Sf9 cells were collected and the optimisation of the his-tagged  $\alpha$ 1 and  $\alpha$ 2 ECDs purification was performed. The baculovirus expression system Bac-to-Bac chosen for these experiments proved to be an adequate technique as more than 90 % of efficiency was reached in our cloning experiments. Growing Sf9 cells in suspension was found to be the most optimal for the Sf9 cell survival and viral infection.

Following optimisation of infection and expression conditions, purification under native conditions of  $\alpha$ 1 and  $\alpha$ 2 ECDs was performed. This was our first priority as we planned to use these purified proteins in proteomics and mass spectrometry experiments aiming at isolation of potential binding partners of these subunits. In this chapter, we have described different steps that were taken in order to obtain partially purified GABA<sub>A</sub>R subunits  $\alpha$ 1 and  $\alpha$ 2 ECDs under native conditions. These included a first purification of the  $\alpha$ 1 and  $\alpha$ 2 ECDs using Tris HCl-based buffer and Probond resin which provided us with considerable amount of extracted proteins, but inadequate purity, due to the presence of abundant contaminating protein. In addition, under these conditions, most of the proteins of interest remained in the pellet (insoluble fraction) after solubilisation and centrifugation. More stringent conditions were subsequently used in order to reduce the amount of contaminating proteins and to increase the yield of proteins of interest in our elution samples following affinity chromatography. In these experiments, we used Ni-NTA agarose beads because their binding affinity for his-tagged proteins is greater than Probond beads. Hypotonic lysis with 20 mM NaH<sub>2</sub>PO<sub>4</sub> and 0.5 % NP-40 was performed in order to reduce the non-specific interactions prior to solubilisation. The presence of a low concentrated detergent in our buffer helped us

to break up membranes and thus, extract more proteins from Sf9 cells without modifying the secondary structure of the proteins. As most of the proteins of interest remained in the pellet, we decided to increase NP-40 concentration and add Deoxycholate (DOC) which helped to extract membrane-bound proteins (Duggan and Stephenson, 1990, Duggan et al., 1991). Once proteins were solubilised in the phosphate buffer containing 2 % NP-40 and 1 % DOC, a significant amount of  $\alpha 1$  and  $\alpha 2$  ECDs was present in the soluble fraction (supernatant) after centrifugation. Because the presence of DOC can interfere with the binding of His-tagged proteins to Ni-NTA beads, we have introduced a dialysis steps to remove DOC from our samples before the binding to Ni-NTA beads. To avoid protein aggregation, the dialysis buffer contained 1 % Triton X-100 and high NaCl concentration (300 mM) (Knight et al., 1998). Then, the binding was performed in the presence of 20 % glycerol in order to conserve the native conformation of the proteins and preserve the non-specific binding to the agarose beads. Finally, elution of bound proteins was carried out with 100 mM EDTA and 250 mM Imidazole which chelate  $\text{Ni}^{2+}$  thus competing with the binding of his-tagged proteins (Hoffmann and Roeder, 1991). This allowed us to collect elution fractions which contained the  $\alpha 1$  and  $\alpha 2$  ECDs in solution. Following elution of proteins, immunoblots were performed in order to assess the affinity chromatography efficiency. When  $\alpha 1$  and  $\alpha 2$  ECDs were revealed by the specific antibodies, they appeared as three different molecular weight bands between 25 and 35 kDa which are likely to result from post-translational modifications such as glycosylation, protein degradation or truncation. Additionally, high molecular weight bands (~80 kDa) were present in the immunoblots. As the purified proteins are sticky and tend to aggregate, these bands are likely to be doublets or triplets of the  $\alpha 1$  or  $\alpha 2$  ECDs. We were only able to partially purify the  $\alpha 1$  and  $\alpha 2$  ECDs from infected Sf9 cells as we could not extract all the proteins by affinity chromatography. This is likely to be caused by protein aggregation which would alter the binding to Ni-NTA beads, thus causing a steric hindrance between the his-tag and the Nickel beads. Additionally, a considerable amount of

protein was lost during the first steps of purification. Although we were able to extract more protein from the pellet with the phosphate buffer than with the Tris-HCl buffer, a considerable amount of protein was present in the supernatant after the second spin before the solubilisation. In addition, some amount of protein was lost throughout the purification steps of the affinity chromatography. Although we decided to load proteins according to the binding capacity of the column, it is possible that due to their stickiness, the ECDs were bound to the beads in a non-specific manner which may be the reason why we had some protein remaining bound to the beads after the elution steps.

# Chapter four

## **4. Investigating the potential synaptic binding partners of the extracellular domains of GABA<sub>A</sub>R subunits $\alpha$ 1 and $\alpha$ 2**

### **4.1 Introduction**

Most cellular processes rely on a multitude of proteins that assemble into multimeric complexes. Thus, a precise understanding of the biological pathways that control cellular events relies on identification and biochemical characterisation of the proteins involved in such multimeric assemblies. In recent years, it has become clear that protein-protein interactions occurring in the synaptic cleft regulate the formation and maintenance of synapses. Examples of these proteins, already mentioned in the Introduction are Neurexin/Neuroigin, NCAMs, Slitrk3/PTP $\delta$  and more recently, GABA<sub>A</sub>Rs  $\alpha$ 1 subunits/Neurexins (Biederer et al., 2002 , Graf et al., 2004, Zhang et al., 2010, Takahashi et al., 2012). These interactions occurring across the synaptic cleft have also been postulated to play an important role during specific recognition of the pre- and postsynaptic elements and initiation of synaptic contacts.

GABA<sub>A</sub>Rs belong to a superfamily of pentameric ligand-gated ion channels (pLGICs) known as the Cys-loop receptors (Grenningloh et al., 1987). Each subunit of the GABA<sub>A</sub>Rs is composed of a large N-terminal extracellular domain of 200-250 amino acids, four transmembrane domains with an M3-4 intracellular loop of 85-255 residues, and a small C-terminal extracellular domain (Karlin and Akabas, 1995).

Of particular interest here are our recent findings that GABA<sub>A</sub>Rs play a structural role during GABAergic synapse formation and are capable of promoting this process in a heterologous co-culture model system (Fuchs et al., 2013). During the course of these experiments, it became clear that in further analysis, particular emphasis should be placed on the structure and function of the extracellular domains of GABA<sub>A</sub>R subunits since these domains are large and exposed in the synaptic cleft and so, might be responsible for the first contacts between the pre- and postsynaptic element.

The first crystallisation of the GABA<sub>A</sub>Rs  $\beta$ 3 homopentamer revealed that GABA<sub>A</sub>R ECDs are composed of structural elements unique to eukaryotic Cys-loop receptors, but more importantly that the highly conserved N-glycans present on the ECDs of all the subunits play an important role in the structural assembly of the receptor, in the signal transduction of GABA<sub>A</sub>R ligands and in the gating process of the receptor (Miller and Aricescu, 2014).

In recent years, identification of multi-subunit protein complexes has been done routinely using proteomics and mass spectrometry due to high sensitivity and accuracy of these techniques (Volkel et al., 2010).

#### **4.1.1 Aims**

In the next set of experiments, our aim was to further investigate the structural role played by the  $\alpha$ 1 and  $\alpha$ 2 subunits during specific GABAergic synapse formation by identifying potential transynaptic binding proteins which could specifically interact, directly or indirectly, with the ECDs of these subunits. These proteins were isolated by proteomics and mass spectrometry.

## **4.2 Methods**

### **4.2.1 Proteomics and Mass spectrometry- First and second round**

The cultures of Sf9 cells grown in suspension were infected and solubilised following the protocol described in the Chapter 3 section 3.2.7. Throughout these experiments, we had to stay in keratin-free environment which is very important for the accuracy of mass spectrometry analysis. Therefore, all the steps were carried out in the laminar flow hood cabinet with gloves.

After solubilisation of proteins from Sf9 cells, Ni-NTA beads were prepared by pipetting 800  $\mu$ l of resuspended beads (50/50 slurry) into one eppendorf tube per affinity chromatography. After they were spun down at 1000 g for 4 min, 400  $\mu$ l of water was added in order to wash the beads. The procedure was repeated one more time. Then, 400  $\mu$ l of binding buffer (50 mM NaH<sub>2</sub>PO<sub>4</sub>, pH 8, 300 mM NaCl, 20 % glycerol, 1

% Triton X-100, and protease inhibitors) was added to the eppendorf tube which was gently inverted and spun down at 1000 g for 4 min. The procedure was repeated one more time. The supernatant was removed and 1 mg of extracted proteins from Sf9 cells infected with  $\alpha 1$  or  $\alpha 2$  bacmid DNA, or control Sf9 cells was added to the beads to bind overnight at 4 °C. The following day, the columns were spun down at 800 g for 2 min and the supernatant after binding was removed. The beads were washed three times in the binding buffer for 5 min with rotation. The last wash was performed with 150 mM NaCl and no glycerol in the buffer and the beads were kept separately on ice until neuronal lysate was ready to be added.

Neuronal lysates were prepared from 6 DIV embryonic cortical neurones (4 x 10 cm dishes) using the lysis buffer containing 50 mM  $\text{NaH}_2\text{PO}_4$ , pH 8.0, 300 mM NaCl, 1 % Triton X-100, protease inhibitors. Subsequently, the cells were scraped with the cell scraper and cell lysates were collected from the bottom of the dish. The plates were washed with 500  $\mu\text{l}$  of lysis buffer and all the lysates were pooled (~ 4 ml total) and solubilised for one hour at 4 °C with rotation. The lysates were spun down for 40 minutes at 10 000 g in the first round of proteomics. The second round of proteomics was performed with high speed centrifugation of lysates at 100 000 g (Beckman-Coulter Table-top ultracentrifuge). Once the supernatant was carefully removed from the pellet, the protein concentration was estimated using Bradford assay. The total yield obtained was ~ 2 mg of protein in 4 ml.

Then, the neuronal extract (420  $\mu\text{g}$  total protein per column) was added to the 400  $\mu\text{l}$  of prepared beads together with 2 mM  $\text{CaCl}_2$  and 1 mM  $\text{MgCl}_2$  to facilitate the binding. The columns were then incubated for 2 h at 4 °C. After the binding was performed, the beads were washed four times with 10 min rotation at 4 °C and spun down at 1000 g for 2 min.

The elution of the bound proteins was carried out with the addition of 200  $\mu\text{l}$  of 0.1 M glycine, pH 2.0 to the beads, and incubation with rotation for 1 h at 4 °C. The columns were then spun down at 1000 g for 2 min and the supernatant was kept on

ice. The beads were resuspended in another 200  $\mu$ l of 0.1 M glycine, pH 2.0 and spun down again. The supernatant after spin was kept on ice. The elution step was repeated two more times in order to detach as much protein as possible from the beads. Then, all the elution fractions were spun down again at 2000 g for 5 min to pellet any remaining beads from the proteins. The supernatants were then gently transferred into new tubes and the methanol/chloroform extraction of the protein was performed as described in the Experimental Procedures Chapter, Section 2.7.

The air-dried proteins were resuspended in 6  $\mu$ l of 2 % SDS and all eluted fractions were pooled together into one tube containing a small amount of 2 % SDS. The tubes were sequentially washed with 5  $\mu$ l of 2 % SDS to collect any remaining proteins and pooled with the first collected fraction. NuPage Sample Buffer (5  $\mu$ l, 4X) and NuPage reducing Agent, (1  $\mu$ l, 10X, Invitrogen) were added to these samples. The samples were heated up at 70 °C for 10 min without boiling and 200 mM iodoacetamide (2  $\mu$ l to make up the total volume of 20  $\mu$ l) was added and incubated in the dark at room temperature for one hour. The samples were loaded onto a NuPage Novex Bis-Tris gel and the electrophoresis was done in MOPS buffer (50 mM MOPS pH 7.7, 50 mM Tris Base, 1 mM EDTA, 0.1% SDS) with NuPage antioxidant (both from Invitrogen), at 200 V for ~1 h.

All the following steps were performed in the fume hood cabinet (Bigneat Containment Technology, Chempac filtration) to avoid any contamination with keratin. Once the gel was removed from the frame and placed carefully in the large sterile tissue culture dish, it was incubated with Instant Blue protein stain, (Expedeon) for 15 min at room temperature with gentle shaking. The Instant Blue was removed and the gel was left to incubate in sterile water overnight to remove any background staining. The gel was washed one more time and a photograph of the gel was taken when the required intensity was achieved.

The bands of interest were cut out of the gel in the laminar flow hood cabinet with protection from direct contact with any potential source of keratin. The gel pieces



were transferred into siliconised low-bind Eppendorf tubes labelled according to the gel lanes. The gel bands were cut into smaller pieces within the tubes to speed up the destaining and digestion.

The bands were destained with 500  $\mu$ l of 50 mM ammonium bicarbonate in EtOH (50:50 ratio) with rotation for 10 min. This step was repeated as many times as necessary until the blue stain disappeared (usually 4 times). Then, 200  $\mu$ l of 200 mM acetonitrile (ACN) was added to the gel pieces and vortexed (Vortex Genie 2, USA Scientific, provided by the Dept of Pharmaceutics, School of Pharmacy) for 10 min. The tubes were centrifuged and the solvent was discarded. This step was repeated three times and samples were air dried or speed vacuum dried. At this step, gel pieces were frozen at  $-20^{\circ}\text{C}$ .

The next step consisted of the in-gel trypsin digestion of proteins. Trypsin is a serine protease enzyme that cleaves peptide chains on the carboxyl end site of amino acids arginine or lysine. The stock of trypsin, (Promega) was prepared to a final concentration of 0.2  $\mu\text{g}/\mu\text{l}$ . Then, 5  $\mu$ l of trypsin was mixed with 20  $\mu$ l of chilled 50 mM ammonium bicarbonate. Next, 10  $\mu$ l of this mixture was added to the gel pieces and was left on ice for 30 min in order for the enzyme to be fully absorbed into the gel. Finally, 50  $\mu$ l of 50 mM ammonium bicarbonate (enough to cover the gel pieces) was added to the gel pieces which were then vortexed and spun down. The mixture of gel pieces, trypsin and ammonium bicarbonate was incubated at  $37^{\circ}\text{C}$  with slow agitation over night in order for the trypsin to digest the proteins contained in the gel pieces into smaller peptides.

To extract the peptides from the gel, 25  $\mu$ l of 5 % formic acid and 50 % of acetonitrile solution mix was added to the gel pieces which were then spun down for one minute at 14,000 g. Next, the tubes were vortexed for 20 min. The supernatants containing the extracted peptides were transferred into a new siliconised tube. Then, 30  $\mu$ l of 100 % ACN was added to the gel pieces, vortexed for 20 min and spun down for 1 min. The supernatant was transferred into the tube containing the extracted

peptides. This step was repeated four times in total in order to increase the yield of extraction of digested peptides. The samples were then dried using the Speed Vac (Dominique Dutscher) for 36 hours at maximum speed until the solvent mixture has completely evaporated (it usually took 1.5 days to dry these samples). After this step, the extracted and dried peptides could be stored at -80 °C for up to six months.

In the final step, the peptides were reconstituted in order to be processed by the mass spectrometer (Q-TOF analyser). We first diluted the peptides in the loading buffer (0.1% formic acid in H<sub>2</sub>O). To avoid overloading the column during mass spec injections, the amount of loading buffer added to the peptides was adapted to their relative concentration estimated by looking at the Instant Blue staining. The tubes were vortexed quickly with 3-4 strokes and spun down for one minute at maximum speed (14,000 g). The supernatant was removed carefully so that 5 µl was left in the tube containing the peptides, and transferred into another set of tubes which were in the fridge until the mass spectrometry analysis was finished.

#### **4.2.2 Mass spectrometry and analysis**

The first round of mass spectrometry was performed using the Mass Spectrometry Facility at the School of Pharmacy and the second round was performed in collaboration with the Swansea University. In both places, a nano ESI (Electrospray ionisation) was used as a source of ionisation followed by Q-TOF (Quadruple Time-of-flight) MS. One blank between each sample was run. To make sure the system was performing, BSA digest standards were injected between each run and their coverage was checked before running our samples. Further standard BSA digest were randomly run throughout the sequence to make sure no problem occurred during the run. In both cases, the Q-TOF mass spectrometer produced a series of .pkl files containing the observed mass- to- charge or m/z ratio and other information regarding the peptides found in each sample. The mass-to-charge ratio (m/z) is a value representing the mass of the ion in relation to its charge.

The analysis of both rounds of proteomics was done using GPM database and MASCOT. The main difference between two rounds was the fact that we introduced a high speed centrifugation step (100 000 g, Beckman-Coulter Table-top ultracentrifuge) in the second round to avoid a possible contamination of solubilised proteins with the membrane fraction.

#### 4.2.2.1 *Analysis with GPM database*

The GPM (global proteome machine) database was designed to store the minimum amount of information necessary to search and retrieve data obtained from the publicly available data analysis. This server is one of the best methods for validating the results of statistical analysis that constitute the final mapping of a list of tandem mass spectra to a list of protein sequences (MS/MS ion search) (Craig et al., 2004).

Each of the .pkl files were individually downloaded onto the GPM website [http://rat.thegpm.org/tandem/thegpm\\_tandem.html](http://rat.thegpm.org/tandem/thegpm_tandem.html) and the conditions presented in the Figure 23 were selected, including a type of residue modification (oxidation), the protein cleavage site (trypsin) and the type of mass spectrometer used (Q-TOF Mass Spectrometer). As there was a probability of mismatch, we decided to set up a tolerated error of 100 parts per million (ppm) equivalent to 0.1 Da. At the end of the search, a log (e) which represents the “peptide sequence to spectrum” matching score is determined for each peptide. The Rat Proteome ENSEMBL was selected as the source of publicly available information. The list of resulting matching proteins was transposed into an Excel table and sorted by increasing log (e) (Appendix).

As a result, GPM produced a list of potential proteins sorted by log (e) matching the peptide sequences found in the sample. The log (e) of each hit is the base -10 log of the expectation that any particular protein assignment was made at random. Thus, the lower the log (e) is, the more accurate the protein assignment is. In addition, GPM results included the total number of tandem mass spectra that can be assigned to one hit together with the molecular mass of the protein sequence, in kilodaltons (kDa).

Finally, GPM assigns an accession number and description of the protein using the ENSEMBL classification.

1. [Human and mouse protein sequence updates, 28 Aug 2014](#) The ENSEMBL protein sequences and SAVs for human and mouse have been updated to correspond to genomes GRCh38 and GRCm38.
2. [Search engine basics 101 #3, 27 Aug 2014](#) Using parent ion mass accuracy histograms to understand deamidation.

**GPM Cyclone, simple search form**

- spectra**
  - ? common, mzXML, mzData, DTA, PKL or MGF only
  - Choose file
  - ? Skyline data file name:
- taxon**
  - ? Select one or more.
  - Eukaryotes  Prokaryotes  Viruses

R. norvegicus (ENSEMBL)	Anaeromyxobacter dehalogenans 2CP 1
R. norvegicus (RefSeq)	Anaeromyxobacter dehalogenans 2CP C
R. norvegicus (UniProt)	Anaeromyxobacter Fw109 5
R. norvegicus (Unigene)	Anaeromyxobacter K
----	Anaplasma centrale Israel
H. sapiens (male, ENSEMBL)	Anaplasma marginale Florida
H. sapiens (female, ENSEMBL)	Anaplasma marginale Maries
M. musculus (male, ENSEMBL)	Anaplasma phagocytophilum HZ

  - 1. Include reversed sequences:  none |  mixed |  only |
  - 2. all <sup>15</sup>N amino acids
- measurement errors**
  - 1. ? Fragment mass error:
- residue modifications**
  - 1. Complete modifications 1:
  - 2. Complete modifications 2:

---

- potential modifications**
  - 
  - 3. Potential modifications:
    - 
    - 
    - 
    -
  - 4. ? Check for known PTMs  yes  no
- refinement specification**
  - 1. ? Potential modifications (unimod):

round 1	round 2
<input type="text" value="none"/>	<input type="text" value="Nethylmaleimide (C)"/>
<input type="text" value="Oxidation (M)"/>	<input type="text" value="Sulfinamide (C)"/>
<input type="text" value="Dioxidation (M)"/>	<input type="text" value="Dioxidation (C)"/>
<input type="text" value="Oxidation (W)"/>	<input type="text" value="Trioxidation (C)"/>
mods: <input type="text" value="15.994915@M,15.994"/>	mods: <input type="text" value="31.98983@M,31.9898"/>
motifs: <input type="text"/>	motifs: <input type="text"/>
  - 2. ? Check for known PTMs  yes  no
  - 3. ? sAPs:  yes  no
  - 4. ? Semi-style cleavage:  yes  no
  - 5. ? Valid expectation: <
- protein cleavage specification**
  - 1. ? Cleavage site:
  - 2. ? Semi-style cleavage:  yes  no
- spectrum conditioning**
  - 1. ? Remove redundant:  yes  no, angle:  (0-90)
  - 2. ? Spectrum synthesis:  yes  no
- predefined methods**
  - 1. ? Method: Select device & parent  $\delta m$ .
    - 
    - 
    - 
    - 
    -
- gpmdb**
  - 1. ? Add to gpmDB:  yes  restricted  no
  - 2. ? Archive MS/MS information  yes  no
  - 3. Anonymous contribution:  yes  no

Hosted by: Beavis Informatics Ltd.

**Figure 23. Screenshot of the GPM online database.** This database research was performed using the GPM which is an online database regularly updated with new mass spectra. We used the Rat Proteome ENSEMBL as a source of information for the matching proteins.

#### 4.2.2.2 *Analysis with MASCOT database*

Mascot (Matrix Science) is a powerful engine which uses mass spectrometry data to identify proteins from the primary sequence database. Like GPM, Mascot uses a probability based scoring. However, it is unique in that it integrates all the proven methods of searching:

- Peptide mass fingerprint: in this method, the only experimental data are peptide mass values.
- Sequence query: in this method, peptide mass data are combined with amino acid sequence and composition information.
- MS/MS ion search: This is the method used by the GPM database which uses un-interpreted MS/MS data from one or more peptide.

As Mascot database is not freely available on the internet, the analysis was performed in the laboratory of Dr. Yuqin Wang, at Swansea University. Each of the files was individually downloaded onto the Mascot program and conditions were selected. As a source of publicly available data, we used the International Protein Index (IPI) Rat database. As there was a probability of mismatch, we decided to set up a tolerated error of 300 parts per million (ppm) equivalent to 0.3 Da.

In Mascot, the ion score is based on the calculated probability,  $P$ , that the observed match between the experimental data and the database sequence is a random event. The protein score is derived from the ion score: it is the sum of the highest ions score for each distinct sequence ([http://www.matrixscience.com/help/interpretation\\_help.html](http://www.matrixscience.com/help/interpretation_help.html)).

Mascot provides the with access to the mass spectrum of a protein of interest from which we could identify the fragment ions and their parent ions as well as other details as shown in the Figure 24. Following the search, the list of resulting matching proteins was transposed into an Excel table and sorted by decreasing protein score (Appendix).

## MASCOT MS/MS Ions Search

<b>Your name</b>	<input type="text" value="jessica arama"/>	<b>Email</b>	<input type="text" value="ucnvjea@live.ucl.ac.uk"/>
<b>Search title</b>	<input type="text" value="PIKA_A2BAND6"/>		
<b>Database(s)</b>	<input type="text" value="Human_EST"/> <input type="text" value="Fungi_EST"/> <input type="text" value="Environmental_EST"/> <input type="text" value="SwissProt"/> <input checked="" type="text" value="NCBIInr"/>	<b>Enzyme</b>	<input type="text" value="Trypsin"/>
<b>Taxonomy</b>	<input type="text" value="All entries"/>	<b>Allow up to</b>	<input type="text" value="2"/> missed cleavages
<b>Fixed modifications</b>	<input type="text" value="--- none selected ---"/>	<b>Quantitation</b>	<input type="text" value="None"/>
<input type="checkbox"/> Display all modifications		<input type="text" value="Acetyl (K)"/> <input type="text" value="Acetyl (N-term)"/> <input type="text" value="Amidated (C-term)"/> <input type="text" value="Amidated (Protein C-term)"/> <input type="text" value="Ammonia-loss (N-term C)"/> <input type="text" value="Biotin (K)"/> <input type="text" value="Biotin (N-term)"/> <input type="text" value="Carbamidomethyl (C)"/> <input type="text" value="Carbamyl (K)"/> <input type="text" value="Carbamyl (N-term)"/> <input type="text" value="Carbamyl (Protein N-term)"/>	
<b>Variable modifications</b>	<input type="text" value="Acetyl (Protein N-term)"/> <input type="text" value="Methylthio (C)"/> <input type="text" value="Oxidation (M)"/>	<b>Peptide tol. ±</b>	<input type="text" value="0.3"/> Da <input type="text" value="# 13C 0"/>
<b>Peptide charge</b>	<input type="text" value="2+"/>	<b>MS/MS tol. ±</b>	<input type="text" value="0.3"/> Da <input checked="" type="radio" value="Monoisotopic"/> Monoisotopic <input type="radio" value="Average"/> Average
<b>Data file</b>	<input type="text" value="ZS_130524_UCL_B_6.pkl"/>	<b>Precursor</b>	<input type="text" value="m/z"/>
<b>Data format</b>	<input type="text" value="Micromass (.PKL)"/>	<b>Error tolerant</b>	<input type="checkbox"/>
<b>Instrument</b>	<input type="text" value="ESI-QUAD-TOF"/>	<b>Report top</b>	<input type="text" value="AUTO"/> hits
<b>Decoy</b>	<input type="checkbox"/>	<input type="button" value="Start Search ..."/> <input type="button" value="Reset Form"/>	

**Figure 24. Screenshot of the MASCOT website similar to the on-site version.** This image shows the parameters of an MS/MS Ion Search on Mascot Website. We performed an on-site search which was more detailed than the online version. In this search, we selected NCBIInr as a reference database, allowed up to 2 Trypsin missed cleavages and selected Acetylation, Methylation or oxidation as variable modifications. In addition, the peptide and MS/ MS tolerances were set up to 0.3 Da.

The two rounds of mass spectrometry experiments were analysed using both the GPM search engine and the MASCOT. In order to have only specific binding proteins, we first compared the proteins which were present in  $\alpha 1$  or  $\alpha 2$  binding assays to those present in the control Sf9 cell extracts binding assays. Those which were present in both were not considered. Those proteins which were isolated with  $\alpha 1$  ECDs were analysed separately from those which were isolated with  $\alpha 2$  ECDs in binding assays. This was done using an Excel macro in the following order:

- Candidate binding proteins specifically isolated using the  $\alpha 1$ -ECD column
- Candidate binding proteins specifically isolated using the  $\alpha 2$ -ECD column
- Candidate binding proteins isolated with both  $\alpha 1$ - and  $\alpha 2$ -ECD columns

This type of analysis was performed with candidate proteins obtained using GPM database separately from candidate obtained using MASCOT. Finally, the candidate proteins found in both databases were pooled together for further analysis.

#### **4.2.3 Binding assays of $\alpha$ 1 and $\alpha$ 2 ECDs**

We conducted a series of binding assays using  $\alpha$ 1 ECD-,  $\alpha$ 2 ECD-, or control Sf9 cell extracts- loaded columns and used 7 DIV cortical and striatal neurone extracts. The cells were infected with  $\alpha$ 1 or  $\alpha$ 2-bacmid DNA and collected using a method described in the Chapter 3, section 3.2.7. Then, the proteins from infected and non-infected Sf9 cells were solubilised and dialysed overnight following the protocol described previously in this chapter, section 4.2.1. The preparation of Ni-NTA columns was done following the protocol described in Chapter 2, section 2.3.7. Briefly, 400  $\mu$ l of beads (50:50 slurry) were transferred into an eppendorf tube, washed with water and incubated over night with the dialysed protein extracts from non-infected or  $\alpha$ 1- or  $\alpha$ 2-infected Sf9 cells. The next day, the cultured neurones were lysed and prepared for binding in the lysis buffer (50 mM NaH<sub>2</sub>PO<sub>4</sub>, pH 8.0, 300 mM NaCl, 1 % Triton X-100, and protease inhibitors) following the protocol described in this chapter, section 4.2.1. Prior to the incubation of the neuronal extracts with the immobilised columns, we performed a “preclear step” which allowed us to decrease the non-specific binding of proteins to Ni-NTA. This step included incubation of Ni-NTA beads with neuronal extracts for 1 h at 4 °C with a ratio of 100  $\mu$ l of beads to 140  $\mu$ g of proteins. Then, the supernatant was collected and bound (~ 400  $\mu$ g of protein per column) to  $\alpha$ 1-ECD-,  $\alpha$ 2-ECD-, or control Sf9-loaded-Ni-NTA columns overnight at 4 °C. The following day, the beads were washed four times with 5 min rotation at 4 °C and spun at 1000 g for 5 min. Next, the proteins bound to  $\alpha$ 1-ECDs- or  $\alpha$ 2-ECDs- or Sf9-loaded-Ni-NTA columns were denatured using 10 % SDS and 5X sample buffer, as described in the Chapter 2, Section 2.8. Once the columns and inputs were boiled for 10 min at 95 °C, the columns were spun for 10 min at 14,000 g in order to pellet the beads. Then, 100  $\mu$ l of the

collected supernatant was loaded on a 8 % SDS PAGE, transferred onto the nitrocellulose membrane and incubated with the specific primary antibodies, followed by HRP-conjugated rabbit light-chain secondary (see Table 12 for details of antibodies used and their dilutions).

#### **4.2.4 Immunohistochemistry**

Immunohistochemistry was performed as described previously (Deuchars et al., 1994). Briefly, E20 brains were isolated from pregnant mouse and fixed in 4% PFA/sucrose overnight at 4 °C. In order to protect the tissue against damages during freezing procedures, the brains were incubated in gradient of sucrose (10, 20 and 30 %) until it penetrated completely (usually one day for each gradient). The brains were cut in 35 µm coronal slices using a cryostat (Leica Biosystem CM1520). Sections were washed twice in PBS for 20 min with rotation. Then, they were washed with 0.3 M glycine for 5 min and washed again twice in PBS for 5 min. The slices were then blocked in 1 % BSA for 30 min and incubated with the primary guinea-pig anti- $\alpha$ 2 antibody overnight at 4 °C (Table 12). The following day, the sections were washed three times in PBS for 10 min. Then, they were blocked and permeabilised in 1 % BSA with 0.2 % Triton for 30 min. The primary mouse anti- GAD-65 and rabbit anti-pikachurin antibodies were added to the brain slices for 3 hours at room temperature (Table 12). The slices were then washed three times in PBS for 10 min and blocked in 1 % BSA for 30 min. The Alexa-conjugated secondary antibodies (Table 12) were added in 1 % BSA for 1 h at room temperature, protected from light. The slices were washed three times in PBS for 5 min and mounted onto coverslips in Vectashield mounting medium (Vectorlabs).

#### **4.2.5 Immunocytochemistry**

The immunocytochemistry was performed as described in Chapter 2, section 2.2. Neurones cultured for 7 or 14 DIV, were fixed using 4 % PFA/sucrose for 12 minutes at room temperature. After fixation, they were incubated with Glycine (0.3 M) in



PBS, in order to quench PFA. After washing, cells were incubated in 1 % BSA in PBS for 1 hour and subsequently incubated overnight at 4 °C with anti- $\alpha$ 2 and anti-pikachurin antibodies, diluted in 1 % BSA in PBS (Table 12). Cultures were then permeabilised by incubating with 1 % BSA, 0.5 % Triton X-100 in PBS for 15 minutes. Neurones were subsequently incubated with anti-GAD-65 and anti-MAP-2 (Table 12) antibodies diluted in 1 % BSA in PBS for 2 hours at room temperature. Following this step, Alexa dye-conjugated secondary antibodies were added and images were analysed using Zeiss 710 Confocal microscope.

#### **4.2.6 Immunoblotting**

Neurones from cortical and striatal cultures at 7 and 14 DIV, and tissue from the embryonic and adult cortex, retina, cerebellum and hippocampus were lysed with 2 % SDS and boiled for 10 min at 95 °C. Then, they were sonicated until the lysates were clear and spun down for 10 min at 14,000 g in order to remove any residual aggregates. Protein concentration of each sample was measured using BCA assay and 200  $\mu$ g of each sample was loaded on a 10 % SDS PAGE. After transfer, the nitrocellulose membrane was incubated with the antibody directed against the N-terminal domain of pikachurin (AA 28-354) (1: 10 000 dilution Wako, Japan; (Sato et al., 2008)) followed by HRP-conjugated rabbit light-chain IgG. The binding of antibodies was visualised using the ECL reagent (GE Healthcare Life Sciences, Amersham ECL western blotting detection system) and recorded using GeneGnome Syngene.

#### **4.2.7 *In vitro* binding assays**

In order to confirm the binding between  $\alpha$ 2 ECD and pikachurin found in the first round of mass spectrometry, a series of binding assays using 6 DIV cortical or striatal neurones were carried out as described previously in this Chapter, Section 4.2.1. Following the binding and elution of proteins, they were separated using SDS/PAGE (8 % gels) and transferred onto the nitrocellulose membrane. Samples were incubated with the antibody directed against the N-terminal domain of pikachurin (AA 28-354)

(1:10 000 dilution Wako, Japan; (Sato et al., 2008)) followed by HRP-conjugated rabbit light-chain IgG and bound proteins were visualised using ECL reagent and recorded using the Syngene GeneGnome.

#### **4.2.8 Co-immunoprecipitation**

The protocol for co-IP was given by Prof. Anne Stephenson, School of Pharmacy. Cultured cortical neurones (6 plates,  $8 \times 10^6$  cells/ plate) were washed twice with ice-cold PBS. The cells were scraped with 500  $\mu$ l of lysis buffer containing 50 mM Tris pH 8.0, 150 mM NaCl, 1 % NP-40, protease inhibitor cocktail. The plates were washed with another 500  $\mu$ l of lysis buffer and the samples were pulled together. The lysate was homogenised using a glass sintered homogeniser (Glass Tenbroeck Tissue Grinder 2 ml, Omni) with 4 to 5 strokes. Protein concentration was measured using Bradford assay and the total yield was 2 mg/ml in 7.5 ml. Extra buffer was added to make it up to a final concentration of 1.5 mg/ml. The neuronal lysate was solubilised for one hour at 4 °C and subsequently spun down at high speed centrifugation (100 000 g) for 40 min at 4 °C. After 10 % of the neuronal lysate was put aside for the input lane (~750  $\mu$ l), the rest was split into four tubes (3 mg/tube) and 5  $\mu$ g of the following antibodies:

- Alpha1 C-terminal sheep antibody (1.5 mg/ml)
- Immune sheep IgG (stock conc. 0.3 mg/ml)
- Alpha2 C-terminal rabbit antibody (PX III at 0.185 mg/ml)
- Immune rabbit IgG (stock conc. 1 mg/ml)

To facilitate the binding,  $MgCl_2$  and  $CaCl_2$  (both at 2 mM final) were added to the mixture which was incubated overnight on a rotating plate at 4 °C.

The following day, the Protein A and G sepharose beads were prepared. As we needed 50  $\mu$ l of slurry per sample, we took 120  $\mu$ l of each type of beads and washed using PBS by vortexing and spinning at 600 g (2500 g) 3 times. The beads were finally resuspended in PBS (50:50 slurry) and 50  $\mu$ l of the mixture was added to the neuronal

extracts incubated with primary antibodies. The Protein G sepharose has a higher affinity for sheep than for rabbit antibodies. Therefore, we added the Protein G sepharose beads to the neuronal lysates which contained the sheep  $\alpha$ 1 antibody as well as the immune sheep IgG. The Protein A sepharose has a higher affinity for rabbit antibodies than for sheep antibodies. Therefore, we added the protein A sepharose beads to the neuronal lysates which contained the rabbit  $\alpha$ 2 antibody as well as the immune rabbit IgG. The samples were further incubated for 1 h at 4 °C on a rotating plate together with the input. The co-IPs were then spun down once for 20 sec at 600 g. The supernatants were removed from each co-IP and discarded. The co-IPs were then washed quickly by adding 1 ml of washing buffer containing 50 mM Tris, pH 8.0, 150 mM NaCl, 2 mM MgCl<sub>2</sub>, 2 mM CaCl<sub>2</sub>, 0.1 % NP 40, protease inhibitors cocktail. The buffer was added carefully down the wall of each tube. After a gentle agitation by flicking the tube and a 5 min spin, the buffer was discarded with caution not to touch the beads. This step was repeated three times. The rest of the washing buffer was removed using a Hamilton syringe.

Finally, the proteins contained in the co-IPs or in the input were precipitated using the methanol/chloroform extraction method described previously in the Chapter 2 Section 2.7. The air dried proteins were then resuspended in 20  $\mu$ l of 3X loading buffer with DTT. The loading buffer was prepared using 1.5  $\mu$ l DTT, 8.5  $\mu$ l H<sub>2</sub>O, 5  $\mu$ l of 3X loading buffer. The input lane was resuspended in 55  $\mu$ l (enough to load twice on a small gel) of 1X loading buffer. Then, all the samples were denatured for 8 min at 75 °C on a 500 g shaker. Small 10 % SDS PAGE gels were loaded using Hamilton syringe. The gels were loaded with an empty space (just loading buffer) between each sample and the control Immune IgG were always loaded before the co-IPs to avoid contamination with spill over which could lead to a false positive result. The gels were run at 20 mA for ~2 h.

The immunoblotting protocol as described in Chapter 2, Section 2.9, was modified to include fewer washes and increase the percentage of milk (Marvel) used as

blocking reagent. After transfer, the membrane was incubated in Block containing 5 % milk in PBS with 0.02 % Tween-20 for 1h at room temperature. Then, rabbit anti-pikachurin antibody was added to 2.5 % milk in PBS with 0.02 % Tween and the membrane was incubated overnight at 4 °C (1: 2500 dilution Wako, Japan; (Sato et al., 2008)). Alternatively, the membrane was incubated with anti  $\alpha$ 1 (1/100 dilution, rabbit anti  $\alpha$ 1 cys- loop; (Fujiyama et al., 2000)) or  $\alpha$ 2 antibody (2  $\mu$ g/ml dilution, rabbit anti  $\alpha$ 2 cys-loop; (Poltl et al., 2003)) in order to confirm the presence of the proteins in the co-IPs.

Then, the membrane was washed three times for 10 min in 2.5 % milk in PBS with 0.02 % Tween-20, and the secondary light chain anti-rabbit HRP antibody (see Table 13 for dilution) prepared in 2.5 % milk in PBS and 0.02 % Tween-20 was added for 1h at room temperature. This incubation was followed by three 10 min washes with 2.5 % milk in PBS and 0.02 % Tween, one 10 min wash in PBS and 0.02 % Tween. The membrane was then incubated for 5 min in ECL and developed using Syngene GeneGNOME.

The second co-IP followed the same protocol but was done with striatal neuronal extracts and in different lysis and washing buffers. In this experiment, we used the anti- $\alpha$ 2 antibody to pull down the GABA<sub>A</sub>RS and anti-rabbit IgG as a control. The lysis buffer contained 10 mM HEPES pH 8.0, 145 mM NaCl, 1 mM CaCl<sub>2</sub>, 2 mM MgCl<sub>2</sub>, 1% Triton X-100, protease inhibitors. The washing buffer contained 10 mM HEPES pH 8.0, 145 mM NaCl, 1 mM CaCl<sub>2</sub>, 2 mM MgCl<sub>2</sub>, 0.1 % Triton, protease inhibitors. In addition, the proteins were loaded on a 7 % polyacrylamide SDS/PAGE.

**Table 12. Antibodies used in immunofluorescence experiments.**

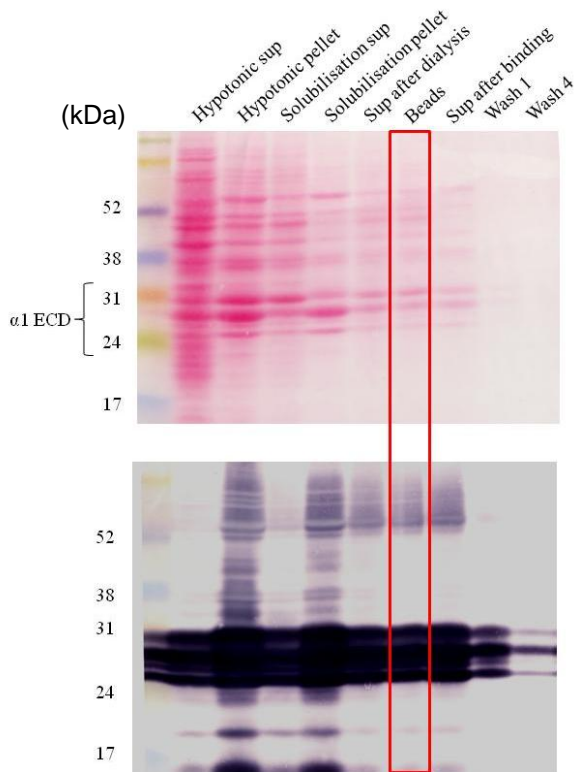
primary antibodies					secondary antibodies		
	specificity	origin	dilutions	source and characterisation	antibodies	dilutions	source
ICC	GABA <sub>A</sub> α2	GP	1:400	Synaptic System 224104	Goat Anti guinea pig cy5	1:750	Alexa Fluor Cy5
	GAD-65	Ms	1:4000	Abcam, ab26113	Goat anti mouse 555	1:750	Alexa Fluor Invitrogen a21422
	pikachurin	Rb	5 µg/ml	Abcam, ab91314	Goat Anti rabbit 405	1:750	Alexa Fluor Invitrogen a31556
IHC	GABA <sub>A</sub> α2	GP	1:400	Synaptic System 224104	Goat Anti guinea pig 488	1:750	Alexa Fluor Invitrogen a11073
	GAD-65	Ms	1:4000	Abcam, ab26113	Goat anti mouse 555	1:750	Alexa Fluor Invitrogen a21422
	pikachurin	Rb	1:2000	(Sato et al., 2008)	Goat Anti rabbit 405	1:750	Alexa Fluor Invitrogen a31556
	MAP2	Chk	1:2500	Abcam, ab92434	Goat Anti chicken 647	1:750	Alexa Fluor Invitrogen a21449

**Table 13. Antibodies used for immunoblotting and co-Immunoprecipitation.**

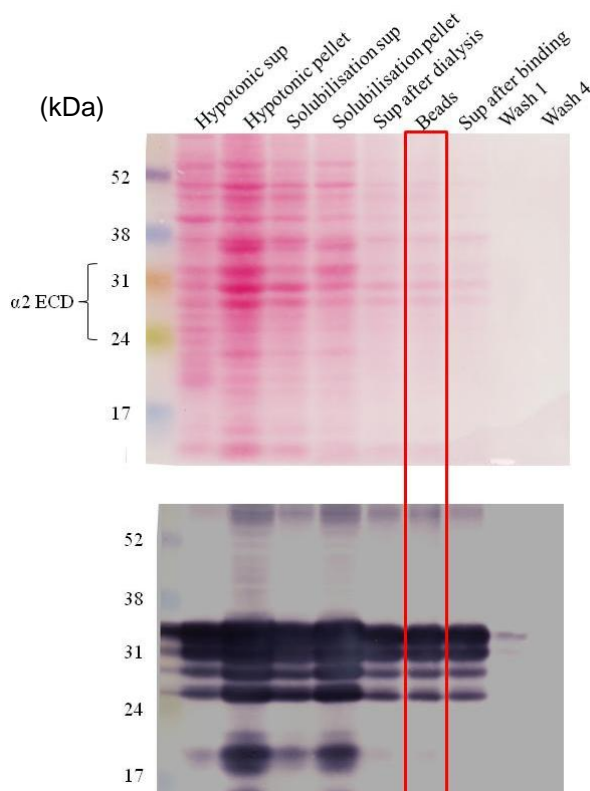
primary antibodies					secondary antibodies		
	specificity	origin	dilutions	source and characterisation	antibodies	dilutions	source
Immunoblot	Neurologin 2	Rb	1:1000	Synaptic System 129203	Anti-Rabbit IgG (H+L) 711-035-152	1:1000	Jackson Immuno Research
	Neurexin 1/2/3	Rb	1:1000	Synaptic System 175003	Same as previously	1:1000	Same as above
	pikachurin	Rb	1:1000	(Sato et al., 2008)	Same as previously	1:1000	Same as above
Co-IPs	pikachurin	Rb	1:2500	(Sato et al., 2008)	Anti-Rabbit IgG, Light Chain Specific 211-032-171	1:1000	Same as above
	α1- cys loop	Shp	1:100	(Fujiyama et al., 2000)	Same as previously	1: 1000	Same as above
	α2 cys-loop	Rb	2 µg/ml	(Poltl et al., 2003)	Same as previously	1:1000	Same as above

### 4.3 Results

The structural role of GABA<sub>A</sub>Rs in specific GABAergic synapse formation is poorly understood. We have hypothesised that the recognition between the presynaptic terminal and the postsynaptic cell involves the GABA<sub>A</sub>R subunits directly or indirectly, via protein-protein interactions within the synaptic cleft. In this chapter, our aim was to identify presynaptic or synaptic cleft-span proteins which specifically bind to the  $\alpha$ 1- or  $\alpha$ 2- ECDs of postsynaptic GABA<sub>A</sub>Rs using proteomics followed by mass spectrometry analysis. Binding assays were carried out with  $\alpha$ 1-,  $\alpha$ 2 extracellular domain (ECD)-, or Sf9 cell extracts-loaded Ni-NTA columns and protein lysates prepared from 6 DIV cultured cortical neurones. Following the binding, the eluted fractions were run on a NuPAGE Bis-Tris 4-12 % gradient gel (Invitrogen) and stained with Coomassie blue. Each gel lane was cut into eighteen pieces according to the molecular weight marker and subjected to in-gel trypsin digestion, extraction and preparation for nano ESI (nano-Electro Spray Ionisation) followed by Q-TOF (Quadrupole Time-Of-Flight analyser) mass spectrometry. Finally, the MS/MS (Tandem Mass Spectrometry) spectra were analysed by two different databases using the precursor ion fingerprinting methods: GPM and MASCOT. The second proteomics analysis was carried using the same conditions as in the first round with exception that the cortical extracts were centrifugated at higher speed (100 000 g) before the binding assays were performed. Figure 24 and 25 show the preparation of  $\alpha$ 1 and  $\alpha$ 2 ECDs from lysates of Sf9 cells expressing these proteins. Following the binding assays, the proteins from cortical neuronal extracts bound to the ECD-columns were eluted and resolved by SDS/PAGE (Figure 26) using NuPAGE Bis-Tris 4-12 % gradient gel (Invitrogen). Each gel lane was cut into eighteen gel pieces and subjected to a series of steps in preparation for mass spectrometry analysis. The presence of proteins in collected fractions was detected using a 6xHis-tag specific antibody followed by incubation with the alkaline phosphatase-conjugated secondary antibody.



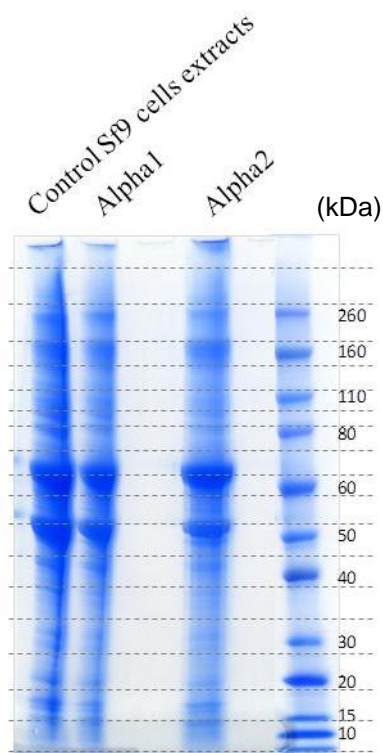
**Figure 24. Preparation of  $\alpha 1$  ECD-Ni-NTA resin used in proteomics.** Fractions collected during the  $\alpha 1$  ECD-Ni-NTA resin preparation were lysed with 2 % SDS. Total of 80  $\mu$ l of each sample was loaded on SDS/PAGE and transferred onto the nitrocellulose membrane. The membrane was then incubated with a mouse anti-6Histag antibody, followed by the incubation with the alkaline phosphatase-conjugated secondary antibody. As expected, the  $\alpha 1$  ECD is detected between 25 and 31 kDa. A significant amount of  $\alpha 1$  ECD was detected bound to the Ni-NTA resin. Weak protein bands detected at higher molecular weight than  $\alpha 1$  are likely to be unknown contaminating proteins which originate from the Sf9 cell extracts and have a high affinity for Ni-NTA. In addition a doublet of the  $\alpha 1$  ECD is probably revealed by the immunoblot around ~52 kDa.



**Figure 25. Purification of  $\alpha 2$  ECD-Ni-NTA resin used in proteomics.** Fractions collected during the  $\alpha 2$  ECD-Ni-NTA resin preparation were lysed with 2 % SDS. Total of 80  $\mu$ l of each sample was loaded on SDS/PAGE and transferred onto the nitrocellulose membrane. The membrane was then incubated with a mouse anti-6xHis-tag antibody, followed by the incubation with the alkaline phosphatase-conjugated secondary antibody. As expected, the  $\alpha 2$  ECD is detected between 25 and 35 kDa. A significant amount of  $\alpha 2$  ECD was detected bound to the Ni-NTA resin. Weak protein bands detected at higher molecular weight than  $\alpha 2$  are likely to be unknown contaminating proteins which originate from the Sf9 cell extracts and have a high affinity for Ni-NTA.

After the electrophoresis, each gel lane was cut into eighteen pieces according to the molecular weight, as shown in the Figure 26. Each gel piece was processed

through destaining, in-gel trypsin digestion and extraction of proteins, and subsequently analysed by Q-TOF Tandem Mass Spectrometry (MS).



**Figure 26. Instant blue staining of proteins from binding assay between ECDs-loaded columns and 6 DIV cortical neurones.** Instant Blue staining of the 4-12 % gradient Nu-PAGE gel representing the samples that were subjected to Mass Spectrometry. After elution from Ni-NTA agarose beads, the proteins were resolved using SDS/PAGE and stained with Instant Blue. Each lanes was cut into 18 bands from the bottom to the top of the gel and prepared for MS.

#### 4.3.1 HSPG Pikachurin was found bound to $\alpha$ 2-ECD-Ni-NTA

##### 4.3.1.1 GPM DB analysis

The GPM database enabled us to compare eluted protein peptides from each gel piece to already known peptides present in data analysis servers such as ENSEMBL, TIGR or UNIGENE. It retrieves information related to the protein matches such as the protein sequence, the accession identifier, the measure of the statistical validity of the identification of the protein. GPM also allowed us to create an Excel file for each band containing details about each of the matches, including the log (e), which is the base -10 log of the expectation that this assignment is stochastic; the log (I), which is the base -10 log of the sum of the intensity of the fragment ion spectra and the molecular mass of the protein sequence in kDa. Once we have obtained MS/MS profiles of all the samples, we have processed them further using GPM database and identified



candidate proteins listed using Excel. The candidate binding proteins of  $\alpha$ 1-ECD,  $\alpha$ 2-ECD and controls were compared and organised in tables according to the following criteria:

1. The  $\alpha$ 1-ECD specific candidate proteins (which are not found in Sf9 controls or  $\alpha$ 2-ECD) from the proteomics experiment 1 (Appendix Table 1).
2. The  $\alpha$ 1-ECD specific candidate proteins (which are not found in Sf9 controls or  $\alpha$ 2-ECD) from the proteomics experiment 2 (Appendix Table 2).
3. The  $\alpha$ 2-ECD specific candidate proteins (which are not found in Sf9 controls or  $\alpha$ 1-ECD) from the proteomics experiment 1 (Appendix Table 3).
4. The  $\alpha$ 2-ECD specific candidate proteins (which are not found in Sf9 controls or  $\alpha$ 1-ECD) from the proteomics experiment 2 (Appendix Table 4).
5. The  $\alpha$ 1-specific candidate proteins found in proteomics 1 and 2 (Appendix Table 5).
6. The  $\alpha$ 2-specific candidate proteins found in proteomics 1 and 2. (Appendix Table 6).
7. The  $\alpha$ 1 and  $\alpha$ 2 common candidate proteins found in proteomics 1 (Appendix Table 7).
8. The  $\alpha$ 1 and  $\alpha$ 2 common candidate proteins found in proteomics 2 (Appendix Table 8).

In order to compare hits between different assays, we used a VBA coded Excel file allowing us to compare the hits according to their accession number. This Excel coded file allowed us to rapidly know which hits were specifically found in  $\alpha$ 1 binding assay and not in  $\alpha$ 2 binding assay, and vice-versa. Then, the resulting protein hits were sorted in decreasing log (e).

In all the Tables (see Appendix) resulting from GPM DS search, matching proteins were assigned with a tolerance of error of 0.1 Da (or 100 ppm). The proteins were identified by their ENSEMBL accession number and their description from the database. According to the GPM, the log (e) is the base -10 log of the expectation that

the assignment was stochastic. The log (I) is the base -10 log of the sum of the fragment ion intensity in the tandem mass spectra used to make this assignment. The % (measured) corresponds to the amino acid coverage of the protein in this assignment. The % (corrected) corresponds to the coverage corrected for peptide sequences that are unlikely to be observed using normal proteomics method. The next column corresponds to the number of unique peptide sequences associated with this protein assignment. The total number of tandem mass spectra that can be assigned to this protein was also determined together with the molecular mass of the protein in kDa (Mr). Finally, GPM provided us with the chromosomal position of the gene related to the protein hit.

A more detailed bibliographic search was then conducted on each of the hits found specifically in the binding assays with  $\alpha$ 1-ECD or  $\alpha$ 2-ECD using protein information from the UniProtKB database. Our aim was to find proteins that would bind specifically to  $\alpha$ 1 or  $\alpha$ 2 ECDs and that this binding would be, potentially of a physiological relevance. We have obtained a large number of candidate proteins with no apparent physiological relevance to GABA<sub>A</sub> receptor function. However, there were a small number of potentially relevant candidates which included perlecan and pikachurin.

#### 4.3.1.2 *MASCOT DB analysis*

The MASCOT database is a powerful search engine which uses mass spectrometry data to identify proteins from primary sequence databases. It is more informative than GPM analysis because it integrates the peptide mass fingerprint, the MS/ MS ion search and the sequence query methods. By combining these three methods, MASCOT provided a high level of confidence, and allowed us to have a detailed description of each hit.

Once the samples from all the eighteen bands for gel lane ( $\alpha$ 1,  $\alpha$ 2 and control Sf9 cell extracts) were processed through Mascot and exported as Excel files, we applied

the same criteria as in the previous section to group them and carefully look for those which showed specificity in binding and potential physiological relevance to GABA<sub>A</sub>R function. The candidate binding proteins of  $\alpha$ 1-ECD,  $\alpha$ 2-ECD and controls were compared and organised in tables according to the following criteria:

1. The  $\alpha$ 1-ECD specific candidate proteins (which are not found in Sf9 controls or  $\alpha$ 2-ECD) from the proteomics experiment 1 (Appendix Table 9).
2. The  $\alpha$ 1-ECD specific candidate proteins (which are not found in Sf9 controls or  $\alpha$ 2-ECD) from the proteomics experiment 2 (Appendix Table 10).
3. The  $\alpha$ 2-ECD specific candidate proteins (which are not found in Sf9 controls or  $\alpha$ 1-ECD) from the proteomics experiment 1 (Appendix Table 11).
4. The  $\alpha$ 2-ECD specific candidate proteins (which are not found in Sf9 controls or  $\alpha$ 1-ECD) from the proteomics experiment 2 (Appendix Table 12).
5. The  $\alpha$ 1-specific candidate proteins found in proteomics 1 and 2 (Appendix Table 13).
6. The  $\alpha$ 2-specific candidate proteins found in proteomics 1 and 2 (Appendix Table 14).
7. The  $\alpha$ 1 and  $\alpha$ 2 common candidate proteins found in proteomics 1 (Appendix Table 15).
8. The  $\alpha$ 1 and  $\alpha$ 2 common candidate proteins found in proteomics 2 (Appendix Table 16)

In order to compare hits between different assays, we used the same Visual Basic for Application (VBA) coded Excel file which allowed us to compare the hits according to their accession number and sort them according to outlined criteria.

In all the Tables resulting from MASCOT search, the protein score is the probability that the observed match is a random event was described for each hits. This score is the result of a  $-10 \log(P)$  where P is the absolute probability. The protein mass representing the observed mass of each individual hits was also provided. The number of matching peptide found in the sample (protein matches) was given. The

proportion of the total protein that is covered by the peptide sequence was also detailed (protein cover). Finally, the experimental m/z value (peptide experimental m/z ratio), and the peptide score which is the ion score, were given.

A more detailed bibliographic search was conducted on each of the hits found specifically in the binding assays with  $\alpha$ 1-ECD or  $\alpha$ 2-ECD resin using protein information from the UniProtKB database. Our aim was to repeat the previous experiment under more stringent conditions which included a high speed centrifugation step at 100 000 g to eliminate a possibility that small pieces of cell membranes were present in our binding assays. Comparing the candidate binding proteins between those obtained with GPM database and Mascot was deemed inappropriate because the criteria for the analysis and the databases used were completely different.

Considering that the role played by Pikachurin in the Ribbon synapse in retina was well documented and that the role of similar heparan sulfate proteoglycans glypicans in glutamatergic synapse formation was also recently demonstrated (Siddiqui et al., 2013), we have decided to further explore the interaction between  $\alpha$ 2 subunit and Pikachurin.

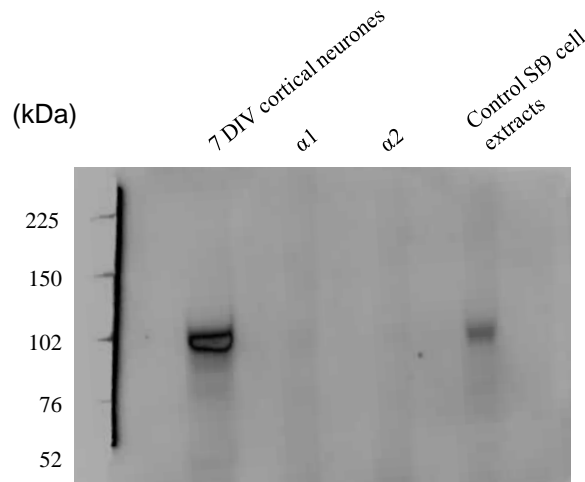
#### **4.3.2 Binding assays of $\alpha$ 1 or $\alpha$ 2 ECDs with Neurexins and Neuroligin**

##### **2**

##### *4.3.2.1 The $\alpha$ 1 and $\alpha$ 2 ECDs do not bind to Neuroligin 2 but bind specifically to Neurexins*

It is now well established that NL2 plays an important role in regulating GABAergic synapse formation (Hoon et al., 2009, Frola et al., 2013, Sun et al., 2013). We wanted to investigate if this role was mediated, at least in part, by the interaction between NL2 and the extracellular domains of  $\alpha$ 1 or  $\alpha$ 2 subunits of GABA<sub>A</sub>Rs. Towards this aim, we performed *in vitro* binding assays using lysates of cultured cortical neurones and  $\alpha$ 1 ECD-,  $\alpha$ 2 ECD-, or Sf9 control lysate- loaded Ni-NTA columns. The *in vitro* binding assays have demonstrated that NL2 does not interact with the

extracellular domains of  $\alpha 1$  or  $\alpha 2$  subunits (Figure 27). NL2 was only found in the input lane containing cortical lysates but not in the lanes containing the  $\alpha 1$ -ECD or  $\alpha 2$ -ECD. A faint band in Sf9 extracts lane was detected at the slightly higher molecular weight likely due to non-specific binding of the primary antibody.

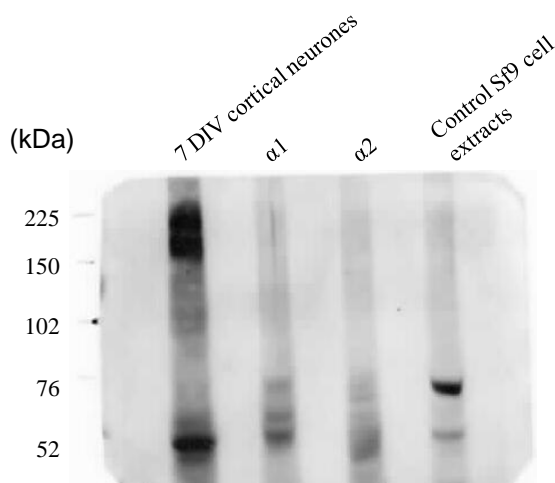


**Figure 27. NL2 does not bind to  $\alpha 1$  or  $\alpha 2$  ECDs.** Detergent-solubilised 7 DIV cortical neurone lysates were incubated with immobilized  $\alpha 1$  or  $\alpha 2$  ECDs purified from Sf9 cells on Ni-NTA columns. Following the binding assays, samples were loaded on an 8 % SDS/PAGE. After transfer, the nitrocellulose membrane was incubated with a specific antibody directed against the N-terminal domain of NL2 (1:1000 dilution Synaptic System) followed by HRP-conjugated rabbit light-chain IgG. Controls were prepared using extracts of Sf9 cells which did not express the extracellular domains of  $\alpha 1$  or  $\alpha 2$  subunits.

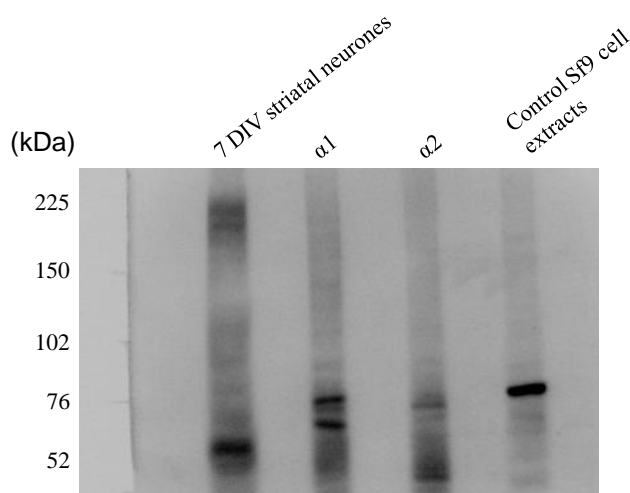
It is known that the interaction between neuroligin 2 (NL2) and neurexins plays an important role during GABAergic synapse formation (Varoqueaux et al., 2004, Huang and Scheiffele, 2008, Hoon et al., 2009). In addition, it has been established that neurexins, the presynaptic partners of NL2, can physically interact with GABA<sub>A</sub>Rs (Zhang et al., 2010). In order to know if the interaction between neurexins and GABA<sub>A</sub>Rs was mediated by the extracellular domains of  $\alpha 1$  and/ or  $\alpha 2$  subunit, we performed another series of binding assays.

In the second set of experiments, we used 7 DIV cortical or striatal neuronal lysates in binding assays with the  $\alpha 1$  ECD or the  $\alpha 2$  ECD to investigate the binding of neurexins. Figure 28 shows that different isoforms of neurexins bind specifically to  $\alpha 1$  or  $\alpha 2$  ECDs and not to control Sf9 cell extracts. Three isoforms of ~55, 60 and 75 kDa bound to  $\alpha 1$  ECDs specifically, while three different bands of ~52, 55 and 58 kDa bound to  $\alpha 2$  ECDs specifically. As the antibody does not allow specific recognition of the different isoforms of neurexins present in the binding assay, we were unable to define specifically which isoforms of Neurexins bind to  $\alpha 1$  or  $\alpha 2$  ECDs.

We also carried out similar binding assays using 7 DIV striatal neuronal lysates. The Figure 29 shows that different Neurexin isoforms to those found in the cortical lysates were bound specifically to  $\alpha 1$  and  $\alpha 2$  ECDs and not to control Sf9 cell extracts. In these assays, two main bands around 60 and 75 kDa were found bound to the  $\alpha 1$  ECD, and two bands around 50 and 75 kDa were found in the presence of  $\alpha 2$  ECDs.



**Figure 28. Neurexins interact with  $\alpha 1$  or  $\alpha 2$  ECDs at 7 DIV in *in vitro* binding assays with cortical neuronal lysates.** Detergent-solubilised 7 DIV cortical neurone lysates were incubated with Ni-NTA immobilized  $\alpha 1$ - or  $\alpha 2$ -ECDs columns. Following the binding, samples were loaded on an 8 % SDS/PAGE. After transfer, the nitrocellulose membrane was incubated with a specific antibody directed against the C-terminal domain of Neurexin 1/2/3 (1:1000 dilution, Table 13) followed by HRP-conjugated rabbit light-chain IgG. Controls were prepared using extracts of Sf9 cells which did not express  $\alpha 1$  or  $\alpha 2$  ECDs.



**Figure 29. Neurexins interact with  $\alpha 1$  or  $\alpha 2$  ECDs in *in vitro* binding assays with striatal neuronal lysates.** Detergent-solubilised 7 DIV striatal neurone lysates were incubated with Ni-NTA immobilized  $\alpha 1$ - or  $\alpha 2$ -ECDs columns. Following the binding, samples were loaded on an 8 % SDS/PAGE. After transfer, the nitrocellulose membrane was incubated with a specific antibody directed against the C-terminal domain of Neurexin 1/2/3 (1:1000 dilution Synaptic System, see Table 13) followed by HRP-conjugated rabbit light-chain IgG. Controls were prepared using extracts of Sf9 cells which did not express  $\alpha 1$  or  $\alpha 2$  ECDs.

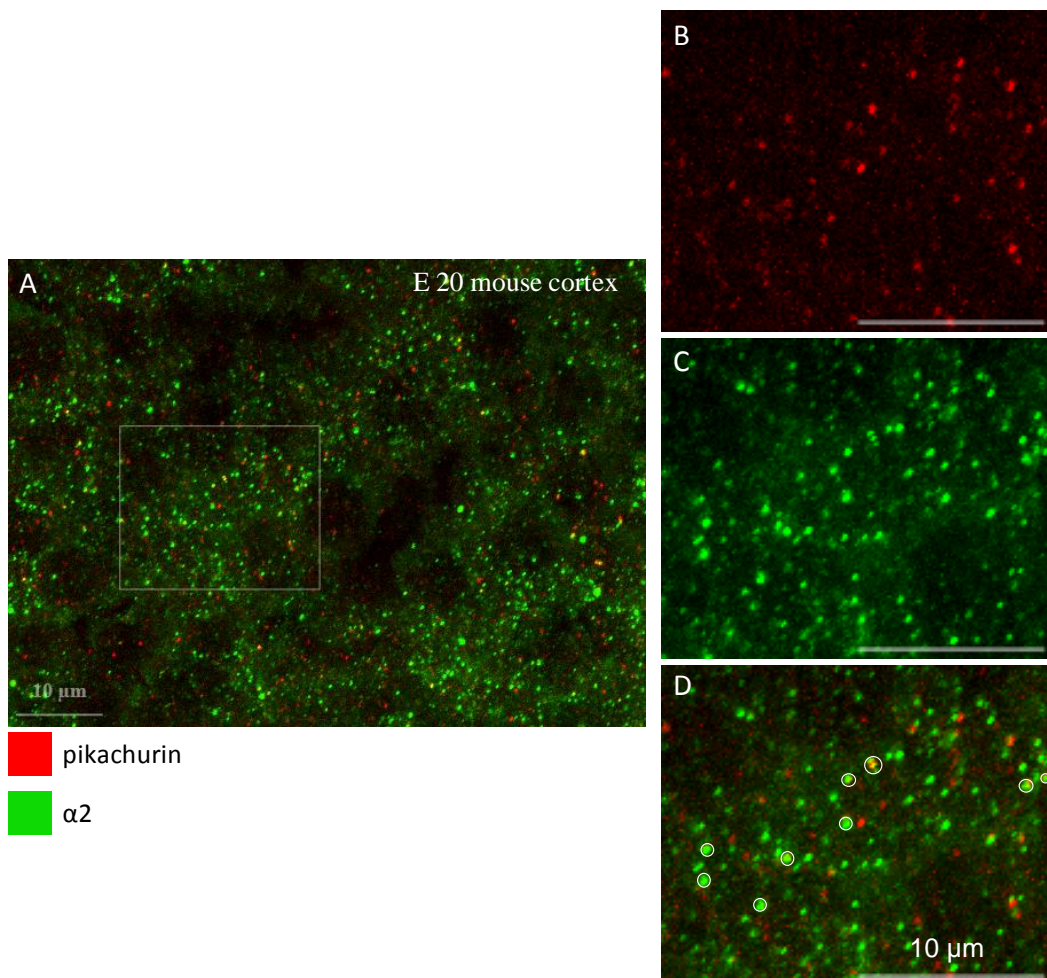
### 4.3.3 Investigating the binding of Pikachurin to the GABA<sub>A</sub>R $\alpha 2$ subunit

#### 4.3.3.1 *Pikachurin is partially co-localised with the GABA<sub>A</sub>R $\alpha 2$ subunit in the embryonic cortex.*

The expression of pikachurin in the retina and its role during ribbon synapse formation has been well characterised (Sato et al., 2008, Katoh et al., 2009, Kanagawa

et al., 2010, Sato, 2010, Han and Townes-Anderson, 2012, Omori et al., 2012). In this subchapter, we wanted to establish the localisation of pikachurin in the brain, the pattern of expression of pikachurin during the brain development, and to confirm the binding with  $\alpha 2$  ECD found in the first round of mass spectrometry.

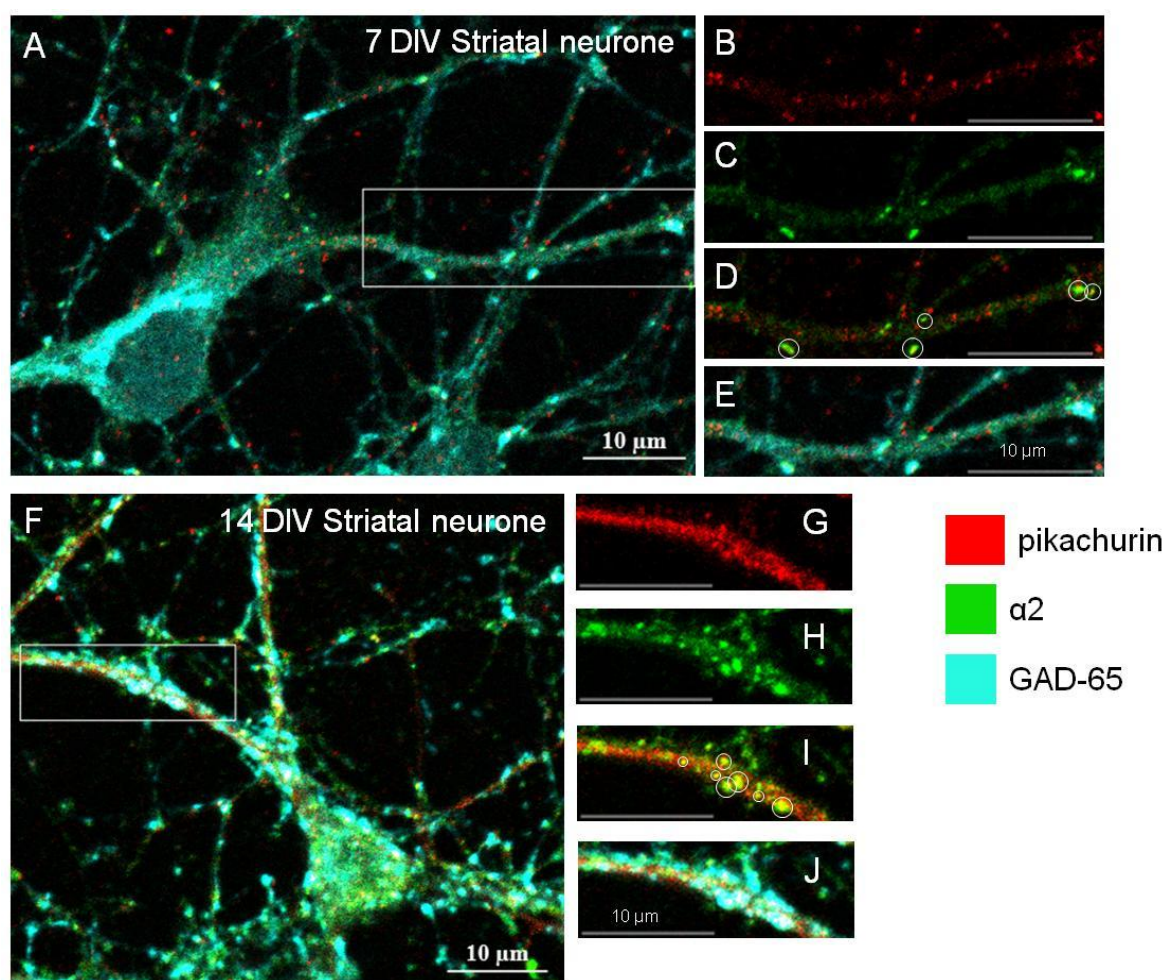
Figure 30 shows an example of staining obtained for pikachurin and the  $\alpha 2$  subunit of GABA<sub>A</sub>Rs using specific antibodies (Table 12) in E20 mouse brain sections. The pattern of pikachurin labelling is punctate and a considerable number of pikachurin puncta was detected in close apposition to the  $\alpha 2$  subunit of GABA<sub>A</sub>Rs throughout the cortical regions.



**Figure 30. pikachurin is expressed in the E 20 mouse brain and is partially co-localised with the  $\alpha 2$  subunit of GABA<sub>A</sub>Rs.** Immunolabelling of pikachurin (red) and GABA<sub>A</sub>Rs  $\alpha 2$  subunit-containing clusters (green) throughout cortical regions of the embryonic mouse brain. **A.** Merged image of an E 20 brain slice representing pikachurin and  $\alpha 2$  staining. **B.** Enlarged image of boxed region in A representing pikachurin staining only. **C.** Enlarged image of boxed region in A representing  $\alpha 2$  positive clusters of GABA<sub>A</sub>Rs. **D.** Enlarged image of boxed region in A in which partially co-localised puncta were circled in white. Scale bar: 10  $\mu$ m.

#### 4.3.3.2 Synaptic localisation of pikachurin in cultured neurones

Expression of pikachurin was analysed in cultured striatal neurones using immunocytochemistry and confocal imaging. Figure 31 shows an example of staining for pikachurin together with the  $\alpha 2$  subunit of GABA<sub>A</sub>Rs subunits and the presynaptic marker GAD-65 using the antibodies described in Table 12. Although the number of co-localised puncta was not quantified, it seems that the proportion of pikachurin puncta co-localised with the  $\alpha 2$ -containing GABA<sub>A</sub>Rs was increased as neurones matured from 7 to 14 DIV. In addition, it is interesting to note that most of the co-localised puncta were synaptic as they were also GAD-65 positive.



**Figure 31. Pikachurin is expressed at GABAergic synaptic contacts and the number of pikachurin puncta is increased from 7 to 14 DIV.** Immunolabelling of pikachurin (red),  $\alpha 2$  subunit-containing GABA<sub>A</sub>Rs (green) and presynaptic GABAergic terminals identified by staining with GAD65 (cyan). **A.** Merged image of a 7 DIV striatal neurone. **B.** Enlarged image of boxed region in A representing pikachurin staining only. **C.** Enlarged image of boxed region in A representing  $\alpha 2$  subunit-containing GABA<sub>A</sub>Rs staining only. **D.** Enlarged image of boxed region



in A representing pikachurin and  $\alpha 2$  subunit-containing GABA<sub>A</sub>Rs stainings. **E.** Enlarged image of boxed region in A representing pikachurin,  $\alpha 2$  and GAD 65 staining. **F.** Merged image of a 14 DIV striatal neurone. **G.** Enlarged image of boxed region in F representing pikachurin staining only. **H.** Enlarged image of boxed region in F representing  $\alpha 2$  subunit-containing GABA<sub>A</sub>Rs staining only. **I.** Enlarged image of boxed region in F representing pikachurin and  $\alpha 2$  subunit-containing GABA<sub>A</sub>Rs stainings. **J.** Enlarged image of boxed region in A representing pikachurin,  $\alpha 2$  and GAD 65 stainings. Scale bars: 10  $\mu$ m.

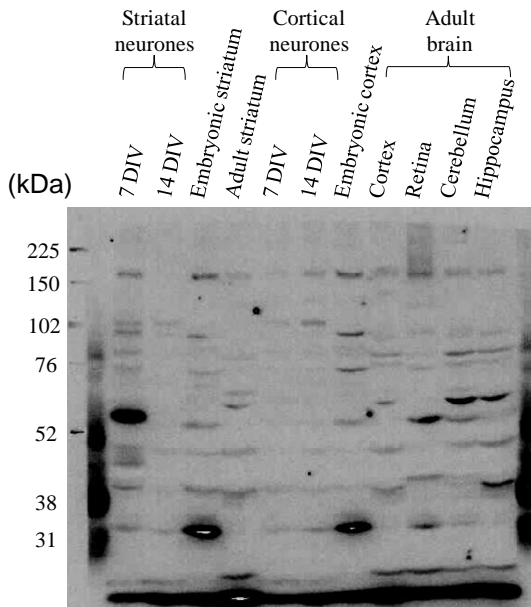
#### 4.3.3.3 *Detection of pikachurin in brain lysates using immunoblotting*

Using a specific antibody directed against the N-terminal domain of pikachurin (AA 28-354), we carried out immunoblotting in order to detect the expression of pikachurin in lysates of striatal and cortical neurones at 7 and 14 DIV but also in the embryonic (E16-18) and adult rat striatum, cortex, adult retina, cerebellum and hippocampus. As shown in the Figure 32, a number of immunoreactive bands were detected at different molecular weights. Pikachurin has previously been found to be cleaved in retina into two fragments: a predominant N-terminal fragment of 60 kDa and another C-terminal fragment of approximately the same molecular weight (which is not detectable with the pikachurin antibody used) (Han and Townes-Anderson, 2012).

As the expression of pikachurin has never been reported in regions other than retina, we were surprised to see so many different bands revealed with this antibody in different neuronal lysates. The expression of pikachurin seemed to be decreased from 7 to 14 DIV in rat striatal cultures with a predominant band ~60 kDa which is not present at 14 DIV. The expression of pikachurin in the embryonic striatum was very similar to the expression in the embryonic cortex with a predominant band around 35 kDa. In addition, the pattern of bands in the adult striatum was very similar to the pattern detected in the adult cortex with a main band ~40 kDa. While the expression of pikachurin in the cortical primary cultures seems quite low at both stages, it is the first time that we detected a band around 110 kDa, probably representing the full length pikachurin. The expression of pikachurin in the adult retina confirmed the reported band of ~60 kDa. However, other unexpected bands around 33 and 40 kDa were also observed. A predominant band around 65 kDa was found in both the adult cerebellum

and hippocampus, although another highly expressed band around 40 kDa was only present in the hippocampus. In addition, the strong low molecular weight band (~10 kDa) could be reflecting a high level of degradation of the protein.

Overall, these results suggest that pikachurin may be processed differently in the brain than in the retina. The specificity of detection of pikachurin with the available antibody remains to be confirmed.

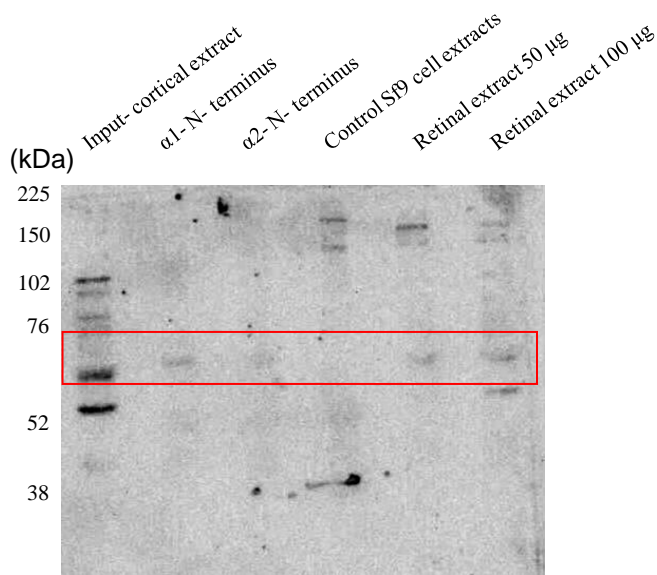


**Figure 32. Pikachurin is expressed in cortical and striatal primary cultures, and in different brain regions.** Samples were prepared using 2 % SDS, boiled, sonicated and spun down. Proteins (200 µg/lane) were resolved using SDS/PAGE (10 % gel). After transfer onto the nitrocellulose membrane, the samples were incubated with the antibody directed against the N-terminal domain of pikachurin (AA 28-354) (1: 10 000 dilution Wako, Japan; (Sato et al., 2008)) followed by HRP-conjugated anti-rabbit light-chain IgG. The immunoblot shows that different immunoreactive bands can be detected in striatal and cortical primary cultures and across the adult and embryonic brain (n=2).

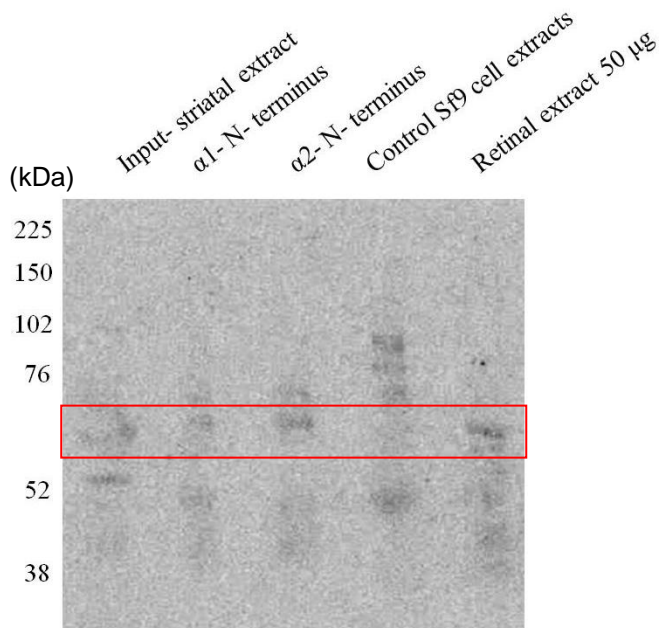
#### 4.3.3.4 *In vitro* binding of pikachurin to $\alpha$ 1- or $\alpha$ 2-ECD-Ni-NTA columns

Binding of pikachurin to GABA<sub>A</sub>Rs was investigated using lysates of cultured cortical and striatal neurones and  $\alpha$ 1- and  $\alpha$ 2-ECDs-loaded Ni-NTA resin. The Sf9 cell extracts were also loaded onto Ni-NTA beads and incubated with neuronal extracts as a control for non-specific binding. In addition, 50 and 100 µg of rat retinal extracts were also included in order to control for the specificity of the pikachurin antibody. Figure 33 shows that an immunoreactive band of 60 kDa (red box) found in the input lane containing cortical extracts, and in the retinal extract lane, is also present in lanes containing the  $\alpha$ 1 and  $\alpha$ 2 ECDs but is not present in the control Sf9 cell extracts. Thus, in this experiment, a pikachurin fragment of 60 kDa expressed in cortical neurones at early developmental stages, is able to specifically bind to the  $\alpha$ 1 and  $\alpha$ 2 ECDs. Figure

34 shows that a fragment of 60 kDa (red box) found in the input lane representing the 6 DIV striatal extracts, and in the retinal extract lane, is present bound to  $\alpha 1$  and  $\alpha 2$  ECDs but is not present in the control binding assay. Thus, in this experiment, a fragment of 60 kDa of pikachurin, expressed in striatal neurones at early developmental stages, is able to specifically bind the  $\alpha 1$  and  $\alpha 2$  ECDs.



**Figure 33. *In vitro* binding of pikachurin to purified  $\alpha 1$  and  $\alpha 2$  ECDs incubated with extracts of cultured cortical neurones.** Detergent-solubilised 6 DIV cortical neuronal lysates were incubated with Ni-NTA-immobilised  $\alpha 1$  or  $\alpha 2$  ECDs and analysed by SDS/PAGE. After transfer, the nitrocellulose membrane was incubated with a specific antibody directed against the N-terminal domain of pikachurin (AA 28-354) (1:10 000 dilution Wako, Japan) followed by HRP-conjugated rabbit light-chain IgG. Controls were prepared using extracts of Sf9 cells which did not express  $\alpha 1$  or  $\alpha 2$  ECDs. Retinal extract were used as controls for detection of pikachurin immunoreactivity.



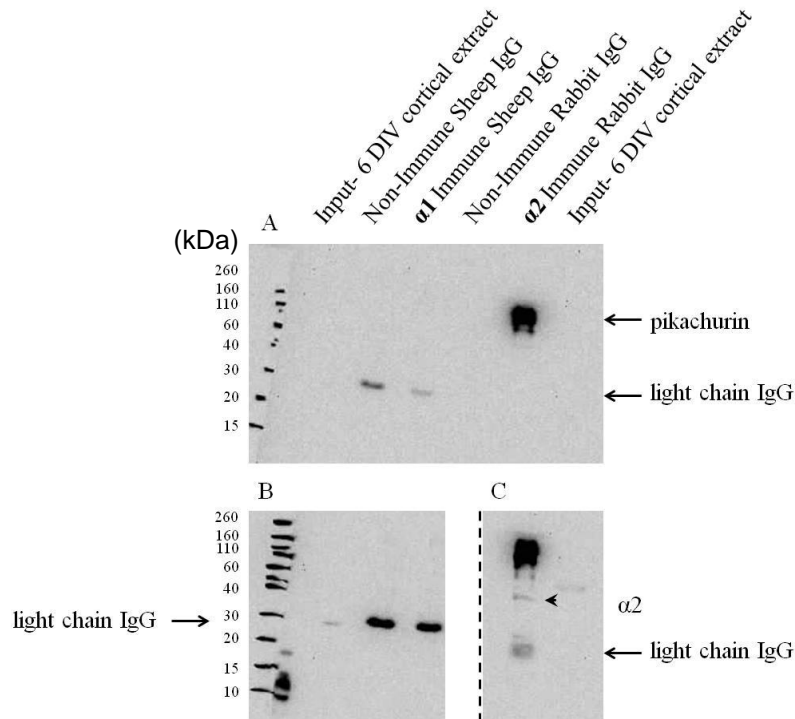
**Figure 34. *In vitro* binding of pikachurin to purified extracellular domains of GABA<sub>A</sub>R  $\alpha 1$  and  $\alpha 2$  subunits using 6 DIV striatal cultures.** Detergent-solubilised 6 DIV striatal neuronal lysates were incubated with Ni-NTA-immobilised  $\alpha 1$  or  $\alpha 2$  ECDs and analysed by SDS/PAGE. After transfer, the nitrocellulose membrane was incubated with a specific antibody directed against the N-terminal domain of pikachurin (AA 28-354) (1:10 000 dilution Wako, Japan) followed by HRP-conjugated rabbit light-chain IgG. Controls were prepared using extracts of Sf9 cells which did not express  $\alpha 1$  or  $\alpha 2$  ECDs. Retinal extract were used as controls for detection of pikachurin immunoreactivity.

#### 4.3.3.5 *Co-immunoprecipitation of pikachurin with the $\alpha 2$ subunit of GABA<sub>A</sub>Rs*

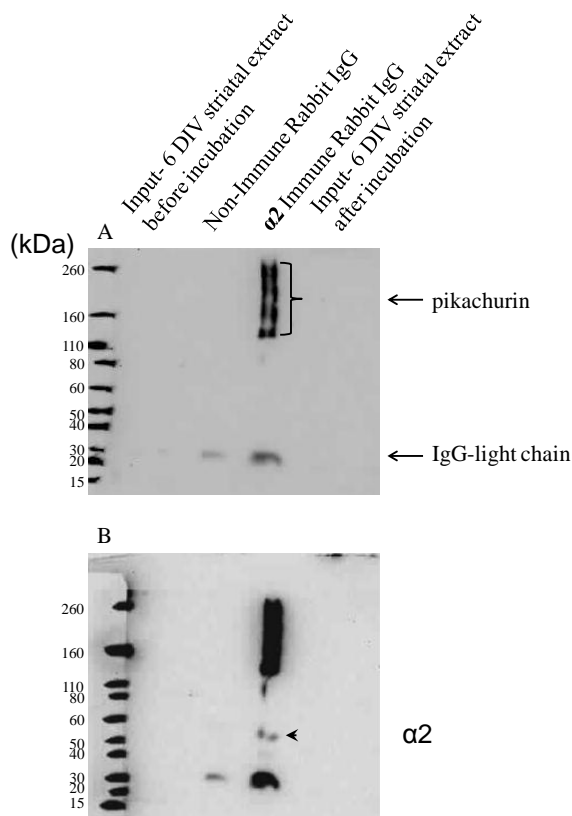
Co-immunoprecipitation experiments were carried out using lysates of cultured cortical or striatal neurones in order to study further the interaction between pikachurin and GABA<sub>A</sub>Rs. The lysates were incubated with the rabbit anti  $\alpha 2$  C-terminal specific (Duggan et al., 1991), sheep  $\alpha 1$  C-terminal specific (Pollard et al., 1993) antibodies or non-immune rabbit or sheep IgGs. The protein complexes bound to the sheep  $\alpha 1$  antibody or control sheep IgG were pulled down with Protein G-Sepharose beads, while complexes bound to the rabbit  $\alpha 2$  antibody or control rabbit IgG were pulled down with Protein A-Sepharose. The co-IPs were loaded on a 12 % SDS/PAGE and transferred onto the nitrocellulose membrane which was subsequently probed with the rabbit anti-pikachurin antibody. Figure 35A shows that pikachurin was co-immunoprecipitated only with  $\alpha 2$  antibody as the band of ~110 kDa. As a control for the efficiency of co-IP, the membrane was cut and each part was probed with either the anti  $\alpha 1$ - or  $\alpha 2$ -specific antibodies. Figure 35B demonstrates that  $\alpha 1$  subunit (~51 kDa) was not efficiently immunoprecipitated in this experiment. However, the Figure 35C demonstrates that  $\alpha 2$  (~51 kDa) was efficiently immunoprecipitated in this experiment (arrow). We noticed that in this experiment, the light chain of sheep IgG cross-reacted with the anti rabbit HRP antibody.

The lysates of cultured striatal neurones were incubated with the rabbit anti  $\alpha 2$  C-terminal antibody or the non-immune rabbit IgG (Figure 36). After incubation with Protein G-Sepharose, the co-IP was loaded on a 7 % SDS PAGE in order to allow a better separation of high molecular weight proteins. The Figure 36A shows that pikachurin was co-immunoprecipitated with the  $\alpha 2$  antibody and was not present in the non-immune rabbit IgG. In addition, the lower acrylamide percentage allowed us to differentiate four different molecular weight bands of pikachurin from 110 to 260 kDa. This could be due to the presence of different fragments in the protein complex, the presence of oligomers or different degree of glycosylation as suggested in (Han and

Townes-Anderson, 2012). Similarly to the previous experiment, the membrane was restriped and re-probed with the anti- $\alpha 2$  loop antibody. As shown in The Figure 36B,  $\alpha 2$  subunit was present in the immunocomplex together with pikachurin.



**Figure 35. Pikachurin interacts with the alpha 2-containing GABA<sub>A</sub> receptors in cortical extracts and can be co-immunoprecipitated using specific antibodies.** Detergent-solubilised 6 DIV cortical extracts were incubated with the rabbit anti  $\alpha 2$  C-terminal specific sheep  $\alpha 1$  C-terminal specific antibody or non-immune rabbit or sheep IgG. The protein complexes were pulled down with Protein G-Sepharose in the case of sheep IgG, or Protein A-Sepharose in the case of rabbit IgG. Proteins were resolved using a 4-12 % NuPAGE gradient gel and transferred onto the nitrocellulose membrane. **A.** The membrane was probed with the rabbit anti-pikachurin antibody (1:2500 dilution, Wako, Japan; followed by HRP-conjugated rabbit light-chain IgG (1:1000). **B.** After restriping, the membrane was cut into two parts. The left part was incubated with the rabbit anti  $\alpha 1$  N-terminal specific antibody (1:300 dilution) followed by HRP- conjugated rabbit light-chain IgG (1:1000). The arrow shows the light chain IgG at ~25 kDa. **C.** The right part of the membrane was incubated with the rabbit anti  $\alpha 2$  intracellular loop specific antibody (2  $\mu$ g/ml dilution). The arrowhead shows the  $\alpha 2$  subunit at ~51 kDa.



**Figure 36 Pikachurin interacts with the alpha 2-containing GABA<sub>A</sub> receptors in 6 DIV striatal extracts and can be co-immunoprecipitated using specific antibodies.** Detergent-solubilised 6 DIV striatal extracts were incubated with the rabbit anti  $\alpha 2$  C-terminal specific antibody or non-immune rabbit IgG. The protein complexes were pulled down with Protein A-Sepharose. Proteins were resolved using a 4-12 % NuPAGE gradient gel and transferred onto the nitrocellulose membrane. **A.** The membrane was probed with the rabbit anti-pikachurin antibody (1:2500 dilution, Wako, Japan; followed by HRP-conjugated rabbit light-chain IgG (1:1000). **B.** After restripping, the membrane was incubated with the rabbit anti  $\alpha 2$  intracellular loop specific antibody (2  $\mu$ g/ml dilution). The arrowhead shows the  $\alpha 2$  subunit at ~51 kDa.

#### 4.4 Discussion

In this chapter, our aim was to establish the optimal conditions for proteomics and tandem mass spectrometry analysis of proteins that bind to the extracellular domains of GABA<sub>A</sub>R  $\alpha 1$  and  $\alpha 2$  subunits. These experiments were based on our hypothesis that the extracellular domains of GABA<sub>A</sub> receptor subunits interact with specific proteins residing in the synaptic cleft and that identification of these proteins could lead to a better understanding of specific GABAergic synapse formation.

To do so, we performed two rounds of proteomics and mass spectrometry analysis and analysed the candidate binding proteins using two independent approaches.

The first round of proteomics revealed a large number of candidate binding proteins which were analysed using free online-based analysis software the Global Proteome Machine (GPM). Subsequently this experiment was analysed using Mascot on-site based analysis software at Swansea University. The two databases provided us

with different outputs and allowed us to compare the relevance of these outputs. The GPM database is based on the use of the Rat Proteome ENSEMBL database. It has provided us with the  $\log(e)$  value of each hit representing the matching score between the peptide sequence of the hit protein (from the database) and the experimental sequence read in the experimental MS/MS spectrum. In contrast, the Mascot database is based on the International Protein Index Rat Database and provided us with the protein score of each hit which is based on the calculated probability,  $P$ , that the observed match between the experimental data and the database sequence is a random event. Similarly, a second round of mass spectrometry and proteomics was performed and analysed with both databases GPM and Mascot. The analysis of the first round with GPM database allowed us to identify a list of proteins that were specifically found in the  $\alpha 1$  and  $\alpha 2$ -ECD-column and which were absent from the control binding assay. Among them, we identified two proteins which belong to the heparan sulfate proteoglycans (HSPG) family, perlecan and pikachurin, which were detected bound to the  $\alpha 1$ -ECD- and  $\alpha 2$ -ECD-, respectively. Interestingly, these two proteins were not retrieved when we analysed the first round with Mascot, suggesting that the identification of the experimental peptides and the peptides referenced within the database are different. Potentially, this divergence could be explained by the different referring databases used by the software (Rat Proteome ENSEMBL was used by GPM, and international protein index (IPI) rat proteome was used by Mascot). Additionally, this could be due to different flexibility of the software in assigning a peak from the tandem MS/MS spectrum to a theoretical peptide. This was supported by the fact that the list of proteins retrieved after Mascot analysis was much longer than the list of proteins identified with GPM, suggesting a much less stringent screening performed by Mascot software.

In addition, the proteins identified in the second round differed considerably from the one found in the first round and we could not retrieve perlecan or pikachurin with either software analysis of this round. This could be due to the high speed

centrifugation step which was introduced in this round, thus probably changing the protein content of the lysate prior the binding assays with  $\alpha 1$ - or  $\alpha 2$ -ECDs loaded columns. This could also be due to the fact that the reproducibility of mass spectrometry experiments in general is the matter of intensive debate as it involves multiple steps and many factors that determine the final outcomes are not always possible to control (Wang et al., 1998).

Considering pikachurin as a potential hit was of high risk as the log (e) it was pulled out with was relatively low, that we did not replicate its presence in the second round of proteomics and mass spectrometry, and the lack of information of the role of this protein in the brain. However, the low log (e) for pikachurin identification leaves us with less than 1 % of chance that the assignment was random. Although pikachurin has been described well in retina, its abundance in the brain and its role has not been investigated so far, although the mRNA for pikachurin was detected in the brain in the original cloning paper (Sato et al., 2008).

We were unable to perform experiments with perlecan due to time constrains, but it would be interesting to test if perlecan binds to the  $\alpha 1$  or  $\alpha 2$  ECDs by co-immunoprecipitation.

As a second part in this chapter, we performed a series of binding assay in order to have a better understanding of the potential presynaptic partners of  $\alpha 1$  and  $\alpha 2$  ECDs already proposed in the literature. In addition, we used co-immunoprecipitation techniques to confirm the binding of the GABA<sub>A</sub>R  $\alpha 2$  subunit ECDs with pikachurin.

In our experiments, NL2 did not bind to the ECDs of  $\alpha 1$  or  $\alpha 2$  GABA<sub>A</sub>R subunits. This result was in accordance with the literature as NL2 is mostly thought to be interacting with neurexins at the presynaptic site and with gephyrin at the postsynaptic site in promoting GABA<sub>A</sub>R synaptic clustering (Graf et al., 2004, Varoqueaux et al., 2006, Pouloupoulos et al., 2009, Kang et al., 2014). As it has already been suggested, neurexins are thought to be interacting with the extracellular domain of the  $\alpha 1$  subunit (Zhang et al., 2010). However, little is known about the capacity of individual subtypes



of  $\alpha$  subunits or other GABA<sub>A</sub>R subunits to bind different isoform of neurexins. In our binding assays with 6 DIV cortical neurones, we observed a differential binding of neurexin isoforms to  $\alpha 1$  or  $\alpha 2$  ECDs, suggesting that they may be interacting in a very specific way. To identify the specific partners would require a very long time given that there are ~ 3000 different splice variants of neurexin reported (Missler and Südhof, 1998).

Finally, we characterised the expression of pikachurin in the developing and adult brain, and its binding to the ECD of the GABA<sub>A</sub>R  $\alpha 2$  subunit. Our preliminary characterisation included immunohistochemical analysis of pikachurin expression in the embryonic mouse brain. In addition, we assessed the expression of pikachurin in cultured medium spiny neurones by immunocytochemistry and across embryonic and adult brain lysates by immunoblotting with pikachurin-specific antibodies. Together, our results demonstrated that in the embryonic brain, pikachurin can be found co-localised with the  $\alpha 2$  subunit and the presynaptic marker GAD-65 at some GABAergic synapses. In addition, the expression of pikachurin and its co-localisation with the  $\alpha 2$  subunit at synaptic contacts appear to be increased as the neurones mature in culture. Interestingly, the immunoblotting revealed that many isoforms of this protein can be detected in brain lysates and some of these isoforms can also be detected in retinal lysates (~60 kDa isoforms) which were used as a control. Binding of pikachurin was also detected *in vitro*, although it seemed weaker than across brain region lysates. Nevertheless, the co-immunoprecipitation experiments have confirmed that pikachurin interacts specifically with the  $\alpha 2$  subunit of GABA<sub>A</sub>Rs.

To further this research, our aim will be to characterise the nature of the interaction between pikachurin and the GABA<sub>A</sub>R receptor  $\alpha 2$  subunit to determine whether the binding is direct or indirect. In addition, we aim to map the binding sites in the  $\alpha 2$  ECD and also in pikachurin. It would also be interesting to investigate the localisation of pikachurin in the embryonic and adult brain, characterise the time course of expression of pikachurin during brain development and to compare this with the time

course of GABAergic synapse formation. Once the structural characteristics of the binding are established, it would be important to study GABAergic synapse formation in pikachurin knock-out (KO) mice, or look at the expression of pikachurin in GABA<sub>A</sub>R subunit  $\alpha$ 2 KO mice.

# Chapter five

## 5. GABAergic synapse formation: study of embryonic MSNs development

### 5.1 Introduction

During the embryonic brain development, the telencephalon gives rise to the striatum and the globus pallidus (Jain et al., 2001). The ventral telencephalon is divided into two transient structures which are present at the mid-stages of the embryonic rat brain development, the ganglionic eminences (Olsson et al., 1998). While the striatum is derived from the lateral ganglionic eminence, the globus pallidus is derived from the medial ganglionic eminences (Marin et al., 2000).

The GABAergic medium spiny neurones (MSNs) account for ~ 95 % of all neurones contained in the striatum. The striatum is a central part of the basal ganglia, a group of nuclei involved in the selection and execution of voluntary movements, as well as cognitive, associative and emotional aspects of motor behaviour (Albin et al., 1989, Mink and Thach, 1993). Virtually the whole of the cortical mantle projects in a topographic manner onto the striatum. This cortical information is processed by the projecting medium spiny neurones within the striatum, and passed via the *direct* and *indirect* pathways to the output nuclei of the basal ganglia, the internal segment of the globus pallidus and the *Substantia Nigra pars reticulata* (SNpr) (Bolam et al., 2000). The basal ganglia transmit the signal by the projections of these output nuclei to the thalamus and then back to the cortex or subcortical premotor regions (Bolam et al., 2000).

In addition, the MSNs receive an important dopaminergic innervation from the *Substantia Nigra pars compacta* (SNpc) which promotes the structural plasticity of MSNs during the development of basal ganglia circuits (Fisone et al., 2007, Fasano et al., 2013). Interestingly, it has been shown that via activation of D1- and D2- receptors, dopamine limits the extent of collateral inhibitory synaptogenesis between medium spiny neurones (Goffin et al., 2010).

The loss of MSNs from the striatum of patients with Huntington's disease is manifested in profound changes in motor movements (Rikani et al., 2014). In Parkinson's disease, the loss of dopaminergic neurones from the SNpc modifies the activity of the striatum and results in motor disturbances (Lewis et al., 2003). Thus, understanding the functioning of the striatum is of tremendous physiological and pathophysiological importance.

In order to understand how the striatum functions it is important to understand how the cellular components of the striatum develop and are regulated. To investigate the development of MSNs we have isolated them from the embryonic striatum and cultured them for up to 14 DIV. These cultured neurones have been shown to express a number of the *in vivo* markers of MSNs including D<sub>1</sub> and D<sub>2</sub> dopamine receptors, GAD, Ca<sup>2+</sup> binding proteins, cannabinoid receptors, and K<sup>+</sup> channels (Falk et al., 2006). Furthermore, these neurones have been shown to form GABAergic synapses by axon collaterals and generate spontaneous GABAergic currents through activation of the ligand-gated channels GABA<sub>A</sub>Rs by the neurotransmitter GABA (Kowalski et al., 1995).

GABA<sub>A</sub>Rs are heteropentamers usually composed of two  $\alpha$ , two  $\beta$  and one  $\gamma$  subunit. The main subunits expressed at GABAergic synapses in the projecting MSNs are the  $\alpha$ 1-2,  $\beta$ 2 and  $\gamma$ 2 subunits (Fujiyama et al., 2000). Depending on the type of  $\alpha$  subunit incorporated in the postsynaptic GABA<sub>A</sub>Rs, the regional expression, physiological and functional properties of the GABAergic synapse will differ (Nusser et al., 1996, Fritschy and Panzanelli, 2014). More specifically, it has been shown that while the  $\alpha$ 1 subunit is expressed in the somatic and dendritic synapses of MSNs, the  $\alpha$ 3 subunit expression was restricted to the perisomatic synapses, a region mostly contacted by local axon collaterals. In contrast, the  $\alpha$ 2 subunit was mostly present in dendritic compartments where striatal MSNs contact MSNs from the globus pallidus (Gross et al., 2011). Thus, due to the kinetic properties conferred by each individual  $\alpha$  subunit, this specific distribution is likely to contribute differentially to both physiological

and pathological patterns of activity in this complex neuronal network of basal ganglia medium spiny neurones (Gross et al., 2011).

Immunocytochemical studies have revealed that the scaffolding protein gephyrin is present at postsynaptic densities of GABAergic synapses (Kneussel and Betz, 2000). In the brain, this protein is enriched at postsynaptic sites which contain GABA<sub>A</sub>R subtypes composed of  $\alpha(1-3)$ ,  $\beta(2-3)$  and  $\gamma 2$  subunits (Jacob et al., 2008). It has been shown that gephyrin binds directly to GABA<sub>A</sub>R via the intracellular loop of the  $\alpha 1-3$  GABA<sub>A</sub>R subunits (Tretter et al., 2008, Mukherjee et al., 2011, Tretter et al., 2011). In doing so, gephyrin plays a central role in the formation of functional GABAergic synapse as it is responsible for the clustering of GABA<sub>A</sub>R into the postsynaptic membrane, enabling the synaptic inhibition to be fast and strong (Tyagarajan and Fritschy, 2014).

Elucidating the way the heterogeneity and clustering of GABA<sub>A</sub>R are regulated during MSNs development will lead us to a better understanding of the way MSNs communicate with each other, and in doing so, contribute to the functioning of the striatum.

### **5.1.1 Aims**

In this part of the thesis, our main goal was to characterise the formation of  $\alpha 1$  and/or  $\alpha 2$ -containing clusters of GABA<sub>A</sub>R and their association with the presynaptic GABAergic terminals. The key questions that we wanted to address are:

1. What is the expression pattern of these subtypes of GABA<sub>A</sub>R throughout the development of medium spiny neurones *in vitro*?
2. Are all  $\alpha 1$  and  $\alpha 2$  GABA<sub>A</sub>R clusters inserted in synaptic contacts?
3. Is gephyrin involved in the formation of GABAergic synapses incorporating different subtypes of GABA<sub>A</sub>R?

## **5.2 Methods**

### **5.2.1 Primary cultures of MSNs**

Neurons were prepared as described in Chapter 2, Section 2.1

### **5.2.2 Immunocytochemistry**

Immunocytochemistry was performed as described in Chapter 2, Section 2.2. Neurons cultured for 7 or 14 DIV, were fixed using 4 % PFA/ sucrose for 12 minutes at room temperature. After fixation, they were incubated with Glycine (0.3 M) in PBS, in order to quench PFA. After washing, cells were incubated in 1 % BSA in PBS for 1 hour and subsequently incubated with anti-  $\alpha 1$  and anti-  $\alpha 2$  antibodies, specifically binding to their N-terminal extracellular domains, diluted in 1 % BSA in PBS overnight (14-16 hours) at 4 °C (Table 14). Cultures were then permeabilised by incubating with 1 % BSA, 0.5 % Triton X-100 in PBS for 15 minutes. Neurons were subsequently incubated with mouse anti- GAD-65 or gephyrin and chicken anti- MAP-2 antibodies (see Table 14 for dilutions) diluted in 1 % BSA in PBS for 2 hours at room temperature. Following this step, conjugated secondary antibodies were added as described in Chapter 2, Section 2.2 (antibodies used in these experiments are described in the Table 14).

### **5.2.3 Confocal analysis**

Immunolabelling was analysed using Zeiss LSM 710 confocal microscope with a Plan-Apochromat 63x/1.4 Oil DIC lens. Threshold for each channel was calculated from the background staining intensity and then removed from the image. To count the density and size of  $\alpha 1$ - and  $\alpha 2$ - containing GABA<sub>A</sub> receptor clusters or gephyrin clusters, puncta were defined as immunoreactive profiles greater than 0.1  $\mu\text{m}^2$ , with the mean intensity of each cluster equal or higher than double the standard deviation of intensity which was indicated by the Zen 2009 Programme. The defined clusters were encircled and their properties noted by hand. The density and size of  $\alpha 1$  clusters were first calculated, followed by the  $\alpha 2$  clusters. Then,  $\alpha 1$  clusters which were mixed with

$\alpha 2$  (minimum of 50 % overlapping) were separated from  $\alpha 1$  clusters and analysed as a separate group. The same process was applied for  $\alpha 2$  mixed clusters. Because the proportion of  $\alpha 1$  and  $\alpha 2$  clusters was different among mixed clusters, these populations were kept and analysed separately, although in most of the cases, they represented the same population of mixed clusters. Therefore, we did not separate these two types of mixed clusters when we analysed their co-localisation with gephyrin.

#### **5.2.4 Analysis of synaptic parameters**

As a criterion for synaptically localised clusters, I determined whether these clusters were in close apposition with the presynaptic marker GAD-65. A minimum of 50 % overlap was used to estimate the close apposition between the postsynaptic clusters and the presynaptic GAD-65 positive terminals. The same overlapping criterion was used to determine the density and ratio of  $\alpha 1$  and/or  $\alpha 2$ - containing clusters co-localised with gephyrin. The total density of GAD-65 immunoreactive puncta forming contacts along the first 20  $\mu\text{m}$  length of primary dendrites was counted to determine the density of presynaptic inputs.

#### **5.2.5 Statistical analysis**

Once all the parameters were measured, they were copied into an Excel file and sorted into different groups according to their size, co-localisation with GAD-65 and kind, single or mixed clusters:

- All  $\alpha 1$  single clusters
- $\alpha 1$  single clusters which are co-localised with GAD-65
- All  $\alpha 2$  single clusters
- $\alpha 2$  single clusters which are co-localised with GAD-65
- All  $\alpha 1$  mixed clusters
- $\alpha 1$  mixed clusters which are co-localised with GAD-65
- All  $\alpha 2$  mixed clusters
- $\alpha 2$  mixed clusters which are co-localised with GAD-65



- All gephyrin clusters
- $\alpha 1$  single clusters which are co-localised with gephyrin
- $\alpha 2$  single clusters which are co-localised with gephyrin
- mixed clusters which are co-localised with gephyrin

Subsequently, the data was analysed using Origin Pro 9.0 32 Bit software. Normal (Gaussian) distribution of the pooled data was first tested using the Shapiro-Wilk and Kolmogorov-Smirnov tests. Since the data did not follow a normal distribution and the categories were independent, non-parametric statistical analysis was carried out using the Mann Whitney test with an interval of confidence of 95 %. Because they represent a robust measure of central tendency when distributions are not normally distributed, the medians and their interquartile range (IQR) were used to describe the data and evaluate statistical dispersion. With the groups following normal distribution, statistical analysis was done using two sample Student's t-test. The synaptic and total densities of clusters were evaluated along the length of 20  $\mu\text{m}$  of primary dendrite for each cell. The percentage of synaptic clusters over the total population was determined for each dendrite.

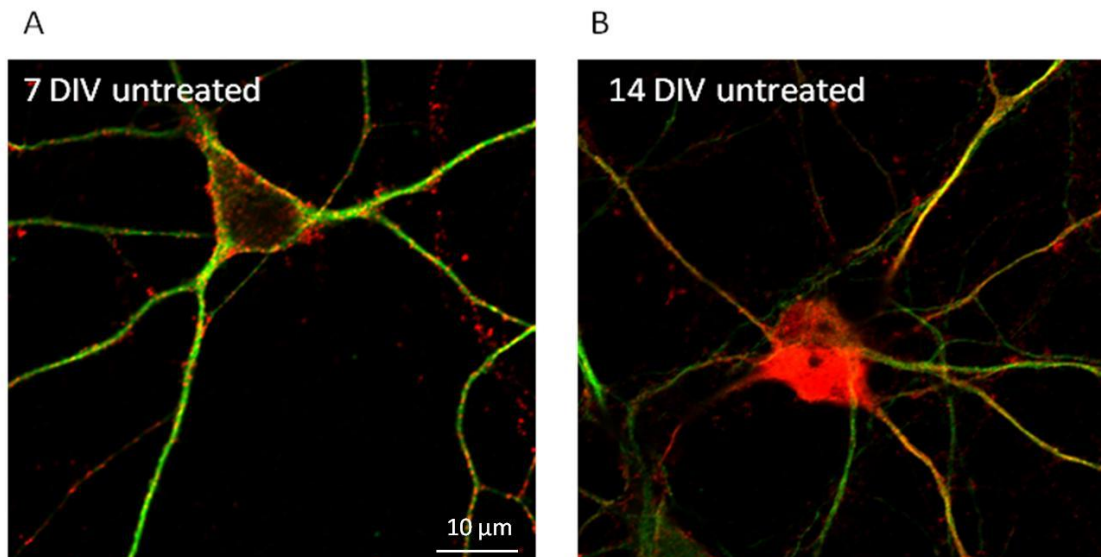
**Table 14. Antibodies used for immunocytochemical analysis of MSNs in culture**

primary antibodies				secondary antibodies		
specificity	origin	dilutions	source and characterisation	antibodies	dilutions	source
GABA <sub>A</sub> α1	Rabbit	1:200	Duggan, MJ, Stephenson AF., 1990. <i>J Biol Chem</i>	Goat anti rabbit 405	1:750	Alexa Fluor Invitrogen a31556
GABA <sub>A</sub> α2	Guinea-pig	1:400	Synaptic System 224104	Goat Anti guinea pig 488	1:750	Alexa Fluor Invitrogen a11073
GAD65	Mouse	1:4000	Abcam, ab26113	Goat anti mouse 555	1:750	Alexa Fluor Invitrogen a21422
MAP2	Chicken	1:2500	Abcam, ab92434	Goat Anti chicken 488	1:750	Alexa Fluor Invitrogen a11039
Gephyrin	Mouse	1:500	Synaptic System, 147111	Goat Anti-mouse 555	1:750	Alexa Fluor Invitrogen a21422

### 5.3 Results

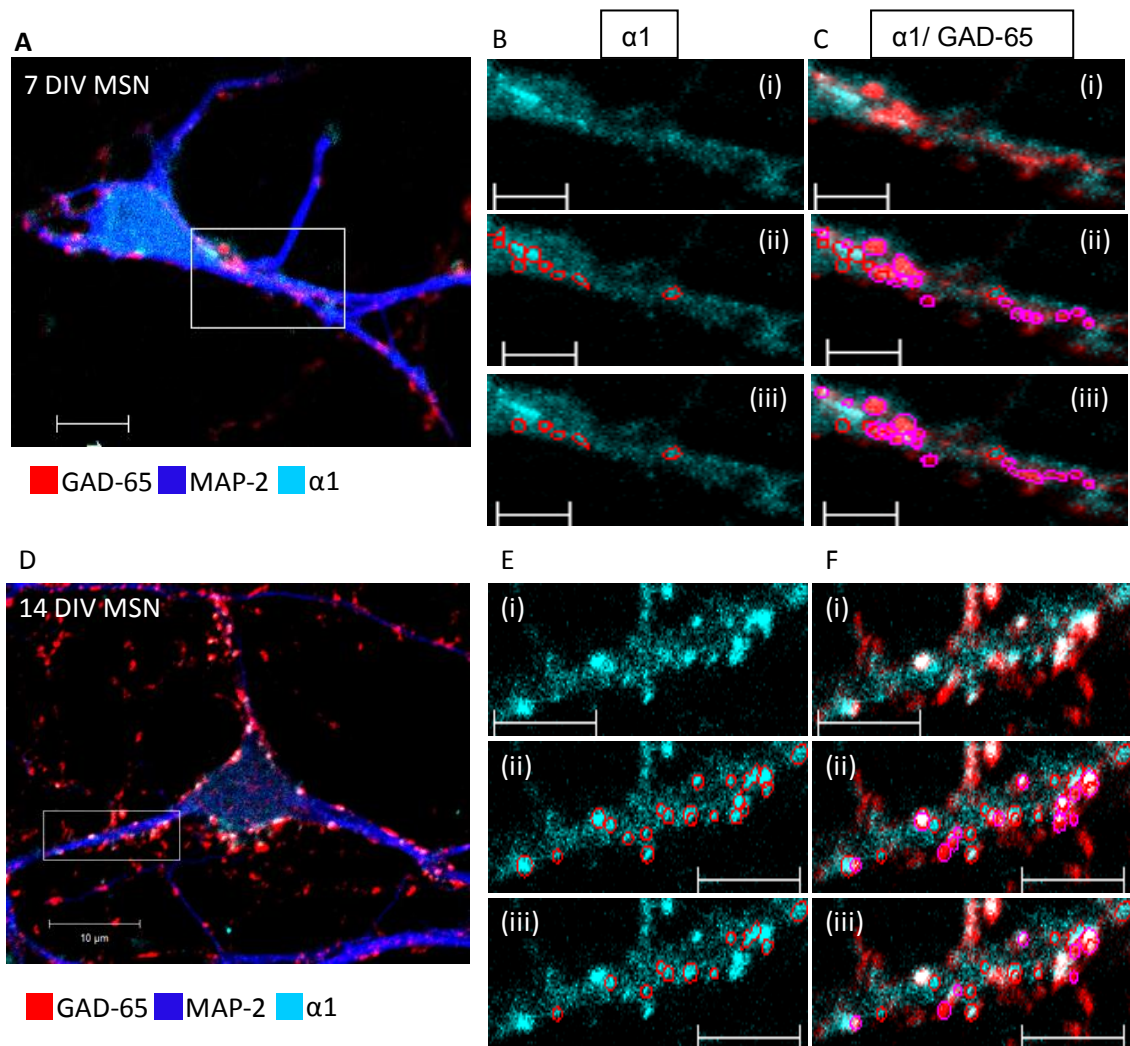
#### 5.3.1 A specific decrease in the total density of α1 single and mixed GABA<sub>A</sub>R clusters is observed from 7 to 14 DIV

Cultured embryonic (E16-18) striatal neurones form a homogeneous population of the precursors of GABAergic medium spiny neurones (MSNs) (Goffin et al., 2010). Although formation of synapses between these neurones has been partially characterised in our laboratory, how specific α1- and α2-containing synapses are established is currently unknown. Cultured embryonic MSNs were previously characterised by immuno-reactivity for DARPP-32 (Dopamine- and cyclic AMP-Regulated Phosphoprotein), a well-established marker of these neurones (Greengard et al., 1999). Striatal tissue from embryonic E17 rat brains was dissected, dissociated and cultured from 7 to 14 DIV. Following staining, the fluorescence of DARPP-32 was increased in all the cells during development. This confirmed that a homogeneous population of GABAergic MSN precursors was cultured (Figure 37).

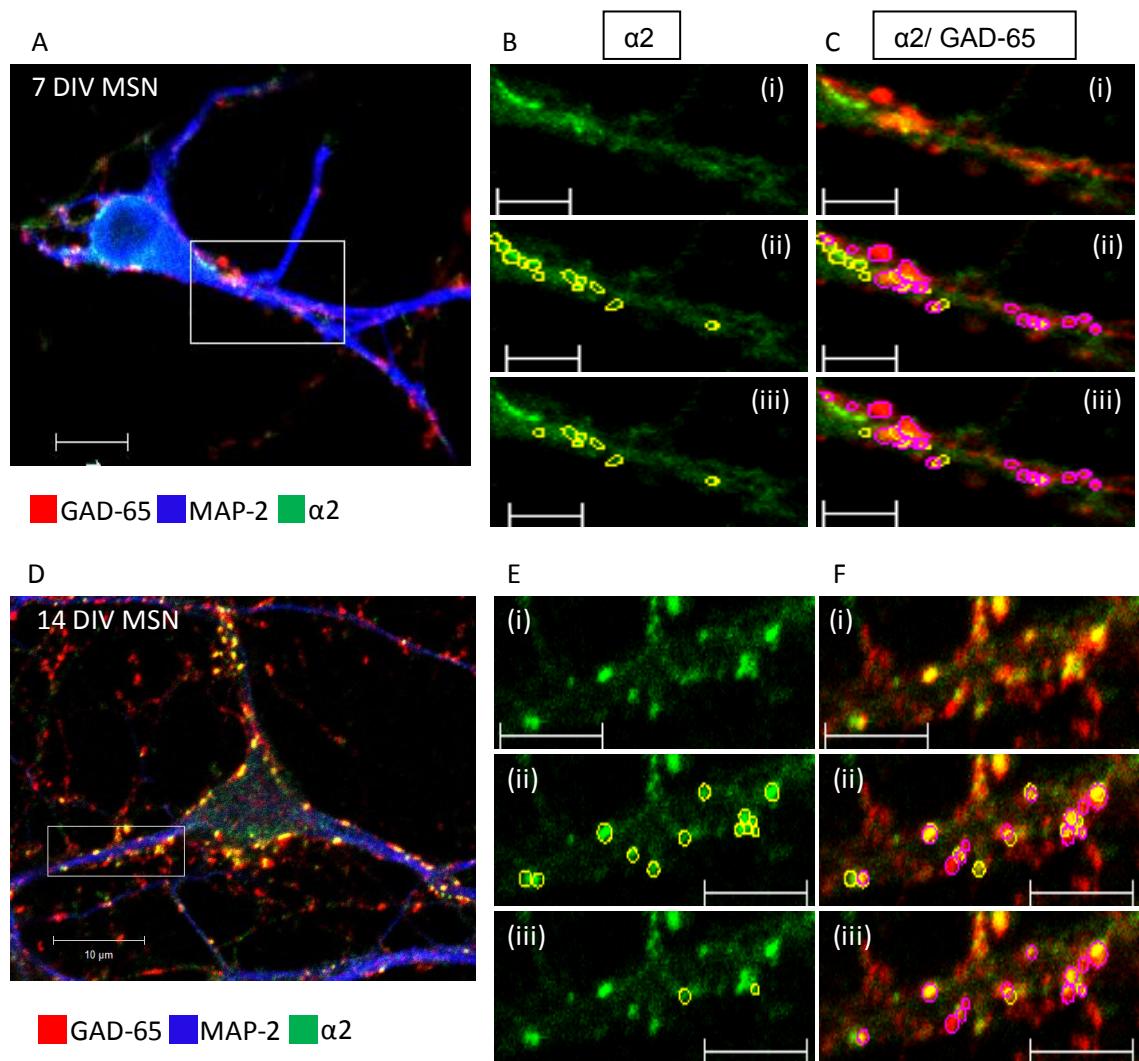


**Figure 37. The expression of DARPP-32 is increased during development of cultured embryonic MSNs (Arama et al., in preparation).** Immunolabelling of cultured embryonic MSNs representing the level of expression of DARPP-32 (red) and MAP-2 (green) from 7 to 14 DIV. **A.** Merged image of a 7 DIV striatal neurone immunostained for DARPP-32 and MAP-2. **B.** Merged image of 14 DIV striatal neurones immunostained for DARPP-32 and MAP-2.

In order to study specific synapse formation, striatal neurones were cultured for 7 or 14 days and synapse formation was analysed using immunocytochemistry and confocal imaging. Figure 38, 39 and 40 show the same couple of neurones stained for  $\alpha 1$  and/or  $\alpha 2$  extracellular domains of GABA<sub>A</sub>Rs subunits, the presynaptic marker GAD-65 and MAP-2, using the antibodies described in table 14. The total density of  $\alpha 1$  single-,  $\alpha 2$  single- or  $\alpha 1/\alpha 2$  mixed subunits- containing GABA<sub>A</sub>R clusters, and the density of synaptic clusters in each groups were determined using the Zen 2009 programme. Synaptic receptor clusters were defined as those closely apposed to the presynaptic GAD-65 positive terminals.

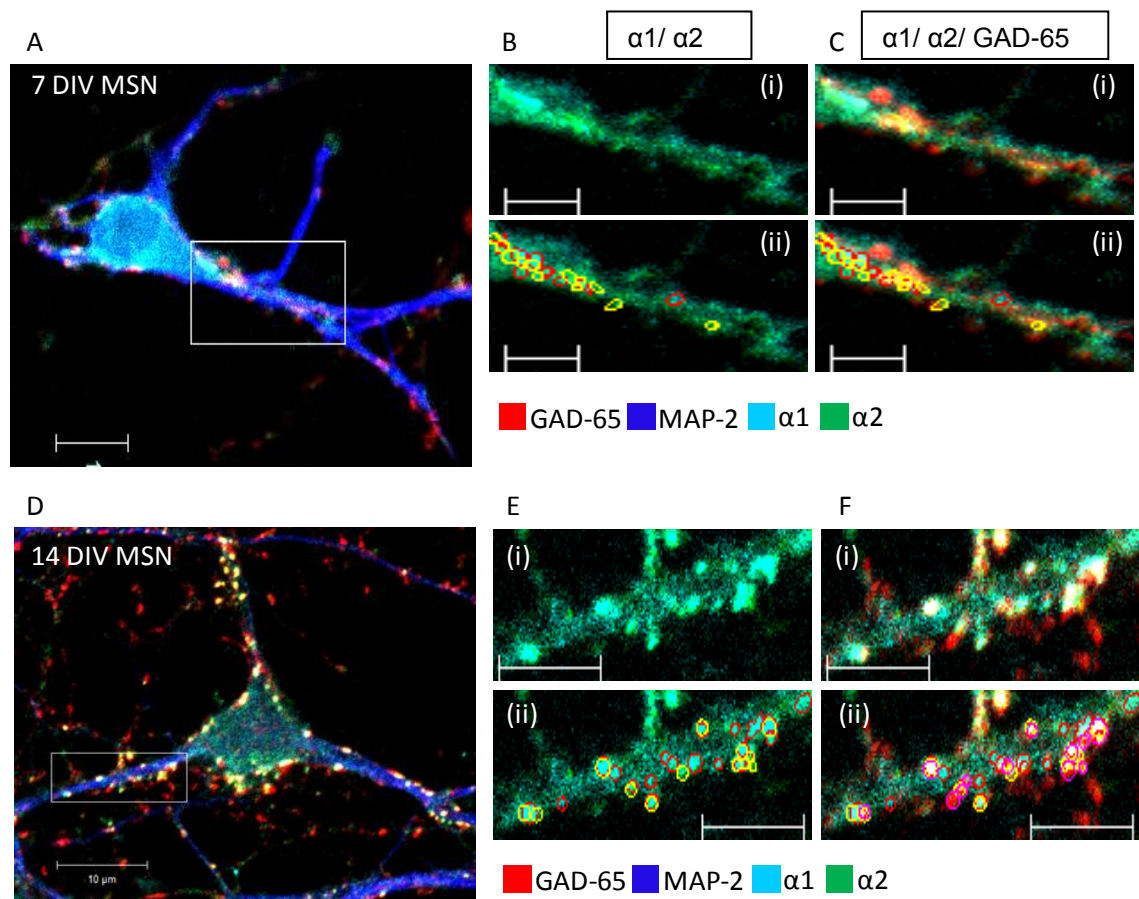


**Figure 38. The density and size of  $\alpha 1$  containing GABA<sub>A</sub>R clusters are modified from 7 to 14 DIV.** Immunolabelling of GABA<sub>A</sub>R  $\alpha 1$  subunit-containing clusters (cyan) and presynaptic GABAergic terminals (red) along primary dendrites (blue) of cultured MSNs. **A.** Merged image of a 7 DIV striatal neurone (scale bar: 10  $\mu$ m). **B. (i)** Enlarged image of boxed region in A representing  $\alpha 1$  staining only. **(ii)** Analysis of image B(i) in which all  $\alpha 1$  clusters are circled in red. **(iii)** Analysis of image B(i) in which only  $\alpha 1$  single clusters that are not associated with  $\alpha 2$  clusters are circled in red (scale bar: 5  $\mu$ m). **C. (i)** Enlarged image of boxed region in A representing  $\alpha 1$  positive clusters and presynaptic GAD-65 positive nerve terminals. **(ii)** Analysis of image C(i) in which all  $\alpha 1$  clusters were circled in red and presynaptic terminals were circled in purple. **(iii)** Analysis of image C(i) in which only  $\alpha 1$  single clusters were circled in red and presynaptic terminals were circled in purple (scale bar: 5  $\mu$ m). **D.** Merged image of a 14 DIV striatal neurone (scale bar: 10  $\mu$ m). **E. (i)** Enlarged image of boxed region in D representing  $\alpha 1$  staining only. **(ii)** Analysis of image E(i) in which all  $\alpha 1$  clusters are circled in red. **(iii)** Analysis of image E(i) in which only  $\alpha 1$  single clusters that are not associated with  $\alpha 2$  clusters are circled in red (scale bar: 5  $\mu$ m). **F. (i)** Enlarged image of boxed region in D representing  $\alpha 1$  positive clusters and presynaptic GAD-65 positive nerve terminals. **(ii)** Analysis of image F(i) in which all  $\alpha 1$  clusters were circled in red and presynaptic terminals were circled in purple. **(iii)** Analysis of image F(i) in which only  $\alpha 1$  single clusters were circled in red and presynaptic terminals were circled in purple (scale bar: 5  $\mu$ m).



**Figure 39. The density and size of  $\alpha 2$  containing GABA<sub>A</sub>R clusters are modified from 7 to 14 DIV.** Immunolabelling of GABA<sub>A</sub>R  $\alpha 2$  subunit-containing clusters (green) and presynaptic GABAergic terminals (red) along primary dendrites (blue) of cultured MSNs. **A.** Merged image of a 7 DIV striatal neurone (scale bar: 10  $\mu$ m). **B. (i)** Enlarged image of boxed region in A representing  $\alpha 2$  staining only. **(ii)** Analysis of image B(i) in which all  $\alpha 2$  clusters are circled in yellow. **(iii)** Analysis of image B(i) in which only  $\alpha 2$  single clusters that are not associated with  $\alpha 1$  clusters are circled in yellow. **C. (i)** Enlarged image of boxed region in A representing  $\alpha 2$  positive clusters and presynaptic GAD-65 positive nerve terminals. **(ii)** Analysis of image C(i) in which all  $\alpha 2$  clusters were circled in yellow and presynaptic terminals were circled in purple. **(iii)** Analysis of image C(i) in which only  $\alpha 2$  single clusters were circled in yellow and presynaptic terminals were circled in purple (scale bar: 5  $\mu$ m). **D.** Merged image of a 14 DIV striatal neurone (scale bar: 10  $\mu$ m). **E. (i)** Enlarged image of boxed region in D representing  $\alpha 2$  staining only. **(ii)** Analysis of image E(i) in which all  $\alpha 2$  clusters are circled in yellow. **(iii)** Analysis of image E(i) in which only  $\alpha 2$  single clusters that are not associated with  $\alpha 2$  clusters are circled in yellow (scale bar: 5  $\mu$ m). **F. (i)** Enlarged image of boxed region in D representing  $\alpha 2$  positive clusters and presynaptic GAD-65 positive nerve terminals. **(ii)** Analysis of image F(i) in which all  $\alpha 2$  clusters were circled in yellow and presynaptic terminals were circled in purple. **(iii)** Analysis of image F(i) in which only  $\alpha 2$  single clusters were circled in yellow and presynaptic terminals were circled in purple (scale bar: 5  $\mu$ m).

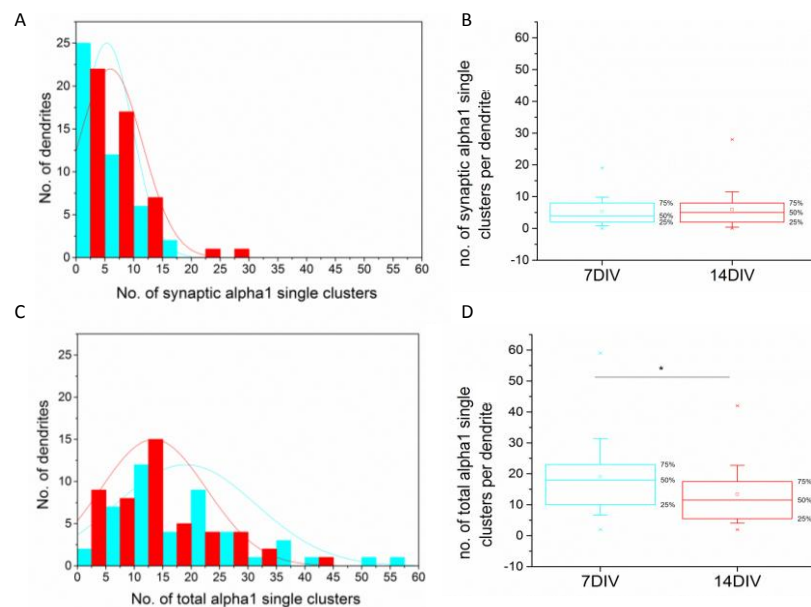




**Figure 40. The density and size of  $\alpha 1$  and  $\alpha 2$  containing GABA<sub>A</sub>R clusters (mixed clusters) are modified from 7 to 14 DIV.** Immunolabelling of GABA<sub>A</sub>R  $\alpha 1$  and  $\alpha 2$  subunit-containing clusters (mixed clusters, cyan and green) and presynaptic GABAergic terminals (red) along primary dendrites (blue) of cultured MSNs. **A.** Merged image of a 7 DIV striatal neurone (scale bar: 10  $\mu$ m). **B. (i)** Enlarged image of boxed region in A representing  $\alpha 1$  and  $\alpha 2$  staining. **(ii)** Analysis of image B(i) in which all mixed  $\alpha 1$  clusters are circled in red and  $\alpha 2$  clusters are circled in yellow (scale bar: 5  $\mu$ m). **C. (i)** Enlarged image of boxed region in A representing  $\alpha 2$  positive clusters and presynaptic GAD-65 positive nerve terminals. **(ii)** Analysis of image C(i) in which all  $\alpha 2$  clusters were circled in yellow and presynaptic terminals were circled in purple (scale bar: 5  $\mu$ m). **D.** Merged image of a 14 DIV striatal neurone (scale bar: 10  $\mu$ m). **E. (i)** Enlarged image of boxed region in D representing  $\alpha 1$  and  $\alpha 2$  staining. **(ii)** Analysis of image E(i) in which mixed  $\alpha 1$  clusters are circled in red and  $\alpha 2$  clusters are circled in yellow (scale bar: 5  $\mu$ m). **F. (i)** Enlarged image of boxed region in D representing mixed  $\alpha 1$  and  $\alpha 2$  clusters and presynaptic GAD-65 positive nerve terminals. **(ii)** Analysis of image F(i) in which mixed  $\alpha 1$  were circled in red, mixed  $\alpha 2$  clusters were circled in yellow and presynaptic terminals were circled in purple (scale bar: 5  $\mu$ m).

Developing MSNs undergo specific changes in the density of  $\alpha 1$  single,  $\alpha 2$  single,  $\alpha 1$  mixed and  $\alpha 2$  mixed clusters of GABA<sub>A</sub>R from 7 to 14 DIV. The density of synaptic and total  $\alpha 1$  single clusters of GABA<sub>A</sub>R per defined length of primary dendrite (the first 20  $\mu$ m from the cell body) was estimated from 7 to 14 DIV (Figure 41). At 7 DIV, the median density of synaptic  $\alpha 1$  single clusters was 4 (8.5-2) compared to 5 (8-2) at 14 DIV (p value= 0.78, Mann Whitney test; n=45 dendrites analysed in 7 DIV-

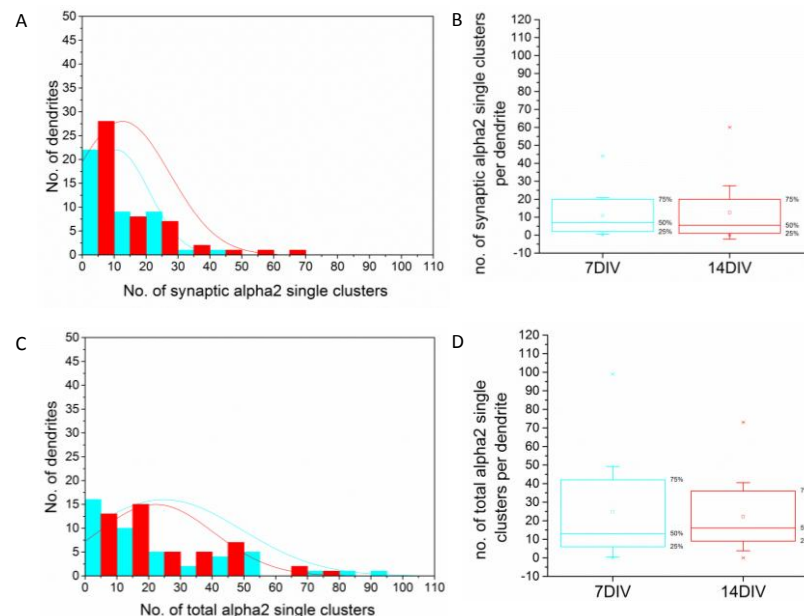
cultured neurones, and n=48 dendrites analysed in 14 DIV-cultured neurones). In contrast, the median density of total  $\alpha 1$  single clusters was 18 (25-10) at 7 DIV compared to 11.5 (17.75-5.25) at 14 DIV (p value=0.024, Mann Whitney test; n=45 dendrites analysed in 7 DIV-cultured neurones, and n=48 dendrites analysed in 14 DIV-cultured neurones). This demonstrates that while the density of synaptic  $\alpha 1$  single clusters remains unchanged, the total density of  $\alpha 1$  single clusters decreases significantly. This indicates that the extrasynaptic  $\alpha 1$ -containing GABA<sub>A</sub>R clusters are down-regulated from 7 to 14 DIV.



**Figure 41. The total density of  $\alpha 1$  single clusters per primary dendrite of MSNs is decreased from 7 to 14 DIV.** The density of  $\alpha 1$ -containing GABA<sub>A</sub> receptors clusters ( $\alpha 1$  single clusters) along the first 20  $\mu\text{m}$  of primary dendrite was counted in MSN cultures after 7 and 14 DIV. **A.** Histogram shows the distribution of synaptic  $\alpha 1$  single cluster densities (n=42 and n=48 dendrites, respectively, from two independent experiments). **B.** Box-plot displays the median density (50% of the population) of synaptic  $\alpha 1$  single clusters. **C.** Histogram shows the distribution of total  $\alpha 1$  single cluster densities (n=45 and n=48 dendrites, respectively, from two independent experiments). **D.** The box plot displays the median density of total  $\alpha 1$  single clusters. Statistical analysis was performed using Mann Whitney test: \* corresponds to p-value <0.05.

In addition, we analysed the density of  $\alpha 2$  single clusters in these cultures. The density of synaptic and total  $\alpha 2$  single cluster of GABA<sub>A</sub>Rs per defined length of primary dendrite (the first 20  $\mu\text{m}$  from the cell body) was estimated from 7 to 14 DIV (Figure 42). At 7 DIV, the median density of synaptic  $\alpha 2$  single clusters was 7 (20-2)

compared to 5.5 (20.5-1) at 14 DIV ( $p$  value=0.84, Mann Whitney test;  $n=42$  dendrites analysed in 7 DIV-cultured neurones,  $n=48$  dendrites analysed at 14 DIV-cultured neurones). Similarly, the median density of total  $\alpha 2$  single clusters was 13 (44.5-6) at 7 DIV compared to 16 (36.5-9) at 14 DIV ( $p$  value=0.98, Mann Whitney test  $n=45$  dendrites analysed in 7 DIV-cultured neurones;  $n=48$  dendrites analysed at 14 DIV-cultured neurones). This demonstrates that the density of synaptic and total  $\alpha 2$  single clusters remains unchanged, and is already determined at 7 DIV.

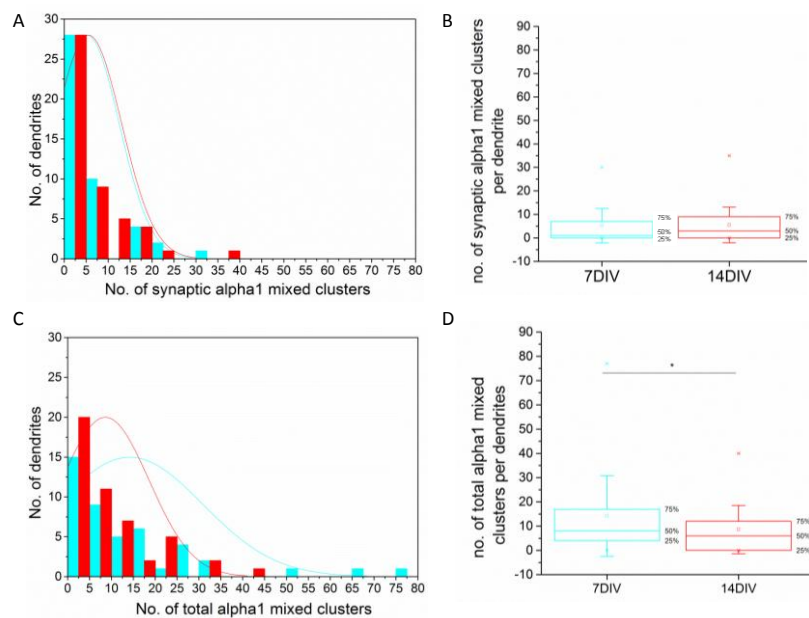


**Figure 42. The density of synaptic and total  $\alpha 2$  single clusters per primary dendrites of MSNs remains unchanged from 7 to 14 DIV.** The density of  $\alpha 2$ -containing GABA<sub>A</sub> receptors clusters ( $\alpha 2$  single clusters) along the first 20  $\mu\text{m}$  of primary dendrite was counted in MSN cultures after 7 and 14 DIV. **A.** Histogram shows the distribution of synaptic  $\alpha 2$  single cluster density ( $n=42$  and  $n=48$  dendrites, respectively, from two independent experiments). **B.** Box-plot displays the median density (50% of the population) of synaptic  $\alpha 2$  single cluster density. **C.** Histogram shows the distribution of total  $\alpha 2$  single cluster density ( $n=45$  and  $n=48$  dendrites, respectively, from two independent experiments). **D.** The box plot displays the median density of total  $\alpha 2$  single clusters. Statistical analysis was performed using Mann Whitney test.

While imaging these neurones, we have noticed that both  $\alpha 1$  and  $\alpha 2$  single clusters were often found in close proximity to each other along the primary dendrites. Therefore, we decided to analyse the density of mixed clusters per dendritic length. The mixed clusters, which contained a majority of  $\alpha 1$  clusters, were defined as  $\alpha 1$  mixed clusters while the mixed clusters containing a majority of  $\alpha 2$  clusters were

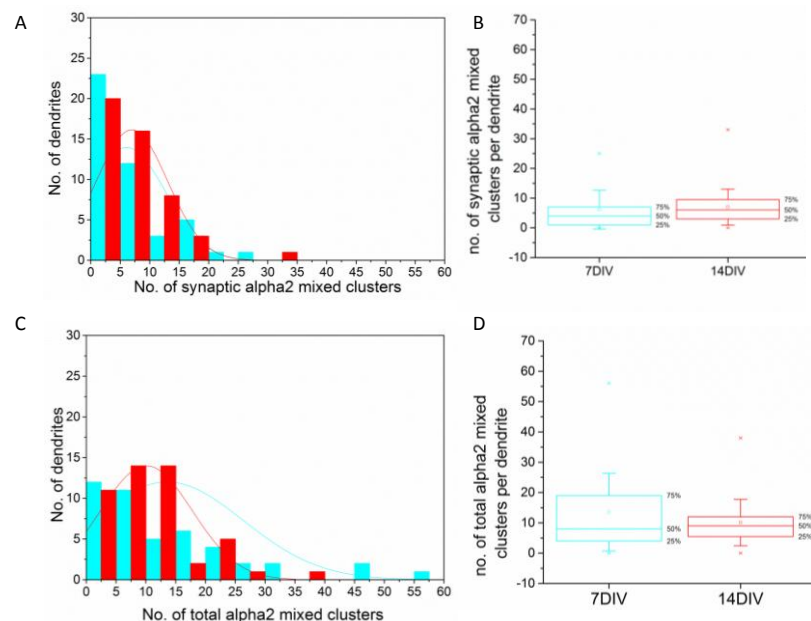


defined as  $\alpha 2$  mixed clusters. The density of synaptic and total  $\alpha 1$  mixed clusters of  $GABA_A$ Rs per defined length of primary dendrite (the first 20  $\mu m$  from the cell body) was estimated from 7 to 14 DIV (Figure 43). At 7 DIV, the median density of synaptic  $\alpha 1$  mixed clusters was 1 (7.5-0) compared to 3 (9-0) at 14 DIV (p value=0.85, Mann Whitney test; n=42 dendrites analysed in 7 DIV-cultured neurones; n=48 dendrites analysed in 14 DIV-treated neurones). In contrast, the median density of total  $\alpha 1$  mixed clusters was 8 (18-3.5) at 7 DIV compared to 6 (12-0) at 14 DIV (p value=0.04, Mann Whitney test; n=45 dendrites analysed in 7 DIV-cultured neurones; n=48 dendrites analysed at 14 DIV-cultured neurones). This demonstrates that while the density of synaptic  $\alpha 1$  mixed clusters remains unchanged, the total density of  $\alpha 1$  mixed clusters is significantly decreased from 7 to 14 DIV. Similarly to  $\alpha 1$  single clusters, this suggests that the extra-synaptic  $\alpha 1$  mixed clusters are down-regulated from 7 to 14 DIV.



**Figure 43. The density of  $\alpha 1$  mixed clusters per primary dendrite of MSNs is decreased from 7 to 14 DIV.** The density of  $\alpha 1/\alpha 2$ -containing  $GABA_A$  receptors clusters ( $\alpha 1$  mixed clusters) along the first 20  $\mu m$  of primary dendrite was counted in MSN cultures after 7 and 14 DIV. **A.** Histogram shows the distribution of synaptic  $\alpha 1$  mixed cluster density (n=45 and n=48 dendrites, respectively, from two independent experiments). **B.** Box-plot displays the median density (50% of the population) of synaptic  $\alpha 1$  mixed clusters. **C.** Histogram shows the distribution of total  $\alpha 1$  mixed cluster density (n=45 and n=48 dendrites, respectively, from two independent experiments). **D.** Box-plot displays the median density of total  $\alpha 1$  mixed clusters. Statistical analysis was performed using Mann Whitney test: \* corresponds to p-value <0.05.

We have also analysed the population of mixed clusters which contained predominantly  $\alpha 2$  clusters ( $\alpha 2$  mixed clusters). The density of synaptic and total  $\alpha 2$  mixed clusters of GABA<sub>A</sub>Rs per defined length of primary dendrite (the first 20  $\mu\text{m}$  from the cell body) was estimated from 7 to 14 DIV (Figure 44). At 7 DIV, the median density of synaptic  $\alpha 2$  mixed clusters was 4 (8-1) compared to 6 (9.75-3) at 14 DIV ( $p$  value=0.20, Mann Whitney test;  $n=45$  dendrites analysed in 7 DIV-cultured neurones;  $n=48$  dendrites analysed in 14 DIV-cultured neurones). The median density of total  $\alpha 2$  mixed clusters was 8 (19.5-4) at 7 DIV compared to 9 (12-5.25) at 14 DIV ( $p$  value=0.46, Mann Whitney test;  $n=45$  dendrites analysed in 7 DIV-cultured neurones;  $n=48$  dendrites analysed in 14 DIV-cultured neurones). This demonstrates that the density of synaptic and total  $\alpha 2$  mixed clusters remains unchanged from 7 to 14 DIV. Similarly to  $\alpha 2$  single clusters, the density of  $\alpha 2$  mixed clusters per dendritic length is already determined at 7 DIV.



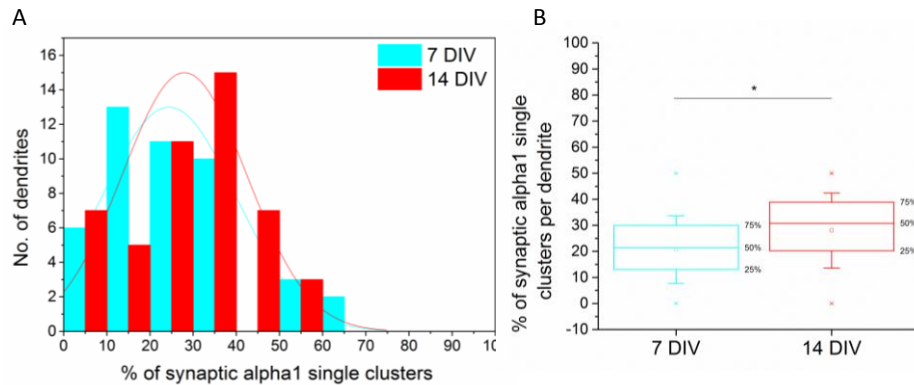
**Figure 44. The density of synaptic and total  $\alpha 2$  mixed clusters per primary dendrite of MSNs remains unchanged from 7 to 14 DIV.** The density of  $\alpha 2/\alpha 1$ -containing GABA<sub>A</sub> receptors clusters ( $\alpha 2$  mixed clusters) along the 20  $\mu\text{m}$  of primary dendrite was counted in MSN cultures after 7 and 14 DIV. **A.** Histogram shows the distribution of synaptic  $\alpha 2$  mixed cluster densities ( $n=42$  and  $n=48$  dendrites, respectively, from two independent experiments). **B.** Box-plot displays the median density (50% of the population) of synaptic  $\alpha 2$  mixed clusters. **C.** Histogram shows the distribution of total  $\alpha 2$  mixed cluster density ( $n=45$  and  $n=48$  dendrites, respectively, from two independent experiments). **D.** Box-plot displays the median density of total  $\alpha 2$  mixed clusters. Statistical analysis was performed using Mann Whitney test.

**Table 15. The total density of  $\alpha 1$  single and mixed clusters per primary dendrite of MSNs is significantly decreased from 7 to 14 DIV**

Density of clusters		7-14 DIV	P < 0.05
$\alpha 1$ single clusters	Synaptic	↘	No
	Total	↘	Yes
$\alpha 2$ single clusters	Synaptic	↘	No
	Total	↘	No
$\alpha 1$ mixed clusters	Synaptic	↘	No
	Total	↘	Yes
$\alpha 2$ mixed clusters	Synaptic	↘	No
	Total	↘	No

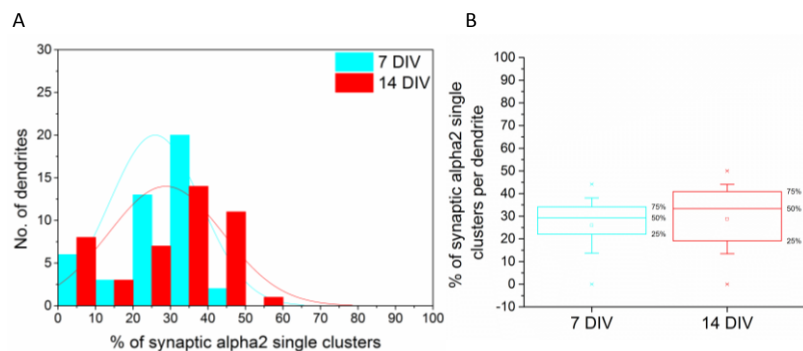
### **5.3.2 The percentage of synaptic over the total GABA<sub>A</sub>R clusters is modified from 7 to 14 DIV**

Despite the observed decrease in the total density of  $\alpha 1$  single and  $\alpha 1$  mixed clusters, the density of synaptic  $\alpha 1$  clusters, or the density of different types of  $\alpha 2$  clusters per dendrite did not seem to significantly change during development of MSNs *in vitro*. In order to analyse further these changes in cluster populations, we estimated the proportion of synaptic clusters as a percentage of total clusters in each population from 7 to 14 DIV. The proportion of  $\alpha 1$  single clusters as a percentage of total  $\alpha 1$  single clusters (the first 20  $\mu\text{m}$  from the cell body) was calculated (Figure 45). At 7 DIV, the median percentage of synaptic/ total  $\alpha 1$  single clusters was 21.42 (11.13-30) % compared to 30.78 (19.19-38.88) % at 14 DIV ( $p$  value=0.006, Mann Whitney test;  $n=45$  dendrites analysed in 7 DIV-cultured neurones, and  $n=48$  dendrites analysed in 14 DIV-cultured neurones). Despite the apparent stability in the density of synaptic  $\alpha 1$  single clusters per dendrite, their contribution to the overall density of  $\alpha 1$  single clusters is significantly increased from 7 to 14 DIV, due to a significant decrease in the density of total  $\alpha 1$  single clusters (Table 15).



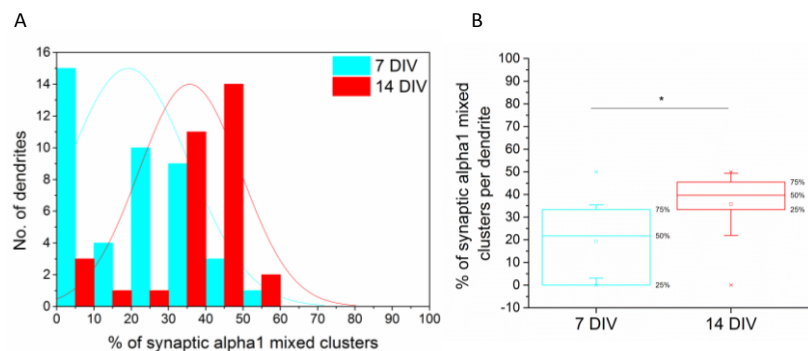
**Figure 45. The percentage of synaptic over the total  $\alpha 1$  single clusters is increasing from 7 to 14 DIV.** The percentage of synaptic over the total  $\alpha 1$  single clusters amongst the total population of  $\alpha 1$  single clusters along the 20  $\mu\text{m}$  of primary dendrite was estimated in MSNs cultures after 7 and 14 DIV. **A.** Histogram shows the distribution of the ratios between synaptic and total  $\alpha 1$  single clusters per dendrite ( $n=45$  and  $n=48$  dendrites, respectively, from two independent experiments). **B.** Box-plot displays the median percentage of synaptic over the total  $\alpha 1$  single clusters per dendrite. Statistical analysis was performed using Mann-Whitney test: \* corresponds to  $p$ -value  $< 0.05$ .

In addition, the proportion of synaptic  $\alpha 2$  single clusters as a percentage of total  $\alpha 2$  single per defined length of primary dendrite (the first 20  $\mu\text{m}$  from the cell body) was calculated (Figure 46). At 7 DIV, the median percentage of synaptic/ total  $\alpha 2$  single clusters was 29.28 (22.05-34.13) % compared to 33.33 (18.63-41.09) % at 14 DIV ( $p$  value=0.11, Mann Whitney test;  $n=44$  dendrites analysed in 7 DIV-cultured neurones, and  $n=44$  dendrites analysed in 14 DIV-cultured neurones). This indicates that, similarly to the density of synaptic  $\alpha 2$  single clusters per dendrite, the proportion of synaptic/ total  $\alpha 2$  single clusters is not changed from 7 to 14 DIV.



**Figure 46. The percentage of synaptic over the total  $\alpha 2$  single clusters remains stable from 7 to 14 DIV.** The percentage of synaptic over the total  $\alpha 2$  single clusters amongst the total population of  $\alpha 2$  single clusters along the 20  $\mu\text{m}$  of primary dendrite was estimated in MSNs cultures after 7 and 14 DIV. **A.** Histogram shows the distribution of ratios of synaptic/total  $\alpha 2$  single clusters per dendrite ( $n=44$  analysed dendrites, in both developmental stages, from two independent experiments). **B.** Box-plot displays the median percentage of synaptic over the total  $\alpha 2$  single clusters per dendrite. Statistical analysis was performed using Mann Whitney test.

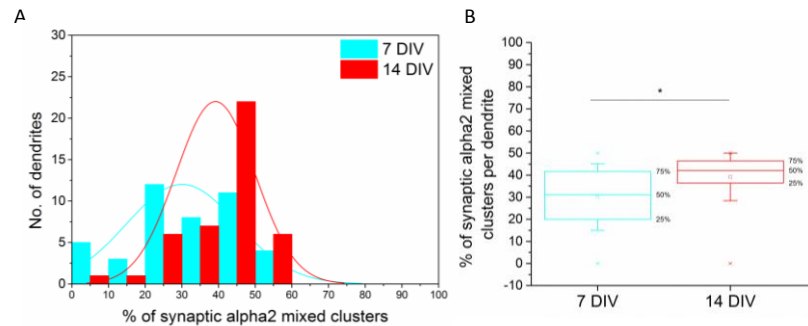
Following the previous analysis, we have also analysed changes in the proportion of synaptic mixed clusters as a percentage of total mixed clusters during MSN development. The proportion of synaptic  $\alpha 1$  mixed clusters as a percentage of total  $\alpha 1$  mixed clusters of GABA<sub>A</sub>Rs per defined length of primary dendrite (the first 20  $\mu\text{m}$  from the cell body) was estimated from 7 to 14 DIV (Figure 47). The median percentage of synaptic over the total  $\alpha 1$  mixed clusters was 21.71 (0-33.33) % at 7 DIV compared to 39.64 (33.3-45.45) % at 14 DIV ( $p$  value= $1.46 \times 10^{-5}$ , Mann Whitney test;  $n=42$  dendrites analysed in 7 DIV-cultured neurones, and  $n=32$  dendrites analysed in 14 DIV-cultured neurones). This demonstrates that, because the density of synaptic  $\alpha 1$  mixed clusters remains unchanged and the total density of  $\alpha 1$  mixed clusters is significantly decreased from 7 to 14 DIV, the percentage of synaptic over the total  $\alpha 1$  mixed clusters of GABA<sub>A</sub>Rs is significantly increased from 7 to 14 DIV.



**Figure 47. The percentage of synaptic over the total  $\alpha 1$  mixed clusters per primary dendrites of MSNs is increased from 7 to 14 DIV.** The percentage of synaptic over the total  $\alpha 1$  mixed clusters amongst the total population of  $\alpha 1$  mixed clusters along the 20  $\mu\text{m}$  of primary dendrite was estimated in MSN cultures after 7 and 14 DIV. **A.** Histogram shows the distribution of the ratios between synaptic and total  $\alpha 1$  mixed clusters per dendrite ( $n=45$  and  $n=48$  dendrites, respectively, from two independent experiments). **B.** Box-plot displays the median percentage of synaptic over the total  $\alpha 1$  mixed clusters per dendrite. Statistical analysis was performed using Mann-Whitney test: \* corresponds to  $p$ -value  $< 0.05$ .

We analysed changes in mixed clusters which contained a predominant density of  $\alpha 2$  clusters in these cultures ( $\alpha 2$  mixed clusters). The proportion of synaptic  $\alpha 2$  mixed clusters as a percentage of total  $\alpha 2$  mixed clusters of GABA<sub>A</sub>Rs per defined length of primary dendrite (the first 20  $\mu\text{m}$  from the cell body) was estimated from 7 to 14 DIV (Figure 48). The median percentage of synaptic over the total  $\alpha 2$  mixed clusters

was 31.03 (20- 41.66) % at 7 DIV compared to 42.10 (36.36- 46.47) % at 14 DIV (p value=0.003, Mann Whitney test; n=43 dendrites analysed in 7 DIV-cultured neurones; n=43 dendrites analysed in 14 DIV-cultured neurones). This demonstrates that although the density of synaptic and total  $\alpha 2$  mixed clusters remains unchanged from 7 to 14 DIV, the percentage of synaptic over the total  $\alpha 2$  mixed clusters of GABA<sub>A</sub>Rs is increased from 7 to 14 DIV.



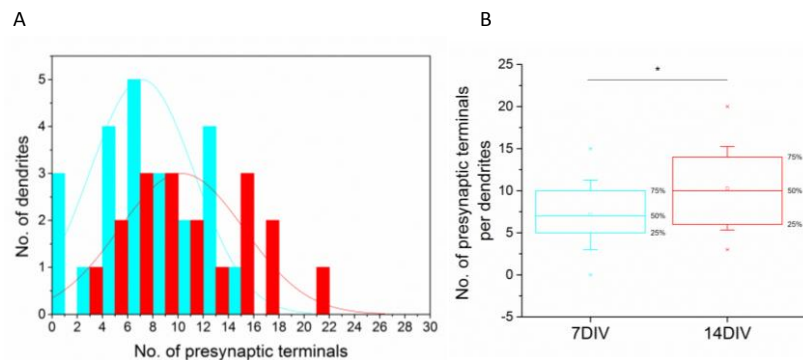
**Figure 48. The percentage of synaptic over the total  $\alpha 2$  mixed clusters is increased from 7 to 14 DIV.** The percentage of synaptic over the total  $\alpha 2$  mixed clusters amongst the total population of  $\alpha 2$  mixed clusters along the 20  $\mu$ m of primary dendrite was estimated in MSN cultures after 7 and 14 DIV. **A.** Histogram shows the distribution of the ratios between synaptic and total  $\alpha 2$  mixed clusters per dendrite (n=43 dendrites analysed, in both developmental stages, from two independent experiments). **B.** Box-plot displays the median percentage of synaptic over the total  $\alpha 2$  mixed clusters per dendrite. Statistical analysis was performed using Mann-Whitney test: \* corresponds to p-value < 0.05.

**Table 16. The percentage of synaptic over the total number of all subtypes of GABA<sub>A</sub>R clusters is increased from 7 to 14 DIV**

	7-14 DIV	P value < 0.05
% (synaptic/total) $\alpha 1$ single clusters	↗	Yes
% (synaptic/total) $\alpha 2$ single clusters	↘	No
% (synaptic/total) $\alpha 1$ mixed clusters	↗	Yes
% (synaptic/total) $\alpha 2$ mixed clusters	↗	Yes

### 5.3.3 The connectivity between MSNs is increased during development of GABAergic synapse

To investigate further GABAergic synapse formation, we investigated if the changes in GABA<sub>A</sub>Rs cluster that we observed were accompanied by changes in the density of presynaptic terminals forming contacts with the primary dendrites. The total density of GAD-65 positive terminals per defined length of primary dendrite (the first 20 μm from the cell body) was estimated from 7 to 14 DIV (Figure 49). At 7 DIV, the mean density of presynaptic terminals was 7.13 (±0.86) (the median was 7 (5-10)) at 7 DIV compared to 10.27 (±1.16) (the median was 10 (6-14.25)) at 14 DIV (p value=0.03, Two sample t-test; n=23 dendrites analysed in 7 DIV-cultured neurones, and n=18 dendrites analysed in 14 DIV-cultured neurones). This indicates that the density in the first 20 μm of presynaptic contacts increases from 7 to 14 DIV.



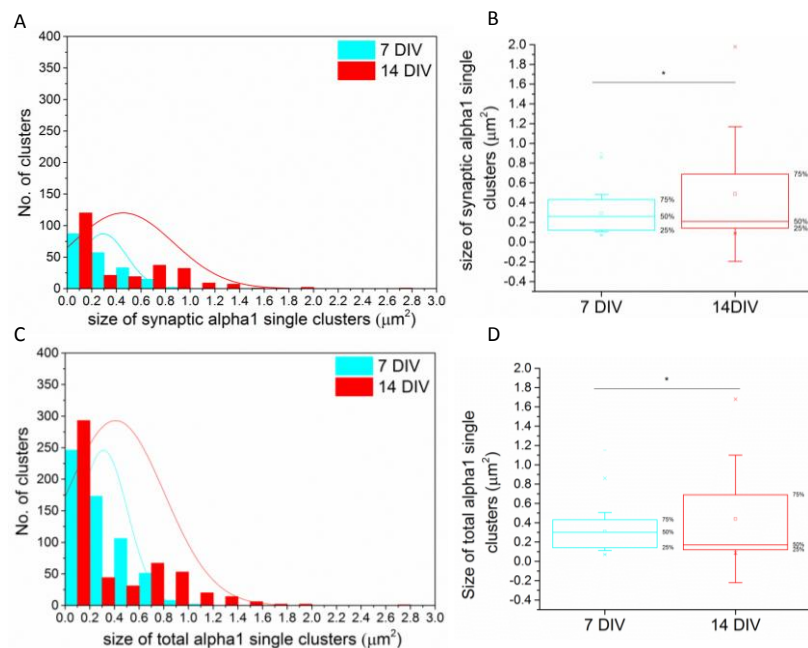
**Figure 49. The density of presynaptic terminals making contacts with primary dendrites is increased from 7 to 14 DIV.** The density of presynaptic terminals along the 20 μm of primary dendrite was counted in MSN cultures after 7 and 14 DIV. **A.** Histogram shows the distribution of the density of presynaptic inputs (n=23 and n=18 dendrites, respectively, from two independent experiments). **B.** Box-plot displays the mean density (dot in the middle of the box) and median (50% of the population) of presynaptic terminals. Statistical analysis was performed using Two-sample T-test: \* corresponds to p-value < 0.05.

### 5.3.4 Developmental changes in the size of GABA<sub>A</sub>R clusters are determined by the type of α subunit incorporated

During their development in culture from 7 to 14 DIV, MSNs undergo prominent changes in the size of α1 single, α2 single, α1 mixed and α2 mixed GABA<sub>A</sub>R clusters. The size of synaptic and total α1 single clusters of GABA<sub>A</sub>Rs per defined length of primary dendrite (the first 20 μm from the cell body) was estimated from 7 to



14 DIV (Figure 50). At 7 DIV, the median size of synaptic  $\alpha 1$  single clusters was 0.26 (0.43-0.12)  $\mu\text{m}^2$  compared to 0.21 (0.7-0.14)  $\mu\text{m}^2$  at 14 DIV ( $p$  value=0.0017, Mann Whitney test;  $n=194$  clusters analysed in 7 DIV-cultured neurones, and  $n=250$  clusters analysed in 14 DIV-cultured neurones). Similarly, the median size of total  $\alpha 1$  single clusters was 0.3 (0.43-0.14)  $\mu\text{m}^2$  at 7 DIV compared to 0.17 (0.69-0.12)  $\mu\text{m}^2$  at 14 DIV ( $p$  value=0.62, Mann Whitney test;  $n=586$  clusters analysed in 7 DIV-cultured neurones, and  $n=533$  clusters analysed in 14 DIV-cultured neurones). This demonstrates that the size of synaptic and total  $\alpha 1$  single clusters is reduced although their density remains stable during development. In contrast, the size and the density of total  $\alpha 1$  single clusters are both decreased from 7 to 14 DIV.

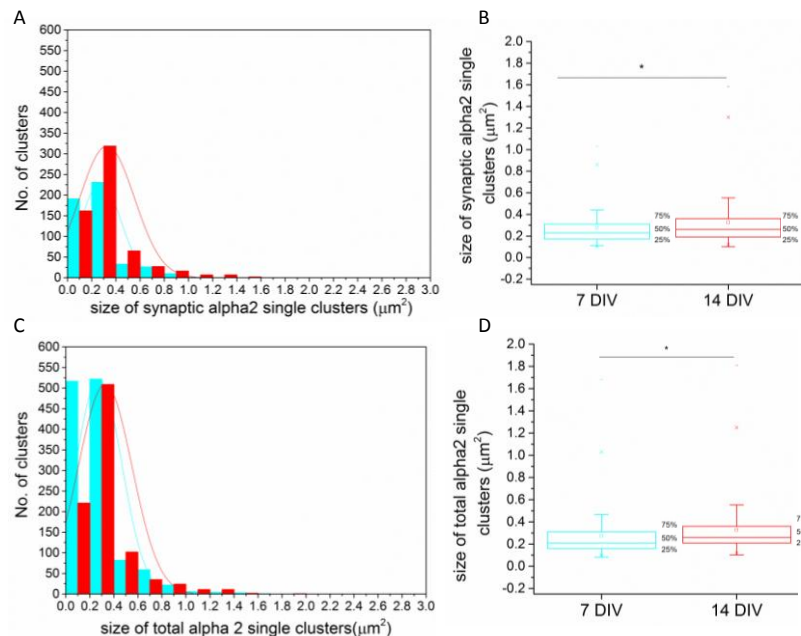


**Figure 50. The size of synaptic and total  $\alpha 1$  single clusters is decreased from 7 to 14 DIV.** The size of  $\alpha 1$  -containing  $\text{GABA}_A$  receptors clusters ( $\alpha 1$  single clusters) along the 20  $\mu\text{m}$  of primary dendrite was measured in MSN cultures after 7 and 14 DIV. **A.** Histogram shows the distribution of synaptic  $\alpha 1$  single cluster sizes ( $n=194$  and  $n=250$  clusters, respectively, from two independent experiments). **B.** Box-plot displays the median size (50 % of the population) of synaptic  $\alpha 1$  single clusters. **C.** Histogram shows the distribution of total  $\alpha 1$  single cluster sizes ( $n=586$  and  $n=333$  clusters, respectively, from two independent experiments). **D.** The box plot displays the population of total  $\alpha 1$  single cluster size. Statistical analysis was performed using Mann Whitney test: \* corresponds to  $p$ -value  $< 0.05$ .

In addition, we analysed the size of  $\alpha 2$  single clusters in these cultures. The size of synaptic and total  $\alpha 2$  single clusters of  $\text{GABA}_A$ Rs per defined length of primary dendrite (the first 20  $\mu\text{m}$  from the cell body) was estimated from 7 to 14 DIV (Figure

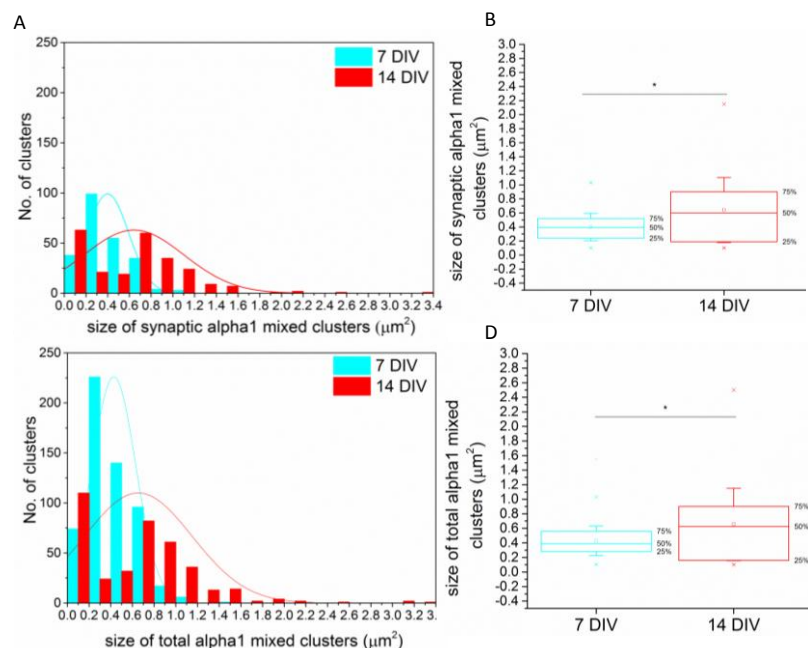


51). At 7 DIV, the median size of synaptic  $\alpha 2$  single clusters was 0.23 (0.31-0.17)  $\mu\text{m}^2$  compared to 0.26 (0.36 - 0.19)  $\mu\text{m}^2$  at 14 DIV (p value=  $5.74 \times 10^{-6}$ , Mann Whitney test; n= 492 clusters analysed in 7 DIV-cultured neurones, compared to n=605 clusters analysed in 14 DIV-cultured neurones). Similarly, the median size of total  $\alpha 2$  single clusters was 0.21 (0.31 - 0.16)  $\mu\text{m}^2$  at 7 DIV compared to 0.26 (0.36 - 0.21)  $\mu\text{m}^2$  at 14 DIV (p value=  $6.19 \times 10^{-19}$ , Mann Whitney test; n= 1216 clusters analysed in 7 DIV-cultured neurones, compared to n= 916 clusters analysed in 14 DIV-cultured neurones). This demonstrates that while the density of synaptic and total  $\alpha 2$  single clusters remains unchanged during development of MSNs, their sizes are significantly increasing, possibly due to an increased synthesis and insertion of  $\alpha 2$ -containing GABA<sub>A</sub>Rs into the plasma membrane.



**Figure 51. The size of synaptic and total  $\alpha 2$  single clusters is increased from 7 to 14 DIV.** The size of  $\alpha 2$  -containing GABA<sub>A</sub> receptors clusters ( $\alpha 2$  single clusters) along the 20  $\mu\text{m}$  of primary dendrite was measured in MSNs cultures after 7 and 14 DIV. **A.** Histogram shows the distribution of synaptic  $\alpha 2$  single cluster sizes (n=492 and n=605 clusters, respectively, from two independent experiments). **B.** Box-plot displays the median size (50 % of the population) of synaptic  $\alpha 2$  single clusters. **C.** Histogram shows the distribution of total  $\alpha 2$  single cluster sizes (n=1216 and n=916 clusters, respectively, from two independent experiments). **D.** The box plot displays the population of total  $\alpha 2$  single cluster sizes. Statistical analysis was performed using Mann Whitney test: \* corresponds to p-value < 0.05.

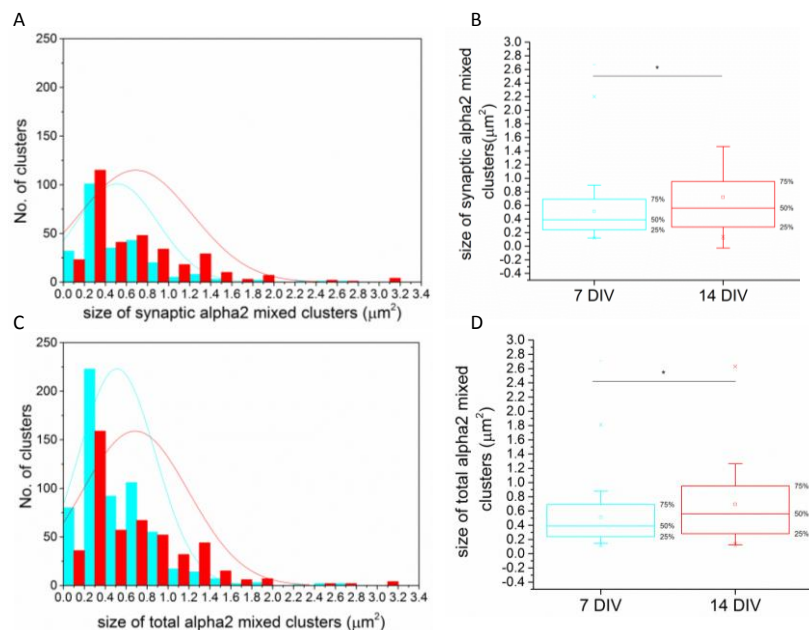
As described, previously, we have identified that  $\alpha 1$  and  $\alpha 2$  single clusters were in proximity to each other, showing a significant overlap, along primary dendrites. Therefore, together with their density, we decided to analyse the changes in the size of  $\alpha 1$  mixed and  $\alpha 2$  mixed GABA<sub>A</sub>R clusters at 7 and 14 DIV. The size of synaptic and total  $\alpha 1$  mixed clusters of GABA<sub>A</sub>R per defined length of primary dendrite (the first 20  $\mu\text{m}$  from the cell body) was estimated from 7 to 14 DIV (Figure 52). At 7 DIV, the median size of synaptic  $\alpha 1$  mixed clusters was 0.39 (0.52-0.24)  $\mu\text{m}^2$  at 7 DIV compared to 0.6 (0.9-0.19)  $\mu\text{m}^2$  at 14 DIV (p value= $1.73 \times 10^{-8}$ , Mann Whitney test; n=234 clusters analysed in 7 DIV-cultured neurones, and n=234 clusters analysed in 14 DIV-cultured neurones). Similarly, the median size of total  $\alpha 1$  mixed clusters was 0.39 (0.56-0.28)  $\mu\text{m}^2$  at 7 DIV compared to 0.625 (0.9-0.16)  $\mu\text{m}^2$  at 14 DIV (p value= $1.11 \times 10^{-10}$ , Mann Whitney test; n=560 clusters analysed in 7 DIV-cultured neurones and n=384 clusters analysed in 14 DIV-cultured neurones). This indicates that the size of  $\alpha 1$  mixed clusters is increasing while their density is decreasing, suggesting that this population of clusters is undergoing significant developmental changes as MSNs differentiate *in vitro*.



**Figure 52. The size of synaptic and total  $\alpha 1$  mixed clusters is increased from 7 to 14 DIV.** The size of  $\alpha 1/\alpha 2$ -containing GABA<sub>A</sub> receptors clusters ( $\alpha 1$  mixed clusters) along the 20  $\mu\text{m}$  of primary dendrite was measured in MSNs cultures at 7 and 14 DIV. **A.** Histogram shows the distribution of synaptic  $\alpha 1$  mixed cluster sizes (n=234 and n=243 clusters, respectively, from two independent experiments). **B.** Box-plot displays the median size (50 % of the population) of

synaptic  $\alpha 1$  mixed clusters. **C.** Histogram shows the distribution of total  $\alpha 1$  mixed cluster sizes (n=560 and n=384 clusters, respectively, from two independent experiments). **D.** The box plot displays the population of total  $\alpha 1$  mixed cluster sizes. Statistical analysis was performed using Mann Whitney test: \* corresponds to p-value <0.05.

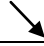







Additionally, the size of synaptic and total  $\alpha 2$  mixed clusters of GABA<sub>A</sub>Rs per defined length of primary dendrite (the first 20  $\mu\text{m}$  from the cell body) was estimated from 7 to 14 DIV (Figure 53). At 7 DIV, the median size of synaptic  $\alpha 2$  mixed clusters was 0.39 (0.69-0.24)  $\mu\text{m}^2$  at 7 DIV compared to 0.56 (0.95-0.28)  $\mu\text{m}^2$  at 14 DIV (p value=2.9x10<sup>-5</sup>, Mann Whitney test; n=252 clusters analysed in 7 DIV-cultured neurones and n=335 clusters analysed in 14 DIV-cultured neurones). Similarly, the median size of total  $\alpha 2$  mixed clusters was 0.39 (0.69-0.24)  $\mu\text{m}^2$  at 7 DIV compared to 0.56 (0.95-0.28)  $\mu\text{m}^2$  at 14 DIV (p value=2.83x10<sup>-8</sup>, Mann Whitney test; n=604 clusters analysed in 7 DIV-cultured neurones, and n=483 clusters analysed in 14 DIV-cultured neurones). This indicates that, although their density remains stable during development, the size of synaptic and total  $\alpha 2$  mixed clusters is increased as MSNs develop *in vitro*, possibly due to increased synthesis and insertion of  $\alpha 2$ -containing GABA<sub>A</sub>Rs into the plasma membrane.



**Figure 53. The size of synaptic and total  $\alpha 2$  mixed clusters is increased from 7 to 14 DIV.** The size of  $\alpha 2/\alpha 1$ -containing GABA<sub>A</sub> receptors clusters ( $\alpha 2$  mixed clusters) along the 20  $\mu\text{m}$  of primary dendrite was measured in MSNs cultures at 7 and 14 DIV. **A.** Histogram shows the distribution of synaptic  $\alpha 2$  mixed cluster sizes (n=252 and n=335 clusters, respectively, from two

independent experiments). **B.** Box-plot displays the median size (50 % of the population) of synaptic  $\alpha 2$  mixed clusters. **C.** Histogram shows the distribution of total  $\alpha 2$  mixed cluster sizes (n=604 and n=483 clusters, respectively, from two independent experiments). **D.** Box- plot displays the population of total  $\alpha 2$  mixed cluster sizes. Statistical analysis was performed using Mann Whitney test: \* corresponds to p-value <0.05.

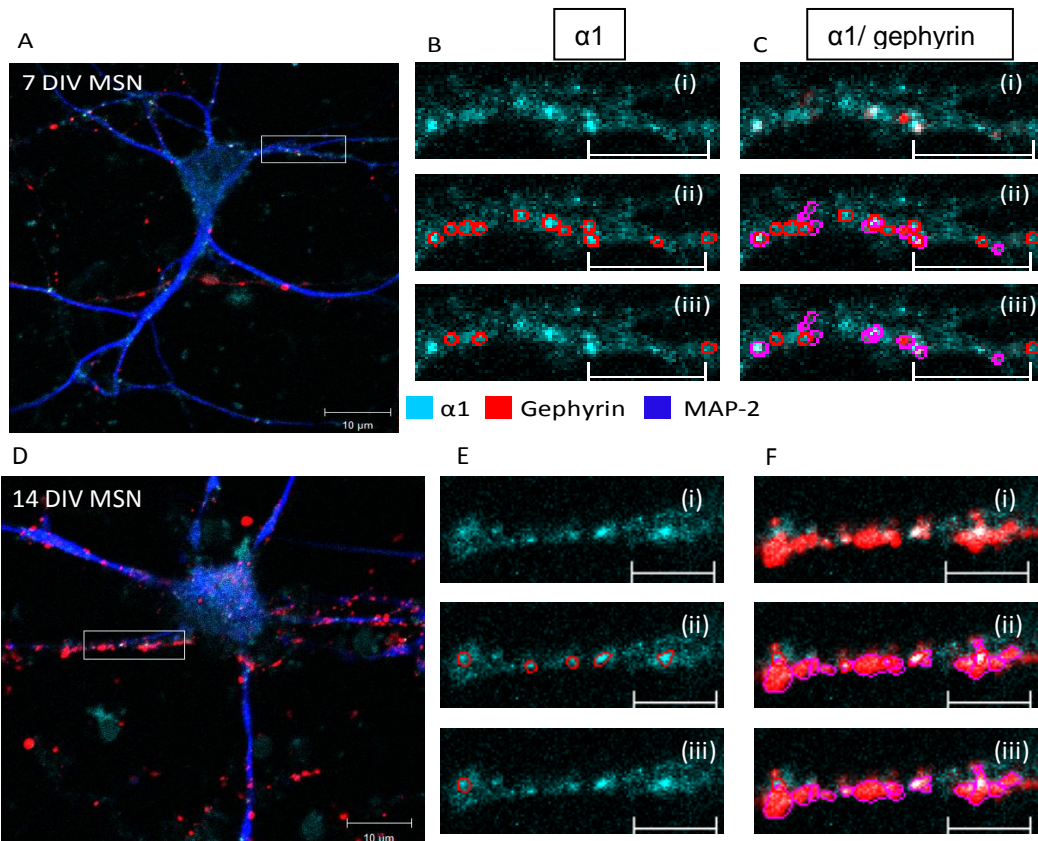
**Table 17. Significant increase in the size of all  $\alpha 2$ - containing GABA<sub>A</sub>R clusters in MSNs from 7 to 14 DIV.**

Size of clusters ( $\mu\text{m}^2$ )		7-14 DIV	P < 0.05
$\alpha 1$ single clusters	Synaptic		Yes
	Total		No
$\alpha 2$ single clusters	Synaptic		Yes
	Total		Yes
$\alpha 1$ mixed clusters	Synaptic		Yes
	Total		Yes
$\alpha 2$ mixed clusters	Synaptic		Yes
	Total		Yes

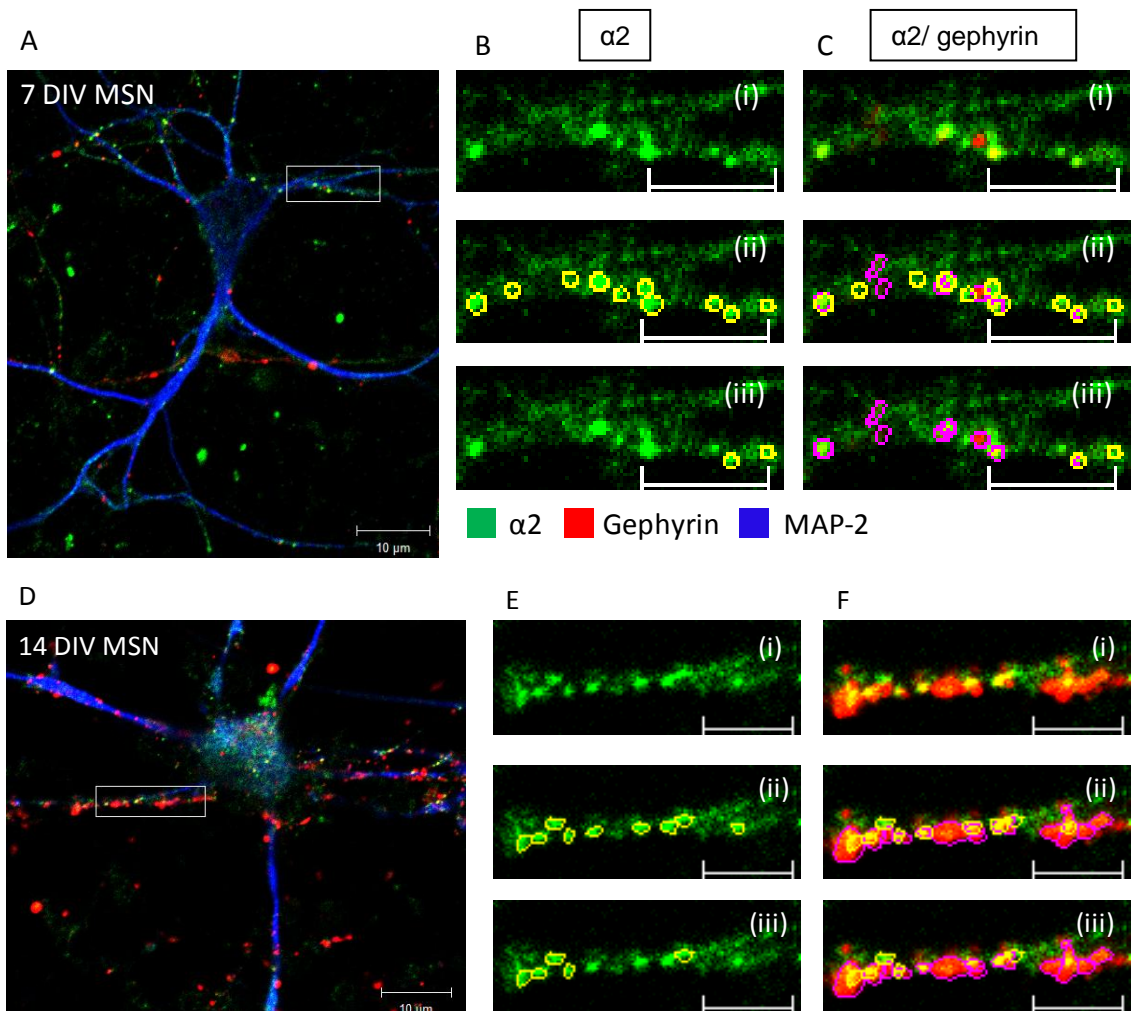
### 5.3.5 The density and size of gephyrin clusters are increased from 7 to 14 DIV

It is now well established that the scaffolding protein gephyrin plays a central role in the maintenance and stability of GABAergic synapses (Yu et al., 2007). However, how the properties of gephyrin clusters change during development of GABAergic synapses is currently unclear. As described previously, embryonic MSNs were cultured for 7 or 14 DIV, and synapse formation was analysed using immunocytochemistry and confocal imaging. Figure 54, 55 and 56 show examples of staining for  $\alpha 1$  and/or  $\alpha 2$  extracellular domains of GABA<sub>A</sub>R subunits, the postsynaptic protein gephyrin and MAP-2, using the antibodies described in Table 14. The total density of gephyrin clusters was determined using Zen 2009 programme. In order to study specific synapse formation, striatal neurones were cultured for 7 or 14 days and synapse formation was analysed using immunocytochemistry and confocal imaging. Figure 54, 55 and 56 show the same couple of neurones stained for  $\alpha 1$  and/or  $\alpha 2$

extracellular domains of GABA<sub>A</sub>R subunits, the postsynaptic protein gephyrin and MAP-2, using the antibodies described in table 14. The total density and the size of gephyrin clusters, and their co-localisation with GABA<sub>A</sub>R subunits  $\alpha$ 1 and  $\alpha$ 2 were determined using the Zen 2009 programme.

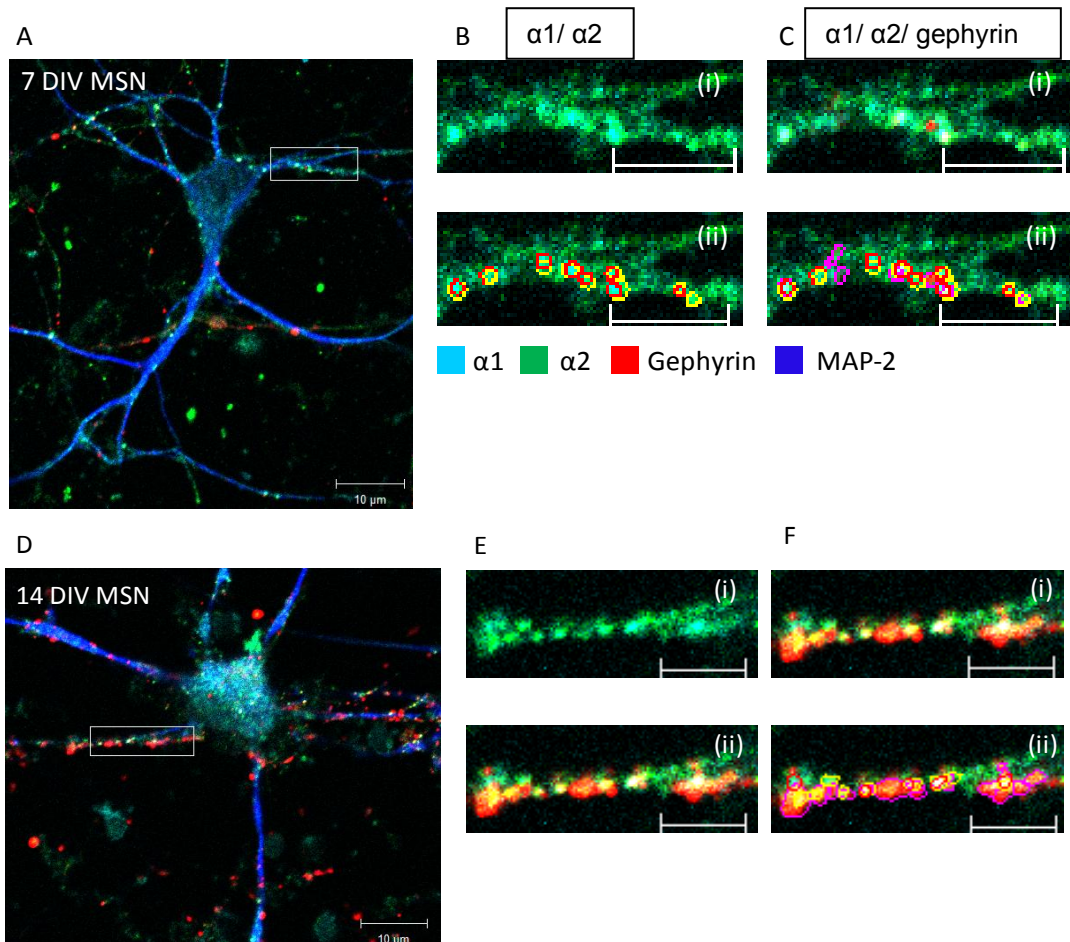


**Figure 54. The density and size of gephyrin clusters, as well as the density of  $\alpha$ 1 clusters co-localising with gephyrin are increased from 7 to 14 DIV.** Immunolabelling of GABA<sub>A</sub>R  $\alpha$ 1 subunit-containing clusters (cyan) and gephyrin (red) along primary dendrites (blue) of cultured MSNs. **A.** Merged image of a 7 DIV striatal neurone (scale bar: 10  $\mu$ m). **B (i)** Enlarged image of boxed region in A representing  $\alpha$ 1 staining only. **(ii)** Analysis of image B(i) in which all  $\alpha$ 1 clusters are circled in red. **(iii)** Analysis of image B(i) in which only  $\alpha$ 1 single clusters that are not associated with  $\alpha$ 2 clusters are circled in red (scale bar: 5  $\mu$ m). **C (i)** Enlarged image of boxed region in A representing  $\alpha$ 1 positive clusters and gephyrin clusters. **(ii)** Analysis of image C(i) in which all  $\alpha$ 1 clusters were circled in red and gephyrin clusters were circled in purple. **(iii)** Analysis of image C(i) in which only  $\alpha$ 1 single clusters were circled in red and gephyrin clusters were circled in purple (scale bar: 5  $\mu$ m). **D.** Merged image of a 14 DIV striatal neurone (scale bar: 10  $\mu$ m). **E (i)** Enlarged image of boxed region in D representing  $\alpha$ 1 staining only. **(ii)** Analysis of image E(i) in which all  $\alpha$ 1 clusters are circled in red. **(iii)** Analysis of image E(i) in which only  $\alpha$ 1 single clusters that are not associated with  $\alpha$ 2 clusters are circled in red (scale bar: 5  $\mu$ m). **F (i)** Enlarged image of boxed region in D representing  $\alpha$ 1 positive clusters and gephyrin clusters. **(ii)** Analysis of image F(i) in which all  $\alpha$ 1 clusters were circled in red and gephyrin clusters were circled in purple. **(iii)** Analysis of image F(i) in which only  $\alpha$ 1 single clusters were circled in red and gephyrin clusters were circled in purple (scale bar: 5  $\mu$ m).



**Figure 55. The density of  $\alpha 2$  clusters co-localising with gephyrin is increased from 7 to 14 DIV.** Immunolabelling of GABA<sub>A</sub>Rs  $\alpha 2$  subunit-containing clusters (green) and gephyrin (red) along primary dendrites (blue) of cultured MSNs. **A.** Merged image of a 7 DIV striatal neurone (scale bar: 10  $\mu$ m). **B (i)** Enlarged image of boxed region in A representing  $\alpha 2$  staining only. **(ii)** Analysis of image B(i) in which all  $\alpha 2$  clusters are circled in red. **(iii)** Analysis of image B(i) in which only  $\alpha 2$  single clusters that are not associated with  $\alpha 1$  clusters are circled in red (scale bar: 5  $\mu$ m). **C (i)** Enlarged image of boxed region in A representing  $\alpha 2$  positive clusters and gephyrin clusters. **(ii)** Analysis of image C(i) in which all  $\alpha 2$  clusters were circled in red and gephyrin clusters were circled in purple. **(iii)** Analysis of image C(i) in which only  $\alpha 2$  single clusters were circled in red and gephyrin clusters were circled in purple (scale bar: 5  $\mu$ m). **D.** Merged image of a 14 DIV striatal neurone (scale bar: 10  $\mu$ m). **E (i)** Enlarged image of boxed region in D representing  $\alpha 2$  staining only. **(ii)** Analysis of image E(i) in which all  $\alpha 2$  clusters are circled in red. **(iii)** Analysis of image E(i) in which only  $\alpha 2$  single clusters that are not associated with  $\alpha 1$  clusters are circled in red (scale bar: 5  $\mu$ m). **F (i)** Enlarged image of boxed region in D representing  $\alpha 2$  positive clusters and gephyrin clusters. **(ii)** Analysis of image F(i) in which all  $\alpha 2$  clusters were circled in red and gephyrin clusters were circled in purple. **(iii)** Analysis of image F(i) in which only  $\alpha 2$  single clusters were circled in red and gephyrin clusters were circled in purple (scale bar: 5  $\mu$ m).

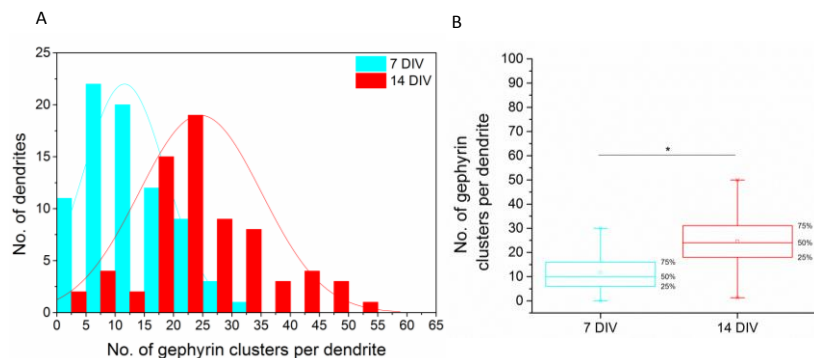




**Figure 56. The density of mixed clusters co-localising with gephyrin is increased from 7 to 14 DIV.** Immunolabelling of GABA<sub>A</sub>Rs  $\alpha 1$  and  $\alpha 2$  subunit-containing clusters (mixed clusters, cyan and green) and gephyrin clusters (red) along primary dendrites (blue) of cultured MSNs. **A.** Merged image of a 7 DIV striatal neurone (scale bar: 10  $\mu\text{m}$ ). **B (i)** Enlarged image of boxed region in A representing  $\alpha 1$  and  $\alpha 2$  staining. **(ii)** Analysis of image B(i) in which all mixed  $\alpha 1$  clusters are circled in red and  $\alpha 2$  clusters are circled in yellow (scale bar: 5  $\mu\text{m}$ ). **C (i)** Enlarged image of boxed region in A representing  $\alpha 2$  positive clusters and gephyrin clusters. **(ii)** Analysis of image C(i) in which all  $\alpha 2$  clusters were circled in yellow and presynaptic terminals were circled in purple (scale bar: 5  $\mu\text{m}$ ). **D.** Merged image of a 14 DIV striatal neurone (scale bar: 10  $\mu\text{m}$ ). **E (i)** Enlarged image of boxed region in D representing  $\alpha 1$  and  $\alpha 2$  staining. **(ii)** Analysis of image E(i) in which mixed  $\alpha 1$  clusters are circled in red and  $\alpha 2$  clusters are circled in yellow (scale bar: 5  $\mu\text{m}$ ). **F (i)** Enlarged image of boxed region in D representing mixed  $\alpha 1$  and  $\alpha 2$  clusters and gephyrin clusters. **(ii)** Analysis of image F(i) in which mixed  $\alpha 1$  were circled in red, mixed  $\alpha 2$  clusters were circled in yellow and gephyrin clusters were circled in purple (scale bar: 5  $\mu\text{m}$ ).

The density of gephyrin clusters per defined length of primary dendrite (the first 20  $\mu\text{m}$  from the cell body) was estimated from 7 to 14 DIV (Figure 57). At 7 DIV, the median density of gephyrin clusters was 10 (6 - 16.25) compared to 24 (17.75 - 31) at 14 DIV ( $p$  value=  $1.87 \times 10^{-13}$ , Mann Whitney test;  $n = 78$  dendrites analysed in 7 DIV-cultured neurones, and  $n = 70$  dendrites analysed in 14 DIV-cultured neurones). This demonstrates that the density of gephyrin clusters is increased from 7 to 14 DIV,

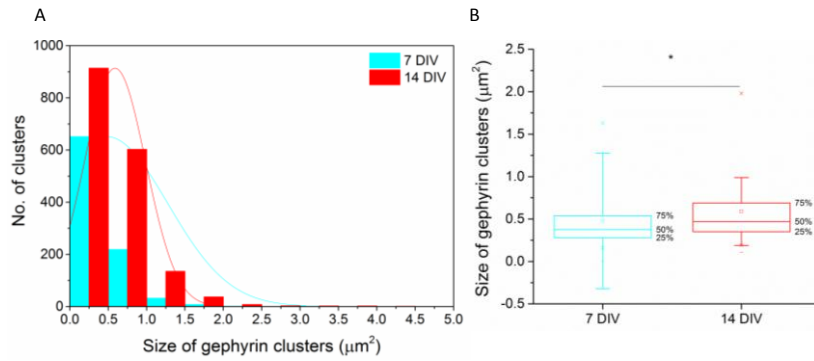
possibly due to a progressive accumulation of gephyrin at synaptic and extrasynaptic sites where GABA<sub>A</sub>Rs are clustered, as neurones mature *in vitro*.



**Figure 57. The density of gephyrin clusters per dendrite is increased from 7 to 14 DIV.** The density of gephyrin clusters along the 20  $\mu\text{m}$  of primary dendrite was counted in MSN cultures after 7 and 14 DIV. The total density of gephyrin clusters is increasing from 7 to 14 DIV. **A.** Histogram shows the distribution of total gephyrin clusters ( $n=78$  and  $n=70$  dendrites, respectively, from two different experiments). **B.** Box-plot displays the median density (50 % of the population) of gephyrin clusters. Statistical analysis was performed using Mann Whitney test: \* corresponds to  $p\text{-value} < 0.05$ .

In addition, we investigated changes in the size of gephyrin clusters during development of MSNs. The size of gephyrin clusters per defined length of primary dendrite (the first 20  $\mu\text{m}$  from the cell body) was estimated from 7 to 14 DIV (Figure 58). At 7 DIV, the median size of gephyrin clusters was 0.375 (0.28-0.54)  $\mu\text{m}^2$  compared to 0.47 (0.35-0.695)  $\mu\text{m}^2$  at 14 DIV ( $p\text{ value}=7.9 \times 10^{-19}$ , Mann Whitney test;  $n=914$  clusters analysed in 7 DIV-cultured neurones,  $n=1706$  clusters analysed in 14 DIV-cultured neurones). This demonstrates that not only the density, but also the size of gephyrin clusters increases as neurones mature *in vitro*, possibly due to an increased synthesis of gephyrin proteins.





**Figure 58. The size of gephyrin clusters is increased from 7 to 14 DIV.**

The size of gephyrin clusters along the 20 µm of primary dendrite was measured in MSNs cultures after 7 and 14 DIV. **A.** Histogram shows the distribution of gephyrin clusters (n=76 and n=68 clusters, respectively, from two different experiments). **B.** Box-plot displays the median size (50 % of the population) of gephyrin. Statistical analysis was performed using Mann Whitney test: \* corresponds to p-value < 0.05.

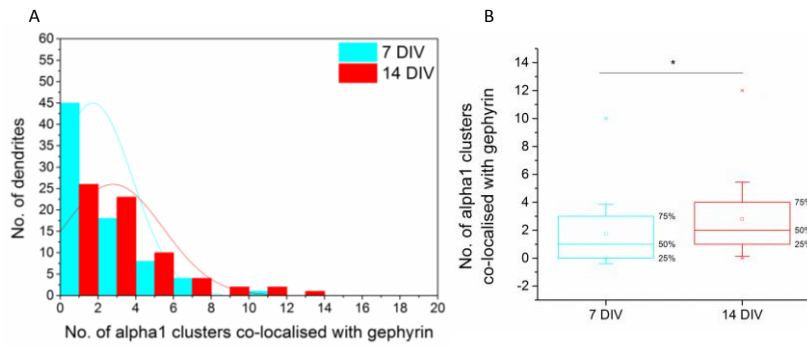
**Table 18. The density and size of gephyrin clusters are increased from 7 to 14 DIV**

Gephyrin clusters	7-14 DIV	P < 0.05
Density of clusters	↗	Yes
Size of clusters	↗	Yes

### 5.3.6 The density of α1, α2 and α1/α2 mixed GABA<sub>A</sub>R clusters co-localising with gephyrin is increased from 7 to 14 DIV

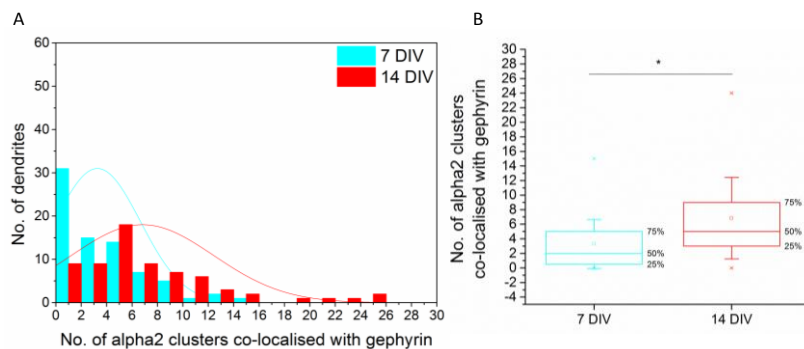
To correlate changes in α1- and/or α2- containing GABA<sub>A</sub>R clusters with changes in gephyrin clusters during development, we analysed the degree of co-localisation between these proteins from 7 to 14 DIV.

The density of α1 clusters co-localised with gephyrin clusters per defined length of primary dendrite (the first 20 µm from the cell body) was estimated from 7 to 14 DIV (Figure 59). At 7 DIV, the median density of α1 clusters which are co-localised with gephyrin was 1 (0-3) compared to 2 (1-4) at 14 DIV (p-value=0.003, Mann Whitney test; n=76 dendrites analysed in 7 DIV-cultured neurones, and n=68 dendrites analysed in 14 DIV-cultured neurones). This result indicates that the co-localisation between α1 containing GABA<sub>A</sub>Rs clusters and gephyrin is increasing from 7 to 14 DIV.



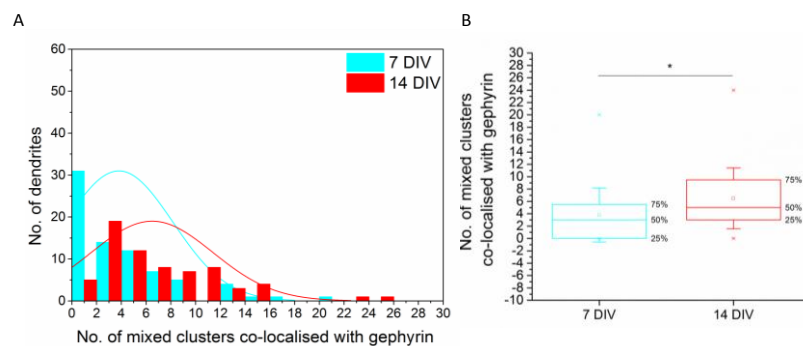
**Figure 59. The density of  $\alpha 1$  clusters co-localising with gephyrin is increased from 7 to 14 DIV.** The density of  $\alpha 1$  clusters co-localising with gephyrin was estimated along the 20  $\mu\text{m}$  of primary dendrites in MSN cultures after 7 and 14 DIV. **A.** Histogram shows the distribution of the density of  $\alpha 1$ -containing GABA<sub>A</sub>R clusters per dendrite co-localising with gephyrin (n=76 and n=68 dendrites, respectively, from two different experiments). **B.** Box-plot displays the median density (50 % of total population) of  $\alpha 1$  clusters co-localised with gephyrin. Statistical analysis was performed using Mann Whitney test: \* corresponds to p-value < 0.05.

The density of  $\alpha 2$  clusters co-localised with gephyrin clusters per defined length of primary dendrite (the first 20  $\mu\text{m}$  from the cell body) was estimated from 7 to 14 DIV (Figure 60). At 7 DIV, the median density of  $\alpha 2$  clusters which are co-localised with gephyrin was 2 (0.25-5) compared to 5 (3-9) at 14 DIV (p-value=5.19.10<sup>-6</sup>, Mann Whitney test; n=76 dendrites analysed in 7 DIV-cultured neurones, and n=68 dendrites analysed in 14 DIV-cultured neurones). This result indicates that the co-localisation between  $\alpha 2$  containing GABA<sub>A</sub>R clusters and gephyrin is increased in MSNs from 7 to 14 DIV.



**Figure 60. The density of  $\alpha 2$  clusters co-localising with gephyrin is increased from 7 to 14 DIV.** The density of  $\alpha 2$  clusters co-localising with gephyrin was estimated along the 20  $\mu\text{m}$  of primary dendrites in MSN cultures after 7 and 14 DIV. **A.** Histogram shows the distribution of the density of  $\alpha 2$ -containing GABA<sub>A</sub>R clusters per dendrite co-localising with gephyrin (n=76 and n=68 dendrites, respectively, from two different experiments). **B.** Box-plot displays the median density (50 % of total population) of  $\alpha 2$  clusters co-localised with gephyrin. Statistical analysis was performed using Mann Whitney test: \* corresponds to p-value < 0.05.

As previously explained, some of the  $\alpha 1$  and  $\alpha 2$  containing clusters were found in close apposition with each other along primary dendrites of MSNs. We were interested to study how the co-localisation between gephyrin and these mixed clusters would change during synapse maturation. The density of  $\alpha 1/\alpha 2$  mixed clusters co-localised with gephyrin clusters per defined length of primary dendrite (the first 20  $\mu\text{m}$  from the cell body) was estimated from 7 to 14 DIV (Figure 61). At 7 DIV, the median density of  $\alpha 1/\alpha 2$  mixed clusters which are co-localised with gephyrin was 3 (0-5.75) compared to 5 (3-9.75) at 14 DIV ( $p$ -value= $7.3 \cdot 10^{-5}$ , Mann Whitney test;  $n=76$  dendrites analysed in 7 DIV-cultured neurones, and  $n=68$  dendrites analysed in 14 DIV-cultured neurones). This result indicates that the co-localisation between  $\alpha 1/\alpha 2$  containing GABA<sub>A</sub>R clusters and gephyrin is increased in MSNs from 7 to 14 DIV.



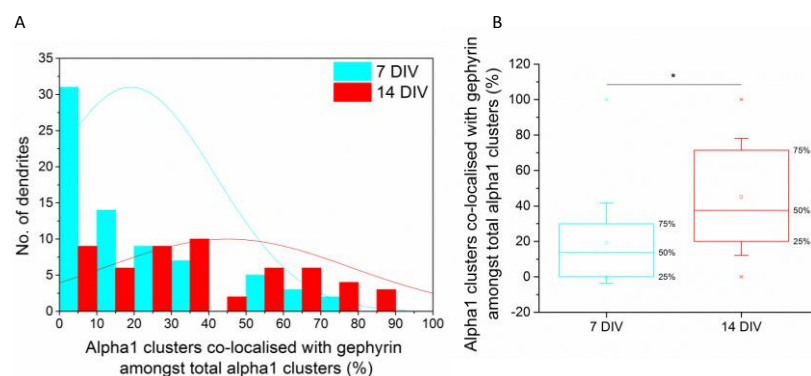
**Figure 61. The density of  $\alpha 1/\alpha 2$  mixed clusters co-localising with gephyrin is increased from 7 to 14 DIV.** The density of  $\alpha 1/\alpha 2$  mixed clusters co-localising with gephyrin was estimated along the 20  $\mu\text{m}$  of primary dendrites in MSN cultures after 7 and 14 DIV. **A.** Histogram shows the distribution of the density of  $\alpha 1/\alpha 2$  containing GABA<sub>A</sub>R clusters per dendrite co-localising with gephyrin ( $n=76$  and  $n=68$  dendrites, respectively, from two different experiments). **B.** Box-plot displays the median density (50 % of total population) of mixed clusters co-localised with gephyrin. Statistical analysis was performed using Mann Whitney test: \* corresponds to  $p$ -value < 0.05.

**Table 19. The density of all types of GABA<sub>A</sub>R clusters co-localising with gephyrin are increased from 7 to 14 DIV**

Density of GABA <sub>A</sub> Rs clusters co-localising with gephyrin	7 to 14 DIV	$P < 0.05$
$\alpha 1$ clusters	↗	Yes
$\alpha 2$ clusters	↗	Yes
$\alpha 1/\alpha 2$ mixed clusters	↗	Yes

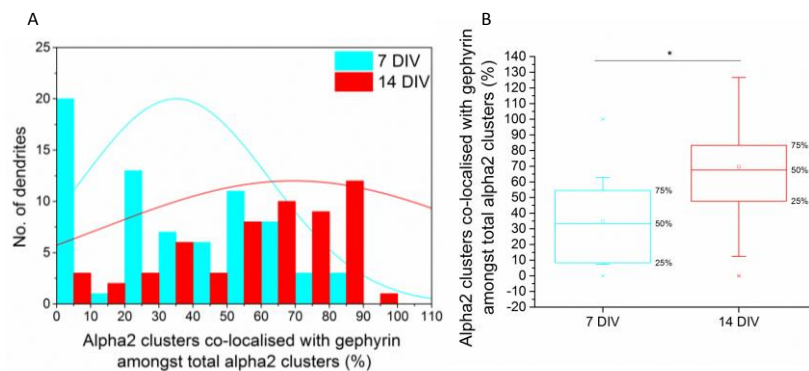
### 5.3.7 The proportion of GABA<sub>A</sub>R clusters co-localising with gephyrin as a percentage of the the total GABA<sub>A</sub>R clusters is increased from 7 to 14 DIV.

As previously described, the density of  $\alpha$ -containing GABA<sub>A</sub>R clusters co-localising with gephyrin increases during MSNs development from 7 to 14 DIV. To understand further these changes, we investigated if, within their respective populations, the percentage of  $\alpha$ 1-,  $\alpha$ 2- or  $\alpha$ 1/ $\alpha$ 2 mixed- containing GABA<sub>A</sub>R clusters co-localising with gephyrin was also changed. The percentage of  $\alpha$ 1 containing GABA<sub>A</sub>R clusters overlapping with gephyrin amongst total  $\alpha$ 1 clusters per defined length of primary dendrite (the first 20  $\mu$ m from the cell body) was calculated from 7 to 14 DIV (Figure 62). At 7 DIV, 13.66 (0-30.58) % of the total  $\alpha$ 1 clusters population was co-localised with gephyrin compared to 37.5 (20-72.07) % at 14 DIV (p- value=  $1.00 \cdot 10^{-6}$ , Mann Whitney test; n=72 dendrites analysed in 7 DIV-cultured neurones, and n=65 dendrites analysed in 14 DIV-cultured neurones). Together with previous data, this shows that not only the density of  $\alpha$ 1 clusters co-localising with gephyrin is increased, but also, that the percentage of  $\alpha$ 1 clusters co-localised with gephyrin is increased amongst all  $\alpha$ 1 clusters in MSNs from 7 to 14 DIV.



**Figure 62. The percentage of  $\alpha$ 1 clusters co-localising with gephyrin is increased from 7 to 14 DIV.** The percentage of  $\alpha$ 1 clusters co-localising with gephyrin was estimated along the 20  $\mu$ m of primary dendrites in MSN cultures after 7 and 14 DIV. **A.** Histogram shows the distribution of the ratio of  $\alpha$ 1 containing GABA<sub>A</sub>R clusters co-localising with gephyrin amongst total  $\alpha$ 1 clusters (n=72 and n=65 dendrites, respectively, from two different experiments). **B.** Box-plot displays the median percentage (50 % of total population) of  $\alpha$ 1 clusters co-localised with gephyrin amongst total  $\alpha$ 1 clusters. Statistical analysis was performed using Mann Whitney test: \* corresponds to p-value < 0.05.

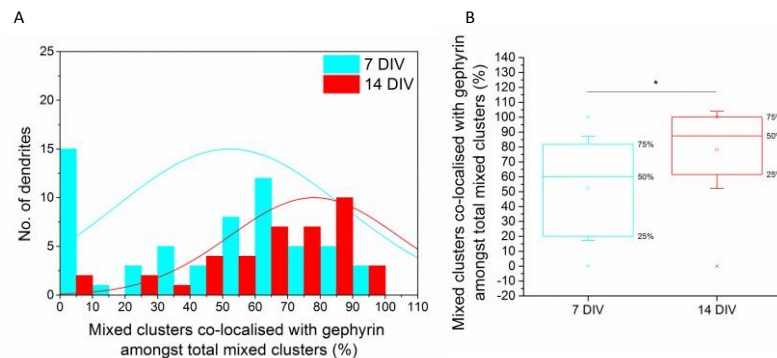
The percentage of  $\alpha 2$ -containing GABA<sub>A</sub>R clusters overlapping with gephyrin amongst total  $\alpha 2$  clusters per defined length of primary dendrite (the first 20  $\mu\text{m}$  from the cell body) was calculated from 7 to 14 DIV (Figure 63). At 7 DIV, 33.33 (8.17-54.79) % of the total  $\alpha 2$  clusters population was co-localised with gephyrin compared to 67.54 (46.59-83.33) % at 14 DIV (p-value=1.74.10<sup>-8</sup>, Mann Whitney test; n=74 dendrites analysed in 7 DIV-cultured neurones, and n=68 dendrites analysed in 14 DIV-cultured neurones). Together with previous data, this shows that not only the density of  $\alpha 2$  clusters co-localising with gephyrin is increasing, but also, that the percentage of  $\alpha 2$  clusters co-localised with gephyrin is increased amongst all  $\alpha 2$  clusters in MSNs from 7 to 14 DIV.



**Figure 63. The percentage of  $\alpha 2$  clusters co-localising with gephyrin is increased from 7 to 14 DIV.** The ratio of  $\alpha 2$  clusters co-localising with gephyrin was estimated along the 20  $\mu\text{m}$  of primary dendrites in MSN cultures after 7 and 14 DIV. **A.** Histogram shows the distribution of the ratio of  $\alpha 2$  containing GABA<sub>A</sub>R clusters co-localising with gephyrin amongst total  $\alpha 2$  clusters (n=74 and n=68 dendrites, respectively, from two different experiments). **B.** Box-plot displays the median percentage (50 % of total population) of  $\alpha 2$  clusters co-localised with gephyrin amongst total  $\alpha 2$ . Statistical analysis was performed using Mann Whitney test: \* corresponds to p-value < 0.05.

The percentage of mixed  $\alpha 1/\alpha 2$ -containing GABA<sub>A</sub>R clusters overlapping with gephyrin amongst total mixed clusters per defined length of primary dendrite (the first 20  $\mu\text{m}$  from the cell body) was calculated from 7 to 14 DIV (Figure 64). At 7 DIV, 60 (20-81.81) % of the total mixed clusters population were co-localised with gephyrin compared to 87.5 (61.15-100) % at 14 DIV (p-value=7.8.10<sup>-6</sup>, Mann Whitney test; n=71 dendrites analysed in 7 DIV-treated cultures, and n=66 dendrites analysed in 14 DIV-cultured neurones). Together with previous data, this shows that not only the density of

mixed clusters co-localising with gephyrin is increasing, but also, that the percentage of mixed clusters co-localised with gephyrin is increased amongst all mixed clusters in MSNs from 7 to 14 DIV.



**Figure 64. The percentage of mixed  $\alpha 1/\alpha 2$  clusters co-localising with gephyrin is increased from 7 to 14 DIV.** The percentage of mixed clusters co-localising with gephyrin was estimated along the 20  $\mu\text{m}$  of primary dendrites in MSN cultures after 7 and 14 DIV. **A.** Histogram shows the distribution of the ratios of mixed  $\alpha 1/\alpha 2$ -containing GABA<sub>A</sub>R clusters co-localising with gephyrin amongst total mixed clusters (n=71 and n=66 dendrites, respectively, from two different experiments). **B.** Box-plot displays the median ratio (50 % of total population) of mixed clusters co-localised with gephyrin amongst total mixed clusters. Statistical analysis was performed using Mann Whitney test: \* corresponds to p-value < 0.05.

**Table 20. The percentage of all subtypes of GABA<sub>A</sub>R clusters co-localising with gephyrin is increased from 7 to 14 DIV**

percentage of GABA <sub>A</sub> Rs co-localising with gephyrin	7 to 14 DIV	p < 0.05
$\alpha 1$ clusters	↗	Yes
$\alpha 2$ clusters	↗	Yes
$\alpha 1/\alpha 2$ mixed clusters	↗	Yes

#### 5.4 Discussion

Synaptic plasticity is exhibited at both excitatory and inhibitory synapses; however the cellular and molecular mechanisms underlying inhibitory synaptic plasticity are more elusive than those regulating plasticity at excitatory synapses. In the central nervous system, fast inhibitory neuronal transmission is mainly mediated by GABA<sub>A</sub>Rs. Many studies support the fact that the density of synaptic receptor determines the strength of the GABAergic synaptic transmission (Bannai et al., 2009). Among other

factors, the membrane insertion or removal rate of GABA<sub>A</sub>Rs is now considered to be a major determinant in the regulation of the density of receptors at inhibitory synapses (Moss and Smart, 2001). Although the total density of receptors at the synapse plays a major role in determining the synaptic strength, the insertion and internalisation of GABA<sub>A</sub>Rs occur at the extrasynaptic sites (Bogdanov et al., 2006, Luo et al., 2013b, Fritschy and Panzanelli, 2014). Single particle tracking, pulse chase imaging and electrophysiology have revealed that the lateral diffusion between synaptic and extrasynaptic sites is the main mechanism involved in targeting of the receptor to synapses (Triller and Choquet, 2005, Bogdanov et al., 2006) .

It is becoming increasingly clear that GABA<sub>A</sub>R  $\alpha$  subunits not only influence GABA<sub>A</sub>R physiology, pharmacology, and biological function, but also mediate the synaptic and extrasynaptic localisation of these receptor subtypes via distinct protein-protein interactions (Tretter et al., 2011). In this chapter, our aim was to investigate developmental changes of  $\alpha$ 1 and/or  $\alpha$ 2 containing GABA<sub>A</sub>R clusters in MSNs.

The co-localisation of GABA<sub>A</sub>R subunits with the presynaptic marker GAD-65 or with the postsynaptic scaffolding protein gephyrin was explored in order to distinguish the synaptic clusters from the extrasynaptic clusters. By combining immunocytochemistry and confocal microscopy, we were able to establish that in developing GABAergic neurones, differential changes occur in  $\alpha$ 1-,  $\alpha$ 2-, or  $\alpha$ 1/2-GABA<sub>A</sub>R clusters. These results suggest that as MSNs mature *in vitro*, the overall density of synaptic contact is increased and the distribution of  $\alpha$ 1 and/or  $\alpha$ 2 containing clusters is modified throughout the development.

Although the total density of  $\alpha$ 1-containing GABA<sub>A</sub>R (single and mixed) clusters was decreased, the density of synaptic  $\alpha$ 1-containing GABA<sub>A</sub>R clusters remained unchanged, suggesting that only the density of extrasynaptic  $\alpha$ 1-containing GABA<sub>A</sub>Rs was down regulated. This decrease in the density of extrasynaptic clusters may be the result of an increased internalisation from extrasynaptic pools as neurones mature *in vitro*, mediated by clathrin-dependent mechanism as it was shown in Kittler et al.,

(Kittler et al., 2000). Additionally, the median size of synaptic  $\alpha 1$  containing clusters ( $\alpha 1$  single) was decreased from 7 to 14 DIV. This could further support the down-regulation observed in the density of extrasynaptic clusters. To test this hypothesis, it would be interesting to test how the clathrin-dependent internalisation of  $\alpha 1$ -containing GABA<sub>A</sub>Rs is regulated during the development of MSNs in culture.

In contrast, while the density of  $\alpha 2$ -containing GABA<sub>A</sub>R clusters (synaptic or extrasynaptic) remained unchanged, their size was significantly increased as neuronal maturation progressed. Interestingly, our results suggest that maturing MSNs tend to favour the formation and stabilisation of predominantly  $\alpha 2$ -containing GABA<sub>A</sub>R clusters than the  $\alpha 1$ -containing GABA<sub>A</sub>R clusters. These results are in accordance with the distribution of GABA<sub>A</sub>R subunits *in vivo* in the adult striatum, in which the  $\alpha 2$  subunit is more prominently present than the  $\alpha 1$  subunit (Fritschy and Mohler, 1995).

In these experiments, we have characterised subcellular distribution of GABA<sub>A</sub>R clusters along the first 20  $\mu\text{m}$  of primary dendrites. Although the  $\alpha 2$  subunits are also highly expressed in the axon initial segment (AIS) where axo-axonic interneurons make synapses (Kasugai et al., 2010), we focused our study on the subunit composition of the dendritic arborisation of MSNs. However, investigating the regional expression and clustering properties of GABA<sub>A</sub>Rs subunits in the AIS and more distal regions during development of MSNs would also be interesting.

Our results show that the density of  $\alpha 1$  and  $\alpha 2$ -containing synapses did not change during the development of MSNs *in vitro*, suggesting that the repartition of different synapses was already established at early developmental stage. However, remodelling of extrasynaptic sites was observed as the total density of  $\alpha 1$ -containing clusters decreased, suggesting that the density of  $\alpha 1$ -containing extrasynaptic sites was decreasing from 7 to 14 DIV. Although we did not directly compare the density of  $\alpha 1$  clusters to the density of  $\alpha 2$  clusters of GABA<sub>A</sub>R, the numbers indicated a higher density of  $\alpha 2$ -containing GABA<sub>A</sub>R clusters along dendrites. This is further supported by the *in vivo* study (Gross et al., 2011) in which it was demonstrated that while  $\alpha 1$  subunit



expression is spread over the MSN cell body and processes, the density of the  $\alpha 2$  subunit is higher in the dendritic compartments.

Interestingly, we observed an overall increase in the density of presynaptic inputs contacting primary dendrites although the density of synaptic clusters did not change. This could reflect an increase in newly formed synapses which either do not contain any GABA<sub>A</sub>Rs yet or contain another  $\alpha$  subunit such as  $\alpha 3$  or  $\alpha 5$  subunits.

In addition, we were interested in looking at the change in size of clusters. Our results indicated that most of the  $\alpha 2$ -containing GABA<sub>A</sub>R cluster ( $\alpha 2$  single,  $\alpha 1/2$  mixed,  $\alpha 2/1$  mixed) sizes were increased in MSN synapses from 7 to 14 DIV, suggesting that the size of  $\alpha 2$ -containing clusters is more likely to play an important role in synapse maturation and maintenance than the density of clusters.

We established the development of GABA<sub>A</sub>R interacting proteins which also play an important role during GABAergic synapse formation. Therefore, we looked at how the postsynaptic scaffolding protein, gephyrin, clustered throughout the development of MSNs, given that gephyrin is known to bind  $\alpha 1$ ,  $\alpha 2$  and  $\alpha 3$  subunits via their intracellular loops (Tretter et al., 2008, Mukherjee et al., 2011, Tretter et al., 2011). Although gephyrin-independent clustering also exists, it is mediated by radixin and it seems to play an important role in clustering of  $\alpha 5$  subunits of GABA<sub>A</sub>R (Loebrich et al., 2006). Thus, the main anchoring protein of GABA<sub>A</sub>Rs in our culture system is likely to be gephyrin.

Our data show that the density and the size of gephyrin clusters are increased as neurones mature *in vitro*. The co-localisation of gephyrin clusters with different subtypes of GABA<sub>A</sub>Rs was also established. Our results suggested that both the gephyrin clusters co-localising with  $\alpha 1$  and/or  $\alpha 2$ -containing-GABA<sub>A</sub>Rs were increased in size and in density. Gephyrin clustering is essential to GABA<sub>A</sub>Rs clustering and is dependent on the subtype of GABA<sub>A</sub>R clusters (Tyagarajan and Fritschy, 2014). The specificity of gephyrin clustering was established in a series of studies in which knock outs (KO) of GABA<sub>A</sub>R subtype genes were carried out. In *Gabra1* KO (encoding the

GABA<sub>A</sub>R  $\alpha$ 1 subunits), the gephyrin clustering was greatly reduced in Purkinje cells, while the  $\alpha$ 3/gephyrin co-localised clusters were sevenfold increased, suggesting a profound network reorganisation in absence of  $\alpha$ 1 subunit which could explain the moderate behavioural consequences observed (Kralic et al., 2006). In addition, knock out of *gabra3* (encoding the GABA<sub>A</sub>R  $\alpha$ 3 subunit) revealed large aggregates of gephyrin localised at the cell surface, suggesting that GABA<sub>A</sub>R are required for gephyrin clustering and GABAergic synapse maintenance cells (Studer et al., 2006, Tyagarajan and Fritschy, 2014). Intriguingly, although gephyrin clustering is significantly reduced in CA1 pyramidal cells of *Gabra2* KO mouse,  $\alpha$ 1-containing clusters appear normal (Tyagarajan and Fritschy, 2014). Thus, postsynaptic clustering of gephyrin at GABAergic synapses depends on interactions between gephyrin and different subtypes of GABA<sub>A</sub>Rs, which suggests that these receptors have a fundamental role in determining the molecular composition and function of the postsynaptic membrane.

# Chapter six

## 6. The regulation of GABAergic synapse formation by GABA signalling

### 6.1 Introduction

Medium spiny neurones (MSNs) are the main neuronal type present in the striatum, representing 95 % of the total neuronal population. They are the principal output neurones of the striatum and also the sites receiving cortical inputs. Thus, they play a crucial role in the input-output operations of the striatum (Bolam et al., 2000). These neurones, not only project to other basal ganglia nuclei, but also communicate with each other by an extensive local plexus of axon collateral branches (Wilson and Groves, 1980). Until recently, there was no direct physiological evidence for functional inhibitory interactions between spiny neurones projections. However, simultaneous intracellular recordings from pairs of spiny projection neurones revealed that GABA<sub>A</sub>R-mediated synaptic connections existed between striatal spiny projection neurones (Tunstall et al., 2002). Further characterisation of this network provided evidence that MSNs projecting in the globus pallidus of the behaving rat, fired tens of action potentials (APs) per second (Benhamou et al., 2012). More interestingly, although this was a low firing frequency at which short term depression would be almost complete, this sparse and synaptically depressed network can significantly affect postsynaptic firing patterns *in vitro* (Bugaysen et al., 2013). Thus, for the first time, it has been shown that the unitary GABAergic synapses composing this network of MSN axon collaterals play an important role in the information processing within the striatum. However, the extent of collateral inhibition is a matter of debate as it is believed that in the striatum, most of the inhibition is mediated by fast spiking interneurones (Planert et al., 2010).

In the previous chapter, we investigated the development of cultured embryonic MSNs and the characteristics of specific GABAergic synapse formation. In this culture system, the MSNs compose a network of axon collateral inhibitory connections which

are also predominant throughout the different nuclei composing the basal ganglia (Tunstall et al., 2002).

Understanding the functionality of such network and the role played by GABA<sub>A</sub>R activity in transducing the GABA signalling during GABAergic synapse formation, is of crucial importance if we are to understand how this network is established. The effects of neuronal activity during GABAergic synapse formation has been a matter of debate for some time. To investigate the role played by neuronal activity during GABAergic synapse formation, mature hippocampal neuron cultures (14-21 DIV) were treated with tetrodotoxin (TTX) to block synaptic activity non-selectively (Penschuck et al., 1999). This treatment resulted in a loss of 30 % of the  $\alpha 1$ ,  $\alpha 2$  and  $\gamma 2$  subunit immunoreactivity after 1- and 12-hours treatment and induced the GABA<sub>A</sub>R subunit staining to vanish from the cell surface. This result provided one of the first pieces of evidence that neuronal activity regulated the cell surface expression of GABA<sub>A</sub>Rs but was not playing a prominent role in the establishment of neuron-specific expression patterns of GABA<sub>A</sub>R subtypes in the developing brain.

This result was further emphasised when hippocampal neurones treated with TTX during the period of synaptogenesis resulted in a reduction in the number of GABAergic presynaptic terminals and of the efficacy of these synapses (Hartman et al., 2006). This reduction in GABAergic synapse number was visible within 5 days after activity suppression, suggesting a general retardation of the GABAergic synaptogenesis provoked by the blockade of neuronal activity. Interestingly, the reduction in synapse number was accompanied by a reduction in the amplitude and the frequency of mIPSCs.

This was further supported when it was shown that excitatory neuronal activity controls the amount of GABA<sub>A</sub>Rs at inhibitory synapses by regulation of their synaptic accumulation and diffusion dynamics (Bannai et al., 2009). In this paper, the increase of excitation reduced the size of synaptic GABA<sub>A</sub>R clusters and depolarising currents decreased mIPSC amplitude. Although this paper might appear contradictory to the

previous ones, it could also reveal an antihomeostatic regulation of excitation-inhibition which, if altered, is involved in pathological conditions such as status epilepticus (Bannai et al., 2009).

In addition, slices from P7 rat hippocampus were cultured by Marty and colleagues for 13 days in the presence of bicuculline to increase neuronal activity, or DNQX, to decrease neuronal activity (Marty et al., 2004). While an increase in activity produced an augmentation of the density of individual  $\alpha 1$  or  $\alpha 2$ -containing GABA<sub>A</sub>R clusters, a decrease in neuronal activity triggered in contrast, a decrease in the density of these receptors. Interestingly, the size of the clusters was inversely regulated, with bicuculline decreasing the size of the clusters and DNQX increasing it. These results indicated that in the hippocampus, neuronal activity regulates the mean size of GABA<sub>A</sub>Rs and gephyrin-immunoreactive clusters by modifying specifically the density of synapses containing small clusters of receptors (Marty et al., 2004). Finally, this was confirmed when an increase in the amplitude and frequency of mIPSCs, accompanied by an increase in the size of  $\gamma 2$  subunit clusters and of GAD-65 puncta, were observed when hippocampal cultures were exposed to depolarising conditions (Rannals and Kapur, 2011).

Although many studies have shown the role played by neuronal activity during GABAergic synapse formation and in homeostatic regulation of networks, the role of GABA<sub>A</sub>R activity during GABAergic synapse formation has never been studied in the context of purely GABAergic systems.

Towards this aim, we utilised the model system of embryonic striatal cultures (described in the previous chapter) and treated MSNs with bicuculline which is a competitive GABA antagonist but is also classified as an allosteric inhibitor of GABA<sub>A</sub>Rs (Birnie et al., 2000).

### **6.1.1 Aims**

In this chapter, our aims were:

1. To determine if GABA signalling regulates the pattern of expression of different subtypes of receptors during the establishment and maintenance of the GABAergic synapses, by analysing the size and density of GABA<sub>A</sub>R clusters containing  $\alpha$ 1 and/or  $\alpha$ 2 subunit in presence and absence of bicuculline.
2. To establish whether these changes were accompanied by modifications of the connectivity between MSNs and in gephyrin clustering.

## **6.2 Methods**

### **6.2.1 Primary cultures of medium spiny neurones**

Striatal cultures were prepared as described in Chapter 2, Section 2.1.

### **6.2.2 Treatments with bicuculline**

To analyse the role of GABA signalling during GABAergic synapse development, E17 striatal neurones were cultured and treated with control (DMSO) or 50  $\mu$ M bicuculline after 4 and 6 DIV and fixed at 7 DIV. Another batch of neurones were treated with the same concentration of bicuculline after 7, 9 and 11 DIV and fixed at 14 DIV. The same time points were used to treat medium spiny neurone cultures with 25  $\mu$ M bicuculline.

### **6.2.3 Immunocytochemistry**

Immunocytochemistry was performed as described in Chapter 2, section 2.2. Neurones cultured for 7 or 14 DIV, were fixed using 4 % PFA/ sucrose for 12 minutes at room temperature. After fixation, they were incubated with glycine (0.3 M) in PBS, in order to quench PFA. After washing in PBS, cells were incubated in 1 % BSA in PBS for 1 hour and subsequently incubated with anti-  $\alpha$ 1 and anti-  $\alpha$ 2 antibodies, specifically binding to their N-terminal extracellular domains, diluted in 1 % BSA in PBS overnight (14-16 hours) at 4 °C (Table 21). Cultures were then permeabilised by incubating with 1 % BSA, 0.5 % Triton X-100 in PBS for 15 minutes. Neurones were subsequently

incubated with GAD-65 and MAP-2 (Table 21) antibodies diluted in 1 % BSA in PBS for 2 hours at room temperature. Following this step, Alexa Fluor-conjugated secondary antibodies were added as described in Chapter 2, Section 2.2 (antibodies used in these experiments are described in the Table 21).

#### **6.2.4 Analysis of images using confocal microscopy**

Immunolabelling was analysed using Zeiss LSM 710 with a Plan-Apochromat 63x/1.4 Oil DIC lens. Threshold for each channel was calculated from the background staining intensity and then removed from the image.

##### *6.2.4.1 Analysis of bicuculline treatment on cell survival*

In order to know if bicuculline had an effect on cell survival, we counted the density of cells per image after treatment with 50 or 25  $\mu\text{M}$  bicuculline from 4 to 7 DIV and from 7 to 14 DIV. Tile-scan (large field) images (3072 x 2048 pixels) were taken using confocal microscopy. Subsequently, the density of cells per image was counted using merge staining and statistical analysis was performed

##### *6.2.4.2 Confocal analysis*

To establish the density and size of  $\alpha 1$ - and  $\alpha 2$ - containing GABA<sub>A</sub> receptor clusters along the 20  $\mu\text{m}$  of each primary dendrite, puncta were defined as immunoreactive profiles greater than 0.1  $\mu\text{m}^2$ , with the mean intensity of each cluster equal or higher than double the standard deviation of intensity which was indicated by the Zen 2009 Programme. The defined clusters were encircled and their properties noted by hand. For each condition, the density and size of  $\alpha 1$  clusters were first calculated, followed by the  $\alpha 2$  clusters. Then,  $\alpha 1$  clusters which were mixed with  $\alpha 2$  (minimum of 50 % overlapping) were separated from  $\alpha 1$  clusters and analysed as a separate group. The same process was applied for  $\alpha 2$  mixed clusters. Because the density of  $\alpha 1$  and  $\alpha 2$  clusters was different among mixed clusters, these populations were kept and analysed separately, although in most of the cases, they represented the same population of mixed clusters.



#### 6.2.4.3 *Analysis of synaptic parameters*

As a criterion for synaptically localised clusters, I determined whether these clusters were in close apposition to the presynaptic marker GAD-65. A minimum of 50 % overlap was used to estimate the close apposition between the postsynaptic clusters and the presynaptic GAD-65 positive terminals. The total density of GAD-65 immunoreactive puncta forming contacts along the first 20  $\mu\text{m}$  length of primary dendrites was counted to determine the density of presynaptic inputs per dendrite

#### 6.2.5 **Statistical analysis**

Once all the parameters for each condition were measured, they were copied into an Excel file and sorted into different groups according to their size, co-localisation with GAD-65 and kind, single or mixed clusters:

- All  $\alpha 1$  single clusters
- $\alpha 1$  single clusters which are co-localised with GAD-65
- All  $\alpha 2$  single clusters
- $\alpha 2$  single clusters which are co-localised with GAD-65
- All  $\alpha 1$  mixed clusters
- $\alpha 1$  mixed clusters which are co-localised with GAD-65
- All  $\alpha 2$  mixed clusters
- $\alpha 2$  mixed clusters which are co-localised with GAD-65

Subsequently, the data were statistically analysed using Origin Pro 9.0 32 Bit software. Normality tests were performed first using Shapiro-Wilk and Kolmogorov-Smirnov tests. After normality tests were performed on each of the groups, non parametric statistical analysis was executed on unpaired data as the groups were not normally distributed (non- Gaussian distribution) and independent. The most adapted test to use was Mann Whitney test performed with an interval of confidence of 95 %. Because they are robust measure of central tendency when distributions are not normally distributed, medians and their interquartile range (IQR) were used to describe the data and evaluate

statistical dispersion. Similar approach was used to analyse the density of presynaptic terminals forming contacts along the first 20  $\mu\text{m}$  of primary dendrites. After normality tests were performed, Mann-Whitney test was used to evaluate if the density of presynaptic terminals per dendrite was changing after bicuculline treatment compared to DMSO. The total density of clusters was evaluated along the 20  $\mu\text{m}$  of primary dendrite of each cells. The density of synaptic clusters was also evaluated for the same dendrite. The percentage of synaptic clusters was determined by the proportion of synaptic clusters as a percentage of the total clusters for each dendrite. The new populations (% of synaptic clusters/total) were tested for normality and subsequently compared using parametric (Student's t-test) or non-parametric statistical tests (Mann-Whitney).

**Table21. Antibodies used for immunocytochemistry performed on medium spiny neurone cultures**

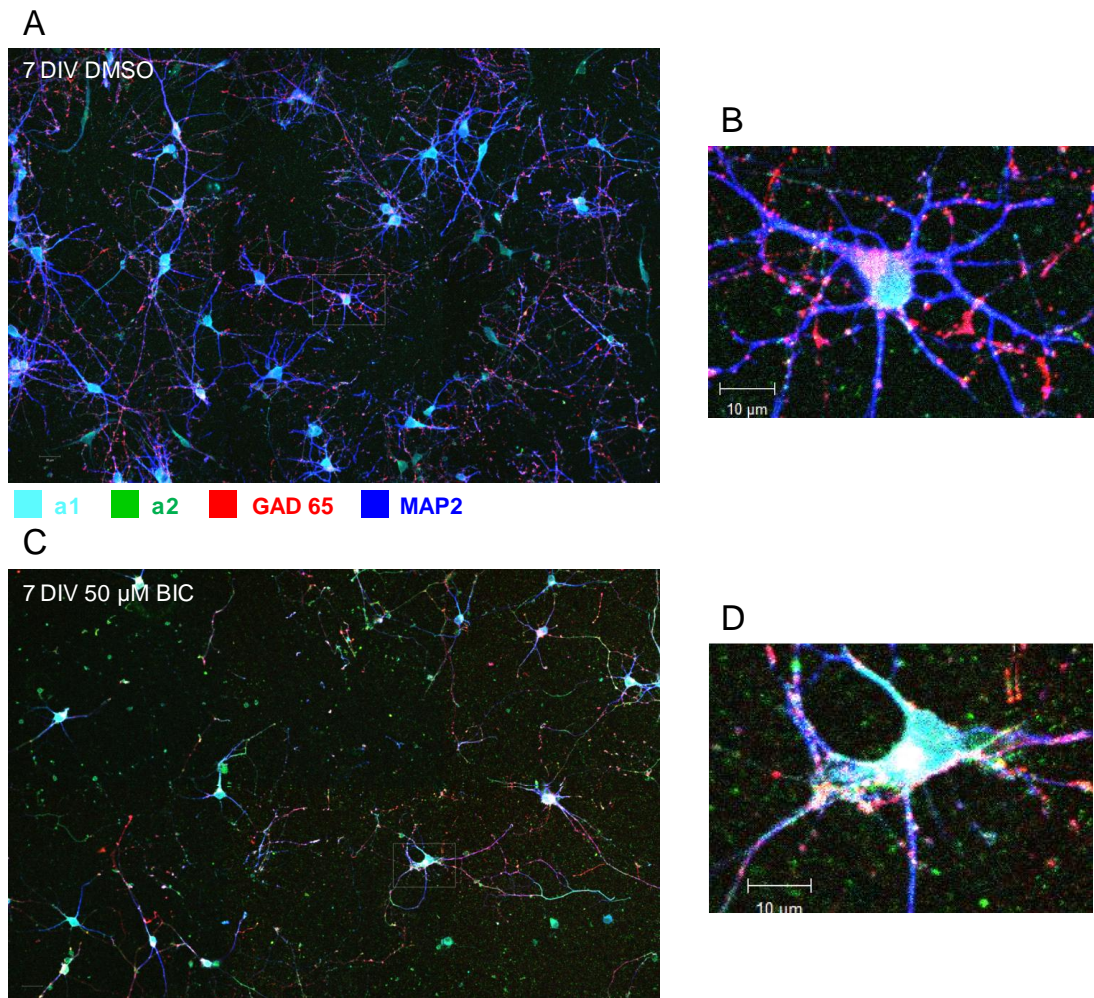
primary antibodies				secondary antibodies		
specificity	origin	dilutions	source and characterisation	antibodies	dilutions	source
GABA <sub>A</sub> $\alpha$ 1	Rabbit	1:200	Duggan, MJ, Stephenson AF., 1990. <i>J Biol Chem</i>	Goat anti rabbit 405	1:750	Alexa Fluor Invitrogen a31556
GABA <sub>A</sub> $\alpha$ 2	Guinea-pig	1:400	Synaptic System 224104	Goat Anti guinea pig 488	1:750	Alexa Fluor Invitrogen a11073
GAD65	Mouse	1:4000	Abcam, ab26113	Goat anti mouse 555	1:750	Alexa Fluor Invitrogen a21422
MAP2	Chicken	1:2500	Abcam, ab92434	Goat Anti chicken 488	1:750	Alexa Fluor Invitrogen a11039

## 6.3 Results

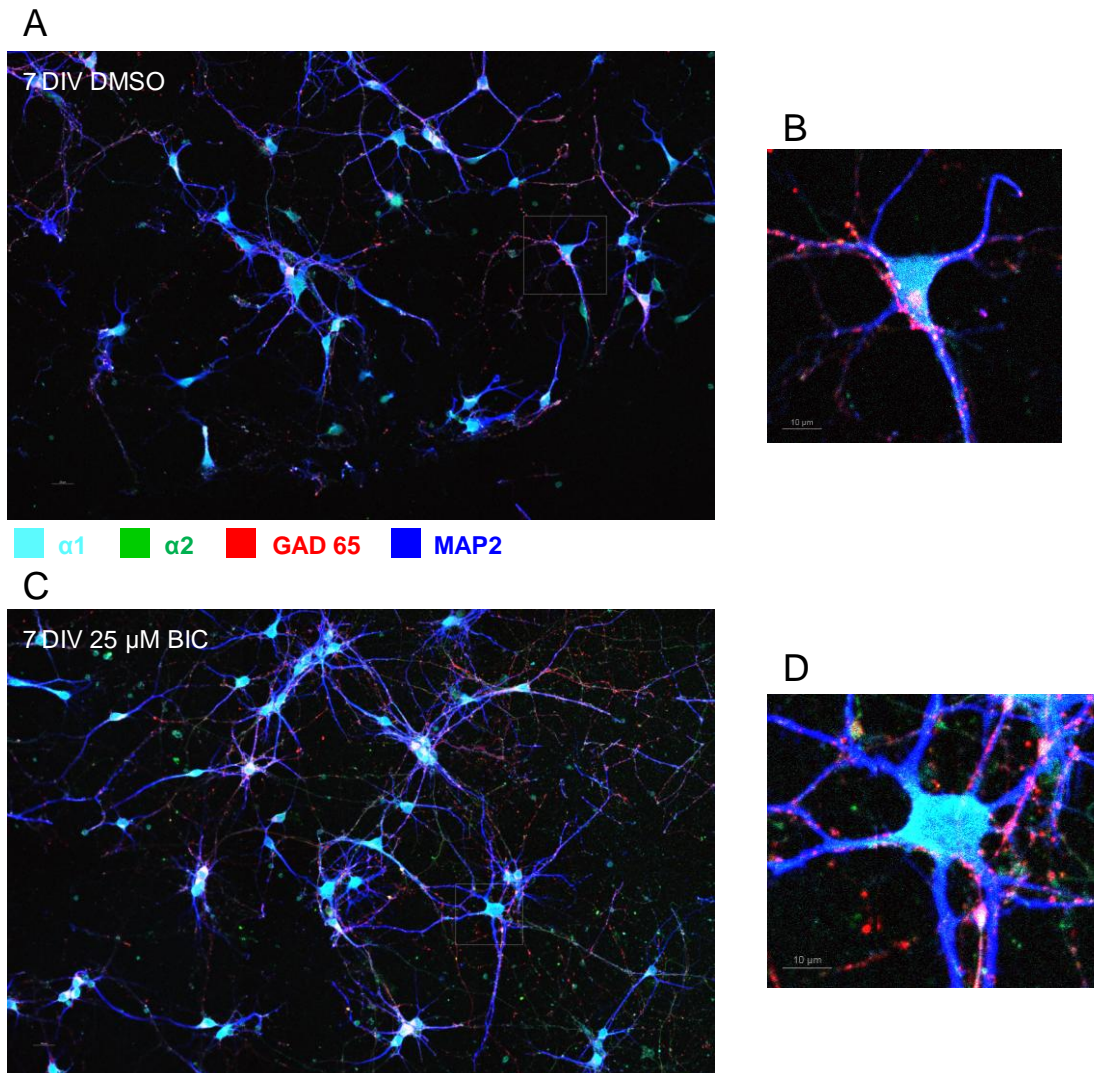
### 6.3.1 Treatment of MSN cultures with bicuculline from 4-7 DIV

#### 6.3.1.1 Treatment of medium spiny neurones with 50 $\mu$ M bicuculline from 4 to 7 DIV provoked cell death

Cultured embryonic (E16-18) striatal neurones form an homogeneous population of the precursors of GABAergic medium spiny neurones (Goffin et al., 2010). In the previous chapter, we were interested in how specific  $\alpha$ 1- and  $\alpha$ 2-containing synapses are established during GABAergic synapse development. In the present chapter, we investigated if activity of GABA<sub>A</sub> receptors influenced the proper positioning and the assembly of different types of inhibitory synapses. To investigate this, we have suppressed the GABA<sub>A</sub> receptor activity in the medium spiny neurone cultures using a competitive antagonist bicuculline over two periods of time. We have chronically treated medium spiny neurones with 50 or 25  $\mu$ M bicuculline from 4 to 7 days *in vitro* (DIV). As a control, we have treated neurones at the same period of time with an equivalent amount of DMSO (dimethyl sulfoxide), a polar solvent in which bicuculline was initially prepared in. Figure 65 is a large field image of medium spiny neurones treated from 4 to 7 DIV with 50  $\mu$ M bicuculline or DMSO. This figure shows examples of staining for  $\alpha$ 1 and  $\alpha$ 2 extracellular domains of GABA<sub>A</sub>Rs subunits, the intracellular presynaptic marker GAD-65 and MAP-, using the antibodies described in Table 19. The total density of cells per image was counted using the Zen 2009 programme. Figure 66 is a large field image of medium spiny neurones treated from 7 to 14 DIV with 50  $\mu$ M bicuculline or DMSO. These figures show examples of staining for  $\alpha$ 1 and  $\alpha$ 2 extracellular domains of GABA<sub>A</sub>Rs subunits, the intracellular presynaptic marker GAD-65 and MAP-, using the antibodies described in Table 19. The total density of cells per image was counted using the Zen 2009 programme.



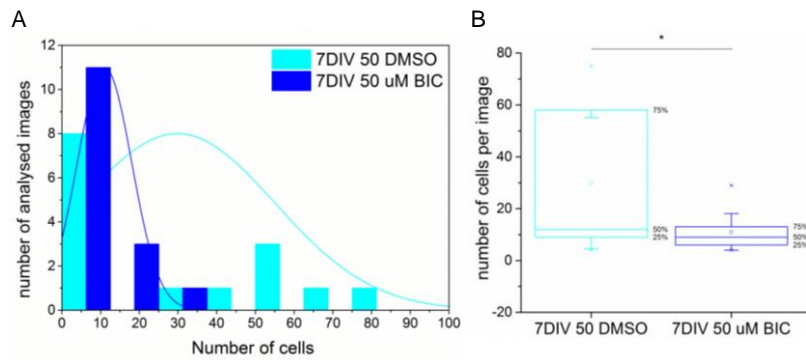
**Figure 65. The density of cells is decreasing with 50 µM bicuculline treatment from 4 to 7 DIV compared to DMSO.** Immunolabelling of GABA<sub>A</sub> receptors α1, α2 subunit containing clusters (respectively cyan and green) and presynaptic GABAergic terminals (red) along primary dendrites (blue) of cultured medium spiny neurones. **A.** Merged tile-scan image of a 7 DIV striatal culture treated with DMSO. **B.** Enlarged image of boxed region in A. **C.** Merged tile-scan image of a 7 DIV striatal culture treated with 50 µM bicuculline **D.** Enlarged image of boxed region in C.



**Figure 66. The density of cells is not affected by 25  $\mu\text{M}$  bicuculline treatment from 4 to 7 DIV compared to DMSO.** Immunolabelling of GABA<sub>A</sub> receptors  $\alpha$ 1,  $\alpha$ 2 subunit containing clusters (respectively cyan and green) and presynaptic GABAergic terminals (red) along primary dendrites (blue) of cultured medium spiny neurones. **A.** Merged tile-scan image of a 7 DIV striatal culture treated with DMSO. **B.** Enlarged image of boxed region in A. **C.** Merged tile-scan image of a 7 DIV striatal culture treated with 25  $\mu\text{M}$  bicuculline **D.** Enlarged image of boxed region in C.

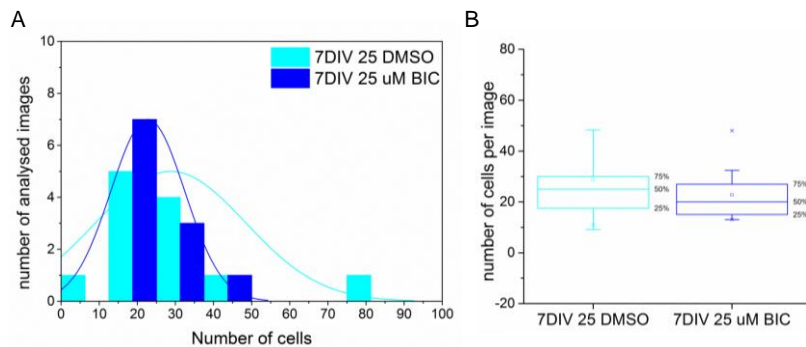
The median density of cells per image was estimated after treatment with 50  $\mu\text{M}$  bicuculline or control (Figure 67). At 7 DIV, the median density of cells per image was 12 (9-58) with control treatment compared to 6 (9-13) with 50  $\mu\text{M}$  bicuculline treatment ( $p$  value < 0.05, Mann Whitney test,  $n=15$  images analysed with control or bicuculline treatment at 7 DIV). This demonstrates that the density of cells is significantly decreased by 50  $\mu\text{M}$  bicuculline treatment compared to DMSO from 4 to 7 DIV.





**Figure 67. The density of cells per image is significantly decreased after treatment with 50  $\mu$ M bicuculline from 4 to 7 DIV.** The density of medium spiny neurones per tile scan images was counted in presence of DMSO or 50  $\mu$ M bicuculline from 4-7 DIV. **A.** Histogram shows the distribution of the density of cells per image in presence of DMSO or 50  $\mu$ M bicuculline added at 4 and 6 DIV (n=15 images analysed respectively, from two independent experiments). **B.** The box plot displays the density of cells per image in presence of DMSO or 50  $\mu$ M bicuculline added at 4 and 6 DIV. Statistical analysis was performed using Mann Whitney test: \* corresponds to p-value <0.05.

The median density of cells per image was estimated after treatment with 25  $\mu$ M bicuculline or control (Figure 68). At 7 DIV, the median density of cells per image was 25 (16.75-30) with control treatment compared to 20 (15-27) with 25  $\mu$ M bicuculline treatment. (p value > 0.05, Mann Whitney test, n=12 images of control-treated neurones analysed; n=11 images of bicuculline-treated neurones analysed). This demonstrates that the density of cells is not affected by 25  $\mu$ M bicuculline compared to DMSO treatment from 4 to 7 DIV.

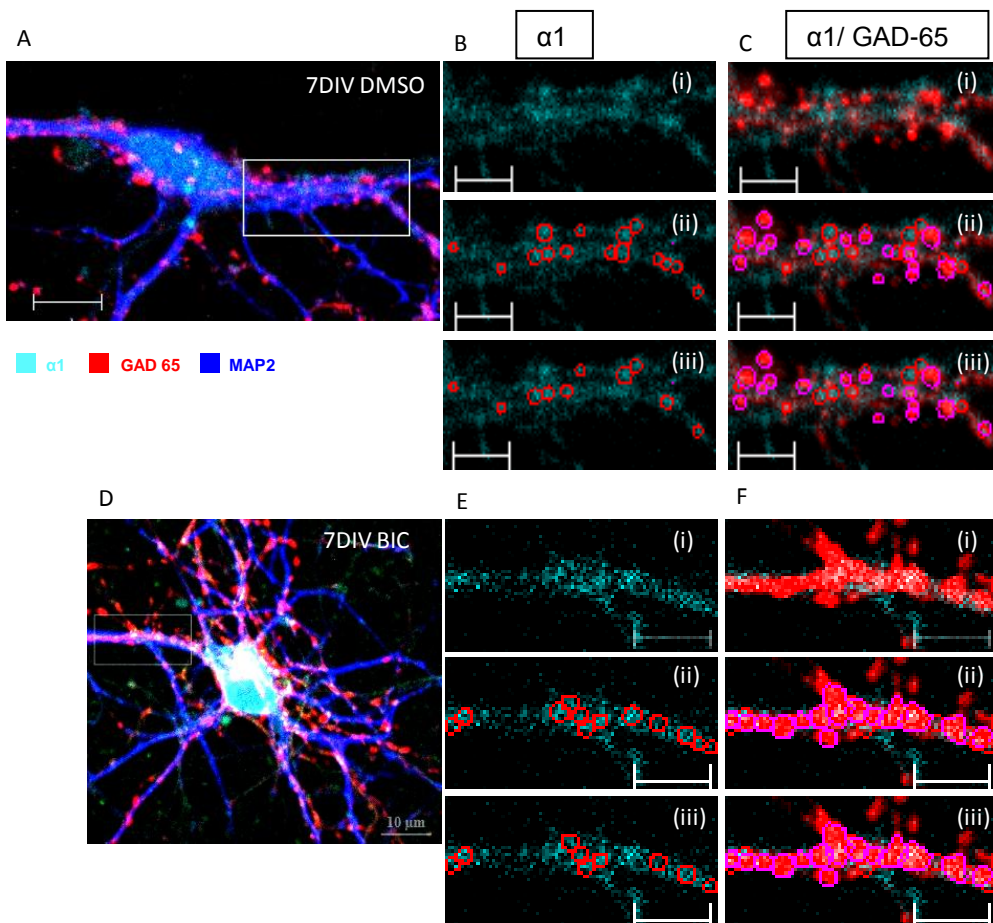


**Figure 68. The density of cells per image is not changing after treatment with 25  $\mu$ M bicuculline from 4 to 7 DIV.** The density of medium spiny neurones per tile scan images was counted in presence of DMSO or 25  $\mu$ M bicuculline from 4-7 DIV. **A.** Histogram shows the distribution of the density of cells per image in presence of DMSO or 25  $\mu$ M bicuculline added at 4 and 6 DIV (n=12 and n=11 images analysed respectively, from two independent experiments). **B.** The box plot displays the density of cells per image in presence of DMSO or 25  $\mu$ M bicuculline added at 4 and 6 DIV. Statistical analysis was performed using Mann Whitney test.

6.3.1.2 *The density of GABA<sub>A</sub>Rs per dendrite was not affected after 25 μM bicuculline treatment from 4 to 7 DIV.*

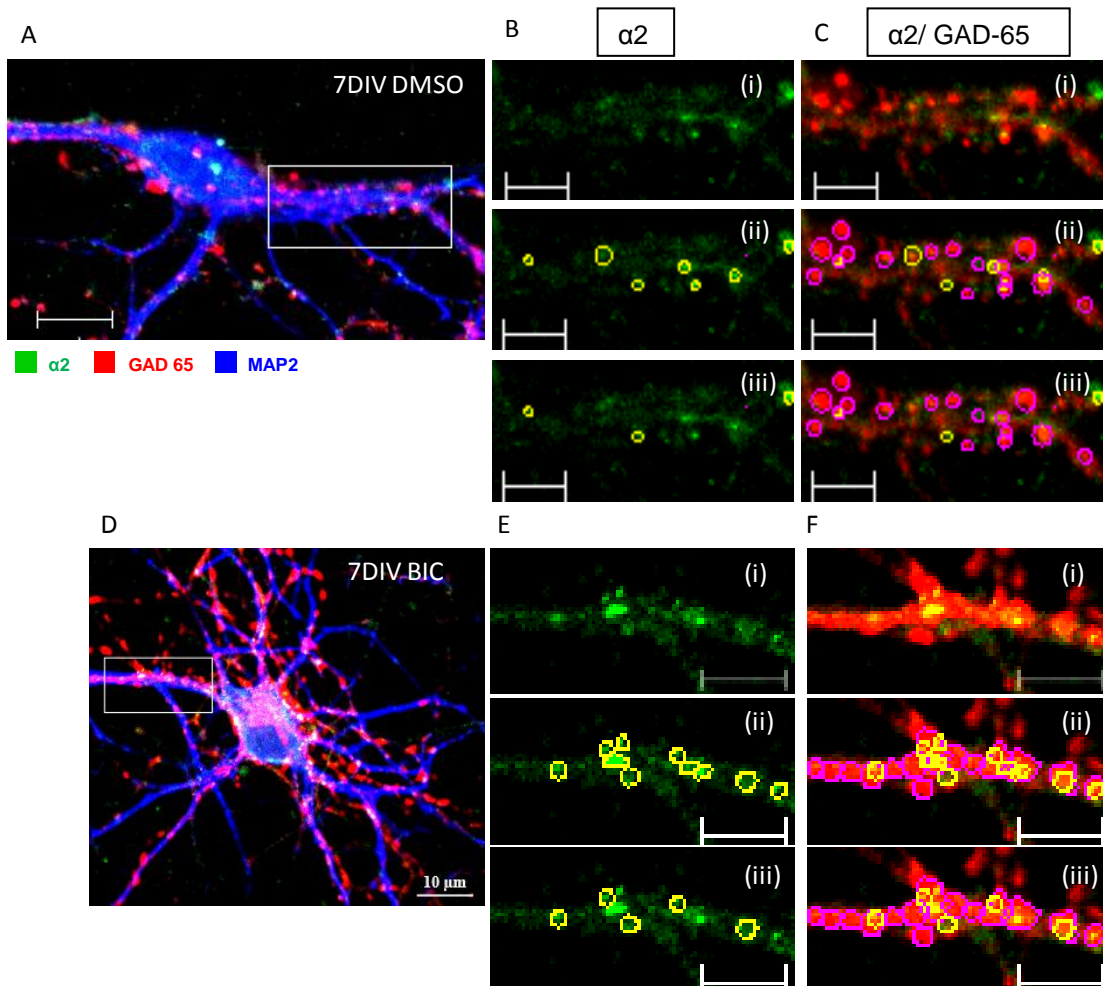
Developing medium spiny neurones treated with 25 μM bicuculline did not change the density of α1 single, α2 single, α1 mixed and α2 mixed clusters of GABA<sub>A</sub>Rs from 4 to 7 days in culture (DIV).

Figure 69, 70 and 71 represent medium spiny neurones treated from 4 to 7 DIV with 25 μM bicuculline or DMSO. This figure shows examples of staining for α1 and α2 extracellular domains of GABA<sub>A</sub>Rs subunits, the intracellular presynaptic marker GAD-65 and MAP-, using the antibodies described in Table 21. The total density of cells per image was counted using the Zen 2009 programme.



**Figure 69. The density of α1 clusters is not affected by the 25 μM bicuculline treatment.** Immunolabelling of GABA<sub>A</sub>Rs α1 subunit-containing clusters (cyan) and presynaptic GABAergic terminals (red) along primary dendrites (blue) of cultured medium spiny neurones. **A.** Merged image of a 7 DIV striatal neurone treated with DMSO (scale bar: 10 μm). **B.(i)** Enlarged image of boxed region in A representing α1 staining only. **(ii)** Analysis of image B(i) in which all α1 clusters are circled in red. **(iii)** Analysis of image B(i) in which only α1 single clusters that are not associated with α2 clusters are circled in red (scale bar: 5 μm). **C.(i)** Enlarged image of boxed

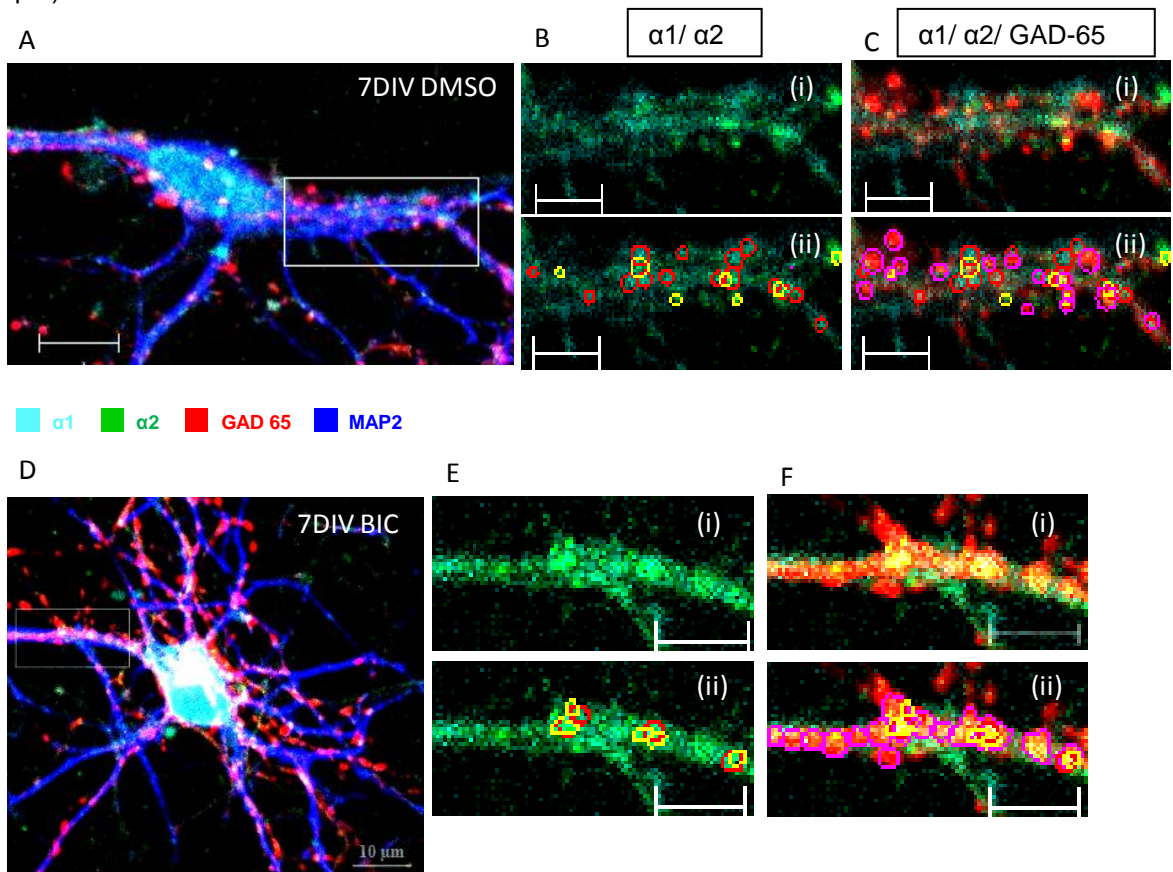
region in A representing  $\alpha 1$  positive clusters and presynaptic GAD-65 positive nerve terminals. **(ii)** Analysis of image C(i) in which all  $\alpha 1$  clusters were circled in red and presynaptic terminals were circled in purple. **(iii)** Analysis of image C(i) in which only  $\alpha 1$  single clusters were circled in red and presynaptic terminals were circled in purple (scale bar: 5  $\mu\text{m}$ ). **D.** Merged image of a 14 DIV striatal neurone (scale bar: 10  $\mu\text{m}$ ). **E.(i)** Enlarged image of boxed region in D representing  $\alpha 1$  staining only. **(ii)** Analysis of image E(i) in which all  $\alpha 1$  clusters are circled in red. **(iii)** Analysis of image E(i) in which only  $\alpha 1$  single clusters that are not associated with  $\alpha 2$  clusters are circled in red (scale bar: 5  $\mu\text{m}$ ). **F.(i)** Enlarged image of boxed region in D representing  $\alpha 1$  positive clusters and presynaptic GAD-65 positive nerve terminals. **(ii)** Analysis of image F(i) in which all  $\alpha 1$  clusters were circled in red and presynaptic terminals were circled in purple. **(iii)** Analysis of image F(i) in which only  $\alpha 1$  single clusters were circled in red and presynaptic terminals were circled in purple (scale bar: 5  $\mu\text{m}$ ).



**Figure 70. The density of  $\alpha 2$  clusters is not affected by the 25  $\mu\text{M}$  bicuculline treatment.** Immunolabelling of GABA<sub>A</sub>Rs  $\alpha 2$  subunit-containing clusters (green) and presynaptic GABAergic terminals (red) along primary dendrites (blue) of cultured medium spiny neurones. **A.** Merged image of a 7 DIV striatal neurone treated with DMSO (scale bar: 10  $\mu\text{m}$ ). **B.(i)** Enlarged image of boxed region in A representing  $\alpha 2$  staining only. **(ii)** Analysis of image B(i) in which all  $\alpha 2$  clusters are circled in yellow. **(iii)** Analysis of image B(i) in which only  $\alpha 2$  single clusters that are not associated with  $\alpha 1$  clusters are circled in yellow (scale bar: 5  $\mu\text{m}$ ). **C.(i)** Enlarged image of boxed region in A representing  $\alpha 2$  positive clusters and presynaptic GAD-65 positive nerve terminals. **(ii)** Analysis of image C(i) in which all  $\alpha 2$  clusters were circled in yellow and presynaptic terminals were circled in purple. **(iii)** Analysis of image C(i) in which only  $\alpha 2$  single clusters were circled in yellow and presynaptic terminals were circled in purple (scale bar: 5  $\mu\text{m}$ ). **D.** Merged image of a 14 DIV striatal neurone (scale bar: 10  $\mu\text{m}$ ). **E.(i)** Enlarged image of boxed region in D representing  $\alpha 2$  staining only. **(ii)** Analysis of image E(i) in which all  $\alpha 2$  clusters are circled in yellow. **(iii)** Analysis of image E(i) in which only  $\alpha 2$  single clusters that are



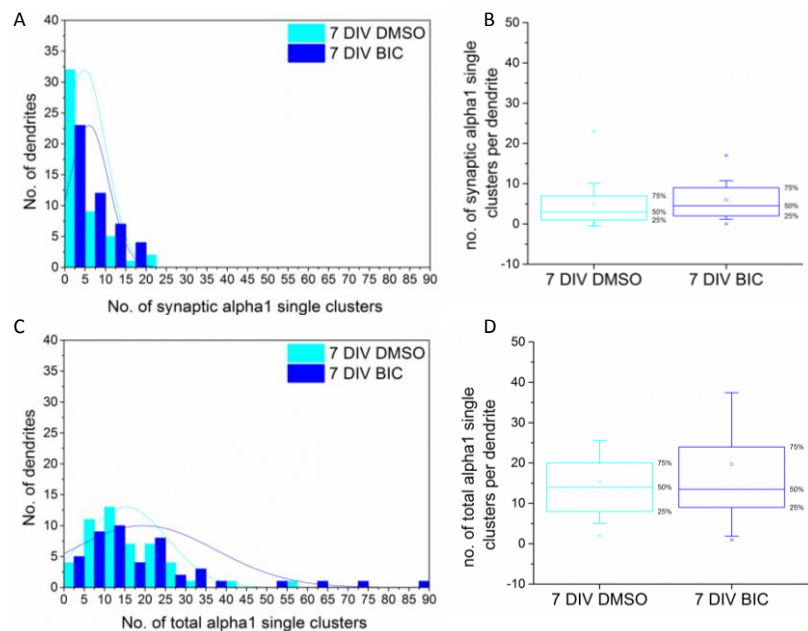
not associated with  $\alpha 1$  clusters are circled in yellow (scale bar: 5  $\mu\text{m}$ ). **F.(i)** Enlarged image of boxed region in D representing  $\alpha 2$  positive clusters and presynaptic GAD-65 positive nerve terminals. **(ii)** Analysis of image F(i) in which all  $\alpha 2$  clusters were circled in yellow and presynaptic terminals were circled in purple. **(iii)** Analysis of image F(i) in which only  $\alpha 2$  single clusters were circled in yellow and presynaptic terminals were circled in purple (scale bar: 5  $\mu\text{m}$ ).



**Figure 71. The density of  $\alpha 1/\alpha 2$  mixed clusters is not affected by the 25  $\mu\text{M}$  bicuculline treatment.** Immunolabelling of GABA<sub>A</sub>Rs  $\alpha 1/\alpha 2$  subunit-containing clusters (cyan and green) and presynaptic GABAergic terminals (red) along primary dendrites (blue) of cultured medium spiny neurones. **A.** Merged image of a 7 DIV striatal neurone treated with DMSO (scale bar: 10  $\mu\text{m}$ ). **B.(i)** Enlarged image of boxed region in A representing  $\alpha 1$  and  $\alpha 2$  staining. **(ii)** Analysis of image B(i) in which all  $\alpha 1$  and  $\alpha 2$  clusters are respectively circled in red and yellow (scale bar: 5  $\mu\text{m}$ ). **C.(i)** Enlarged image of boxed region in A representing  $\alpha 1$ ,  $\alpha 2$  positive clusters and presynaptic GAD-65 positive nerve terminals. **(ii)** Analysis of image C(i) in which all  $\alpha 1$  and  $\alpha 2$  clusters were respectively circled in red and yellow and presynaptic terminals were circled in purple. **D.** Merged image of a 14 DIV striatal neurone (scale bar: 10  $\mu\text{m}$ ). **E.(i)** Enlarged image of boxed region in D representing  $\alpha 1$  and  $\alpha 2$  staining. **(ii)** Analysis of image E(i) in which all  $\alpha 1$  and  $\alpha 2$  clusters were respectively circled in red and yellow (scale bar: 5  $\mu\text{m}$ ). **F.(i)** Enlarged image of boxed region in D representing  $\alpha 1$ ,  $\alpha 2$  positive clusters and presynaptic GAD-65 positive nerve terminals. **(ii)** Analysis of image F(i) in which all  $\alpha 1$  and  $\alpha 2$  clusters were respectively circled in red and yellow and presynaptic terminals were circled in purple (scale bar: 5  $\mu\text{m}$ ).

The density of synaptic and total  $\alpha 1$  single clusters of GABA<sub>A</sub>Rs was estimated per defined length of primary dendrite (the first 20  $\mu\text{m}$  from the cell body) after treatment with DMSO or 25  $\mu\text{M}$  bicuculline from 4 to 7 DIV (Figure 72). The median density of synaptic  $\alpha 1$  single clusters was 3 (7-1) with DMSO treatment, compared to

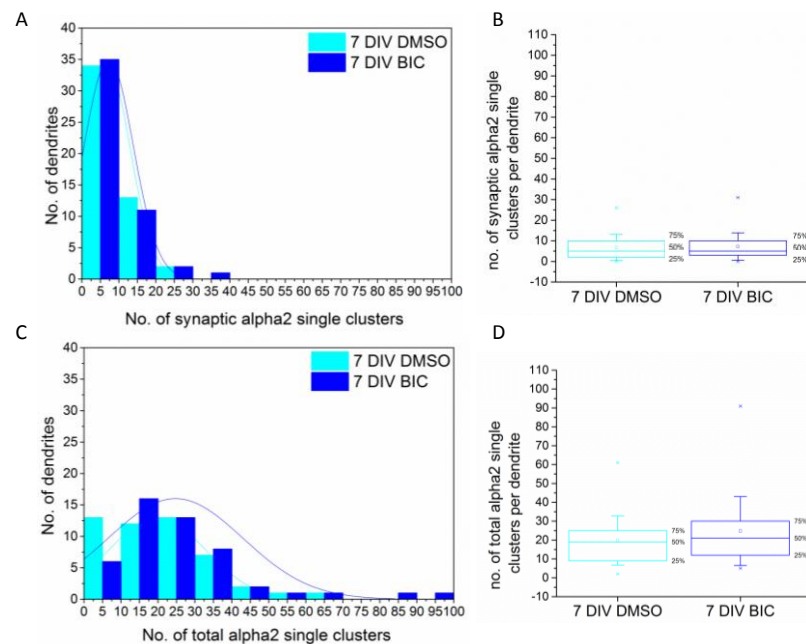
4.5 (9.25-2) with bicuculline treatment ( $p$  value =0.09, Mann Whitney test,  $n=49$  dendrites analysed from DMSO treated cultures and  $n=46$  dendrites analysed from bicuculline treated neurones). Similarly, the median density of total  $\alpha 1$  single clusters was 14 (20.5-8) with DMSO treatment, compared to 13.5 (24-8.75) with bicuculline treatment ( $p$  value=0.47, Mann Whitney test,  $n=49$  dendrites analysed from DMSO treated cultures and  $n=46$  dendrites analysed from bicuculline treated neurones). This demonstrates that the synaptic and total densities of  $\alpha 1$  single clusters are not affected by the treatment, indicating that the regulation of the density of these types of clusters is independent of GABA<sub>A</sub>R activity at this developmental stage.



**Figure 72. The density of synaptic and total  $\alpha 1$  clusters is not affected by treatment with 25  $\mu\text{M}$  bicuculline.** The density of  $\alpha 1$ -containing GABA<sub>A</sub> receptors clusters ( $\alpha 1$  single clusters) along the 20  $\mu\text{m}$  of primary dendrite was counted in medium spiny neurone cultures in presence of DMSO or 25  $\mu\text{M}$  bicuculline from 4 to 7 DIV. **A.** Histogram shows the distribution of synaptic  $\alpha 1$  single clusters densities in presence of DMSO or 25  $\mu\text{M}$  bicuculline from 4 to 7 DIV ( $n=49$  and  $n=46$  dendrites respectively from two independent experiments). **B.** box plot displays the median density (50 % of the population) of synaptic  $\alpha 1$  single clusters in presence of DMSO or 25  $\mu\text{M}$  bicuculline from 4 to 7 DIV. **C.** Histogram shows the distribution of total  $\alpha 1$  single clusters density in presence of DMSO or 25  $\mu\text{M}$  bicuculline from 4 to 7 DIV ( $n=49$  and  $n=46$  dendrites respectively from two independent experiments). **D.** Box plot displays the median density (50 % of the population) of total  $\alpha 1$  single clusters in presence of DMSO or 25  $\mu\text{M}$  bicuculline from 4 to 7 DIV. Statistical analysis was performed using Mann Whitney test.

We were also interested to analyse the density of  $\alpha 2$  single clusters in presence of DMSO or 25  $\mu\text{M}$  bicuculline from 4 to 7 DIV. The density of synaptic and total  $\alpha 2$  single clusters of GABA<sub>A</sub>Rs was estimated per defined length of primary dendrite (the first 20

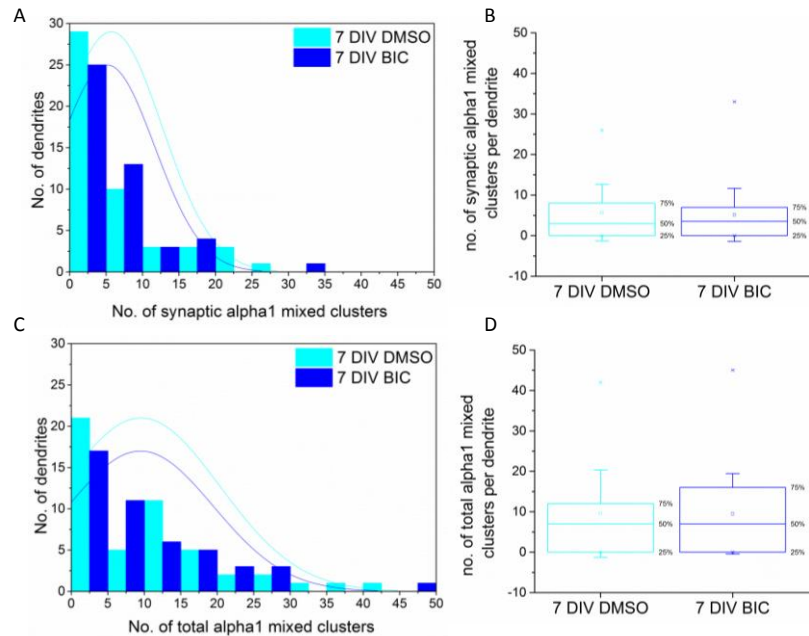
$\mu\text{m}$  from the cell body) after treatment with DMSO or 25  $\mu\text{M}$  bicuculline (Figure 73). The median density of synaptic  $\alpha 2$  single clusters was 5 (11-2) with DMSO treatment, compared to 5 (10.5-3) with bicuculline treatment (p value=0.60, Mann Whitney test, n=49 dendrites analysed from DMSO treated cultures and n=49 dendrites analysed from bicuculline treated neurones). Similarly, the median density of total  $\alpha 2$  single clusters was 19 (27-9) with DMSO treatment, compared to 21 (30.5-11.5) with bicuculline treatment (p value=0.18, Mann Whitney test, n=49 dendrites analysed from DMSO treated cultures and n=49 dendrites analysed from bicuculline treated neurones). This demonstrates that similarly to  $\alpha 1$  single clusters, the synaptic and total densities of  $\alpha 2$  single clusters are not affected by the treatment, indicating that the regulation of the density of these types of clusters is independent of GABA<sub>A</sub>R activity at this developmental stage.



**Figure 73. The density of synaptic and total  $\alpha 2$  clusters is not affected by treatment with 25  $\mu\text{M}$  bicuculline.** The density of  $\alpha 2$ -containing GABA<sub>A</sub> receptors clusters ( $\alpha 2$  single clusters) along the 20  $\mu\text{m}$  of primary dendrite was counted in medium spiny neurone cultures in presence of DMSO or 25  $\mu\text{M}$  bicuculline from 4 to 7 DIV. **A.** Histogram shows the distribution of synaptic  $\alpha 2$  single clusters densities in presence of DMSO or 25  $\mu\text{M}$  bicuculline from 4 to 7 DIV (n=49 and n=46 dendrites respectively from two independent experiments). **B.** box plot displays the median density (50 % of the population) of synaptic  $\alpha 2$  single clusters in presence of DMSO or 25  $\mu\text{M}$  bicuculline from 4 to 7 DIV. **C.** Histogram shows the distribution of total  $\alpha 2$  single clusters density in presence of DMSO or 25  $\mu\text{M}$  bicuculline from 4 to 7 DIV (n=49 and n=46 dendrites respectively from two independent experiments). **D.** Box plot displays the median density (50 %

of the population) of total  $\alpha 2$  single clusters in presence of DMSO or 25  $\mu\text{M}$  bicuculline from 4 to 7 DIV. Statistical analysis was performed using Mann Whitney test.

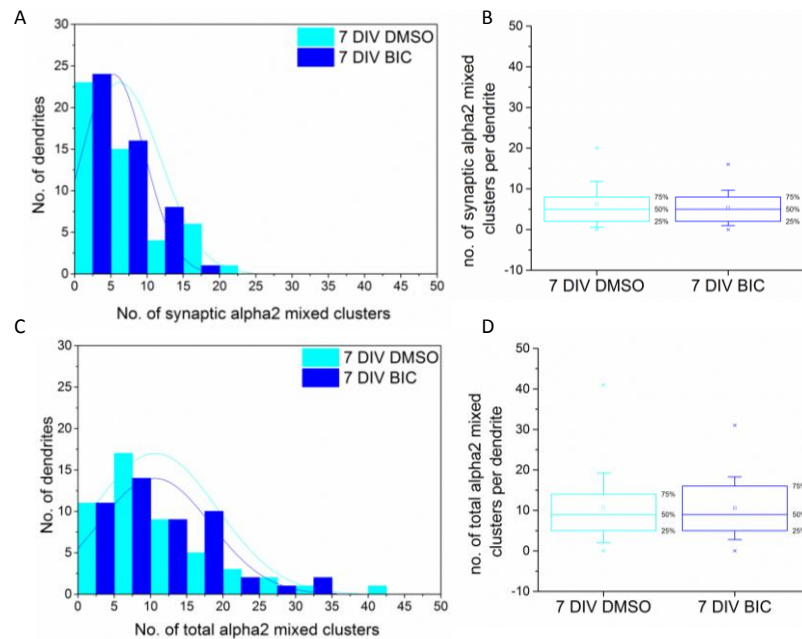
As explained in the previous chapter, we have observed two types of  $\alpha 1/\alpha 2$  mixed clusters. The mixed clusters which contained a majority of  $\alpha 1$  clusters were defined as  $\alpha 1$  mixed clusters while the mixed clusters containing a majority of  $\alpha 2$  clusters were defined as  $\alpha 2$  mixed clusters. The density of synaptic and total  $\alpha 1$  mixed clusters of  $\text{GABA}_A\text{Rs}$  was estimated per defined length of primary dendrite (the first 20  $\mu\text{m}$  from the cell body) after treatment with DMSO or 25  $\mu\text{M}$  bicuculline from 4 to 7 DIV (Figure 74). The median density of synaptic  $\alpha 1$  mixed clusters was 3 (8.5-0) with DMSO treatment, compared to 3.5 (7-0) with bicuculline treatment (p value=0.79, Mann Whitney test, n=49 dendrites analysed from DMSO treated cultures and n=46 dendrites analysed from bicuculline treated neurones). Similarly, the median density of total  $\alpha 1$  mixed clusters was 7 (14.5-0) with DMSO treatment, compared to 7 (16-0) with bicuculline treatment (p value=0.93, Mann Whitney test, n=49 dendrites analysed from DMSO treated cultures and n=46 dendrites analysed from bicuculline treated neurones). This demonstrates that the synaptic and total densities of  $\alpha 1$  mixed clusters are not affected by the treatment, indicating that the regulation of the density of these types of clusters is independent of the  $\text{GABA}_A\text{Rs}$  activity at this developmental stage.



**Figure 74. The density of synaptic and total  $\alpha 1$  clusters is not affected by treatment with 25  $\mu\text{M}$  bicuculline.** The density of  $\alpha 1/\alpha 2$ -containing GABA<sub>A</sub> receptors clusters ( $\alpha 1$  mixed clusters) along the 20  $\mu\text{m}$  of primary dendrite was counted in medium spiny neurone cultures in presence of DMSO or 25  $\mu\text{M}$  bicuculline from 4 to 7 DIV. **A.** Histogram shows the distribution of synaptic  $\alpha 1$  mixed clusters densities in presence of DMSO or 25  $\mu\text{M}$  bicuculline from 4 to 7 DIV (n=49 and n=46 dendrites respectively from two independent experiments). **B.** box plot displays the median density (50 % of the population) of synaptic  $\alpha 1$  mixed clusters in presence of DMSO or 25  $\mu\text{M}$  bicuculline from 4 to 7 DIV. **C.** Histogram shows the distribution of total  $\alpha 1$  mixed clusters density in presence of DMSO or 25  $\mu\text{M}$  bicuculline from 4 to 7 DIV (n=49 and n=46 dendrites respectively from two independent experiments). **D.** Box plot displays the median density (50 % of the population) of total  $\alpha 1$  mixed clusters in presence of DMSO or 25  $\mu\text{M}$  bicuculline from 4 to 7 DIV. Statistical analysis was performed using Mann-Whitney test.

We have also analysed the population of mixed clusters which contained a predominant density of  $\alpha 2$  clusters ( $\alpha 2$  mixed). The density of synaptic and total  $\alpha 2$  mixed clusters of GABA<sub>A</sub>Rs was estimated per defined length of primary dendrite (the first 20  $\mu\text{m}$  from the cell body) after treatment with DMSO or 25  $\mu\text{M}$  bicuculline from 4 to 7 DIV (Figure 75). The median density of synaptic  $\alpha 2$  mixed clusters was 5 (8.5-2) with DMSO treatment, compared to 5 (8.5-2) with bicuculline treatment (p value=0.71, Mann-Whitney test, n=49 dendrites analysed from DMSO treated cultures and n=49 dendrites analysed from bicuculline treated neurones). Similarly, the median density of total  $\alpha 2$  mixed clusters was 9 (14.5-5) with DMSO treatment, compared to 9 (16-5) with bicuculline treatment (p value=0.92, Mann-Whitney test, n=49 dendrites analysed from DMSO treated cultures and n=49 dendrites analysed from bicuculline treated

neurones). This demonstrates that the synaptic and total densities of  $\alpha 2$  mixed clusters are not affected by the treatment, indicating that the regulation of the density of these types of clusters is independent of the  $GABA_A$ Rs activity at this developmental stage.



**Figure 75. The densities of synaptic and total  $\alpha 2$  clusters are not affected by treatment with 25  $\mu M$  bicuculline.** The density of  $\alpha 1/\alpha 2$ -containing  $GABA_A$  receptors clusters ( $\alpha 2$  mixed clusters) along the 20  $\mu m$  of primary dendrite was counted in medium spiny neurone cultures in presence of DMSO or 25  $\mu M$  bicuculline from 4 to 7 DIV. **A.** Histogram shows the distribution of synaptic  $\alpha 2$  mixed clusters densities in presence of DMSO or 25  $\mu M$  bicuculline from 4 to 7 DIV (n=49 and n=49 dendrites respectively from two independent experiments). **B.** Box plot displays the median density (50 % of the population) of synaptic  $\alpha 2$  mixed clusters in presence of DMSO or 25  $\mu M$  bicuculline from 4 to 7 DIV. **C.** Histogram shows the distribution of total  $\alpha 2$  mixed clusters density in presence of DMSO or 25  $\mu M$  bicuculline from 4 to 7 DIV (n=49 and n=46 dendrites respectively from two independent experiments). **D.** Box plot displays the median density (50 % of the population) of total  $\alpha 2$  mixed clusters in presence of DMSO or 25  $\mu M$  bicuculline from 4 to 7 DIV. Statistical analysis was performed using Mann Whitney test.

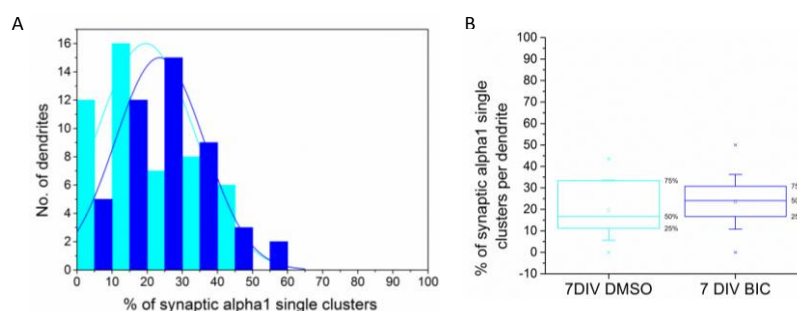
**Table 22. The density of  $GABA_A$ R clusters is not affected by 25  $\mu M$  treatment from 4 to 7 DIV**

Density of clusters		7 DIV DMSO/ BIC	Significant
$\alpha 1$ single clusters	Synaptic	↔	No
	Total		No
$\alpha 2$ single clusters	Synaptic		No
	Total		No
$\alpha 1$ mixed clusters	Synaptic		No
	Total		No
$\alpha 2$ mixed clusters	Synaptic		No
	Total		No



### 6.3.1.3 *The proportion of synaptic clusters as a percentage of the total clusters was not affected by 25 $\mu$ M bicuculline treatment from 4 to 7 DIV*

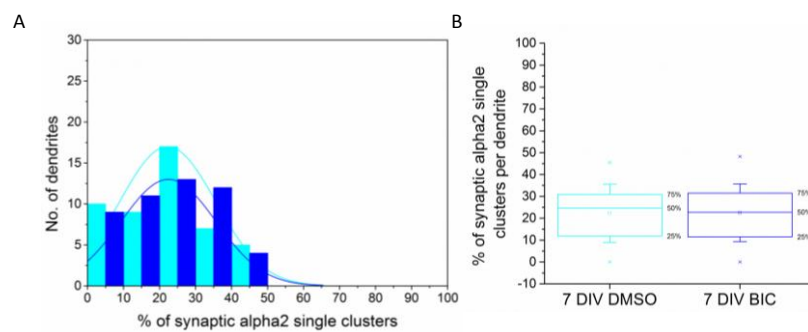
Despite the fact that the densities of all types of clusters were not affected by the treatment, we analysed further these changes in cluster populations. We estimated the proportion of synaptic clusters as a percentage of the total clusters in each population treated from 4 to 7 DIV. The proportion of synaptic  $\alpha$ 1 single as a percentage of the total  $\alpha$ 1 single clusters of GABA<sub>A</sub>Rs per defined length of primary dendrite (the first 20  $\mu$ m from the cell body) was calculated after treatment from 4 to 7 DIV (Figure 76). The median percentage of synaptic amongst total  $\alpha$ 1 single clusters was 16.66 (10.10-33.33) % with DMSO treatment compared to 24.06 (16.03-30.88) % with bicuculline treatment ((p value=0.15, Mann Whitney test, n=49 dendrites analysed after DMSO treatment and n=46 dendrites analysed after bicuculline treatment). Similarly to the density of synaptic  $\alpha$ 1 single clusters per dendrite, the percentage between the synaptic and the total  $\alpha$ 1 single clusters is not altered by bicuculline (Table 23).



**Figure 76. The percentage of synaptic/total  $\alpha$ 1 single clusters is not changed after treatment with 25  $\mu$ M bicuculline from 4 to 7 DIV.** The percentage of synaptic  $\alpha$ 1 single clusters amongst the total population of  $\alpha$ 1 single clusters along the 20  $\mu$ m of primary dendrite was estimated in medium spiny neurones cultures treated with DMSO or 25  $\mu$ M bicuculline from 4 to 7 DIV. **A.** Histogram shows the distribution of the percentages of synaptic/total  $\alpha$ 1 single clusters per dendrite after treatment with DMSO or bicuculline from 4 to 7 DIV (n=49 and n=46 dendrites respectively, from two independent experiments). **B.** Box-plot displays the median percentage (50 % of the represented population) of synaptic/total  $\alpha$ 1 single clusters per dendrite after treatment with DMSO or bicuculline from 4 to 7 DIV. Statistical analysis was performed using Mann-Whitney test.

In addition, the proportion of synaptic  $\alpha$ 2 single as a percentage of the total  $\alpha$ 2 single clusters of GABA<sub>A</sub>Rs per defined length of primary dendrite was calculated after

treatment with DMSO or 25  $\mu\text{M}$  bicuculline (Figure 77). After treatment with DMSO from 4 to 7 DIV, the median percentage of synaptic/total  $\alpha 2$  single clusters was 24.62 (31.31-11.45) % compared to 22.72 (32.92-11.26) % after treatment with bicuculline ( $p$  value=0.93, Mann Whitney test,  $n=48$  dendrites analysed after treatment with DMSO and  $n=49$  dendrites analysed after treatment with 25  $\mu\text{M}$  bicuculline). This indicates that, similarly to the density of synaptic  $\alpha 2$  single clusters per dendrite, the percentage of  $\alpha 2$  single clusters/total density of clusters is not changing with 25  $\mu\text{M}$  treatment of bicuculline.

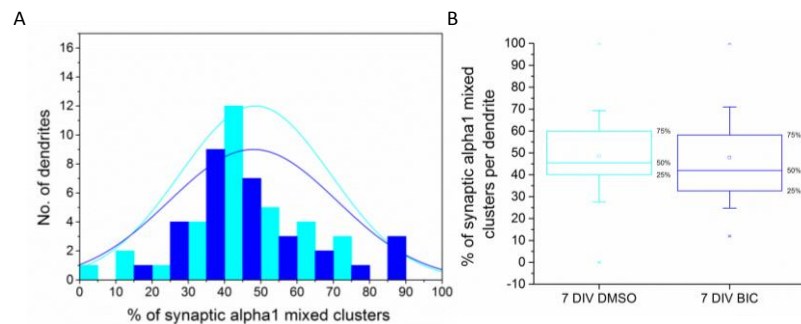


**Figure 77. The percentage of synaptic/total  $\alpha 2$  single clusters is not changed after treatment with 25  $\mu\text{M}$  bicuculline from 4 to 7 DIV.** The percentage of synaptic  $\alpha 2$  single clusters amongst the total population of  $\alpha 2$  single clusters along the 20  $\mu\text{m}$  of primary dendrite was estimated in medium spiny neurones cultures treated with DMSO or 25  $\mu\text{M}$  bicuculline from 4 to 7 DIV. **A.** Histogram shows the distribution of the percentages of synaptic/total  $\alpha 2$  single clusters per dendrite after treatment with DMSO or bicuculline from 4 to 7 DIV ( $n=48$  and  $n=49$  dendrites respectively, from two independent experiments). **B.** Box-plot displays the median percentage (50 % of the represented population) of synaptic/total  $\alpha 2$  single clusters per dendrite after treatment with DMSO or bicuculline from 4 to 7 DIV. Statistical analysis was performed using Mann-Whitney test.

Following the previous analysis, we analysed changes in the proportion of synaptic mixed clusters as a percentage of total mixed clusters during medium spiny neurones development. ). The proportion of synaptic  $\alpha 1$  mixed as a percentage of the total  $\alpha 1$  mixed clusters of  $\text{GABA}_A\text{Rs}$  per defined length of primary dendrite (the first 20  $\mu\text{m}$  from the cell body) was calculated after treatment with DMSO or 25  $\mu\text{M}$  bicuculline (Figure 78). After treatment with DMSO from 4 to 7 DIV, the median percentage of synaptic/total  $\alpha 1$  mixed clusters was 45.52 (39.09-60) % after treatment with DMSO compared to 41.98 (32.33-41.98) % after treatment with 25  $\mu\text{M}$  bicuculline ( $p$  value=0.43, Mann Whitney test,  $n=34$  dendrites analysed after treatment with DMSO



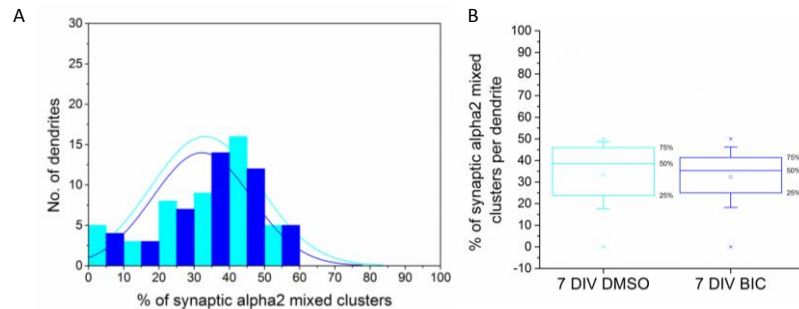
and n=32 dendrites analysed after treatment with 25  $\mu$ M bicuculline). This demonstrates that, the percentage of synaptic/total  $\alpha$ 1 mixed clusters of GABA<sub>A</sub>Rs per defined length of primary dendrite is not altered by treatment with 25  $\mu$ M bicuculline, possibly because GABA signalling is not involved in regulating this parameter at early stages of development.



**Figure 78. The percentage of synaptic/total  $\alpha$ 1 mixed clusters is not changed after treatment with 25  $\mu$ M bicuculline from 4 to 7 DIV.** The percentage of synaptic  $\alpha$ 1 mixed clusters amongst the total population of  $\alpha$ 1 mixed clusters along the 20  $\mu$ m of primary dendrite was estimated in medium spiny neurones cultures treated with DMSO or 25  $\mu$ M bicuculline from 4 to 7 DIV. **A.** Histogram shows the distribution of the percentages of synaptic/total  $\alpha$ 1 mixed clusters per dendrite after treatment with DMSO or bicuculline from 4 to 7 DIV (n=34 and n=32 dendrites respectively, from two independent experiments). **B.** Box-plot displays the median percentage (50 % of the represented population) of synaptic/total  $\alpha$ 1 mixed clusters per dendrite after treatment with DMSO or bicuculline from 4 to 7 DIV. Statistical analysis was performed using Mann-Whitney test.

We estimated changes in mixed clusters which contained a predominant density of  $\alpha$ 2 clusters in these cultures ( $\alpha$ 2 mixed clusters). The proportion of synaptic  $\alpha$ 2 mixed as a percentage of the total  $\alpha$ 2 mixed clusters of GABA<sub>A</sub>Rs per defined length of primary dendrite (the first 20  $\mu$ m from the cell body) was calculated after treatment with DMSO or 25  $\mu$ M bicuculline (Figure 79). After treatment with DMSO from 4 to 7 DIV, the median percentage of synaptic/total  $\alpha$ 2 mixed clusters was 38.53 (23.51-45.99) % after treatment with DMSO compared to 35.29 (25-41.74) % after treatment with 25  $\mu$ M bicuculline (p value=0.46, Mann-Whitney test, n=46 dendrites analysed after treatment with DMSO and n=45 dendrites analysed after treatment with 25  $\mu$ M bicuculline). This demonstrates that, the percentage of synaptic/total  $\alpha$ 2 mixed clusters of GABA<sub>A</sub>Rs per defined length of primary dendrite is not altered by treatment with 25  $\mu$ M bicuculline. As

stated before, it is possibly because GABA signalling is not involved in regulating this parameter at early stages of development.



**Figure 79. The percentage of synaptic/total  $\alpha 2$  mixed clusters is not changed after treatment with 25  $\mu\text{M}$  bicuculline from 4 to 7 DIV.** The percentage of synaptic  $\alpha 2$  mixed clusters amongst the total population of  $\alpha 2$  mixed clusters along the 20  $\mu\text{m}$  of primary dendrite was estimated in medium spiny neurones cultures treated with DMSO or 25  $\mu\text{M}$  bicuculline from 4 to 7 DIV. **A.** Histogram shows the distribution of the percentages of synaptic/total  $\alpha 2$  mixed clusters per dendrite after treatment with DMSO or bicuculline from 4 to 7 DIV ( $n=46$  and  $n=45$  dendrites respectively, from two independent experiments). **B.** Box-plot displays the median percentage (50 % of the represented population) of synaptic/total  $\alpha 2$  mixed clusters per dendrite after treatment with DMSO or bicuculline from 4 to 7 DIV. Statistical analysis was performed using Mann-Whitney test.

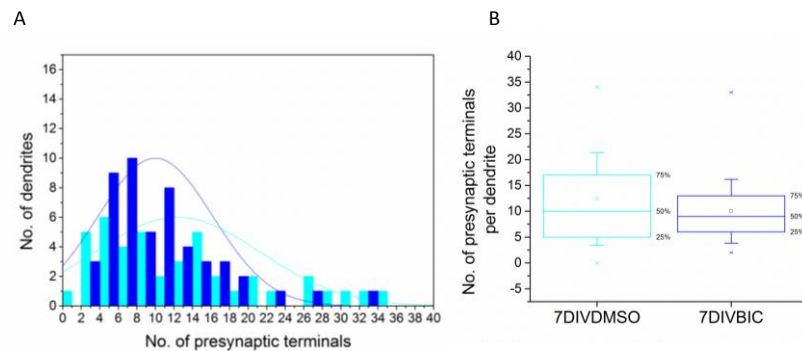
**Table 23. The percentage of synaptic/total density of clusters is in overall unchanged by 25  $\mu\text{M}$  bicuculline treatment from 4 to 7 DIV**

	7 DIV DMSO/ BIC	Significant
% (synaptic/total) $\alpha 1$ single clusters	↗	No
% (synaptic/total) $\alpha 2$ single clusters	↘	No
% (synaptic/total) $\alpha 1$ mixed clusters	↘	No
% (synaptic/total) $\alpha 2$ mixed clusters	↘	No

#### 6.3.1.4 *The connectivity between medium spiny neurones was not changed after treatment with 25 $\mu\text{M}$ bicuculline from 4 to 7 DIV*

To investigate further the role of GABA signalling in GABAergic synapse formation, we applied 25  $\mu\text{M}$  bicuculline in MSN cultures from 4 to 7 DIV and estimated if activity of GABA<sub>A</sub>Rs would regulate the density of presynaptic terminals forming contacts with the primary dendrites at early stages of development. The total density of GAD-65 positive terminals per defined length of primary dendrite (the first 20  $\mu\text{m}$  from the cell body) was estimated after treatment with DMSO or 25  $\mu\text{M}$  bicuculline from 4 to 7 DIV

(Figure 80). After DMSO treatment, the median density of presynaptic terminals was 10 (5-17) compared to 9 (5.75-13) after treatment with bicuculline ( $p$  value  $> 0.05$  Mann Whitney test,  $n=43$  dendrites analysed after treatment with DMSO and  $n=50$  dendrites analysed after treatment with 25  $\mu\text{M}$  bicuculline from 4 to 7 DIV). This indicates that the density of presynaptic contacts per dendrite is not regulated by GABA signalling at early developmental stages.

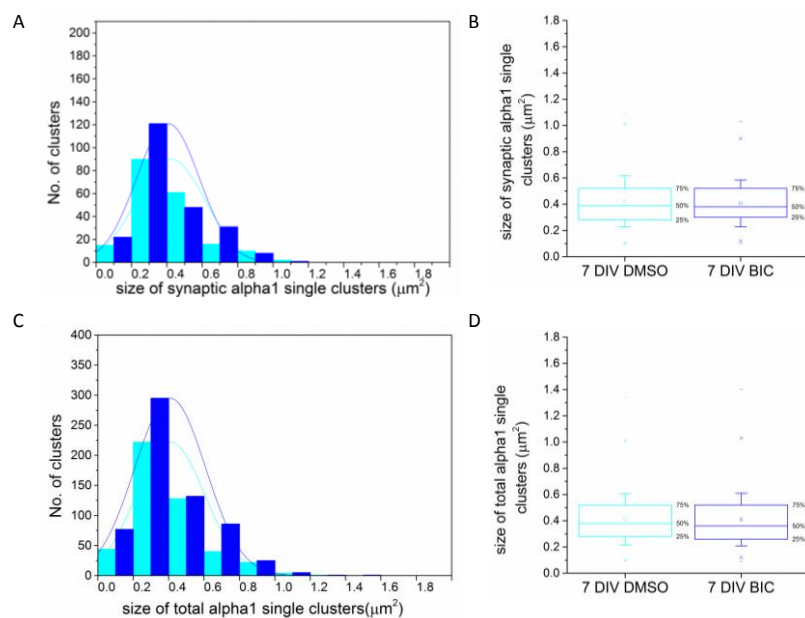


**Figure 80. The density of presynaptic terminals making contacts with primary dendrites is not changed after treatment with 25  $\mu\text{M}$  bicuculline from 4 to 7 DIV.** The density of presynaptic terminals along the 20  $\mu\text{m}$  of primary dendrite was counted in medium spiny neurones cultures after 7 and 14 DIV. **A.** Histogram shows the distribution of the density of presynaptic inputs after treatment with DMSO or 25  $\mu\text{M}$  bicuculline from 4 to 7 DIV ( $n=43$  and  $n=50$  dendrites respectively, from two independent experiments). **B.** Box-plot displays the median density of presynaptic terminals after treatment with DMSO or 25  $\mu\text{M}$  bicuculline from 4 to 7 DIV. Statistical analysis was performed using Mann Whitney test.

### 6.3.1.5 *The size of $\alpha 2$ -containing GABA<sub>A</sub>R clusters is decreased after treatment with 25 $\mu\text{M}$ bicuculline from 4 to 7 DIV*

During their development in culture, while treated with DMSO or 25  $\mu\text{M}$  bicuculline, medium spiny neurones underwent changes in the size of GABA<sub>A</sub>R cluster. The size of synaptic and total  $\alpha 1$  single clusters of GABA<sub>A</sub>Rs per defined length of primary dendrite (the first 20  $\mu\text{m}$  from the cell body) was estimated after treatment with DMSO or 25  $\mu\text{M}$  bicuculline (Figure 81). After treatment with DMSO, the median size of synaptic  $\alpha 1$  single clusters was 0.39  $\mu\text{m}^2$  (0.52-0.28) compared to 0.38  $\mu\text{m}^2$  (0.52-0.3) with 25  $\mu\text{M}$  bicuculline from 4 to 7 DIV ( $p$  value =0.56, Mann Whitney test,  $n=194$  clusters analysed after DMSO treatment and  $n=231$  clusters analysed after treatment with 25

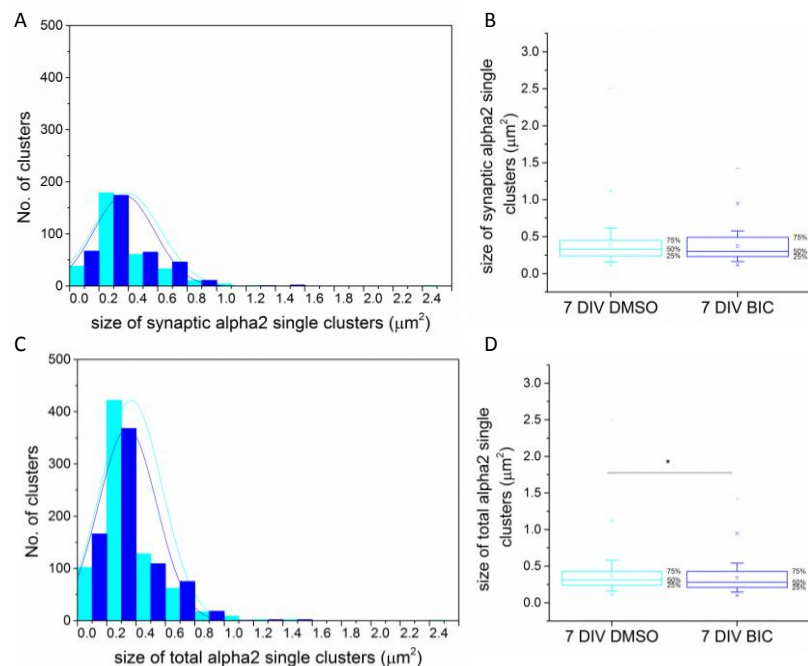
$\mu\text{M}$  bicuculline). Similarly, the median size of total  $\alpha 1$  single clusters was  $0.38 \mu\text{m}^2$  (0.52-0.28) after treatment with DMSO compared to  $0.36 \mu\text{m}^2$  (0.52-0.26) after treatment with  $25 \mu\text{M}$  bicuculline ( $p$  value =0.74, Mann Whitney test,  $n=461$  clusters analysed after DMSO treatment and  $n=622$  clusters analysed after treatment with  $25 \mu\text{M}$  bicuculline). This demonstrates that the size of synaptic and total  $\alpha 1$  single clusters is not altered by treatment with  $25 \mu\text{M}$  bicuculline from 4 to 7 DIV. This might be because at this early stage of development, the size of  $\alpha 1$  single GABA<sub>A</sub>Rs is not dependent on GABA signalling.



**Figure 81. The size of synaptic and total  $\alpha 1$  single clusters is not altered by treatment from 4 to 7 DIV.** The size of  $\alpha 1$ -containing GABA<sub>A</sub> receptors clusters ( $\alpha 1$  single clusters) along the  $20 \mu\text{m}$  of primary dendrite was measured in medium spiny neurones cultures after treatment with DMSO or  $25 \mu\text{M}$  bicuculline. **A.** Histogram shows the distribution of synaptic  $\alpha 1$  single clusters sizes after treatment with DMSO or  $25 \mu\text{M}$  bicuculline ( $n=194$  and  $n=231$  clusters respectively, from two independent experiments). **B.** Box-plot displays the median size (50 % of the population) of synaptic  $\alpha 1$  single clusters after treatment with DMSO or  $25 \mu\text{M}$  bicuculline. **C.** Histogram shows the distribution of total  $\alpha 1$  single clusters sizes after treatment with DMSO or  $25 \mu\text{M}$  bicuculline ( $n=461$  and  $n=622$  clusters respectively, from two independent experiments). **D.** The box plot displays the population of total  $\alpha 1$  single clusters sizes after treatment with DMSO or  $25 \mu\text{M}$  bicuculline. Statistical analysis was performed using Mann Whitney test.

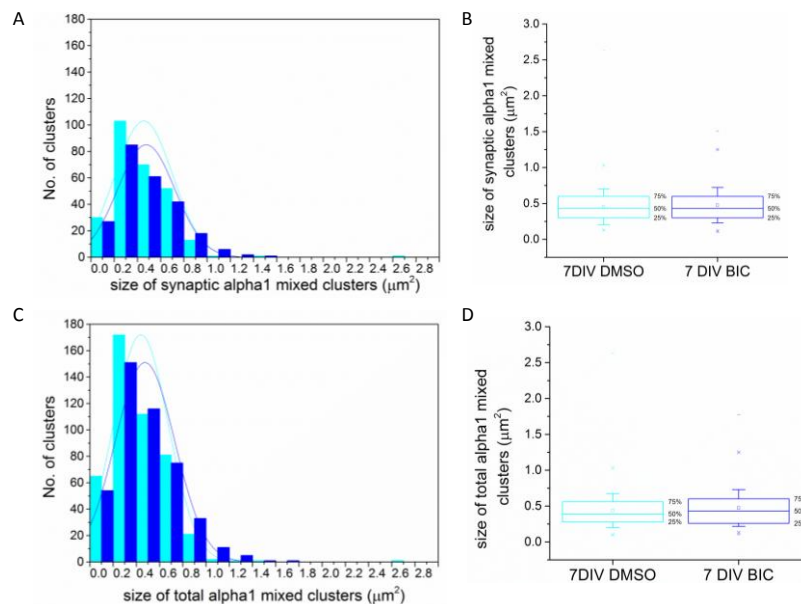
The size of synaptic and total  $\alpha 2$  single clusters of GABA<sub>A</sub>Rs per defined length of primary dendrite (the first  $20 \mu\text{m}$  from the cell body) was estimated after treatment with DMSO or  $25 \mu\text{M}$  bicuculline (Figure 82). After treatment with DMSO, the median size of synaptic  $\alpha 2$  single clusters was  $0.33 \mu\text{m}^2$  (0.45-0.24) compared to  $0.3 \mu\text{m}^2$  (0.49-0.23)

with 25  $\mu\text{M}$  bicuculline from 4 to 7 DIV (p value=0.13 Mann Whitney test, n=328 clusters analysed after DMSO treatment and n=366 clusters analysed after treatment with 25  $\mu\text{M}$  bicuculline). Similarly, the median size of total  $\alpha 2$  single clusters was 0.31  $\mu\text{m}^2$  (0.43-0.24) after treatment with DMSO compared to 0.28  $\mu\text{m}^2$  (0.43-0.21) after treatment with 25  $\mu\text{M}$  bicuculline (p value= $2.6 \times 10^{-5}$ , Mann Whitney test, n=745 clusters analysed after DMSO treatment and n=741 clusters analysed after treatment with 25  $\mu\text{M}$  bicuculline). This demonstrates that the size of total  $\alpha 2$  single clusters is decreased by the treatment with 25  $\mu\text{M}$  bicuculline from 4 to 7 DIV, suggesting that at this early stage of development, the size of extrasynaptic  $\alpha 2$ -containing GABA<sub>A</sub>Rs is regulated by the depolarising GABA signalling.



**Figure 82. The size of total  $\alpha 2$  single clusters is decreased by treatment from 4 to 7 DIV.** The size of  $\alpha 2$  -containing GABA<sub>A</sub> receptors clusters ( $\alpha 2$  single clusters) along the 20  $\mu\text{m}$  of primary dendrite was measured in medium spiny neurones cultures after treatment with DMSO or 25  $\mu\text{M}$  bicuculline. **A.** Histogram shows the distribution of synaptic  $\alpha 2$  single clusters sizes after treatment with DMSO or 25  $\mu\text{M}$  bicuculline (n=328 and n=366 clusters respectively, from two independent experiments). **B.** Box-plot displays the median size (50 % of the population) of synaptic  $\alpha 2$  single clusters after treatment with DMSO or 25  $\mu\text{M}$  bicuculline. **C.** Histogram shows the distribution of total  $\alpha 2$  single clusters sizes after treatment with DMSO or 25  $\mu\text{M}$  bicuculline (n=745 and n=741 clusters respectively, from two independent experiments). **D.** The box plot displays the population of total  $\alpha 2$  single clusters sizes after treatment with DMSO or 25  $\mu\text{M}$  bicuculline. Statistical analysis was performed using Mann Whitney test.

The size of synaptic and total  $\alpha 1$  mixed clusters of GABA<sub>A</sub>Rs per defined length of primary dendrite (the first 20  $\mu\text{m}$  from the cell body) was estimated after treatment with DMSO or 25  $\mu\text{M}$  bicuculline (Figure 83). After treatment with DMSO, the median size of synaptic  $\alpha 1$  mixed clusters was 0.43  $\mu\text{m}^2$  (0.6-0.3) compared to 0.43  $\mu\text{m}^2$  (0.6-0.3) with 25  $\mu\text{M}$  bicuculline from 4 to 7 DIV (p value =0.43 Mann Whitney test, n=271 clusters analysed after DMSO treatment and n=242 clusters analysed after treatment with 25  $\mu\text{M}$  bicuculline). Similarly, the median size of total  $\alpha 1$  mixed clusters was 0.39  $\mu\text{m}^2$  (0.56-0.28) after treatment with DMSO compared to 0.43  $\mu\text{m}^2$  (0.6-0.26) after treatment with 25  $\mu\text{M}$  bicuculline (p value=0.07, Mann Whitney test, n=456 clusters analysed after DMSO treatment and n=447 clusters analysed after treatment with 25  $\mu\text{M}$  bicuculline). This demonstrates that the size of synaptic and total  $\alpha 1$  mixed clusters is not altered by treatment with 25  $\mu\text{M}$  bicuculline from 4 to 7 DIV. This might be because at this early stage of development, the size of  $\alpha 1$  mixed GABA<sub>A</sub>Rs is not dependent on GABA signalling.

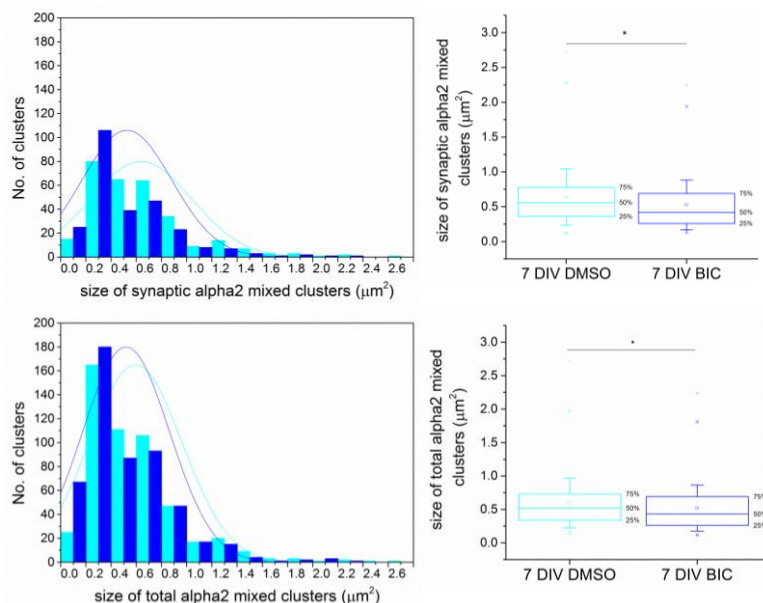


**Figure 83. The size of synaptic and total  $\alpha 1$  mixed clusters is not altered by treatment from 4 to 7 DIV.** The size of  $\alpha 1/\alpha 2$ -containing GABA<sub>A</sub> receptors clusters ( $\alpha 1$  mixed clusters) along the 20  $\mu\text{m}$  of primary dendrite was measured in medium spiny neurones cultures after treatment with DMSO or 25  $\mu\text{M}$  bicuculline. **A.** Histogram shows the distribution of synaptic  $\alpha 1$  mixed clusters sizes after treatment with DMSO or 25  $\mu\text{M}$  bicuculline (n=456 and n=447 clusters respectively, from two independent experiments). **B.** Box-plot displays the median size (50 % of the population) of synaptic  $\alpha 1$  mixed clusters after treatment with DMSO or 25  $\mu\text{M}$  bicuculline.



**C.** Histogram shows the distribution of total  $\alpha 1$  mixed clusters sizes after treatment with DMSO or 25  $\mu\text{M}$  bicuculline ( $n=271$  and  $n=242$  clusters respectively, from two independent experiments). **D.** The box plot displays the population of total  $\alpha 1$  mixed clusters sizes after treatment with DMSO or 25  $\mu\text{M}$  bicuculline. Statistical analysis was performed using Mann Whitney test.

The size of synaptic and total  $\alpha 2$  mixed clusters of  $\text{GABA}_A$ Rs per defined length of primary dendrite (the first 20  $\mu\text{m}$  from the cell body) was estimated after treatment with DMSO or 25  $\mu\text{M}$  bicuculline (Figure 84). After treatment with DMSO, the median size of synaptic  $\alpha 2$  mixed clusters was  $0.56 \mu\text{m}^2$  (0.79-0.36) compared to  $0.42 \mu\text{m}^2$  (0.69-0.26) with 25  $\mu\text{M}$  bicuculline from 4 to 7 DIV ( $p$  value= $2.8 \times 10^{-5}$ , Mann Whitney test,  $n=298$  clusters analysed after DMSO treatment and  $n=263$  clusters analysed after treatment with 25  $\mu\text{M}$  bicuculline). Similarly, the median size of total  $\alpha 2$  mixed clusters was  $0.52 \mu\text{m}^2$  (0.73-0.34) after treatment with DMSO compared to  $0.43 \mu\text{m}^2$  (0.69-0.26) after treatment with 25  $\mu\text{M}$  bicuculline ( $p$  value= $2.69 \times 10^{-5}$ , Mann Whitney test,  $n=511$  clusters analysed after DMSO treatment and  $n=517$  clusters analysed after treatment with 25  $\mu\text{M}$  bicuculline). This demonstrates that the size of total  $\alpha 2$  mixed clusters is decreased by treatment with 25  $\mu\text{M}$  bicuculline from 4 to 7 DIV, possibly due to a regulation by GABA signalling of the size of a specific subtype of clusters containing  $\alpha 2$  clusters predominantly.



**Figure 84. The size of synaptic and total  $\alpha 2$  mixed clusters is decreased by treatment from 4 to 7 DIV.** The size of  $\alpha 2/\alpha 1$ -containing  $\text{GABA}_A$  receptors clusters ( $\alpha 2$  mixed clusters) along the 20  $\mu\text{m}$  of primary dendrite was measured in medium spiny neurones cultures after

treatment with DMSO or 25  $\mu\text{M}$  bicuculline. **A.** Histogram shows the distribution of synaptic  $\alpha 2$  mixed clusters sizes after treatment with DMSO or 25  $\mu\text{M}$  bicuculline (n=298 and n=263 clusters respectively, from two independent experiments). **B.** Box-plot displays the median size (50 % of the population) of synaptic  $\alpha 2$  mixed clusters after treatment with DMSO or 25  $\mu\text{M}$  bicuculline. **C.** Histogram shows the distribution of total  $\alpha 2$  mixed clusters sizes after treatment with DMSO or 25  $\mu\text{M}$  bicuculline (n=511 and n=517 clusters respectively, from two independent experiments). **D.** The box plot displays the population of total  $\alpha 2$  mixed clusters sizes after treatment with DMSO or 25  $\mu\text{M}$  bicuculline. Statistical analysis was performed using Mann Whitney test: \* corresponds to  $p < 0.05$ .

**Table 24. The size of  $\alpha 2/\alpha 1$  mixed- containing  $\text{GABA}_A\text{R}$  clusters is decreased by 25  $\mu\text{M}$  treatment from 4 to 7 DIV**

Size of clusters ( $\mu\text{m}^2$ )		7 DIV DMSO/ BIC	Significant
$\alpha 1$ single clusters	Synaptic		No
	Total		No
$\alpha 2$ single clusters	Synaptic		No
	Total		Yes
$\alpha 1$ mixed clusters	Synaptic		No
	Total		No
$\alpha 2$ mixed clusters	Synaptic		Yes
	Total		Yes

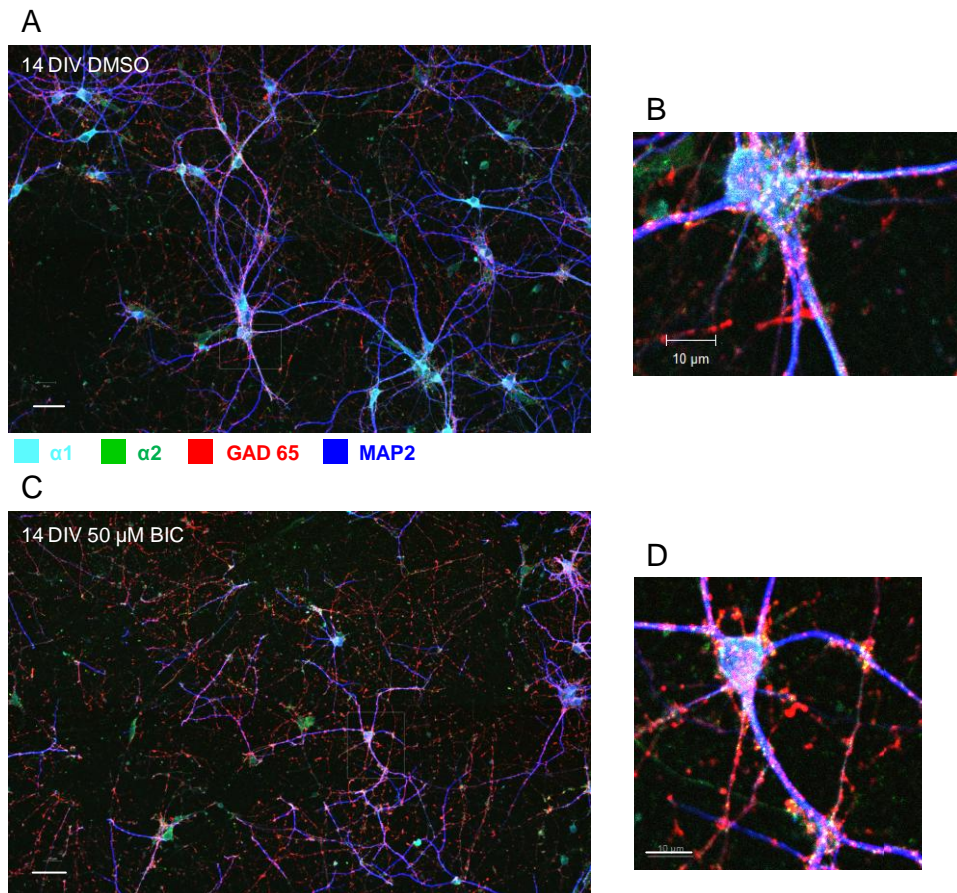
### 6.3.2 Treatment of MSN cultures with bicuculline from 7-14 DIV

#### 6.3.2.1 Treatment of medium spiny neurones with 50 $\mu\text{M}$ bicuculline from 7 to 14 DIV provoked cell death

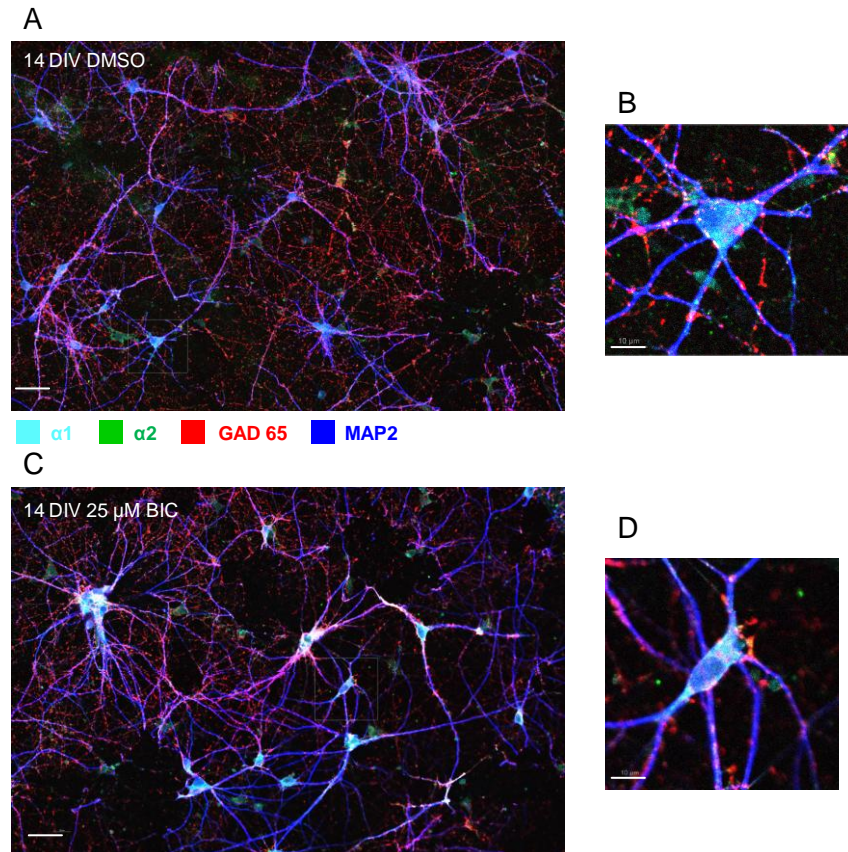
In order to know if activity of  $\text{GABA}_A\text{Rs}$  would play a different role at later developmental stages, when synapses are formed and mature, we have chronically treated medium spiny neurones with 50 or 25  $\mu\text{M}$  bicuculline from 7 to 14 days *in vitro* (DIV). As a control, we have treated neurones at the same period of time with an equivalent amount of DMSO. Figure 85 is a large field images of medium spiny neurones treated from 7 to 14 DIV with 50  $\mu\text{M}$  bicuculline or DMSO. Figure 86 is a large field images of medium spiny neurones treated from 7 to 14 DIV with 25  $\mu\text{M}$  bicuculline or DMSO. These figures show examples of staining for  $\alpha 1$  and  $\alpha 2$



extracellular domains of GABA<sub>A</sub>Rs subunits, the intracellular presynaptic marker GAD-65 and MAP-, using the antibodies described in table 19. The total density of cells per image was counted using the Zen 2009 programme.

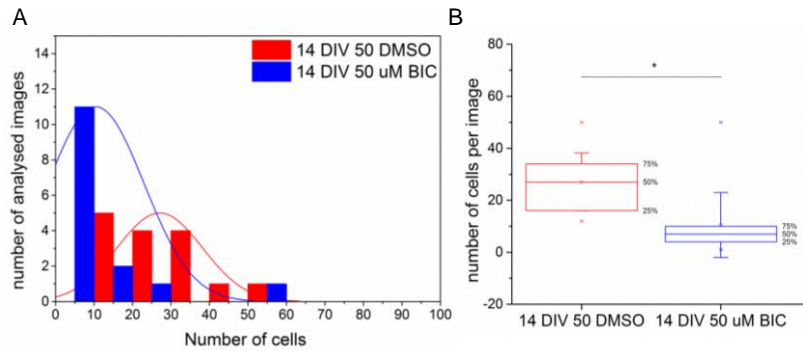


**Figure 85. The density of cells is decreased by 50 μM bicuculline treatment from 7 to 14 DIV compared to DMSO.** Immunolabelling of GABA<sub>A</sub> receptors α1, α2 subunit containing clusters (respectively cyan and green) and presynaptic GABAergic terminals (red) along primary dendrites (blue) of cultured medium spiny neurones. **A.** Merged tile-scan image of a 14 DIV striatal culture treated with DMSO (scale bar: 20 μm). **B.** Enlarged image of boxed region in A (scale bar: 10 μm). **C.** Merged tile-scan image of a 14 DIV striatal culture treated with 50 μM bicuculline (scale bar: 20 μm). **D.** Enlarged image of boxed region in C (scale bar: 10 μm).



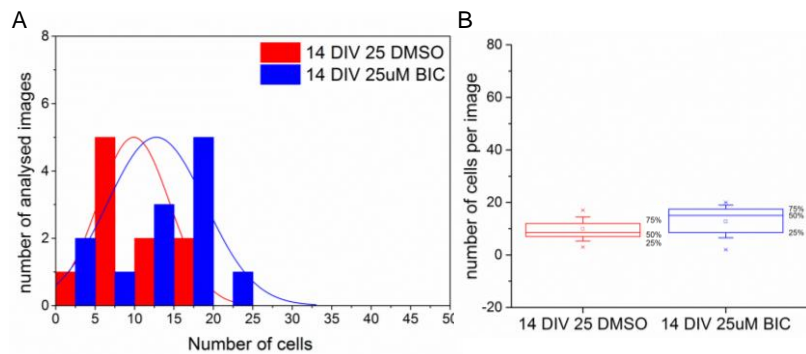
**Figure 86. The density of cells is not affected by 25  $\mu\text{M}$  bicuculline treatment from 7 to 14 DIV compared to DMSO.** Immunolabelling of GABA<sub>A</sub> receptors  $\alpha 1$ ,  $\alpha 2$  subunit containing clusters (respectively cyan and green) and presynaptic GABAergic terminals (red) along primary dendrites (blue) of cultured medium spiny neurones. **A.** Merged tile-scan image of a 14 DIV striatal culture treated with DMSO (scale bar: 20  $\mu\text{m}$ ). **B.** Enlarged image of boxed region in A (scale bar: 10  $\mu\text{m}$ ). **C.** Merged tile-scan image of a 14 DIV striatal culture treated with 25  $\mu\text{M}$  bicuculline (scale bar: 20  $\mu\text{m}$ ). **D.** Enlarged image of boxed region in C (scale bar: 10  $\mu\text{m}$ ).

The median density of cells per image was estimated after treatment with 50  $\mu\text{M}$  bicuculline or control (Figure 87). At 7 DIV, the median density of cells per image was 27 (34-16) with control treatment compared to 7 (10-4) with 50  $\mu\text{M}$  bicuculline treatment ( $p$  value= $1.87 \times 10^{-4}$ , Mann Whitney test,  $n=15$  images analysed with control or bicuculline treatment at 14 DIV). This demonstrates that the density of cells is significantly decreased by 50  $\mu\text{M}$  bicuculline treatment compared to DMSO from 7-14 DIV.



**Figure 87. The density of cells per image is significantly decreased after treatment with 50 µM bicuculline from 7 to 14 DIV.** The density of medium spiny neurones per tile scan images was counted in presence of DMSO or 50 µM bicuculline from 7-14 DIV. **A.** Histogram shows the distribution of the density of cells per image in presence of DMSO or 50 µM bicuculline added at 7,9 and 11 DIV (n=15 images analysed respectively, from two independent experiments). **B.** Box plot displays the density of cells per image in presence of DMSO or 50 µM bicuculline added at 7 and 14 DIV. Statistical analysis was performed using Mann Whitney test: \* corresponds to p-value <0.05.

The median density of cells per image was estimated after treatment with 25 µM bicuculline or control (Figure 88). At 14 DIV, the median density of cells per image was 8.5 (13.25-6.75) with control treatment compared to 15 (15.75-7.75) with 25 µM bicuculline treatment (p value=0.22, Mann Whitney test, n=15 images analysed). This demonstrates that the density of cells is not affected by 25 µM bicuculline compared to DMSO treatment from 7 to 14 DIV.

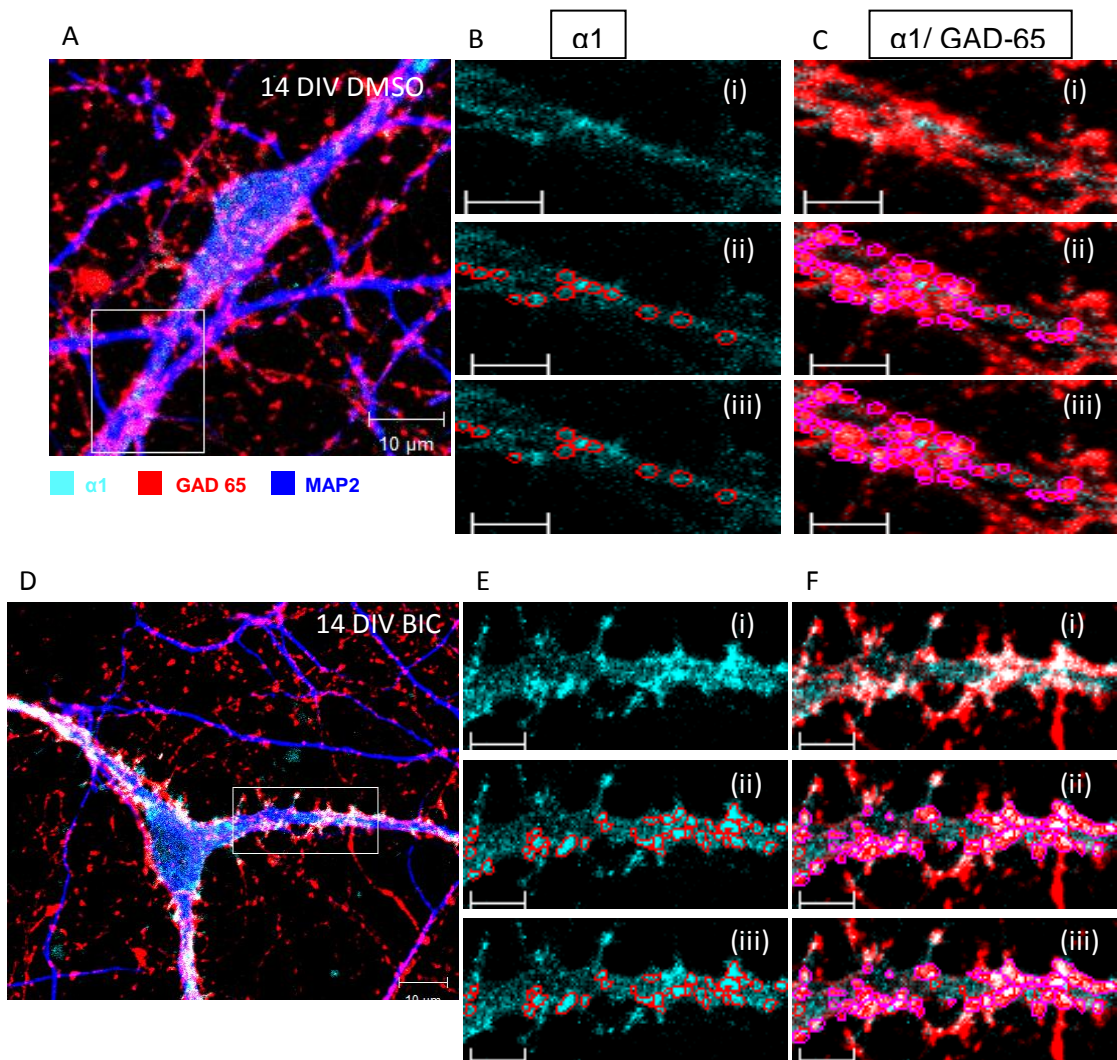


**Figure 88. The density of cells per image is not changed after treatment with 25 µM bicuculline from 7 to 14 DIV.** The density of medium spiny neurones per tile scan images was counted in presence of DMSO or 25 µM bicuculline from 7-14 DIV. **A.** Histogram shows the distribution of the density of cells per image in presence of DMSO or 25 µM bicuculline added at 7, 9 and 11 DIV (n=15 images analysed, from two independent experiments). **B.** Box plot displays the density of cells per image in presence of DMSO or 25 µM bicuculline added at 7, 9 and 11 DIV. Statistical analysis was performed using Mann Whitney test.

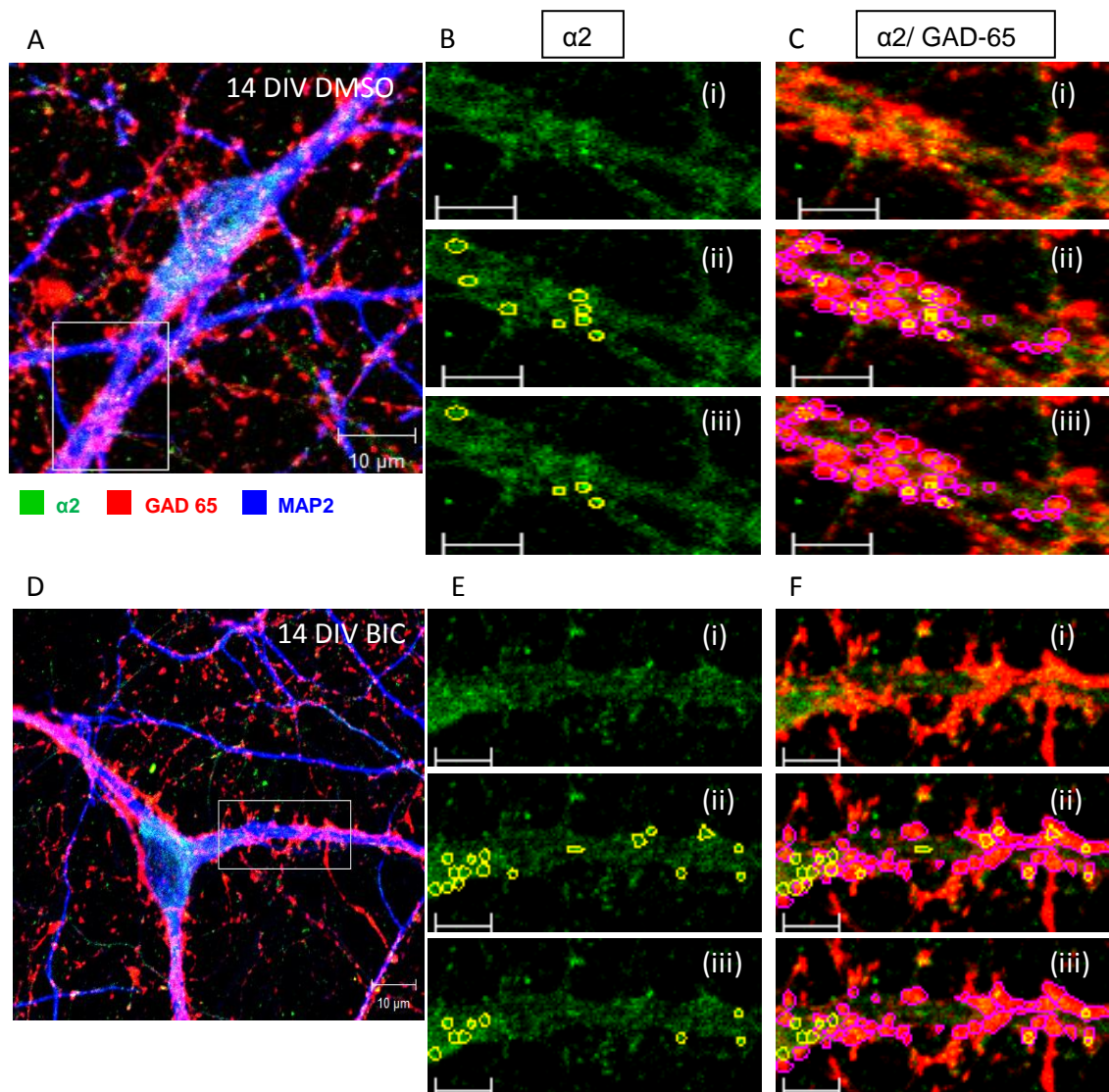
*6.3.2.2 The density of synaptic  $\alpha 2$  single GABA<sub>A</sub>R clusters per dendrite was increased after 25  $\mu$ M bicuculline treatment from 7 to 14 DIV.*

An increase in density of synaptic  $\alpha 2$  single clusters was the only change in density of clusters observed after treatment of medium spiny neurones with 25  $\mu$ M bicuculline from 7 to 14 DIV. Figure 89, 90 and 91 represent MSN medium spiny neurones treated from 7 to 14 DIV with 25  $\mu$ M bicuculline or DMSO. This figure shows examples of staining for  $\alpha 1$  and  $\alpha 2$  extracellular domains of GABA<sub>A</sub>Rs subunits, the intracellular presynaptic marker GAD-65 and MAP-, using the antibodies described in Table 21. The total density of cells per image was counted using the Zen 2009 programme.



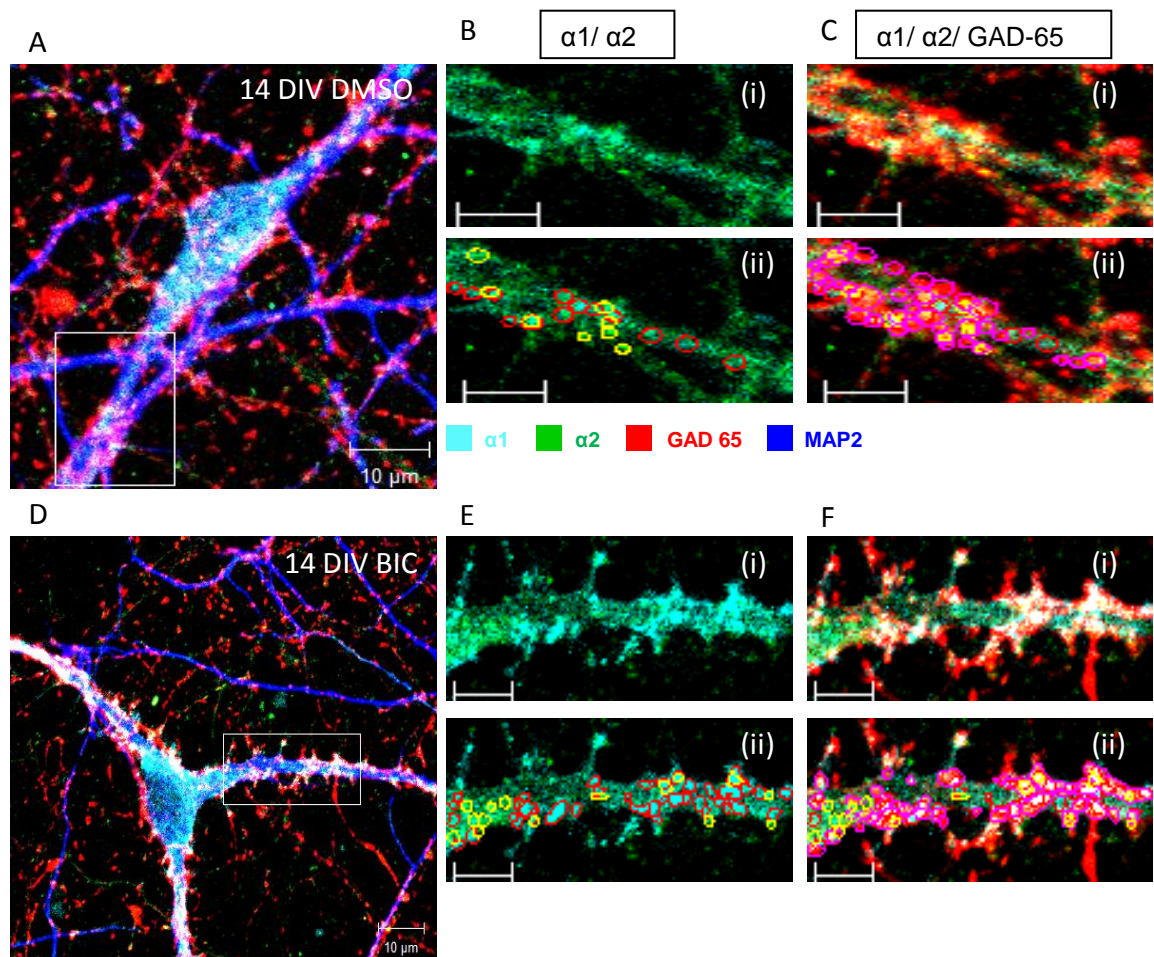


**Figure 89. The density of  $\alpha 1$  clusters is not affected by the 25  $\mu\text{M}$  bicuculline treatment.** Immunolabelling of GABA<sub>A</sub>Rs  $\alpha 1$  subunit-containing clusters (cyan) and presynaptic GABAergic terminals (red) along primary dendrites (blue) of cultured medium spiny neurones. **A.** Merged image of a 14 DIV striatal neurone treated with DMSO (scale bar: 10  $\mu\text{m}$ ). **B.(i)** Enlarged image of boxed region in A representing  $\alpha 1$  staining only. **(ii)** Analysis of image B(i) in which all  $\alpha 1$  clusters are circled in red. **(iii)** Analysis of image B(i) in which only  $\alpha 1$  single clusters that are not associated with  $\alpha 2$  clusters are circled in red (scale bar: 5  $\mu\text{m}$ ). **C.(i)** Enlarged image of boxed region in A representing  $\alpha 1$  positive clusters and presynaptic GAD-65 positive nerve terminals. **(ii)** Analysis of image C(i) in which all  $\alpha 1$  clusters were circled in red and presynaptic terminals were circled in purple. **(iii)** Analysis of image C(i) in which only  $\alpha 1$  single clusters were circled in red and presynaptic terminals were circled in purple (scale bar: 5  $\mu\text{m}$ ). **D.** Merged image of a 14 DIV striatal neurone treated with 25  $\mu\text{M}$  bicuculline (scale bar: 10  $\mu\text{m}$ ). **E.(i)** Enlarged image of boxed region in D representing  $\alpha 1$  staining only. **(ii)** Analysis of image E(i) in which all  $\alpha 1$  clusters are circled in red. **(iii)** Analysis of image E(i) in which only  $\alpha 1$  single clusters that are not associated with  $\alpha 2$  clusters are circled in red (scale bar: 5  $\mu\text{m}$ ). **F.(i)** Enlarged image of boxed region in D representing  $\alpha 1$  positive clusters and presynaptic GAD-65 positive nerve terminals. **(ii)** Analysis of image F(i) in which all  $\alpha 1$  clusters were circled in red and presynaptic terminals were circled in purple. **(iii)** Analysis of image F(i) in which only  $\alpha 1$  single clusters were circled in red and presynaptic terminals were circled in purple (scale bar: 5  $\mu\text{m}$ ).



**Figure 90. The density of synaptic  $\alpha 2$  single clusters is increased by the 25  $\mu\text{M}$  bicuculline treatment.** Immunolabelling of GABA<sub>A</sub>Rs  $\alpha 2$  subunit-containing clusters (green) and presynaptic GABAergic terminals (red) along primary dendrites (blue) of cultured medium spiny neurones. **A.** Merged image of a 14 DIV striatal neurone treated with DMSO (scale bar: 10  $\mu\text{m}$ ). **B.(i)** Enlarged image of boxed region in A representing  $\alpha 2$  staining only. **(ii)** Analysis of image B(i) in which all  $\alpha 2$  clusters are circled in yellow. **(iii)** Analysis of image B(i) in which only  $\alpha 2$  single clusters that are not associated with  $\alpha 1$  clusters are circled in yellow (scale bar: 5  $\mu\text{m}$ ). **C.(i)** Enlarged image of boxed region in A representing  $\alpha 2$  positive clusters and presynaptic GAD-65 positive nerve terminals. **(ii)** Analysis of image C(i) in which all  $\alpha 2$  clusters were circled in yellow and presynaptic terminals were circled in purple. **(iii)** Analysis of image C(i) in which only  $\alpha 2$  single clusters were circled in yellow and presynaptic terminals were circled in purple (scale bar: 5  $\mu\text{m}$ ). **D.** Merged image of a 14 DIV striatal neurone treated with 25  $\mu\text{M}$  bicuculline (scale bar: 10  $\mu\text{m}$ ). **E.(i)** Enlarged image of boxed region in D representing  $\alpha 2$  staining only. **(ii)** Analysis of image E(i) in which all  $\alpha 2$  clusters are circled in yellow. **(iii)** Analysis of image E(i) in which only  $\alpha 2$  single clusters that are not associated with  $\alpha 1$  clusters are circled in yellow (scale bar: 5  $\mu\text{m}$ ). **F.(i)** Enlarged image of boxed region in D representing  $\alpha 2$  positive clusters and presynaptic GAD-65 positive nerve terminals. **(ii)** Analysis of image F(i) in which all  $\alpha 2$  clusters were circled in yellow and presynaptic terminals were circled in purple. **(iii)** Analysis of image F(i) in which only  $\alpha 2$  single clusters were circled in yellow and presynaptic terminals were circled in purple (scale bar: 5  $\mu\text{m}$ ).

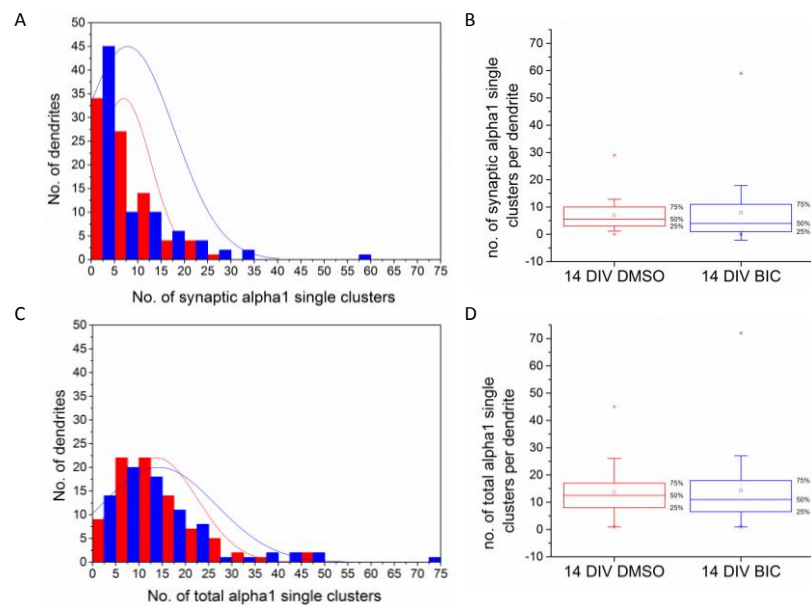




**Figure 91. The density of  $\alpha 1/\alpha 2$  mixed clusters is not affected by the 25  $\mu\text{M}$  bicuculline treatment.** Immunolabelling of GABA<sub>A</sub>R $\alpha 1/\alpha 2$  subunit-containing clusters (cyan and green) and presynaptic GABAergic terminals (red) along primary dendrites (blue) of cultured medium spiny neurones. **A.** Merged image of a 14 DIV striatal neurone treated with DMSO (scale bar: 10  $\mu\text{m}$ ). **B.(i)** Enlarged image of boxed region in A representing  $\alpha 1$  and  $\alpha 2$  staining. **(ii)** Analysis of image B(i) in which all  $\alpha 1$  and  $\alpha 2$  clusters are respectively circled in red and yellow (scale bar: 5  $\mu\text{m}$ ). **C.(i)** Enlarged image of boxed region in A representing  $\alpha 1$ ,  $\alpha 2$  positive clusters and presynaptic GAD-65 positive nerve terminals. **(ii)** Analysis of image C(i) in which all  $\alpha 1$  and  $\alpha 2$  clusters were respectively circled in red and yellow and presynaptic terminals were circled in purple (scale bar: 5  $\mu\text{m}$ ). **D.** Merged image of a 14 DIV striatal neurone treated with 25  $\mu\text{M}$  bicuculline (scale bar: 10  $\mu\text{m}$ ). **E.(i)** Enlarged image of boxed region in D representing  $\alpha 1$  and  $\alpha 2$  staining. **(ii)** Analysis of image E(i) in which all  $\alpha 1$  and  $\alpha 2$  clusters were respectively circled in red and yellow (scale bar: 5  $\mu\text{m}$ ). **F.(i)** Enlarged image of boxed region in D representing  $\alpha 1$ ,  $\alpha 2$  positive clusters and presynaptic GAD-65 positive nerve terminals. **(ii)** Analysis of image F(i) in which all  $\alpha 1$  and  $\alpha 2$  clusters were respectively circled in red and yellow and presynaptic terminals were circled in purple (scale bar: 5  $\mu\text{m}$ ).

The density of synaptic and total  $\alpha 1$  single clusters of GABA<sub>A</sub>R $\alpha 1$  was estimated per defined length of primary dendrite (the first 20  $\mu\text{m}$  from the cell body) after treatment with DMSO or 25  $\mu\text{M}$  bicuculline from 7 to 14 DIV (Figure 92). The median density of synaptic  $\alpha 1$  single clusters was 5.5 (10-3) with DMSO treatment, compared to 4 (11-1) with bicuculline treatment (p value=0.22, Mann Whitney test, n=84 dendrites analysed

from DMSO treated cultures and n=80 dendrites analysed from bicuculline treated neurones). Similarly, the median density of total  $\alpha 1$  single clusters was 12.5 (17-8) with DMSO treatment, compared to 11 (18-6.25) with bicuculline treatment (p value=0.51, Mann Whitney test, n=84 dendrites analysed from DMSO treated cultures and n=80 dendrites analysed from bicuculline treated neurones). This demonstrates that the synaptic and total densities of  $\alpha 1$  single clusters are not affected by the treatment, indicating that the regulation of the density of these types of clusters is independent of the GABA<sub>A</sub>Rs activity at this developmental stage.

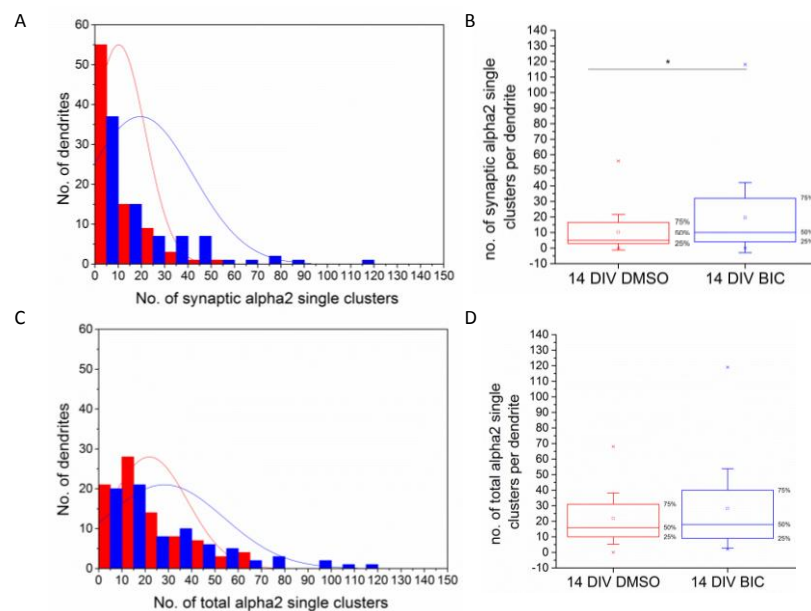


**Figure 92. The density of synaptic and total  $\alpha 1$  clusters is not affected by treatment with 25  $\mu\text{M}$  bicuculline from 7 to 14 DIV.** The density of  $\alpha 1$ -containing GABA<sub>A</sub> receptors clusters ( $\alpha 1$  single clusters) along the 20  $\mu\text{m}$  of primary dendrite was counted in medium spiny neurone cultures in presence of DMSO or 25  $\mu\text{M}$  bicuculline from 7 to 14 DIV. **A.** Histogram shows the distribution of synaptic  $\alpha 1$  single clusters densities in presence of DMSO or 25  $\mu\text{M}$  bicuculline from 7 to 14 DIV (n=84 and n=79 dendrites respectively from two independent experiments). **B.** Box plot displays the median density (50 % of the population) of synaptic  $\alpha 1$  single clusters in presence of DMSO or 25  $\mu\text{M}$  bicuculline from 7 to 14 DIV. **C.** Histogram shows the distribution of total  $\alpha 1$  single clusters density in presence of DMSO or 25  $\mu\text{M}$  bicuculline from 7 to 14 DIV (n=85 and n=79 dendrites respectively from two independent experiments). **D.** Box plot displays the median density (50 % of the population) of total  $\alpha 1$  single clusters in presence of DMSO or 25  $\mu\text{M}$  bicuculline from 7 to 14 DIV. Statistical analysis was performed using Mann Whitney test.

We analysed the density of  $\alpha 2$  single clusters in presence of DMSO or 25  $\mu\text{M}$  bicuculline from 7 to 14 DIV. The density of synaptic and total  $\alpha 2$  single clusters of GABA<sub>A</sub>Rs was estimated per defined length of primary dendrite (the first 20  $\mu\text{m}$  from the cell body) after treatment with DMSO or 25  $\mu\text{M}$  bicuculline from 7 to 14 DIV (Figure

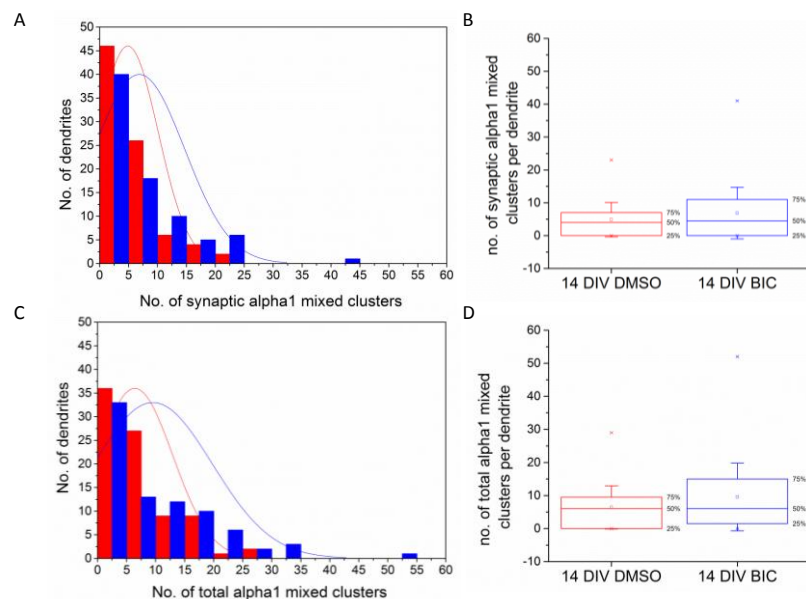


93). The median density of synaptic  $\alpha 2$  single clusters was 5 (16.75-3) with DMSO treatment, compared to 10 (32-4) with bicuculline treatment (p value=0.003, Mann Whitney test, n=84 dendrites analysed from DMSO treated cultures and n=79 dendrites analysed from bicuculline treated neurones). Similarly, the median density of total  $\alpha 2$  single clusters was 16 (31-9.5) with DMSO treatment, compared to 18 (40-9) with bicuculline treatment (p value=0.32, Mann Whitney test, n=85 dendrites analysed from DMSO treated cultures and n=79 dendrites analysed from bicuculline treated neurones). This demonstrates that similarly to  $\alpha 1$  single clusters, the synaptic and total densities of  $\alpha 2$  single clusters are not affected by the treatment, indicating that the regulation of the density of these types of clusters is independent of the GABA<sub>A</sub>Rs activity at this developmental stage.



**Figure 93. The density of synaptic  $\alpha 2$  single clusters is increased by treatment with 25  $\mu\text{M}$  bicuculline from 7 to 14 DIV.** The density of  $\alpha 2$ -containing GABA<sub>A</sub> receptors clusters ( $\alpha 2$  single clusters) along the 20  $\mu\text{m}$  of primary dendrite was counted in medium spiny neurone cultures in presence of DMSO or 25  $\mu\text{M}$  bicuculline from 7 to 14 DIV. **A.** Histogram shows the distribution of synaptic  $\alpha 2$  single clusters densities in presence of DMSO or 25  $\mu\text{M}$  bicuculline from 7 to 14 DIV (n=84 and n=79 dendrites respectively from two independent experiments). **B.** Box plot displays the median density (50 % of the population) of synaptic  $\alpha 2$  single clusters in presence of DMSO or 25  $\mu\text{M}$  bicuculline from 7 to 14 DIV. **C.** Histogram shows the distribution of total  $\alpha 2$  single clusters density in presence of DMSO or 25  $\mu\text{M}$  bicuculline from 7 to 14 DIV (n=85 and n=79 dendrites respectively from two independent experiments). **D.** Box plot displays the median density (50 % of the population) of total  $\alpha 2$  single clusters in presence of DMSO or 25  $\mu\text{M}$  bicuculline from 7 to 14 DIV. Statistical analysis was performed using Mann Whitney test: \* corresponds to p < 0.05.

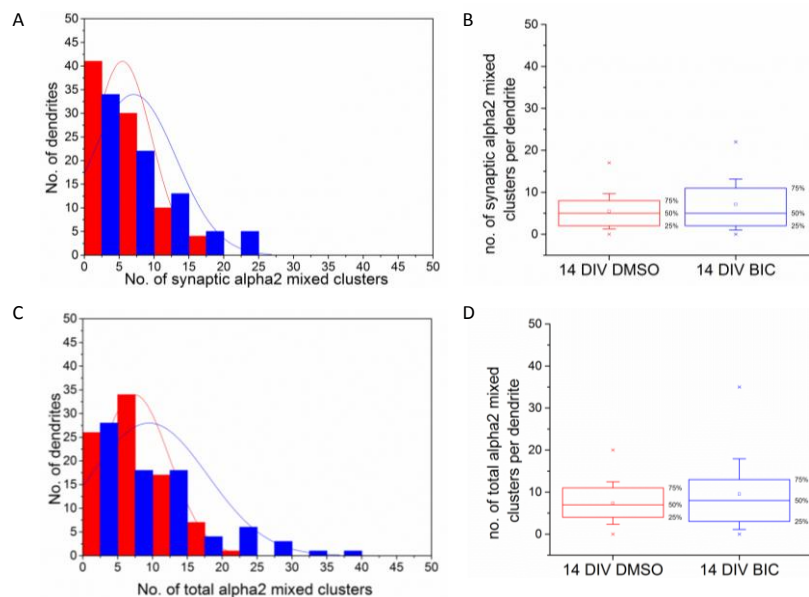
As explained in the previous chapter, we have observed two types of  $\alpha 1/\alpha 2$  mixed clusters. The mixed clusters which contained a majority of  $\alpha 1$  clusters were defined as  $\alpha 1$  mixed clusters while the mixed clusters containing a majority of  $\alpha 2$  clusters were defined as  $\alpha 2$  mixed clusters. The density of synaptic and total  $\alpha 1$  mixed clusters of  $GABA_A$ Rs was estimated per defined length of primary dendrite (the first 20  $\mu m$  from the cell body) after treatment with DMSO or 25  $\mu M$  bicuculline from 7 to 14 DIV (Figure 94). The median density of synaptic  $\alpha 1$  mixed clusters was 4 (7-0) with DMSO treatment, compared to 4.5 (11-0) with bicuculline treatment (p value=0.20, Mann Whitney test, n=84 dendrites analysed from DMSO treated cultures and n=80 dendrites analysed from bicuculline treated neurones). Similarly, the median density of total  $\alpha 1$  mixed clusters was 6 (9.75-0) with DMSO treatment, compared to 6 (15-1.25) with bicuculline treatment (p value=0.11, Mann Whitney test, n=84 dendrites analysed from DMSO treated cultures and n=80 dendrites analysed from bicuculline treated neurones). This demonstrates that the synaptic and total densities of  $\alpha 1$  mixed clusters are not affected by the treatment, indicating that the regulation of the density of these types of clusters is independent of the  $GABA_A$ Rs activity at this developmental stage.



**Figure 94. The density of synaptic and total  $\alpha 1$  mixed clusters is not affected by treatment with 25  $\mu M$  bicuculline from 7 to 14 DIV.** The density of  $\alpha 1/\alpha 2$ -containing  $GABA_A$  receptors clusters ( $\alpha 1$  mixed clusters) along the 20  $\mu m$  of primary dendrite was counted in medium spiny neurone cultures in presence of DMSO or 25  $\mu M$  bicuculline from 7 to 14 DIV. **A.**

Histogram shows the distribution of synaptic  $\alpha 1$  mixed clusters densities in presence of DMSO or 25  $\mu\text{M}$  bicuculline from 7 to 14 DIV ( $n=84$  and  $n=80$  dendrites respectively from two independent experiments). **B.** Box plot displays the median density (50 % of the population) of synaptic  $\alpha 1$  mixed clusters in presence of DMSO or 25  $\mu\text{M}$  bicuculline from 7 to 14 DIV. **C.** Histogram shows the distribution of total  $\alpha 1$  mixed clusters density in presence of DMSO or 25  $\mu\text{M}$  bicuculline from 7 to 14 DIV ( $n=84$  and  $n=80$  dendrites respectively from two independent experiments). **D.** Box plot displays the median density (50 % of the population) of total  $\alpha 1$  mixed clusters in presence of DMSO or 25  $\mu\text{M}$  bicuculline from 7 to 14 DIV. Statistical analysis was performed using Mann Whitney test.

We have analysed the population of mixed clusters which contained a predominant density of  $\alpha 2$  clusters ( $\alpha 2$  mixed) after treatment with DMSO or 25  $\mu\text{M}$  bicuculline from 7 to 14 DIV (Figure 95). The median density of synaptic  $\alpha 2$  mixed clusters was 5 (8-2) with DMSO treatment, compared to 5 (11-2) with bicuculline treatment ( $p$  value= 0.22, Mann Whitney test,  $n=85$  dendrites analysed from DMSO treated cultures and  $n=79$  dendrites analysed from bicuculline treated neurones). Similarly, the median density of total  $\alpha 2$  mixed clusters was 7 (11-3.5) with DMSO treatment, compared to 8 (13-3) with bicuculline treatment. This demonstrates that the synaptic and total densities of  $\alpha 2$  mixed clusters are not affected by the treatment, indicating that the regulation of the density of these types of clusters is independent of the  $\text{GABA}_A$ Rs activity at this developmental stage.



**Figure 95. The density of synaptic and total  $\alpha 2$  mixed clusters is not affected by treatment with 25  $\mu\text{M}$  bicuculline from 7 to 14 DIV.** The density of  $\alpha 1/\alpha 2$ -containing  $\text{GABA}_A$  receptors clusters ( $\alpha 2$  mixed clusters) along the 20  $\mu\text{m}$  of primary dendrite was counted in medium spiny neurone cultures in presence of DMSO or 25  $\mu\text{M}$  bicuculline from 7 to 14 DIV. **A.** Histogram shows the distribution of synaptic  $\alpha 2$  mixed clusters densities in presence of DMSO

or 25  $\mu\text{M}$  bicuculline from 7 to 14 DIV (n=85 and n=79 dendrites respectively from two independent experiments). **B.** Box plot displays the median density (50 % of the population) of synaptic  $\alpha 2$  mixed clusters in presence of DMSO or 25  $\mu\text{M}$  bicuculline from 7 to 14 DIV. **C.** Histogram shows the distribution of total  $\alpha 2$  mixed clusters density in presence of DMSO or 25  $\mu\text{M}$  bicuculline from 7 to 14 DIV (n=85 and n=79 dendrites respectively from two independent experiments). **D.** Box plot displays the median density (50 % of the population) of total  $\alpha 2$  mixed clusters in presence of DMSO or 25  $\mu\text{M}$  bicuculline from 7 to 14 DIV. Statistical analysis was performed using Mann Whitney test.

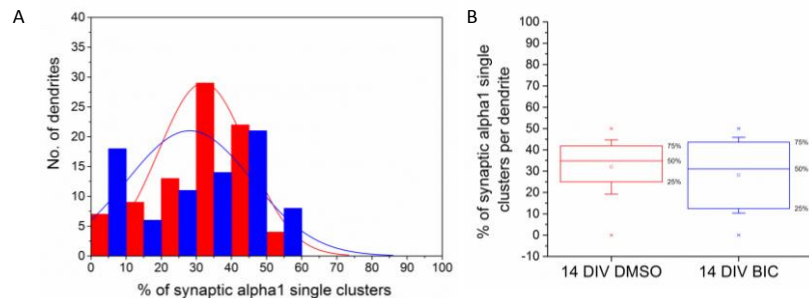
**Table 25. The density of synaptic  $\alpha 2$  single GABA<sub>A</sub>R clusters is increased after treatment with 25  $\mu\text{M}$  bicuculline treatment compared to DMSO from 7 to 14 DIV**

Density of clusters		14 DIV DMSO/ BIC	Significant
$\alpha 1$ single clusters	Synaptic		No
	Total		No
$\alpha 2$ single clusters	Synaptic		No
	Total		Yes
$\alpha 1$ mixed clusters	Synaptic		No
	Total		No
$\alpha 2$ mixed clusters	Synaptic		No
	Total		No

**6.3.2.3** *The proportion of synaptic as a percentage of total  $\alpha 2$  single GABA<sub>A</sub> receptor clusters was increased after treatment with 25  $\mu\text{M}$  bicuculline from 7 to 14 DIV*

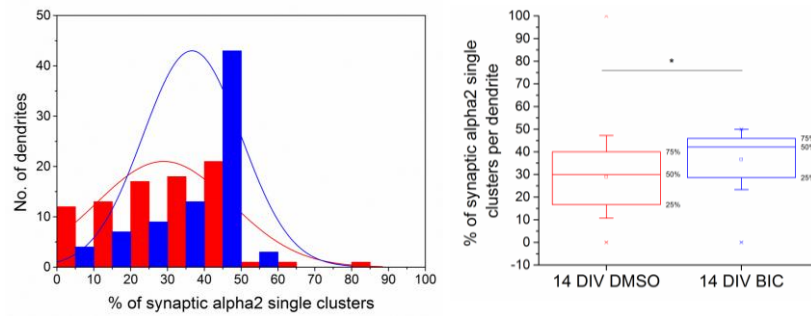
The densities of all types of clusters might not be affected by the treatment. However, the proportion of synaptic clusters as a percentage of the total population may vary indicating a redistribution of clusters. We estimated the proportion of synaptic clusters as a percentage of total density of clusters in each population treated from 7 to 14 DIV). The proportion of synaptic  $\alpha 1$  single clusters as a percentage of the total  $\alpha 1$  single clusters of GABA<sub>A</sub>Rs per defined length of primary dendrite (the first 20  $\mu\text{m}$  from the cell body) was calculated after treatment with DMSO or 25  $\mu\text{M}$  bicuculline from 7 to 14 DIV (Figure 96). The median percentage of synaptic amongst total  $\alpha 1$  single clusters was 34.8 (41.9-25) % with DMSO treatment compared to 31 (43.6-12.1) %

with bicuculline treatment ( $p=0.42$ , Mann Whitney test,  $n=84$  dendrites analysed after DMSO treatment and  $n=78$  dendrites analysed after bicuculline treatment). Similarly to the density of synaptic  $\alpha 1$  single clusters per dendrite, the percentage between the synaptic and the total  $\alpha 1$  single clusters is not altered by bicuculline (Table 26).



**Figure 96. The percentage of synaptic/total  $\alpha 1$  single clusters is not changed after treatment with 25  $\mu\text{M}$  bicuculline from 7 to 14 DIV.** The percentage of synaptic  $\alpha 1$  single clusters amongst the total population of  $\alpha 1$  single clusters along the 20  $\mu\text{m}$  of primary dendrite was estimated in medium spiny neurones cultures treated with DMSO or 25  $\mu\text{M}$  bicuculline from 7 to 14 DIV. **A.** Histogram shows the distribution of the percentages of synaptic/total  $\alpha 1$  single clusters per dendrite after treatment with DMSO or bicuculline from 7 to 14 DIV ( $n=84$  and  $n=78$  dendrites respectively, from two independent experiments). **B.** Box-plot displays the median percentage (50 % of the represented population) of synaptic/total  $\alpha 1$  single clusters per dendrite after treatment with DMSO or bicuculline from 7 to 14 DIV. Statistical analysis was performed using Mann- Whitney test.

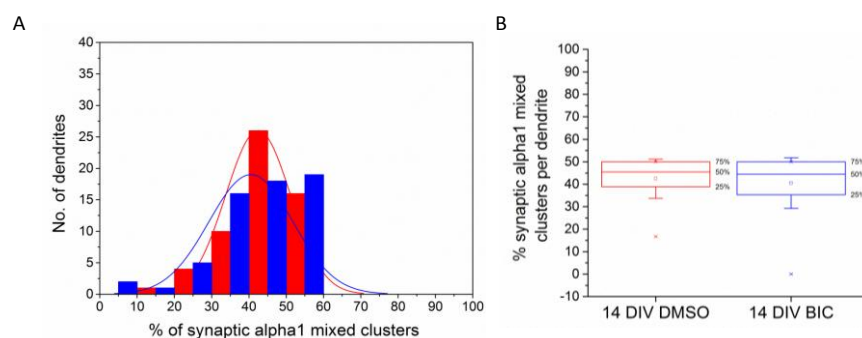
In addition, the proportion of synaptic  $\alpha 2$  single clusters as a percentage of the total  $\alpha 2$  single clusters of GABA<sub>A</sub>Rs per defined length of primary dendrite (the first 20  $\mu\text{m}$  from the cell body) was calculated after treatment with DMSO or 25  $\mu\text{M}$  bicuculline (Figure 97). After treatment with DMSO from 7 to 14 DIV, the median percentage of synaptic/total  $\alpha 2$  single clusters was 30 (40-16.3) % compared to 42.1 (42.9-28.6) % after treatment with bicuculline ( $p$  value=  $1.01 \times 10^{-4}$ , Mann Whitney test,  $n=85$  dendrites analysed after treatment with DMSO and  $n=79$  dendrites analysed after treatment with 25  $\mu\text{M}$  bicuculline). This indicates that, similarly to the density of synaptic  $\alpha 2$  single clusters per dendrite, the percentage of  $\alpha 2$  single clusters/total density of clusters increases with 25  $\mu\text{M}$  treatment of bicuculline.



**Figure 97. The percentage of synaptic/total  $\alpha 2$  single clusters is not changed after treatment with 25  $\mu\text{M}$  bicuculline from 7 to 14 DIV**

The percentage of synaptic  $\alpha 2$  single clusters amongst the total population of  $\alpha 2$  single clusters along the 20  $\mu\text{m}$  of primary dendrite was estimated in medium spiny neurones cultures treated with DMSO or 25  $\mu\text{M}$  bicuculline from 7 to 14 DIV. **A.** Histogram shows the distribution of the percentages of synaptic/total  $\alpha 2$  single clusters per dendrite after treatment with DMSO or bicuculline from 7 to 14 DIV ( $n=85$  and  $n=79$  dendrites respectively, from two independent experiments). **B.** Box-plot displays the median percentage (50 % of the represented population) of synaptic/total  $\alpha 2$  single clusters per dendrite after treatment with DMSO or bicuculline from 7 to 14 DIV. Statistical analysis was performed using Mann-Whitney test.

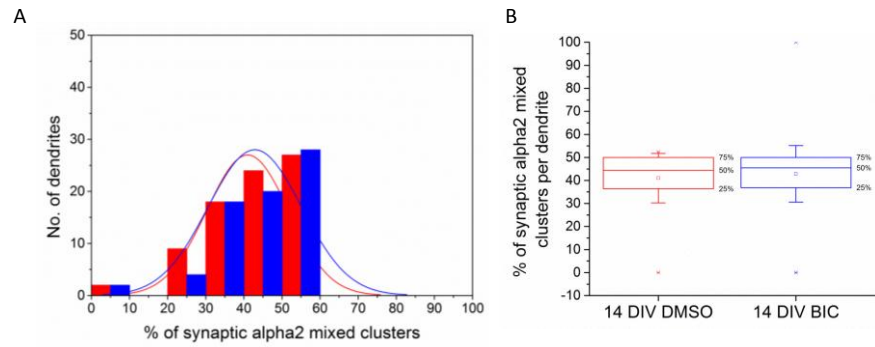
Following the previous analysis, we have also analysed changes in the percentage of synaptic mixed clusters over total mixed clusters during medium spiny neurones development. The proportion of synaptic  $\alpha 1$  mixed clusters as a percentage of the total  $\alpha 1$  mixed clusters of GABA<sub>A</sub>Rs per defined length of primary dendrite (the first 20  $\mu\text{m}$  from the cell body) was calculated after treatment with DMSO or 25  $\mu\text{M}$  bicuculline (Figure 98). After treatment with DMSO from 7 to 14 DIV, the median percentage of synaptic/total  $\alpha 1$  mixed clusters was 45.45 (50-38.2) % after treatment with DMSO compared to 44.4 (50-34.3) % after treatment with 25  $\mu\text{M}$  bicuculline ( $p$  value=0.58, Mann-Whitney test,  $n=57$  dendrites analysed after treatment with DMSO and  $n=61$  dendrites analysed after treatment with 25  $\mu\text{M}$  bicuculline). This demonstrates that, the percentage of synaptic/total  $\alpha 1$  mixed clusters of GABA<sub>A</sub>Rs per defined length of primary dendrite is not altered by treatment with 25  $\mu\text{M}$  bicuculline, possibly because GABA signalling is not involved in regulating this parameter at early stages of development.



**Figure 98. The percentage of synaptic/total  $\alpha 1$  mixed clusters is not changed after treatment with 25  $\mu\text{M}$  bicuculline from 7 to 14 DIV.** The percentage of synaptic  $\alpha 1$  mixed clusters amongst the total population of  $\alpha 1$  mixed clusters along the 20  $\mu\text{m}$  of primary dendrite was estimated in medium spiny neurones cultures treated with DMSO or 25  $\mu\text{M}$  bicuculline from 7 to 14 DIV. **A.** Histogram shows the distribution of the percentages of synaptic/total  $\alpha 1$  mixed clusters per dendrite after treatment with DMSO or bicuculline from 7 to 14 DIV ( $n=57$  and  $n=61$  dendrites respectively, from two independent experiments). **B.** Box-plot displays the median percentage (50 % of the represented population) of synaptic/total  $\alpha 1$  mixed clusters per dendrite after treatment with DMSO or bicuculline from 7 to 14 DIV. Statistical analysis was performed using Mann-Whitney test.

We analysed mixed clusters which contained a predominant density of  $\alpha 2$  clusters in these cultures ( $\alpha 2$  mixed clusters). The proportion of synaptic  $\alpha 2$  mixed clusters as a percentage of the total  $\alpha 2$  mixed clusters of  $\text{GABA}_A\text{Rs}$  per defined length of primary dendrite (the first 20  $\mu\text{m}$  from the cell body) was calculated after treatment with DMSO or 25  $\mu\text{M}$  bicuculline (Figure 99). After treatment with DMSO from 7 to 14 DIV, the median percentage of synaptic/total  $\alpha 2$  mixed clusters was 44.4 (50-36.4) % after treatment with DMSO compared to 45.4 (50-36.2) % after treatment with 25  $\mu\text{M}$  bicuculline ( $p$  value=0.4, Mann-Whitney test,  $n=80$  dendrites analysed after treatment with DMSO and  $n=73$  dendrites analysed after treatment with 25  $\mu\text{M}$  bicuculline). This demonstrates that, the percentage of synaptic/total  $\alpha 2$  mixed clusters of  $\text{GABA}_A\text{Rs}$  per defined length of primary dendrite is not altered by treatment with 25  $\mu\text{M}$  bicuculline. As stated before, it is possibly because GABA signalling is not involved in regulating this parameter at early stages of development.





**Figure 99. The percentage of synaptic/total  $\alpha 2$  mixed clusters is not changed after treatment with 25  $\mu\text{M}$  bicuculline from 7 to 14 DIV.** The percentage of synaptic  $\alpha 2$  mixed clusters amongst the total population of  $\alpha 2$  mixed clusters along the 20  $\mu\text{m}$  of primary dendrite was estimated in medium spiny neurones cultures treated with DMSO or 25  $\mu\text{M}$  bicuculline from 7 to 14 DIV. **A.** Histogram shows the distribution of the percentages of synaptic/total  $\alpha 2$  mixed clusters per dendrite after treatment with DMSO or bicuculline from 7 to 14 DIV (n=80 and n=73 dendrites respectively, from two independent experiments). **B.** Box-plot displays the median percentage (50 % of the represented population) of synaptic/total  $\alpha 2$  mixed clusters per dendrite after treatment with DMSO or bicuculline from 7 to 14 DIV. Statistical analysis was performed using Mann-Whitney test.

**Table 26. The percentage of synaptic/total  $\alpha 2$  single GABA<sub>A</sub>R clusters is decreased by 25  $\mu\text{M}$  bicuculline treatment from 7 to 14 DIV**

	14 DIV DMSO/ BIC	Significant
% (synaptic/total) $\alpha 1$ single clusters	-->	No
% (synaptic/total) $\alpha 2$ single clusters	->	Yes
% (synaptic/total) $\alpha 1$ mixed clusters	-->	No
% (synaptic/total) $\alpha 2$ mixed clusters	->	No

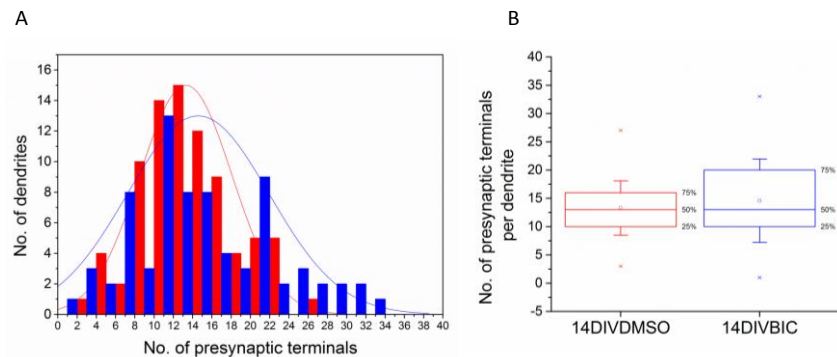
#### 6.3.2.4 *The connectivity between medium spiny neurones was not changed after treatment with 25 $\mu\text{M}$ bicuculline from 7 to 14 DIV*

To investigate further the role of GABA signalling in GABAergic synapse formation, we applied 25  $\mu\text{M}$  bicuculline in MSN cultures from 7 to 14 DIV and estimated if activity of GABA<sub>A</sub>Rs would regulate the density of presynaptic terminals forming contacts with the primary dendrites at early stages of development.

The total density of GAD-65 positive terminals per defined length of primary dendrite (the first 20  $\mu\text{m}$  from the cell body) was estimated after treatment with DMSO or 25  $\mu\text{M}$  bicuculline from 7 to 14 DIV (Figure 100). After DMSO treatment, the median density of



presynaptic terminals was 13 (20-10) compared to 13 (16-9) after treatment with bicuculline (p value=0.48, Mann Whitney test, n=74 dendrites analysed after treatment with DMSO and n=82 dendrites analysed after treatment with 25  $\mu$ M bicuculline from 7 to 14 DIV). This indicates that the density of presynaptic contacts per dendrite is not regulated by GABA signalling at early developmental stages.

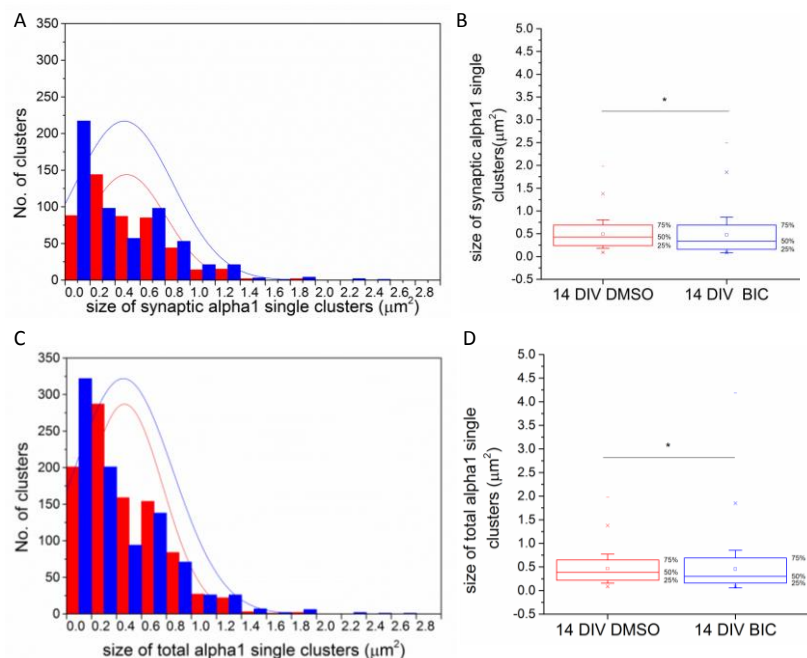


**Figure 100. The density of presynaptic terminals making contacts with primary dendrites is not changed after treatment with 25  $\mu$ M bicuculline from 7 to 14 DIV.** The density of presynaptic terminals along the 20  $\mu$ m of primary dendrite was counted in medium spiny neurones cultures after 7 and 14 DIV. A. Histogram shows the distribution of the density of presynaptic inputs after treatment with DMSO or 25  $\mu$ M bicuculline from 7 to 14 DIV (n=74 and n=82 dendrites respectively, from two independent experiments). B. Box-plot displays the median density of presynaptic terminals after treatment with DMSO or 25  $\mu$ M bicuculline from 7 to 14 DIV. Statistical analysis was performed using Mann Whitney test.

### 6.3.2.5 *$\alpha$ subunit-specific effects on cluster size of bicuculline treatment from 7 to 14 DIV*

During their development in culture, while treated with DMSO or 25  $\mu$ M bicuculline, medium spiny neurones underwent changes in the size of GABA<sub>A</sub>R clusters. The size of synaptic and total  $\alpha$ 1 single clusters of GABA<sub>A</sub>Rs per defined length of primary dendrite (the first 20  $\mu$ m from the cell body) was estimated after treatment with DMSO or 25  $\mu$ M bicuculline (Figure 101). After treatment with DMSO, the median size of synaptic  $\alpha$ 1 single clusters was 0.43  $\mu$ m<sup>2</sup> (0.69-0.24) compared to 0.34  $\mu$ m<sup>2</sup> (0.69-0.16) with 25  $\mu$ M bicuculline from 7 to 14 DIV (p value=0.002, Mann Whitney test, n=481 clusters analysed after DMSO treatment and n=576 clusters analysed after treatment with 25  $\mu$ M bicuculline). Similarly, the median size of total  $\alpha$ 1 single clusters was 0.39  $\mu$ m<sup>2</sup> (0.65-0.22) after treatment with DMSO compared to 0.3  $\mu$ m<sup>2</sup> (0.69-0.16) after

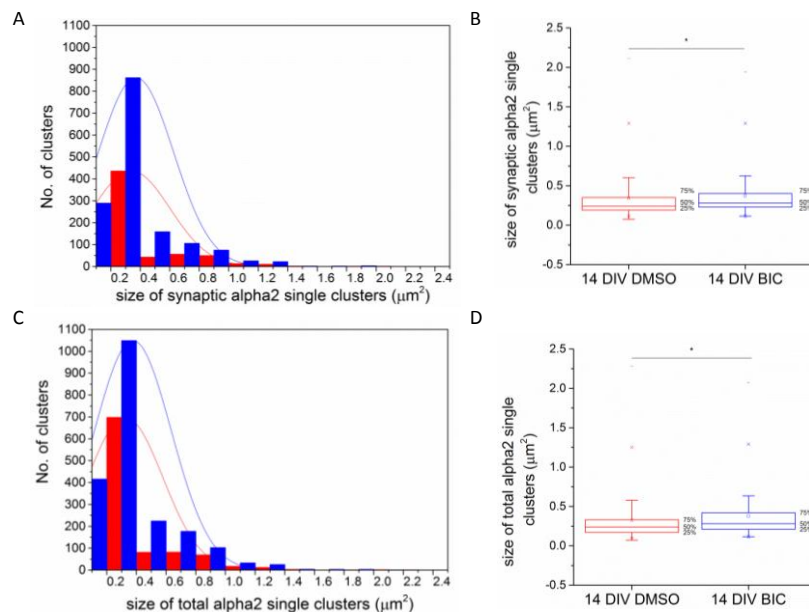
treatment with 25  $\mu\text{M}$  bicuculline ( $p$  value= $2.77 \times 10^{-4}$ , Mann Whitney test,  $n=940$  clusters analysed after DMSO treatment and  $n=898$  clusters analysed after treatment with 25  $\mu\text{M}$  bicuculline). This demonstrates that the size of synaptic and total  $\alpha 1$  single clusters is decreased by the treatment with 25  $\mu\text{M}$  bicuculline from 7 to 14 DIV, possibly due to regulation by GABA signalling of the size of a specific subtype of cluster less predominant in the culture at this developmental stage, containing mostly  $\alpha 1$  subunit.



**Figure 101. The size of synaptic and total  $\alpha 1$  single clusters is decreased by treatment from 7 to 14 DIV.** The size of  $\alpha 1$ -containing  $\text{GABA}_A$  receptors clusters ( $\alpha 1$  single clusters) along the 20  $\mu\text{m}$  of primary dendrite was measured in medium spiny neurones cultures after treatment with DMSO or 25  $\mu\text{M}$  bicuculline. **A.** Histogram shows the distribution of synaptic  $\alpha 1$  single clusters sizes after treatment with DMSO or 25  $\mu\text{M}$  bicuculline ( $n=481$  and  $n=576$  clusters respectively, from two independent experiments). **B.** Box-plot displays the median size (50% of the population) of synaptic  $\alpha 1$  single clusters after treatment with DMSO or 25  $\mu\text{M}$  bicuculline. **C.** Histogram shows the distribution of total  $\alpha 1$  single clusters sizes after treatment with DMSO or 25  $\mu\text{M}$  bicuculline ( $n=481$  and  $n=576$  clusters respectively, from two independent experiments). **D.** Box plot displays the population of total  $\alpha 1$  single clusters sizes after treatment with DMSO or 25  $\mu\text{M}$  bicuculline. Statistical analysis was performed using Mann Whitney test.

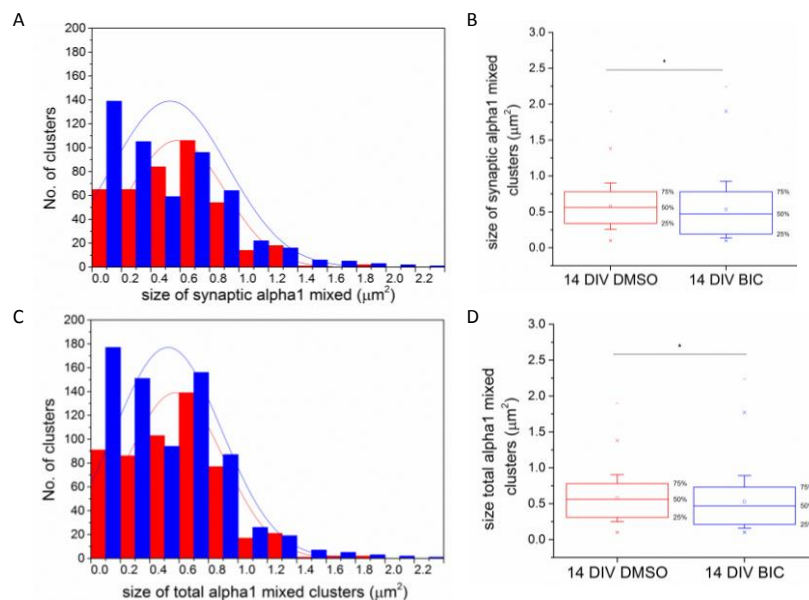
The size of synaptic and total  $\alpha 2$  single clusters of  $\text{GABA}_A$ Rs per defined length of primary dendrite (the first 20  $\mu\text{m}$  from the cell body) was estimated after treatment with DMSO or 25  $\mu\text{M}$  bicuculline (Figure 102). After treatment with DMSO, the median size

of synaptic  $\alpha 2$  single clusters was  $0.24 \mu\text{m}^2$  (0.35-0.19) compared to  $0.28 \mu\text{m}^2$  (0.4-0.23) with  $25 \mu\text{M}$  bicuculline from 7 to 14 DIV ( $p$  value= $2.91 \times 10^{-12}$  Mann Whitney test,  $n=859$  clusters analysed after DMSO treatment and  $n=1546$  clusters analysed after treatment with  $25 \mu\text{M}$  bicuculline). Similarly, the median size of total  $\alpha 2$  single clusters was  $0.24 \mu\text{m}^2$  (0.33-0.17) after treatment with DMSO compared to  $0.28 \mu\text{m}^2$  (0.42-0.21) after treatment with  $25 \mu\text{M}$  bicuculline ( $p$  value= $1.14 \times 10^{-22}$ , Mann Whitney test,  $n=1397$  clusters analysed after DMSO treatment and  $n=2038$  clusters analysed after treatment with  $25 \mu\text{M}$  bicuculline). This demonstrates that the size of synaptic and total  $\alpha 2$  single clusters is increased by treatment with  $25 \mu\text{M}$  bicuculline from 7 to 14 DIV, suggesting that the lack of activity provoked compensatory mechanisms favouring the insertion of  $\alpha 2$ -containing  $\text{GABA}_A$ Rs.



**Figure 102. The size of synaptic and total  $\alpha 2$  single clusters is increased by treatment from 7 to 14 DIV.** The size of  $\alpha 2$ -containing  $\text{GABA}_A$  receptors clusters ( $\alpha 2$  single clusters) along the  $20 \mu\text{m}$  of primary dendrite was measured in medium spiny neurones cultures after treatment with DMSO or  $25 \mu\text{M}$  bicuculline. **A.** Histogram shows the distribution of synaptic  $\alpha 2$  single clusters sizes after treatment with DMSO or  $25 \mu\text{M}$  bicuculline ( $n=859$  and  $n=1546$  clusters respectively, from two independent experiments). **B.** Box-plot displays the median size (50 % of the population) of synaptic  $\alpha 2$  single clusters after treatment with DMSO or  $25 \mu\text{M}$  bicuculline. **C.** Histogram shows the distribution of total  $\alpha 2$  single clusters sizes after treatment with DMSO or  $25 \mu\text{M}$  bicuculline ( $n=1397$  and  $n=2038$  clusters respectively, from two independent experiments). **D.** Box plot displays the population of total  $\alpha 2$  single clusters sizes after treatment with DMSO or  $25 \mu\text{M}$  bicuculline. Statistical analysis was performed using Mann Whitney test.

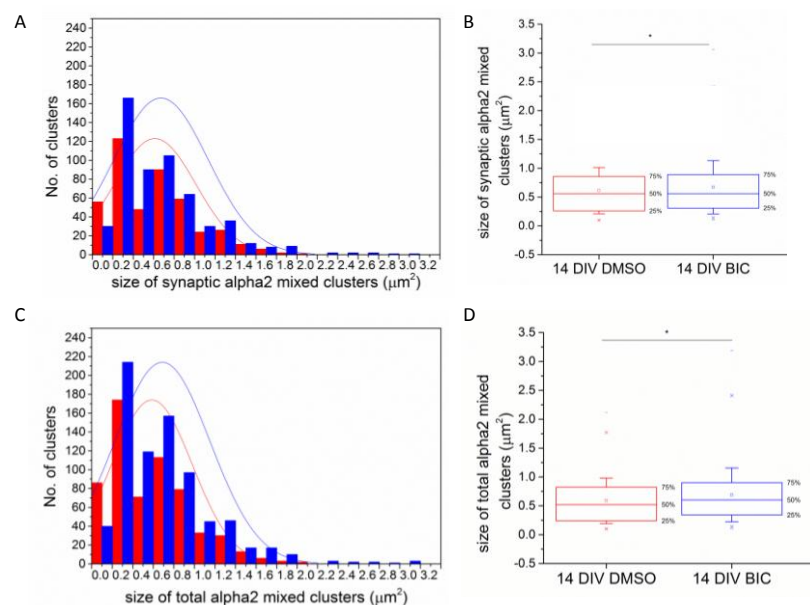
The size of synaptic and total  $\alpha 1$  mixed clusters of GABA<sub>A</sub>Rs per defined length of primary dendrite (the first 20  $\mu\text{m}$  from the cell body) was estimated after treatment with DMSO or 25  $\mu\text{M}$  bicuculline (Figure 103). After treatment with DMSO, the median size of synaptic  $\alpha 1$  mixed clusters was 0.56  $\mu\text{m}^2$  (0.78-0.34) compared to 0.47  $\mu\text{m}^2$  (0.78-0.19) with 25  $\mu\text{M}$  bicuculline from 7 to 14 DIV ( $p$  value=0.002, Mann Whitney test,  $n=409$  clusters analysed after DMSO treatment and  $n=518$  clusters analysed after treatment with 25  $\mu\text{M}$  bicuculline). Similarly, the median size of total  $\alpha 1$  mixed clusters was 0.56  $\mu\text{m}^2$  (0.78-0.33) after treatment with DMSO compared to 0.47  $\mu\text{m}^2$  (0.73-0.21) after treatment with 25  $\mu\text{M}$  bicuculline ( $p$  value= $6.88 \times 10^{-4}$ , Mann Whitney test,  $n=539$  clusters analysed after DMSO treatment and  $n=729$  clusters analysed after treatment with 25  $\mu\text{M}$  bicuculline). This demonstrates that the size of synaptic and total  $\alpha 1$  mixed clusters is decreased by treatment with 25  $\mu\text{M}$  bicuculline from 7 to 14 DIV, possibly due to regulation by GABA signalling of the size of a specific subtype of cluster less predominant in the culture at this developmental stage, containing mostly  $\alpha 1$  subunit.



**Figure 103. The size of synaptic and total  $\alpha 1$  mixed clusters is decreased by treatment from 7 to 14 DIV.** The size of  $\alpha 1/\alpha 2$ -containing GABA<sub>A</sub> receptors clusters ( $\alpha 1$  mixed clusters) along the 20  $\mu\text{m}$  of primary dendrite was measured in medium spiny neurones cultures after treatment with DMSO or 25  $\mu\text{M}$  bicuculline. **A.** Histogram shows the distribution of synaptic  $\alpha 1$  mixed clusters sizes after treatment with DMSO or 25  $\mu\text{M}$  bicuculline ( $n=409$  and  $n=518$  clusters respectively, from two independent experiments). **B.** Box-plot displays the median size (50 % of the population) of synaptic  $\alpha 1$  mixed clusters after treatment with DMSO or 25  $\mu\text{M}$  bicuculline.

**C.** Histogram shows the distribution of total  $\alpha 1$  mixed clusters sizes after treatment with DMSO or 25  $\mu\text{M}$  bicuculline ( $n=539$  and  $n=729$  clusters respectively, from two independent experiments). **D.** Box plot displays the population of total  $\alpha 1$  mixed clusters sizes after treatment with DMSO or 25  $\mu\text{M}$  bicuculline. Statistical analysis was performed using Mann Whitney test.



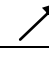



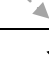
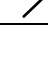
The size of synaptic and total  $\alpha 2$  mixed clusters of GABA<sub>A</sub>Rs per defined length of primary dendrite (the first 20  $\mu\text{m}$  from the cell body) was estimated after treatment with DMSO or 25  $\mu\text{M}$  bicuculline (Figure 104). After treatment with DMSO, the median size of synaptic  $\alpha 2$  mixed clusters was  $0.56 \mu\text{m}^2$  (0.86-0.26) compared to  $0.56 \mu\text{m}^2$  (0.73-21) with 25  $\mu\text{M}$  bicuculline from 7 to 14 DIV ( $p$  value=0.04, Mann Whitney test,  $n=446$  clusters analysed after DMSO treatment and  $n=558$  clusters analysed after treatment with 25  $\mu\text{M}$  bicuculline). The median size of total  $\alpha 2$  mixed clusters was  $0.52 \mu\text{m}^2$  (0.82-0.24) after treatment with DMSO compared to  $0.6 \mu\text{m}^2$  (0.9-0.34) after treatment with 25  $\mu\text{M}$  bicuculline ( $p$  value= $5.7 \times 10^{-6}$ , Mann Whitney test,  $n=610$  clusters analysed after DMSO treatment and  $n=773$  clusters analysed after treatment with 25  $\mu\text{M}$  bicuculline). This demonstrates that the size of total  $\alpha 2$  mixed clusters is increased by treatment with 25  $\mu\text{M}$  bicuculline from 7 to 14 DIV, suggesting that the lack of activity provoked compensatory mechanisms favouring the insertion of  $\alpha 2$ -containing GABA<sub>A</sub>Rs.



**Figure 104. The size of synaptic and total  $\alpha 2$  mixed clusters is increased by treatment from 7 to 14 DIV.** The size of  $\alpha 2/\alpha 1$ -containing GABA<sub>A</sub> receptors clusters ( $\alpha 2$  mixed clusters) along the 20  $\mu\text{m}$  of primary dendrite was measured in medium spiny neurones cultures after treatment with DMSO or 25  $\mu\text{M}$  bicuculline. **A.** Histogram shows the distribution of synaptic  $\alpha 2$  mixed clusters sizes after treatment with DMSO or 25  $\mu\text{M}$  bicuculline ( $n=446$  and  $n=558$  clusters respectively, from two independent experiments). **B.** Box-plot displays the median size (50 % of

the population) of synaptic  $\alpha 2$  mixed clusters after treatment with DMSO or 25  $\mu\text{M}$  bicuculline. **C.** Histogram shows the distribution of total  $\alpha 2$  mixed clusters sizes after treatment with DMSO or 25  $\mu\text{M}$  bicuculline ( $n=610$  and  $n=773$  clusters respectively, from two independent experiments). **D.** Box plot displays the population of total  $\alpha 2$  mixed clusters sizes after treatment with DMSO or 25  $\mu\text{M}$  bicuculline. Statistical analysis was performed using Mann Whitney test: \* corresponds to  $p < 0.05$ .

**Table 27. The size of  $\alpha 2$ -containing GABA<sub>A</sub>R clusters is increased while the size of  $\alpha 1$ -containing GABA<sub>A</sub>R clusters is decreased by the 25  $\mu\text{M}$  treatment from 7 to 14 DIV.**

Size of clusters ( $\mu\text{m}^2$ )		14 DIV DMSO/ BIC	Significant ( $p < 0.05$ )
$\alpha 1$ single clusters	Synaptic		Yes
	Total		Yes
$\alpha 2$ single clusters	Synaptic		Yes
	Total		Yes
$\alpha 1$ mixed clusters	Synaptic		Yes
	Total		Yes
$\alpha 2$ mixed clusters	Synaptic		Yes
	Total		Yes

#### 6.4 Discussion

It has now been well established that GABA is the first neurotransmitter released in the embryonic brain (Ben-Ari et al., 2007). Due to high expression of the chloride co-transporter NKCC1 and low expression of the chloride extruder KCC2 in the embryonic brain, opening of the GABA<sub>A</sub> receptors leads to a decrease of chloride intracellular concentration, thus resulting in a depolarising current (Ben-Ari et al., 2007). These depolarising potentials have been shown to contribute to proper axonal wiring of the developing brain (Fritschy and Panzanelli, 2014). In the adult brain, the expression of the chloride transporter NKCC1 is lower and the KCC2 becomes the predominant chloride extruder leading to hyperpolarising currents and influx of chloride when GABA<sub>A</sub>Rs are activated (Ben-Ari et al., 2007). However, it is important to remember that at any developmental stage, the main effect of GABA signalling is to increase the

membrane conductance opposed to the influx of positively charged ions into the postsynaptic cell induced by other neurotransmitters signalling.

Although the role played by neuronal activity on diffusion properties, size and efficacy of GABA<sub>A</sub>Rs has been widely studied (Saliba et al., 2007, Bannai et al., 2009), little is known about the effect of GABA signalling during the construction of GABAergic synapses. It has been shown that in mature hippocampal cultures, the excitatory activity decreases the GABA<sub>A</sub>R and gephyrin cluster sizes and reduces GABAergic miniature inhibitory postsynaptic currents (mIPSCs) (Bannai et al., 2009). At the synapse, homeostatic plasticity has been observed as an increase or a decrease in synaptic strength following corresponding changes in neuronal network activity (Cline, 2005). Although studies of activity-dependent changes at excitatory synapses have furthered our understanding of homeostatic mechanisms, the effects of chronic activity changes at inhibitory synapses is not as clearly defined. Studies of homeostatic plasticity at inhibitory synapses have shown decreased synaptic strength following chronic activity blockade (Hartman et al., 2006). This work suggested that presynaptic mechanisms regulate homeostatic plasticity during 9 days treatments of activity blockade in hippocampal cultures. More recently, Rannals et al., demonstrated that in hippocampal neurones challenged by chronic depolarisation, an increase of inhibitory postsynaptic GABA<sub>A</sub>R expression followed by an increase in the presynaptic marker GAD-65 were observed (Rannals and Kapur, 2011). These increases were paralleled to increase in synaptic strength measured by mIPSC amplitude, confirming that postsynaptic mechanisms were in play. In addition, the rate of internalisation of GABA<sub>A</sub>Rs was slowed down.

These experiments have been conducted in a mixed culture environment where glutamatergic and GABAergic neurones are contacting each other, hence providing excellent conditions to study homeostatic regulations. But what are the effects mediated by GABA<sub>A</sub>Rs signal transduction on GABAergic synapse development when

depolarising GABA is the only neurotransmitter present in the embryonic and postnatal brain, and when GABA becomes hyperpolarising later on?

Prior to our experiments, calcium imaging was performed in our culture model in order to confirm that the switch of GABA signalling observed *in vivo* during GABAergic synapse maturation was also present in our culture model. This experiment showed that activation of GABA<sub>A</sub>Rs by the agonist muscimol from 4 to 7 DIV induced intracellular calcium increase. In contrast, when GABA<sub>A</sub>R activity was triggered by addition of muscimol in MSN cultures from 7 to 14 DIV, no increase in intracellular calcium was observed. These results indicated that at early developmental stages, activating GABA<sub>A</sub>Rs caused a depolarisation of MSNs, which was not observed at later developmental stages, suggesting that GABA<sub>A</sub> receptor activation caused hyperpolarisation (Arama et al., manuscript in preparation).

Additionally, electrophysiology recordings have been performed in the MSN cultures. When recorded from 4 to 7 DIV, MSNs only exhibited mIPSCs and spontaneous inhibitory postsynaptic currents (sIPSCs), reflecting the immature stage of development they were in. However, action potential-(AP) driven activity was recorded in 12 DIV neurones, suggesting that MSNs attained their maturity and GABAergic synapses were stabilised enough to mediate AP-triggered neurotransmitter release (Arama et al., manuscript in preparation).

GABA<sub>A</sub>R subtypes are thought to subserve individual functions in GABAergic synaptic transmission. The existence of different combinations of subunits probably contributes to synaptic variety and sensitivity to the endogenous GABA. This is emphasised by extrasynaptic receptors being 20 times more sensitive to GABA than synaptic receptors (Saxena and Macdonald, 1996). In the study by Bohme et al., it was demonstrated that a specific four amino-acid motif present in the N-terminal extracellular domain of the  $\alpha$ 1-6 subunits controls the sensitivity to GABA of GABA<sub>A</sub>Rs (Bohme et al., 2004). By exchanging this 4aa motif, they were able to transfer these sensitivity properties from one  $\alpha$  subunit type to another. It was already known that  $\alpha$ 1



had the highest affinity for GABA of all the synaptic  $\alpha$  subunits (Ebert et al., 1994). When different  $\alpha$  subunits in combination with the  $\beta 3$  and  $\gamma 2$  subunits were expressed in HEK 293, the  $EC_{50}$  of the chloride currents induced by GABA was determined. In decreasing order of affinity for GABA, it was shown that  $\alpha 6 > \alpha 1 > \alpha 2 > \alpha 4 > \alpha 5 > \alpha 3$  (Bohme et al., 2004). The exchange of four amino acids between  $\alpha 1$ ,  $\alpha 3$ ,  $\alpha 4$  and  $\alpha 5$  subunits resulted in the exact transfer of their respective GABA sensitivities. Interestingly, when the four amino acids of  $\alpha 2$  subunit were exchanged, a drastic loss in GABA sensitivity was observed, potentially explained by a conformational change only occurring in this synaptic subunit. In addition, the motif exchange in the  $\alpha 6$  subunit resulted in the partial transfer of the GABA sensitivity, suggesting that another motif only present in the  $\alpha 6$  subunits could explain its highly sensitivity to GABA (Bohme et al., 2004).

Considering all these criteria, to investigate the effects of  $GABA_A$ R activity during maturation of GABAergic synapses, we have suppressed the  $GABA_A$  receptor activity in the medium spiny neurone cultures using a competitive antagonist bicuculline from 4 to 7 days *in vitro* (DIV) or from 7 to 14 DIV. As a control, we have treated neurones in parallel with an equivalent amount of DMSO, a polar solvent in which bicuculline was initially dissolved.

Our results demonstrated that the addition of 50  $\mu$ M bicuculline to MSN cultures at any developmental stages had deleterious effects on cell survival, causing a prominent loss of MSNs. We concluded that at this dose, bicuculline is toxic. This was likely to be a consequence of the complete inhibition of  $GABA_A$ R activity which had irreversible effects on cell survival. Thus, we decided to treat MSNs with bicuculline at 25  $\mu$ M dose which was sufficient to block GABAergic activity (established in electrophysiological recordings) without causing toxicity.

Once these conditions were confirmed, GABAergic synapse formation was analysed during maturation of MSNs *in vitro*. When neurones were chronically treated from 4 to 7 DIV, the density of  $GABA_A$ R clusters was not affected. This result indicated

that at this early developmental stage, the density of GABA<sub>A</sub>R clusters per dendrite is not regulated by the depolarising GABA signalling. In contrast, under the same conditions, the median size of all  $\alpha$ 2-single or mixed clusters was decreased. This suggests that at early developmental stages, GABA<sub>A</sub>R activity is important for clustering  $\alpha$ 2-containing GABA<sub>A</sub>R clusters specifically and that in absence of this signalling, the  $\alpha$ 2-containing GABA<sub>A</sub>R clusters are down-regulated. Additionally, the density of presynaptic terminals contacting dendrites of MSNs was not affected by blocking GABA<sub>A</sub>R, suggesting that at early developmental stages in culture, wiring between MSNs is not regulated by GABA signalling. Other mechanisms such as adhesion molecules recognition between the pre and postsynaptic elements could be at the origin of GABAergic wiring.

When neurones were chronically treated from 7 to 14 DIV with 25  $\mu$ M bicuculline, different phenotypes were observed. At a time when GABA is hyperpolarising, blocking this signal increased the density and the size of  $\alpha$ 2-containing GABA<sub>A</sub>R clusters. In contrast, the size of  $\alpha$ 1-containing GABA<sub>A</sub>R clusters was decreased significantly upon this treatment. As observed in early developmental stage treatments, the density of GAD-65 positive terminals contacting MSN dendrites was not altered by blocking GABA signalling. These results suggest that when MSNs are deprived of GABA signalling at a time it becomes hyperpolarising; compensatory mechanisms involving clustering of GABA<sub>A</sub>R clusters are preferentially driven towards the formation of the  $\alpha$ 2-containing synapses. The  $\alpha$ 2-containing receptors function is probably broader as they are known to be involved in diverse processes such as reward and alcohol/drug abuse, schizophrenic symptomatology, depression and chronic pain (Engin et al., 2012). However, so many implications could not be directly reflecting the reason why the formation of  $\alpha$ 2-containing receptors is promoted in the absence of GABA signalling in MSNs. This increase of the  $\alpha$ 2-containing GABA<sub>A</sub>R clusters clustering in a GABA signalling-deprived context could be explained by the fact that this subunit is preferentially localised to proximal dendrites of MSNs (Gross et al., 2011). Considering that we only

characterised synapse formation in the region of proximal dendrite, different regulatory mechanisms could be occurring at the same time in the soma or axons of MSNs and may involve a modulation of other GABA<sub>A</sub>R subtypes.

In addition, the fact that  $\alpha$ 1-containing synapses were down-regulated in absence of GABA signalling suggested that at this developmental stage, when GABA is hyperpolarising,  $\alpha$ 1-containing synapses are promoted and maintained by GABA<sub>A</sub>R activity. This was confirmed in the previous chapter in which we showed that the size of  $\alpha$ 1 mixed cluster is increased from 7 to 14 DIV. Potentially, this could be explained by the fact that  $\alpha$ 1 subunit has the highest GABA sensitivity of all synaptic  $\alpha$  subunits (Bohme et al., 2004), and so, is the most efficient subunit in transducing the GABA signalling. Nevertheless, when GABA signalling is blocked, the  $\alpha$ 2 subunit, which is the most prominent subunit in the striatum (Fritschy and Mohler, 1995), is preferentially incorporated into GABA<sub>A</sub>R clusters. It would be interesting to further the relevance of such mechanisms in an *in vivo* model where GABA signalling is altered and to confirm these results with pharmacology and electrophysiological recordings.

# Chapter seven

## **7. The formation of GABAergic synapses is enhanced in the presence of the exogenous extracellular domains (ECDs) of GABA<sub>A</sub> R $\alpha$ 1 and $\alpha$ 2 subunits**

### **7.1 Introduction**

While in the previous chapter, we studied the role played by the activity of GABA<sub>A</sub>Rs, in the present chapter, we investigated the structural role played by GABA<sub>A</sub>Rs during GABAergic synapse formation.

Structural heterogeneity of GABA<sub>A</sub>Rs is thought to be the basis of their physiological and pharmacological heterogeneity (Olsen and Sieghart, 2009). Each subunit of the GABA<sub>A</sub>Rs is composed of a large N-terminal extracellular domain of 200-250 amino acids, four transmembrane domains with an M3-4 intracellular loop of 85-255 residues, and a small C-terminal extracellular domain (Karlin and Akabas, 1995).

Many studies have focused on the role played by the intracellular loop of GABA<sub>A</sub>R  $\alpha$  subunits, showing their role in intracellular protein-protein interactions involved in the clustering and stability of GABA<sub>A</sub>Rs at synapses by binding to Gephyrin and Neuroligin 2 (Kneussel et al., 1999, Jacob et al., 2005, Tretter et al., 2008, Pouloupoulos et al., 2009, Mukherjee et al., 2011, Tretter et al., 2011). However, little is known about the structural role played by the extracellular domains of GABA<sub>A</sub> receptor subunits.

Assembly of GABA<sub>A</sub>Rs into pentamers involves the initial formation of  $\alpha\beta$  subunit heterodimers. The N-terminal extracellular domains of  $\alpha$  and  $\beta$  subunits associate within the luminal part of the endoplasmic reticulum with two chaperone proteins involved in the folding control quality called Binding Immunoglobulin Protein (BiP) and Calnexin (Connolly et al., 1996a, Kleizen and Braakman, 2004, Arancibia-Carcamo and Kittler, 2009, Luscher et al., 2011). In addition, GABA binding sites and binding sites for clinically important drugs such as benzodiazepines, are also located in the N-terminal extracellular domain (Homanics et al., 1997). While the GABA binding site is located between the extracellular domains of  $\alpha$  and  $\beta$  subunits, the benzodiazepine binding site is located in a pocket between the ECDs of  $\alpha$  and  $\gamma$  subunits (Ernst et al.,

2003, Henschel O, 2008, Olsen and Sieghart, 2008). The binding of each of these molecules between the GABA<sub>A</sub>R subunits causes a conformational change in the receptor, opens the channel gate and allows the entrance (or exit) of chloride ions into the postsynaptic cell (Macdonald and Olsen, 1994).

Using radioligand binding assays and electrophysiology combined with mutagenesis, four amino acids within the extracellular domain of the  $\alpha$  subunits have been shown to mediate the distinct sensitivity to GABA (Bohme et al., 2004). The exchange of the whole motif between different subunit conferred the respective GABA sensitivity for most receptors. This study provided a better understanding of the mechanistic features responsible for the molecular diversity of GABAergic synapses and hence, emphasized on the important role played by individual  $\alpha$  subunits in the transmission of the GABAergic signal.

In addition, the first crystallisation of the GABA<sub>A</sub>R  $\beta$ 3 homopentamer revealed that GABA<sub>A</sub>R ECDs are composed of structural elements unique to eukaryotic Cys-loop receptors, but more importantly that the highly conserved N-glycans present on the ECDs of all the subunits play an important role in the structural assembly of the receptor, in the signal transduction of GABA<sub>A</sub>R ligands and in gating process of the receptor (Miller and Aricescu, 2014).

Finally, it has recently been shown that GABA<sub>A</sub>Rs play a structural role during GABAergic synapse formation and are capable to promote this process in a heterologous co-culture model system (Fuchs et al., 2013). A particular interest should be focused on the structure and function of the extracellular domains of GABA<sub>A</sub>R subunits in this process since these domains are present in the synaptic cleft and so, they may be responsible for initiation of first contact between the pre- and postsynaptic elements.

Together, these data suggest that the extracellular domains play an important role in the global functioning of the GABA<sub>A</sub>Rs. In the last chapter of my thesis, we aimed to define and investigate the role played by the ECDs of  $\alpha$ 1 and  $\alpha$ 2 subunits

during specific GABAergic synapse formation. Purified  $\alpha 1$  and  $\alpha 2$  ECDs from infected Sf9 cells under sterile conditions, and prepared Sf9 cell protein extracts.

### **7.1.1 Aims**

In this chapter, our aims were:

1. We proved that purified  $\alpha 1$  and  $\alpha 2$  ECDs were glycosylated using deglycosylation enzyme assay.
2. We have treated embryonic MSN cultures with the purified  $\alpha 1$  or  $\alpha 2$  ECDs, and applied Sf9 cell protein extracts as a control.
3. We have investigated the structural role played by the exogenous  $\alpha 1$  or  $\alpha 2$  ECDs during GABAergic synapse formation by analysing the density, size and synaptic location of GABA<sub>A</sub>R clusters.

## **7.2 Methods**

### **7.2.1 Purification of ECDs under sterile conditions**

Cultures of Sf9 cells grown in suspension and infected with baculovirus stocks were spun down and resuspended in the filtered lysis buffer containing 20 mM NaH<sub>2</sub>PO<sub>4</sub> pH 8.0, 0.5 % NP-40 and protease inhibitors cocktail. After three freeze/thaw cycles, lysates were centrifuged at 10,000 g for 15 min at 4 °C using a MIKRO 22R Hettich Zentrifugen centrifuge (14,000 g rotor). The pellets were collected and resuspended in the filter-sterilised solubilisation buffer containing 50 mM NaH<sub>2</sub>PO<sub>4</sub>, 150 mM NaCl pH 8.0, 2 % NP-40, 1 % DOC. Subsequently, the samples were homogenised with a sintered-glass homogeniser (4-5 strokes on ice) and incubated for 90 min on a rotating plate at 4 °C to solubilise. After rotating, the proteins were spun at 10,000 g for 15 min at 4 °C; the pellets were resuspended in the solubilisation buffer and snap-frozen for further analysis. The supernatant containing the proteins was dialysed against the dialysis buffer containing 50 mM NaH<sub>2</sub>PO<sub>4</sub>, 300 mM NaCl, pH 8, 1 % Triton X-100. The following day, 1 mg of total protein was added to sterile 0.2 ml resin columns (HisPur Ni-NTA spin column, 0.2 ml resin bed, Thermo Scientific)

prepared in filtered binding buffer (dialysis buffer with the addition of 20 % sterile glycerol). The proteins were incubated for binding overnight at 4 °C with rotation. The Ni-NTA agarose columns were chosen because they are composed of nitrilotriacetic acid (NTA), a tetradentate chelating ligand, in highly cross-linked 6 % agarose matrix. NTA binds Ni<sup>2+</sup> ions by four co-ordination sites which allow 6 Histidine-tagged proteins to bind with micro molar affinity. The binding capacity of the resin is 5-10 mg of recombinant protein per ml of resin. The following day, three washes were performed in 400 µl binding buffer and two more washes were carried out with the same buffer in the absence of Triton X-100, in order to remove any trace of this non-ionic detergent from the proteins. Subsequently, columns were incubated on a rotating plate, overnight at room temperature with 400 µl of the elution buffer containing 50 mM NaH<sub>2</sub>PO<sub>4</sub>, 300 mM NaCl, pH 6.0, 100 mM EDTA, 500 mM imidazole, and protease inhibitors cocktail. The next day, columns were spun and the first elution fraction (E1) was collected. Two subsequent elutions were also carried out for 10 min at room temperature (E2 and E3). Finally, elution fractions were dialysed overnight at 4 °C in PBS containing 300 mM NaCl. The protein concentration was measured using the Bradford Assay; small aliquots of protein samples were prepared and snap frozen in liquid nitrogen. At each stage of purification, small fractions of samples were collected, denatured in 2 % SDS and analysed by SDS/PAGE and immunoblotting with the Histidine-tag specific antibody (see Chapter 2, section 2.8-2.9 for immunoblotting details). As a control, we have eluted proteins from non-infected Sf9 cells in parallel with the samples containing α1 and α2 ECDs.

### **7.2.2 Deglycosylation of ECDs**

In the amino-acid sequence of the α1 and α2 ECDs there are two and three N-glycosylation sites, respectively (Miller and Aricescu, 2014). Deglycosylation experiments were performed under denaturing conditions with 20 µg of purified α1 and α2 ECDs using the glycoprotein, deglycosylation kit, Millipore). The Sf9 cell extracts



and Bovine fetuin protein were run alongside the ECDs, as positive controls. Samples were dissolved in 5 X reaction buffer (250 mM sodium phosphate buffer, pH 7) and denaturation solution containing 2 % SDS/ 1M  $\beta$ -mercaptoethanol, pH 7.0 and boiled at 100 °C for 5 min. After cooling, Triton X-100 detergent solution was added in excess in order to complex any free SDS which could reduce the rate of the N-glycosidase F cleavage. Then, 1  $\mu$ l of each enzyme was added (see list below) and incubated with the proteins for 3 hours at 37 °C. Although there is no evidence that the  $\alpha$ 1 and  $\alpha$ 2 ECDs are O-glycosylated, we used a mixture of the following deglycosylation enzymes to test if the purified ECDs incorporated any oligosaccharides:

- N-glycosidase F: this enzyme cleaves all asparagine-linked complex, hybrid, or high mannose oligosaccharides.
- Endo- $\alpha$ -N-acetylgalactosaminidase: this enzyme cleaves serine- or threonine-linked unsubstituted Gal $\beta$ 1,3GalNaca.
- The  $\alpha$ 2-3,6,8,9-Neuraminidase: this enzyme cleaves all the non-reducing terminal branched and unbranched sialic acids.
- The  $\beta$ 1,4-Galactosidase: this enzyme releases only  $\beta$ 1,4-linked, non-reducing terminal galactose from complex carbohydrates and glycoproteins.
- The  $\beta$ -N-Acetylglucosaminidase: this enzyme cleaves all non-reducing terminal  $\beta$ -linked-N-acetylglucosamine residues from complex carbohydrates and glycoproteins.

Each of the reactions was loaded on two different 12 % SDS/PAGE. Then, they were transferred onto the nitrocellulose membrane and, after blocking with 1.5 % milk/TBS-Tween 20, membranes were incubated with the Histidine-tag specific antibodies in 1.5 % milk/ TBS-Tween 20 overnight at 4 °C. After washing, the membranes were incubated with an alkaline-phosphatase conjugated secondary antibody and the immuno-reactivity was visualised using a colour reaction based on NBT/ BCIP substrate (see chapter 2, sections 2.8-2.9 for details on immunoblotting).

### 7.2.3 Treatment of MSN cultures with $\alpha 1$ or $\alpha 2$ ECDs

To analyse the role of the N-terminal extracellular domains of  $\alpha 1$  and  $\alpha 2$  GABA<sub>A</sub>R subunits during synapse formation, E17 striatal neurones were cultured and treated from 4 to 7 DIV or 7 to 14 DIV with 5  $\mu$ g of the eluted control Sf9 cell extracts or  $\alpha 1$  ECDs or  $\alpha 2$  ECDs. In the first set of treatments, these reagents were added at 4 and 6 DIV and the cells were fixed at 7 DIV. In the second set of experiment, neurones were treated with 5  $\mu$ g of control Sf9 cell extracts or  $\alpha 1$  ECDs or  $\alpha 2$  ECDs at 7, 9 and 11 DIV and subsequently fixed at 14 DIV.

### 7.2.4 Immunocytochemistry

Immunocytochemistry was performed as described in the Chapter 2, Section 2.2. Neurones cultured for 7 or 14 DIV were fixed using 4 % PFA/ sucrose for 12 min at room temperature. After fixation, they were incubated with 0.3 M glycine in PBS in order to quench the PFA. After washing, cells were incubated in 2 % BSA in PBS for 1 h and subsequently incubated with specific antibodies. In order to visualise the binding of the exogenous  $\alpha 1$  or  $\alpha 2$  ECDs, neurones were incubated with rabbit anti- $\alpha 1$  and guinea-pig anti- $\gamma 2$ , or guinea-pig anti- $\alpha 2$  and rabbit anti- $\gamma 2$  antibodies, respectively (Figure 107 and 108 for treatment from 4 to 7 DIV; Figure 118 and 119 for treatment from 7 to 14 DIV), each specifically binding to the N-terminal domains of the corresponding subunit, diluted in 2 % BSA in PBS, overnight at 4 °C (14- 16 h, Table 28). Neurones were then permeabilised by incubation with 0.1 % Triton X-100 / 2 % BSA in PBS for 15 min. They were subsequently incubated with chicken anti-MAP2 antibody (see Table 26 for dilutions) diluted in 2 % BSA in PBS for 2 h at room temperature. Following this step, fluorescently-labelled secondary antibodies were added as described in the Chapter 2, Section 2.2 (Table 28).

In a second set of experiments (Figures 109 and 120), immunolabelling was done using a mouse anti-6Histag proteins antibody in combination with the guinea-pig anti- $\gamma 2$  subunit antibody overnight at 4 °C. The following day, neurones were permeabilised

as described above and incubated with chicken anti-MAP2 and rabbit anti-VGAT antibodies for 2 h, followed by incubation with fluorescently labelled secondary antibodies which were added as described in the Chapter 2, Section 2.2 (antibodies used in these experiments are described in Table 26).

In a third set of experiments (Figures 110 and 121), neurones treated with the ECDs, were fixed and stained with the guinea-pig anti- $\gamma 2$  antibody specifically binding to the extracellular domain of  $\gamma 2$  subunit, overnight at 4 °C. The following day, neurones were permeabilised as described above and incubated with mouse anti-GAD-65 and chicken anti-MAP2 antibodies (See Table 26 for description). The protocol previously described for immunocytochemistry was followed throughout the staining.

In a fourth set of experiments (Figures 117 and 128), neurones treated with the ECDs were fixed and stained with the guinea-pig anti- $\gamma 2$  antibody specifically binding to the extracellular domain of  $\gamma 2$  subunit, overnight at 4 °C. The following day, neurones were permeabilised as described above and incubated with mouse anti- gephyrin, rabbit anti-VGAT and chicken anti-MAP2 antibodies (see Table 26 for description). The protocol previously described for immunocytochemistry was followed throughout the staining. In all four sets of experiments, immunolabelling was analysed using Zeiss LSM 710 with a Plan-Apochromat 63x/ 1.4 Oil DIC lens. Threshold for each channel was calculated from the background intensity and then removed from the image, as described in the Chapter 2, Section 2.2.

### **7.2.5 Analysis of synaptic parameters**

To estimate the density and size of  $\gamma 2$ -containing GABA<sub>A</sub>R clusters, puncta were defined as immunoreactivity greater than 0.1  $\mu\text{m}^2$ , with the mean intensity of each cluster equal or higher than double the standard deviation of intensity as indicated by the Zen 2009 programme. The defined clusters were circled and their sizes noted by

hand. The total density of  $\gamma 2$ -positive clusters and GAD-65-positive presynaptic terminals were analysed using Excel and Origin programmes.

#### **7.2.6 Statistical analysis**

Subsequently, the data was analysed using Origin Pro 9.0 32 Bit software. Normal (Gaussian) distribution of the pooled data was first tested using the Shapiro-Wilk and Kolmogorov-Smirnov tests. Since the data did not follow a normal distribution and the categories were independent, non-parametric statistical analysis was carried out using the Mann Whitney test with an interval of confidence of 95 %. Because they represent a robust measure of central tendency when distributions are not normally distributed, the medians and their interquartile range (IQR) were used to describe the data and evaluate statistical dispersion. With the groups following normal distribution, statistical analysis was done using two sample Student's t-test. The total density of clusters was evaluated along the length of 20  $\mu\text{m}$  of primary dendrite for each cell. The density of synaptic clusters was also evaluated along the 20  $\mu\text{m}$  of dendrites for each cell in a whole population of clusters. The proportion of synaptic clusters was determined as a percentage of the total clusters for each dendrite. The proportion of the synaptic clusters/total clusters was tested as above and subsequently compared using parametric (Student's t-test) or non-parametric statistical tests (Mann-Whitney).

**Table 28. Antibodies used for immunocytochemical analysis of GABA<sub>A</sub>R clusters and presynaptic terminals in MSN cultures**

Primary antibodies				Secondary antibodies		
Specificity	Origin	dilutions	Source and characterisation	Antibodies (host: Goat)	Dilutions	Source (Alexa Fluor, Invitrogen)
GABA <sub>A</sub> α1	Rb	1:200	(Duggan and Stephenson, 1990)	Anti-rabbit 555	1:750	A31556
GABA <sub>A</sub> γ2	Gp	1:3000	(Fujiyama et al., 2000)	Anti-guinea-pig 488	1:750	A11073
GABA <sub>A</sub> α2	Gp	1:250	Synaptic System, 224104	Anti-guinea-pig 488	1:750	A11073
GABA <sub>A</sub> γ2	Rb	1:500	Synaptic System, 224003	Anti-rabbit 555	1:750	A31556
6xHis-tag	Ms	1:500	GeneTex 3H2201	Anti-mouse 555	1:750	A21422
VGAT	Rb	1:500	Synaptic System, 131013	Anti-rabbit 555	1:750	A31556
GAD-65	Ms	1:4000	Abcam, ab26113	Anti-mouse 555	1:750	A21422
MAP2	Ch	1:2500	Abcam, ab92434	Anti-chicken 647	1:750	A21469
Gephyrin	Ms	1:500	Synaptic System, 147111	Anti-mouse 405	1:750	A31553

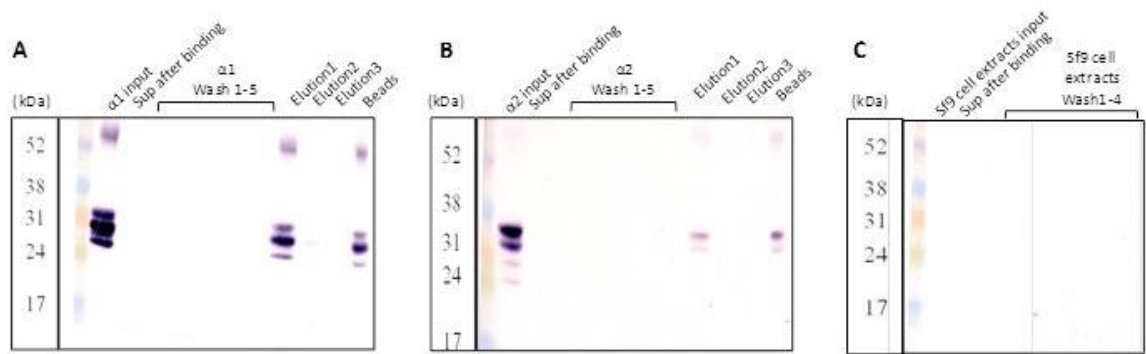
### 7.3 Results

GABA<sub>A</sub>Rs, the essential functional components of the inhibitory synapses in the brain, have recently been demonstrated to play a structural role during synapse formation by promoting the adhesion of inhibitory axon terminals (Fuchs et al., 2013). The aim of the present study was to investigate whether these synaptogenic effects may be mediated by the large N-terminal extracellular domains (ECDs) of GABA<sub>A</sub>Rs. Towards this aim, we have cloned and expressed the glycosylated N-terminal ECDs of the α1 and α2 subunits of GABA<sub>A</sub>Rs (α1 and α2 ECDs) using the Bac-to-Bac CT-TOPO expression system in Sf9 cells (see Chapter 3).

### 7.3.1 Purification of $\alpha 1$ and $\alpha 2$ ECDs under sterile condition

In the present chapter, we have established a protocol for the purification of these two proteins and confirmed that they were glycosylated proteins. In order to test whether these ECDs would affect the formation of synaptic contacts, we treated developing MSN cultures, at different time intervals, with the purified  $\alpha 1$  and  $\alpha 2$  ECDs. As the purified ECDs were added throughout the development of MSNs, these proteins had to be purified under sterile conditions. Therefore, we decided to use pre-stacked Ni-NTA columns and all the steps of purification of  $\alpha 1$ ,  $\alpha 2$  ECDs and control Sf9 cell extracts were carried out under sterile conditions. As we tried to purify these proteins in a sufficient amount, each step of the protocol was changed and optimised until the best extraction, binding and elution conditions were reached. One of the most important steps was to completely remove Triton X-100 from our samples to avoid lysis of cells and cell death. Once these steps were optimised, 5  $\mu\text{g}$  (0.38  $\mu\text{M}$ ) of the  $\alpha 1$ ,  $\alpha 2$  ECDs and control Sf9 cell extracts were added to the cell culture.

Figure 105 shows the protein distribution of  $\alpha 1$  and  $\alpha 2$  ECDs through purification after transferring onto a nitrocellulose membrane and immunoblotting with anti-Histidine Tag antibody. Both  $\alpha 1$  and  $\alpha 2$  ECDs were present in the input lane indicating that we were able to extract a considerable amount of proteins from Sf9 infected cells. Proteins were not detected in the supernatant after binding, indicating that the binding step was efficient and that the binding was within the binding capacity of the column. A significant amount of each protein was found in the first elution fraction indicating that bound proteins were efficiently eluted from the column at this step. However, some quantity of  $\alpha 1$  and  $\alpha 2$  ECDs was found bound to beads even after the third elution, indicating that this fraction was not efficiently removed from the column under these elution conditions.



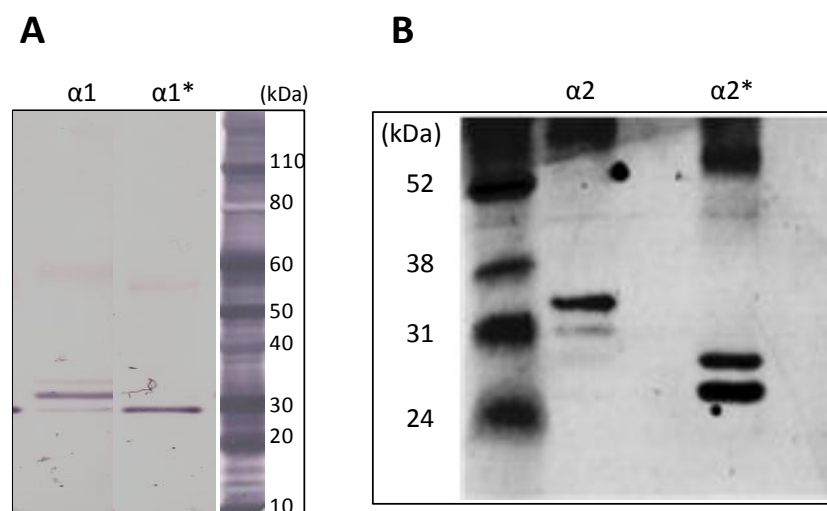
**Figure 105. The purification of extracellular domains of  $\alpha 1$  and  $\alpha 2$  subunits of GABA<sub>A</sub>Rs using Ni-NTA pre-stack columns.** Immunoblot analysis of fractions collected during the purification of  $\alpha 1$  and  $\alpha 2$  ECDs as Histidine-tagged proteins. Non-infected Sf9 cell extracts were used as a negative control throughout the experiment. Samples were collected throughout the purification and lysed with 2 % SDS. Total of 80  $\mu$ l of each sample was loaded on the SDS/PAGE and transferred onto the nitrocellulose membrane. The membranes were then incubated with a mouse anti-6xHis-tag antibody, followed by the incubation with the alkaline phosphatase-conjugated secondary antibody. **A.** Immunoblot showing the purification steps of  $\alpha 1$  ECDs. **B.** Immunoblot showing the purification steps of  $\alpha 2$  ECDs. The first lane represents the extracts of  $\alpha 1$ - or  $\alpha 2$ - baculovirus infected Sf9 cells. The second lane shows the supernatant after binding. The five next lanes represent the washing steps of the column after binding. The three next lanes represent the elution steps from the Ni-NTA column (E1-3). The last lane shows the remaining ECDs left bound to the beads after the last elution. **C.** Immunoblot showing the purification steps of non-infected Sf9 cell extracts. The first lane represents the extracts from non- infected Sf9 cells. The second lane shows the supernatant after binding. The four next lanes represent the washing steps of the column after binding with the extracts from non- infected Sf9 cells.

### 7.3.2 Deglycosylation of $\alpha 1$ and $\alpha 2$ ECDs

As observed previously, our purification experiments have revealed different molecular weight bands immunoreactive with the 6xHis-tag-specific and  $\alpha 1$  and  $\alpha 2$ -extracellular domains-specific antibodies. Sequence analysis using Uniprot Knowledgebase (UniprotKB) has suggested that the extracellular domains of  $\alpha 1$  and  $\alpha 2$  GABA<sub>A</sub>R subunits incorporate potential glycosylation sites for N-linked oligosaccharides (source for  $\alpha 1$  subunit: <http://www.uniprot.org/uniprot/P62812>; source for  $\alpha 2$  subunit: <http://www.uniprot.org/uniprot/P26048>). These two mouse sequences contained two or three glycosylation sites each:  $\alpha 1$  ECD could potentially be glycosylated on Asn 37 and Asn 137, while  $\alpha 2$  ECD could potentially be glycosylated on Asn 38 and Asn 138, and maybe Asn 114 (only found in the rat sequence so far). The deglycosylation experiments were performed using the glycoprotein deglycosylation kit from Millipore. This kit contains all enzymes and reagents needed to remove all N-linked and O-linked oligosaccharides from glycoproteins. The

deglycosylation was performed in denaturing conditions with 20  $\mu$ g of  $\alpha$ 1 and  $\alpha$ 2 ECDs, and samples were analysed using immunoblotting with anti- $\alpha$ 1 or  $\alpha$ 2 extracellular domains-specific antibodies.

Figure 106 shows the purified  $\alpha$ 1 and  $\alpha$ 2 ECDs incubated in absence or in presence of the deglycosylating enzymes. Both  $\alpha$ 1 and  $\alpha$ 2 ECDs are recognised by their specific antibodies, respectively, as indicated by the typical pattern of two or three bands detected in both immunoblots. In both cases, the pattern of bands changed after incubating the extracellular domains with deglycosylating enzymes, and the bands were detected at the lowest molecular weight. This shift to the lowest molecular weight observed after incubation indicated the efficient removal of glycosylation groups from purified  $\alpha$ 1 and  $\alpha$ 2 ECDs. In both  $\alpha$ 1 and  $\alpha$ 2 ECD immunoblots, the highest molecular weight band is likely to represent the isoform containing N-linked oligosaccharides at all the potential glycosylated sites, while the middle molecular weight band(s) is likely to represent the isoform(s) only partly glycosylated. Finally, the lowest bands of the two extracellular domains of  $\alpha$ 1 and  $\alpha$ 2 GABA<sub>A</sub>R subunits detected at the predicted molecular weight (between 26 and 27 kDa) likely represent the isoforms which were not glycosylated.



**Figure 106. The  $\alpha$ 1 and  $\alpha$ 2 ECD purified from infected Sf9 cells are glycosylated.** Immunoblot analysis following incubation of the purified  $\alpha$ 1 (A) or  $\alpha$ 2 ECDs (B) in absence or in presence of deglycosylating enzyme mix. After incubation, samples (20  $\mu$ g) were collected and loaded on the SDS/PAGE and transferred onto the nitrocellulose membranes. The membranes were then incubated with anti-histidine tag specific antibody, followed by the incubation with the



alkaline phosphatase-conjugated secondary antibodies. Representative blots from two independent experiments.

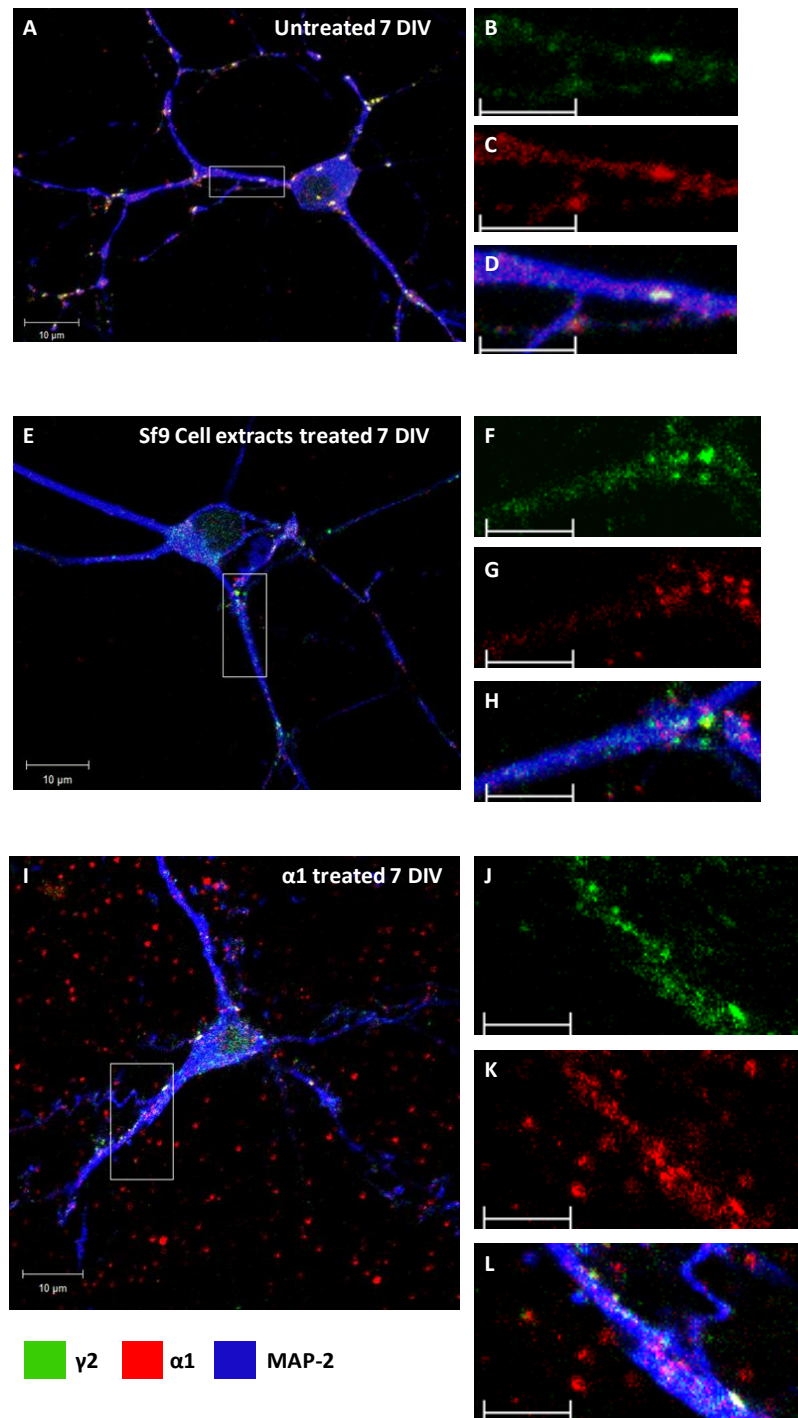
### **7.3.3 Treatment of 4-7 DIV MSN cultures with purified $\alpha 1$ or $\alpha 2$ ECDs**

#### *7.3.3.1 Treatment of MSN cultures with $\alpha 1$ or $\alpha 2$ ECDs from 4 to 7 DIV revealed that the exogenous proteins adhere to the neuronal cell surface*

We have demonstrated that we were able to purify glycosylated  $\alpha 1$  and  $\alpha 2$  ECDs by affinity chromatography using Ni-NTA resin columns. Our next aim was to investigate how the addition of these proteins to the MSN in culture affects the formation of GABAergic synapses. We have decided to test this by adding 5  $\mu\text{g}$  of the purified proteins to cultured MSNs from 4 to 7 DIV. Subsequently, synapse formation was analysed using immunocytochemistry and confocal imaging.

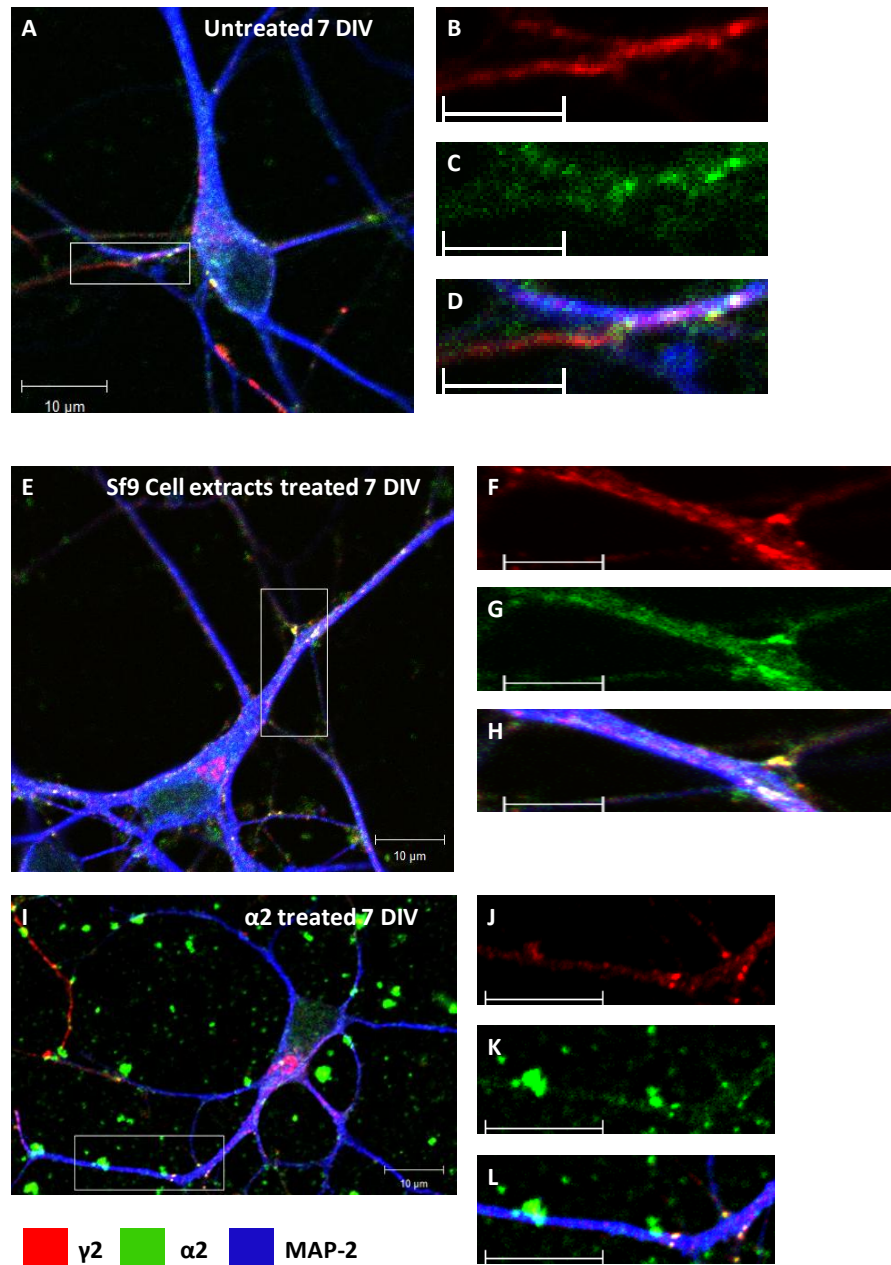
Figure 107 shows an example of each of i) untreated 7 DIV neurones (A-D), ii) neurones treated from 4 to 7 DIV with control Sf9 cell extracts (E-H), and iii) neurones treated with the  $\alpha 1$  ECDs (I-L). After fixation, these neurones were stained with the rabbit anti- $\alpha 1$  extracellular domain and guinea-pig anti- $\gamma 2$  extracellular domain specific antibodies. After permeabilisation, they were incubated with the chicken anti-MAP2 specific antibody. Similarly, Figure 108 shows an example of each of i) untreated 7 DIV neurones (A-D), ii) neurones treated from 4 to 7 DIV with the control Sf9 cell extracts (E-H), and iii) neurones treated with the  $\alpha 2$  ECDs (I-L). After fixation, these neurones were stained with the guinea-pig anti- $\alpha 2$  extracellular domain and rabbit anti- $\gamma 2$  extracellular domain specific antibodies. After permeabilisation, they were incubated with the chicken anti- MAP2 specific antibody (see Table 28 for details). Figure 109 shows an example of each of i) 7 DIV neurones treated from 4 to 7 DIV with control Sf9 cell extracts (A-E), ii) neurones treated from 4 to 7 DIV with  $\alpha 1$  ECDs (F-J), and iii) neurones treated from 4 to 7 DIV with  $\alpha 2$  ECDs (K-O). After fixation, these neurones were stained with the mouse anti-6xHis-tag proteins and guinea-pig anti- $\gamma 2$  extracellular domain specific antibodies. After permeabilisation, they were incubated with the chicken anti-MAP2 and rabbit anti-VGAT specific antibodies (see Table 26 for

details). The adhesion of the exogenous  $\alpha 1$  and  $\alpha 2$  ECDs to the cell surface of MSNs was visualised using confocal microscopy after immunolabelling with the N-terminal specific antibodies. The added proteins were present in the extracellular space and also on the surface of cultured neurones, but with this antibody combinations, they were not distinguishable from the endogenous subunit of receptors (Figure 107 and 108). To visualise the localisation of the exogenous  $\alpha 1$  and  $\alpha 2$  ECDs, we decided to stain neurones with the anti-6xHis-tagged proteins together with anti- $\gamma 2$  extracellular domain specific antibodies (Figure 110). This immunolabelling confirmed that the exogenous ECDs adhered to the cell surface of MSNs and were also sparsely distributed in the extracellular space.

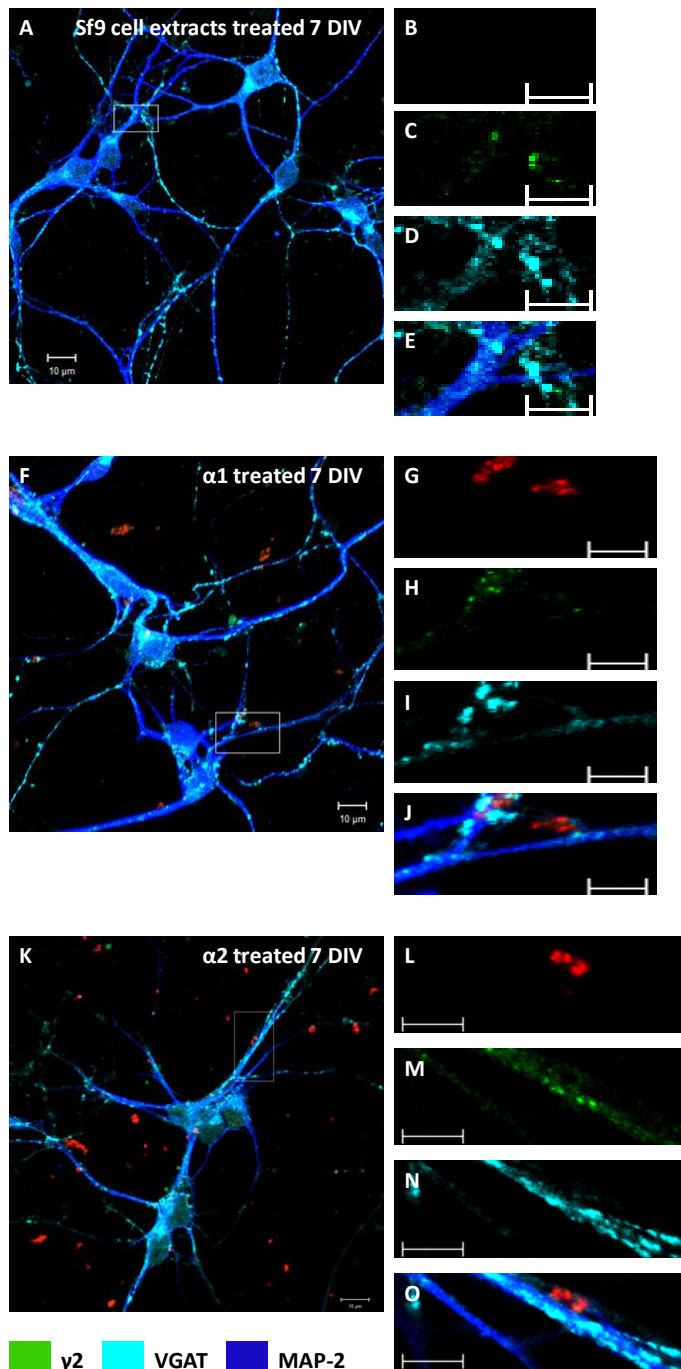


**Figure 107. The exogenous  $\alpha 1$  ECDs adhere to the cell surface of MSNs treated from 4 to 7 DIV but are not distinguishable from endogenous  $\alpha 1$ -containing  $GABA_A$ Rs.** Immunolabelling of  $GABA_A$ Rs containing the  $\gamma 2$  subunit (green) and the  $\alpha 1$  subunit (red) at the cell surface of cultured MSNs. Somatodendritic compartment is labelled with the MAP2 antibody (blue). **A.** Merged image of a 7 DIV MSN untreated (scale bar=10  $\mu$ m). **B.** Enlarged image of the boxed region in A representing  $\gamma 2$  staining only. **C.** Enlarged image of the boxed region in A representing  $\alpha 1$  staining only. **D.** Enlarged image of the boxed region in A showing all the three channels (scale bar=5  $\mu$ m). **E.** Merged image of a 7 DIV MSN treated with control Sf9 cell extracts (scale bar=10  $\mu$ m). **F.** Enlarged image of the boxed region in E representing  $\gamma 2$  staining only. **G.** Enlarged image of the boxed region in E representing  $\alpha 1$  staining only. **H.** Enlarged image of the boxed region in E showing all the three channels (scale bar=5  $\mu$ m). **I.** Merged image of a 7 DIV MSN treated with the  $\alpha 1$  ECDs (scale bar=10  $\mu$ m). **J.** Enlarged image of the boxed region in I representing  $\gamma 2$  staining only. **K.** Enlarged image of the boxed region in I

representing  $\alpha 1$  staining only. L. Enlarged image of the boxed region in I representing all the three channels (scale bar=5  $\mu\text{m}$ ).



**Figure 108. The exogenous  $\alpha 2$  ECDs adhere to the cell surface of MSNs treated from 4 to 7 DIV but are not distinguishable from endogenous  $\alpha 2$ - containing GABA<sub>A</sub>Rs.** Immunolabelling of GABA<sub>A</sub>Rs containing the  $\gamma 2$  subunit (red) and the  $\alpha 2$  subunit (green) at the cell surface of cultured MSNs. Somatodendritic compartment is labelled with the MAP2 antibody (blue). **A.** Merged image of a 7 DIV MSN untreated (scale bar=10  $\mu\text{m}$ ). **B.** Enlarged image of the boxed region in A representing  $\gamma 2$  staining only. **C.** Enlarged image of the boxed region in A representing  $\alpha 2$  staining only. **D.** Enlarged image of the boxed region in A showing all the three channels (scale bar=5  $\mu\text{m}$ ). **E.** Merged image of a 7 DIV MSN treated with control Sf9 cell extracts (scale bar=10  $\mu\text{m}$ ). **F.** Enlarged image of the boxed region in E representing  $\gamma 2$  staining only. **G.** Enlarged image of the boxed region in E representing  $\alpha 2$  staining only. **H.** Enlarged image of the boxed region in E showing all the three channels (scale bar=5  $\mu\text{m}$ ). **I.** Merged image of a 7 DIV MSN treated with the  $\alpha 2$  ECDs (scale bar=10  $\mu\text{m}$ ). **J.** Enlarged image of the boxed region in I representing  $\gamma 2$  staining only. **K.** Enlarged image of the boxed region in I representing  $\alpha 2$  staining only. **L.** Enlarged image of the boxed region in I representing all the three channels (scale bar=5  $\mu\text{m}$ ).



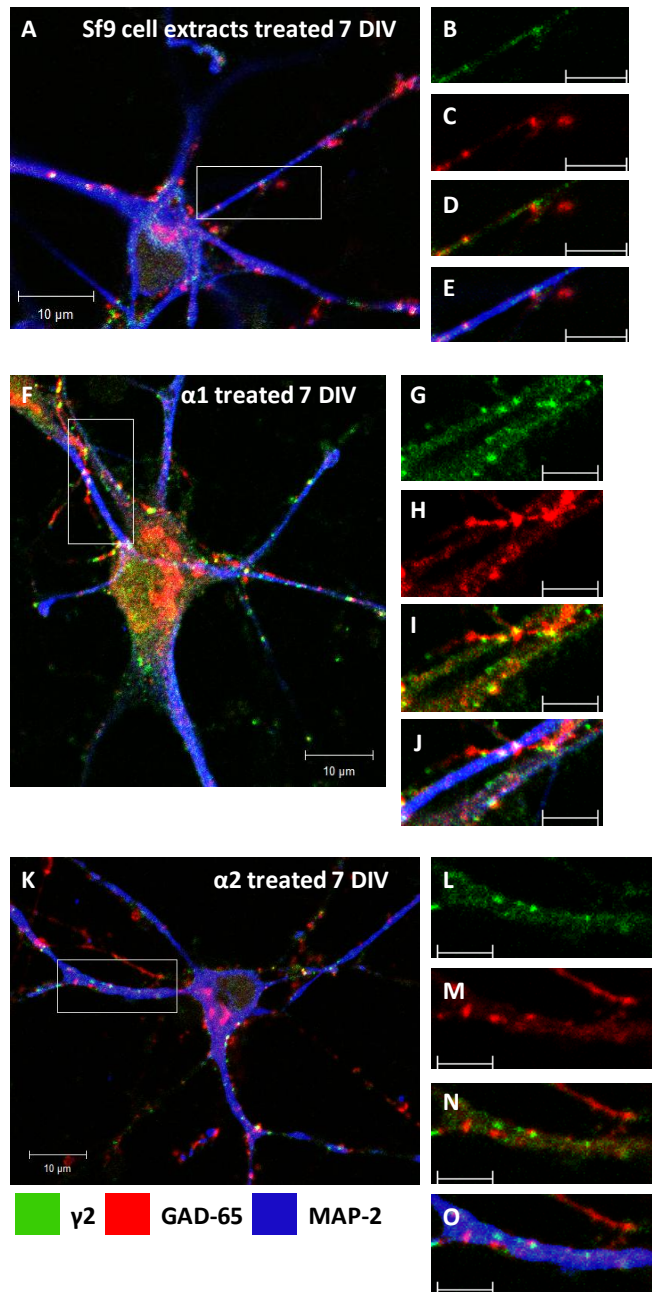
**Figure 109.** The histidine-tagged  $\alpha 1$  and  $\alpha 2$  ECDs adhere to the cell surface of medium spiny neurones treated from 4 to 7 DIV. Immunolabelling of the exogenous  $\alpha 1$  and  $\alpha 2$  ECDs using 6xHis-tag antibody (red),  $\gamma 2$ -containing GABA<sub>A</sub>Rs (green) and the VGAT positive presynaptic terminals (cyan). The somatodendritic tree is labelled with the MAP2 antibody (blue). **A.** Merged image of a 7 DIV MSN treated with control Sf9 cell extracts (scale bar=10  $\mu$ m). **B.** Enlarged image of the boxed region in A representing 6xHis-tag proteins staining only. **C.** Enlarged image of the boxed region in A representing  $\gamma 2$  staining only. **D.** Enlarged image of the boxed region in A representing VGAT staining only. **E.** Enlarged image of the boxed region in A representing all three channels (scale bar=5  $\mu$ m). **F.** Merged image of a 7 DIV MSN treated with the  $\alpha 1$  ECDs (scale bar=10  $\mu$ m). **G.** Enlarged image of the boxed region in F representing 6xHis-tag proteins staining only. **H.** Enlarged image of the boxed region in F representing  $\gamma 2$  staining only. **I.** Enlarged image of the boxed region in F representing VGAT staining only. **J.** Enlarged image of the boxed region in F representing all the three channels (scale bar=5  $\mu$ m). **K.** Merged image of a 7 DIV MSN treated with the  $\alpha 2$  ECDs (scale bar=10  $\mu$ m). **L.** Enlarged image of the boxed region in K representing 6xHis-tag proteins staining only. **M.** Enlarged

image of the boxed region in K representing  $\gamma 2$  staining only. **N.** Enlarged image of the boxed region in K representing VGAT staining only. **O.** Enlarged image of the boxed region in K representing all the three channels (scale bar=5  $\mu\text{m}$ ).

**7.3.3.2**      *The total density of  $\gamma 2$ -containing GABA<sub>A</sub>Rs per dendrite of MSNs is increased after the treatment with  $\alpha 1$  or  $\alpha 2$  ECDs from 4 to 7 DIV*

It has been established that the  $\gamma 2$  subunit is mostly found at synaptic contacts (Somogyi et al., 1996). To test if the addition of  $\alpha 1$  or  $\alpha 2$  ECDs affects the formation of synapses, developing MSNs were treated with the control Sf9 cell extracts,  $\alpha 1$  ECDs or  $\alpha 2$  ECDs from 4 to 7 DIV, fixed and immunolabelled with  $\gamma 2$ -, GAD-65- and MAP2-specific antibodies (Figure 110). The properties of  $\gamma 2$ -containing GABA<sub>A</sub>R clusters, i.e. the total density and the size, were analysed using confocal imaging.

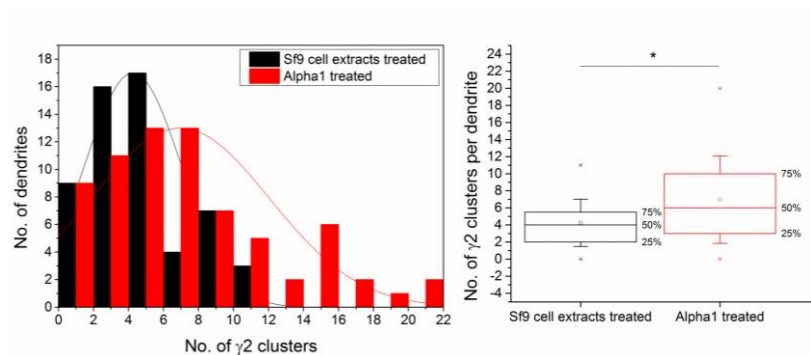




**Figure 110. The density and the size of  $\gamma 2$ -containing  $GABA_A$ R clusters are increased after the treatment of MSNs with the  $\alpha 1$  or  $\alpha 2$  ECDs from 4 to 7 DIV.** Immunolabelling of  $GABA_A$ Rs containing the  $\gamma 2$  subunit (green) and of the presynaptic terminals containing GAD-65 (red) along the primary dendrites of cultured MSNs stained for MAP2 (blue). **A.** Merged image of a 7 DIV striatal neurone treated with control Sf9 cell extracts (scale bar=10  $\mu$ m). **B.** Enlarged image of the boxed region in A representing  $\gamma 2$  staining only. **C.** Enlarge image of boxed region in A representing GAD-65 staining only. **D.** Enlarged image of the boxed region in A representing  $\gamma 2$  and GAD-65 staining. **E.** Enlarged image of the boxed region in A showing all the three channels (scale bar=5  $\mu$ m). **F.** Merged image of a 7 DIV striatal neurone treated with  $\alpha 1$  ECD (scale bar=10 $\mu$ m). **G.** Enlarged image of the boxed region in F representing  $\gamma 2$  staining only. **H.** Enlarged image of the boxed region in F representing GAD-65 staining only. **I.** Enlarged image of the boxed region in F representing  $\gamma 2$  and GAD-65 staining. **J.** Enlarged image of the boxed region in F showing all the three channels (scale bar= 5 $\mu$ m). **K.** Merged image of a 7 DIV striatal neurone treated with the  $\alpha 2$  ECDs (scale bar= 10 $\mu$ m). **L.** Enlarged image of the boxed region in K representing  $\gamma 2$  staining only. **M.** Enlarged image of the boxed region in K representing GAD-65 staining only. **N.** Enlarged image of the boxed region in K representing  $\gamma 2$

and GAD-65 staining. **O**. Enlarged image of the boxed region in K showing all the three channels (scale bar=5 $\mu$ m).

The density of  $\gamma$ 2- containing GABA<sub>A</sub>R clusters was estimated per defined length of primary dendrite (the first 20  $\mu$ m from the cell body) after treatment with the control Sf9 cell extracts or  $\alpha$ 1 ECDs from 4 to 7 DIV (Figure 111). The median density of  $\gamma$ 2 clusters was 4 (5.75-2) with the control Sf9 cell extracts treatment, compared to 6 (10-3) with the  $\alpha$ 1 ECD treatment ( $p$  value=0.003, Mann-Whitney test;  $n$ =56 dendrites, and  $n$ =71 dendrites, respectively). This demonstrates that the total density of  $\gamma$ 2 clusters is increased by the treatment, indicating that the exogenous  $\alpha$ 1 ECDs promote either the insertion of the  $\gamma$ 2 subunit-containing GABA<sub>A</sub>Rs or their clustering, or both, at this developmental stage.

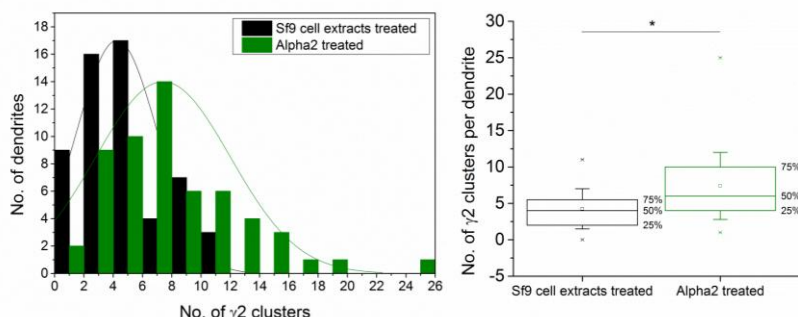


**Figure 111. The density of  $\gamma$ 2-containing GABA<sub>A</sub>R clusters per primary dendrite of MSNs is increased by the treatment with  $\alpha$ 1 ECDs from 4 to 7 DIV.** The density of  $\gamma$ 2-containing GABA<sub>A</sub>R clusters along the first 20  $\mu$ m of primary dendrites was counted in MSN cultures in the presence of control Sf9 cell extracts or  $\alpha$ 1 ECDs from 4 to 7 DIV. **A**. Histogram shows the distribution of  $\gamma$ 2 cluster densities per dendrite in the presence of control Sf9 cell extracts or  $\alpha$ 1 ECDs ( $n$ =56 and  $n$ =71 dendrites, respectively, from two independent experiments). **B**. Box plot displays the median density (50 % of the population) of  $\gamma$ 2 clusters in the presence of control Sf9 cell extracts or  $\alpha$ 1 ECDs. Statistical analysis was performed using Mann-Whitney test: \* corresponds to  $p < 0.05$ .

The density of  $\gamma$ 2-containing GABA<sub>A</sub>R clusters was estimated per defined length of primary dendrite (the first 20  $\mu$ m from the cell body) after the treatment with the control Sf9 cell extracts or  $\alpha$ 2 ECDs from 4 to 7 DIV (Figure 112). The median density of  $\gamma$ 2 clusters was 4 (5.75-2) with the control Sf9 cell extracts treatment, compared to 6 (10-4) with the  $\alpha$ 2 ECDs treatment ( $p$  value= $4.21 \times 10^{-5}$ , Mann-Whitney test;  $n$ =56 dendrites, and  $n$ =57 dendrites, respectively). This demonstrates that the total density of  $\gamma$ 2



clusters is increased by the treatment, indicating that the exogenous  $\alpha 2$  ECDs promote either the insertion of the  $\gamma 2$  subunit-containing GABA<sub>A</sub>Rs or their clustering, or both, at this developmental stage.



**Figure 112. The density of  $\gamma 2$ -containing GABA<sub>A</sub>R clusters per primary dendrite of MSNs is increased by the treatment with  $\alpha 2$  ECDs from 4 to 7 DIV.** The density of  $\gamma 2$ -containing GABA<sub>A</sub>R clusters along the first 20  $\mu\text{m}$  of primary dendrites was counted in MSN cultures in the presence of control Sf9 cell extracts or  $\alpha 2$  ECDs from 4 to 7 DIV. **A.** Histogram shows the distribution of  $\gamma 2$  cluster densities per dendrite in the presence of Sf9 cell extracts or  $\alpha 2$  ECDs ( $n=56$  and  $n=57$  dendrites, respectively, from two independent experiments). **B.** Box plot displays the median density (50 % of the population) of  $\gamma 2$  clusters in the presence of Sf9 cell extracts or  $\alpha 2$  ECDs. Statistical analysis was performed using Mann-Whitney test: \* corresponds to  $p < 0.05$ .

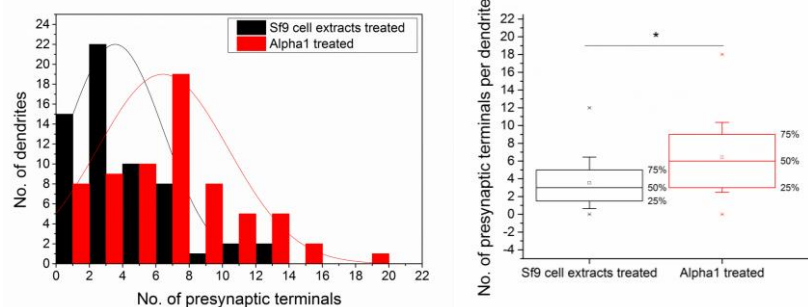
**Table 29. The density of  $\gamma 2$ -containing GABA<sub>A</sub>R clusters per primary dendrite of MSN is increased by the  $\alpha 1$  or  $\alpha 2$  ECD treatments from 4 to 7 DIV**

	Density of $\gamma 2$ clusters at 7 DIV	P < 0.05
Sf9 cell extracts- Vs. $\alpha 1$ -treated neurones	↗	Yes
Sf9 cell extracts- Vs. $\alpha 2$ -treated neurones	↗	Yes

### 7.3.3.3 *The connectivity between MSNs is increased by the $\alpha 1$ or $\alpha 2$ ECD treatments from 4 to 7 DIV*

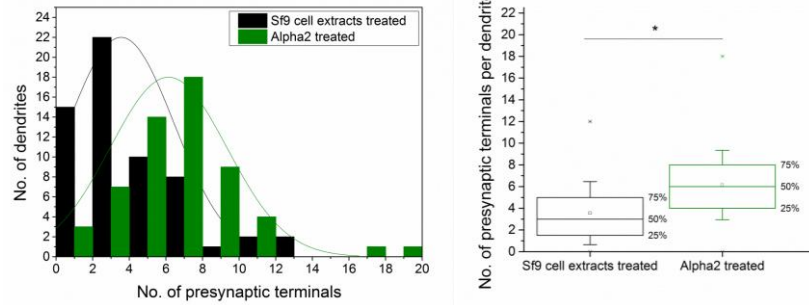
To investigate further the structural role of GABA<sub>A</sub>Rs in GABAergic synapse formation, we applied extracellular domains of  $\alpha 1$  or  $\alpha 2$  subunits of GABA<sub>A</sub>Rs to MSN cultures from 4 to 7 DIV and estimated if the exogenous ECDs affect the density of presynaptic terminals forming contacts with the primary dendrites in these cultures. The total density of GAD-65 positive terminals per defined length of primary dendrite (the

first 20  $\mu\text{m}$  from the cell body) was estimated after the treatment with control Sf9 cell extracts or  $\alpha 1$  ECDs from 4 to 7 DIV (Figure 113). After the control Sf9 cell extracts treatment, the median density of presynaptic terminals was 3 (5 - 1.25) compared to 6 (9 - 3) after the treatment with  $\alpha 1$  ECDs (p value =  $5.34 \times 10^{-6}$ , Mann-Whitney test; n=60 dendrites, and n=67 dendrites, respectively). This indicates that the density of presynaptic contacts per 20  $\mu\text{m}$  primary dendrite is increased by the treatment with  $\alpha 1$  ECDs from 4 to 7 DIV, indicating that the connectivity between MSNs could be regulated by  $\alpha 1$  ECDs early in development.



**Figure 113. The density of presynaptic terminals per primary dendrite of MSNs is increased after the  $\alpha 1$  ECD treatments from 4 to 7 DIV.** The density of presynaptic terminals along the first 20  $\mu\text{m}$  of primary dendrites was counted in MSN cultures after the treatment with control Sf9 cell extracts or  $\alpha 1$  ECDs from 4 to 7 DIV. **A.** Histogram shows the distribution of the density of presynaptic inputs after the treatment with control Sf9 cell extracts or  $\alpha 1$  ECDs (n=60 and n=67 dendrites, respectively, from two independent experiments). **B.** Box plot displays the median density of presynaptic terminals after the treatment with control Sf9 cell extracts or  $\alpha 1$  ECDs. Statistical analysis was performed using Mann-Whitney test: \* corresponds to p<0.05.

The total density of GAD-65 positive terminals per defined length of primary dendrite (the first 20  $\mu\text{m}$  from the cell body) was estimated after the treatment with control Sf9 cell extracts or  $\alpha 2$  ECDs from 4 to 7 DIV (Figure 114). After the Sf9 cell extracts treatment, the median density of presynaptic terminals was 3 (5 - 1.25) compared to 6 (8 - 4) after the treatment with  $\alpha 2$  ECDs (p value =  $1.72 \times 10^{-6}$ , Mann-Whitney test; n=60 dendrites, and n=57 dendrites, respectively). This indicates that the density of presynaptic contacts per dendrite is increased by the treatment with  $\alpha 2$  ECDs from 4 to 7 DIV, indicating that the connectivity between MSNs could be regulated by  $\alpha 2$  ECDs early in development.

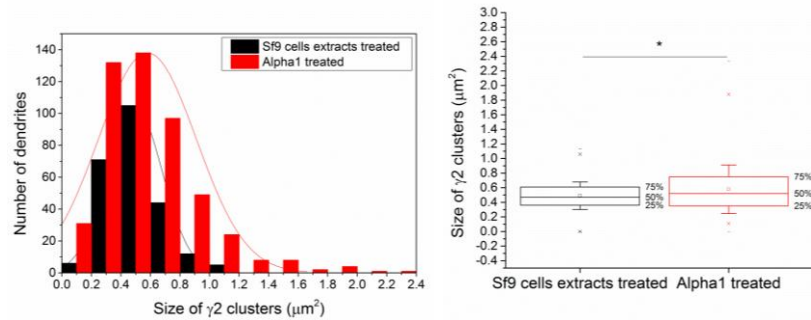


**Figure 114. The density of presynaptic terminals per primary dendrite of MSNs is increased after the  $\alpha 2$  ECD treatments from 4 to 7 DIV.**

The density of presynaptic terminals along the first 20  $\mu\text{m}$  of primary dendrites was counted in MSN cultures after the treatment with control Sf9 cell extracts or  $\alpha 2$  ECDs from 4 to 7 DIV. **A.** Histogram shows the distribution of the density of presynaptic inputs after the treatment with control Sf9 cell extracts or  $\alpha 2$  ECDs ( $n=60$  and  $n=57$  dendrites, respectively, from two independent experiments). **B.** Box plot displays the median density of presynaptic terminals after the treatment with control Sf9 cell extracts or  $\alpha 2$  ECDs. Statistical analysis was performed using Mann-Whitney test: \* corresponds to  $p < 0.05$ .

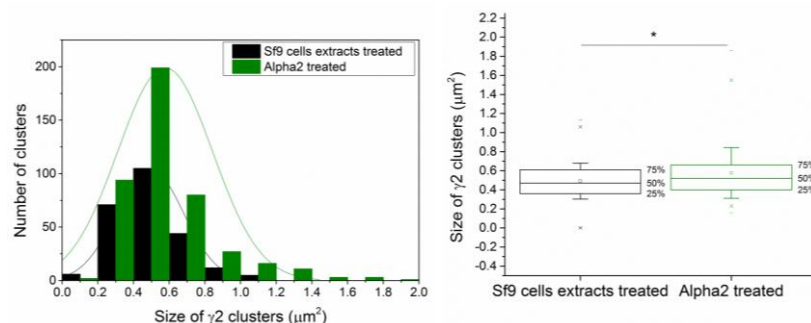
#### 7.3.3.4 *The size of $\gamma 2$ -containing GABA<sub>A</sub>Rs is increased after the treatment with $\alpha 1$ or $\alpha 2$ ECDs from 4 to 7 DIV*

We estimated whether the addition of the  $\alpha 1$  or  $\alpha 2$  ECDs affects the size of the  $\gamma 2$ -containing GABA<sub>A</sub>R clusters in MSNs treated from 4 to 7 DIV. The size of  $\gamma 2$ -containing GABA<sub>A</sub>R clusters per defined length of primary dendrite (the first 20  $\mu\text{m}$  from the cell body) was estimated after the treatment with control Sf9 cell extracts or  $\alpha 1$  ECDs from 4 to 7 DIV (Figure 115). After the treatment with control Sf9 cell extracts, the median size of  $\gamma 2$  clusters was 0.47 (0.61 - 0.36)  $\mu\text{m}^2$  compared to 0.52 (0.75 - 0.35)  $\mu\text{m}^2$  with  $\alpha 1$  ECDs ( $p$  value=0.01, Mann-Whitney test;  $n=243$  clusters, and  $n=495$  clusters, respectively). This demonstrates that the size of  $\gamma 2$ -containing GABA<sub>A</sub>R clusters is increased by the treatment with  $\alpha 1$  ECDs from 4 to 7 DIV. This suggests that at this early stage of development, the exogenous  $\alpha 1$  ECDs could promote the clustering of synaptic GABA<sub>A</sub>Rs.



**Figure 115. The size of  $\gamma_2$ -containing GABA<sub>A</sub>R clusters is increased by the treatment with  $\alpha_1$  ECDs from 4 to 7 DIV.** The size of  $\gamma_2$ -containing GABA<sub>A</sub>R clusters along the first 20  $\mu\text{m}$  of primary dendrites was measured in MSN cultures after the treatment with control Sf9 cell extracts or  $\alpha_1$  ECDs from 4 to 7 DIV. **A.** Histogram shows the distribution of sizes of  $\gamma_2$  clusters per dendrite after the treatment with control Sf9 cell extracts or  $\alpha_1$  ECDs (n=243 and n=495 clusters, respectively, from two independent experiments). **B.** Box plot displays the median size (50 % of the population) of  $\gamma_2$  clusters after the treatment with control Sf9 cell extracts or  $\alpha_1$  ECDs. Statistical analysis was performed using Mann-Whitney test: \* corresponds to  $p < 0.05$ .

The size of  $\gamma_2$ -containing GABA<sub>A</sub>R clusters per defined length of primary dendrite (the first 20  $\mu\text{m}$  from the cell body) was estimated after the treatment with control Sf9 cell extracts or  $\alpha_2$  ECD from 4 to 7 DIV (Figure 116). After the treatment with control Sf9 cell extracts, the median size of  $\gamma_2$  clusters was 0.47 (0.61 - 0.36)  $\mu\text{m}^2$  compared to 0.52 (0.66 - 0.40)  $\mu\text{m}^2$  with  $\alpha_2$  ECDs ( $p$  value= $4.35 \times 10^{-4}$ , Mann-Whitney test; n=243 clusters, and n=436 clusters, respectively). This demonstrates that the size of  $\gamma_2$ -containing GABA<sub>A</sub>R clusters is increased by the treatment with  $\alpha_2$  ECDs from 4 to 7 DIV. This suggests that at this early stage of development, the exogenous  $\alpha_2$  ECDs could promote the clustering of synaptic GABA<sub>A</sub>Rs.



**Figure 116. The size of  $\gamma_2$ -containing GABA<sub>A</sub>R clusters is increased by the treatment with  $\alpha_2$  ECDs from 4 to 7 DIV.** The size of  $\gamma_2$ -containing GABA<sub>A</sub>R clusters along the first 20  $\mu\text{m}$  of primary dendrites was measured in MSN cultures after the treatment with the control Sf9 cell extracts or  $\alpha_2$  ECDs from 4 to 7 DIV. **A.** Histogram shows the distribution of sizes of  $\gamma_2$  clusters per dendrite after the treatment with control Sf9 cell extracts or  $\alpha_2$  ECDs (n=243 and n=436 clusters, respectively, from two independent experiments). **B.** Box plot displays the median size (50 % of the population) of  $\gamma_2$  clusters after the treatment with control Sf9 cell extracts or  $\alpha_2$  ECDs. Statistical analysis was performed using Mann-Whitney test: \* corresponds to  $p < 0.05$ .

**Table 30. The size of  $\gamma 2$ -containing GABA<sub>A</sub>R clusters per primary dendrite of MSN is increased by the treatment with  $\alpha 1$  or  $\alpha 2$  ECDs from 4 to 7 DIV**

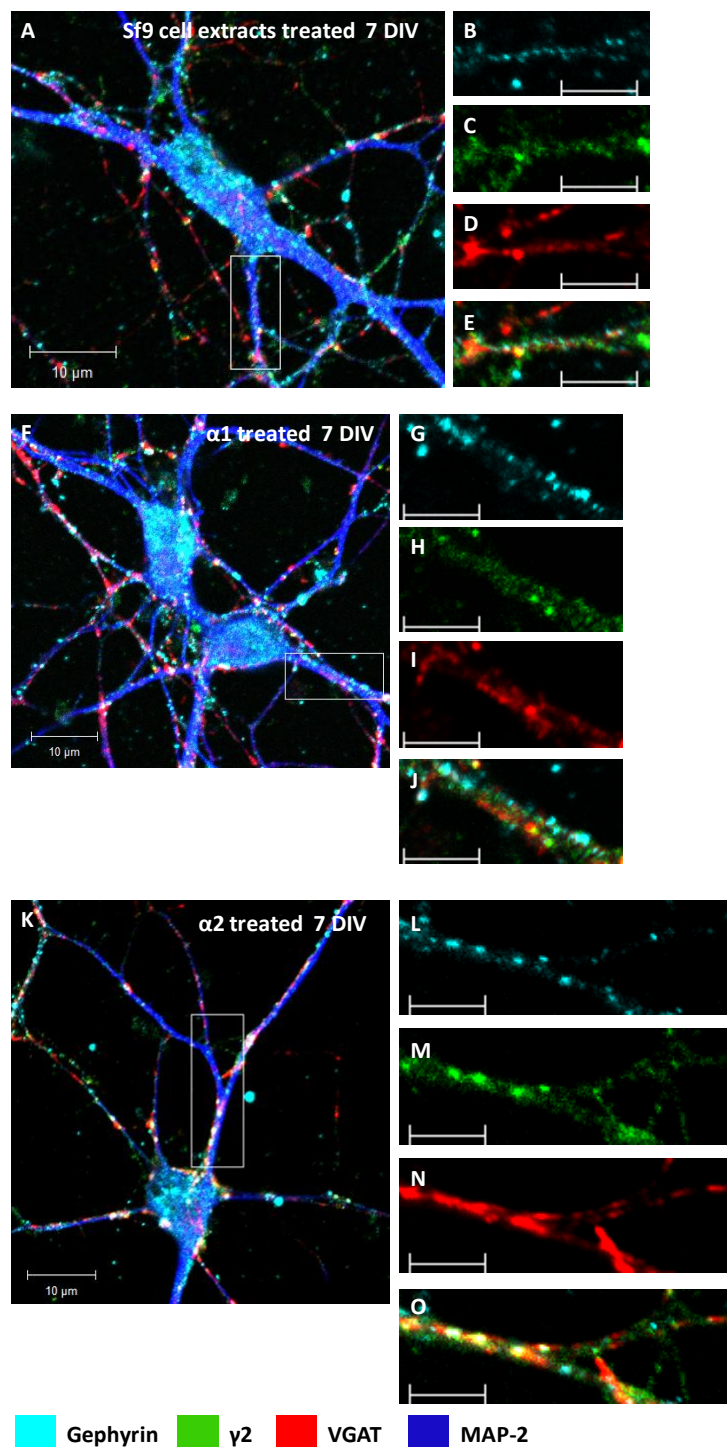
	Size of $\gamma 2$ clusters at 7 DIV	P < 0.05
Sf9 cell extracts- Vs. $\alpha 1$ -treated neurones	↗	Yes
Sf9 cell extracts- Vs. $\alpha 2$ -treated neurones	↗	Yes

### 7.3.3.5 Analysis of gephyrin clusters in MSN following the treatments with $\alpha 1$ or $\alpha 2$ ECDs from 4 to 7 DIV

It has been established that, together with the  $\gamma 2$  subunit, the scaffolding protein gephyrin clusters contributes to the anchoring of GABA<sub>A</sub>Rs at inhibitory synapses (Essrich et al., 1998, Jacob et al., 2005). In cultured neurones, it has been shown that this protein facilitated  $\alpha 2$ -containing GABA<sub>A</sub>R clustering by a direct interaction with a 10 amino acid sequence in the cytoplasmic loop of the  $\alpha 2$  subunit (Tretter et al., 2008).

In the present chapter, we were interested to establish whether the treatment with  $\alpha 1$  or  $\alpha 2$  ECDs would alter gephyrin clustering process during GABAergic synapse formation. Therefore, we decided to perform immunolabelling with the gephyrin specific antibody in MSN cultures treated with the control Sf9 cell extracts,  $\alpha 1$  or  $\alpha 2$  ECDs. Developing MSNs treated with the control Sf9 cell extracts,  $\alpha 1$  ECDs or  $\alpha 2$  ECDs from 4 to 7 DIV were immunolabelled with the mouse anti-gephyrin, rabbit anti-VGAT, guinea-pig anti- $\gamma 2$  and chicken anti-MAP2 specific antibodies. Changes in the density and size of gephyrin clusters were analysed by confocal microscopy (Figure 117).

From this preliminary experiment, gephyrin clusters appeared to increase in both the size and the density after the treatment with  $\alpha 1$  ECDs or  $\alpha 2$  ECDs compared to Sf9 cell extracts treatment from 4 to 7 DIV. This would be consistent with the observed changes in the  $\gamma 2$ -containing GABA<sub>A</sub>R clusters after treatment. However, statistical analysis must be performed to confirm these results.



**Figure 117.** The density and the size of gephyrin clusters appear to be increased after the treatment of MSN cultures with the  $\alpha 1$  or  $\alpha 2$  ECDs from 4 to 7 DIV. Immunolabelling of gephyrin (cyan),  $\gamma 2$  subunit (green) and the presynaptic marker VGAT (red). The somatodendritic compartment is labelled with the MAP2 antibody (blue). **A.** Merged image of a 7 DIV striatal neurone treated with the control Sf9 cell extracts (scale bar=10 $\mu$ m). **B.** Enlarged image of the boxed region in A representing gephyrin staining only. **C.** Enlarge image of boxed region in A representing  $\gamma 2$  staining only. **D.** Enlarged image of the boxed region in A representing VGAT staining only. **E.** Enlarged image of the boxed region in A showing all the three channels (scale bar=5 $\mu$ m). **F.** Merged image of a 7 DIV striatal neurone treated with the  $\alpha 1$  ECDs (scale bar=10 $\mu$ m). **G.** Enlarged image of the boxed region in F representing gephyrin staining only. **H.** Enlarged image of the boxed region in F representing  $\gamma 2$  staining only. **I.** Enlarged image of the boxed region in F representing VGAT staining. **J.** Enlarged image of the boxed region in F showing all the three channels (scale bar=5 $\mu$ m). **K.** Merged image of a 7 DIV

MSN treated with the  $\alpha 2$  ECDs (scale bar=10 $\mu$ m). **L.** Enlarged image of the boxed region in K representing gephyrin staining only. **M.** Enlarged image of the boxed region in K representing  $\gamma 2$  staining only. **N.** Enlarged image of the boxed region in K representing VGAT staining. **O.** Enlarged image of the boxed region in K showing all the three channels (scale bar=5 $\mu$ m).

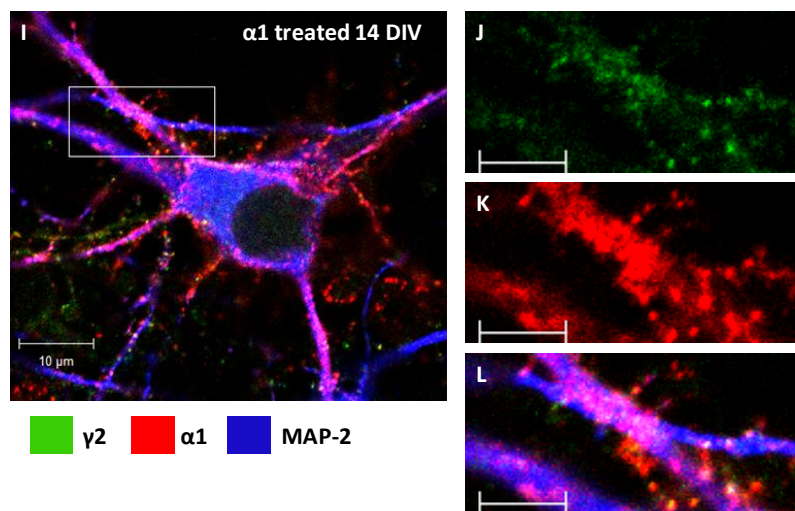
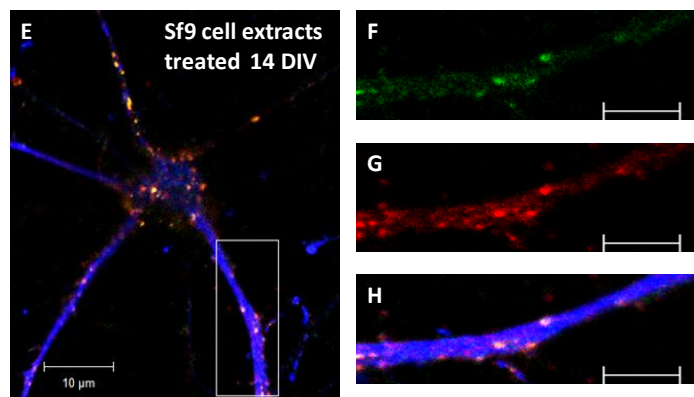
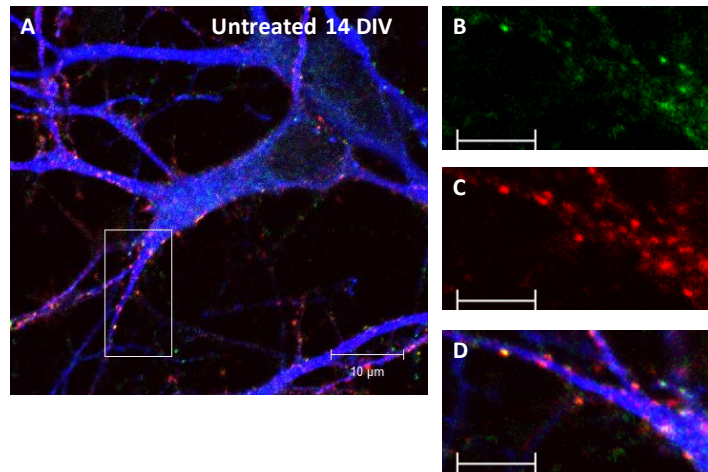
### **7.3.4 Treatment of 7-14 DIV MSN cultures with purified $\alpha 1$ or $\alpha 2$ ECDs**

*7.3.4.1 The treatment of MSN cultures with purified  $\alpha 1$  or  $\alpha 2$  ECDs from 7 to 14 DIV revealed that the exogenous proteins are adhering to the neuronal cell surface*

In parallel to our previous study in which the effect of the treatment of MSN cultures with  $\alpha 1$  ECDs or  $\alpha 2$  ECDs was established at early developmental stages, we have decided to test the effects of the addition of 5  $\mu$ g of the purified proteins to MSNs starting from 7 to 14 DIV. Subsequently, synapse formation was analysed using immunocytochemistry and confocal imaging. Figure 118 shows an example of each of i) untreated 14 DIV neurones (A-D), ii) neurones treated from 7 to 14 DIV with control Sf9 cell extracts (E-H), and iii) neurones treated with the  $\alpha 1$  ECDs (I-L). After fixation, these neurones were stained with the rabbit anti-  $\alpha 1$  subunit and guinea-pig anti- $\gamma 2$  subunit specific antibodies. After permeabilisation, they were incubated with chicken anti-MAP2 specific antibody. Similarly, Figure 119 shows an example of i) untreated 14 DIV neurones (A-D), ii) neurones treated from 7 to 14 DIV with control Sf9 cell extracts (E-H), and iii) neurones treated with the  $\alpha 2$  ECDs (I-L). After fixation, these neurones were stained with the guinea-pig anti- $\alpha 2$  and rabbit anti- $\gamma 2$  specific antibodies. After permeabilisation, they were incubated with the chicken anti-MAP2 specific antibody (see Table 26 for details). Figure 120 shows an example of each of i) 14 DIV neurones treated from 7 to 14 DIV with control Sf9 cell extracts (A-E), ii) neurones treated from 7 to 14 DIV with  $\alpha 1$  ECDs (F-J), and iii) neurones treated from 7 to 14 DIV with  $\alpha 2$  ECDs (K-O). After fixation, these neurones were stained with the mouse anti-6xHis-tag proteins and guinea-pig anti- $\gamma 2$  subunit specific antibodies. After permeabilisation, they were incubated with the chicken anti-MAP2 and rabbit anti-VGAT specific antibodies (see Table 26 for details). The adhesion of the exogenous  $\alpha 1$  and  $\alpha 2$  ECDs to the cell

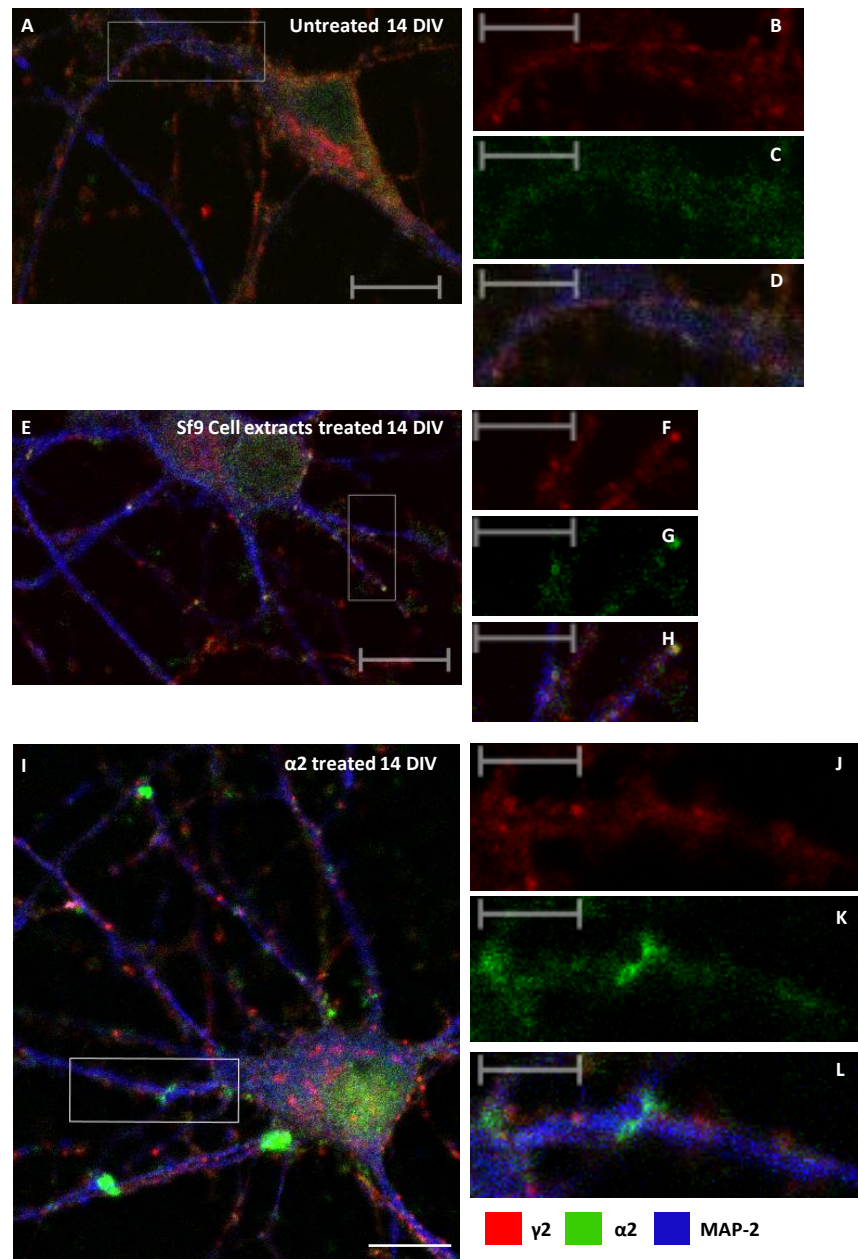
surface of MSNs was visualised using confocal microscopy after immunolabelling with the N-terminal specific antibodies. The added proteins were present in the extracellular space and also on the surface of cultured neurones, but they were not distinguishable from the endogenous receptors using this antibody combinations (Figure 118 and 119). To visualise the localisation of the exogenous  $\alpha 1$  and  $\alpha 2$  ECDs, we decided to stain neurones with anti-6xHis-tagged proteins together with anti- $\gamma 2$  subunit specific antibodies (Figure 121). This immunolabelling confirmed that the exogenous ECDs adhered to the cell surface of MSNs and were also sparsely distributed in the extracellular space.





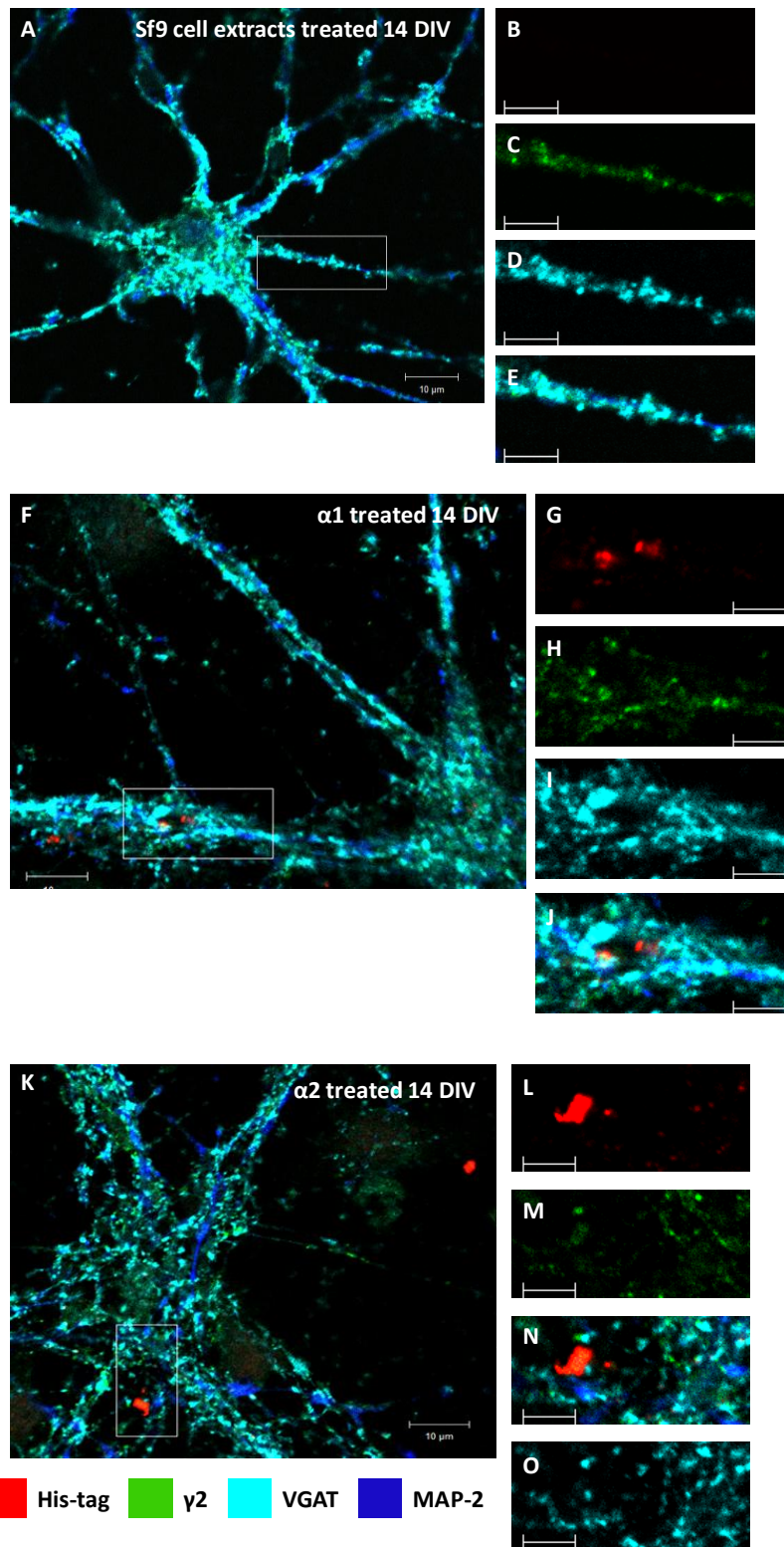
**Figure 118.** The exogenous  $\alpha 1$  ECDs adhere to the cell surface of MSNs treated from 7 to 14 DIV but are not distinguishable from the endogenous  $\alpha 1$ -containing GABA<sub>A</sub>Rs. Immunolabelling of GABA<sub>A</sub>Rs containing  $\gamma 2$  subunit (green) and the  $\alpha 1$  subunit (red) at the cell surface of cultured MSNs. Somatodendritic compartment is labelled with the MAP2 antibody (blue). **A.** Merged image of an untreated 14 DIV MSN (scale bar=10  $\mu$ m). **B.** Enlarged image of the boxed region in A representing  $\gamma 2$  staining only. **C.** Enlarged image of the boxed region in A representing  $\alpha 1$  staining only. **D.** Enlarged image of the boxed region in A showing all the three channels (scale bar=5  $\mu$ m). **E.** Merged image of a 14 DIV MSN treated with the control Sf9 cell extracts (scale bar=10  $\mu$ m). **F.** Enlarged image of the boxed region in E representing  $\gamma 2$  staining only. **G.** Enlarged image of the boxed region in E representing  $\alpha 1$  staining only. **H.** Enlarged

image of the boxed region in E showing all the three channels (scale bar=5  $\mu$ m). **I.** Merged image of a 14 DIV MSN treated with the  $\alpha$ 1 ECDs (scale bar=10  $\mu$ m). **J.** Enlarged image of the boxed region in I representing  $\gamma$ 2 staining only. **K.** Enlarged image of the boxed region in I representing  $\alpha$ 1 staining only. **L.** Enlarged image of the boxed region in I representing all the three channels (scale bar=5  $\mu$ m).



**Figure 119.** The exogenous  $\alpha$ 2 ECDs adhere to the cell surface of MSNs treated from 7 to 14 DIV but are not distinguishable from endogenous  $\alpha$ 2- containing GABA<sub>A</sub>Rs. Immunolabelling of GABA<sub>A</sub>Rs containing  $\gamma$ 2 subunit (red) and the  $\alpha$ 2 subunit (green) at the cell surface of cultured MSNs. Somatodendritic compartment is labelled with the MAP2 antibody (blue). **A.** Merged image of an untreated 14 DIV MSN (scale bar=10  $\mu$ m). **B.** Enlarged image of the boxed region in A representing  $\gamma$ 2 staining only. **C.** Enlarged image of the boxed region in A representing  $\alpha$ 2 staining only. **D.** Enlarged image of the boxed region in A showing all the three channels (scale bar=5  $\mu$ m). **E.** Merged image of a 14 DIV MSN treated with the control Sf9 cell extracts (scale bar=10  $\mu$ m). **F.** Enlarged image of the boxed region in E representing  $\gamma$ 2 staining only. **G.** Enlarged image of the boxed region in E representing  $\alpha$ 2 staining only. **H.** Enlarged image of the boxed region in E showing all the three channels (scale bar=5  $\mu$ m). **I.** Merged image of a 14 DIV MSN treated with the  $\alpha$ 2 ECDs (scale bar=10  $\mu$ m). **J.** Enlarged image of the boxed region in I representing  $\gamma$ 2 staining only. **K.** Enlarged image of the boxed region in I representing  $\alpha$ 2 staining only. **L.** Enlarged image of the boxed region in I representing all the three channels (scale bar=5  $\mu$ m).

representing  $\alpha 2$  staining only. L. Enlarged image of the boxed region in I representing all the three channels (scale bar=5  $\mu$ m).



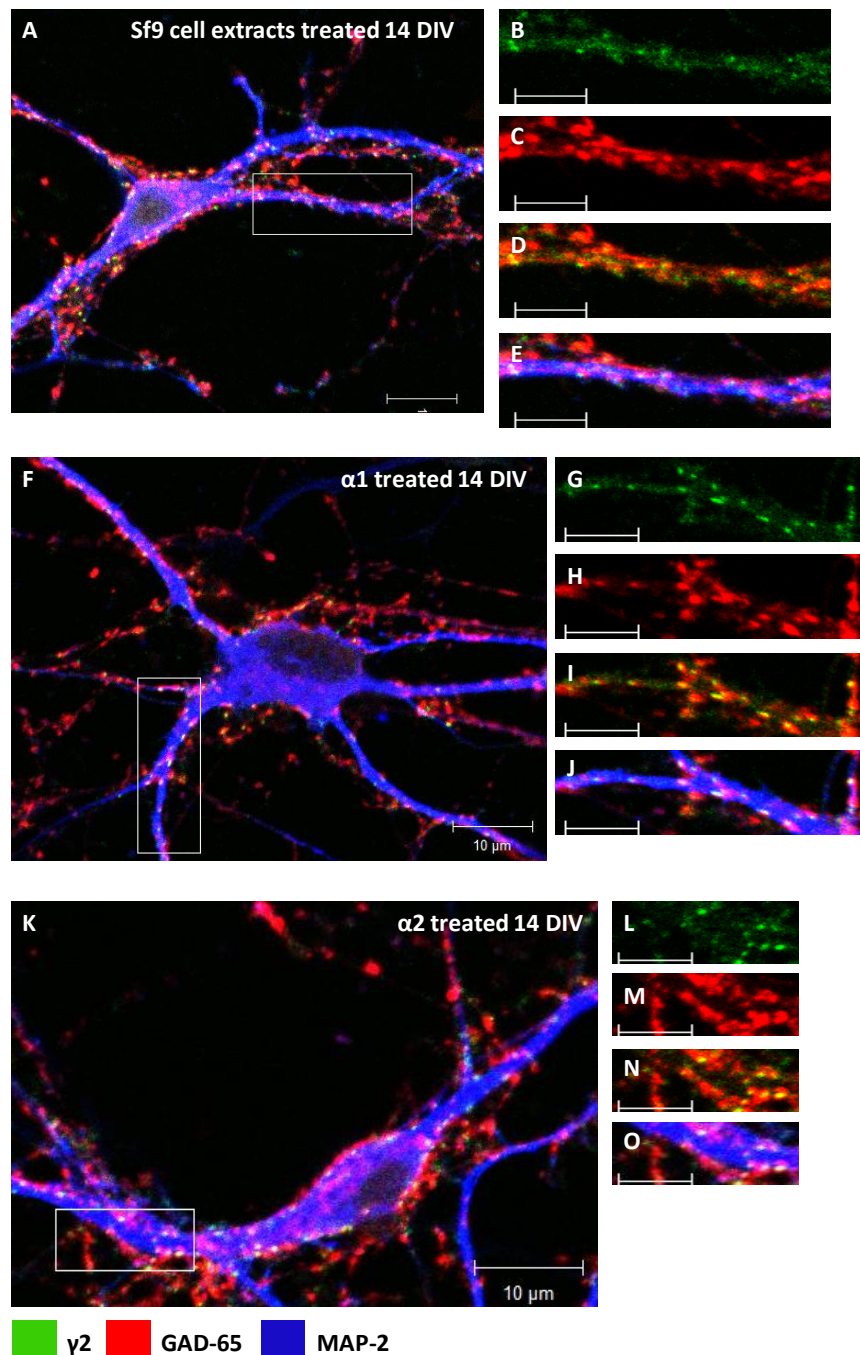
**Figure 120. The histidine-tagged  $\alpha 1$  and  $\alpha 2$  ECDs adhere to the cell surface of MSNs treated from 7 to 14 DIV.** Immunolabelling of the exogenous  $\alpha 1$  and  $\alpha 2$  ECDs using 6xHis-tag antibody (red),  $\gamma 2$ -containing GABA<sub>A</sub>Rs (green) and VGAT positive presynaptic terminals (cyan). The somatodendritic tree is labelled with the MAP2 antibody (blue). **A.** Merged image of a 14 DIV MSN treated with the control Sf9 cell extracts (scale bar=10  $\mu$ m). **B.** Enlarged image of the boxed region in A representing 6xHis-tag proteins staining only. **C.** Enlarged image of the

boxed region in A representing  $\gamma 2$  staining only. **D.** Enlarged image of the boxed region in A representing VGAT staining only. **E.** Enlarged image of the boxed region in A representing all three channels (scale bar=5  $\mu\text{m}$ ). **F.** Merged image of a 14 DIV MSN treated with the  $\alpha 1$  ECDs (scale bar=10  $\mu\text{m}$ ). **G.** Enlarged image of the boxed region in F representing 6xHis-tag proteins staining only. **H.** Enlarged image of the boxed region in F representing  $\gamma 2$  staining only. **I.** Enlarged image of the boxed region in F representing VGAT staining only. **J.** Enlarged image of the boxed region in F representing all the three channels (scale bar=5  $\mu\text{m}$ ). **K.** Merged image of a 14 DIV MSN treated with the  $\alpha 2$  ECDs (scale bar=10  $\mu\text{m}$ ). **L.** Enlarged image of the boxed region in K representing 6xHis-tag proteins staining only. **M.** Enlarged image of the boxed region in K representing  $\gamma 2$  staining only. **N.** Enlarged image of the boxed region in K representing VGAT staining only. **O.** Enlarged image of the boxed region in K representing all the three channels (scale bar=5  $\mu\text{m}$ ).

#### 7.3.4.2 *The total density of $\gamma 2$ -containing GABA<sub>A</sub>Rs per dendrite of MSNs is increased after the treatment with $\alpha 1$ or $\alpha 2$ ECDs from 7 to 14 DIV*

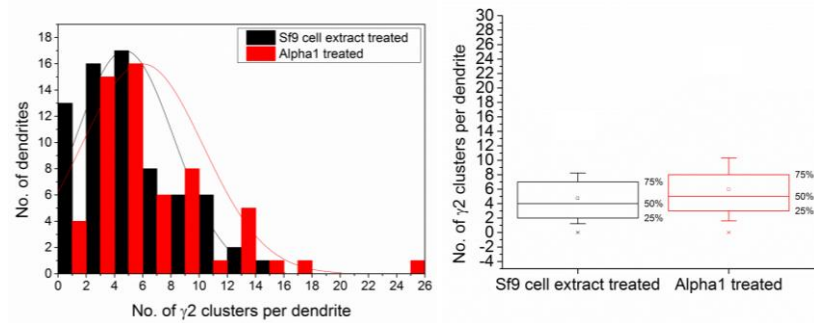
Following the treatments of MSN from 7 to 14 DIV, the total density of  $\gamma 2$  clusters per dendrite was counted, and their size estimated using the Zen 2009 Programme. Developing MSNs treated with Sf9 cell extracts,  $\alpha 1$  ECD or  $\alpha 2$  ECD from 7 to 14 DIV were immunolabelled with the  $\gamma 2$ -, GAD-65- and MAP2-specific antibodies, and the properties of  $\gamma 2$ -containing GABA<sub>A</sub>R clusters were analysed using confocal imaging (Figure 121). The density of  $\gamma 2$ -containing GABA<sub>A</sub>R clusters was estimated per defined length of primary dendrite (the first 20  $\mu\text{m}$  from the cell body) after treatment with the control Sf9 cell extracts or  $\alpha 1$  ECD from 7 to 14 DIV (Figure 122). The median density of  $\gamma 2$  clusters was 4 (7 - 2) with the Sf9 cell extracts treatment, compared to 5 (8 - 3) with the  $\alpha 1$  ECD treatment ( $p$  value=0.08, Mann-Whitney test;  $n=69$  dendrites, and  $n=58$  dendrites, respectively). This demonstrates that the total density of  $\gamma 2$  clusters did not change significantly, indicating that the effects of exogenous  $\alpha 1$  ECDs are less pronounced at this developmental stage.





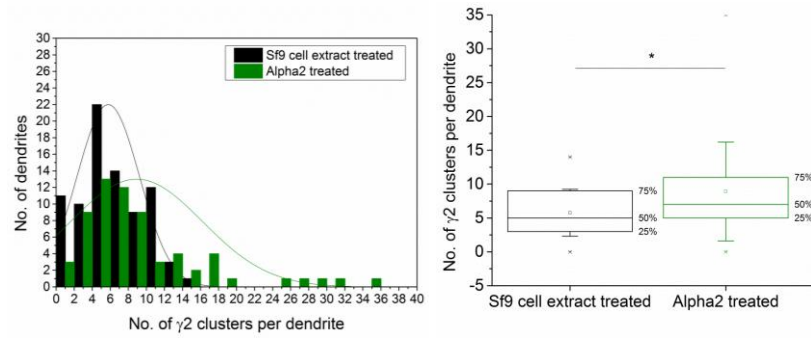
**Figure 121. Immunolabelling of the  $\gamma 2$ -containing GABA<sub>A</sub>R clusters in MSN cultures following the treatments with control Sf9 cell extracts,  $\alpha 1$  or  $\alpha 2$  ECDs from 7 to 14 DIV.** Immunolabelling of GABA<sub>A</sub>R containing the  $\gamma 2$  subunit (green) and of the presynaptic marker GAD-65 (red) along the primary dendrites of cultured MSNs stained for MAP2 (blue). **A.** Merged image of a 14 DIV striatal neurone treated with the control Sf9 cell extracts (scale bar=10  $\mu$ m). **B.** Enlarged image of the boxed region in A representing  $\gamma 2$  staining only. **C.** Enlarge image of boxed region in A representing GAD-65 staining only. **D.** Enlarged image of the boxed region in A representing  $\gamma 2$  and GAD-65 staining. **E.** Enlarged image of the boxed region in A showing all the three channels (scale bar=5  $\mu$ m). **F.** Merged image of a 14 DIV striatal neurone treated with  $\alpha 1$  ECDs (scale bar=10  $\mu$ m). **G.** Enlarged image of the boxed region in F representing  $\gamma 2$  staining only. **H.** Enlarged image of the boxed region in F representing GAD-65 staining only. **I.** Enlarged image of the boxed region in F representing  $\gamma 2$  and GAD-65 staining. **J.** Enlarged image of the boxed region in F showing all the three channels (scale bar=5  $\mu$ m). **K.** Merged image of a 14 DIV striatal neurone treated with the  $\alpha 2$  ECDs (scale bar=10  $\mu$ m). **L.** Enlarged image of the boxed region in K representing  $\gamma 2$  staining only. **M.** Enlarged image of the boxed region in K representing GAD-65 staining only. **N.** Enlarged image of the boxed region in K

representing  $\gamma 2$  and GAD-65 staining. **O**. Enlarged image of the boxed region in K showing all the three channels (scale bar=5  $\mu\text{m}$ ).



**Figure 122. The density of  $\gamma 2$ -containing GABA<sub>A</sub>R clusters per primary dendrite of MSNs remains unchanged after the treatment with  $\alpha 1$  ECDs from 7 to 14 DIV.** The density of  $\gamma 2$ -containing GABA<sub>A</sub>R clusters along the first 20  $\mu\text{m}$  of primary dendrites was counted in MSN cultures in the presence of control Sf9 cell extracts or  $\alpha 1$  ECDs from 7 to 14 DIV. **A**. Histogram shows the distribution of  $\gamma 2$  cluster densities in the presence of control Sf9 cell extracts or  $\alpha 1$  ECDs ( $n=81$  and  $n=59$  dendrites, respectively, from two independent experiments). **B**. Box plot displays the median density (50 % of the population) of  $\gamma 2$  clusters in the presence of control Sf9 cell extracts or  $\alpha 1$  ECDs. Statistical analysis was performed using Mann-Whitney test: \* corresponds to  $p < 0.05$ .

The density of  $\gamma 2$ -containing GABA<sub>A</sub>R clusters was estimated per defined length of primary dendrite (the first 20  $\mu\text{m}$  from the cell body) after the treatment with control Sf9 cell extracts or  $\alpha 2$  ECDs from 7 to 14 DIV (Figure 123). The median density of  $\gamma 2$  clusters was 5 (9-3) with the control Sf9 cell extracts treatment, compared to 7 (11.5 - 4.5) with the  $\alpha 2$  ECDs treatment ( $p$  value=0.01, Mann-Whitney test;  $n=82$ , and  $n=65$  dendrites, respectively). This demonstrates that the total density of  $\gamma 2$  clusters is increased by the treatment, indicating that the exogenous  $\alpha 2$  ECDs promote either the insertion of the  $\gamma 2$  subunit-containing GABA<sub>A</sub>Rs or their clustering, or both, at this developmental stage.



**Figure 123. The density of  $\gamma_2$ -containing GABA<sub>A</sub>R clusters per primary dendrite of MSNs is increased by the treatment with  $\alpha_2$  ECDs from 7 to 14 DIV.** The density of  $\gamma_2$ -containing GABA<sub>A</sub>R clusters along the first 20  $\mu\text{m}$  of primary dendrites was counted in MSN cultures in the presence of control Sf9 cell extracts or  $\alpha_2$  ECDs from 7 to 14 DIV. **A.** Histogram shows the distribution of  $\gamma_2$  cluster densities in the presence of control Sf9 cell extracts or  $\alpha_2$  ECDs (n=82 and n=65 dendrites, respectively, from two independent experiments). **B.** Box plot displays the median density (50 % of the population) of  $\gamma_2$  clusters in the presence of control Sf9 cell extracts or  $\alpha_2$  ECDs. Statistical analysis was performed using Mann-Whitney test: \* corresponds to  $p < 0.05$ .

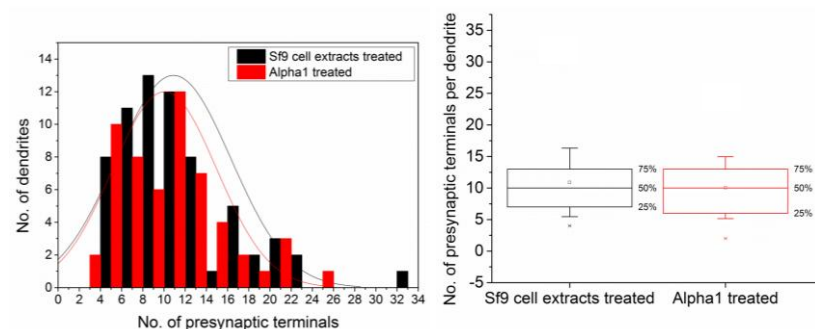
**Table 31. The density of  $\gamma_2$ -containing GABA<sub>A</sub>R clusters per primary dendrite of MSN is increased by the  $\alpha_2$  ECD treatments from 7 to 14 DIV**

	Density of $\gamma_2$ clusters at 7 DIV	P < 0.05
Sf9 cell extracts- Vs. $\alpha_1$ -treated neurones	↗	No
Sf9 cell extracts- Vs. $\alpha_2$ -treated neurones	↘	Yes

#### 7.3.4.3 The connectivity between MSNs is increased by the $\alpha_2$ ECD treatments from 7 to 14 DIV

To investigate further the structural role of GABA<sub>A</sub>Rs in GABAergic synapse formation at later developmental stages, we applied  $\alpha_1$  or  $\alpha_2$  ECDs to MSN cultures from 7 to 14 DIV and estimated if the exogenous ECDs affected the density of presynaptic terminals forming contacts with the primary dendrites in these cultures. The total density of GAD-65 positive terminals per defined length of primary dendrite (the first 20  $\mu\text{m}$  from the cell body) was estimated after the treatment with the control Sf9 cell extracts or  $\alpha_1$  from 7 to 14 DIV (Figure 124). After the treatment with the control Sf9 cell extracts, the median density of presynaptic terminals was 10 (13 - 7) compared to 10 (13 - 6) after the treatment with  $\alpha_1$  ECDs ( $p$  value =0.52, Mann-Whitney test; n=66 dendrites analysed in Sf9 cell extracts- treated cultures, and n=56 dendrites

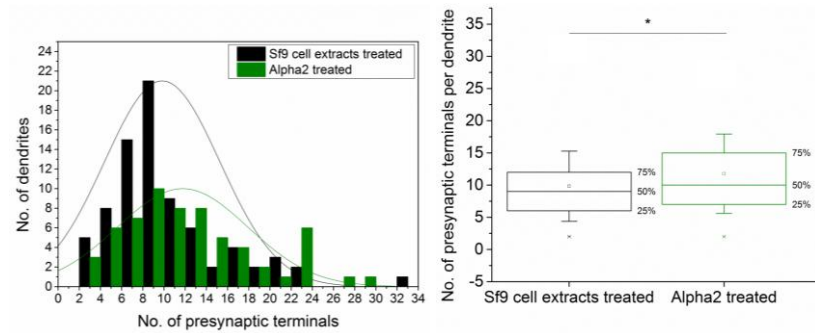
analysed in  $\alpha 1$  ECDs- treated cultures). This indicates that the density of presynaptic contacts did not change following the treatment with  $\alpha 1$  ECDs from 7 to 14 DIV. This result indicates that the effects of  $\alpha 1$  ECDs on the connectivity between MSNs is less prominent at this later stage of development.



**Figure 124. The density of presynaptic terminals per primary dendrite of MSNs remains unchanged after the  $\alpha 1$  ECDs treatment from 7 to 14 DIV.** The density of presynaptic terminals along the first 20  $\mu\text{m}$  of primary dendrites was counted in MSN cultures after the treatment with the control Sf9 cell extracts or  $\alpha 1$  ECDs from 7 to 14 DIV. **A.** Histogram shows the distribution of the density of presynaptic inputs per dendrites after the treatment with control Sf9 cell extracts or  $\alpha 1$  ECDs (n=66 and n=56 dendrites, respectively, from two independent experiments). **B.** Box plot displays the median density of presynaptic terminals after the treatments with control Sf9 cell extracts or  $\alpha 1$  ECDs. Statistical analysis was performed using Mann-Whitney test.

The total density of GAD-65 positive terminals per defined length of primary dendrite (the first 20  $\mu\text{m}$  from the cell body) was estimated after the treatment with the control Sf9 cell extracts or  $\alpha 2$  ECDs from 7 to 14 DIV (Figure 125). After the Sf9 cell extract treatments, the median density of presynaptic terminals was 9 (12 - 6) compared to 10 (15.25 - 7) after the treatment with  $\alpha 2$  ECDs ( $p$  value =0.038, Mann-Whitney test; n=78 dendrites analysed in Sf9 cell extracts-treated cultures, and n=62 dendrites analysed in  $\alpha 2$  ECDs-treated cultures). This indicates that the density of presynaptic contacts per dendrite is increased by the treatment with  $\alpha 2$  ECDs from 7 to 14 DIV, indicating that the connectivity between MSNs could be also regulated by  $\alpha 2$  ECDs later in development.

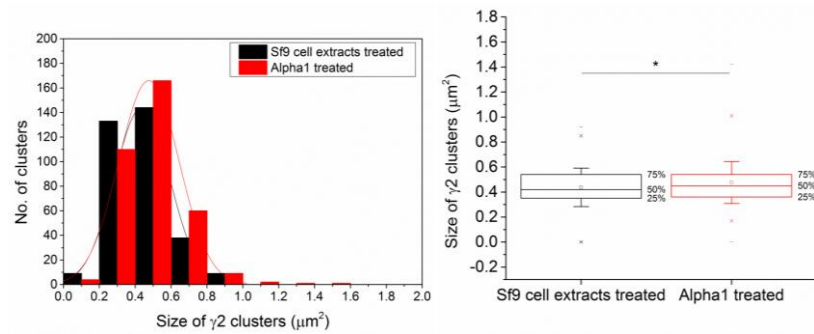




**Figure 125.** The density of presynaptic terminals per primary dendrite of MSNs is increased after the  $\alpha 2$  ECDs treatment from 7 to 14 DIV. The density of presynaptic terminals along the first 20  $\mu\text{m}$  of primary dendrites was counted in MSN cultures after the treatment with control Sf9 cell extracts or  $\alpha 2$  ECDs from 7 to 14 DIV. **A.** Histogram shows the distribution of the density of presynaptic inputs per dendrites after the treatment with control Sf9 cell extracts or  $\alpha 2$  ECDs ( $n=78$  and  $n=62$  dendrites, respectively, from two independent experiments). **B.** Box plot displays the median density of presynaptic terminals per dendrite after the treatment with control Sf9 cell extracts or  $\alpha 2$  ECDs. Statistical analysis was performed using Mann-Whitney test: \* corresponds to  $p < 0.05$ .

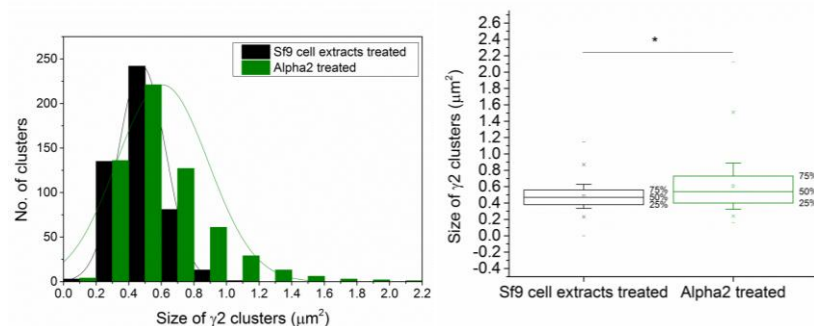
#### 7.3.4.4 *The size of the $\gamma 2$ -containing GABA<sub>A</sub>Rs is increased after the treatment with $\alpha 1$ or $\alpha 2$ ECDs from 7 to 14 DIV*

We were also interested to investigate whether the addition of the  $\alpha 1$  or  $\alpha 2$  ECDs affects the size of the  $\gamma 2$ -containing GABA<sub>A</sub>R clusters in MSNs treated from 7 to 14 DIV. The size of  $\gamma 2$ -containing GABA<sub>A</sub>R clusters per defined length of primary dendrite (the first 20  $\mu\text{m}$  from the cell body) was estimated after the treatment with  $\alpha 1$  ECDs from 7 to 14 DIV (Figure 126). After the treatment with control Sf9 cell extracts, the median size of  $\gamma 2$  clusters was 0.42 (0.54 - 0.35)  $\mu\text{m}^2$  compared to 0.45 (0.55 - 0.36)  $\mu\text{m}^2$  with  $\alpha 1$  ECDs ( $p$  value=0.003, Mann-Whitney test;  $n=333$  clusters, and  $n=353$  clusters, respectively). This demonstrates that the size of  $\gamma 2$ -containing GABA<sub>A</sub>R clusters is increased by the treatment with  $\alpha 1$  ECDs from 7 to 14 DIV. This suggests that even at this later stage of development, the exogenous  $\alpha 1$  ECDs could promote the clustering of synaptic GABA<sub>A</sub>Rs.



**Figure 126. The size of the  $\gamma_2$ -containing GABA<sub>A</sub>R clusters is increased by the treatment with  $\alpha_1$  ECDs from 7 to 14 DIV.** The size of the  $\gamma_2$ -containing GABA<sub>A</sub>R clusters along the first 20  $\mu\text{m}$  of primary dendrites was measured in MSN cultures after the treatment with control Sf9 cell extracts or  $\alpha_1$  ECDs from 7 to 14 DIV. **A.** Histogram shows the distribution of  $\gamma_2$  cluster sizes after the treatment with the control Sf9 cell extracts or  $\alpha_1$  ECDs (n=333 and n=353 clusters, respectively, from two independent experiments). **B.** Box plot displays the median size (50 % of the population) of  $\gamma_2$  clusters after the treatment with the control Sf9 cell extracts or  $\alpha_1$  ECDs. Statistical analysis was performed using Mann-Whitney test: \* corresponds to  $p < 0.05$ .

The size of the  $\gamma_2$ -containing GABA<sub>A</sub>R clusters per defined length of primary dendrite (the first 20  $\mu\text{m}$  from the cell body) was estimated after the treatment with  $\alpha_2$  ECDs from 7 to 14 DIV (Figure 127). After the treatment with control Sf9 cell extracts, the median size of  $\gamma_2$  clusters was 0.47 (0.56 - 0.38)  $\mu\text{m}^2$  compared to 0.54 (0.73 - 0.4)  $\mu\text{m}^2$  with  $\alpha_2$  ECDs ( $p$  value= $4.82 \times 10^{-12}$ , Mann-Whitney test; n=475 clusters, and n=603 clusters, respectively). This demonstrates that the size of  $\gamma_2$ -containing GABA<sub>A</sub>R clusters is increased by the treatment with  $\alpha_2$  ECDs from 7 to 14 DIV. This suggests that even at this later stage of development, the exogenous  $\alpha_2$  ECDs could promote clustering of synaptic GABA<sub>A</sub>Rs.



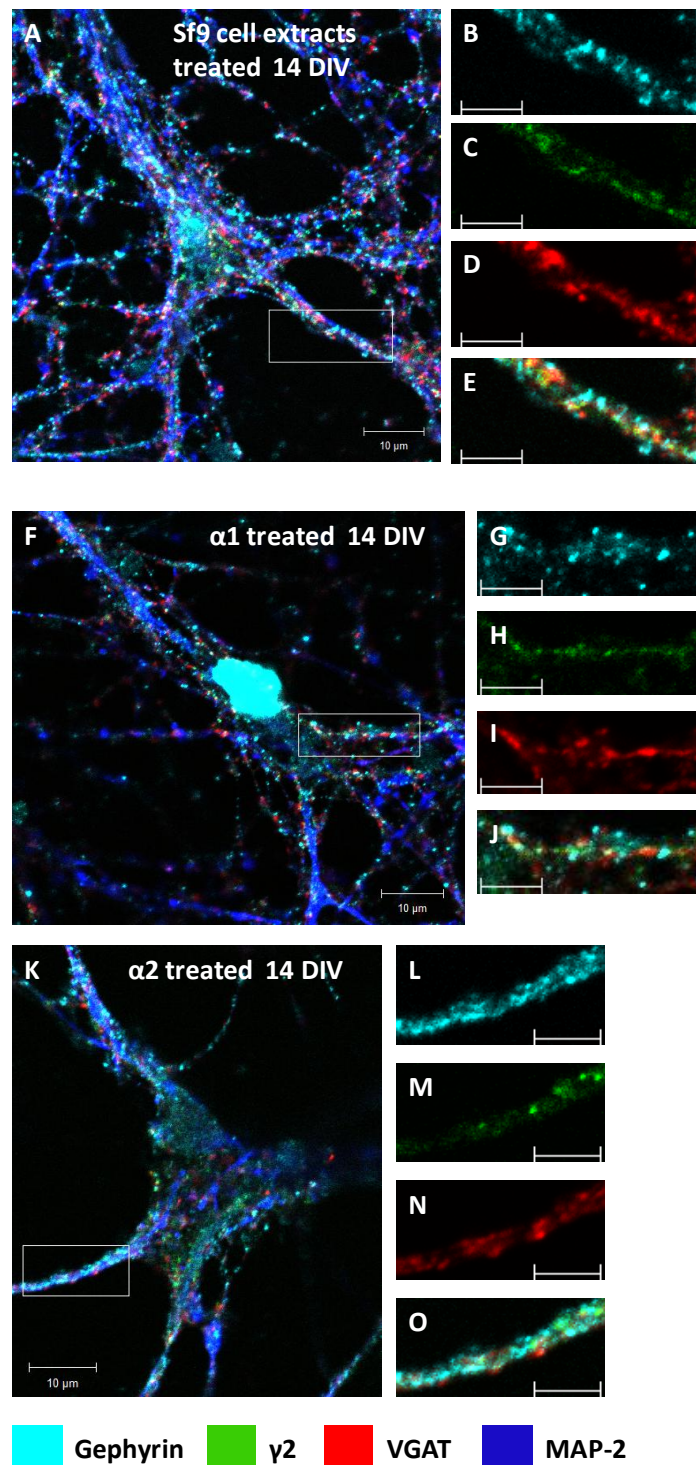
**Figure 127. The size of  $\gamma_2$ -containing GABA<sub>A</sub>R clusters is increased by the treatment with  $\alpha_2$  ECD from 7 to 14 DIV.** The size of  $\gamma_2$ -containing GABA<sub>A</sub>R clusters along the first 20  $\mu\text{m}$  of primary dendrites was measured in MSN cultures after the treatment with the control Sf9 cell extracts or  $\alpha_2$  ECDs from 7 to 14 DIV. **A.** Histogram shows the distribution of  $\gamma_2$  cluster sizes after the treatment with control Sf9 cell extracts or  $\alpha_2$  ECDs (n=475 and n=603 clusters, respectively, from two independent experiments). **B.** Box plot displays the median size (50 % of the population) of  $\gamma_2$  clusters after the treatment with control Sf9 cell extracts or  $\alpha_2$  ECDs. Statistical analysis was performed using Mann-Whitney test: \* corresponds to  $p < 0.05$ .

**Table 32. The size of  $\gamma$ 2-containing GABA<sub>A</sub>R clusters per primary dendrite of MSNs is increased by the treatment with  $\alpha$ 1 or  $\alpha$ 2 ECD from 7 to 14 DIV.**

	Size of $\gamma$ 2 clusters at 7 DIV	P < 0.05
Sf9 cell extracts- Vs. $\alpha$ 1-treated neurones	↗	Yes
Sf9 cell extracts- Vs. $\alpha$ 2-treated neurones	↗	Yes

*7.3.4.5 Analysis of gephyrin clusters in MSNs following the treatments with  $\alpha$ 1 or  $\alpha$ 2 ECDs from 7 to 14 DIV*

Developing MSNs treated with the control Sf9 cell extracts,  $\alpha$ 1 ECDs or  $\alpha$ 2 ECDs from 7 to 14 DIV, were immunolabelled with the mouse anti-gephyrin, rabbit anti-VGAT, guinea-pig anti- $\gamma$ 2 and chicken anti-MAP2 specific antibodies. Changes in density and size of gephyrin clusters were analysed by confocal microscopy (Figure 128). From this preliminary experiments, gephyrin clusters seem to be increased in size after the  $\alpha$ 2 ECDs treatment compared to control Sf9 cell extracts treatment from 7 to 14 DIV. However, statistical analysis must be performed to confirm these observations.



**Figure 128. The density of gephyrin clusters appears to be increased after the treatments of MSN with the  $\alpha 2$  ECDs from 7 to 14 DIV.** Immunolabelling of gephyrin (cyan),  $\gamma 2$  subunit (green) and the presynaptic marker VGAT (red). The somatodendritic compartment is labelled with the MAP2 antibody (blue). **A.** Merged image of a 14 DIV striatal neurone treated with the control Sf9 cell extracts (scale bar=10 $\mu$ m). **B.** Enlarged image of the boxed region in A representing gephyrin staining only. **C.** Enlarge image of boxed region in A representing  $\gamma 2$  staining only. **D.** Enlarged image of the boxed region in A representing VGAT staining only. **E.** Enlarged image of the boxed region in A showing all the three channels (scale bar=5 $\mu$ m). **F.** Merged image of a 14 DIV striatal neurone treated with  $\alpha 1$  ECDs (scale bar=10 $\mu$ m). **G.** Enlarged image of the boxed region in F representing gephyrin staining only. **H.** Enlarged image of the boxed region in F representing  $\gamma 2$  staining only. **I.** Enlarged image of the boxed region in F representing VGAT staining. **J.** Enlarged image of the boxed region in F showing all the three

channels (scale bar=5 $\mu$ m). **K.** Merged image of a 14 DIV striatal neurone treated with the  $\alpha$ 2 ECDs (scale bar=10 $\mu$ m). **L.** Enlarged image of the boxed region in K representing gephyrin staining only. **M.** Enlarged image of the boxed region in K representing  $\gamma$ 2 staining only. **N.** Enlarged image of the boxed region in K representing VGAT staining. **O.** Enlarged image of the boxed region in K showing all the three channels (scale bar=5 $\mu$ m).

#### **7.4 Discussion**

GABA<sub>A</sub>Rs are the essential functional postsynaptic components of GABAergic synapses in the mammalian brain (Sieghart, 2006). Gene deletion studies of the most abundant subunits of GABA<sub>A</sub>Rs in mice have demonstrated specific structural changes in inhibitory synapse formation (Fritschy et al., 2012). To investigate whether GABA<sub>A</sub>Rs alone could promote inhibitory synapse formation, Fuchs et al. developed a model in which GABA<sub>A</sub>Rs were expressed in HEK 293 cells and co-cultured with GABAergic medium spiny neurones (Fuchs et al., 2013). In this study, it was showed that when stably transfected into HEK 293 cells, the  $\alpha$ 1/ $\beta$ 2/ $\gamma$ 2 GABA<sub>A</sub>Rs were able to promote synaptic contact formation and functional maturation. Interestingly, the density of synaptic inputs on the surface of transfected HEK cells and synaptic strength were reinforced when GABA<sub>A</sub>Rs were co-transfected with NL2. However, molecular mechanisms that mediate this process are currently unknown.

We hypothesised at the start of these experiments that amongst different domains, due to their architecture and their presence in the extracellular space, the large N-terminal extracellular domains of GABA<sub>A</sub>R subunits is likely to play a role in the recognition process between the pre and postsynaptic terminals. It is now well recognised that amongst all the subunits, the diversity of  $\alpha$  subunits is the best candidate to explain the physiological and regional diversity of GABA<sub>A</sub>Rs and hence, the specificity of GABAergic synapses present throughout the brain (Fritschy and Panzanelli, 2014).

In this chapter, our aim was to identify the structural role played by the extracellular domains of  $\alpha$ 1 and  $\alpha$ 2 GABA<sub>A</sub>R subunits during specific GABAergic synapse formation.

To do so, we have utilised the  $\alpha 1$  and  $\alpha 2$  extracellular domains (ECDs) produced in Sf9 cells which were purified under sterile conditions. In order to study the specific role of each domain during GABAergic synapse formation, we applied 5 $\mu$ g of  $\alpha 1$  or  $\alpha 2$  ECDs to MSN cultures from 4 to 7 DIV or from 7 to 14 DIV. Using immunocytochemistry and confocal microscopy, we have been able to study the effects of these treatments on GABA<sub>A</sub>R clusters density, size and synaptic localisation along the first 20  $\mu$ m of primary dendrites of MSNs.

Prior to the treatment, we wanted to confirm that the purified extracellular domains were glycosylated as we knew that glycosylation plays a major role in the extracellular domain function and protein-protein interactions (Miller and Aricescu, 2014). Thus we performed deglycosylation assay in which the purified  $\alpha 1$  and  $\alpha 2$  ECDs were incubated with deglycosylation enzymes. After incubation, the degree of glycosylation was assessed by immunoblotting. As expected, the immunoblots confirmed that both  $\alpha 1$  ECD and  $\alpha 2$  ECD were glycosylated.

In addition, before synapse formation analysis was carried out, we observed that at both developmental stages 7 and 14 DIV, the  $\alpha 1$  and  $\alpha 2$  exogenous ECDs adhered to the neuronal cell surface along dendrites of most of the cultured neurones.

The treatments of MSNs with  $\alpha 1$  or  $\alpha 2$  ECDs resulted in an increase in synapse formation and in GABA<sub>A</sub>R clustering, suggesting synaptogenic effects of these domains. We found that when MSNs were treated with either ECD, the density and size of  $\gamma 2$ -containing GABA<sub>A</sub>R clusters were increased as well as the connectivity between MSNs, in comparison with the neurones treated with extracts from non-infected Sf9 cells. Interestingly, when MSNs were treated from 7 to 14 DIV, the density of  $\gamma 2$ -containing clusters and the MSNs connectivity was increased with the  $\alpha 2$  ECDs treatment, but not with the  $\alpha 1$  ECDs treatment.

These results suggested that at early developmental stages, when synapses are still immature, both the  $\alpha 1$  and  $\alpha 2$  ECDs have the capacity to promote synapse formation, while later on during development, when synaptic contact are made and

synapses are becoming functional, only the  $\alpha 2$  ECDs were able to promote the increase of functional synapses. These synaptogenic effects of the extracellular domains of  $\alpha 1$  and  $\alpha 2$  ECDs could be explained by different mechanisms.

The N-terminal extracellular domain of  $\alpha$ ,  $\beta$  and  $\gamma$  subunits plays a crucial role during GABA<sub>A</sub>R assembly in the ER. When expressed in heterologous systems, each of the individual subunits are able to form homomers or dimers (Connolly et al., 1996b, Luscher et al., 2011). Thus,  $\alpha$  subunits are capable of oligomerisation via their N-terminal extracellular domains. However, very little is known about the existence and relevance of homomers of any GABA<sub>A</sub>R subunits *in vivo*. In our model, the oligomerisation of the exogenous extracellular domains with the endogenous, surface-expressed GABA<sub>A</sub>R subunits could be potentially one of the mechanisms that could mediate the increase in GABA<sub>A</sub>R clusters size and synaptic contact formation, observed after treatment. Hence, by adhering to the cell surface of neurones, the exogenous domains would oligomerise with endogenous receptors making the clusters larger and thus, stabilising their association with the presynaptic terminals and promoting formation of synaptic contacts.

Alternatively, oligomerisation with endogenous receptors could block their activation by GABA and thus, could lead to compensatory mechanisms similar to those observed in the previous result chapter. Electrophysiological recordings would help us to explore this possibility. By recording postsynaptic currents, we would be able to know if the strength of synapses has been increased or decreased after the treatment.

Additionally, the synaptogenic effects observed after treatment with  $\alpha 1$  or  $\alpha 2$  ECDs at early developmental stages, could be explained by the potential interaction of these domains with some presynaptic proteins involved in specific GABAergic synapse formation. By adhering to the cell surface of neurones, and being available for trans-synaptic interactions, the exogenous domains could attract presynaptic proteins to bind and this process itself could lead to a further recruitment of the endogenous GABA<sub>A</sub>Rs to these sites either from the extrasynaptic or intracellular receptor pools.

All together, these results could be linked with the previous findings showing that  $\alpha 2$ -containing GABA<sub>A</sub>R clusters are the most readily available for modulation by GABA signalling and also are the most abundant types of receptors in the adult striatum. The role played by the potentially  $\alpha 2$  subunit-interacting protein pikachurin would be interesting to study under the treatment of developing MSNs with the  $\alpha 2$  ECDs. In addition, to understand further the role played by these glycosylated domains, it would be interesting to treat MSN cultures with deglycosylated ECDs and determine if the synaptogenic effects of these domains are still observed. Additionally, it would be of interest to determine the exact amino acid sequence in  $\alpha 1$  and  $\alpha 2$  ECDs which is necessary for these synaptogenic effects to occur. Finally, it would be important to establish the synaptogenic effects of other GABA<sub>A</sub>R subunits such as  $\beta$  and  $\gamma$  which probably also play an important role in the GABAergic synapse formation.

In conclusion, by investigating the role of GABA<sub>A</sub>R subunits  $\alpha 1$  and  $\alpha 2$  in GABAergic synapse formation, a better understanding of the role of each subunit was established. We found that as MSNs mature *in vitro*, the formation of  $\alpha 2$ -containing synapses is predominantly promoted as the median size of  $\alpha 2$ -containing GABA<sub>A</sub>R clusters was increased from 7 to 14 DIV. It would be interesting to establish if these newly inserted subunits are readily available from extrasynaptic pools or the result of intracellular mechanisms. On the second hand, it would be interesting to understand if this specificity towards the formation of  $\alpha 2$ -containing receptors is related to the pharmacological properties of this particular  $\alpha$  subunit, or is related to the structure of this subunit promoting specific intracellular pathways activated by specific protein-protein interactions. We found that the Heparan sulfate proteoglycan pikachurin was able to bind the extracellular domain of  $\alpha 2$  subunit at early developmental stages. The role of pikachurin in the striatum will have to be established, and the relevance of its binding to  $\alpha 2$  subunit ECD during synapse formation will need to be further confirmed.



# Chapter eight

## 8. Discussion

GABA<sub>A</sub>Rs are the main receptors in the brain transducing inhibitory signals. These signals play a crucial role in regulating the proper functioning of the mammalian brain. The networks of GABAergic neurones are involved in a very wide range of functions from cognitive perception to motor control or breathing. Although they play a central role in the functioning of GABAergic synapses, little is known about the role played by individual subunits composing the GABA<sub>A</sub> heteropentamers during GABAergic synapse formation. In this thesis, my main goal was to investigate the role played by the extracellular domains of GABA<sub>A</sub>R  $\alpha$ 1 and  $\alpha$ 2 subunits during the formation and maturation of GABAergic synapses. In addition, we also studied the role played by GABA<sub>A</sub>Rs activity in regulating GABA<sub>A</sub> receptor clustering and synaptic localisation. The  $\alpha$ 1 and  $\alpha$ 2 subunits are of particular interest because they are widely expressed throughout the brain and their expression varies dramatically during the brain development, hence playing a pivotal role during GABAergic synapse formation. The extracellular domains of GABA<sub>A</sub>R  $\alpha$  subunits incorporate the GABA and benzodiazepine binding sites, but also may play a central role in transynaptic interactions, as they are situated in the synaptic cleft.

To investigate the role of  $\alpha$ 1 and  $\alpha$ 2 subunits during synapse formation, we have first expressed and purified their extracellular domains (ECDs) using the baculovirus/Sf9 cells expression system. We have then utilised these purified ECDs in order to address two important questions: Are there presynaptic or synaptic cleft proteins with which  $\alpha$ 1 and  $\alpha$ 2 ECDs could specifically interact? Do these domains play any direct structural role during GABAergic synapse formation in the embryonic neuronal cultures?

In addition, we were interested in understanding the role of GABA<sub>A</sub>R activity during GABAergic synapse development. To do so, we have treated embryonic MSNs cultures with the GABA antagonist bicuculline, and studied the effect of GABA signalling blockade on GABAergic synapse formation and stabilisation.

### **8.1 The HSPG protein pikachurin binds to the extracellular domain of GABA<sub>A</sub>R $\alpha$ 2 subunit**

In the first chapter, the optimisation of expression and purification of  $\alpha$ 1 and  $\alpha$ 2 ECDs enabled us to investigate the potential binding partners of the  $\alpha$ 1 and  $\alpha$ 2 subunits. Proteomics and mass spectrometry experiments revealed a large density of candidate binding proteins, but only some of these proteins were chosen to be studied further because of their known involvement in synaptic function. One of these proteins was pikachurin, a heparin sulfate proteoglycan which was shown to play an important role in synapse formation in retina (Sato, 2010). We were able to demonstrate that this protein can be co-immunoprecipitated with the  $\alpha$ 2 subunit from neuronal lysates and that it is highly co-localised with this subunit of GABA<sub>A</sub>Rs at synapses. Supporting our findings, a recent study showed that similar HSPG contribute to the excitatory synapse formation by interacting with Leucine rich repeated transmembrane neuronal protein (LRRTMs) and promoting their synaptogenic effects (Siddiqui et al., 2013). LRRTMs were first identified in fibroblast-neurone co-culture model where they were able to mediate excitatory presynaptic and postsynaptic differentiation (Linhoff et al., 2009). In the manuscript by Siddiqui et al., it was shown that the synaptogenic effects observed on dentate gyrus granule cells mediated by LRRTM4 required the presence of HSPGs (Siddiqui et al., 2013). In addition, when glycosylated, pikachurin has been shown to interact with the dystroglycan protein complex and regulate the apposition between the dendrites of bipolar neurones and photoreceptor in the ribbon synapse in retina (Sato et al., 2008, Sato, 2010, Hu et al., 2011, Omori et al., 2012). The protein Agrin is another HSPGs known to play a central role during NMJ formation (Wu et al., 2010). In the brain, this transmembrane protein is released following proteolytic cleavage triggered by neural activity in the hippocampus (Matsumoto-Miyai et al., 2009). It has been shown that *in vitro*, agrin may be implicated in the regulation of dendrite extension and clustering of GABA<sub>A</sub>Rs (Ferreira, 1999). In addition, it was showed that agrin is present at GABAergic synapses and treating cultures with agrin significantly increased

the total cluster area of  $\alpha$ -DG and  $\beta$ 3 GABA<sub>A</sub>Rs (Pribrag et al., 2014). The treatment was also sufficient to increase mIPSC amplitude. These data suggest that ligand-induced signalling through DG or ligand-induced clustering of DG is sufficient to increase GABA<sub>A</sub>R cluster size and GABAergic neurotransmission. In this paper, it was demonstrated that the dystroglycan subunits  $\alpha$  and  $\beta$  ( $\alpha$ DG and  $\beta$ DG), gephyrin and  $\alpha$ 1 and  $\beta$ 2/3 subunits of GABA<sub>A</sub>Rs can be co-immunoprecipitated as a supramolecular complex (Pribrag et al., 2014). However, Lévi et al. showed that DG is not necessary for GABAergic synapse formation and is recruited after the appearance of GABA<sub>A</sub>R clusters in hippocampal neurones, suggesting that DG is not required for GABA<sub>A</sub>R clustering (Lévi et al., 2002). Thus, DG could contribute to synapse stabilisation rather than synapse formation, as it does in the neuromuscular junction (NMJ), by contributing to activity-dependent regulation of the density of synaptic GABA<sub>A</sub>Rs. To test this possibility, Pribrag et al., showed that by increasing neuronal firing in hippocampal culture they were able to promote GABAergic synapse formation (Pribrag et al., 2014). By applying 10  $\mu$ M bicuculline for 24 hours or by elevating extracellular K<sup>+</sup> concentration, they observed homeostatic increase in the total cluster area of GABA<sub>A</sub>R  $\beta$ 3 subunit and increased levels of  $\gamma$ 2 subunits, but also an increase in the total cluster area of functionally glycosylated  $\alpha$ -DG. These results suggested a homeostatic up-regulation of GABA<sub>A</sub>Rs and DG consistent with a function for DG in GABA<sub>A</sub>Rs clustering and stabilisation (Panzanelli et al., 2011).

All together, this data give us directions to follow to study further the interaction between the  $\alpha$ 2 GABA<sub>A</sub>R subunits and Pikachurin and to understand better the role played by pikachurin in GABAergic synapse formation and homeostatic plasticity as a potential upstream regulator of the DG complex at GABAergic synapses. To further the understanding of the role of this interaction during brain development, it would be very helpful to study GABAergic synapse formation in the brain of pikachurin knock-out (KO) mice (Kanagawa et al., 2010).

## **8.2 The $\alpha$ 2-containing synapses are favoured compared to $\alpha$ 1-containing synapses during maturation of GABAergic MSNs *in vitro***

In the third chapter of this thesis, the structural analysis of embryonic MSN cultures allowed us to understand further how GABAergic synapses are formed and maintained throughout *in vitro* development. In our study, we were interested in looking at the change in size of clusters. Our results indicated that  $\alpha$ 2-containing GABA<sub>A</sub>R cluster ( $\alpha$ 2 single,  $\alpha$ 1/2 mixed,  $\alpha$ 2/1 mixed clusters) sizes were increased in MSN synapses from 7 to 14 DIV while the size of single  $\alpha$ 1 synaptic clusters was decreased. Although we did not directly compare the density of  $\alpha$ 1 clusters to the density of  $\alpha$ 2 clusters of GABA<sub>A</sub>Rs, the densities indicated a higher density of  $\alpha$ 2-containing GABA<sub>A</sub>R clusters along dendrites. These results are in accordance with the distribution of GABA<sub>A</sub>R subunits *in vivo* in the adult striatum, in which the  $\alpha$ 2 subunit is more prominently present than the  $\alpha$ 1 subunit (Fritschy and Mohler, 1995). This is further supported by a study showing that *in vivo* the density of  $\alpha$ 2-containing synapses is higher in the proximal dendrites of MSNs, while the  $\alpha$ 1-containing receptors are widely spread over the perisomatic and dendritic regions (Gross et al., 2011). Due to their different affinity for zolpidem, the  $\alpha$ 1 and  $\alpha$ 2/3-containing GABA<sub>A</sub>Rs were distinguished by using 100 nM or 400 nM of this hypnotic drug, respectively. In this paper, the authors were able to show that in the globus pallidus, the specific subcellular distribution of  $\alpha$ 1 and  $\alpha$ 3 subunits is believed to be related to the innervation by axon collaterals of other GP neurones, while the presence of  $\alpha$ 2-containing synapses in proximal dendrites of MSNs would be related to the striatal innervation (Gross et al., 2011).

A dissociated culture system using striatal and cortical neurones was used to describe the axon collateral-mediated inhibition (Lalchandani and Vicini, 2013). Interestingly, it was shown that in 14 DIV MSN cultures, autaptic currents were found in 50 % of MSNs at 7-8 DIV and 57 % of MSNs at 13-16 DIV (Lalchandani and Vicini, 2013). All together, these data suggest that via axon collateral inhibition, MSNs shape

neurone firing and striatal output of the striatum. They also suggest that these inhibitory inputs are probably mediated by  $\alpha 2$ -containing synapses.

However, which molecular mechanisms are at the origin of the formation of such synapses, remains unclear. In the light of the first two chapters of this thesis, we could hypothesise that formation of these synapses may be, at least in part, promoted by the interaction between the HSPG Pikachurin and the  $\alpha 2$  ECDs of GABA<sub>A</sub>Rs. The role of this interaction could be established by studying the GABAergic synapse formation in cultured MSNs from Pikachurin Knock-Out mice.

### **8.3 Activity-dependent regulation of GABAergic synapse formation**

GABA<sub>A</sub> receptor heterogeneity is based on the combinatorial assembly of a large family of subunits into distinct receptor subtypes. This suggests that genetic programs established during ontogeny govern the expression of GABA<sub>A</sub>R subtypes (Penschuck et al., 1999). The role played by neuronal activity on the expression levels of GABA<sub>A</sub>R subtypes was tested in the hippocampus *in vitro* and *in vivo* (Penschuck et al., 1999). As this paper and many others have shown, the activity-dependent mechanisms regulate GABA<sub>A</sub>R clustering and thereby, help to regulate homeostatic plasticity in the brain (Hartman et al., 2006, Saliba et al., 2007, Bannai et al., 2009, Muir and Kittler, 2014). But what do we know about the role played by GABA signalling during GABAergic synapse formation and maturation? It is now well established that GABA<sub>A</sub>R-mediated signalling plays a pivotal role in mediating activity-dependent synapse formation. In the embryonic brain, GABA acts as a trophic factor that depolarises neuronal progenitors and early post mitotic granule cells, enabling network activity to regulate cell proliferation, survival and growth (Dieni et al., 2013). Following the appearance of glutamatergic synapses, a switch in GABA signalling from an excitatory to an inhibitory signal is observed. However, whether depolarising or hyperpolarising, GABA<sub>A</sub>R-mediated signalling occurs in two different modes termed phasic and tonic inhibition. While phasic inhibition refers to conventional synaptic

transmission, in which GABA is released from the presynaptic terminals and activates low-affinity postsynaptic GABA<sub>A</sub>Rs, tonic inhibition refers to the activation of high-affinity extrasynaptic GABA<sub>A</sub>Rs by low ambient concentrations of GABA (Nusser and Mody, 2002, Luo et al., 2013b). In addition, perisynaptic GABA<sub>A</sub> receptors mediate an intermediate form of inhibition that is mediated *in vivo* by the NPY-positive basket cells (English et al., 2012). The subunit composition of GABA<sub>A</sub>Rs that mediate striatal tonic inhibition is of crucial interest in understanding the underlying factors that control MSN output and neuronal excitability (Luo et al., 2013b).

Due to precise dissection of the embryonic striatal region at the stage when the dopaminergic neurones are the only input received (Goffin et al., 2010), our MSNs culture model presents unique features of purely GABAergic culture. In addition, no interneurones are present in these embryonic cultures as they would normally appear during the postnatal brain development (Kawaguchi, 1993). It is also important to note that *in vivo*, the MSNs are projecting out of the striatum, primarily targeting other areas of the basal ganglia. In contrast, in our model system, MSNs are “forced” to synapse with each other as they have no other possible cells to target. That has been confirmed by electrophysiological recordings (data not shown), which showed that MSNs are able to promote action-potential driven activity from 12 DIV.

Other roles played by GABA have been investigated. For the first time, Chattopadhyaya and colleagues demonstrated a function of GABA in regulating GABAergic innervation in the postnatal brain, when GABA is inhibitory (Chattopadhyaya et al., 2007). By using conditional knock down of GAD-67 but not GAD-65 in basket interneurones of the visual cortex, they showed a cell autonomous deficit in axon branching, perisomatic synapse formation around pyramidal neurones and complexity of the innervation fields. As intracellular GABA levels are modulated by neuronal activity, these results implicated GAD-67-mediated GABA synthesis in activity dependent regulation of inhibitory patterns. These results showed that GABA acts

beyond its classical role in inhibitory transmission in the adolescent brain and regulates the maturation of inhibitory synapses and innervation patterns, thus revealing a new effect of GABA function different from its early trophic action in the prenatal brain (Huang and Scheiffele, 2008). GABA is the main neurotransmitter released in our culture model. Thus, any activity-dependent mechanism, whether excitatory or inhibitory, triggering phasic or tonic inhibition, would be altered by the treatment with 25  $\mu$ M bicuculline. In our experiments, we found differential alterations of GABAergic synapses depending on the developmental stages the bicuculline was applied at, but also depending on the subtype of GABA<sub>A</sub>Rs observed. Our results suggest that at early developmental stages, when excitatory, GABA signalling promotes the formation of  $\alpha$ 2-containing clusters specifically. However, from 7 to 14 DIV, blocking GABA signalling caused compensatory mechanisms favouring the formation of  $\alpha$ 2-containing synapses and decreasing the formation of  $\alpha$ 1-containing synapses. Potentially, this could be explained by the fact that  $\alpha$ 2 subunit is the most abundant subunit present in the striatum (Fujiyama et al., 2000), thereby,  $\alpha$ 2-containing GABA<sub>A</sub>Rs are probably readily available in MSNs *in vitro*. This could also be explained by the pharmacological properties of  $\alpha$ 2-containing GABA<sub>A</sub>Rs which kinetics of deactivation are slower than  $\alpha$ 1-containing receptors, thus are probably more appropriated to an environment where GABA is the main neurotransmitter (Brussaard et al., 1997).

#### **8.4 The N-terminal extracellular domains of $\alpha$ 1 and $\alpha$ 2 GABA<sub>A</sub>R subunits have synaptogenic effects**

Treating MSN cultures with  $\alpha$ 1 or  $\alpha$ 2 ECDs at immature and mature developmental stages has revealed that GABA<sub>A</sub>Rs can play a structural role during GABAergic formation and maintenance, and that this structural role is mediated by the large N-terminal extracellular domains of  $\alpha$ 1 and  $\alpha$ 2 subunits. Although both types of exogenous  $\alpha$ 1 and  $\alpha$ 2 ECDs had synaptogenic effects during formation of synapses (compared to Sf9 cell extracts treatment), only the  $\alpha$ 2 exogenous ECDs were capable



of promoting functional synapse formation at more mature stages, when neurones were able to form functional synapses. This was confirmed by monitoring an increase in  $\gamma 2$ -containing GABA<sub>A</sub>R clusters following treatment with  $\alpha 2$  ECDs from 7 to 14 DIV. These findings are preliminary and would need extensive work in order to establish the mechanisms that mediate the observed synaptogenic effects. The modification of gephyrin clustering during these treatments would be important to analyse even though the binding between  $\alpha$  subunits and gephyrin is mediated by intracellular domains (Tretter et al., 2008). As the ECDs adhere to the cell surface of neurones, the increase in synapse formation could be due to oligomerisation of the exogenous and endogenous receptors, making them more “attractive” for presynaptic terminals. The synaptogenic effects could also be due to pikachurin interaction (or another presynaptic protein) with GABA<sub>A</sub>R which could enhance the stability of synapses by the presence of  $\alpha 2$  ECDs in mature cultured neurones.

The final Table 33 provides an overview of our results. Firstly, we wanted to establish what subtypes of GABA<sub>A</sub>R were predominantly expressed during the formation of GABAergic synapses between MSNs *in vitro*. From 7 to 14 DIV, MSNs showed an increase in the size of  $\alpha 2$ -containing GABA<sub>A</sub>R clusters and a decrease in the density of  $\alpha 1$ -containing GABA<sub>A</sub>R clusters. Thus, as they mature, MSNs tend to promote the formation of  $\alpha 2$ -containing synapses, suggesting an important role played by this subunit in the striatal GABAergic synapse formation. These findings are supported by the expression pattern of GABA<sub>A</sub>R in the adult striatum *in vivo*, which is known to express high levels of  $\alpha 2$  subunits and low levels of  $\alpha 1$  subunits of GABA<sub>A</sub>R (Fujiyama et al., 2000).

By treating purely GABAergic MSN cultures with the GABA<sub>A</sub>R antagonist bicuculline, we tried to establish the role played by GABA<sub>A</sub>R activity during GABAergic synapse formation. We have analysed the way MSNs responded to the GABA-deprived environment and concluded that while the size of  $\alpha 1$ -containing clusters was decreased, the size and the density of  $\alpha 2$ -containing GABA<sub>A</sub>R was increased. This

suggested that compensatory mechanisms involving  $\alpha 2$ -containing receptors were triggered in GABAergic activity-deprived environment. In addition, this revealed that the lack of activity induced a down-regulation of  $\alpha 1$ -containing receptors. However, the link between GABAergic activity and the regulation of postsynaptic GABA<sub>A</sub>Rs including  $\alpha 1$  or  $\alpha 2$  subunits remains to be elucidated.

The extracellular domains (ECDs) of GABA<sub>A</sub>Rs are large glycosylated domains and are exposed in the synaptic cleft. Thus, we hypothesised that they might play an important structural role during the initiation of GABAergic synapse formation by interacting with presynaptic proteins. We focused our study on  $\alpha 1$  and  $\alpha 2$  subunits because  $\alpha$  subunits are known to provide the GABA<sub>A</sub>Rs with specific kinetics and physiological properties (Olsen and Sieghart, 2009) and also because they are the most predominant subunits expressed throughout the formation of the striatum (Fujiyama et al., 2000). We decided to screen for a protein that would specifically bind the ECDs of  $\alpha 1$  or  $\alpha 2$  subunits using proteomics and mass spectrometry. As a result, we found that a heparan sulfate proteoglycans pikachurin was specifically binding the ECD of  $\alpha 2$  subunit. The expression of pikachurin was established across embryonic and adult brain areas *in vivo*, but also in the MSN cultures *in vitro*. In addition, co-localisation of pikachurin with synaptic  $\alpha 2$ -containing GABA<sub>A</sub>Rs was observed in the E20 brain. This binding was confirmed by binding assays and co-immunoprecipitation between the two proteins. However, the binding site where this interaction occurs and the role played by this interaction during GABAergic synapse formation has not been established yet.

Finally, we treated MSNs with purified  $\alpha 1$  or  $\alpha 2$  ECDs in early synapse formation stages (from 4 to 7 DIV) or during synapse stabilisation (from 7 to 14 DIV). These experiments showed that  $\alpha 1$  and  $\alpha 2$  ECDs were capable of promoting synapse formation at early developmental stages, although  $\alpha 2$  ECDs and not  $\alpha 1$  ECDs were able to promote synapse formation and stabilisation. This suggested that  $\alpha 1$  but mostly  $\alpha 2$  ECDs had synaptogenic effects on synapse formation and stabilisation,

emphasising the structural role played by these domains. However, the mechanisms by which these exogenous domains would trigger synapse formation remain unclear.

In conclusion, these results suggest that the extracellular domains of GABA<sub>A</sub>Rs play a role in both activity-dependent and structure-dependent functions. Interestingly, similarities shared by these mechanisms exist. Indeed, formation of  $\alpha$ 2-containing synapses is facilitated during normal development together with the accumulation of gephyrin at postsynaptic sites. In addition, the formation of  $\alpha$ 2-containing GABA<sub>A</sub>Rs is promoted when the system is deprived of GABAergic currents, possibly as compensatory mechanism. Finally, both the  $\alpha$ 1 and the  $\alpha$ 2 exogenous ECDs were able to increase the density of GABA<sub>A</sub>Rs and the density of functional GABAergic synapses per dendrites. These results are interestingly linked with each other as they both suggest a dominant structural and functional role of  $\alpha$ 2-containing GABA<sub>A</sub>Rs during the formation of GABAergic synapses in the embryonic basal ganglia. All together, our data show a prominent structural and physiological role of the  $\alpha$ 2 subunit in the striatum cultures which may lead us to a better understanding of the particular abundance of the GABA<sub>A</sub>R  $\alpha$ 2 subunit in the adult striatum.

### **8.5 *Limits of the analysis of GABAergic synapses***

In the result chapters 5, 6 and 7 of this thesis, we were interested in understanding the role played by  $\alpha$ 1 and  $\alpha$ 2 GABA<sub>A</sub>R subunits at the early stages of GABAergic synapse formation. To do so, we have cultured GABAergic medium spiny neurones at different developmental stages, fixed them with 4% (w/v) paraformaldehyde, performed immunostaining, and analysed the synaptic contacts under different treatments and conditions. Although we conducted a thorough and detailed study of synaptic contact formation in these three chapters, the inherent variability of the experiments depends on many different parameters. What are the technical limits and bias of these three result chapters?

The paraformaldehyde preserves the tissue by cross-linking proteins and maintains the relative positions of cellular structures. However, we noticed that it provoked a slight membrane disruption which could potentially alter the staining and interfere with the precision of the analysis. Indeed, the fixation with paraformaldehyde provoked an uncontrolled permeabilisation of the membrane which then led in some cases, to unwanted intracellular staining.

The primary and secondary antibodies used throughout immunolabelling sometimes lack of specificity, resulting in a misleading staining. In this thesis, the specificity of the antibodies used was already characterised. The rabbit antibody directed against the  $\alpha 1$  subunit of GABA<sub>A</sub>Rs was developed and characterised by Duggan and colleagues (Duggan and Stephenson, 1989), while the other antibodies were commercially available and also previously tested in the laboratory. However, the specificity of some conjugated secondary antibodies was unclear and some would cross-react with the MSN cultures. To prevent this trouble and determine which conjugated antibody to use, the MSN cultures were stained in the absence of primary antibodies and in the presence of secondary antibodies only (data not shown).

Immunolabelling was analysed using Zeiss LSM 710 confocal microscope with a Plan-Apochromat 63x/1.4 Oil DIC lens. Selecting cells could sometimes trigger a bias as the selection should be done randomly throughout the coverslip. However, the density of cells was not always even across the field. Some neurones were isolated from the rest of the network and showed different morphology compared to the group of neighbouring cells. To be consistent with the study of synapse formation within a GABAergic network, we selected the cells that were included within a network of neighbouring MSNs and avoided to image isolated neurones.

Although several washings were performed at different stages of the immunostaining, and a thorough control of the specificity of antibodies was done, background staining was inevitable. Therefore, the image was modified before the measurement of clusters was performed. First, the background staining intensity was

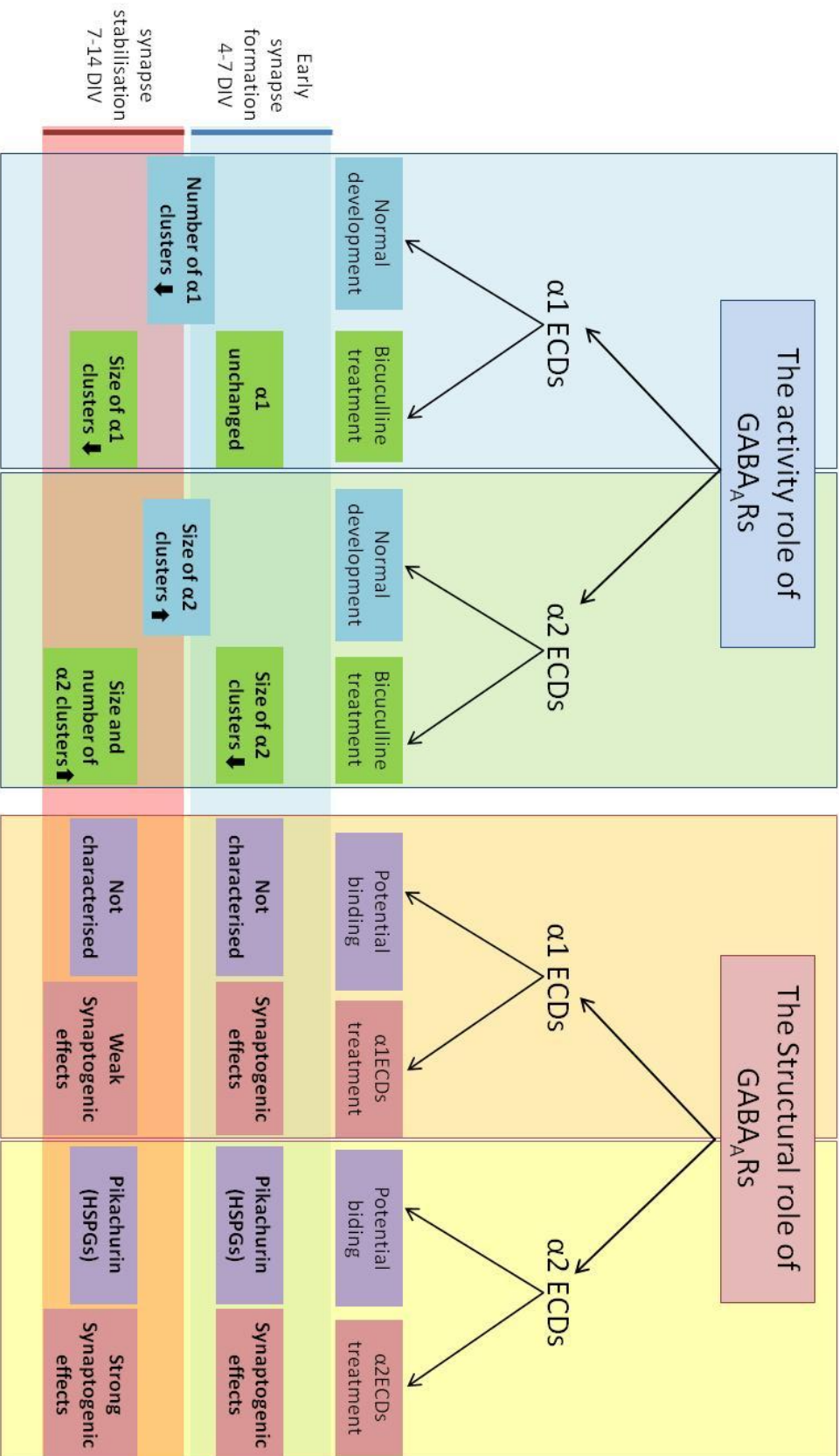
measured from a circle randomly placed in the extracellular space. Subsequently, the average intensity threshold of the image was adjusted for each channel so that any staining with lower or equal intensity to the background was removed from the image. Although the value of the background intensity could vary depending on where the circle was placed in the extracellular space, it was similar across the image.

In order to establish the density and size of  $\alpha 1$ - and  $\alpha 2$ -containing GABA<sub>A</sub> receptor clusters or gephyrin clusters, puncta were defined as immunoreactive profiles greater than  $0.1 \mu\text{m}^2$ , with the mean intensity of each cluster equal or higher than double the standard deviation of intensity which was indicated by the Zen 2009 Programme. These criteria were previously defined (Goffin et al., 2010) and allowed us to determine which puncta could be classified as a cluster with more restriction and precision.

The density and size of  $\alpha 1$  clusters were first calculated, followed by the  $\alpha 2$  clusters. Then,  $\alpha 1$  clusters which were co-localised with  $\alpha 2$  clusters ( $\alpha 1$  mixed clusters) were separated from  $\alpha 1$  clusters and analysed as a separate group. The same selection was applied to  $\alpha 2$  mixed clusters. A minimum of 50 % overlap between the two stainings was defined by eye. Although this method could decrease the strength of our results because it is subjective, the estimation was consistently and carefully performed throughout the analysis and carried by the same experimenter. The same criterion was applied to identify synaptic clusters which were in close apposition to the GAD-65-positive presynaptic nerve terminal and also to determine the density and proportion of  $\alpha 1$  and  $\alpha 2$ -containing clusters co-localised with gephyrin.

All together, a careful look at the way the analysis was carried throughout these three result chapters reveals technical limits and some bias. However, care and precision were maintained throughout the experiments, supporting the strength of the data. It would certainly be a major improvement if this analysis was carried by a specifically designed program adapted to our experiments.

**Table 33: Activity and structural role of GABA<sub>A</sub>R subunits  $\alpha 1$  and  $\alpha 2$  ECDs during GABAergic synapse formation.**



Activity and Structural role of GABA<sub>A</sub>R subunits  $\alpha 1$  and  $\alpha 2$  ECDs during GABAergic synapse formation

## 9. Bibliography

- Ahnert-Hilger G, Jahn R (2011) CLC-3 spices up GABAergic synaptic vesicles. *Nat Neurosci* 14:405-407.
- Albin RL, Young AB, Penney JB (1989) The functional anatomy of basal ganglia disorders. *Trends in neurosciences* 12:366-375.
- Ali A, Thomson A (2008) Synaptic alpha 5 subunit-containing GABAA receptors mediate IPSPs elicited by dendrite-preferring cells in rat neocortex. *Cereb Cortex* 18(6):1260-71.
- Arancibia-Carcamo I, Kittler JT (2009) Regulation of GABA<sub>A</sub> receptor membrane trafficking and synaptic localization. *Pharmacology and Therapeutics* 123:17-31.
- Bannai H, Lévi S, Schweizer C, Inoue T, Launey T, Racine V, Sibarita J-B, Mikoshiba K, Triller A (2009) Activity-dependent tuning of inhibitory neurotransmission based on GABA<sub>A</sub>R diffusion dynamics. *Neuron* 62:670-682.
- Bedford FK, Kittler JT, Muller E, Thomas P, Uren JM, Merlo D, Wisden W, Triller A, Smart TG, Moss SJ (2001) GABA(A) receptor cell surface number and subunit stability are regulated by the ubiquitin-like protein Plic-1. *Nature Neuroscience* 4:908-916.
- Ben-Ari Y, Gaiarsa JL, Tysio R, Khazipov R (2007) GABA: a pioneer transmitter that excites immature neurons and generates primitive oscillations. *Physiology Review* 1215–1284.
- Benhamou L, Bronfeld M, Bar-Gad I, Cohen D (2012) Globus pallidus external segment neuron classification in freely moving rats: A comparison to primates. *PLoS one* 7:e45421.
- Benson JA, Löw K, Keist R, Mohler H, Rudolph U (1998) Pharmacology of recombinant gamma-aminobutyric acid<sub>A</sub> receptors rendered diazepam-insensitive by point-mutated alpha-subunits. *FEBS Letter* 431(3): p. 400-404.
- Bevan MD, Booth PA, Eaton SA, Bolam JP (1998) Selective innervation of neostriatal interneurons by a subclass of neuron in the globus pallidus of the rat. *The Journal of neuroscience : the official journal of the Society for Neuroscience* 18:9438-9452.
- Biederer T, Sara Y, Mozhayeva M, Atasoy D, Liu X, Kavalali ET, Südhof TC (2002 ) SynCAM, a synaptic adhesion molecule that drives synapse assembly. *Science* 297(5586):1525-31.
- Birnir B, Eghbali M, Everitt AB, Gage PW (2000) Bicuculline, pentobarbital and diazepam modulate spontaneous GABAA channels in rat hippocampal neurons. *British journal of pharmacology* 131:695-704.
- Blake DJ, Weir A, Newey SE, Davies KE (2002) Function and genetics of dystrophin and dystrophin-related proteins in muscle. *Physiol Rev* 82(2):291-329.
- Bogdanov Y, Michels G, Armstrong-Gold C, Haydon PG, Lindstrom J, Pangalos M, Moss SJ (2006) Synaptic GABAA receptors are directly recruited from their extrasynaptic counterparts. *The EMBO journal* 25:4381-4389.
- Bohme I, Rabe H, Luddens H (2004) Four amino acids in the alpha subunits determine the gamma-aminobutyric acid sensitivities of GABAA receptor subtypes. *J Biol Chem* 279:35193-35200.
- Bolam JP, Hanley JJ, Booth PA, Bevan MD (2000) Synaptic organisation of the basal ganglia. *Journal of anatomy* 196 ( Pt 4):527-542.
- Bormann J (2000) the 'ABC' of GABA receptors. *Trends in pharmacological sciences* 21: p. 16-19.

- Bowery NG, Bettler B, Froestl W, Gallagher JP, Marshall F, Raiteri M, Bonner TI, Enna SJ (2002) International Union of Pharmacology. XXXIII. Mammalian gamma-Aminobutyric Acid B Receptors: Structure and Function. *Pharmacological reviews* 54: p. 247-264.
- Bracci E, Centonze D, Bernardi G, Calabresi P (2002) Dopamine excites fast-spiking interneurons in the striatum. *J Neurophysiol* 87:2190-2194.
- Brandon NJ, Jovanovic JN, Colledge M, Kittler JT, Brandon JM, Scott JD, Moss SJ (2003) A-kinase anchoring protein 79/150 facilitates the phosphorylation of GABA(A) receptors by cAMP-dependent protein kinase via selective interaction with receptor beta subunits. *Molecular and Cellular Neuroscience* 22:87-97.
- Breitbach K, Jarvis DL (2001) Improved glycosylation of a foreign protein by Tn-5B1-4 cells engineered to express mammalian glycosyltransferases. *Biotechnology and bioengineering* 74:230-239.
- Brewer GJ, Torricelli JR, Evege EK, Price PJ (1993) Optimized survival of hippocampal neurons in B27-supplemented Neurobasal, a new serum-free medium combination. *Journal of neuroscience research* 35:567-576.
- Brünig I, Scotti E, Sidler C, Fritschy J (2002) Intact sorting, targeting, and clustering of gamma-aminobutyric acid A receptor subtypes in hippocampal neurons in vitro. *Journal of Comparative Neurology* 443:43-55.
- Brussaard AB, Kits KS, Baker RE, Willems WP, Leyting-Vermeulen JW, Voorn P, Smit AB, Bicknell RJ, Herbison AE (1997) Plasticity in fast synaptic inhibition of adult oxytocin neurons caused by switch in GABA(A) receptor subunit expression. *Neuron* 19:1103-1114.
- Budreck EC, Scheiffele P (2007) Neuroligin-3 is a neuronal adhesion protein at GABAergic and glutamatergic synapses. *Eur J Neurosci* 26(7):1738-48.
- Bugaysen J, Bar-Gad I, Korngreen A (2013) Continuous Modulation of Action Potential Firing by a Unitary GABAergic Connection in the Globus Pallidus In Vitro. *The Journal of Neuroscience* 33:12805-12809.
- Cascio M, Shenkel S, Grodzicki RL, Sigworth FJ, Fox RO (2001) Functional reconstitution and characterization of recombinant human alpha 1-glycine receptors. *J Biol Chem* 276:20981-20988.
- Castro LR, Brito M, Guiot E, Polito M, Korn CW, Herve D, Girault JA, Paupardin-Tritsch D, Vincent P (2013) Striatal neurones have a specific ability to respond to phasic dopamine release. *The Journal of physiology* 591:3197-3214.
- Chattopadhyaya B, Di Cristo G, Wu CZ, Knott G, Kuhlman S, Fu Y, Palmiter RD, Huang ZJ (2007) GAD67-mediated GABA synthesis and signaling regulate inhibitory synaptic innervation in the visual cortex. *Neuron* 54:889-903.
- Chen ZW, Olsen RW (2007) GABAA receptor associated proteins: a key factor regulating GABAA receptor function. *Journal of Neurochemistry* 100:279-294.
- Chevalier G, Deniau JM (1990) Disinhibition as a basic process in the expression of striatal functions. *Trends in neurosciences* 13:277-280.
- Chubykin AA, Atasoy D, Etherton MR, Brose N, Kavalali ET, Gibson JR, Südhof TC (2007) Activity-dependent validation of excitatory versus inhibitory synapses by neuroligin-1 versus neuroligin-2. *Neuron* 54(6):919-31.
- Ciccarone VC, Polayes DA, Luckow VA (1998) Generation of Recombinant Baculovirus DNA in E.coli Using a Baculovirus Shuttle Vector. *Methods in molecular medicine* 13:213-235.



- Cline H (2005) Synaptogenesis: A Balancing Act between Excitation and Inhibition. *Current Biology* 15:R203-R205.
- Collins GG (1972) GABA-2-oxoglutarate transaminase, glutamate decarboxylase and the half-life of GABA in different areas of rat brain. *Biochemistry and Pharmacology* 21(21): p. 2849-58.
- Collinson N, Kuenzi FM, Jarolimek W, Maubach KA, Cothliff R, Sur C, Smith A, Otu FM, Howell O, Atack JR, McKernan RM, Seabrook GR, Dawson GR, Whiting PJ, Rosahl TW (2002) Enhanced learning and memory and altered GABAergic synaptic transmission in mice lacking the alpha 5 subunit of the GABAA receptor. *J Neurosci* 22(13):5572-80.
- Connolly CN, Krishek BJ, McDonald BJ, Smart TG, Moss SJ (1996a) Assembly and cell surface expression of heteromeric and homomeric gamma-aminobutyric acid type A receptors. *Journal of Biological Chemistry* 271:89-96.
- Connolly CN, Wooltorton JR, Smart TG, Moss SJ (1996b) Subcellular localization of gamma-aminobutyric acid type A receptors is determined by receptor beta subunits. *Proc Natl Acad Sci U S A* 93:9899-9904.
- Conti F, DeBiasi S, Minelli A, Rothstein JD, Melone M (1998a) EAAC1, a high-affinity glutamate transporter, is localized to astrocytes and gabaergic neurons besides pyramidal cells in the rat cerebral cortex. *Cereb Cortex* 8:108-116.
- Conti F, Melone M, De Biasi S, Minelli A, Brecha NC, Ducati A (1998b) Neuronal and glial localization of GAT-1, a high-affinity gamma-aminobutyric acid plasma membrane transporter, in human cerebral cortex: with a note on its distribution in monkey cortex. *J Comp Neurol* 396:51-63.
- Craig AM, Banker G, Chang W, McGrath ME, Serpinskaya AS (1996) Clustering of gephyrin at GABAergic but not glutamatergic synapses in cultured rat hippocampal neurons. *J Neurosci* 16(10):3166-77.
- Craig R, Cortens JP, Beavis RC (2004) Open source system for analyzing, validating, and storing protein identification data. *Journal of proteome research* 3:1234-1242.
- Crestani F, Lorez M, Baer K, Essrich C, Benke D, Laurent JP, Belzung C, Fritschy JM, Lüscher B, Mohler H (1999) Decreased GABA<sub>A</sub>-receptor clustering results in enhanced anxiety and a bias for threat cues. *Nature Neuroscience* 2:833 - 839.
- Danglot L, Triller A, Bessis A (2003) Association of gephyrin with synaptic and extrasynaptic GABAA receptors varies during development in cultured hippocampal neurons. *Mol Cell Neurosci* 23(2):264-78.
- Deacon TW, Pakzaban P, Isacson O (1994) The lateral ganglionic eminence is the origin of cells committed to striatal phenotypes: neural transplantation and developmental evidence. *Brain Res* 668:211-219.
- Dehorter N, Guigoni C, Lopez C, Hirsch J, Eusebio A, Ben-Ari Y, Hammond C (2009) Dopamine-deprived striatal GABAergic interneurons burst and generate repetitive gigantic IPSCs in medium spiny neurons. *The Journal of neuroscience : the official journal of the Society for Neuroscience* 29:7776-7787.
- Deuchars J, West DC, Thomson AM (1994) Relationships between morphology and physiology of pyramid-pyramid single axon connections in rat neocortex in vitro. *The Journal of physiology* 478:423-435.
- Dieni CV, Chancey JH, Overstreet-Wadiche LS (2013) Dynamic functions of GABA signaling during granule cell maturation. *Frontiers in Neural Circuits* 6.

Doig NM, Moss J, Bolam JP (2010) Cortical and thalamic innervation of direct and indirect pathway medium-sized spiny neurons in mouse striatum. *The Journal of neuroscience : the official journal of the Society for Neuroscience* 30:14610-14618.

Duggan MJ, Pollard S, Stephenson FA (1991) Immunoaffinity purification of GABA<sub>A</sub> receptor alpha-subunit iso-oligomers. Demonstration of receptor populations containing alpha 1 alpha 2, alpha 1 alpha 3, and alpha 2 alpha 3 subunit pairs. *J Biol Chem* 266:24778-24784.

Duggan MJ, Stephenson FA (1989) Bovine gamma-aminobutyric acidA receptor sequence-specific antibodies: identification of two epitopes which are recognised in both native and denatured gamma-aminobutyric acidA receptors. *J Neurochem* 53:132-139.

Duggan MJ, Stephenson FA (1990) Biochemical evidence for the existence of gamma-aminobutyrateA receptor iso-oligomers. *J Biol Chem* 265:3831-3835.

Durieux PF, Schiffmann SN, de Kerchove d'Exaerde A (2011) Targeting neuronal populations of the striatum. *Frontiers in Neuroanatomy* 5.

Ebert B, Wafford KA, Whiting PJ, Krosgaard-Larsen P, Kemp JA (1994) Molecular pharmacology of gamma-aminobutyric acid type A receptor agonists and partial agonists in oocytes injected with different alpha, beta, and gamma receptor subunit combinations. *Molecular pharmacology* 46:957-963.

Edwards RH (2007) The neurotransmitter cycle and quantal size. *Neuron* 55:835-858.

Elster L, Schousboe A, Olsen RW (2000) Stable GABA(A) receptor intermediates in SF-9 cells expressing alpha1, beta2 and gamma2 subunits. *Journal of neuroscience research* 61:193-205.

Engin E, Liu J, Rudolph U (2012) alpha2-containing GABA(A) receptors: a target for the development of novel treatment strategies for CNS disorders. *Pharmacology & therapeutics* 136:142-152.

English DF, Ibanez-Sandoval O, Stark E, Tecuapetla F, Buzsaki G, Deisseroth K, Tepper JM, Koos T (2012) GABAergic circuits mediate the reinforcement-related signals of striatal cholinergic interneurons. *Nat Neurosci* 15:123-130.

Erlander M, Tillakaratne N, Feldblum S, Patel N, Tobin A (1991) Two genes encode distinct glutamate decarboxylases. *Neuron* 7:91-100.

Ernst M, Brauchart D, Boresch S, Sieghart W (2003) Comparative modeling of GABA(A) receptors: limits, insights, future developments. *Neuroscience* 119(4):933-43.

Essrich C, Lorez M, Benson JA, Fritschy JM, Luscher B (1998) Postsynaptic clustering of major GABA<sub>A</sub> receptor subtypes requires the gamma 2 subunit and gephyrin. *Nat Neurosci* 1:563-571.

Fairless R, Masius H, Rohlmann A, Heupel K, Ahmad M, Reissner C, Dresbach T, Missler M (2008) Polarized targeting of neurexins to synapses is regulated by their C-terminal sequences. *J Neurosci* 28(48):12969-81.

Falk T, Zhang S, Erbe EL, Sherman SJ (2006) Neurochemical and electrophysiological characteristics of rat striatal neurons in primary culture. *J Comp Neurol* 494:275-289.

Farrar S, Whiting P, Bonnert T, McKernan R (1999) Stoichiometry of a ligand-gated ion channel determined by fluorescence energy transfer. *Journal of Biological Chemistry* 274:10111-10104.

Fasano C, Bourque MJ, Lapointe G, Leo D, Thibault D, Haber M, Kortleven C, Desgroseillers L, Murai KK, Trudeau LE (2013) Dopamine facilitates dendritic spine formation by cultured striatal

medium spiny neurons through both D1 and D2 dopamine receptors. *Neuropharmacology* 67:432-443.

Ferreira A (1999) Abnormal synapse formation in agrin-depleted hippocampal neurons. *Journal of cell science* 112 ( Pt 24):4729-4738.

Fisone G, Hakansson K, Borgkvist A, Santini E (2007) Signaling in the basal ganglia: postsynaptic and presynaptic mechanisms. *Physiology & behavior* 92:8-14.

Folch J, Ascoli I, Lees M, Meath JA, Le BN (1951) Preparation of lipide extracts from brain tissue. *J Biol Chem* 191:833-841.

Fritschy J, Brünig I (2003) Formation and plasticity of GABAergic synapses: physiological mechanisms and pathophysiological implications. *Pharmacol Ther* 98(3):299-323.

Fritschy J, Paysan J, Enna A, Mohler H (1994) Switch in the expression of rat GABAA-receptor subtypes during postnatal development: an immunohistochemical study. *J Neurosci* 14(9):5302-24.

Fritschy JM, Mohler H (1995) GABAA-receptor heterogeneity in the adult rat brain: differential regional and cellular distribution of seven major subunits. *J Comp Neurol* 359:154-194.

Fritschy JM, Panzanelli P (2014) GABAA receptors and plasticity of inhibitory neurotransmission in the central nervous system. *Eur J Neurosci* 39:1845-1865.

Fritschy JM, Panzanelli P, Tyagarajan SK (2012) Molecular and functional heterogeneity of GABAergic synapses. *Cellular and molecular life sciences : CMLS* 69:2485-2499.

Frola E, Patrizi A, Goetz T, Medrihan L, Petrini EM, Barberis A, Wulff P, Wisden W, Sassoe-Pognetto M (2013) Synaptic competition sculpts the development of GABAergic axo-dendritic but not perisomatic synapses. *PloS one* 8:e56311.

Fuchs C, Abitbol K, Burden JJ, Mercer A, Brown L, Iball J, Anne Stephenson F, Thomson AM, Jovanovic JN (2013) GABA(A) receptors can initiate the formation of functional inhibitory GABAergic synapses. *Eur J Neurosci* 38:3146-3158.

Fujiyama F, Fritschy JM, Stephenson FA, Bolam JP (2000) Synaptic localization of GABA(A) receptor subunits in the striatum of the rat. *J Comp Neurol* 416:158-172.

Galanopoulou AS (2010) Mutations affecting GABAergic signaling in seizures and epilepsy. *Pflugers Archiv : European journal of physiology* 460:505-523.

Gangarossa G, Espallergues J, Mailly P, De Bundel D, De Kerchove D'Exaerde A, Hervé D, Girault J-A, Valjent E, Krieger P (2013) Spatial distribution of D1R- and D2R-expressing medium-sized spiny neurons differs along the rostral-caudal axis of the mouse dorsal striatum. *Frontiers in Neural Circuits* 7.

Gerfen CR, Surmeier DJ (2011) Modulation of striatal projection systems by dopamine. *Annual review of neuroscience* 34:441-466.

Gittis AH, Kreitzer AC (2012) Striatal microcircuitry and movement disorders. *Trends in neurosciences* 35:557-564.

Goffin D, Ali AB, Rampersaud N, Harkavyi A, Fuchs C, Whitton PS, Nairn AC, Jovanovic JN (2010) Dopamine-dependent tuning of striatal inhibitory synaptogenesis. *The Journal of neuroscience : the official journal of the Society for Neuroscience* 30:2935-2950.

Graf ER, Zhang X, Jin SX, Linhoff MW, Craig AM (2004) Neurexins induce differentiation of GABA and glutamate postsynaptic specializations via neuroligins. *Cell* 119:1013-1026.

- Greengard P, Allen PB, Nairn AC (1999) Beyond the Dopamine Receptor: the DARPP-32/Protein Phosphatase-1 Cascade. *Neuron* 23:435-447.
- Grenningloh G, Gundelfinger E, Schmitt B, Betz H, Darlison MG, Barnard EA, Schofield PR, Seeburg PH (1987) Glycine vs GABA receptors. *Nature* 330:25-26.
- Gross A, Sims R, Swinny J, Sieghart W, Bolam J, Stanford I (2011) Differential localization of GABA(A) receptor subunits in relation to rat striatopallidal and pallidopallidal synapses. *Eur J Neurosci* 33(5):868-78.
- Günther U, Benson J, Benke D, Fritschy J, Reyes G, Knoflach F, Crestani F, Aguzzi A, Arigoni M, Lang Y (1995) Benzodiazepine-insensitive mice generated by targeted disruption of the gamma 2 subunit gene of gamma-aminobutyric acid type A receptors. *Proc Natl Acad Sci USA* 92:7749–7753.
- Han J, Townes-Anderson E (2012) Cell specific post-translational processing of pikachurin, a protein involved in retinal synaptogenesis. *PLoS one* 7:e50552.
- Hartman KN, Pal SK, Burrone J, Murthy VN (2006) Activity-dependent regulation of inhibitory synaptic transmission in hippocampal neurons. *Nat Neurosci* 9:642-649.
- Harvey K, Duguid I, Alldred M, Beatty S, Ward H, Keep N, Lingenfelter S, Pearce B, Lundgren J, Owen M, Smart T, Lüscher B, Rees M, Harvey R (2004) The GDP-GTP exchange factor collybistin: an essential determinant of neuronal gephyrin clustering. *J Neurosci* 24(25):5816-26.
- Henschel O GK, Bordey A. (2008) GABA<sub>A</sub> receptors, anesthetics and anticonvulsants in brain development. *CNS Neurol Disord Drug Targets* (2):211-24.
- Hille B (2001) *Ion channels of excitable membranes*. Sunderland, Mass.: Sinauer Associates.
- Hines R, Davies P, Moss S, Maguire J (2011) functional regulation of GABA<sub>A</sub> Receptors in nervous system pathologies. *current Opinion in Cell Biology* 22: p. 1-7.
- Hoffmann A, Roeder RG (1991) Purification of his-tagged proteins in non-denaturing conditions suggests a convenient method for protein interaction studies. *Nucleic acids research* 19:6337-6338.
- Homanics G, DeLorey T, Firestone L, Quinlan J, Handforth A, Harrison N, Krasowski M, Rick C, Korpi E, Mäkelä R, Brilliant M, Hagiwara N, Ferguson C, Snyder K, Olsen R (1997) Mice devoid of gamma-aminobutyrate type A receptor beta3 subunit have epilepsy, cleft palate, and hypersensitive behavior. *Proc Natl Acad Sci USA* 94:4143-4148.
- Hoon M, Bauer G, Fritschy JM, Moser T, Falkenburger BH, Varoqueaux F (2009) Neuroligin 2 controls the maturation of GABAergic synapses and information processing in the retina. *The Journal of Neuroscience* 29:8039-8050.
- Hu H, Li J, Zhang Z, Yu M (2011) Pikachurin interaction with dystroglycan is diminished by defective O-mannosyl glycosylation in congenital muscular dystrophy models and rescued by LARGE overexpression. *Neuroscience letters* 489:10-15.
- Huang J, Scheiffele P (2008) GABA and neuroligin signaling: linking synaptic activity and adhesion in inhibitory synapse development. *Current Opinion Neurobiology* 18:77-83.
- Jacob TC, Bogdanov YD, Magnus C, Saliba RS, Kittler JT, Haydon PG, Moss SJ (2005) Gephyrin regulates the cell surface dynamics of synaptic GABA<sub>A</sub> receptors. *The Journal of Neuroscience* 25:10469-10478.
- Jacob TC, Moss SJ, Jurd R (2008) GABA(A) receptor trafficking and its role in the dynamic modulation of neuronal inhibition. *Nat Rev Neurosci* 9:331-343.

- Jain M, Armstrong R, Barker R, Rosser A (2001) Cellular and molecular aspects of striatal development. *Brain Research Bulletin* 55:533-540.
- Janssen M, Yasuda R, Vicini S (2011) GABAA receptor  $\beta 3$  subunit expression regulates tonic current in developing striatopallidal medium spiny neurons. *frontiers in cellular neurosciences* 5.
- Jin H, Wu H, Osterhaus G, Wei J, Davis K, Sha D, Floor E, Hsu CC, Kopke RD, Wu JY (2003) Demonstration of functional coupling between gamma -aminobutyric acid (GABA) synthesis and vesicular GABA transport into synaptic vesicles. *Proc Natl Acad Sci U S A* 100:4293-4298.
- Jung MJ, Lippert B, Metcalf BW, Schechter PJ, Bohlen P, Sjoerdsma A (1977) The effect of 4-amino hex-5-ynoic acid (gamma-acetylenic GABA, gamma-ethynyl GABA) a catalytic inhibitor of GABA transaminase, on brain GABA metabolism in vivo. *J Neurochem* 28:717-723.
- Kanagawa M, Omori Y, Sato S, Kobayashi K, Miyagoe-Suzuki Y, Takeda S, Endo T, Furukawa T, Toda T (2010) Post-translational maturation of dystroglycan is necessary for pikachurin binding and ribbon synaptic localization. *J Biol Chem* 285:31208-31216.
- Kandel ER (2013) *Principles of neural science*. New York: McGraw-Hill Medical.
- Kanematsu T, Yamaguchi T, Nagahama H, Yoshimura K, Hidaka K, Matsuda M, Takeuchi H, Misumi Y, Nakayama K, Yamamoto T, Akaike N, Hirata M, Nakayama K. (2002) Role of the PLC-related, catalytically inactive protein p130 in GABA(A) receptor function. *EMBO Journal* 21:1004-1011.
- Kang Y, Ge Y, Cassidy RM, Lam V, Luo L, Moon KM, Lewis R, Molday RS, Wong RO, Foster LJ, Craig AM (2014) A combined transgenic proteomic analysis and regulated trafficking of neuroligin-2. *J Biol Chem*.
- Kang Y, Zhang X, Dobie F, Wu H, Craig AM (2008) Induction of GABAergic postsynaptic differentiation by alpha-neurexins. *J Biol Chem* 283(4):2323-34.
- Karlin A, Akabas MH (1995) Toward a structural basis for the function of nicotinic acetylcholine receptors and their cousins. *Neuron* 15:1231-1244.
- Kasugai Y, Swinny JD, Roberts JD, Dalezios Y, Fukazawa Y, Sieghart W, Shigemoto R, Somogyi P (2010) Quantitative localisation of synaptic and extrasynaptic GABAA receptor subunits on hippocampal pyramidal cells by freeze-fracture replica immunolabelling. *Eur J Neurosci* 32:1868-1888.
- Katoh K, Omori Y, Furukawa T (2009) [Extracellular matrix protein, Pikachurin, is required for photoreceptor ribbon synapse formation]. *Tanpakushitsu kakusan koso Protein, nucleic acid, enzyme* 54:1166-1172.
- Kawaguchi Y (1993) Physiological, morphological, and histochemical characterization of three classes of interneurons in rat neostriatum. *The Journal of Neuroscience* 13:4908-4923.
- Keller C, Yuan X, Panzanelli P, Martin M, Alldred M, Sassoè-Pognetto M, Lüscher B (2004) The gamma2 subunit of GABA(A) receptors is a substrate for palmitoylation by GODZ. *Journal of Neuroscience* 24:5881-5891.
- Kins S, Betz H, Kirsch J (2000) Collybistin, a newly identified brain-specific GEF, induces submembrane clustering of gephyrin. *Nat Neurosci* 3(1):22-9.
- Kittler J, Chen G, Honing S, Bogdanov Y, McAinsh K, Arancibia-Carcamo I, Jovanovic J, Pangalos M, Haucke V, Yan Z, Moss S (2005) Phospho-dependent binding of the clathrin AP2 adaptor complex to GABAA receptors regulates the efficacy of inhibitory synaptic transmission. *Proc Natl Acad Sci U S A* 102:14871-14876.

Kittler J, Chen G, Kukhtina V, Vahedi-Faridi A, Gu Z, Tretter V, Smith K, McAinsh K, Arancibia-Carcamo I, Saenger W, Haucke V, Yan Z, Moss S (2008) Regulation of synaptic inhibition by phospho-dependent binding of the AP2 complex to a YECL motif in the GABAA receptor gamma2 subunit. *Proc Natl Acad Sci U S A* 9.

Kittler J, Delmas P, Jovanovic J, Brown D, Smart T, Moss S (2000) Constitutive endocytosis of GABAA receptors by an association with the adaptin AP2 complex modulates inhibitory synaptic currents in hippocampal neurons. *Journal of Neuroscience* 20:7972-7977.

Kittler J, Rostaing P, Schiavo G, Fritschy J, Olsen R, Triller A, Moss S (2001) The subcellular distribution of GABARAP and its ability to interact with NSF suggest a role for this protein in the intracellular transport of GABA(A) receptors. *Molecular and Cellular Neuroscience* 18:13-25.

Kittler J, Thomas P, Tretter V, Bogdanov Y, Haucke V, Smart T, Moss S (2004) Huntingtin-associated protein 1 regulates inhibitory synaptic transmission by modulating gamma-aminobutyric acid type A receptor membrane trafficking. *Proc Natl Acad Sci U S A* 101:12736-12741.

Klausberger T, Roberts J, Somogyi P (2002) Cell type- and input-specific differences in the number and subtypes of synaptic GABA(A) receptors in the hippocampus. *Journal of Neuroscience* 22:2513-2521.

Kleizen B, Braakman I (2004 ) Protein folding and quality control in the endoplasmic reticulum. *Current Opinion in Cell Biology* 4:343-349.

Kneussel M, Betz H (2000) Receptors, gephyrin and gephyrin-associated proteins: novel insights into the assembly of inhibitory postsynaptic membrane specializations. *Journal of Physiology* 525:1-9.

Kneussel M, Brandstätter J, Laube B, Stahl S, Müller U, Betz H (1999) Loss of postsynaptic GABA(A) receptor clustering in gephyrin-deficient mice. *J Neurosci* 19(21):9289-97.

Knight AR, Hartnett C, Marks C, Brown M, Gallager D, Tallman J, Ramabhadran TV (1998) Molecular size of recombinant alpha1beta1 and alpha1beta1gamma2 GABAA receptors expressed in Sf9 cells. *Receptors & channels* 6:1-18.

Knuesel I, Bornhauser B, Zuellig R, Heller F, Schaub M, Fritschy J (2000) Differential expression of utrophin and dystrophin in CNS neurons: an in situ hybridization and immunohistochemical study. *J Comp Neurol* 422(4):594-611.

Knuesel I, Mastrocola M, Zuellig R, Bornhauser B, Schaub M, Fritschy J (1999) Short communication: altered synaptic clustering of GABAA receptors in mice lacking dystrophin (mdx mice). *Eur J Neurosci* 11(12):4457-62.

Koos T, Tepper JM (2002) Dual cholinergic control of fast-spiking interneurons in the neostriatum. *The Journal of neuroscience : the official journal of the Society for Neuroscience* 22:529-535.

Korpi ER, Mihalek RM, Sinkkonen ST, Hauer B, Hevers W, Homanics GE, Sieghart W, Luddens H (2002) Altered receptor subtypes in the forebrain of GABA(A) receptor delta subunit-deficient mice: recruitment of gamma 2 subunits. *Neuroscience* 109:733-743.

Kowalski C, Crest M, Vuillet J, Pin T, Gola M, Nieoullon A (1995) Emergence of a synaptic neuronal network within primary striatal cultures seeded in serum-free medium. *Neuroscience* 64:979-993.

Kralic JE, Korpi ER, O'Buckley TK, Homanics GE, Morrow AL (2002) Molecular and pharmacological characterization of GABA(A) receptor alpha1 subunit knockout mice. *The Journal of pharmacology and experimental therapeutics* 302:1037-1045.

- Kralic JE, Sidler C, Parpan F, Homanics GE, Morrow AL, Fritschy JM (2006) Compensatory alteration of inhibitory synaptic circuits in cerebellum and thalamus of gamma-aminobutyric acid type A receptor alpha1 subunit knockout mice. *J Comp Neurol* 495:408-421.
- Kueh S, Head S, Morley J (2008) GABA(A) receptor expression and inhibitory post-synaptic currents in cerebellar Purkinje cells in dystrophin-deficient mdx mice. *Clin Exp Pharmacol Physiol* 35(2):207-10.
- Kuriyama K, Haber B, Siskin B, Roberts E (1966) The gamma-aminobutyric acid system in rabbit cerebellum. *Proc Natl Acad Sci U S A* 55:846-852.
- Lalchandani RR, Vicini S (2013) Inhibitory collaterals in genetically identified medium spiny neurons in mouse primary corticostriatal cultures. *Physiological reports* 1:e00164.
- Laurie D, Wisden W, Seeburg P (1992) The distribution of thirteen GABAA receptor subunit mRNAs in the rat brain. III. Embryonic and postnatal development. *Journal of Neuroscience* 12:4151-4172.
- Leisman G, Braun-Benjamin O, Melillo R (2014) Cognitive-motor interactions of the basal ganglia in development. *Frontiers in systems neuroscience* 8:16.
- Lévi S, Grady RM, Henry MD, Campbell KP, Sanes JR, Craig AM (2002) Dystroglycan is selectively associated with inhibitory GABAergic synapses but is dispensable for their differentiation. *J Neurosci* 22(11):4274-85.
- Lévi S, Logan SM, Tovar KR, Craig AM (2004) Gephyrin is critical for glycine receptor clustering but not for the formation of functional GABAergic synapses in hippocampal neurons. *J Neurosci* 24(1):207-17.
- Lévi S, Schweizer C, Bannai H, Pascual O, Charrier C, Triller A (2008) Homeostatic regulation of synaptic GlyR numbers driven by lateral diffusion. *Neuron* 59(2):261-73.
- Lewis SJ, Caldwell MA, Barker RA (2003) Modern therapeutic approaches in Parkinson's disease. *Expert reviews in molecular medicine* 5:1-20.
- Linhoff MW, Lauren J, Cassidy RM, Dobie FA, Takahashi H, Nygaard HB, Airaksinen MS, Strittmatter SM, Craig AM (2009) An unbiased expression screen for synaptogenic proteins identifies the LRRTM protein family as synaptic organizers. *Neuron* 61:734-749.
- Llinás RR, Ribary U, Jeanmonod D, Kronberg E, Mitra PP (1999) Thalamocortical dysrhythmia: A neurological and neuropsychiatric syndrome characterized by magnetoencephalography. *Proceedings of the National Academy of Sciences* 96:15222-15227.
- Loeblich S, Bähring R, Katsuno T, Tsukita S, Kneussel M (2006) Activated radixin is essential for GABAA receptor alpha5 subunit anchoring at the actin cytoskeleton. *EMBO J* 25(5):987-99.
- Löw K, Crestani F, Keist R, Benke D, Brünig I, Benson JA, Fritschy JM, Rüllicke T, Bluethmann H, Möhler H, Rudolph U (2000) Molecular and neuronal substrate for the selective attenuation of anxiety. *Science* 290:131-134.
- Luo R, Janssen MJ, Partridge JG, Vicini S (2013a) Direct and GABA-mediated indirect effects of nicotinic ACh receptor agonists on striatal neurones. *The Journal of physiology* 591:203-217.
- Luo R, Partridge JG, Vicini S (2013b) Distinct roles of synaptic and extrasynaptic GABAA receptors in striatal inhibition dynamics. *Frontiers in Neural Circuits* 7.
- Luscher B, Fuchs T, Kilpatrick C (2011) GABA<sub>A</sub> Receptor trafficking-mediated plasticity of inhibitory synapses. *Neuron* 70.

- Lüscher B, Keller C (2004) Regulation of GABAA receptor trafficking, channel activity, and functional plasticity of inhibitory synapses. *Pharmacology and Therapeutics* 102:195-221.
- Macdonald R, Olsen R (1994) GABAA receptor channels. *Annu Rev Neurosci* 17:569-602.
- Mallet N, Le Moine C, Charpier S, Gonon F (2005) Feedforward inhibition of projection neurons by fast-spiking GABA interneurons in the rat striatum in vivo. *The Journal of Neuroscience* 25:3857-3869.
- Marin O, Anderson SA, Rubenstein JL (2000) Origin and molecular specification of striatal interneurons. *The Journal of Neuroscience* 20:6063-6076.
- Mariner R, Jackson AW, 3rd, Levitas A, Hagerman RJ, Braden M, McBogg PM, Smith AC, Berry R (1986) Autism, mental retardation, and chromosomal abnormalities. *Journal of autism and developmental disorders* 16:425-440.
- Marty S, Wehrle R, Fritschy JM, Sotelo C (2004) Quantitative effects produced by modifications of neuronal activity on the size of GABAA receptor clusters in hippocampal slice cultures. *Eur J Neurosci* 20:427-440.
- Matsumoto-Miyai K, Sokolowska E, Zurlinden A, Gee CE, Luscher D, Hettwer S, Wolfel J, Ladner AP, Ster J, Gerber U, Rulicke T, Kunz B, Sonderegger P (2009) Coincident pre- and postsynaptic activation induces dendritic filopodia via neurotrypsin-dependent agrin cleavage. *Cell* 136:1161-1171.
- McClellan A, Twyman R (1999) Receptor system response kinetics reveal functional subtypes of native murine and recombinant human GABAA receptors. *Journal of Physiology* 515:711-727.
- McIntire S, Reimer R, Schuske K, Edwards R, Jorgensen E (1997) Identification and characterization of the vesicular GABA transporter. *Nature* 389(6653):870-6.
- McKernan R, Rosahl T, Reynolds D, Sur C, Wafford K, Atack J, Farrar S, Myers J, Cook G, Ferris P, Garrett L, Bristow L, Marshall G, Macaulay A, Brown N, Howell O, Moore K, Carling R, Street L, Castro J, Ragan C, Dawson G, Whiting P (2000) Sedative but not anxiolytic properties of benzodiazepines are mediated by the GABA(A) receptor alpha1 subtype. *Nature Neuroscience* 3:587-592.
- Mhatre MC, Pena G, Sieghart W, Ticku MK (1993) Antibodies specific for GABAA receptor alpha subunits reveal that chronic alcohol treatment down-regulates alpha-subunit expression in rat brain regions. *J Neurochem* 61:1620-1625.
- Miller PS, Aricescu AR (2014) Crystal structure of a human GABA receptor. *Nature*.
- Minelli A, DeBiasi S, Brecha NC, Zuccarello LV, Conti F (1996) GAT-3, a high-affinity GABA plasma membrane transporter, is localized to astrocytic processes, and it is not confined to the vicinity of GABAergic synapses in the cerebral cortex. *The Journal of Neuroscience* 16:6255-6264.
- Mink JW, Thach WT (1993) Basal ganglia intrinsic circuits and their role in behavior. *Current opinion in neurobiology* 3:950-957.
- Missler M, Südhof T (1998) Neurexins: three genes and 1001 products. *Trends Genet* 14(1):20-6.
- Missler M, Zhang W, Rohlmann A, Kattenstroth G, Hammer R, Gottmann K, Südhof T (2003) Alpha-neurexins couple Ca<sup>2+</sup> channels to synaptic vesicle exocytosis. *Nature* 26;423(6943):939-48.



- Mohler H, Fritschy JM, Rudolph U (2002) A new benzodiazepine pharmacology. *The Journal of pharmacology and experimental therapeutics* 300:2-8.
- Mohler H, Knoflach F, Paysan J, Motejlek K, Benke D, Lüscher B, Fritschy J (1995) Heterogeneity of GABAA-receptors: cell-specific expression, pharmacology, and regulation. *Neurochem Res* 20(5):631-6.
- Moss SJ, Smart TG (2001) Constructing inhibitory synapses. *Nat Rev Neurosci* 2:240-250.
- Muir J, Kittler J (2014) Plasticity of GABAA receptor diffusion dynamics at the axon initial segment. *Frontiers in Cellular Neuroscience* 8.
- Mukherjee J, Kretschmannova K, Gouzer G, Maric HM, Ramsden S, Tretter V, Harvey K, Davies PA, Triller A, Schindelin H, Moss SJ (2011) The residence time of GABA(A)Rs at inhibitory synapses is determined by direct binding of the receptor alpha1 subunit to gephyrin. *The Journal of Neuroscience* 31:14677-14687.
- Nusser Z, Ahmad Z, Tretter V, Fuchs K, Wisden W, Sieghart W, Somogyi P (1999) Alterations in the expression of GABAA receptor subunits in cerebellar granule cells after the disruption of the alpha6 subunit gene. *Eur J Neurosci* 11:1685-1697.
- Nusser Z, Mody I (2002) Selective modulation of tonic and phasic inhibitions in dentate gyrus granule cells. *J Neurophysiol* 87(5):2624-8.
- Nusser Z, Sieghart W, Benke D, Fritschy J, Somogyi P (1996) Differential synaptic localization of two major gamma-aminobutyric acid type A receptor alpha subunits on hippocampal pyramidal cells. *Proc Natl Acad Sci U S A* 93:11939-11944.
- Nyíri G, Freund T, Somogyi P (2001) Input-dependent synaptic targeting of alpha(2)-subunit-containing GABA(A) receptors in synapses of hippocampal pyramidal cells of the rat. *Eur J Neurosci* 13:428-442.
- Obeso JA, Marin C, Rodriguez-Oroz C, Blesa J, Benitez-Temino B, Mena-Segovia J, Rodriguez M, Olanow CW (2008) The basal ganglia in Parkinson's disease: current concepts and unexplained observations. *Annals of neurology* 64 Suppl 2:S30-46.
- Olsen R, Sieghart W (2008) International Union of Pharmacology. LXX. Subtypes of gamma-aminobutyric acid(A) receptors: classification on the basis of subunit composition, pharmacology, and function. *Pharmacol Rev* 60(3):243-60.
- Olsen RW, Sieghart W (2009) GABAA receptors: subtypes provide diversity of function and pharmacology. *Neuropharmacology* 56:141-148.
- Olsson M, Bjorklund A, Campbell K (1998) Early specification of striatal projection neurons and interneuronal subtypes in the lateral and medial ganglionic eminence. *Neuroscience* 84:867-876.
- Omori Y, Araki F, Chaya T, Kajimura N, Irie S, Terada K, Muranishi Y, Tsujii T, Ueno S, Koyasu T, Tamaki Y, Kondo M, Amano S, Furukawa T (2012) Presynaptic dystroglycan-pikachurin complex regulates the proper synaptic connection between retinal photoreceptor and bipolar cells. *The Journal of Neuroscience* 32:6126-6137.
- Ornstein L (1964) Disc eletrophoresis.I. background and theory. *Annals of the New York Academy of Sciences* 121:321-349.
- Ortells M, Lunt G (1995) evolutionary history of the ligand- gated ion-channel superfamily of receptors. *Trends Neuroscience* 18:121-127.

- Panzanelli P, Gunn BG, Schlatter MC, Benke D, Tyagarajan SK, Scheiffele P, Belelli D, Lambert JJ, Rudolph U, Fritschy JM (2011) Distinct mechanisms regulate GABAA receptor and gephyrin clustering at perisomatic and axo-axonic synapses on CA1 pyramidal cells. *The Journal of physiology* 589:4959-4980.
- Papadopoulos T, Korte M, Eulenburg V, Kubota H, Retiounskaia M, Harvey R, Harvey K, O'Sullivan G, Laube B, Hülsmann S, Geiger J, Betz H (2007) Impaired GABAergic transmission and altered hippocampal synaptic plasticity in collybistin-deficient mice. *EMBO J* 26(17):3888-99.
- Pauly MC, Piroth T, Dobrossy M, Nikkhah G (2012) Restoration of the striatal circuitry: from developmental aspects toward clinical applications. *Front Cell Neurosci* 6:16.
- Peng Z, Hauer B, Mihalek RM, Homanics GE, Sieghart W, Olsen RW, Houser CR (2002) GABA(A) receptor changes in delta subunit-deficient mice: altered expression of alpha4 and gamma2 subunits in the forebrain. *J Comp Neurol* 446:179-197.
- Penschuck S, Paysan J, Giorgetta O, Fritschy JM (1999) Activity-dependent regulation of GABAA receptors. *Annals of the New York Academy of Sciences* 868:654-666.
- Picconi B, Piccoli G, Calabresi P (2012) Synaptic dysfunction in Parkinson's disease. *Advances in experimental medicine and biology* 970:553-572.
- Pillai-Nair N, Panicker A, Rodriguiz R, Gilmore K, Demyanenko G, Huang J, Wetsel W, Maness P (2005) Neural cell adhesion molecule-secreting transgenic mice display abnormalities in GABAergic interneurons and alterations in behavior. *The Journal of Neuroscience* 25(18):4659-71.
- Pirker S, Schwarzer C, Sperk G (2000) GABA(A) receptors: immunocytochemical distribution of 13 subunits in the adult rat brain. *Neuroscience* 101(4):815-50.
- Planert H, Szydlowski SN, Hjorth JJJ, Grillner S, Silberberg G (2010) Dynamics of Synaptic Transmission between Fast-Spiking Interneurons and Striatal Projection Neurons of the Direct and Indirect Pathways. *The Journal of Neuroscience* 30:3499-3507.
- Plenz D (2003) When inhibition goes incognito: feedback interaction between spiny projection neurons in striatal function. *Trends in neurosciences* 26:436-443.
- Pollard S, Duggan MJ, Stephenson FA (1993) Further evidence for the existence of alpha subunit heterogeneity within discrete gamma-aminobutyric acidA receptor subpopulations. *J Biol Chem* 268:3753-3757.
- Poltl A, Hauer B, Fuchs K, Tretter V, Sieghart W (2003) Subunit composition and quantitative importance of GABA(A) receptor subtypes in the cerebellum of mouse and rat. *J Neurochem* 87:1444-1455.
- Poulopoulos A, Aramuni G, Meyer G, Soykan T, Hoon M, Papadopoulos T, Zhang M, Paarmann I, Fuchs C, Harvey K, Jedlicka P, Schwarzacher SW, Betz H, Harvey RJ, Brose N, Zhang W, Varoqueaux F (2009) Neuroligin 2 drives postsynaptic assembly at perisomatic inhibitory synapses through gephyrin and collybistin. *Neuron* 63:628-642.
- Pribiag H, Peng H, Shah WA, Stellwagen D, Carbonetto S (2014) Dystroglycan mediates homeostatic synaptic plasticity at GABAergic synapses. *Proc Natl Acad Sci U S A* 111:6810-6815.
- Prior P, Schmitt B, Grenningloh G, Pribilla I, Multhaup G, Beyreuther K, Maulet Y, Werner P, Langosch D, Kirsch J (1992) Primary structure and alternative splice variants of gephyrin, a putative glycine receptor-tubulin linker protein. *Neuron* 8:1161-1170.

- Rannals MD, Kapur J (2011) Homeostatic strengthening of inhibitory synapses is mediated by the accumulation of GABA(A) receptors. *The Journal of Neuroscience* 31:17701-17712.
- Rao A, Cha EM, Craig AM (2000) Mismatched appositions of presynaptic and postsynaptic components in isolated hippocampal neurons. *The Journal of Neuroscience* 20:8344-8353.
- Rathenberg J, Kittler J, Moss S (2004) Palmitoylation regulates the clustering and cell surface stability of GABAA receptors. *Mol Cell Neurosci* 26(2):251-7.
- Raymond S, Weintraub L (1959) Acrylamide gel as a supporting medium for zone electrophoresis. *Science* 130:711.
- Reyes A, Lujan R, Rozov A, Burnashev N, Somogyi P, Sakmann B (1998) Target-cell-specific facilitation and depression in neocortical circuits. *Nat Neurosci* 1:279-285.
- Reynolds JNJ, Wickens JR (2004) The corticostriatal input to giant aspiny interneurons in the rat: a candidate pathway for synchronising the response to reward-related cues. *Brain Research* 1011:115-128.
- Rikani AA, Choudhry Z, Choudhry AMBBS, Rizvi N, Ikram H, Mobassarrah NJ, Tulli S (2014) The mechanism of degeneration of striatal neuronal subtypes in Huntington disease. *Annals of neurosciences* 21:112-114.
- Rivera C, Voipio J, Payne J, Ruusuvuori E, Lahtinen H, Lamsa K, Pirvola U, Saarma M, Kaila K (1999) The K<sup>+</sup>/Cl<sup>-</sup> co-transporter KCC2 renders GABA hyperpolarizing during neuronal maturation. *Nature* 397:251-5.
- Ronner HE, Ponten SC, Stam CJ, Uitdehaag BMJ (2009) Inter-observer variability of the EEG diagnosis of seizures in comatose patients. *Seizure* 18:257-263.
- Roth FC, Draguhn A (2012) GABA Metabolism and Transport: Effects on Synaptic Efficacy. *Neural Plasticity* 2012.
- Rudolph U, Crestani F, Benke D, Brünig I, Benson JA, Fritschy JM, Martin JR, Bluethmann H, Möhler H (1999) Benzodiazepine actions mediated by specific gamma-aminobutyric acid(A) receptor subtypes. *Nature* 401:796-800.
- Rudolph U, Crestani F, Möhler H (2001) GABA(A) receptor subtypes: dissecting their pharmacological functions. *Trends in pharmacological sciences* 22:188-194.
- Saliba R, Michels G, Jacob T, Pangalos M, Moss S (2007) Activity-dependent ubiquitination of GABA(A) receptors regulates their accumulation at synaptic sites. *Journal of Neuroscience* 27:13341-13351.
- Sato S (2010) [Essential role of pikachurin, a novel dystroglycan-binding protein, in bipolar dendrite connection to photoreceptor ribbon synapse in the retina]. *Nippon Ganka Gakkai zasshi* 114:955-967.
- Sato S, Omori Y, Katoh K, Kondo M, Kanagawa M, Miyata K, Funabiki K, Koyasu T, Kajimura N, Miyoshi T, Sawai H, Kobayashi K, Tani A, Toda T, Usukura J, Tano Y, Fujikado T, Furukawa T (2008) Pikachurin, a dystroglycan ligand, is essential for photoreceptor ribbon synapse formation. *Nat Neurosci* 11:923-931.
- Saxena N, Macdonald R (1994) Assembly of GABAA receptor subunits: role of the delta subunit. *the Journal of Neuroscience* 14(11 Pt 2):7077-86.
- Saxena NC, Macdonald RL (1996) Properties of putative cerebellar gamma-aminobutyric acid A receptor isoforms. *Molecular pharmacology* 49:567-579.

- Schweizer C, Balsiger S, Bluethmann H, Mansuy I, Fritschy J, Mohler H, Luscher B (2003) The gamma2 subunit of GABAA receptors is required for maintenance of receptors at mature synapses. *Molecular and Cellular Neuroscience* 24:442–450.
- Siddiqui TJ, Tari PK, Connor SA, Zhang P, Dobie FA, She K, Kawabe H, Wang YT, Brose N, Craig AM (2013) An LRRTM4-HSPG complex mediates excitatory synapse development on dentate gyrus granule cells. *Neuron* 79:680-695.
- Sieghart W (2006) Structure, pharmacology, and function of GABAA receptor subtypes. *Advances in pharmacology (San Diego, Calif)* 54:231-263.
- Sieghart W, Fuchs K, Tretter V, Ebert V, Jechlinger M, Hoeger H, Adamiker D (1999) Structure and subunit composition of GABAA receptors. *Neurochemistry international* 34:379-385.
- Sieghart W, Sperk G (2002) Subunit composition, distribution and function of GABA(A) receptor subtypes. *Curr Top Med Chem* 2(8):795-816.
- Singer HS, Minzer K (2003) Neurobiology of Tourette's syndrome: concepts of neuroanatomic localization and neurochemical abnormalities. *Brain and Development* 25:S70-S84.
- Smith GE, Summers MD, Fraser MJ (1983) Production of human beta interferon in insect cells infected with a baculovirus expression vector. *Molecular and cellular biology* 3:2156-2165.
- Soghomonian J, Martin D (1998) Two isoforms of glutamate decarboxylase: why? *Trends in pharmacological sciences* 19:500-505.
- Somogyi P, Fritschy JM, Benke D, Roberts JD, Sieghart W (1996) The gamma 2 subunit of the GABAA receptor is concentrated in synaptic junctions containing the alpha 1 and beta 2/3 subunits in hippocampus, cerebellum and globus pallidus. *Neuropharmacology* 35:1425-1444.
- Srinivasan S, Nichols CJ, Lawless GM, Olsen RW, Tobin AJ (1999) Two invariant tryptophans on the alpha1 subunit define domains necessary for GABA(A) receptor assembly. *J Biol Chem* 274:26633-26638.
- Studer R, von Boehmer L, Haenggi T, Schweizer C, Benke D, Rudolph U, Fritschy JM (2006) Alteration of GABAergic synapses and gephyrin clusters in the thalamic reticular nucleus of GABAA receptor alpha3 subunit-null mice. *Eur J Neurosci* 24:1307-1315.
- Sumita K, Sato Y, Iida J, Kawata A, Hamano M, Hirabayashi S, Ohno K, Peles E, Hata Y (2007) Synaptic scaffolding molecule (S-SCAM) membrane-associated guanylate kinase with inverted organization (MAGI)-2 is associated with cell adhesion molecules at inhibitory synapses in rat hippocampal neurons. *J Neurochem* 100:154-166.
- Sun C, Zhang L, Chen G (2013) An unexpected role of neuroligin-2 in regulating KCC2 and GABA functional switch. *Molecular brain* 6:23.
- Sur C, Wafford K, Reynolds D, Hadingham K, Bromidge F, Macaulay A, Collinson N, O'Meara G, Howell O, Newman R, Myers J, Atack J, Dawson G, McKernan R, Whiting P, Rosahl T (2001) Loss of the major GABA(A) receptor subtype in the brain is not lethal in mice. *J Neurosci* 21(10):3409-18.
- Takahashi H, Katayama K, Sohya K, Miyamoto H, Prasad T, Matsumoto Y, Ota M, Yasuda H, Tsumoto T, Aruga J, Craig AM (2012) Selective control of inhibitory synapse development by Slitrk3-PTPdelta trans-synaptic interaction. *Nat Neurosci* 15:389-398, s381-382.
- Taylor PM, Connolly CN, Kittler JT, Gorrie GH, Hosie A, Smart TG, Moss SJ (2000) Identification of residues within GABA(A) receptor alpha subunits that mediate specific assembly with receptor beta subunits. *The Journal of Neuroscience* 20:1297-1306.

- Tepper J, Bolam J (2004) Functional diversity and specificity of neostriatal interneurons. *Current Opinion Neurobiology* 14:685-692.
- Thomas P, Mortensen M, Hosie A, Smart T (2005) Dynamic mobility of functional GABAA receptors at inhibitory synapses. *Nat Neurosci* 8(7):889-97.
- Thomson A, Bannister A, Hughes D, Pawelzik H (2000) Differential sensitivity to Zolpidem of IPSPs activated by morphologically identified CA1 interneurons in slices of rat hippocampus. *Eur J Neurosci* 12(2):425-36.
- Thomson A, Jovanovic J (2010) Mechanisms underlying synapse-specific clustering of GABA(A) receptors. *Eur J Neurosci* 31:2193-2203.
- Towbin H, Staehlen T, Gordon J (1979) Electrophoretic transfer of proteins from polyacrylamide gels to nitrocellulose sheets: procedure and some applications. *Proc Natl Acad Sci USA* 76 pp. 4350-4354.
- Tretter V, Ehya N, Fuchs K, Sieghart W (1997) Stoichiometry and assembly of a recombinant GABAA receptor subtype. *Journal of Neuroscience* 17:2728-2737.
- Tretter V, Hauer B, Nusser Z, Mihalek RM, Hoyer H, Homanics GE, Somogyi P, Sieghart W (2001) Targeted disruption of the GABA(A) receptor delta subunit gene leads to an up-regulation of gamma 2 subunit-containing receptors in cerebellar granule cells. *J Biol Chem* 276:10532-10538.
- Tretter V, Jacob T, Mukherjee J, Fritschy J, Pangalos M, Moss S (2008) The clustering of GABA(A) receptor subtypes at inhibitory synapses is facilitated via the direct binding of receptor alpha 2 subunits to gephyrin. *Journal of Neuroscience* 28:1356-1365.
- Tretter V, Kerschner B, Milenkovic I, Ramsden SL, Ramerstorfer J, Saiepour L, Maric HM, Moss SJ, Schindelin H, Harvey RJ, Sieghart W, Harvey K (2011) Molecular basis of the gamma-aminobutyric acid A receptor alpha3 subunit interaction with the clustering protein gephyrin. *J Biol Chem* 286:37702-37711.
- Tretter V, Moss SJ (2008) GABA(A) Receptor Dynamics and Constructing GABAergic Synapses. *Frontiers in molecular neuroscience* 1:7.
- Triller A, Choquet D (2005) Surface trafficking of receptors between synaptic and extrasynaptic membranes: and yet they do move! *Trends in neurosciences* 28:133-139.
- Tunstall MJ, Oorschot DE, Kean A, Wickens JR (2002) Inhibitory interactions between spiny projection neurons in the rat striatum. *J Neurophysiol* 88:1263-1269.
- Tyagarajan SK, Fritschy JM (2014) Gephyrin: a master regulator of neuronal function? *Nat Rev Neurosci* 15:141-156.
- Unwin N (1993) Neurotransmitter action: opening of ligand-gated ion channels. *Cell* 72: p. Suppl:31-41.
- van Oers MM, Pijlman GP, Vlak JM (2014) Thirty years of baculovirus-insect cell protein expression: From dark horse to mainstream technology. *The Journal of general virology*.
- Varoqueaux F, Aramuni G, Rawson RL, Mohrmann R, Missler M, Gottmann K, Zhang W, Sudhof TC, Brose N (2006) Neuroligins determine synapse maturation and function. *Neuron* 51:741-754.
- Varoqueaux F, Jamain S, Brose N (2004) Neuroligin 2 is exclusively localized to inhibitory synapses. *Eur J Cell Biol* 83(9):449-56.

Varoqueaux F SA, Rhee JS, Brose N, Enk C, Reim K, Rosenmund C., T. (2002) Total arrest of spontaneous and evoked synaptic transmission but normal synaptogenesis in the absence of Munc13-mediated vesicle priming. *Proc Natl Acad Sci U S A* 99(13): p. 9037-9042.

Vicini S, Ferguson C, Prybylowski K, Kralic J, Morrow A, Homanics G (2001) GABA(A) receptor alpha1 subunit deletion prevents developmental changes of inhibitory synaptic currents in cerebellar neurons. *Journal of Neuroscience* 21:3009-3016.

Volkel P, Le Faou P, Angrand PO (2010) Interaction proteomics: characterization of protein complexes using tandem affinity purification-mass spectrometry. *Biochemical Society transactions* 38:883-887.

Wang H, Bedford F, Brandon N, Moss S, Olsen R (1999) GABA(A)-receptor-associated protein links GABA(A) receptors and the cytoskeleton. *Nature* 397:69-72.

Wang Z, Russon L, Li L, Roser DC, Long SR (1998) Investigation of spectral reproducibility in direct analysis of bacteria proteins by matrix-assisted laser desorption/ionization time-of-flight mass spectrometry. *Rapid Communications in Mass Spectrometry* 12:456-464.

Wassef A, Baker J, Kochan LD (2003) GABA and schizophrenia: a review of basic science and clinical studies. *Journal of clinical psychopharmacology* 23:601-640.

Wickens JR, Alexander ME, Miller R (1991) Two dynamic modes of striatal function under dopaminergic-cholinergic control: simulation and analysis of a model. *Synapse (New York, NY)* 8:1-12.

Wilhelm S, Gröbler, B., Gluch, M. and Heinz, H. Confocal laser scanning microscopy principles. ZEISS Jena.

Wilson C, Kawaguchi Y (1996) The origins of two-state spontaneous membrane potential fluctuations of neostriatal spiny neurons. *The Journal of Neuroscience* 16:2397-2410.

Wilson CJ, Groves PM (1980) Fine structure and synaptic connections of the common spiny neuron of the rat neostriatum: a study employing intracellular inject of horseradish peroxidase. *J Comp Neurol* 194:599-615.

Wingrove P, Safo P, Wheat L, Thompson S, Wafford K, Whiting P (2002) Mechanism of alpha-subunit selectivity of benzodiazepine pharmacology at gamma-aminobutyric acid type A receptors. *European Journal of Pharmacology* 437:31-39.

Wisden W, Seeburg P (1992) GABAA receptor channels: from subunits to functional entities. *Curr Opin Neurobiol* 2(3):263-9.

Wu H, Xiong WC, Mei L (2010) To build a synapse: signaling pathways in neuromuscular junction assembly. *Development (Cambridge, England)* 137:1017-1033.

Yu W, Jiang M, Miralles CP, Li RW, Chen G, de Blas AL (2007) Gephyrin clustering is required for the stability of GABAergic synapses. *Molecular and cellular neurosciences* 36:484-500.

Zhang C, Atasoy D, Arac D, Yang X, Fucillo MV, Robison AJ, Ko J, Brunger AT, Sudhof TC (2010) Neurexins physically and functionally interact with GABA(A) receptors. *Neuron* 66:403-416.

## 10. Appendix

**Table 1. Proteomics round 1: Hits identified in the  $\alpha 1$  ECDs-binding assay and absent from the  $\alpha 2$  ECDs- binding assay analysed with GPM.**

Accession	Hits	log(e)	log(l)	Mr
ENSRNOP00000033950	Ubiquitin-like modifier-activating enzyme	-53.6	3.14	117.7
ENSRNOP00000060177	Tubulin beta-5 chain Source: UniProtKB	-26.4	3.19	24.3
ENSRNOP00000031061	Transcription intermediary factor 1-beta	-23.5	2.82	88.9
ENSRNOP00000061208	Glyceraldehyde-3-phosphate dehydroge	-23.4	2.72	35.7
ENSRNOP00000005990	Alpha-actinin-1 (Alpha-actinin cytoskelet	-20.5	2.73	102.5
ENSRNOP00000013305	Serine/threonine-protein phosphatase 2E	-17.5	2.72	58.6
ENSRNOP00000062817	type I keratin KA11 IPR016044 FIPR018	-12.8	2.64	52.6
ENSRNOP00000005285	Keratin, type I cytoskeletal 14 (Cytoker	-12.5	2.46	52.7
ENSRNOP00000012640	Keratin, type II cytoskeletal 75 (Cytoker	-12.4	4.13	59
ENSRNOP00000024895	similar to 2610301G19Rik protein (RGD	-11.8	2.23	102.7
ENSRNOP00000033922	no protein text annotation availableIPR0	-10.2	3.3	76.9
ENSRNOP00000013629	AP-2 complex subunit beta (Adapter-rel	-8.9	2.31	105.6
ENSRNOP00000011484	NADH dehydrogenase (ubiquinone) 1 alp	-8.6	1.97	15.2
ENSRNOP00000014004	importin 7 IPR016024 ARM-type foldIPR	-8.2	2.39	119.4
ENSRNOP00000031020	Complement component 1 Q subcompo	-7.6	3.2	31
ENSRNOP00000003277	General vesicular transport factor p115 (	-6.9	2.02	107.1
ENSRNOP00000004725	Gamma-aminobutyric acid receptor sub	-6.6	2.15	51.7
sp CASB_BOVIN	Beta-casein; Contains: Casoparan; Cor	-5.5	3	25.1
ENSRNOP00000015083	Arginase-2, mitochondrial Precursor (EC	-5.5	2.28	38.7
ENSRNOP00000037110	60S ribosomal protein L11 Source: UniP	-5	2.3	20.2
ENSRNOP000000036123	No description	-5	2.3	90.5
ENSRNOP00000018149	GTPase activating protein (SH3 domain)	-4.7	1.77	51.8
ENSRNOP00000026696	Stress-70 protein, mitochondrial Precurs	-4.5	2.28	73.7
ENSRNOP00000053926	translocase of inner mitochondrial memt	-4.2	2.18	14.3
ENSRNOP00000004370	Phenylalanyl-tRNA synthetase alpha ch	-3.6	2.42	57.7
ENSRNOP00000006890	Tetratricopeptide repeat protein 35 (TPR	-3.4	2	34.8
ENSRNOP00000023606	V-type proton ATPase subunit d 1 IPR0	-3	2.28	40.3
ENSRNOP00000014859	no protein text annotation availableIPR0	-2.6	2.42	123.6
ENSRNOP00000010419	EH domain-containing protein 3 Source:	-2.4	2.24	60.8
sp CASK_BOVIN	Kappa-casein; Contains: Casoxin-C; Co	-2.2	2.7	21.3
ENSRNOP000000052297	RAP1, GTP-GDP dissociation stimulat	-2.1	1.99	61.9
ENSRNOP00000004956	Collagen alpha-1(III) chain Source: UniP	-2	2.38	138.9
ENSRNOP00000046203	Voltage-dependent anion-selective chan	-1.8	2.25	30.9
ENSRNOP00000026881	immunity-related GTPase family, Q IPR	-1.7	2.93	59.2
ENSRNOP00000024198	Bifunctional protein NCOAT (Nuclear cyt	-1.7	2.12	107
ENSRNOP00000027145	RNA-binding protein 34 (RNA-binding mx	-1.6	2.1	47.6
ENSRNOP00000033847	RAB, member of RAS oncogene family-I	-1.6	2.28	26.3
sp CAS2_BOVIN	Alpha-S2-casein; Contains: Casocidin-1	-1.6	2.36	26
ENSRNOP00000017805	Neutral cholesterol ester hydrolase 1 (N	-1.6	1.68	45.8
ENSRNOP00000038639	tubulin tyrosine ligase-like family, memb	-1.6	2.55	73.9
ENSRNOP00000006361	Vesicle-fusing ATPase (EC 3.6.4.6)(N-e	-1.6	2.21	82.6
ENSRNOP00000020568	cartilage acidic protein 1 IPR001881 EG	-1.5	2.11	70.4
ENSRNOP00000019935	No description available.Protein Family:	-1.5	2.17	125.8
ENSRNOP00000034954	perlecan (heparan sulfate proteoglycan 2	-1.5	2.05	375
ENSRNOP00000006628	COMM domain containing 9 IPR009886	-1.4	1.67	22
ENSRNOP00000029833	Gliomedin Source: UniProtKB/Swiss-Pr	-1.4	2.75	59.3
ENSRNOP00000052173	no protein text annotation availableIPR0	-1.3	2.59	30.6
ENSRNOP00000022555	kinesin family member 11 IPR001752 Ki	-1.3	2.79	118.2
ENSRNOP00000014191	cDNA sequence BC024139 (BC024139)	-1.1	1.62	85.9
ENSRNOP00000012853	Hydroxymethylglutaryl-CoA lyase, mitoc	-1.1	0.92	34.2

**Table 2. Proteomics round 2: Hits identified in the  $\alpha$ 1 ECDs-binding assay and absent from the  $\alpha$ 2 ECDs- binding assay analysed with GPM.**

Accession	Hits	log(e)	log(l)	Mr
ENSRNOP00000008504	Hspa2:p , Heat shock-related 70 kDa	-82.7	5.74	69.6
ENSRNOP000000023447	Acly:p , ATP-citrate synthase ( EC 2	-81.6	4.94	121
ENSRNOP000000022892	Atp5a1:p , ATP synthase subunit alp	-45.3	4.71	59.8
ENSRNOP000000015535	Aldoc:p , Fructose-bisphosphate ald	-30.5	4.52	39.3
ENSRNOP00000004725	Gabra1:p , Gamma-aminobutyric aci	-29.8	4.5	51.7
ENSRNOP000000020681	Vapa:p , Vesicle-associated membra	-27.4	4.17	27.8
ENSRNOP000000010512	Tmed10:p , transmembrane emp24 d	-26.5	4.53	24.8
ENSRNOP00000001227	Cct6a:p , T-complex protein 1 subuni	-23.7	4.52	58
ENSRNOP000000045650	Sodium/potassium-transporting ATPa	-21.7	4.16	113
ENSRNOP00000002037	Psmb1:p , Proteasome subunit beta	-20.2	4.54	26.4
ENSRNOP000000018711	Cap1:p , Adenylyl cyclase-associate	-16.8	5.15	51.6
ENSRNOP000000015779	Eif5a2:p , no protein text annotation a	-15.1	4.28	16.8
ENSRNOP000000059233	Nckap1:p ,	-14	3.75	125
ENSRNOP000000022779	Actr1b:p , ARP1 actin-related protein	-13.7	4.03	42.3
ENSRNOP000000001201	Hsph1:p ,	-11.9	3.95	96.4
ENSRNOP000000025086	Nup93:p , Nuclear pore complex prot	-11.3	3.4	93.2
ENSRNOP000000026297	Cleavage and polyadenylation specifi	-11	3.32	26.2
ENSRNOP000000018934	RGD1562948:p ,	-11	4.15	35.8
ENSRNOP000000059847	Actbl2:p , beta-actin-like protein 2 [ S	-10.7	4.15	41.9
ENSRNOP000000048250	Hemoglobin subunit beta-1	-9.9	4.06	16
ENSRNOP000000008337	Aco1:p ,	-9.5	4.18	98.1
ENSRNOP000000056260	Rps14:p , 40S ribosomal protein S14	-9.1	4.29	16.3
ENSRNOP000000026016	Ctnnb1:p , Catenin beta-1 (Beta-cate	-7.9	4.07	85.4
ENSRNOP000000061544	Fubp1:p ,	-7.5	4.48	67.2
ENSRNOP000000008329	Sec61b:p , Sec61 beta subunit [ Sou	-6.4	3.02	10
ENSRNOP000000025794	Sod2:p , Superoxide dismutase [Mn]	-5.8	3.83	24.7
ENSRNOP000000006190	Ppp1cb:p , Serine/threonine-protein p	-5.5	3.11	37.2
ENSRNOP000000028020	budding uninhibited by benzimidazole	-5	3.32	67.7
ENSRNOP000000018145	Mvd:p , Diphosphomevalonate decarb	-4.9	3.93	43.9
ENSRNOP000000030902	Rpl38:p ,	-4.9	3.1	8.2
ENSRNOP000000012842	Uchl3:p , Ubiquitin carboxyl-terminal	-4.9	3.87	26.1
ENSRNOP00000006607	Actr2:p , Actin-related protein 2 (Acti	-4.7	4.18	44.7
ENSRNOP000000002478	Dynamin-1-like protein ( EC 3.6.5.5 )	-4.7	3.23	83.9
ENSRNOP000000022574	Stmn1:p , Stathmin Source: UniProt	-4.6	4.25	17.3
ENSRNOP000000020940	Aldh18a1:p , pyrroline-5-carboxylate	-4.1	3.93	87.3
ENSRNOP000000061516	Arpc5:p ,	-4	3.7	16.3
ENSRNOP000000016495	Atp6v1e1:p , V-type proton ATPase s	-4	3.51	26.1
ENSRNOP000000024471	Ndufab1:p , acyl carrier protein, mitoc	-4	3.84	17.5
ENSRNOP000000012425	Ndufs3:p , NADH dehydrogenase [ S	-4	3.79	30.2
ENSRNOP000000019405	Arpc5l:p ,	-3.9	3.79	17.1
ENSRNOP000000025224	Rpsa:p , 40S ribosomal protein SA	-3.8	3.94	32.8
ENSRNOP000000020402	Sae1:p , no protein text annotation a	-3.8	3.72	38.5
ENSRNOP000000029702	DEAD (Asp-Glu-Ala-Asp) box polype	-3.7	3.18	34.3
ENSRNOP000000020478	Pdia3:p , Protein disulfide-isomerase	-3.7	3.8	56.6
ENSRNOP000000004438	Cops3:p , COP9 signalosome compl	-3.6	3.85	47.8
ENSRNOP000000004520	Actin-related protein 3 (Actin-like prot	-3.5	3.2	47.3
ENSRNOP000000009999	kinesin family member 3a [ Source: f	-3.3	3.28	80.2
ENSRNOP000000008328	LOC100359421:p ,	-3.3	4.69	15.4
ENSRNOP000000015218	Sec11a:p , Signal peptidase complex	-3.1	3.02	20.6
ENSRNOP000000026021	Fbl:p , rRNA 28#39;-O-methyltransfe	-3	3.68	34.2
ENSRNOP000000037163	Sec24b:p , SEC24 family, member B	-3	2.62	135
ENSRNOP000000046491	Hnrpd:p , Heterogeneous nuclear ribc	-2.9	3.54	38.2
ENSRNOP000000007567	Ndufa4:p , NADH dehydrogenase (ub	-2.9	3.16	9.3
ENSRNOP00000001675	Pcbp3:p ,	-2.9	3.74	33.8
ENSRNOP000000028687	Prdx5:p , Peroxiredoxin-5, mitochonc	-2.9	3.82	22.2
ENSRNOP000000057942	heterogeneous nuclear ribonucleopro	-2.8	3.5	30.3
ENSRNOP000000015757	Psmc3:p , 26S protease regulatory s	-2.6	4.02	49.5
ENSRNOP000000044122	Fam190a:p ,	-2.5	3.82	79.7
ENSRNOP000000007351	Snrpf:p , small nuclear ribonucleopro	-2.5	3.43	9.7
ENSRNOP000000014250	Syn1:p , Synapsin-1 (Synapsin I) Sou	-2.5	3.3	73.9
ENSRNOP000000004942	Tmed7:p , transmembrane emp24 pro	-2.4	3.21	25.5
ENSRNOP000000046414	Cytochrome c oxidase subunit 2 Sou	-2.3	4.22	25.9
ENSRNOP000000019737	Ctla:p , Clathrin light chain A (Lca). S	-2.2	3.37	27
ENSRNOP000000010956	Cul5:p , Cullin-5 (CUL-5)(Vasopressin	-2.1	3.48	90.8
ENSRNOP000000023526	Ndufs8:p , NADH dehydrogenase ubi	-2.1	3.87	24
ENSRNOP00000002358	Psmc2:p , 26S proteasome non-ATP	-2.1	3.75	100
ENSRNOP000000001609	RGD1303003:p , ES1 protein homolo	-2.1	3.3	28.2
ENSRNOP000000021514	Uqcrc2:p , Cytochrome b-c1 complex	-2.1	3.73	48.4
ENSRNOP000000007100	Ywhae:p , 14-3-3 protein epsilon (14-	-2.1	3.77	29.2
ENSRNOP000000031281	Usp32:p , ubiquitin specific protease	-1.9	3.27	162
ENSRNOP000000027828	Fam189b:p ,	-1.8	3.11	71.8



**Table 3. Proteomics round 1: Hits identified in the  $\alpha 2$  ECDs-binding assay and absent from the  $\alpha 1$  ECDs- binding assay analysed with GPM.**

Accession	Hits	log(e)	log(l)	Mr
ENSRNOP00000010811	Protein NDRG1 Source: UniProt	-23.9	2.54	42.9
ENSRNOP00000004895	protein canopy homolog 2 IPR0	-12.1	2.63	20.7
ENSRNOP00000012842	Ubiquitin carboxyl-terminal hydr	-11.7	2.77	25.8
ENSRNOP00000058898		-9.4	3.46	29.3
ENSRNOP00000002091	Neuromodulin (Axonal membran	-5.3	2.14	23.6
ENSRNOP00000015234	40S ribosomal protein S9 Sourc	-3.8	2.24	22.6
ENSRNOP00000010087	Proteasomal ubiquitin receptor A	-3.8	2.39	42.1
ENSRNOP00000027305	Elongation factor 1-gamma (EF-	-3.7	2.41	50
ENSRNOP00000028576	EH domain-containing protein 1	-3.6	1.7	55.4
ENSRNOP00000017942	UPF0160 protein MYG1, mitoch	-3.3	2.24	42.9
ENSRNOP00000043519	Moesin Source: UniProtKB/Swis	-3	2.29	67.6
ENSRNOP00000022854	Protein phosphatase 1 regulator	-2.7	2.21	41.3
ENSRNOP00000014609	Serine/threonine-protein phosph	-2.6	2.17	76.1
ENSRNOP00000014780	Glycyl-tRNA synthetase Fragme	-2.4	2.08	81.7
ENSRNOP00000007554	Vesicle-associated membrane p	-2.1	3.07	26.9
ENSRNOP00000000599	AH receptor-interacting protein (	-2.1	2.76	37.6
ENSRNOP00000054270	Uncharacterized protein Source:	-1.9	2.4	161.3
ENSRNOP00000003840	PH domain leucine-rich repeat p	-1.6	2.9	183.5
ENSRNOP00000005122	arsA arsenite transporter, ATP-k	-1.6	2.52	39
ENSRNOP00000028117	Small conductance calcium-acti	-1.6	2.49	81.3
ENSRNOP00000004942	transmembrane emp24 protein t	-1.5	2.61	25.5
ENSRNOP00000018711	Adenylyl cyclase-associated pro	-1.5	1.72	51.6
ENSRNOP00000024404	integrin alpha L IPR013517 FG-C	-1.5	1.97	127.6
ENSRNOP00000008356	Calumenin Precursor (Crocabin	-1.3	2.4	37
ENSRNOP00000059909	Actin-related protein 3 Source: U	-1.3	1.79	47.3
ENSRNOP00000041192	Pikachurin Precursor (EGF-like,	-1.3	2.53	110.5
ENSRNOP00000047793	ret proto-oncogene isoform a S	-1.2	2.39	124.2
ENSRNOP00000049627	Ac2-008 Source: UniProtKB/TrE	-1.2	2.75	24.5
ENSRNOP00000013073	aldo-keto reductase family 1, m	-1.2	2.81	36.1
ENSRNOP00000043232	Protein sel-1 homolog 1 Precurs	-1.2	2.42	88.5
ENSRNOP00000017776	G protein-coupled receptor 124	-1.2	2.93	143.2
ENSRNOP00000022622	leucine rich repeat containing 36	-1.2	2.19	84.1
ENSRNOP00000008274	galectin-related protein IPR0089	-1.1	2.32	18.9
ENSRNOP00000024762	Shootin-1 Source: UniProtKB/S	-1.1	2.16	70.4

**Table 4. Proteomics round 2: Hits identified in the  $\alpha 2$  ECDs-binding assay and absent from the  $\alpha 1$  ECDs-binding assay analysed with GPM.**

Accession	Hits	log(e)	log(l)	Mr
ENSRNOP00000	Gcn111:p , GCN1 general control of ami	-81	4.84	292.5
ENSRNOP00000	Rab2a:p , Ras-related protein Rab-2A S	-52	5.1	21.7
ENSRNOP00000	Fam49b:p , family with sequence simila	-45.9	4.97	36.8
ENSRNOP00000	Nme1:p , Nucleoside diphosphate kinas	-41.3	5.32	17.2
ENSRNOP00000	spectrin beta chain, brain 1 [ Source: Re	-34.7	4.46	273.3
ENSRNOP00000	Eif5a:p , Eukaryotic translation initiation	-23	4.84	16.8
ENSRNOP00000	40S ribosomal protein S5 [Contains 40S	-22.8	4.72	22.9
ENSRNOP00000	Capza2:p , F-actin-capping protein subu	-19.7	4.27	32.9
ENSRNOP00000	Rps21:p , 40S ribosomal protein S21 Sc	-15.2	4.01	9.1
ENSRNOP00000	Cct2:p , T-complex protein 1 subunit bel	-13.5	4.1	57.4
ENSRNOP00000	Nme2:p , Nucleoside diphosphate kinas	-13.1	4.31	17.3
ENSRNOP00000	Glrx3:p , Glutaredoxin-3 Source: UniPro	-11.8	3.96	37.8
ENSRNOP00000	Flna:p , no protein text annotation availa	-10	3.49	280.3
ENSRNOP00000	Arf4:p , ADP-ribosylation factor 4 Sourc	-9.9	4.65	20.4
ENSRNOP00000	no protein information available	-9.7	3.51	14.8
ENSRNOP00000	Prdx3:p , thioredoxin-dependent peroxid	-9.3	4.37	28.3
ENSRNOP00000	Arf5:p , ADP-ribosylation factor 5 Sourc	-8.9	4.66	20.5
ENSRNOP00000	Eif4g1:p , no protein text annotation ava	-8.1	3.48	175.6
ENSRNOP00000	Npm3:p ,	-8.1	3.85	18.9
ENSRNOP00000	Nup205:p , nucleoporin 205 [ Source: Ri	-7.3	3.44	227.1
ENSRNOP00000	Map1b:p , Microtubule-associated prote	-7.1	3.51	269.5
ENSRNOP00000	Usp24:p ,	-6	3.02	293.8
ENSRNOP00000	triple functional domain (PTPRF interact	-5.8	3.57	348.1
ENSRNOP00000	Psmf7:p , proteasome (prosome, macro	-5.5	2.94	36.5
ENSRNOP00000	Asna1:p ,	-5.1	2.07	38.8
ENSRNOP00000	Got1:p , Aspartate aminotransferase, cy	-5	3.26	46.4
ENSRNOP00000	Eef1b2:p , eukaryotic translation elonga	-4.7	3.78	24.7
ENSRNOP00000	Npm1:p , Nucleophosmin Source: UniPr	-4.7	2.72	32.5
ENSRNOP00000	Cox5b:p , Cytochrome c oxidase subun	-4.1	3.71	13.9
ENSRNOP00000	Rps20:p , 40S ribosomal protein S20 Sc	-4	4.18	13.4
ENSRNOP00000	RGD1311659:p , similar to Proteasome	-3.9	3.68	27.9
ENSRNOP00000	no protein text annotation available	-3.7	3.15	29.2
ENSRNOP00000	Cnpy2:p , protein canopy homolog 2 [ S	-3.6	3.86	20.7
ENSRNOP00000	Triosephosphate isomerase	-3.6	4.11	26.4
ENSRNOP00000	Ppp2r2a:p , Serine/threonine-protein pho	-3.4	3.62	51.6
ENSRNOP00000	Cnot1:p , RGD1308009 protein Fragmer	-3.3	3.22	266.7
ENSRNOP00000	sp CAS1_BOVIN Alpha-S1-casein; Bos d 8; Contains: An	-2.9	3.79	24.5
ENSRNOP00000	Fa2h:p ,	-2.9	3.52	42.6
ENSRNOP00000	Ldhd:p , L-lactate dehydrogenase B cha	-2.9	4.46	36.6
ENSRNOP00000	Nduf2:p , NADH dehydrogenase [ubiqui	-2.7	4.37	27.4
ENSRNOP00000	Aldoa:p , Fructose-bisphosphate aldolase	-2.6	2.5	39.3
ENSRNOP00000	Fndc3b:p , no protein text annotation av	-2.5	3.33	132.7
ENSRNOP00000	RGD1303066:p ,	-2.5	2.96	47.3
ENSRNOP00000	Sumo2:p , Small ubiquitin-related modifi	-2.4	4.16	10.9
ENSRNOP00000	LOC296300:p , similar to zinc finger pro	-2.2	4.5	45.8
ENSRNOP00000	Col4a1:p , collagen alpha-1(IV) chain [ S	-2.1	3.73	160.5
ENSRNOP00000	Psmf1:p , Proteasome subunit alpha ty	-2.1	2.84	29.5
ENSRNOP00000	Rab5b:p , RAB5B, member RAS oncog	-2.1	3.7	23.7
ENSRNOP00000	RGD1560648:p , Protein DJ-1 (Parkinso	-2.1	3.58	20
ENSRNOP00000	Adprh:p , [Protein ADP-ribosylarginine] l	-2	3.72	39.9
ENSRNOP00000	Pafah1b2:p , platelet-activating factor ac	-1.6	3.63	25.6
ENSRNOP00000	Sec24a:p , SEC24 family, member A [ S	-1.6	3.62	118.8
ENSRNOP00000	Asah1:p , Acid ceramidase Precursor ( <i>A</i>	-1.5	3.58	44.4
ENSRNOP00000	COX15 homolog, cytochrome c oxidase	-1.5	3.69	45.9
ENSRNOP00000	Lrrc38:p ,	-1.4	2.91	32.4
ENSRNOP00000	Col11a2:p ,	-1.3	3.87	158.9
ENSRNOP00000	Mfsd2:p ,	-1.2	3.76	58.6
ENSRNOP00000	Psmf11:p ,	-1.2	3.75	49.6
ENSRNOP00000	No description &nbsp;	-1.1	3.02	106.5
ENSRNOP00000	Rab26:p , RAS-RELATED PROTEIN RA	-1.1	3.53	28.2
ENSRNOP00000	RGD1564142:p ,	-1.1	3.95	337.5
ENSRNOP00000	RGD1562747:p , similar to RIKEN cDNA	-1	3.87	19.8

**Table 5: Hits identified in the  $\alpha 1$  ECDs-binding assay and absent from the  $\alpha 2$  ECDs-binding assay analysed with GPM found in Proteomics round 1 and 2**

Accession	Description	log(e)	log(l)	Mr
ENSRNOP00000004725	Gabra1:p , Gamma-amin	-29.8	4.5	51.7

**Table 6: Hits identified in the  $\alpha 2$  ECDs-binding assay and absent from the  $\alpha 1$  ECDs-binding assay analysed with GPM found in Proteomics round 1 and 2**

Accession	Description	log(e)	log(l)	Mr
ENSRNOP00000004895	Cnpy2:p , protein canopy homolog 2	-3.6	3.86	20.7

**Table 7. Proteomics round 1: Hits identified in the  $\alpha 1$  ECDs- binding assay and present in the  $\alpha 2$  ECDs- binding assay analysed with GPM.**

Accession	Hits	log(e)	log(l)	Mr
ENSRNOP00000008504	Heat shock-related 70 kDa prote	-63.7	3.58	69.6
ENSRNOP00000025064	78 kDa glucose-regulated protei	-20.5	3.19	72.3
ENSRNOP00000049998	Tubulin alpha-3 chain Source: U	-11.7	2.74	49.9
ENSRNOP00000015851	NADH-ubiquinone oxidoreductas	-8.1	2.6	79.4
ENSRNOP00000031564	tubulin, alpha-like 3 IPR002452	-5.2	2.36	49.9
ENSRNOP00000037217	F-actin-capping protein subunit $\alpha$	-4.8	2.19	32.9
ENSRNOP00000057097	Protein RUFY3 (Rap2-interacting	-4.2	2.18	74.3
ENSRNOP00000018009	protein kinase C substrate 80K-I	-3.3	3.1	59.2
ENSRNOP00000003667	similar to RIKEN cDNA 261002C	-3.3	2.39	22.4
ENSRNOP00000024306	26S proteasome non-ATPase re	-2.5	1.29	105.6
ENSRNOP00000025794	Superoxide dismutase , mitochc	-2.5	2.37	24.7
ENSRNOP000000051848	sp K1C15_SHEEP  Keratin, type I cytoskeletal 15;	-2.4	2.34	48.7
ENSRNOP000000051848	mitochondrial ribosomal protein	-2.4	2.37	29.4
ENSRNOP00000010674	Tyrosyl-tRNA synthetase, cytop	-2.3	1.93	63
ENSRNOP000000055173	no protein text annotation availa	-2.1	2.42	31.7
ENSRNOP00000028440	no protein text annotation availa	-1.1	2.39	136.3

**Table 8. Proteomics round 2: Hits identified in the  $\alpha 1$  ECDs- binding assay and present in the  $\alpha 2$  ECDs- binding assay analysed with GPM.**

Accession	Hits	log(e)	log(l)	Mr
ENSRNOP00000042382	Spectrin alpha chain, brain (Spectrin, non-	-95.4	4.75	284.5
ENSRNOP00000063671	Crmp1:p , Dihydropyrimidinase-related pro	-74.3	5.86	62.2
ENSRNOP00000022951	Plexin-A1 Precursor (Plexin-1)(Plex 1) [ So	-35.5	4.1	211
ENSRNOP00000018005	Psm5:p , Proteasome subunit beta type-	-34.1	4.77	28.5
ENSRNOP00000028484	Proteasome subunit beta type-4 Precursor	-28.5	4.96	29.2
ENSRNOP00000026373	Gnao1:p , Guanine nucleotide-binding prot	-18.8	4.93	40
ENSRNOP00000027305	Eef1g:p , Elongation factor 1-gamma (EF-	-17.7	4.68	50
ENSRNOP00000008608	Mif:p , Macrophage migration inhibitory fac	-15.9	4.64	12.5
ENSRNOP00000024863	Taldo1:p , Transaldolase ( EC 2.2.1.2 ) So	-13.1	3.91	37.4
ENSRNOP00000020322	ldh1:p , Isocitrate dehydrogenase [NADP]	-10.4	3.93	46.7
ENSRNOP00000027226	no protein text annotation available	-8.4	5.52	14.4
ENSRNOP00000025282	Ppp1ca:p , Serine/threonine-protein phosph	-5.9	3.81	37.5
ENSRNOP00000010753	Psm3:p , No description &nbsp;sp;	-4.6	2.9	28.4
ENSRNOP00000044971	Ddah1:p , N(G),N(G)-dimethylarginine dim	-4.1	3.1	31.4
ENSRNOP00000045992	Myl12b:p , Myosin regulatory light chain 1	-3.7	3.88	19.8
ENSRNOP00000001738	Sarcoplasmic/endoplasmic reticulum calci	-3.2	3.19	110.2
ENSRNOP00000006856	no protein information available	-2.1	4.08	81.1
ENSRNOP00000018646	Snrpd1:p , no description available	-1.9	4.17	13.3
ENSRNOP00000027774	Pafah1b3:p ,	-1.6	2.99	25.8

**Table 9. Proteomics round 1: Hits identified in the  $\alpha$ 1 ECDs- binding assay and absent from  $\alpha$ 2 ECDs- binding assay analysed with MASCOT.**

prot_acc	Hits	prot_score	prot_mass	prot_matches	prot_cover	pep_query	pep_exp_mz	pep_score
IPI00734561	Hsp90b1 Isoform 2 of Endoplasmic	222	74162	7	12.1	122	508.2581	5.33
IPI00287835	Hba-a2 Hemoglobin subunit alpha-1/2	221	15319	12	57	106	409.7324	5.36
IPI00557715	Glyceraldehyde-3-phosphate dehydrogenase (Fr	126	45771	4	9.5	390	685.3758	57.34
IPI00213463	Actn4 Alpha-actinin-4	112	104849	6	7	337	608.358	13.76
IPI00201410	Ppp3ca Isoform 1 of Serine/threonine-protein pho	75	58606	4	9.4	150	536.8204	0.53
IPI00817078	Proteasome subunit alpha type	73	19524	3	20.1	472	817.9443	39.47
IPI00421539	Aco2 Aconitate hydratase, mitochondrial	69	85380	4	7.2	249	634.834	16.96
IPI00382233	Acat3 Ab2-076	67	103244	3	2.7	359	436.6032	25.61
IPI00200773	Actn3 Uncharacterized protein	66	102948	2	2.7	342	622.3861	4.97
IPI00231829	Arg2 Arginase-2, mitochondrial	65	38616	1	4.2	493	786.4208	64.98
IPI00203723	Arg2 Arginase-related protein	65	37776	1	4.4	493	786.4208	64.98
IPI00210233	Fdt1 Squalene synthase	64	48075	1	3.4	335	738.3983	64
IPI00370073	Krt17 Keratin, type I cytoskeletal 17	61	48093	6	13.6	66	405.2244	1.7
IPI00199865	Farsa Phenylalanyl-tRNA synthetase alpha chain	60	57684	2	2.2	251	655.3625	25.74
IPI00561918	Uncharacterized protein (Fragment)	60	34410	2	8.8	333	615.3471	3.61
IPI00201403	Ppm1a Protein phosphatase 1A	58	42390	1	4.7	513	678.0007	58.25
IPI00778370	Uncharacterized protein	53	33108	2	7.7	245	594.8339	53.08
IPI00554194	Calu calumenin isoform b	51	37124	2	4.1	229	640.8072	45.13
IPI00382267	Ilf2 Interleukin enhancer-binding factor 2	51	51348	2	4.5	125	521.3234	51.42
IPI00230775	Tpm2 Isoform 1 of Tropomyosin beta chain	50	32817	2	9.2	344	622.3338	50.01
IPI00191354	Tpm3 Uncharacterized protein	50	33129	2	7.7	344	622.3338	50.01
IPI00551673	Krt10 Uncharacterized protein	47	57598	2	4.6	169	545.7702	46.71
IPI00764232	LOC687295 Uncharacterized protein	46	14258	1	8.2	330	629.3278	46.22
IPI00869568	Vps35 maternal embryonic message 3	44	91669	7	9.9	103	492.8252	23.93
IPI00764841	Slc25a31 Uncharacterized protein	42	35231	3	8.1	445	723.8742	11.91
IPI00363182	Slc25a6 ADP/ATP translocase 2-like	42	33155	5	12.4	327	610.3417	4.77
IPI00208170	Tmt112 hypothetical protein LOC293700	40	14118	1	10.4	505	759.4155	39.58
IPI00366247	Ttc35 Tetratricopeptide repeat protein 35	38	34847	1	4.4	417	740.3746	38.24
IPI00476086	Atp6v0d1 Uncharacterized protein	37	40275	2	6.8	312	615.8455	7.33
IPI00199980	Psmb7 Proteasome subunit beta type-7	37	29908	1	3.6	162	508.7786	37.42
IPI00957729	LOC100363716;LOC100359928 microtubule-assc	35	17616	3	16.9	47	546.2952	7.38
IPI00371269	Rab5b Uncharacterized protein	35	23660	3	11.6	198	543.3011	2.46
IPI00190943	Glaf Isoform 1 of Glial fibrillary acidic protein	32	49927	2	5.6	234	639.3619	31.8
IPI00369480	RGD1565010 otubain 1-like	31	31059	1	3.3	148	525.8023	31.17
IPI00362534	Ddx3x Uncharacterized protein	30	73100	1	1.8	233	646.376	29.66
IPI00205374	Hmgcl Hydroxymethylglutaryl-CoA lyase, mitoch	30	34170	1	4.3	430	763.9011	29.92
IPI00951917	LOC100362339 Uncharacterized protein	30	16108	2	12.4	169	485.81	2.49
IPI00203574	Hsbp1 Hsp70-binding protein 1	29	39166	1	3.1	347	649.3559	29.46
IPI00210564	Lsm5 Uncharacterized protein	29	9931	2	20.9	566	1019.0818	20.49
IPI00365595	Asap2 Uncharacterized protein (Fragment)	28	103130	1	0.9	149	487.2804	27.8
IPI00470254	Ezr Ezrin	28	69348	2	3.6	152	552.8027	27.67
IPI00372976	Gga3 Uncharacterized protein	28	78710	1	1.7	296	679.389	28.38
IPI00212186	RGD1562259 ribosomal protein S20-like	28	13368	2	10.1	407	450.9318	0.73
IPI00367724	Hcfc1 Uncharacterized protein	27	209022	1	0.8	517	873.5378	27.44
IPI00198904	Mat2b Methionine adenosyltransferase 2 subunit	27	37351	1	3.6	278	585.8649	27.36
IPI00369788	RGD1561230;LOC100360876 Uncharacterized pr	27	77710	1	2.1	433	839.4315	26.95
IPI00192586	Csnk2a1 Casein kinase II subunit alpha	26	45045	1	4.6	467	622.3495	25.75
IPI00390762	MGC95210 Uncharacterized protein	26	58048	1	2.4	439	700.8768	25.51
IPI00230917	Rpl18 60S ribosomal protein L18	25	21645	1	6.9	376	673.3804	24.69
IPI00957926	Arhgap42 Rho-type GTPase-activating protein FL	24	94449	1	1.1	167	519.7761	24.4
IPI00213457	Atp6v1c1 V-type proton ATPase subunit C 1	24	43873	5	9.9	147	538.8046	2.78
IPI00191485	Pkd1 Uncharacterized protein	24	465927	1	0.3	271	746.2993	24.43
IPI00422076	Thbs1 Thrombospondin 1	24	129588	1	0.9	228	639.9035	24.19
IPI00368799	Esf1 ESF1 homolog	23	97474	1	1.1	320	604.3825	23.15
IPI00553976	LOC682097 LOC682097 protein (Fragment)	23	19269	1	5.9	177	629.3079	22.51
IPI00212838	Otud3 Uncharacterized protein	23	44104	3	5.6	195	566.7824	0.4
IPI00778032	Rap1gds1 Uncharacterized protein (Fragment)	23	61874	2	4	129	514.3114	21.4
IPI00191728	Calr Calreticulin	22	47966	1	3.6	403	595.6175	22.07
IPI00360340	Ehd1 EH domain-containing protein 1	22	60565	3	6.6	278	684.8395	5.95
IPI00364866	Erp44 Uncharacterized protein	22	46848	1	3.2	336	493.9234	22.21
IPI00192912	Rcn1 Uncharacterized protein	22	38067	2	5.8	37	400.7701	17.26
IPI00359278	Cnr1p1 CB1 cannabinoid receptor-interacting prot	21	18647	1	9.8	475	856.9562	21.32
IPI00189759	Ndufa10i1 NADH dehydrogenase (ubiquinone) 1 $\epsilon$	20	40519	2	7.3	263	575.3272	19.97
IPI00195109	Shmt2 Serine hydroxymethyltransferase	20	55730	1	2.2	370	648.3566	20.38
IPI00366924	RGD1560073 Uncharacterized protein	19	18747	2	10.9	202	555.3392	18.86
IPI00565628	Wdr62 Uncharacterized protein (Fragment)	19	157952	1	0.8	384	671.3588	19.34
IPI00959479	Ckap2l Uncharacterized protein	17	82658	2	1.6	272	697.3962	8.39
IPI00366007	Eif4g2 Uncharacterized protein (Fragment)	17	102379	2	2.5	229	513.3304	5.34
IPI00188196	Pde4a Isoform 1 of cAMP-specific 3-,5--cyclic p	17	93380	2	3.1	270	495.8849	17.38
IPI00367636	RGD1566373 ribosomal protein L36a-like	16	13668	4	8.4	198	582.3254	16.34
IPI00325195	Cpz Carboxypeptidase Z	15	73035	3	3.7	57	696.4081	14.94
IPI00207390	Anxa3 Annexin A3	14	36341	1	5.9	562	541.0974	14.28
IPI00200751	Flnn Folliculin	14	64081	3	4.7	551	903.4465	14.28
IPI00201057	Hk2 Hexokinase-2	14	102478	3	3.5	286	563.3101	6.28
IPI00363160	Seps1 selenide, water dikinase 1	14	42865	1	3.8	417	560.6511	13.94
IPI00358065	Mrlp44 Uncharacterized protein	13	37417	1	2.1	56	839.4248	13.47
IPI00202428	Pde4b Isoform 1 of cAMP-specific 3-,5--cyclic p	13	83322	1	1.8	454	495.8925	13.23
IPI00389624	Tsen2 tRNA-splicing endonuclease subunit Sen2	13	52918	1	1.5	56	839.4248	13.47

**Table 10 Proteomics round 2: Hits identified in the  $\alpha$ 1 ECDs- binding assay and absent from the  $\alpha$ 2 ECDs- binding assay analysed with MASCOT.**

prot_acc	Hits	prot_score	prot_mass	prot_matches	prot_cover	pep_query	pep_exp_mz	pep_score
IPI00656375	RGD1562758 glyceraldehyde-3-phosph	359	35834	12	18	64	435.2771	19.98
IPI00328017	Map2 Microtubule-associated protein	336	198705	12	7.3	118	494.2996	33.78
IPI00960040	LOC680097 histone cluster 1, H2ae-like	236	51695	13	19.9	59	425.7722	26.43
IPI00958096	LOC100360950 GF20391-like isoform 1	205	24560	8	31.5	103	477.3126	25.09
IPI00206406	Ppp3r1 Isoform 1 of Calcineurin subunit	158	19288	4	25.9	68	400.737	14.5
IPI00231955	Calm2;Calm3;Calm1 Calmodulin	158	16827	5	27.5	127	478.7761	32.8
IPI00951891	Ap1b1 Uncharacterized protein	138	103888	7	7.7	97	461.2837	4.92
IPI00209258	Sptan1 Uncharacterized protein	125	284865	10	3.9	68	415.7481	5.67
IPI00959265	LOC100363379;LOC100365936 peroxin	118	22150	7	30.2	62	416.2454	42.22
IPI00363265	Hspa9 Stress-70 protein, mitochondrial	107	73812	3	6	173	667.4033	49.08
IPI00192642	Gabra1 Gamma-aminobutyric acid rece	100	51721	5	10.1	60	449.285	13.49
IPI00230897	Hbb Hemoglobin subunit beta-1	95	15969	4	27.9	95	456.7762	24.61
IPI00362229	Actr1b ARP1 actin-related protein 1 hor	91	42255	2	8.2	264	767.4379	65.73
IPI00869806	Actr1a Alpha-centractin	91	42587	2	8.2	264	767.4379	65.73
IPI00203723	Arg2 Arginase-related protein	86	37776	1	4.4	217	786.4623	86.04
IPI00231829	Arg2 Arginase-2, mitochondrial	86	38616	1	4.2	217	786.4623	86.04
IPI00191444	Capzb Uncharacterized protein	81	31326	3	10.5	124	554.8489	20.1
IPI00203730	Ras12-9 GTP-binding nuclear protein Ra	78	24436	2	10.2	100	508.3192	68.06
IPI00369913	Sarm1 Uncharacterized protein	77	79638	1	2.2	317	864.5264	76.55
IPI00679210	Microtubule-associated protein	74	35874	6	15.7	50	431.2434	33.77
IPI00188924	Uqcrc2 Cytochrome b-c1 complex subu	73	48366	1	2.2	166	609.8629	72.62
IPI00325912	Ctnnb1 Catenin beta-1	73	85400	2	4.2	224	693.4071	57.77
IPI00208286	Uchl3-ps1;Uchl3 Ubiquitin carboxyl-term	72	26107	1	5.7	229	762.3955	71.95
IPI00188330	Ndufs8 Uncharacterized protein	71	23955	1	5.2	204	637.3755	70.82
IPI00394032	Tom1l2 Uncharacterized protein	70	55610	1	2.6	237	737.4757	69.92
IPI00190348	Hist1h2bc histone H2B	70	13882	2	19	126	477.3047	32.91
IPI00196987	Adrbk1 Beta-adrenergic receptor kinase	69	79734	1	2.6	361	1022.0796	68.96
IPI00362072	Actr2 Actin-related protein 2	64	44705	1	3	218	677.3986	63.5
IPI00359978	Rps28 40S ribosomal protein S28	63	7836	2	17.4	232	680.8837	46.6
IPI00339164	Mtor Serine/threonine-protein kinase m	63	288610	2	0.9	190	605.3741	5.14
IPI00214192	Sh3gl1 Endophilin-A2	61	41466	1	1.9	61	436.2566	61.05
IPI00768793	LOC680322 Histone H2A	61	14202	8	40.8	59	425.7722	26.43
IPI00366436	Eif3s6ip Eukaryotic translation initiation	61	66668	2	3.2	45	404.2386	10.32
IPI00230837	Ywhab Isoform Long of 14-3-3 protein b	60	28037	3	19.1	64	452.2774	40.98
IPI00363489	Nudt21 Cleavage and polyadenylation s	60	26224	1	12.8	379	1038.969	59.59
IPI00188249	Bri3bp Uncharacterized protein	58	28298	1	3.6	185	569.3382	58.13
IPI00201500	Rps14 40S ribosomal protein S14	57	16249	1	7.3	147	527.7986	57.44
IPI00231639	Gstm1 Glutathione S-transferase Mu 1	57	25897	1	7.3	312	895.532	56.9
IPI00200069	Sfxn3 Sideroflexin-3	56	35411	1	4	201	760.9496	56.2
IPI00362534	Ddx3x Uncharacterized protein	56	73100	1	1.8	156	646.4171	56.1
IPI00195123	Atp5o ATP synthase subunit O, mitoch	56	23383	2	8.5	93	444.2736	31.53
-----								
IPI00911298	RGD1566243 hypothetical protein LOC	19	56497	1	2.4	242	694.4314	19.19
IPI00213299	Mapre1 Microtubule-associated protein	19	29985	1	6.7	315	612.3682	18.99
IPI00365340	Cpne7 Uncharacterized protein	19	62067	1	2.5	237	767.9626	19.48
IPI00231967	Arff6 ADP-ribosylation factor 6	18	20069	1	8	316	803.44	17.68
IPI00208240	Unc13c protein unc-13 homolog C	17	249310	1	0.8	323	1038.6261	17.03
IPI00454355	Slc2a3 Slc2a3 protein	17	35764	1	3.6	213	479.65	16.57
IPI00360057	Prkd3 Uncharacterized protein	17	33563	1	4.4	265	793.9805	16.87
IPI00781221	L-lactate dehydrogenase (Fragment)	16	37205	1	4.1	229	818.4702	15.56
IPI00781234	RGD1562937 Uncharacterized protein	15	15406	1	12	294	861.0014	15.08
IPI00358443	Fkbp4 Peptidyl-prolyl cis-trans isomera	15	51418	2	2.8	254	725.9031	13.79
IPI00896207	Extl2 Uncharacterized protein	15	37260	1	4.6	235	843.4513	14.55



**Table 11. Proteomics round 1: Hits identified in the  $\alpha 2$  ECDs- binding assay and absent from the  $\alpha 1$  ECDs- binding assay analysed with MASCOT.**

prot_acc	Hits	prot_score	prot_mass	prot_matches	prot_cover	pep_query	pep_exp_mz	pep_score
IPI00960040	LOC680097 histone cluster 1, H2ae	169	51695	12	13.5	129	425.7731	0.09
IPI00231192	LOC689064;LOC100134871;Hbb He	154	15972	12	44.9	145	459.7599	7.98
IPI00213546	Hspa11 Heat shock 70 kDa protein 1	121	70505	5	8	316	614.8395	45.17
IPI00205163	Cnpy2 Uncharacterized protein	74	20696	3	12.1	170	524.7864	19.04
IPI00367633	RGD1560350 hypothetical protein L	70	16841	1	8.4	347	643.3766	69.51
IPI00364262	Gars glycyl-tRNA synthetase	63	81741	2	3.3	350	657.8705	2.78
IPI00470317	Eef1g Elongation factor 1-gamma	60	50029	2	4.8	32	488.2887	2.4
IPI00358083	Ppp1r7 Protein phosphatase 1 regul	59	41271	1	3.1	298	634.895	59.2
IPI00371003	Krt25 Keratin, type I cytoskeletal 25	58	48913	2	4	245	545.7838	57.5
IPI00382241	Bco2 Ab2-079	56	54389	2	3.7	122	487.7673	16.65
IPI00188666	Krt27 Keratin, type I cytoskeletal 27	45	49078	1	2	239	545.7855	44.81
IPI00189404	Hddc3 Uncharacterized protein	43	20242	2	9.5	523	881.4503	11.1
IPI00365487	Eif3g Eukaryotic translation initiati	43	35629	1	4.1	369	687.8865	42.65
IPI00195999	RGD1560831 Uncharacterized prote	42	26613	1	3.7	247	546.8006	41.88
IPI00565381	LOC100363177;LOC100365139 Fer	41	20748	3	22.4	341	695.3793	3.27
IPI00200539	RGD1563551 mCG49427-like	41	19206	1	5.4	131	494.7804	40.85
IPI00207014	Krt19 Keratin, type I cytoskeletal 19	41	44609	4	7.9	96	404.2112	29.97
IPI00201528	Tsta3 GDP-L-fucose synthase	41	35774	1	3.7	287	564.8538	40.91
IPI00325281	Eef1a2 Elongation factor 1-alpha 2	40	50422	2	4.1	159	488.294	10.72
IPI00357947	Tbc1d20 Uncharacterized protein	40	45855	1	2.5	257	587.3081	40.23
IPI00368131	LOC100364984;LOC100360253 Unc	39	24644	2	11.2	386	658.8458	38.85
IPI00192216	Rab33b ras-related protein Rab-33B	39	25736	1	4.8	386	658.8458	38.85
IPI00196795	Rab15 Ras-related protein Rab-15	39	24268	1	5.2	386	658.8458	38.85
IPI00203760	Rab39 Uncharacterized protein	39	24905	1	5.1	386	658.8458	38.85
IPI00202238	Ndufb10 Uncharacterized protein	36	20845	1	6.8	461	735.4121	35.92
IPI00389636	Ppp2r1b Uncharacterized protein	36	76057	1	1.7	230	621.8909	36
IPI00231495	Map1lc3b Isoform 2 of Microtubule-c	35	14590	2	16.8	127	420.2794	35.18
IPI00191288	Cox4nb Neighbor of COX4	35	23390	1	4.3	150	481.2766	35.04
IPI00763927	Tcp111 T-complex protein 11-like p	35	56217	1	2.4	291	672.9058	34.69
IPI00358229	Abhd8 Uncharacterized protein	35	48337	2	2.3	121	571.8611	35.2
IPI00231650	Hist1h1d Histone H1.2	34	21974	1	5	257	554.2986	34.42
IPI00363763	RGD1311558 Isoform 1 of Shootin-1	34	71402	1	1.7	241	629.363	34.5
IPI00192612	Has1 Uncharacterized protein	33	65683	1	1.4	62	435.7863	32.55
IPI00205128	Ubl4 Ubiquitin-like protein 4A	32	17780	1	5.1	122	487.7673	32.26
IPI00358383	Pcdhb21 protocadherin beta-11	32	82822	1	1.6	310	650.3462	31.54
IPI00421802	Krt40 Keratin, type I cytoskeletal 40	30	48265	2	3.7	96	404.2112	29.97
IPI00421798	Krt32 Uncharacterized protein	30	51150	2	5.1	96	404.2112	29.97
IPI00948302	Atp5c1 ATP synthase gamma chain	29	32975	4	9.7	107	432.7598	14.22
IPI00201399	Alad Delta-aminolevulinic acid dehy	29	36008	2	6.4	217	524.8174	28.64
IPI00192234	Adrm1 Uncharacterized protein	29	32713	2	4.9	422	766.4308	28.73
IPI00210405	Met C-met/hepatocyte growth factor	29	15177	2	412	2	1478.8064	19
IPI00388143	LOC689656 Uncharacterized protei	28	38220	2	5.2	99	537.2172	28.12
IPI00949165	Copz1 Uncharacterized protein	27	20185	1	7.9	444	832.9532	26.61
IPI00212314	Msn Moesin	26	67697	2	3.3	251	552.8117	25.66
IPI00369635	Rdx Radixin	26	68501	3	4.6	238	538.3167	0.14
IPI00368617	Arhgef2 Rho guanine nucleotide exc	25	111840	2	1.9	90	439.7678	25.05
IPI00371863	Kpna5 Importin subunit alpha-6	25	60261	1	1.3	14	421.2471	25
IPI00200486	Khdrbs2 KH domain-containing, RN	23	38831	1	4	300	656.3455	23.4
IPI00454495	Rab31 ras-related protein Rab-31	23	21486	2	10.8	159	488.2841	5.52
IPI00205912	Nono Non-POU domain-containing c	23	54891	1	1.9	163	551.7986	22.93
IPI00476864	Rbm33 Uncharacterized protein	23	136361	2	1.7	145	545.3466	22.77
IPI00363828	Actr3 Uncharacterized protein	22	47164	3	6.7	324	705.4153	22.43
IPI00364414	Kpna3 Uncharacterized protein	22	57737	1	2.5	321	700.4139	21.74
IPI00212479	Hbe2 Uncharacterized protein	21	16378	1	6.8	347	644.8721	21.49
IPI00208197	Adprh [Protein ADP-ribosylarginine]	21	39935	1	2.8	271	551.812	20.54
IPI00362888	Arglu1 Arginine and glutamate-rich p	21	32868	1	4.1	177	417.2262	21.47
IPI00193605	Pfdn1 Uncharacterized protein	20	14247	2	17.2	257	558.3308	18.76
IPI00563558	- Uncharacterized protein	20	91547	1	1.1	200	544.8039	20.18
IPI00365036	Prex1 Uncharacterized protein	19	184560	3	2.1	511	583.9097	6.48
IPI00212365	Akap4 A-kinase anchor protein 4	19	93434	5	2	62	461.7437	7.27
IPI00362386	RGD1560175 similar to hypothetica	18	246437	2	0.7	336	620.8569	18.11
IPI00368084	Bcas3 breast carcinoma amplified s	18	101001	2	1.8	484	911.9341	18.45
IPI00563107	- Uncharacterized protein (Fragment	18	16740	1	9	302	710.8801	17.82
IPI00779103	LOC679154 family with sequence si	17	96613	3	1.1	328	609.3481	0.67
IPI00360078	Eml4 Uncharacterized protein (Frag	16	95649	2	1	250	568.8025	16.04
IPI00210005	Sycp3 Synaptonemal complex prote	16	29714	3	5.8	409	608.318	9
IPI00555187	Cap1 Adenylyl cyclase-associated p	16	51556	1	4	526	1086.6337	16.29
IPI00679252	Gabra2 Uncharacterized protein	15	51089	1	2.7	429	713.3727	15.12
IPI00369982	Mprl27 Uncharacterized protein	15	16014	1	7.3	183	633.2994	15.45
IPI00198781	Chma3 Neuronal acetylcholine rece	15	56960	1	1.4	102	738.426	14.97

**Table 12. Proteomics round 2: Hits identified in the  $\alpha 2$  ECDs- binding assay and absent from the  $\alpha 1$  ECDs- binding assay analysed with MASCOT.**

prot_acc	Hits	prot_score	prot_mass	prot_matches	prot_cover	pep_query	pep_exp_mz	pep_score
IPI00776619	Sptan1 Spectrin alpha chain, brain	429	284462	17	7	113	451.2685	35.78
IPI00360075	Lrpprc Leucine-rich PPR motif-containi	323	156554	13	9.8	73	426.7307	4.23
IPI00957899	LOC100360950 GF20391-like isoform 2	299	21227	9	37	96	451.2356	30.88
IPI00206171	Map2 Isoform MAP2x of Microtubule-as	258	202288	10	6.2	126	479.7794	1.31
IPI00205519	Uggt1 UDP-glucose:glycoprotein gluco	235	176320	12	7.7	77	429.2184	28.96
IPI00364046	Tuba1c Tubulin alpha-1C chain	233	49905	5	15.4	137	508.2849	45.06
IPI00199421	Tsnax Translin-associated protein X	212	32985	3	6.6	394	1038.5846	82.11
IPI00393508	Hist1h2bb Histone H2B	209	13914	5	27	86	477.2898	26.79
IPI00372557	Vars Valyl-tRNA synthetase	207	140280	4	4.7	114	482.2652	38.21
IPI00366405	Fam49b Uncharacterized protein	193	36753	5	17.3	167	569.2819	59.48
IPI00214889	Psmb3 Proteasome subunit beta type-	193	22949	3	12.2	65	446.7494	25.84
IPI00190462	Ppp2cb Serine/threonine-protein phosph	184	35552	5	11	115	480.7332	67.28
IPI00231966	Arf4 ADP-ribosylation factor 4	182	20384	4	15	40	420.7549	16.01
IPI00363440	Plxna2 plexin-A2	178	211469	8	5.1	89	421.2379	6.33
IPI00958044	Hist1h2ai histone cluster 1, H2ae-like	177	28038	8	29.2	76	425.7294	26.58
IPI00777130	Ncam1 Uncharacterized protein (Fragm	177	118504	7	5.8	69	424.2314	26.37
IPI00324893	Ywhaz 14-3-3 protein zeta/delta	175	27754	5	15.5	178	573.7977	1.07
IPI00556932	LOC100359692;LOC100365976 Histone	173	16342	5	27.9	96	451.2356	30.88
IPI00201407	Ppp3cb Serine/threonine-protein phosph	168	59076	5	10.5	187	584.7758	33.55
IPI00203181	Bag6 Isoform 2 of Large proline-rich pr	156	114576	3	3.6	159	557.3309	48.95
IPI00210975	Hyou1 Hypoxia up-regulated protein 1	154	111220	6	5.2	77	430.2513	29.24
IPI00389890	Dnm1 Isoform 5 of Dynamin-1-like prot	150	82488	5	8.7	73	420.2227	33.68
IPI00476899	Eef1b2 Uncharacterized protein	142	24660	4	16.4	117	473.2902	48.6
IPI00392583	Dynlrb1 Dynein light chain roadblock-ty	123	10983	2	21.9	168	558.7708	74.39
IPI00763802	Cyfp2 Uncharacterized protein	121	145440	9	5.6	52	411.7494	16.44
IPI00212776	Rps3 40S ribosomal protein S3	118	26657	3	14.4	157	546.7822	46.01
IPI00194324	Pdhb Pyruvate dehydrogenase E1 com	115	38957	2	4.5	342	874.451	76.21
IPI00201410	Ppp3ca Isoform 1 of Serine/threonine-p	114	58606	4	8.4	187	584.7758	33.55
IPI00212186	RGD1562259 ribosomal protein S20-lik	111	13368	3	19.3	203	624.3007	68.35
IPI00382182	Tsn Da2-35	111	31370	2	6.5	128	537.2587	56.93
IPI00204225	Glx3 Isoform 2 of Glutaredoxin-3	110	31341	1	7.5	312	956.507	109.68
IPI00422001	Lsm2 LSM2 homolog, U6 small nuclea	104	14770	1	14.5	288	1073.019	103.5
IPI00363423	Ckap5 cytoskeleton associated protei	100	196836	4	2.8	192	593.3586	55.5
IPI00197711	Ldha L-lactate dehydrogenase A chain	100	36427	2	7.5	164	565.7925	49.03
IPI00421855	Krt14 Keratin, type I cytoskeletal 14	99	52651	4	5.8	124	495.248	6.28
IPI00829443	Tubb5 Isoform 2 of Tubulin beta-5 chair	98	24256	4	13.7	140	505.2715	9.68
IPI00212523	Park7 Protein DJ-1	96	19961	1	10.1	352	947.5156	95.76
IPI00370090	Krt15 Keratin, type I cytoskeletal 15	93	48840	3	3.6	72	405.2054	32.27
IPI00360079	RGD1307235 Uncharacterized protein	93	134566	3	2.6	64	420.2241	40.96
IPI00369646	Pfas Uncharacterized protein	92	136808	3	3.5	176	582.3154	72.99
IPI00679252	Gabra2 Uncharacterized protein	91	51089	4	9.1	98	453.7376	47.32
IPI00367829	Cyfp1 Uncharacterized protein	86	145164	9	5.3	152	411.7494	16.44
IPI00869546	Xpo7 Uncharacterized protein	86	123947	2	2.4	85	591.3218	42.35
IPI00231134	Gnb2i1 Guanine nucleotide-binding pro	85	35055	3	9.8	148	530.2976	48.25
IPI00206054	Cntn1 Contactin-1	84	113423	4	3.8	99	452.753	27.13
IPI00192246	Cox5a Cytochrome c oxidase subunit 5	84	16119	2	16.4	126	496.7478	36.35
IPI00372857	Sarta Uncharacterized protein	84	22384	3	15.7	64	446.7113	32.17
IPI00371266	Naca nascent polypeptide-associated c	83	23370	1	7	302	807.8847	83.32
IPI00213559	Rtn1 Isoform RTN1-B of Reticulon-1	19	82951	1	1.2	101	491.7809	19.26
IPI00213013	Stip1 Stress-induced-phosphoprotein 1	19	62530	1	1.8	162	569.2872	18.77
IPI00366977	Cpne3 Uncharacterized protein	18	59648	1	1.7	94	450.2577	18.02
IPI00199980	Psmb7 Proteasome subunit beta type-	18	29908	2	6.9	376	1073.5724	18.9
IPI00366038	Atxn2l Atxn2l protein	17	112784	1	0.7	88	488.2571	16.55
IPI00188909	Col1a1 Collagen alpha-1(I) chain	17	137869	1	0.7	118	473.2913	17.23
IPI00389749	Dnm2 Isoform 2 of Dynamin-2	17	98098	3	2.5	90	440.2574	21.74
IPI00325049	Dnm3 Isoform 1 of Dynamin-3	17	97853	5	4.9	67	418.2159	19.33
IPI00211891	Nck2 Uncharacterized protein	17	42883	1	2.1	88	488.2571	16.55
IPI00199691	Nelf Isoform 1 of Nasal embryonic lutei	17	60244	1	1.7	88	488.2571	16.55
IPI00382214	Psmc3 Ab2-371	17	183415	1	0.5	88	488.2571	16.55
IPI00562727	RGD1565071 EG212225 protein-like	17	54929	1	1.8	88	488.2571	16.55
IPI00914757	Slc22a23 Solute carrier family 22 mem	17	74159	1	1	88	488.2571	16.55
IPI00569284	Tet2 Uncharacterized protein	17	213736	1	0.7	217	838.9493	17.21
IPI00778588	Top3a Uncharacterized protein	17	9714	1	9.4	88	488.2571	16.55
IPI00362313	Ubtfl1 Uncharacterized protein	17	46403	1	2.3	88	488.2571	16.55
IPI00869671	Dock9 Uncharacterized protein (Fragm	16	232884	2	1.1	125	532.2596	9.47
IPI00205419	Nf1 Neurofibromin	16	316880	3	1.7	229	651.8948	1.93
IPI00324590	Itgb7 integrin, beta 7	15	87572	1	2.1	300	912.4273	15.29
IPI00213554	Itpka Inositol-trisphosphate 3-kinase A	15	50839	1	5.4	357	1310.6636	15.28
IPI00400495	Neb Uncharacterized protein (Fragmen	14	40598	1	4.8	339	960.0231	14.43
IPI00958465	Uty (Fragment)	13	128187	1	1.3	311	854.5187	13.48

**Table 13: Hits identified in the  $\alpha$ 1 ECDs-binding assay and absent from the  $\alpha$ 2 ECDs-binding assay analysed with Mascot found in Proteomics round 1 and 2**

prot_descr	prot_score	prot_mass	prot_matches	prot_cover	pep_query	pep_exp_mz	pep_score
Tax_Id=10116 Gene_Symbol=Calm2;Calm3;Calm1 Calmodulin	158	16827	5	27.5	313	782.3983	82.45
Tax_Id=10116 Gene_Symbol=Vps35 maternal embryonic message 3	156	91669	6	9.3	178	622.3725	65.35
Tax_Id=10116 Gene_Symbol=Hspa9 Stress-70 protein, mitochondrial	107	73812	3	6	269	797.0264	49.39
Tax_Id=10116 Gene_Symbol=Gabra1 Gamma-aminobutyric acid receptor subunit 1	100	51721	5	10.1	101	509.7872	62.88
Tax_Id=10116 Gene_Symbol=Arg2 Arginase-related protein	86	37776	1	4.4	217	786.4623	86.04
Tax_Id=10116 Gene_Symbol=Arg2 Arginase-2, mitochondrial	86	38616	1	4.2	217	786.4623	86.04
Tax_Id=10116 Gene_Symbol=Ndufs8 Uncharacterized protein	71	23955	1	5.2	204	637.3755	70.82
Tax_Id=10116 Gene_Symbol=Sh3gl1 Endophilin-A2	61	41466	1	1.9	61	436.2566	61.05
Tax_Id=10116 Gene_Symbol=Farsa Phenylalanyl-tRNA synthetase alpha chain	57	57684	1	2.2	195	655.4112	56.94
Tax_Id=10116 Gene_Symbol=Ddx3x Uncharacterized protein	56	73100	1	1.8	156	646.4171	56.1
Tax_Id=10116 Gene_Symbol=Gga3 Uncharacterized protein	52	78710	1	1.7	211	679.4208	52.38
Tax_Id=10116 Gene_Symbol=Sod2 Superoxide dismutase [Mn], mitochondrial	51	24659	2	9.5	251	720.9343	51.47
Tax_Id=10116 Gene_Symbol=- Uncharacterized protein (Fragment)	50	34410	2	9.7	313	895.9964	49.95
Tax_Id=10116 Gene_Symbol=- Uncharacterized protein (Fragment)	47	225547	3	1.4	153	588.8526	46.88
Tax_Id=10116 Gene_Symbol=Calr Calreticulin	45	47966	2	3.8	94	488.2718	41.79
Tax_Id=10116 Gene_Symbol=Map1a Uncharacterized protein	38	324819	1	0.3	151	514.8324	38.14
Tax_Id=10116 Gene_Symbol=Atp6v1c1 V-type proton ATPase subunit C 1	37	43873	2	6.3	287	815.0042	36.83
Tax_Id=10116 Gene_Symbol=- Uncharacterized protein	36	14291	1	9	134	616.3315	36.35
Tax_Id=10116 Gene_Symbol=Atp6v0d1 Uncharacterized protein	36	40275	1	2.8	136	597.3638	35.67
Tax_Id=10116 Gene_Symbol=Ndufs1 NADH-ubiquinone oxidoreductase 75 kDa	35	79362	1	1.9	279	806.4742	34.61
Tax_Id=10116 Gene_Symbol=Ckap2l Uncharacterized protein	32	82658	1	1.6	242	697.3962	31.55
Tax_Id=10116 Gene_Symbol=RGD1565297 RAN binding protein 1-like	31	23722	1	4.4	106	517.7965	31.18
Tax_Id=10116 Gene_Symbol=Cct5 T-complex protein 1 subunit epsilon	29	59499	2	5	366	1070.105	29.46
Tax_Id=10116 Gene_Symbol=Lrrc16a Uncharacterized protein (Fragment)	27	143066	2	1.2	255	858.4806	27.48
Tax_Id=10116 Gene_Symbol=Acat3 Ab2-076	23	103244	2	2.9	191	702.4139	22.71

**Table 14: Hits identified in the  $\alpha$ 2 ECDs-binding assay and absent from the  $\alpha$ 1 ECDs-binding assay analysed with Mascot found in Proteomics round 1 and 2**

prot_descr	prot_score	prot_mass	prot_matches	prot_cover	pep_query	pep_exp_mz	pep_score
Tax_Id=10116 Gene_Symbol=Cap1 Adenylyl cyclase-associated protein 1	110	51556	3	9.9	404	1086.6218	75.45
Tax_Id=10116 Gene_Symbol=Gabra2 Uncharacterized protein	91	51089	4	9.1	259	713.3469	53.09
Tax_Id=10116 Gene_Symbol=Cnpy2 Uncharacterized protein	82	20696	1	6.6	248	722.3796	81.75
Tax_Id=10116 Gene_Symbol=Actr3 Uncharacterized protein	80	47164	5	8.9	233	705.3752	50.13
Tax_Id=10116 Gene_Symbol=Cct5 T-complex protein 1 subunit epsilon	70	59499	2	5.4	402	1070.0732	48.06
Tax_Id=10116 Gene_Symbol=Eef1g Elongation factor 1-gamma	69	50029	3	6.4	185	621.3167	53.67
Tax_Id=10116 Gene_Symbol=RGD1563551 mCG49427-like	66	19206	1	5.4	121	494.755	65.98
Tax_Id=10116 Gene_Symbol=Gars glycyl-tRNA synthetase	58	81741	1	1.1	99	450.238	57.71
Tax_Id=10116 Gene_Symbol=Ppp1r7 Protein phosphatase 1 regulatory subunit 7	53	41271	1	5	384	996.0356	52.8
Tax_Id=10116 Gene_Symbol=Nono Non-POU domain-containing protein 1	42	54891	1	1.9	164	551.7867	42.18
Tax_Id=10116 Gene_Symbol=Map1lc3b Isoform 2 of Microtubule associated protein 1C	37	14590	3	21.6	69	420.2321	38.17
Tax_Id=10116 Gene_Symbol=Ndufs1 NADH-ubiquinone oxidoreductase 75 kDa	36	79362	1	1.8	266	702.3893	36.48
Tax_Id=10116 Gene_Symbol=LOC100365478;LOC685091 high-molecular weight protein 1	32	23327	1	6.9	293	531.5948	31.65
Tax_Id=10116 Gene_Symbol=Pcdhb21 protocadherin beta-11	32	82822	1	1.6	197	650.2932	32.31
Tax_Id=10116 Gene_Symbol=Kpna5 Importin subunit alpha-6	28	60261	1	1.3	66	421.2283	28.34



**Table 15. Proteomics round 1: Hits identified in the  $\alpha$ 1 ECDs- binding assay and present in the  $\alpha$ 2 ECDs- binding assay analysed with MASCOT.**

prot_acc	Hits	prot_score	prot_mass	prot_matches	prot_cover	pep_query	pep_exp_mz	pep_score
IPI00231955	Calm2;Calm3;Calm1 Calmodulin	187	16827	6	26.2	204	547.2468	42
IPI00206624	Hspa5 78 kDa glucose-regulated protein	150	72302	7	9.5	155	493.7789	33.5
IPI00421389	Ndrp1 Protein NDRG1	138	42927	3	11.9	352	676.864	79.4
IPI00373591	Fubp1 Far upstream element-binding	122	67155	7	9.5	234	534.3141	24.96
IPI00358033	Ndufs1 NADH-ubiquinone oxidoreductase	80	79362	3	5.8	229	532.7991	26.42
IPI00215184	Rps25 40S ribosomal protein S25	60	13734	1	8	237	542.8337	60.19
IPI00470301	Cct5 T-complex protein 1 subunit epsilon	57	59499	1	1.8	160	547.2847	57.12
IPI00388209	PrkcsH Uncharacterized protein	55	59181	1	1.9	297	595.3281	54.7
IPI00951116	Hbb 16 kDa protein	53	15955	5	38.1	202	545.8051	9.48
IPI00364376	Mapk1ip1I Uncharacterized protein	50	23640	1	7.1	563	918.954	50.44
IPI00198665	Ssbp3 Uncharacterized protein	48	40395	1	2.6	246	576.3296	48.22
IPI00197585	Myg1 UPF0160 protein MYG1, mitochondrial	44	42862	1	2.6	270	550.3248	44.21
IPI00958235	RGD1565403 nucleoside diphosphate kinase	42	17104	4	33.1	68	741.3911	2.78
IPI00204065	Rufy3 Isoform 1 of Protein RUFY3	42	52873	2	4.7	85	473.7768	3.39
IPI00211593	Sod2 Superoxide dismutase [Mn], mitochondrial	42	24659	1	6.3	454	720.9189	42.24
IPI00192642	Gabra1 Gamma-aminobutyric acid receptor subunit 1	41	51721	2	1.8	160	483.2477	7.76
IPI00198118	Map1a Uncharacterized protein	41	324819	1	0.3	197	514.816	40.84
IPI00958625	LOC100365478;LOC685091 high-mobility group box 1	39	23327	1	6.9	518	531.6066	39.22
IPI00367660	RGD1562502 hypothetical protein LOC100365478	39	22410	1	7.6	501	558.3021	38.73
IPI00213552	Dync1li1 Cytoplasmic dynein 1 light chain 1	38	56757	2	4.6	124	511.3047	0.85
IPI00362341	RGD1565297 RAN binding protein 1-like 1	38	23722	2	5.4	449	691.3418	38.39
IPI00214192	Sh3gl1 Endophilin-A2	36	41466	1	1.9	116	436.2462	35.86
IPI00366327	Lrrc16a Uncharacterized protein (Frag)	35	143066	2	1.2	549	858.4612	35.23
IPI00205693	Atp1a2 Sodium/potassium-transporting ATPase 2	34	112145	1	1.5	509	810.3995	34.42
IPI00421395	RGD1304704 Uncharacterized protein	31	33804	1	2.7	192	511.812	31.07
IPI00188330	Ndufs8 Uncharacterized protein	27	23955	2	9.4	324	612.8325	0.4
IPI00551558	Krt2 Uncharacterized protein	26	69248	1	2	361	627.8218	25.5
IPI00197529	Zfp423 Zinc finger protein 423	25	147131	1	1	404	468.9272	24.62
IPI00203773	Mrp12 Uncharacterized protein	24	29423	1	5.1	416	677.3633	23.58
IPI00188112	Psph Phosphoserine phosphatase	21	24952	1	5.3	389	680.3787	21.41
IPI00363265	Hspa9 Stress-70 protein, mitochondrial	18	73812	1	1.8	358	667.3887	18.21

**Table 16. Proteomics round 2: Hits identified in the  $\alpha$ 1 ECDs- binding assay and present in the  $\alpha$ 2 ECDs- binding assay analysed with MASCOT.**

prot_acc	Hits	prot_score	prot_mass	prot_matches	prot_cover	pep_query	pep_exp_mz	pep_score
IPI00370815	Cct8 Uncharacterized protein	449	59550	17	27.7	89	444.7452	29.92
IPI00554039	RGD1565368 glyceraldehyde-3-phosphate dehydrogenase	436	35760	13	19.5	192	678.843	48.23
IPI00949013	Crmp1 Dihydropyrimidinase-related protein 1	415	62157	14	26.9	75	425.2151	34.77
IPI00767139	Gcn11 GCN1 general control of amino acid starvation 1	350	292886	20	10.2	107	443.2816	20.1
IPI00368347	Uba1 Ubiquitin-like modifier-activating enzyme 1	296	117713	8	9.8	120	492.7536	40.1
IPI00194045	ldh1 Isocitrate dehydrogenase [NADP] cytosolic	286	46705	12	30	38	404.2138	13.6
IPI00231929	Pkm2 Isoform M1 of Pyruvate kinase isozyme 2	283	57781	10	14.7	72	420.7689	16.92
IPI00370456	Psm2 26S proteasome non-ATPase regulatory subunit 2	265	100124	8	11.3	62	412.7318	21.09
IPI00326305	Atp1a1 Sodium/potassium-transporting ATPase 1	262	112982	6	7.5	187	570.3099	4.38
IPI00337168	Cct4 T-complex protein 1 subunit delta	259	58063	12	19.5	61	409.2168	3.99
IPI00339129	Dcl1 Uncharacterized protein	240	46558	8	11.4	168	560.794	36.88
IPI00214665	Acly ATP-citrate synthase isoform 1	222	120704	9	9.1	55	410.7348	8.26
IPI00364311	Gpi Glucose-6-phosphate isomerase	219	62787	7	11.8	67	416.1979	35.9
IPI00372700	Npepps puromycin-sensitive aminopeptidase	216	103279	12	12.6	125	500.2893	4.74
IPI00324741	Pdia3 Protein disulfide-isomerase A3	201	56588	11	19.2	88	444.735	23.06
IPI00188111	Cct6a Uncharacterized protein	199	57981	7	12.1	56	404.221	20.68
IPI00364286	Cct7 Uncharacterized protein	193	59620	11	12.9	66	415.2232	21.81
IPI00339148	Hspd1 60 kDa heat shock protein, mitochondrial	190	60917	4	10.3	100	456.7932	35.5
IPI00339109	LOC100360573;LOC100363860 40S ribosomal protein S25	186	15210	2	16.1	353	1129.0671	110.38
IPI00205372	Stxbp1 Isoform 1 of Syntaxin-binding protein 1	183	67526	5	10.1	121	479.2922	40.32
IPI00204843	Gnao1 Isoform Alpha-2 of Guanine nucleotide-binding protein G(o)1	176	40055	5	14.4	105	446.2444	14.25
IPI00231674	Arf3 ADP-ribosylation factor 3	164	20588	10	24.9	40	420.7549	16.01
IPI00365929	Pdia6 protein disulfide-isomerase A6	162	48730	3	6.1	221	693.8737	113.04
IPI00195818	Ipo9 Uncharacterized protein	160	116575	4	6.3	219	650.3499	83.95
IPI00188686	LOC100364558;LOC100360846 proteasome activator complex 1	160	25287	3	12.6	48	424.2147	74.2
IPI00231965	Arf5 ADP-ribosylation factor 5	158	20517	4	15	40	420.7549	16.01
IPI00191749	Psm1 Proteasome subunit beta type-1	156	26462	3	17.5	158	573.786	76.96
IPI00869818	Sec23a Uncharacterized protein	154	86106	3	3.5	265	701.408	50.35
IPI00869568	Vps35 maternal embryonic message 3	150	91669	9	10.2	55	399.7559	12.92
IPI00358371	RGD1560871 Uncharacterized protein	148	210759	8	3.6	89	421.2379	6.33
IPI00202725	LOC100363012;Rps21 40S ribosomal protein S21	135	9122	2	31.3	173	569.7266	76.43
IPI00768246	Uba2 Uba2 protein	135	70726	6	9.2	100	450.2385	35.18
IPI00471835	Hsph1 Heat shock protein 105 kDa	133	96357	3	4.4	167	560.3088	47.89
IPI00372520	Eef1b2l Uncharacterized protein	129	27952	2	5.9	204	809.4351	79.51
IPI00563746	Glyceraldehyde-3-phosphate dehydrogenase	128	33981	4	12.1	282	890.4225	67.08
IPI00360356	Actbl2 Uncharacterized protein	126	41936	2	9	323	895.9135	125.97
IPI00212512	Psm1 26S proteasome non-ATPase regulatory subunit 1	121	105681	5	3.9	76	428.7498	17.84
IPI00287338	Xpo1 Exportin-1	121	122959	9	8.1	111	475.8008	27.85
IPI00365944	My16l Myosin light polypeptide 6	119	16964	6	25.2	127	498.2792	48.74
IPI00231358	Pfn1 Profilin-1	119	14948	4	35.7	91	445.7508	3.27
IPI00212622	Hadha Trifunctional enzyme subunit alpha	114	82613	4	4.6	129	499.7804	23.02
IPI00769124	Usp42 Ubiquitin carboxyl-terminal hydrolase 42	19	146266	2	2	184	643.8314	7.08
IPI00190020	Atp2a2 Uncharacterized protein	18	114741	2	2.1	117	460.296	11.54
IPI00203214	Eef2 Elongation factor 2	18	95223	3	2.6	164	553.2857	5.47

